AN INVESTIGATION OF ADVANCED OXIDATION PROCESSES IN WATER TREATMENT

GAVIN WYATT SCHWIKKARD

MScEng (Natal); BScEng (Natal)

Submitted in fulfilment of the academic
requirements for the degree of
Doctor of Philosophy
in the
School of Chemical Engineering,
University of Natal, Durban.

February 2001

ABSTRACT

The deteriorating water quality in South Africa and changing legislation requiring the industrial implementation of waste minimisation and pollution prevention technologies has highlighted the need for the investigation of new effluent treatment technologies such as advanced oxidation processes.

This investigation details the evaluation of ultrasound, an emerging advanced oxidation process, to degrade organic compounds during water treatment. The objectives of the investigation included the design of a suitable ultrasonic laboratory reactor to investigate ultrasound chemistry and the sub-processes occurring during sonication. Atrazine was used as a model compound to compare the performance of ultrasound with that of ozone and hydrogen peroxide, already established advanced oxidation processes. Recommendations have also been made for the scale-up of ultrasonic processes.

A 500 mL ultrasonic cell containing an ultrasonic horn as an energy source was designed and constructed. The measurement of hydrogen peroxide concentration was used as a tool to indicate the process conditions under which the formation of free radical reactions during sonication are enhanced. These include the application of oxygen and air sparging or the addition of a commercial source of hydrogen peroxide. It was found that oxygen sparging and a high acoustic power input should be used in ultrasonic processes with a short retention time, and conversely, that air sparging and a lower acoustic energy source should be used in processes with a long retention time. A flow loop system should be considered to maximise oxidation both within and beyond the sonicated zone, gas sparging should only occur within the sonication zone else the degradation of hydrogen peroxide is encouraged. Ultrasound is most effectively applied in water treatment as a pretreatment stage in combination with other technologies and not as a stand-alone process.

Atrazine was used as a model compound to compare the performance of ultrasound with ozone because of its persistence in the environment and resistance to degradation. Atrazine was degraded during sonication and ozonation, degradation increased with the addition of hydrogen peroxide. Ozone decomposition (and hence free radical reactions) was enhanced when ozone was combined with ultrasound or hydrogen peroxide. Enhanced ozone decomposition during ozonation combined with sonication is due to the conditions (high temperatures and pressures) as well as the free radical reactions occurring within the collapsing cavitation bubbles and at the gas-liquid interface. The enhancing effect of combining ultrasound with ozone was greatest at the low ozone concentrations typically applied during water treatment.

Atrazine degradation during sonication and ozonation is predominantly due to the reaction with hydroxyl radicals. Atrazine degradation products identified using gas chromatography and mass spectrometry were deethylatrazine, hydroxyatrazine and deethyldeisopropylatrazine (tentatively identified).

PREFACE

I, Gavin Schwikkard, declare that unless indicated, this thesis is my own work and that it has not been submitted, in whole or in part, for a degree at another University or Institution.

GW SCHWIKKARD

February 2001

ACKNOWLEDGMENTS

I would like to express my thanks and appreciation to the following people and organisations who have contributed to the investigation:

The Water Research Commission and Pollution Research Group for funding the investigation.
Diarec Diamond Sales *cc* for assistance in acquiring the ultrasonic horn.
Umgeni Water for the loan of an ozone generator.
The Foundation for Research Development for personal funding during the investigation.
Sasol for the postponement of my bursary obligation.

My supervisor, Prof. C Buckley, for his dedication, advice and commitment to excellence.
Mr C Brouckaert for advice on process modelling.
Prof. D Mulholland of the School of Chemistry and Applied Chemistry for the use of HPLC equipment.
Mr K Robertson and Mr L Henwood from the workshop of the School of Chemical Engineering for the construction of the ultrasonic cell and for assistance with equipment maintenance.
The laboratory technicians, Ms D Harrison, Ms S Wadley and Mr B Parel, for their technical support.
Ms S Freese from Umgeni Water for advice on setting up the ozone system.
Ms A Hansa from the ML Sultan Technikon for assistance with the identification of degradation products.
Mr R Coetzer from Sasol Technology for assistance and advice with statistical modelling.
Mr I Vorster from the Rand Afrikaans University for mass spectroscopy analysis.

My fellow graduate students for their friendship and experiences we shared learning from one another.
My family, David, Dorothy, Mandy and Joanne, for their continual encouragement and support throughout the investigation.
My wife, Sianne, for performing the HPLC atrazine analysis, assisting with the interpretation of mass spectra and for the sacrifices she made during the writing of this thesis.

And to God, the Father, Son and Holy Spirit, who add meaning to life.

CONTENTS

Contents cont.

Contents cont.

Contents cont.

Contents cont.

Contents cont.

APPENDICES

A. EQUIPMENT CHARACTERISATION

B. ANALYTICAL PROCEDURES

C. ULTRASOUND EXPERIMENTAL DATA

Contents cont.

D. Ozone Experimental Data

E. Atrazine Experimental Data

F. Statistical Analysis

Contents cont.

FIGURES

Figures cont.

Figures cont.

Figures cont.

Figures cont.

Figures cont.

Figures cont.

Figures cont.

TABLES

Tables cont.

Tables cont.

Tables cont.

Tables cont.

Tables cont.

Tables cont.

Tables cont.

Tables cont.

Tables cont.

Tables cont.

Tables cont.

NOMENCLATURE

A	atrazine	
A_{ws}	area of the wetted surface of the vessel	
B	generic chemical compound	
C	concentration	mg L^{-1}
C_A	atrazine concentration	mg L^{-1}
C_B	concentration of chemical compound B	mg L^{-1}
C_i	concentration of a species i in water	mg L^{-1}
C_0	initial concentration	mg L^{-1}
C_P	liquid heat capacity	J kg^{-1} K^{-1}
C^*	liquid-phase ozone concentration	mg L^{-1}
D_{O_3}	ozone diffusivity in water	m^2 s^{-1}
f_A	fraction of radiation absorbed by atrazine	
f_0	ultrasonic resonance frequency	Hz
$\Delta G_f°$	standard Gibbs free energy of formation	J mol^{-1}
$\Delta H_f°$	standard heat of formation	J mol^{-1}
H	Henry's Law constant	atm m^3 mol^{-1}
Ha	dimensionless Hatta number	
$[HO^\bullet]_{SS}$	steady state hydroxyl radical concentration during ozonation	mg L^{-1}
$[HO^-]$	hydroxide ion concentration	mg L^{-1}
hv	ultraviolet radiation	
I	current	ampere
I_a	intensity of adsorbed radiation	Einstein s^{-1}
I_A	atrazine degradation rate due to direct photolysis	mol L^{-1} s^{-1}
I_0	effective intensity of radiation in water	Einstein L^{-1} s^{-1}
k	reaction rate constant	
$k_{HO,B}$	rate constant for the reaction between compound B and HO radicals	M^{-1} s^{-1}
k_d	rate constant for the direct reaction between ozone and a compound	
k_L	liquid-phase mass transfer coefficient	m s^{-1}
k_I	rate constant for the initiation reaction between solute B and hydroxide ions	

Nomenclature cont.

k_S	rate constant for the scavenging reaction between solute *B* and hydroxyl radicals	
L	effective path of radiation in a liquid	cm
LC_{50}	lethal chemical concentration that kills 50 % of a group of animals	mg m^{-3}
LD_{50}	lethal chemical dose that kills 50 % of a group of animals	mg kg^{-1}
m	mass	kg
n	sample size	
$[O_3]$	ozone concentration	mg L^{-1}
p	pressure at distance *r* from bubble centre	Pa
P	external liquid pressure at infinity	Pa
P_A	liquid pressure	Pa
P_0	ultrasonic wave amplitude	m
pH	negative log of the activity of hydrogen ions	
pKa	acid dissociation constant	
P_{O_3}	gas-phase ozone partial pressure	Pa
q	bubble gas pressure at maximum radius	Pa
Q	power	W
r	distance from bubble centre	mm
r_m	distance from bubble centre at which maximum liquid pressure occurs	mm
R	bubble radius	mm
R_m	maximum bubble radius	mm
R_0	bubble radius at time $t = 0$	mm
R^2	coefficient of determination	
s	standard deviation	
S_i	scavenger species in water such as inorganic or organic solutes	
SS_{reg}	variability in data explained by a regression model	
SS_{res}	unexplained variability in data, usually attributed to error	
SS_{total}	total variability in data	
t	time	s
t_D	diffusion time	s
t_R	reaction time	s

Nomenclature cont.

T	temperature	°C
T_{max}	maximum temperature in bubble	°C
T_0	ambient temperature of surrounding liquid	°C
T_v	temperature of the inner vessel wall	°C
u	fluid velocity at distance r from bubble centre	m s^{-1}
V	volume of irradiated solution	m^3
x_i	a sample point	
$\bar{x}$	sample mean	
x_w	thickness of the inner wall	
y_i	a measured dependent variable	
$\widehat{y_i}$	the predicted value of y from a regression model	
$\bar{y}$	the mean of the dependent variable	
Z	volume compression ratio $(R_m/R)^3$	
Greek letters		
ε_i	molar extinction coefficient of a species i in water	mol cm^{-1} s^{-1}
$\in_{600}$	molar absorptivity at a wavelength of 600 nm	M^{-1} cm^{-1}
γ	specific heat ratio of gas in bubble	
π	constant with an approximate value of 3,14159	
Φ_A	quantum yield of atrazine	mol $quantum^{-1}$
$\Phi_{H_2O_2}$	quantum yield of hydrogen peroxide	mol $quantum^{-1}$
ρ	liquid density	kg m^{-3}
σ	liquid surface tension	N m^{-1}
ω	angular frequency	rad s^{-1}
Prefixes		
k	kilo . . . . 10^3	
M	mega . . . 10^6	
m	milli . . . 10^{-3}	
μ	micro . . . 10^{-6}	
n	nano . . . 10^{-9}	
p	pico . . . . 10^{-12}	

ABBREVIATIONS

AEA	Atomic Energy Authority, United Kingdom
amu	atomic mass unit
AR	analytical reagent grade
ASTM	American Society for the Testing of Materials
ATP	adenosine triphosphate
BOD	biological oxygen demand
COD	chemical oxygen demand
DM	Deutsche mark
DMP	2,9-dimethyl-1,10-phenanthroline
DOE	Department of Energy, United States of America
EDTA	ethylenediaminetetraacetic acid
EPA	Environmental Protection Agency, United States of America
ESKOM	Electricity Supply Commission, South Africa
GAC	granular activated carbon
HPLC	high performance liquid chromatography
LAB	laboratory reagent grade
MSDS	Materials Safety Data Sheet
NADP	nicotinamide adenine dinucleotide phosphate
NADPH	reduced form of NADP
NMR	nuclear magnetic resonance spectroscopy
NOM	natural organic matter
RAU	Rand Afrikaans University
SASOL	South African Coal, Oil & Gas Corporation Ltd.
TOC	total organic carbon
UV	ultraviolet
WRC	Water Research Commission, South Africa

GLOSSARY

aerobic	in the presence of oxygen
adsorption	attachment of molecule or ion to a substrate by manipulation of electrical charge or pH
advanced oxidation process	a process that produces sufficient hydroxyl radicals to affect water treatment
anions	atoms that have gained one or more electrons
assimilative capacity	capacity of water to accommodate additional pollutants without a decrease in water quality
biological oxygen demand	oxygen required to meet the metabolic needs of aerobic organisms in water rich in organic matter
biorefractory	resistant to biological degradation
carcinogenic	capable of causing or promoting the development of cancer
cations	atoms that have donated one or more electrons
cavitation	formation, expansion and implosion of bubbles in a liquid
cavitation threshold	acoustic pressure amplitude above which cavitation will be induced
cavitation noise	noise caused by the collapsing cavities during sonication
chemical oxygen demand	oxygen required to oxidise all organic matter in a sample that is susceptible to oxidation by a strong chemical oxidising agent
chemiluminescence	emission of visible light accompanying a chemical reaction
coefficient of determination	the proportion of total variability explained by a regression model
confidence interval	the range around a calculated statistic that contains the true value of the statistic for a particular level of confidence
degrees of freedom	the number of independent parameters associated with an experiment
eutrophication	the enrichment of water bodies (such as dams or lakes) with organic or mineral nutrients so that the resultant growth and decay of algae and other plants significantly depletes the oxygen content of the water
Fenton's reaction	reaction between hydrogen peroxide and ferrous salts producing hydroxyl radicals
fluence	the total radiant ultraviolet energy per cross sectional area of target
fluorescence	emission of visible light from a substance that has absorbed radiation of a shorter wavelength from another source
free radical	atom or molecule that contains one or more unpaired electrons
granular activated carbon	porous material made from the controlled combustion of coal, wood or coconut shells, used for the adsorption of pollutants during water treatment

Glossary cont.

Hatta number	dimensionless group indicating the relative contribution of reaction kinetics to mass transfer effects in gas absorption reactions
heterogeneous	involving more than one phase
homogeneous	only involving one phase
hydrodynamic cavitation	cavitation induced in a flowing liquid system by a pressure variation caused by a change in velocity
hydrophobicity	ratio of hydrophobic groups to hydrophilic groups in a molecule
incandescence	emission of visible light due to high temperatures
in situ	in its original place
in vivo	in the living body
magnetostrictive effect	a material that undergoes a change in dimension during magnetization
mean	the average value of a sample
mineralisation	complete degradation of organic compounds to carbon dioxide and water
mutagenic	capable of causing mutation
oxidant	an oxidising agent
oxidation	a chemical reaction in which a compound loses electrons, a hydrogen atom or gains an oxygen atom
pathogenic	capable of producing disease
photolysis	radiation with ultraviolet light
photophosphorylation	production of ATP
piezoelectric effect	a ceramic material that undergoes a dimensional change when an electric charge is applied across the opposite faces of the material
radiolysis	radiation with X-rays or other high-energy sources
recalcitrant	resistant to biodegradation
rectified diffusion	mechanism for cavity growth in which more gas diffuses into a cavity when it is large in a rarefaction phase than what diffuses out when it is small in a compression phase
regioselective	reactant orientation so as to produce exclusively, or nearly so, one of several potential isomeric products
salinisation	the accumulation of salts in an inland water body (such as a river or dam)
sonication	radiation with sound waves
sonochemistry	the application of ultrasound in chemistry
sonoluminescence	emission of visible light during radiation of a liquid with sound waves

Glossary cont.

spin trap	a diamagnetic molecule that reacts with a short-lived free radical to produce a longer-lived paramagnetic addition product for identification using electron spin resonance
standard deviation	a measure of the spread or variation in sample data, the average distance between a particular point and the sample mean
stripped gas liquor	effluent produced in the quenching of hot gas from coal gasifiers from which organic contaminants have been removed and ammonia and acid gas levels have been reduced
synergism	a greater combined effect than the summation of the individual effects
total organic carbon	organic carbon other than carbon dioxide (inorganic)
ultrasound	sound waves with a frequency above the audible range (16 kHz)

1

INTRODUCTION

Water is the key to development, both present and future (Kasrils, 2000).

1.1 WATER RESOURCES IN SOUTH AFRICA

The address delivered by Ronnie Kasrils, the Minister of Water Affairs and Forestry, on the 17 March 2000 at the Water Week celebrations emphasised that water is key to development (Kasrils, 2000). Technological development will be one of the key drivers ensuring that the 21st century becomes the century of the African Renaissance as projected by President Thabo Mbeki. Development not only entails industrial and economic growth but also the upliftment of the people in the provision of basic services such as potable water, sanitation and electricity. All these facets of development, as outlined by the Minister of Water Affairs at the Water Week celebrations, are reliant on water. South Africa is one of the leading economies in Africa and will thus play a major role in spearheading the upliftment of the African continent. South Africa, however, is not a water-rich country and will have to deal efficiently and manage effectively its limited available water resources not only to ensure its own development but also its role in facilitating the century of the African Renaissance.

The water situation in a country can be categorised, as presented in Table 1.1, in terms of the total annual volume of renewable surface water per head of population (Muller, 2000).

Table 1.1 : Classification of the water situation in a country (Muller, 2000)

Water availability (m^3/person/year)	Category of water situation
< 500	absolute scarcity of water
500 to 1 000	chronic water scarcity: lack of water begins to hamper economic development and human health and welfare
1 000 to 1 700	periodic or regular water stress
> 1 700	will suffer only occasional or local water problems

The total volume of renewable surface water in South Africa is approximately 53 500 million m^3 per annum (O'Keeffe et al., 1992). South Africa, based on the population in 1995 and that projected at the present growth rate for 2025, was classified according to Table 1.1 for 1995 (1 200 m^3 available water per person per year) as a country that experiences periodic or regular water shortages and for 2025 (730 m^3 available water per person per year) as a country that will face chronic water shortages and where economic development will be hindered by the lack of water (Muller, 2000).

Rivers are the most important water source in South Africa, there are few natural lakes and only 45 % of the available groundwater can be utilised economically (Rabie and Day, 1992). River flow is highly variable due to the seasonal changes in rainfall and the uneven distribution across the country. The highest rainfall occurs along the eastern seaboard whereas the greater part of the interior and western portion of the country are arid or semi-arid. The South African average annual rainfall, 497 mm per year, is below the world average of 860 mm (Rabie and Day, 1992). Approximately 65 % of the country receives less than 500 mm of rain per year and 21 % below 200 mm per year. The annual evaporation rate across the country varies between 1 100 and 3 000 mm and is on average greater than the annual rainfall. It is estimated that only about 9 % of rainfall reaches the rivers (Muller, 2000). The variability in flow and high evaporation rate results in only approximately 33 000 million m^3 (62 %) of the annual runoff of 53 500 million m^3 being practically exploitable (O'Keeffe et al., 1992).

Water demand estimates for 1996 indicated that water use, approximately 20 000 million m^3, was almost 40 % of the total available water and 61 % of the economically exploitable water. In 2030 water use is estimated to be approximately 55 % and 80 %, respectively, of the total available and economically exploitable water (Muller, 2000). Projections of the expected total water demand per sector in South Africa (van der Merwe, 1995) are presented in Table 1.2.

Table 1.2 : Estimates of South African water demand per sector in 1990, 2000 and 2010 (van der Merwe, 1995)

Sector	1990		2000		2010	
	million m^3/year	%	million m^3/year	%	million m^3/year	%
municipal and domestic	2,281	12.0	3,220	14.4	4,477	17.3
industrial	1,448	7.6	2,043	9.1	2,961	11.4
mining	511	2.7	582	2.6	649	2.5
power generation	444	2.3	779	3.5	900	3.5
irrigation	9,695	50.9	10,974	48.9	11,885	45.9
stock watering	288	1.5	316	1.4	358	1.4
nature conservation	182	1.0	187	0.8	191	0.7
forestry run-off reduction	1,427	7.5	1,570	7.0	1,700	6.6
estuaries and lakes	2,767	14.5	2,767	12.3	2,767	10.7
Total	**19,043**	**100**	**22,438**	**100**	**25,888**	**100**

The growing water demand in South Africa has traditionally been addressed by increasing water supply with the building of dams and the transfer of water between river catchment basins. Total water storage capacity has been increased from 4 400 million m^3 in 1956 to the present 29 500 million m^3 (Muller, 2000). More dams could possibly be built in the eastern part of the country where rainfall is highest, however, good dam sites are limited and environmental activists would protest the ecological impact of such a dam. Inter-basin transfers have also been used to augment water supplies in areas such as the province of Gauteng where water demand is high. The population census of 1996 indicated that 18 % of South Africa's population lives in Gauteng (Central Statistical Service, 2000). Gauteng is also home to 60 % of the industrial and mining activity in South Africa (van der Merwe, 1995) and 30 % of total electricity consumption (Central Statistical Service, 2000). Water supply to the Gauteng region is supplemented under the Tugela-Vaal Scheme where water is pumped from the upper Tugela River across the Drakensberg watershed into the Sterkfontein Dam from where it is released on demand into the Vaal River system (Laburn, 1995; van der Merwe, 1995). An international venture, the Lesotho Highlands Water Project, is under construction to help meet the projected water demand in Gauteng till the year 2025. Future water supplies could possibly be obtained from the Zambesi River with a pipeline across eastern Botswana or from neighbouring Mozambique (Laburn, 1995; van der Merwe, 1995).

Rivers in South Africa are not only under pressure due to the increasing demand for water but also due to the reducing water quality caused by inadequate effluent treatment and illegal waste discharges. Rapid urbanisation, poor water management and the lack of funding are leading to organic pollution and eutrophication becoming serious problems in many areas (van der Merwe, 1995). Organic pollution in rivers also occurs due to chemicals such as pesticides being carried in irrigation runoff from agricultural lands. Conventional methods of water treatment are not always successful in the degradation of such organic compounds. Investigation of new treatment methods, such as advanced oxidation technologies, is thus required for the degradation of biorefractory organic compounds.

1.2 WATER LEGISLATION IN SOUTH AFRICA

Both the efficient use and effective management of available water resources are required to ensure that economic development is not hindered due to the lack of water and that the whole nation is provided with basic services. Effective management is set in order through the promulgation by government of legislation dealing with water issues. Water legislation has changed significantly with the democratically elected South African government of 1994.

Water management has been evident in South Africa since historic times; tribal laws required that people washed downstream from where drinking water was collected. Jan van Riebeeck, during early colonisation by the Dutch, also decreed that the washing of a soldier's breeches was not allowed to take place upstream of a water off take point. The Union Health Act of 1919 (Act 36 of 1919) was the first national legislation in

South Africa that dealt with water issues; liquid effluent had to be disposed of on land and was not allowed to pollute any surface water (Quibell et al., 1997). Water reuse became inevitable with increasing demand and the Water Act of 1956 (Act 54 of 1956) stipulated that all effluent be returned to the water body from which it was drawn. The effluent, however, had to comply with certain standards (the Uniform Effluent Standards) so as to prevent a decrease in quality of the receiving waters (Quibell et al., 1997). Water legislation, as embodied in the Water Act of 1954, was based on Roman law with the riparian principle of water rights being linked to land ownership (Kidd, 1997b). The Act distinguished between *private* and *public* water where *private* water was defined as that which had risen or fallen naturally on any piece of land; the land owner enjoyed exclusive use of the water but could not pollute it. The linking of water rights to land ownership in a water-scarce country such as South Africa resulted in a significant imbalance in the access to water by the majority of the South African population especially during the apartheid era (Kidd, 1997b).

The Constitution of the new government (the Interim Constitution was enacted with Act 200 of 1993 and the Final Constitution with Act 108 of 1996) included a Bill of Human Rights (Kidd, 1997a). The Constitution declared that everyone has the right to access to sufficient water and to an environment that is not harmful to their health or well-being (RSA, 1996). The mandate of government is thus to address these issues and provide the legal framework within which these rights can be fulfilled.

The right to an adequate supply of safe drinking water is being addressed through the Reconstruction and Development Programme wherein government is committed to providing a basic water supply of 25 L per person per day to within 200 m from a homestead (van der Merwe, 1995). The fulfilment of this constitutional right required the reform of existing water legislation. New water policy was published in the 1997 White Paper on National Water Policy, new legislation was enacted with the Water Services Act (Act 108 of 1997) and the National Water Act (Act 36 of 1998). The Acts ensure that South Africa's water resources are protected and used in a sustainable way that is of benefit to everyone. The definition of *private* or *public* water was abolished and all water whether on land, underground or in surface channels is regarded as part of the common resource (DWAF, 1997). National government is to act as the custodian of the nation's water resources, and water management is to be practised per catchment basin. Water management is to include an environmental reserve that is recognised as the amount of water required by the environment to sustain the integrity of ecosystems (GCIS, 1999; Kidd, 1997b). The slogan of the Department of Water Affairs and Forestry *Some, For All, Forever* summarises the goals of water management in South Africa which is to ensure:

- access to a limited resource,
- on an equitable basis,
- in a sustainable manner, now and in the future (DWAF, 1997).

The right to an environment that is not harmful to a person's health requires that government prevents water pollution so as to protect the quality of water resources in South Africa and ensure the sustainable use of available water resources (DWAF, 1997). Water quality is not only defined by the biological, chemical or physical attributes but, recognising that water resources are dynamic ecosystems, includes indicators such as biotic diversity (GCIS, 1999). The quality of South African water resources is declining primarily due to salinisation, eutrophication and pollution by trace metals and micro-pollutants (Kidd, 1997b; O'Keeffe et al., 1992). Water quality may in the future, especially in places in the interior of the country, become a more important factor in water management than the increasing demand for water (van der Merwe, 1995).

Industrialisation and economic development inevitably lead to pollution and the deterioration in quality of water resources. The allowed environmental impact, however, must be managed so as to ensure sustainable development, in that future development is not jeopardised by the present use of available resources, and a long-term healthy economy (Walmsley, 1995). Water quality management in South Africa was initiated with the Water Act of 1954 that required effluent discharges to comply with the Uniform Effluent Standards. The standards consisted of a general standard applicable throughout the country, a special standard for certain rivers and, later, a phosphate standard applicable to water sources where eutrophication was a problem (Kidd, 1997b; Quibell et al., 1997). Standards were amended with legislation (and made more stringent where necessary) due to the continuing deterioration in water quality. Limitations of the Uniform Effluent Standards included that no incentives were provided for pollution reductions to below the maximum permitted level and that the standards were designed for point pollution sources without accounting for the cumulative impact of several sources on a waterway (Kidd, 1997b).

Water quality management changed in the late 1980s with the adoption of the Receiving Water Quality Objectives (Kidd, 1997b; O'Keeffe et al., 1992; Quibell et al., 1997). The policy was based on the assimilative capacity of effluent-receiving water bodies to dilute or degrade pollutants. Site-specific standards were formulated to govern effluent discharge such that quality specifications of the receiving water, based on the needs of downstream users, were not exceeded. Receiving Water Quality Objectives were managed in conjunction with a pollution-prevention approach. Pollution-prevention strategies had to be incorporated into the design of plants and companies had to show a commitment to the reduction of effluents at source. Administration of the Receiving Water Quality Objectives was limited by the difficulty of establishing the exact needs of downstream users (Kidd, 1997b).

Water quality management in South Africa, since 1995, has changed with the primary objective being to ensure sustainable development. Water resources are to be managed on a catchment basin basis with an integrated approach that secures a healthy, stable water resource base to meet both current and future water needs of South Africa (GCIS, 1999). Some impact on the environment is allowed but the impact is to be controlled and managed within a system of waste minimisation technologies, pollution prevention, recycling and water reuse strategies. The use of low-water or zero-effluent technologies are to be encouraged with the phased-in introduction of effluent charges and the efficient use of water with voluntary as well as mandatory

measures for water conservation (GCIS, 1999). These measures form part of the National Strategy Framework for Water Conservation and Demand Management that is being developed by the Department of Water Affairs and Forestry. This Framework is to provide a motivation for water conservation in South Africa, list the objectives and goals of water conservation and suggest possible water conservation measures (DWAF, 2000). The Waste Discharge Charge System is being developed as part of the Water Conservation Framework in which a user will pay to be able to discharge effluent to a river (DWAF, 2000).

Water quality management policies are being implemented by government so as to ensure that technological development can take place today but not at the expense of water needs of future generations.

1.3 ADVANCED OXIDATION TECHNOLOGIES

Government may introduce legislation to effectively manage water quality and supply, however, daily water usage by people must also change to reflect the true value of water. A culture of water conservation focuses on minimising wastage and includes water recycling. Pollutants not readily degraded using conventional water treatment methods, such as some pesticides and organic compounds, are present in water sources and industrial effluents. Research into new or more efficient water treatment technologies is thus vital to combat deteriorating water quality due to pollution. Trihalomethane by-product formation during chlorination has also initiated research into other water treatment technologies such as advanced oxidation processes (Kuo and Mou, 1997; Peyton, 1990).

The focus on waste minimisation and water conservation will result in the production of concentrated or toxic residues. Techniques need to be developed to responsibly degrade these streams. Advanced oxidation has the potential to degrade (fully or partially) these streams.

Advanced oxidation processes are defined as processes that generate hydroxyl radicals in sufficient quantity to affect water treatment (Glaze et al., 1987; Glaze et al., 1992). These processes include oxidising agents such as ozone, ultraviolet radiation, hydrogen peroxide, Fenton's reagent, ultrasound or combinations thereof (Huang et al., 1993; Sen Gupta et al., 1995; Yue, 1997). Hydroxyl radicals are a powerful oxidant with an oxidation potential, as shown in Table 1.3, second only to molecular fluorine. Typically, a stronger oxidant also exhibits a faster oxidation reaction (Clarke and Knowles, 1982; Huang et al., 1993).

Table 1.3 : Standard oxidation/reduction potentials at 25 °C and 101,3 kPa of selected oxidising agents (Huang et al., 1993; Vanysek, 1998)

Oxidising agent	Redox reaction	E^o (V)
fluorine	$F_2 + 2e^- \rightarrow 2F^-$	2.87
hydroxyl radical	$HO^\bullet + H^+ + e^- \rightarrow H_2O$	2.33
ozone	$O_3 + 2H^+ + 2e^- \rightarrow O_2 + H_2O$	2.08
hydrogen peroxide	$H_2O_2 + 2H^+ + 2e^- \rightarrow 2H_2O$	1.78
chlorine	$Cl_2 + 2e^- \rightarrow 2Cl^-$	1.36

Hydroxyl radicals are not only a stronger oxidant than chlorine, as shown in Table 1.3, but are also less selective than molecular ozone (Glaze et al., 1987; Huang et al., 1993; von Sonntag, 1996). Hydroxyl radicals react with most organic and many inorganic solutes with high rate constants that approach diffusion-controlled limits (Hoigné, 1997; von Sonntag, 1996). Radical scavengers, however, such as bicarbonates, carbonates and natural organic matter decrease the effectiveness of hydroxyl radicals (Masten and Davies, 1994). Typical rate constants for the second-order reaction with hydroxyl radicals are listed in Table 1.4 (Glaze et al., 1992).

Table 1.4 : Rate constants for the reaction between hydroxyl radicals and selected compounds (Glaze et al., 1992)

Compound, *B*	$k_{HO,B}$ (M^{-1} s^{-1})
benzene	$7{,}8 \times 10^9$
toluene	$3{,}0 \times 10^9$
1-butanol	$4{,}2 \times 10^9$
vinyl chloride	$7{,}1 \times 10^9$
trichlorethylene	$4{,}0 \times 10^9$
tetrachloroethylene	$2{,}3 \times 10^9$
chlorobenzene	$4{,}5 \times 10^9$
nitrobenzene	$3{,}9 \times 10^9$

Advanced oxidation processes have the potential for complete oxidation (mineralisation) of organic pollutants to carbon dioxide, water and salts at ambient temperature and pressure (Glaze et al., 1992; Yue, 1992). The processes are also suited for use in combination with other technologies as a pretreatment or polishing step. Partial oxidation of pollutants where reaction conditions or times may not allow for complete oxidation has the potential to produce less refractory compounds that can be degraded biologically (Glaze et al., 1992; Yue, 1992). On-site methods for toxic waste degradation eliminate waste transportation

and handling and thus comply with waste minimisation practises government is requiring industry to implement (Bull and Zeff, 1991).

Advanced oxidation processes have been successfully used to degrade compounds such as methyl *tert*-butyl ether from leaking gasoline tanks, chlorinated organics, aromatics and phenolics (Bull and Zeff, 1991; Glaze, 1987; Kim et al., 1997; Peyton, 1990; Sen Gupta et al., 1995; von Sonntag, 1996).

1.4 PROJECT BACKGROUND

Advanced oxidation research at the University of Natal, Durban, under Prof. Chris Buckley began in 1991 with a project funded by the Water Research Commission entitled *The evaluation of different methods to produce free radicals for the oxidation of organic molecules in industrial effluents and potable water with special reference to CAV-OX®* (Winship, 1999). The project included an evaluation of the advanced oxidation system, CAV-OX®, that employed UV radiation, hydrogen peroxide and hydrodynamic cavitation for the degradation of low-level concentrations of organic pollutants in water (Shah et al., 1999f). Hydroxyl radical formation during hydrodynamic cavitation was compared with that during ultrasonic cavitation. Ultrasound, an emerging advanced oxidation process, was identified as having potential for the treatment of industrial effluents (Shah et al., 1999f; Winship, 1999).

Ultrasonic research was initiated in 1992 as the MSc(Eng) project of Schwikkard (Schwikkard, 1995). The project, partially funded by SASOL, was entitled *An investigation of the sonochemical degradation of hydantoin compounds*. Hydantoin compounds are found in the stripped gas liquor at a petrochemical plant and increase in concentration as the liquor is recycled for cooling purposes. Degradation of hydantoin compounds does not occur during water treatment with the consequence of potential scaling and fouling of heat exchangers. The project investigated 1-methylhydantoin as a model biorefractory compound during sonication in an ultrasonic bath. The 1-methylhydantoin was shown to be degraded during sonication, kinetics of degradation were measured and degradation products were identified using various chromatrographic techniques. It was recommended that an ultrasonic cell using a more powerful ultrasonic source be designed to allow for the measurement of kinetic data required in the scale-up of ultrasonic processes and that ultrasound be evaluated for the treatment of industrial effluent and the preparation of potable water (Schwikkard, 1995).

Advanced oxidation processes such as ozone, UV radiation and ultrasound are electricity-driven and thus attracted interest from ESKOM, the South African electricity supplier. Collaboration with the University of Natal was initiated to investigate and promote the use of ultrasound in potable water and industrial effluent treatment (Faul, 1996a; Faul, 1996b). The project included funding for one of the researchers to attend the Fifth Meeting of the European Society of Sonochemistry in Cambridge, July 1996, and various technical visits to sonochemical research laboratories in the United Kingdom. The visits included that to AEA Technology, Harwell; Coventry University; the Department of Chemistry at the University of Bath and the

Department of Physical and Theoretical Chemistry at Oxford University. Research at Coventry University showed that the required dosage of chlorine during potable water disinfection was significantly decreased when chlorine was used in conjunction with ultrasound; similar results could potentially be expected for the combination of ultrasound with ozone (Faul, 1996a).

A collaborative project between ESKOM and Umgeni Water was undertaken to assess the international status and commercial markets of advanced oxidation processes (Gericke, 1999). It was concluded that despite the sound scientific basis of the technology certain market forces prohibited full commercialisation and that certain fundamental aspects required further research (Gericke, 1999).

Umgeni Water have also investigated, in a project funded by the Water Research Commission, the potential of combining ozone and granular activated carbon as a potential method to treat water from impoundments that are tending to become eutrophic (Pryor and Freese, 2000). The project is entitled *The treatment of eutrophic water using pre- and intermediate ozonation, peroxone and PICA carbon*. The nutrient load in runoff from informal settlements along river banks and pollutants such as pesticides and herbicides in agricultural runoff have contributed to the deterioration in water quality in impoundments in South Africa (Pryor and Freese, 2000). Ozone was shown to reduce the concentration of atrazine, a herbicide known to persist in ground and surface waters, by over 70 %. Atrazine degradation was enhanced when ozonation was followed by absorption on granular activated carbon. Nevertheless, sporadic breakthroughs of atrazine above the European Union recommended limit for herbicides (100 ng L^{-1}) occurred over the 450 d trial (Pryor and Freese, 2000). Ozone has been shown to be effective in significantly reducing the concentration of herbicides such as atrazine in water, however, to ensure that required limits are consistently achieved the application of ozone in combination with other technologies should be investigated.

Ultrasound combined with ozone was thus investigated to follow on from the study by Umgeni Water into atrazine degradation using different technologies. Atrazine, however, was also a good model compound to use in the evaluation of ultrasound in water treatment to degrade organic compounds since atrazine chemistry is well studied and it is difficult to degrade. Atrazine is used extensively in South Africa and is highly persistent in the environment. Atrazine is also relatively safe to handle and is readily available.

1.5 PROJECT OBJECTIVES

The present investigation was initiated to follow-up the recommendations made in the projects described in Section 1.4. The objectives of the investigation are to:

- Design and construct an ultrasonic cell to be used in the evaluation of ultrasound to degrade organic pollutants in water treatment
- Use such equipment to investigate the process mechanism (the sequence of sub-processes whose overall result produces the observed effect) occurring during sonication.

- Investigate the equipment operation and implications for scale-up.
- Compare the performance of ultrasound, an emerging technology in water treatment, with that of ozone, an already established advanced oxidation process.
- Use atrazine as a model organic compound and investigate degradation rates during sonication and ozonation.
- Identify degradation products obtained during the sonication and ozonation of atrazine.

To achieve the objectives, a literature review on ultrasound and ozone was undertaken to gather background information so as to assist in designing the ultrasonic cell and to identify experimental techniques for performing ultrasonic and ozonation research. Literature on the chemistry of atrazine was reviewed and potential degradation mechanisms and products identified. The ultrasonic cell was designed and constructed and a commercially available ozone generator was used for ozone production. Equipment characterisation allowed for the necessary experimental techniques to be mastered, to determine estimates of experimental error and to assure that analytical procedures could be followed reproducibly. The sub-processes occurring during sonication were investigated by varying acoustic power and ozone input and measuring dissolved oxygen, hydrogen peroxide and ozone concentrations. Atrazine degradation kinetics during sonication and ozonation were measured and degradation product samples collected for identification using mass spectrometry.

The purpose and function of an ultrasonic cell (or ultrasonic laboratory reactor) within the context of the development of large-scale ultrasonic equipment for application in water treatment is demonstrated in the reactor design flow diagram shown in Figure 1.1.

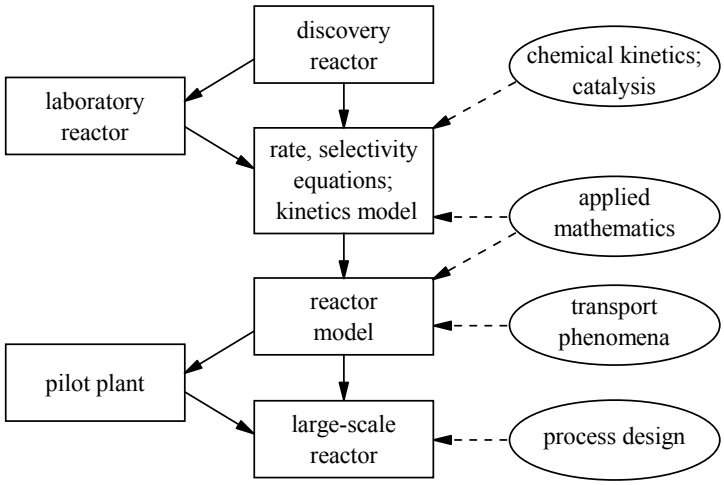

Figure 1.1 : Reactor design flow diagram (Smith, 1970)

The scientific disciplines involved between the discovery of a reaction (or demonstration of a process) and the large-scale reactor for industrial application are shown on the right in Figure 1.1. A laboratory reactor is built to investigate process parameters (such as reaction conditions, catalyst lifetime) and reaction kinetics so

as to obtain reaction rate and conversion/selectivity equations (Smith, 1970). This information is required for a mathematical model to be developed of the large-scale reactor. The model is evaluated with the operation of pilot plant in which questions concerning construction materials, corrosion, operating procedures, instrumentation and control are also investigated. The reactor model can then be used in the design and construction of a large-scale reactor for industrial application (Smith, 1970).

The investigation of the sonochemical degradation of hydantoin compounds in an ultrasonic bath indicated the potential of ultrasound to be used in water treatment specifically for the degradation of biorefractory organic pollutants (Schwikkard, 1995). The next step from such a demonstration of a process, as illustrated in Figure 1.1, is the design of an ultrasonic laboratory reactor (an ultrasonic cell) to investigate reaction kinetics, process operation and implications for scale-up, thus obtaining rate information for the development of a model of a large-scale ultrasonic reactor.

1.6 THESIS OUTLINE

A flow diagram of the thesis outline is presented in Figure 1.2.

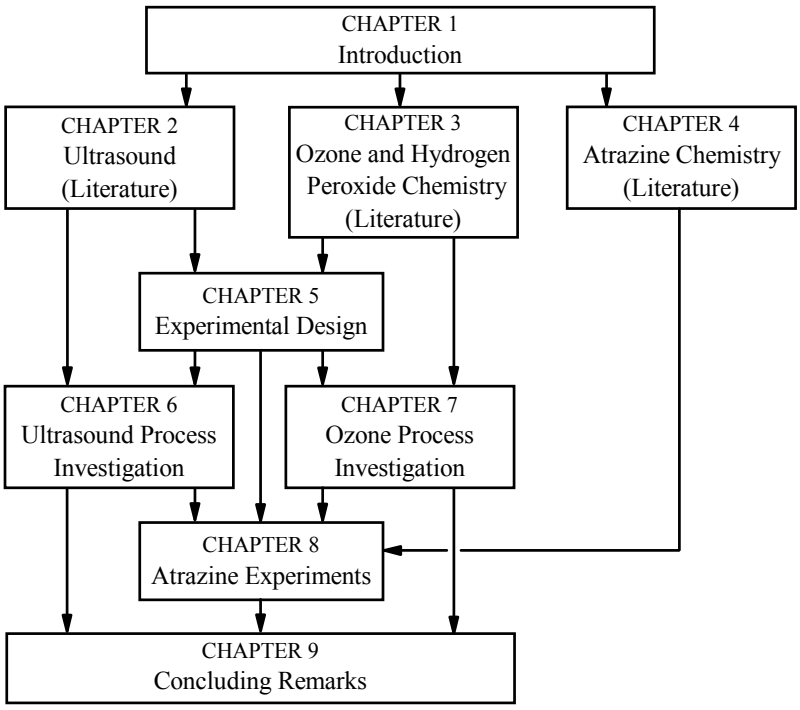

Figure 1.2 : Flow diagram of thesis outline

The water situation in South Africa specifically the increasing demand, the limited supply, the deteriorating water quality and legislation enacted to manage water usage is described in Chapter 1. Advanced oxidation processes are introduced and the development of this project from earlier research projects is also described.

Ultrasound literature is reviewed in Chapter 2. The mechanisms of cavitation and the formation of free radicals during sonication are described. Both chemical and physical effects of ultrasound are discussed and examples are listed of ultrasonic applications in the fields of chemistry, industry and medicine. Details are also provided of commercially available sonochemical equipment. Ozone and hydrogen peroxide literature are reviewed in Chapter 3. This includes the generation of ozone, the kinetics of ozone decomposition and the application of ozone in water treatment. Examples are also given of the application of hydrogen peroxide in water treatment. Atrazine literature is reviewed in Chapter 4. The chapter summarises atrazine chemistry and the behaviour of atrazine in both soil and water systems in the environment. Potential technologies to degrade atrazine are also described.

Equipment and analytical procedures used in the investigation are presented in Chapter 5. This includes a description of the design of the ultrasonic cell and the equipment used for ozone generation. Standard procedures were used to measure ozone concentration whereas an HPLC method was developed to measure atrazine concentration. Methods to measure hydrogen peroxide and dissolved oxygen concentrations are also described.

Characterisation of the ultrasonic cell is presented in Chapter 6. The process mechanisms occurring during sonication were investigated by measuring parameters such as dissolved oxygen concentration, formation and degradation of hydrogen peroxide under saturation with different gases. Implications for scale-up of an ultrasonic process are also considered. The investigation of the fundamentals of ozone chemistry and equipment characterisation, in terms of ozone formation and degradation and hydrogen peroxide formation, is detailed in Chapter 7. Atrazine experiments are discussed in Chapter 8. This includes the degradation of atrazine during sonication and ozonation and the identification of degradation products.

Concluding remarks and recommendations are presented in Chapter 10. Sources referenced during the investigation and Appendices detailing data and calculation procedures are also presented.

2

ULTRASOUND

Ultrasound is defined as sound which is of a frequency above the limit (16 kHz) to which the human ear can respond (Mason, 1990). The effects of ultrasound in a medium are due to the chemical and physical effects caused by ultrasonic cavitation. The literature presented in this chapter describes the enhancement of chemical reactions by ultrasound and the potential for scale-up of industrial applications.

The history of ultrasound is presented in Section 2.1. The formation and classification of ultrasonic cavitation, as well as the phenomena which arise from cavitation, are discussed in Section 2.2. The chemical and physical effects of cavitation, and the mechanisms by which ultrasound influences chemical reactions, are discussed in Section 2.3. Applications of ultrasound in the medical, chemical and industrial fields are presented in Section 2.4. Laboratory ultrasonic equipment and ultrasonic reactors for large-scale operation are described in Section 2.5.

2.1 HISTORY OF ULTRASOUND

The production of ultrasound was made possible with the discovery of the magnetostrictive and piezoelectric effects. James Prescott Joule reported in 1847 that the application of a magnetic field to an iron bar caused the bar to increase in length (Mason, 1976). The magnetostrictive effect is defined as the production of a change in dimension of a magnetic material during magnetisation (Bremner, 1986). Sound waves are thus produced in the surrounding medium when an alternating field, by means of a solenoid, is applied across a ferromagnetic material. Pierre and Jacques Curie discovered the piezoelectric effect in 1880; a pressure applied across certain crystals (such as quartz) was found to produce an electric charge on the surface of the crystal (Mason, 1976). The converse of the effect is that a dimensional change is induced in such a crystal when an electric charge is applied across the opposite faces of the crystal. Sound waves are thus produced in the surrounding medium if an alternating voltage is applied across a piezoelectric crystal (Mason, 1976; Mason, 1990).

Paul Langevin, in 1917, performed the earliest investigation of ultrasound (Mason, 1976). Ultrasound was investigated as a method for submarine detection and the first underwater sound transducer (used mainly for depth determination) was produced. The discovery by Langevin that sound waves killed small fish began research in the 1920's into the biological effects of ultrasound (Alliger, 1975). At that time pioneering work

on the chemical effects of ultrasound was performed by Richards and Loomis. Chemical transformations accelerated by ultrasound included the explosion of nitrogen tri-iodide, the dispersion of mercury, the degassing of liquids, the lowering of the boiling temperature of liquids, the hydrolysis of dimethyl sulfate and the iodine clock reaction (Richards and Loomis, 1927). The emission of light during sonication (sonoluminescence) was first reported by Frenzel and Schultes in 1934 (Harvey, 1939).

An investigation of high speed propeller erosion by Lord Rayleigh (for the British Navy) led to the publishing, in 1917, of a paper describing a mathematical model of the collapse of a pre-existing, spherical cavitation bubble under a steady pressure (Alliger, 1975; Suslick, 1989). These conditions are different to what occurs in an ultrasonic field, however, the concepts presented in the paper formed the basis for the development of ultrasonic cavitation theory (Neppiras, 1984). In 1950, Noltingk and Neppiras published a systematic treatment of the growth and collapse of a gas-filled cavitation bubble in a liquid medium subjected to a sinusoidal ultrasonic pressure wave (Noltingk and Neppiras, 1950).

2.2 CAVITATION

Cavitation is defined as the formation, expansion and collapse of cavities in a liquid (Sirotyuk, 1963). The four types of cavitation are listed below (Shah et al., 1999a; Young, 1989).

- Hydrodynamic cavitation is produced in a flowing liquid due to the pressure variations caused by the system geometry.
- Ultrasonic cavitation is produced in a liquid because of the pressure variations caused by sound waves moving through the liquid.
- Optic cavitation occurs when photons of high intensity light (lasers) are focused on a liquid.
- Particle cavitation occurs when elementary particles (such as protons) are used to rupture a superheated liquid in a bubble chamber.

The formation of ultrasonic cavitation is reviewed in Section 2.2.1; the classification of ultrasonic cavitation as either stable or transient in Section 2.2.2; the theoretical equations of cavitation bubble dynamics in Section 2.2.3 and phenomena which arise from ultrasonic cavitation (sonoluminescence and cavitation noise) in Section 2.2.4.

2.2.1 Formation of ultrasonic cavitation

Sound is transmitted through a liquid by inducing vibrational motion (phases of compression and rarefaction) of the liquid molecules (Mason and Cordemans, 1996). Local pressure variations occur as liquid molecules are stretched apart during a rarefaction phase of a sound wave and pressed together during a compression phase. Cavities are formed in a liquid when the negative pressure created by the rarefaction phase exceeds the tensile strength of the liquid, the molecules of the liquid are stretched beyond the critical molecular distance required to hold the liquid intact (Pandit and Moholkar, 1996; Suslick, 1989). The breakdown in a

liquid to form cavities should happen simultaneously throughout the liquid but generally it occurs only at weak spots or nucleation sites (Sirotyuk, 1963). Microdust particles or dissolved gas (gas-filled crevices in suspended particulate matter or microbubbles from prior cavitation events) act as nucleation sites in the liquid (Apfel, 1984; Roi, 1957). Cavity formation occurs at these weak spots or nucleation sites since the tensile strength of pure liquids is too large for cavitation to be formed solely by the local negative pressure induced by a rarefaction phase of a sound wave (Apfel, 1972; Sirotyuk, 1966; Suslick, 1990).

The cavitation threshold is defined as the sound wave amplitude, depending on frequency, that induces sufficient vibration of liquid molecules to cause cavity formation in the liquid (Crawford, 1963; Webster, 1963). The following parameters affect the cavitation threshold (Mason, 1990; Pandit and Moholkar, 1996; Pestman et al., 1994; Webster, 1963).

- The presence of dissolved gas in a liquid lowers the cavitation threshold as more nucleation sites for cavity formation exist.
- Physical properties of a liquid, such as surface tension, vapour pressure and viscosity, affect the cavitation threshold. A reduction in surface tension (such as with the addition of a surfactant) decreases the cavitation threshold. Liquids with a low vapour pressure do not readily cavitate. Liquids with higher viscosities have greater natural cohesive forces and hence a higher cavitation threshold.
- An increase in temperature lowers the cavitation threshold as many liquid properties, such as density and viscosity, are temperature dependent.
- The cavitation threshold is raised as the external applied pressure is increased. A higher external pressure requires a greater negative pressure in the rarefaction phase of a sound wave for cavity formation to occur.
- The cavitation threshold is raised with an increase in frequency. The rarefaction and compression phases of a sound wave are shortened and insufficient time may be available for a cavity to either grow in a rarefaction phase or collapse in a compression phase.
- Intensity is related to the amplitude of a sound wave, an increase in intensity increases cavitation. However, an optimum intensity exists beyond which a further increase will have no effect since the formation of larger, more stable cavities dampen the passage of sound energy through the liquid.

2.2.2 Classification of cavitation

Cavitation is classified as either stable or transient (Neppiras, 1984). The experimental distinction between stable and transient cavitation is not well defined (Henglein, 1987; Vaughan and Leeman, 1989). However, the lifespan of a stable cavity is longer than that of a transient cavity and stable cavities exist over many acoustic cycles whereas transient cavities exist for only one or two acoustic cycles. Stable cavitation is produced by ultrasonic intensities in the range of 1 to 3 W cm^{-2} whereas transient cavitation is produced by intensities greater than 10 W cm^{-2} (Mason, 1990).

Stable cavities are bubbles that exist for many acoustic cycles and oscillate, often non linearly, about an equilibrium radius that is dependent on the applied ultrasonic field (Henglein, 1987; Riesz et al., 1990a). The lifespan of stable cavities is still short since a cavity which exists for 1 000 acoustic cycles in a 20 kHz ultrasonic field has a lifespan of 0,05 s (Mason, 1990). Stable cavities grow through a process called rectified diffusion in that the amount of gas diffusing in or out a cavity depends on the surface area of the cavity; more gas diffuses into a cavity when it is large, in a rarefaction phase, than diffuses out of a cavity when it is small, in a compression phase (Suslick et al., 1990). The cavities grow to a size at which they become unstable and implode. The implosion is cushioned by the gas and liquid vapour contained in the cavity (Henglein, 1987; Neppiras, 1984).

Transient cavities exist for only one or two acoustic cycles and implode violently during a single compression phase once the cavities have expanded to a size two to three times the equilibrium radius (Riesz et al., 1990a). The lifespan of the cavities is too short for gas dissolved in the liquid to diffuse into the cavities. However, the cavities may contain some vapour from the liquid. The collapse of the cavities is violent, as no gas is present in the cavities to cushion the implosion (Henglein, 1987). Upon implosion, the cavities often disintegrate into numerous smaller cavities providing nuclei for further cavitation (Henglein, 1987). Powerful shock waves are produced and considerable energy is released into the liquid as the cavities implode (Boudjouk, 1986). From theoretical calculations, temperatures and pressures in a gas cavity during the final stages of collapse have been estimated to be in the range of 2 000 to 10 000 K and 100 to 1 000 MPa (Suslick et al., 1986). The high temperatures and pressures in the cavities cause the dissociation of water vapour into hydroxyl and hydrogen radicals (Bremner, 1986; Makino et al., 1982; Riesz et al., 1990a; Todd, 1970; Webster, 1963).

Sonochemical effects are caused by both types of cavitation despite the earlier belief that only transient cavitation enhanced chemical reactions (Ratoarinoro et al., 1992). Although the temperatures and pressures developed in stable cavities are lower then those in collapsing transient cavities (the implosion is cushioned by the gas content in the stable cavity), the lifespan of stable cavities is longer and there is thus a greater potential for influencing chemical reactivity (Mason, 1990).

Vaughan and Leeman have proposed a different system for the classification of cavitation (Vaughan and Leeman, 1989). The system, unlike stable/transient classification, provides for a hierarchy of thresholds of observed cavitation phenomena, such as cavitation noise (or subharmonic emission), sonoluminescence and sonochemical reaction enhancement. The stable/transient mode of classification developed from the theoretical interpretation of the implosion of a gas-less cavity, however, ultrasonic cavitation occurs mostly in gas-saturated liquids; the classification system proposed by Vaughan and Leeman is not dependent on a specific bubble dynamic model (Leeman and Vaughan, 1992). Cavitation is defined as the non-linear pulsation of bubbles in a sound field and is classified as subsonic, gas-phase or liquid-phase cavitation. The classification is performed by comparing the maximum velocity of the bubble wall with the speed of sound in the gas in the bubble and with the speed of sound in the liquid surrounding the bubble. The dynamic

behaviour of the bubble wall is regarded as one of the most important parameters that characterises the interaction of the bubble with the applied sound field (Vaughan and Leeman, 1989).

Subsonic cavitation occurs when the maximum velocity of the bubble wall is lower than both the speed of sound in the gas in the bubble and the speed of sound in the surrounding liquid (Leeman and Vaughan, 1992). Subsonic cavitation is characterised by non-linear motion of the bubble wall and is the threshold for cavitation noise. **Gas-phase** cavitation occurs when the applied acoustic power is increased such that the maximum velocity of the bubble wall becomes greater than the speed of sound in the gas in the bubble (but still less than the speed of sound in the liquid). The gas inside the bubble is shock-excited and significant heating occurs. Gas-phase cavitation marks the threshold for sonochemical reactions between activated species within the gas bubble as well as for sonoluminescence since light emission is associated with the movement of shock waves through a gas. **Liquid-phase** cavitation occurs when the applied acoustic power is further increased such that the maximum velocity of the bubble wall is greater than both the speed of sound in the gas in the bubble and the speed of sound in the surrounding liquid. Shock waves are generated in the liquid surrounding the bubble; high temperatures and pressures accompanying the shock waves lead to sonochemical reactions taking place in the liquid. However, the outward radiating nature of the shock waves cause such reactions to take place in a relatively thin shell of liquid surrounding the bubble (Leeman and Vaughan, 1992).

2.2.3 Equations of cavitation bubble dynamics

One of the earliest systematic treatments of ultrasonic cavities was performed by Noltingk and Neppiras (Noltingk and Neppiras, 1950). The ultrasonic cavitation of a liquid saturated with gas was modelled based on the analysis performed by Rayleigh of the implosion of a gas-less void. A differential analyser was used to solve a non-linear differential equation of motion for the radial behaviour of a gas-filled bubble in an incompressible liquid, acted upon by a sinusoidal varying pressure field. For specific initial conditions, the solutions to the equation were plotted as bubble radius versus time graphs. The pressure distribution in the liquid surrounding a collapsing, gas-filled bubble was also investigated. The following assumptions were made in the model, the liquid was taken to be incompressible, the composition of the gas in the bubble was assumed to be constant during the lifespan of the bubble, the applied ultrasonic pressure was assumed to be exactly sinusoidal and the diameter of the bubble was assumed to be much less than a wavelength of sound (Noltingk and Neppiras, 1950). The hot spot theory for the generation of sonochemical effects developed from the analysis by Noltingk and Neppiras.

The following theoretical derivation of the radial behaviour of a gas-filled bubble in an incompressible liquid, acted upon by a sinusoidal varying pressure field is summarised from the paper published by Noltingk and Neppiras (Noltingk and Neppiras, 1950). The external liquid pressure P at a distance of infinity is equal to the sum of the hydrostatic and acoustic pressures. The external liquid pressure at time t when an ultrasonic wave of amplitude P_0 and frequency $\omega/2\pi$, where ω is the angular frequency, is applied over a liquid pressure, P_A, is

$$P = P_A - P_0 \sin(\omega t) \qquad [2.1]$$

The bubble has an arbitrary radius R_0 at time $t = 0$, and contains gas at the equilibrium pressure of $(P_A + 2\sigma/R_0)$, where σ is the surface tension of the liquid. The kinetic energy $2\pi\rho R^3\left(\frac{dR}{dt}\right)^2$ of the whole mass of liquid with density ρ is equal to the algebraic sum of the work done by the surface tension, gas pressure and liquid pressure at infinity. The energy equation, if the gas changes are isothermal, is

$$2\pi\rho R^3\left(\frac{dR}{dt}\right)^2 = \int_{R_0}^{R}\left\{4\pi R^2\left[P_0 \sin(\omega t) - P_A + \left(P_A + \frac{2\sigma}{R_0}\right)\frac{R_0^3}{R^3}\right] - 8\pi R\sigma\right\}dR \qquad [2.2]$$

The differential equation of motion is found by differentiating with respect to R, giving

$$2R\left[P_0 \sin(\omega t) - P_A + \left(P_A + \frac{2\sigma}{R_0}\right)\frac{R_0^3}{R^3}\right] = 4\sigma + 3\rho R\left(\frac{dR}{dt}\right)^2 + 2\rho R^2\frac{d^2R}{dt^2} \qquad [2.3]$$

Noltingk and Neppiras found that the boundary value of the bubble wall radial velocity (dR/dt) at R_0 did not significantly affect the (t, R) curves produced from numerically solving equation 2.3 (Noltingk and Neppiras, 1950). The radial velocity at R_0 was therefore assumed to be zero.

$$\left(\frac{dR}{dt}\right)_{R=R_0} = 0 \qquad [2.4]$$

The solution of the differential equation for radial motion of a bubble (equation 2.3) over four cycles of pressure is shown in Figure 2.1. The equation was solved numerically for a specific set of initial conditions (P_A, P_0 and R_0) at frequencies of 5 and 15 MHz.

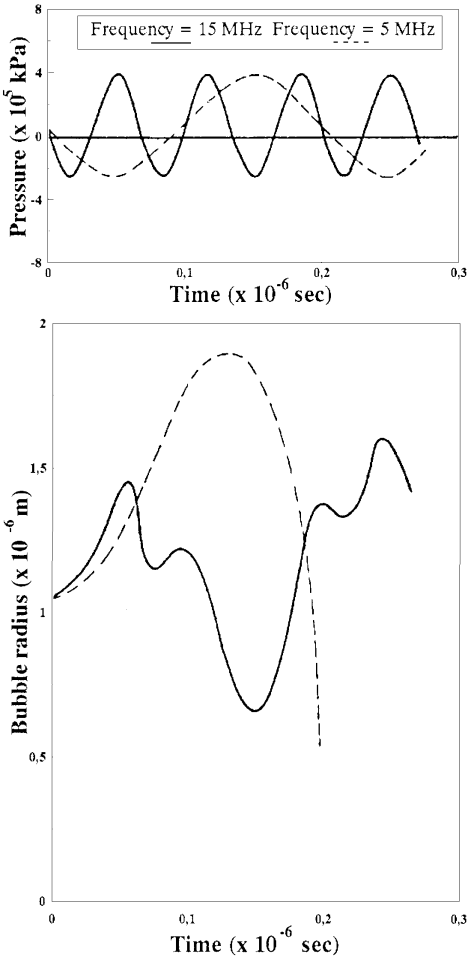

Figure 2.1 : Radius versus time curves for a gas-filled bubble in water in an ultrasonic field with a frequency of 5 MHz (dashed line) or 15 MHz (solid line); P_A = 100 kPa, P_0 = 400 kPa and R_0 = 0,8 μm (Noltingk and Neppiras, 1950)

The radius of a bubble in an ultrasonic field increases to a maximum R_m at which the bubble becomes unstable and begins to collapse. After the bubble radius has reached a maximum, as shown by the dashed line in Figure 2.1, it shrinks with increasing rapidity. The slope of the graph eventually becoming too steep to be traced with the differential analyser as used by Noltingk and Neppiras in solving equation 2.3 (Noltingk and Neppiras, 1950). Noltingk and Neppiras regarded bubble collapse as a prerequisite for cavitation and did not classify a bubble oscillating according to the solid line in Figure 2.1 as cavitating. The system of classifying cavitation as either transient or stable, where stable cavitation was defined as the non-linear oscillation of a bubble, was developed later (Flynn, 1964, in Vaughan and Leeman, 1989). A review published by Neppiras in 1980 used the diagram shown in Figure 2.1 to show the difference in radial motion between stable and transient cavitation (Neppiras, 1980).

Noltingk and Neppiras also investigated the pressure distribution in the liquid surrounding a collapsing bubble (Noltingk and Neppiras, 1950). The energy equation for the collapse of a gas-filled bubble, assuming adiabatic conditions, is

$$\frac{3\rho}{2}\left(\frac{dR}{dt}\right)^2 = P(Z - 1) - q\left(\frac{Z - Z^{\gamma}}{1 - \gamma}\right) \qquad [2.5]$$

where γ is the specific heat ratio of the gas in the bubble and q the gas pressure in the bubble at the maximum radius $R = R_m$. The symbol Z, the volume compression ratio, is defined as $(R_m/R)^3$. The external liquid pressure P is assumed to be constant because bubble collapse is very fast. Surface tension forces are ignored, as they would be insignificant during the collapse as compared with the two opposing pressure terms (Noltingk and Neppiras, 1950).

The pressure distribution in the liquid surrounding a collapsing bubble is obtained by application of the general hydrodynamic equation of motion

$$\frac{\partial u}{\partial t} + u\frac{\partial u}{\partial r} = -\frac{1}{\rho}\frac{dp}{dr} \qquad [2.6]$$

where u is the fluid velocity at a distance r from the centre of a bubble and p is the pressure at r. The partial derivatives, $\frac{\partial u}{\partial t}$ and $\frac{\partial u}{\partial r}$, are found as functions of r and R from the energy equation (equation 2.6) and the continuity equation,

$$R^2\frac{dR}{dt} = r^2\frac{dr}{dt} \qquad [2.7]$$

Noltingk and Neppiras found this to give

$$\frac{dp}{dr} = \frac{R}{3r^2}\left[\frac{qZ^{\gamma}(3\gamma - 4)}{1 - \gamma} + \frac{qZ}{1 - \gamma} - (Z - 4)P\right] + \frac{4R^4}{3r^5}\left[P(Z - 1) - \frac{q(Z - Z^{\gamma})}{1 - \gamma}\right] \qquad [2.8]$$

which upon integration gives

$$p - P = -\frac{R}{3r}\left[\frac{qZ^{\gamma}(3\gamma - 4)}{1 - \gamma} + \frac{qZ}{1 - \gamma} - (Z - 4)P\right] - \frac{R^4}{3r^4}\left[P(Z - 1) - \frac{q(Z - Z^{\gamma})}{1 - \gamma}\right] \qquad [2.9]$$

The function in equation 2.9 was solved by Noltingk and Neppiras for various values of Z and is plotted in Figure 2.2.

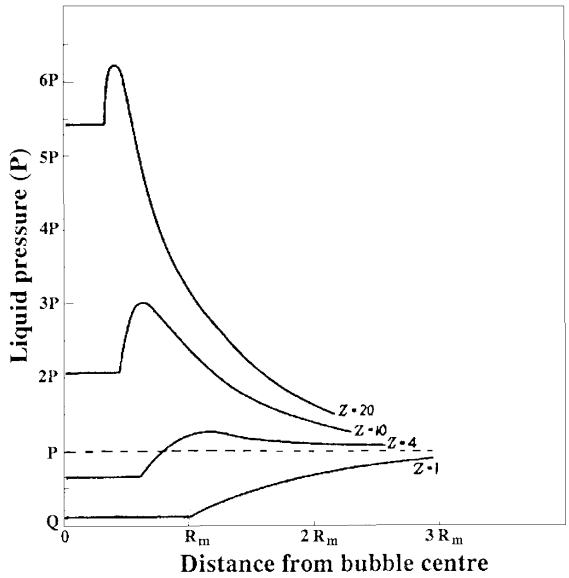

Figure 2.2 : Pressure distribution in the liquid surrounding a collapsing, gas-filled bubble where Z is the volume compression ratio $(R_m/R)^3$ (Noltingk and Neppiras, 1950)

The value of Z (defined as the ratio $(R_m/R)^3$) becomes greater during bubble collapses since the radius R is decreasing whereas R_m is constant. The four lines drawn in Figure 2.2 show the pressure distribution in and around a collapsing gas-filled bubble. The line for $Z = 1$ represents the situation just before the bubble begins to collapse. The horizontal part of the lines indicate the constant gas pressure within the gas bubble; pressure then increases from the bubble surface into the surrounding liquid. The amplitude of the liquid pressure wave increases steeply as the bubble radius decreases and inward velocity increases.

The maximum liquid pressure occurs at a distance r_m from the bubble centre and is obtained by solving for $dp/dr = 0$ in equation 2.8 and then substituting for $r = r_m$ in equation 2.9. This pressure occurs at the bubble surface at minimum radius and for adiabatic collapse is equal to $q(P/3q)^{\gamma}$ (Noltingk and Neppiras, 1950). The maximum liquid pressure was calculated for various ultrasonic frequencies and is plotted in Figure 2.3.

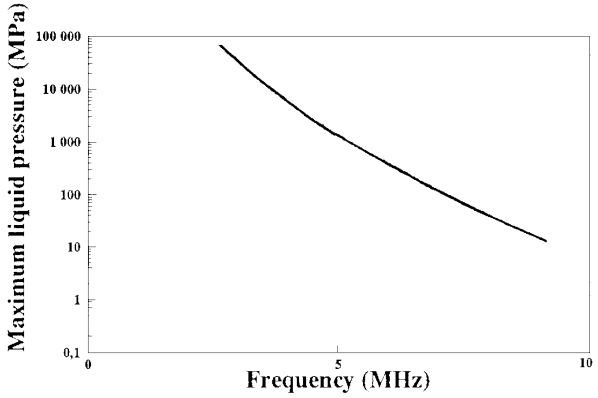

Figure 2.3 : Maximum liquid pressures calculated for different ultrasonic frequencies during bubble collapse under adiabatic conditions; P_0 = 400 kPa and R_0 = 3,2 μm (Noltingk and Neppiras, 1950)

As shown in Figure 2.3 high pressures are produced during the collapse of a gas-filled bubble. These pressures, however, exist for only a fraction of the total collapse time and over a small volume of fluid near the bubble surface. Isothermal gas changes were assumed for bubble growth and adiabatic for bubble collapse (Noltingk and Neppiras, 1950). The assumption of adiabatic conditions for the collapse period implies that gas temperature increases to a high value as bubble radius approaches a minimum. The gas temperature at radius R for adiabatic compression is given by

$$T = T_0\left(\frac{R_m}{R}\right)^{3(\gamma-1)} \qquad [2.10]$$

where T_0 is the ambient temperature of the surrounding liquid. The maximum temperature in the bubble occurs when the bubble radius is a minimum (Noltingk and Neppiras, 1950). The maximum temperature can therefore be calculated from equation 2.10 when R is equal to the minimum radius. At minimum radius equation 2.10 becomes

$$T = T_0\left(\frac{P}{3q}\right)^{3(\gamma-1)} \qquad [2.11]$$

The maximum gas temperature is calculated from equation 2.11 to be 10 000 K when T_0 is 300 K, P is 100 kPa and q is 1 kPa (Noltingk and Neppiras, 1950). The temperature of the bubble surface would effectively be the same as that of the surrounding liquid (T_0) and a steep temperature gradient would exist in the gas adjacent to the bubble wall. The high temperatures confined to the gas in the bubble was proposed to lead to incandescence, accounting for the luminescence observed during ultrasonic cavitation (Noltingk and Neppiras, 1950).

Most of the theory of ultrasonic cavitation has developed from the theoretical analysis performed by Noltingk and Neppiras. Various authors, to model experimental conditions more realistically, have made adaptions to include terms accounting for parameters such as viscosity and compressibility of the liquid medium. The review published by Neppiras in 1980 summarises the ultrasonic cavitation theory (Neppiras, 1980). Whereas the early development of ultrasonic cavitation theory focused on what is now defined as transient cavitation, equations have been published for both stable and transient cavitation (Neppiras, 1980; Shah et al., 1999b; Thompson and Doraiswamy, 1999).

2.2.4 Cavitation phenomena

Sonochemical reaction enhancement, sonoluminescence and cavitation noise are phenomena caused by ultrasonic cavitation (Webster, 1963). Sonoluminescence and cavitation noise are reviewed in Section 2.2.4.1 and Section 2.2.4.2 respectively; sonochemistry is reviewed in Section 2.3.

2.2.4.1 Sonoluminescence

Sonoluminescence is a weak emission of light observed during ultrasonic cavitation in liquids such as water containing dissolved gas (Verrall and Sehgal, 1988). One of the earliest observations of sonoluminescence was by Frenzel and Schultes in 1934 (Harvey, 1939). Sonoluminescence occurs periodically with the frequency of the sound field, one flash per cycle of sound (Saksena and Nyborg, 1970). The occurrence of sonoluminescence has been reported for both continuous (Sehgal et al., 1980a) and pulsed ultrasound (Henglein and Gutiérrez, 1993). The amplitude of an ultrasonic wave must be greater than a certain threshold value before sonoluminescence will occur (Vaughan and Leeman, 1989). Various thermal and electrical theories have been proposed to explain the origin of sonoluminescence.

- The electrical microdischarge theory proposed by Frenkel in 1940 postulates that lens-shaped cavities are formed when a liquid is ruptured by a sound field (Frenkel, 1940, in Webster, 1963). Ions of opposite charge gather on the opposing cavity walls and produce an electric field within the cavity. The electric field becomes stronger as the cavity develops a spherical shape. Emission of light occurs during the growth of the cavity.
- The mechanochemical theory proposed by Weyl and Marboe in 1949 postulates that light emission occurs upon photochemical recombination of ions formed by the mechanical fracture of molecules at the surface of an expanding cavity. Emission of light is independent of dissolved gas and occurs during the growth of a cavity (Weyl and Marboe, 1949, in Verrall and Sehgal, 1988).
- The anion discharge theory was proposed by Degrois and Baldo (Degrois and Baldo, 1974). This theory postulates that light emission occurs when the internal charge of a gaseous bubble is rapidly discharged during bubble compression. Electrons are produced in the bubble when the gas molecules at the gas-liquid interface neutralise the anions in the liquid which are adsorbed onto the external bubble surface. If the total internal charge acquired by the bubble is considered to be constant, the charge density increases upon bubble compression and an outflow of electrons from within the bubble into the liquid medium occurs when the charge density reaches a critical value.

This flow of electrons produces excitation and ionisation of molecules in the liquid phase causing luminescence and other chemical effects (Degrois and Baldo, 1974).

- The hot spot theory proposed by Noltingk and Neppiras in 1950 postulates that sonoluminescence is the result of incandescence of gas in a cavitation bubble (Noltingk and Neppiras, 1950). The adiabatic collapse of a cavitation bubble heats the contents of the bubble to incandescence (the emission of light due to high temperatures). Griffing and Sette extended the hot spot theory by postulating that sonoluminescence was the result of chemiluminescence rather than incandescence (Griffing and Sette, 1955, in Verrall and Sehgal, 1988). Chemiluminescence is the emission of light caused by the recombination of excited and reactive chemical species. These chemical species are formed in the gas bubbles due to the high temperatures created by the adiabatic collapse of the bubble.

The electrical theories developed first (Él'piner, 1960) and most early work, such as that performed by Harvey, concluded that sonoluminescence was of electrical origin (Harvey, 1939). The work published by Parke and Taylor, in 1956, was part of the earliest work which considered the thermal theories to explain the origin of sonoluminescence and other chemical effects of ultrasound (Parke and Taylor, 1956).

A comparison of the sonoluminescent flashes and acoustic pressure pulses generated by the collapsing bubbles established that the light flashes occurred during the final stages of bubble collapse (Kuttruff, 1962, in Verrall and Sehgal, 1988). This disproved the electrical microdischarge and mechanochemical theories that postulated that light emission occurred during bubble growth (Verrall and Sehgal, 1988). The anion discharge theory proposed by Degrois and Baldo was shown by Sehgal and Verrall not be consistent with experimental results (Sehgal and Verrall, 1982). Another electrical theory explaining the occurrence of sonoluminescence and sonochemical reactions has been proposed by Margulis (Margulis, 1985; Margulis, 1992). This theory postulates that light emission occurs during the formation of a small bubble from the breakdown of a large deformed bubble. A large negative charge accumulates at the neck of the smaller bubble as it is pinched off the larger bubble. Charges are equalised when discharge (and light emission) occurs through the small bubble (Margulis, 1985). This theory, however, has been discredited by Suslick and co-workers as also not being consistent with experimental observations (Suslick et al., 1990; Suslick and Kemper, 1993). Suslick and Kemper investigated the sonoluminescence produced during the sonication of silicone oil solutions of $Cr(CO)_6$ (Suslick and Kemper, 1993). Sonoluminescence was found to significantly decrease in the presence of even small amounts of fluorocarbon gases (CF_4 or C_2F_6) even though these gases are capable of supporting electrical discharge. It was concluded that the results were in direct conflict with the electrical theories of sonoluminescence (Suslick and Kemper, 1993).

In an investigation performed by Saksena and Nyborg sonoluminescence was observed from the periodic volume oscillation of a gas bubble in a sound field; one flash of light per cycle of sound (Saksena and Nyborg, 1970). The volume oscillation of a bubble is caused by the compression and rarefaction phases of the sound field. The addition of allyl alcohol, a radical scavenger, quenched the sonoluminescence from a

95:5 v/v glycerine-water mixture (Saksena and Nyborg, 1970). This indicated that free radicals were involved in the formation of sonoluminescence. In support of the hot spot theory, it was concluded that sonoluminescence resulted from the recombination of hydroxyl and hydrogen radicals formed by the adiabatic heating of a bubble during the compression phase of a sound wave (Saksena and Nyborg, 1970).

According to the hot spot theory, gases that have the same specific heat ratio, γ, will reach the same final temperature in the cavity and thus have the same intensity of light emission (Verrall and Sehgal, 1988). However, gases with the same specific heat ratio have been found to give different intensities of sonoluminescence (Young, 1976). The hot spot theory assumes bubble collapse to occur adiabatically and thus ignores heat loss to the surrounding liquid. The model developed by Young to calculate the actual temperature in a cavity during cavity collapse accounts for heat loss due to the thermal conductivity of the gas in the cavity (Young, 1976). Young investigated the sonoluminescence in water saturated with a range of monatomic gases having a similar specific heat ratio but different heat conductivity (Young, 1976). The noble gases studied by Young are listed in Table 2.1.

Table 2.1 : Effect of gas thermal heat conductivity on actual gas temperature in a cavity and on the measured sonoluminescence intensity (Young, 1976)

Gas	Specific heat ratio γ	Thermal heat conductivity ($W\ m^{-1}\ K^{-1}$)	Actual gas temperature (K)	Sonoluminescence intensity (lumen m^{-2})
helium	1.65	$15{,}1 \times 10^{-2}$	815	$1{,}2 \times 10^{-6}$
neon	1.64	$4{,}89 \times 10^{-2}$	1,420	$3{,}2 \times 10^{-6}$
argon	1.65	$1{,}77 \times 10^{-2}$	1,650	30×10^{-6}
krypton	1.67	$1{,}00 \times 10^{-2}$	1,890	50×10^{-6}
xenon	1.67	$0{,}58 \times 10^{-2}$	2,000	125×10^{-6}

Heat conductivity decreases for the gases helium to xenon, as listed in Table 2.1, and thus progressively less heat is lost from the cavities resulting in higher cavity temperatures and greater measured intensities of sonoluminescence (Young, 1976). The work performed by Young supports the hot spot theory for the formation of sonoluminescence (Young, 1976).

Further evidence in support of the hot spot theory was gained from investigations of the sonoluminescence spectra of distilled water saturated with different gases. Sehgal and co-workers investigated the sonoluminescence spectra from water saturated with nitric oxide, NO, and nitrogen dioxide, NO_2 (Sehgal et al., 1980b). The actual temperatures in the gas cavities were calculated (not assuming adiabatic conditions) to be 1 350 K for nitric oxide and 860 K for nitrogen dioxide. The sonoluminescence spectra of nitric oxide- and nitrogen dioxide-saturated water were found to be similar to the spectra from fluorescence and thermal emission of nitrogen dioxide and from $NO + O_3$ chemiluminescence (Sehgal et al., 1980b). It

was concluded that sonoluminescence arose from a similar mechanism; emission occurring from the gas-phase, electronic-excited state of NO_2 (Sehgal et al., 1980b). An investigation of the sonoluminescence spectra from argon-saturated alkali metal salt solutions (sodium and potassium) also concluded that light emission occurred from the de-excitation of excited chemical species in the gas cavities (Sehgal et al., 1979). Light emission was found to occur from the de-excitation of the excited alkali metal atoms (Sehgal et al., 1979). The conditions in the gas cavities excite molecules into high-energy states and light is emitted when the molecules return to their ground states (Suslick, 1989).

It was originally reported that sonoluminescence was only characteristic of transient cavitation and did not occur during stable cavitation (Neppiras and Fill, 1969). The work published by Saksena and Nyborg in 1970 and Crum and Reynolds in 1985 showed that sonoluminescence also occurs during stable cavitation (Saksena and Nyborg, 1970; Crum and Reynolds, 1985).

In another investigation by Sehgal and co-workers, sonoluminescence was observed from water saturated with helium, neon, argon, krypton, oxygen, nitrogen and air (Sehgal et al., 1980a). The solutions were sonicated at ultrasonic frequencies of 333 and 459 kHz. The emission spectra were measured by using single-photon counting techniques and showed a continuum that extended from a wavelength of 240 nm to the near-infrared region (Sehgal et al., 1980a). The spectrum of argon-saturated water sonicated at 333 kHz is shown in Figure 2.4.

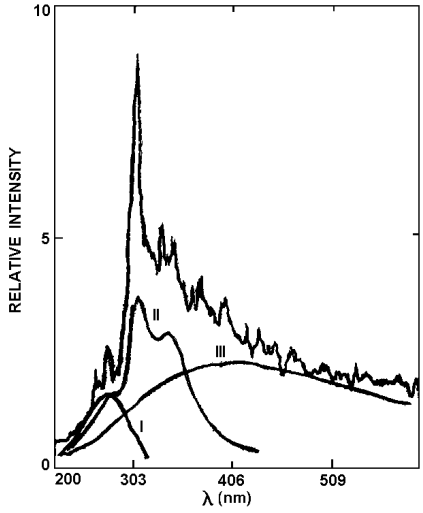

Figure 2.4 : Sonoluminescence spectrum of argon-saturated water sonicated at 333 kHz; I, emission from H_2O^*; II, emission from OH^*; and III, emission from $H^\bullet + HO^\bullet$ reaction (Sehgal et al., 1980a)

The emission spectrum of a solution arises due to the sonoluminescence from both stable and transient cavitation (Sehgal et al., 1980a). The higher temperatures in transient cavities cause electronic excitation. The formation of excited water molecules is followed by either radiative relaxation or dissociation into hydrogen and hydroxyl radicals. The emission in the near-UV region with a peak maximum in the region of

270 nm to 290 nm, shown by curve I in Figure 2.4, is the emission from the transitions from the triplet $^3B_1$ state of water (Sehgal et al., 1980a). Emission below 400 nm, shown by curve II, is due to the electronically exited $OH(\Sigma^+)$ formed by the fragmentation of water in the excited state. The lower temperatures in stable cavities cause vibrational excitation leading to the dissociation of water in the ground state. The radicals formed combine radiately to give a continuum with a broad maximum around 400 nm, shown by curve III in Figure 2.4 (Sehgal et al., 1980a). Selective quenching of hydroxyl radical emission by the addition of nitric acid has also provided chemical evidence for the formation of the excited water molecule, H_2O^* (Sehgal et al., 1980d). The nitric anion, NO_3^-, preferentially scavenges the hydroxyl radicals and uncovers the emission peak, at about 280 nm, from the excited water molecule. In the absence of a hydroxyl radical scavenger, the emission peak for the excited water molecule is hidden by the emission peaks for the excited hydroxyl radicals (Sehgal et al., 1980d).

Various factors influence the intensity of sonoluminescence. An increase in temperature of the bulk solution causes the intensity of sonoluminescence to decrease (Didenko et al., 1994; Sehgal et al., 1980c). By comparing the spectra from neon-saturated water at various temperatures, Sehgal and co-workers concluded that the chemical reactions producing sonoluminescence were not dependent upon ambient temperature, however, the decrease in sonoluminescence was mostly due to a decrease in the degree of cavitation (Sehgal et al., 1980c). Didenko and co-workers investigated the sonoluminescence from argon- saturated water and reasoned that an increase in bulk solution temperature increased the vapour/gas ratio inside the gas cavity (Didenko et al., 1994). This was due to the decrease in gas solubility and hence the water vapour pressure in the gas cavity was raised. The specific heat ratio (γ) of water vapour is lower than that of the noble gases (argon) and hence a lower temperature would be reached in the cavity during cavity collapse; and a lower intensity of sonoluminescence would be produced (Didenko et al., 1994).

For a fixed ultrasonic intensity, sonoluminescence decreases with an increase in frequency (Verrall and Sehgal, 1988). The spectral distribution of the light is also changed with a change in frequency. Sehgal and co-workers measured the spectra for argon-saturated water at frequencies of 333 and 459 kHz (Sehgal et al., 1980a). It was reported that the 310 nm band ascribed to the OH* emission was more pronounced and defined at the lower frequency, and that the continuum band from the radiative recombination of free radicals dominated the spectrum at the higher frequency. It was reasoned that the differences in the spectra were related to the relative change, with frequency, in the distribution of transient and stable cavities (Sehgal et al., 1980a). Chendke and Fogler investigated the intensity of sonoluminescence from nitrogen-saturated water for static pressures ranging from 0,1 to 1,46 MPa (Chendke and Fogler, 1983b). The intensity of sonoluminescence was found to increase with static pressure up to a maximum at about 0,6 MPa. A further increase in static pressure resulted in a decrease in sonoluminescence intensity; at a pressure of 1,4 MPa sonoluminescence was totally suppressed. The initial increase in sonoluminescence was attributed to an increase in the number of gas cavities. The decrease in sonoluminescence at higher static pressures was due to the acoustic pressure being lower than the static pressure and thus too low to initiate cavitation (Chendke

and Fogler, 1983b). The spectral distribution of the light did not change over the pressure range investigated (Chendke and Fogler, 1983b). Investigation of the sonoluminescence of aqueous carbon tetrachloride solutions by Chendke and Fogler also showed that the intensity of sonoluminescence was dependent on static pressure whereas the spectral distribution of light was independent of pressure (Chendke and Fogler, 1983a).

Sonoluminescence has been recorded in non-aqueous liquids. The sonoluminescence intensity of carbon tetrachloride and water mixtures was measured by Chendke and Fogler (Chendke and Fogler, 1983a). The intensity was found to increase with increasing amount of carbon tetrachloride in water; a fully-saturated solution luminesced with an intensity 2,8 times that of pure water. It was concluded that light emission occurred because of chemiluminescence (Chendke and Fogler, 1983a). The sonoluminescence from various hydrocarbons saturated with different gases was measured by Flint and Suslick (Flint and Suslick, 1989). Similar to sonoluminescence from aqueous solutions, sonoluminescence from non-aqueous solutions was found to occur from excited chemical species. Spectral studies showed that light emission from argon-saturated alkanes occurred from excited C_2, C_2H and CH molecules. For nitrogen-saturation, light emission occurred from the excited state of the CN molecule; for oxygen-saturation, light emission occurred from the excited states of the CO_2, CH and OH molecules (Flint and Suslick, 1989). For linear alkanes such as dodecane, decane and octane, sonoluminescence was found to decrease with increasing vapour pressure. This is due to the reduced cavity temperature reached during cavity collapse (Flint and Suslick, 1989).

For both aqueous and non-aqueous liquids sonoluminescence arises from the chemical reactions of high energy species formed during cavity collapse. It is a form of chemiluminescence and is not due to either blackbody radiation or electrical discharge (Suslick, 1990).

2.2.4.2 Cavitation noise

Ultrasound is accompanied by an intense noise. The collapsing cavities act as secondary sources of sound, emitting spherical waves (Neppiras, 1980). The spectral composition of this cavitation noise consists of harmonics and subharmonics of the fundamental ultrasonic frequency and a continuous background or continuum of *white* noise (Roi, 1957). The noise spectra for ultrasonic frequencies varying from 3 kHz to 3,3 MHz was measured by Esche (Esche, 1952, in Webster, 1963). The noise spectrum for an ultrasonic frequency of 15 kHz is shown in Figure 2.5.

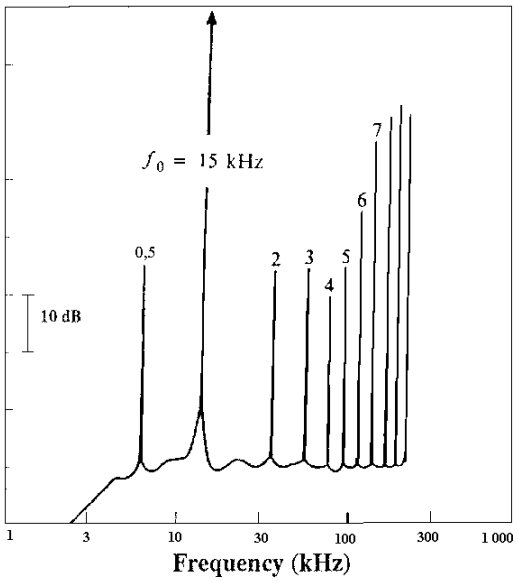

Figure 2.5 : Cavitation noise spectrum for an ultrasonic resonance frequency (f_0) of 15 kHz (Esche, 1952, in Webster, 1963)

The half-order subharmonic line and the higher order harmonic lines of the driving frequency, as well as the continuous background of the noise spectrum, are shown in Figure 2.5. The harmonic lines are caused by the non-linear radial and surface oscillations of the cavities and the continuous portion of the spectrum arises from the violent collapse as well as oscillation of the cavities (Rooney, 1988; Webster, 1963). The subharmonic lines are possibly caused by the parametric amplification of a low-level signal already present in the liquid (Tucker, 1965, in Rooney, 1988), or possibly by the large amplitude radial oscillations of cavities that are unstable to subharmonic response when the resonant frequency of the cavity is half the applied frequency (Rooney, 1988).

The cavitation noise spectra depend on the state of gasification of the liquid, ambient pressure and temperature and ultrasonic intensity and frequency (Neppiras, 1980). Cavitation noise increases with increasing ultrasonic intensity and is greater for transient than stable cavitation (Neppiras, 1980).

2.3 SONOCHEMISTRY

Sonochemistry is the application of ultrasound in chemistry. Sonochemical benefits are caused by the chemical and physical effects that arise from ultrasonic cavitation; chemical effects are reviewed in Section 2.3.1 and physical effects in Section 2.3.2.

2.3.1 Chemical effects

The chemical effects of ultrasonic cavitation are caused by the formation of hydroxyl and hydrogen radicals in the collapsing cavities (Makino et al., 1982). The radicals react with each other and with solutes present

in the liquid medium. The site of these sonochemical reactions (in relation to the collapsing cavity) is reviewed in Section 2.3.1.1 and the effect of dissolved gas on the reactions is reviewed in Section 2.3.1.2.

2.3.1.1 Site of sonochemical reactions

Sonochemical reactions in a cavitating liquid occur in three regions, the gas inside a cavity, the interface between a gas cavity and a liquid and the bulk liquid (Él'piner, 1959; Suslick and Hammerton, 1986). Margulis disagreed with such a system of classification as it was reported that sonochemical reactions were the result of different processes occurring in both the gas and liquid phases, the role of each depending on various factors that changed throughout the process, and thus could not be classified as reactions occurring in separate regions (Margulis, 1969). A diagram of the three regions in a cavitating liquid in which sonochemical reactions take place and the processes that occur in each region are shown in Figure 2.6.

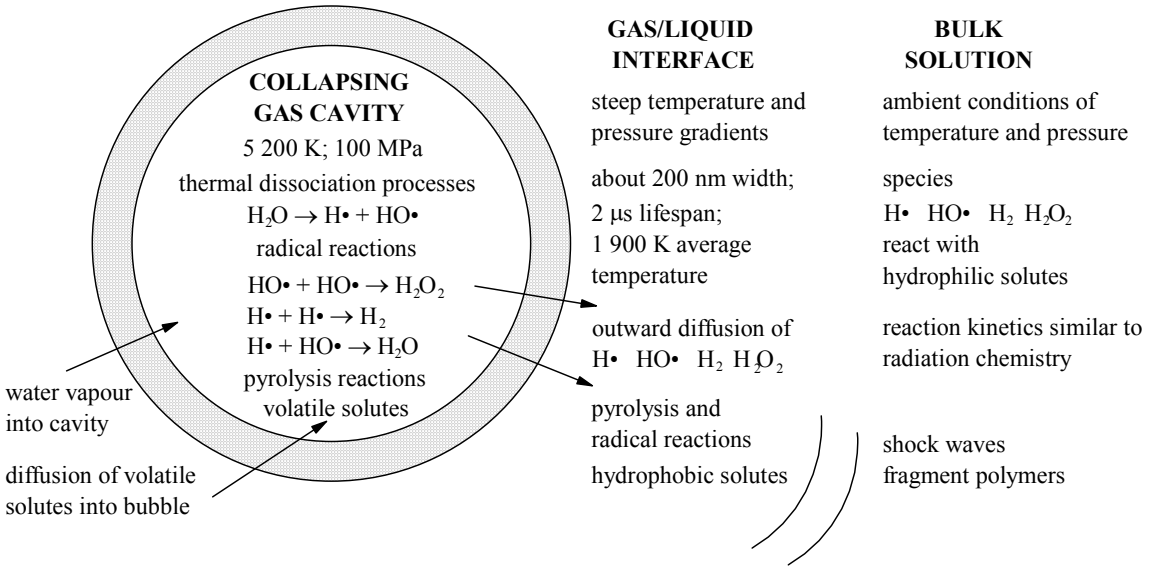

Figure 2.6 : Schematic diagram of the three regions in a cavitating liquid in which chemical reactions take place

The gas inside the collapsing gas cavities is the region where according to the hot spot theory, high temperatures and pressures occur (Noltingk and Neppiras, 1950). Noltingk and Neppiras calculated the maximum temperature in a collapsing cavity to be approximately 10 000 K (Noltingk and Neppiras, 1950). The formula for temperature calculation under adiabatic conditions (equation 2.11) was approximated by Neppiras to be

$$T_{max} = \frac{T_0 P(\gamma - 1)}{q} \qquad [2.12]$$

where T_0 is the ambient temperature of the liquid, q is the gas pressure in the cavity at its maximum radius, γ is the specific heat ratio of the gas in the cavity and P is the external pressure (sum of the hydrostatic and acoustic pressures) of the liquid (Neppiras, 1980). This equation indicates the direct relationship between

the maximum temperature reached in the collapsing cavities and the specific heat ratio of the gas; the higher the specific heat ratio, the higher the temperature (Riesz et al., 1990a). The maximum temperatures calculated for specific heat ratios of 1,67 (for a monatomic gas) and 1,30 (for the triatomic gas N_2O) were 3 015 and 1 350 K, respectively, when T_0 was 300 K and the ratio P/q was 15 (Riesz et al., 1990a).

The work published by Noltingk and Neppiras in 1950 has been followed by the publishing of different equations to calculate the maximum temperature in a collapsing cavity. These theoretical studies begin with the adiabatic collapse of a gas-filled cavity and then apply various corrections for parameters that affect the maximum temperature, such as the gas thermal conductivity, vapour condensation, gas reactions and radial temperature distribution inside the cavity (Suslick et al., 1990). A comparison of calculated maximum temperatures from different hydrodynamic models is shown in Table 2.2.

Table 2.2 : Theoretical maximum temperature in a collapsing cavity calculated from mathematical hydrodynamic models (Suslick et al., 1990)

Authors	Date	Dissolved gas	Maximum temperature (K)
Noltingk and Neppiras	1950	N_2	9,500
Hickling	1963	N_2	3,500
Fogler	1969	CO_2	1,900
Young	1976	Ar	1,650
Fujikawa and Akamatsu	1980	air	6,700
Margulis and Dmitieva	1982	air	5,300

The theoretical temperature values reported in Table 2.2 cannot be compared directly as different initial conditions were assumed in each model and the relative importance of the various corrections are difficult to establish (Suslick et al., 1990). However, the values of the maximum temperature (> 1 500 K) indicate that high temperatures are reached during cavity collapse.

Young showed that the sonoluminescence from a range of noble gases, with the same specific heat ratio, increased with decreasing thermal conductivity (Young, 1976). This indicates that cavity collapse is not completely adiabatic, as assumed by Notingk and Neppiras (1950), and that heat is lost to the surrounding liquid (Riesz et al., 1990a). The amount of heat lost during cavity collapse is dependent on the thermal conductivity of the gas. As reported in Table 2.1, the estimated temperatures during cavity collapse for water saturated with helium, neon, argon, krypton and zenon were 815; 1 420; 1 650; 1 890 and 2 000 K respectively (Young, 1976).

Mišík and co-workers used the temperature dependence of the kinetic deuterium isotope effect (for the cleavage of O-H and O-D bonds, respectively, in H_2O and D_2O molecules) to investigate the cavitation temperature (Misík et al., 1995). The rates of formation of $H^\bullet$ and $D^\bullet$ radicals, caused by the cleavage of O-H and O-D bonds in a mixture of water (H_2O) and D_2O, were measured during sonication by using various spin traps. The ratio of the rates of formation of the $H^\bullet$ and $D^\bullet$ radicals (k_H/k_D) was compared with the ratio of k_H/k_D calculated, at various temperatures, using the semi-classical model of the kinetic isotope effect for $H^\bullet$ and $D^\bullet$ radical formation. The three spin traps gave different cavitation temperatures in the range of 2 000 to 4 000 K (Misík et al., 1995).

Flint and Suslick investigated the maximum cavitation temperature by measuring the sonoluminescence spectra from silicone oil (Flint and Suslick, 1991). Light emission occurred from the excited state of the C_2 molecule. Synthetic spectra were generated, as a function of rotational and vibration temperatures, using diatomic-molecule emission theory and compared with the observed sonoluminescence spectra. From this comparison, the effective cavitation temperature was found to be 5 075 ± 156 K (Flint and Suslick, 1991). In an investigation of the sonochemical ligand substitution rates of volatile metal carbonyls, Suslick and co-workers used comparative rate thermometry to determine that the temperature in a collapsing cavity was approximately 5 200 ± 650 K (Suslick et al., 1986). The actual temperature within a collapsing cavity may be lower than that predicted by the original hot spot theory yet experimental evidence indicates that significantly high temperatures are reached in the cavities.

The high temperatures and pressures in the collapsing cavities cause the thermal dissociation of water vapour, as shown in Scheme 2.1, into hydroxyl $HO^\bullet$ and hydrogen radicals $H^\bullet$ (hydrogen and oxygen atoms are referred to as radicals since they contain an unpaired electron). These radicals have been identified by reaction with spin trapping compounds (Makino et al., 1982; Makino et al., 1983).

$$H_2O \rightarrow HO^\bullet + H^\bullet$$

Scheme 2.1

Hydrogen peroxide formation during sonication was first proposed by Schmitt and co-workers in 1929 to explain the sonochemical formation of iodine from a potassium iodide solution (Schmitt et al., 1929). The decolourisation of potassium permanganate either during sonication or in water that had been sonicated was early proof that hydrogen peroxide was formed during sonication (Flosdorf et al., 1936; Liu and Wu, 1934). This lead to the hypothesis that the action of ultrasonic waves was an *indirect effect*, in that the chemical changes were due to reactive compounds (such as hydroxyl radicals) that were formed from the dissociation of water molecules and not from any direct ultrasonic attack on the solute (Miller, 1950). The sonochemical formation of hydrogen peroxide was proposed to be analogous to the formation of hydrogen peroxide from the radical reactions occurring during radiation chemistry (Weissler, 1959). Hydrogen abstraction from sodium formate during sonication was used to prove the formation of hydrogen radicals during sonication

(Anbar and Pecht, 1964b); similarly, the oxidative deamination of ethylenediamine during sonication was reported as evidence for the formation of hydroxyl radicals during sonication (Anbar and Pecht, 1967). The formation of hydroxyl and hydrogen radicals during sonication has been proposed, and accepted, for many years, however, the electron spin resonance measurements by Makino and co-workers provided the first direct evidence for such formation (Makino et al., 1982; Makino et al., 1983).

Riesz and co-workers showed that the formation of hydroxyl radicals is directly linked to the temperature within a collapsing cavity (Riesz et al., 1990a). The different heat conductivity's of the noble gases was used to obtain different temperatures in the collapsing cavities. The production of hydroxyl radicals in water saturated with the different noble gases increased in the order for decreasing heat conductivity of the gases and thus increasing cavity temperatures (Riesz et al., 1990a). Hydroxyl and hydrogen radicals have been detected in pulsed (Christman et al., 1987) and continuous ultrasound (Makino et al., 1982). The occurrence of sonoluminescence from both stable and transient cavitation indicates that hydroxyl and hydrogen radicals are formed in both types of cavitation, since sonoluminescence arises from radical recombination reactions and excited molecules (Crum and Reynolds, 1985; Verrall and Sehgal, 1988).

Hydroxyl and hydrogen radicals in the gas cavities react either with other radicals producing water, hydrogen peroxide and hydrogen gas, as shown in Scheme 2.2, or with other gaseous components such as volatile organic solutes (Sehgal et al., 1982; Todd, 1970). Fischer and co-workers estimated that approximately 80 % of the radicals formed react to produce water (reaction [a] of Scheme 2.2) in the absence of any volatile solutes (Fischer et al., 1986a). Hart and Henglein also reported that more radicals react to produce water, according to reaction [a] of Scheme 2.2, than hydrogen peroxide, according to reaction [b] of Scheme 2.2 (Hart and Henglein, 1987).

$$H^{\bullet} + HO^{\bullet} \rightarrow H_2O \qquad [a]$$

$$HO^{\bullet} + HO^{\bullet} \rightarrow H_2O_2 \qquad [b]$$

$$H^{\bullet} + H^{\bullet} \rightarrow H_2 \qquad [c]$$

Scheme 2.2

Conditions in a collapsing cavity are not only determined by the specific heat ratio and heat conductivity of the gas but also by the vapour pressure of any volatile solute in the cavity (Suslick et al., 1983). Suslick and co-workers studied the sonochemical ligand substitution rates of volatile metal carbonyls, such as $Fe(CO)_5$, $Cr(CO)_6$, $Mo(CO)_6$ and $W(CO)_6$, to investigate the site of sonochemical reactions (Suslick and Hammerton, 1986; Suslick et al., 1986). The rate constants were found to increase linearly as the vapour pressure of the metal carbonyls increased. This is expected for gas phase reactions, since an increase in vapour pressure would cause an increase in solute concentration in the gas cavity and hence an increase in the rate coefficient (Suslick and Hammerton, 1986; Suslick et al., 1986). Suslick and co-workers also investigated the sonochemistry of non-aqueous liquids (Suslick et al., 1983; Suslick et al., 1984). Two

chemical dosimeters were used to study the sonochemical yields from alkane compounds, radical trapping by diphenylpicrylhydrazyl and decomposition of $Fe(CO)_5$. Both dosimeters indicated a decreasing linear relationship between the log of the sonochemical rate and the solvent vapour pressure (Suslick et al., 1983; Suslick et al., 1984). An increase in vapour pressure increases the solvent vapour in the gas cavity and thus decreases the intensity of the cavity collapse (the collapse is cushioned by the solvent vapour). This reduces the temperature reached during cavity collapse and thus lowers the rate of reaction (Suslick et al., 1983; Suslick et al., 1984). An investigation of the sonochemistry of alcohol-water mixtures by Krishna and co-workers also showed the effect of solvent vapour pressure on cavitation conditions and hence on sonochemical yields (Krishna et al., 1987; Krishna et al., 1989). The degradation of alcohols (such as methanol, ethanol, 1-propanol and 2-propanol) occur through bond cleavage and radical formation caused by thermal dissociation in the gas cavities (Krishna et al., 1987; Krishna et al., 1989). The investigation of the sonochemistry of non-aqueous solvents by Suslick and co-workers and the investigation of alcohol-water mixtures by Krishna and co-workers indicate that the radical reactions occurring inside the collapsing gas cavities are similar to radical reactions occurring during high temperature pyrolysis (Krishna et al., 1987; Krishna et al., 1989; Suslick et al., 1983; Suslick et al., 1984).

The second region where sonochemical reactions take place, as shown in Figure 2.6, is at the interface between the hot gas cavities and the bulk liquid. Large temperature and pressure gradients exist in this region (Riesz and Kondo, 1992). The investigation by Suslick and co-workers of the sonochemical ligand substitution rates of volatile metal carbonyls found that the linear relationship between the sonochemical rate constant and the vapour pressure had a non-zero intercept. This indicated that part of the reaction was not dependent on the vapour pressure and occurred in the liquid, probably at the interfacial region heated by the collapsing gas cavities (Suslick and Hammerton, 1986; Suslick et al., 1986). A conduction model was used to calculate that the interfacial region extended for about 200 nm from the cavity surface, existed for less than 2 μs after the cavity collapsed and had an approximate temperature of 1 900 K (Suslick and Hammerton, 1986; Suslick et al., 1986).

The formation of hydrogen peroxide, water and hydrogen gas, according to the radical reactions listed in Scheme 2.2 also occur at the interface between the hot gas cavity and the bulk liquid. Weissler reported that the yield of hydrogen peroxide decreased, for oxygen- and argon-saturated water, when volatile solutes such as allylthiourea, formic acid or acrylamide were added to the water (Weissler, 1959). Hydrogen peroxide formation was reduced because the reactions listed in Scheme 2.2 are inhibited by the solutes reacting with the hydroxyl and hydrogen radicals. The most volatile solute would produce the largest reduction in hydrogen peroxide formation if the reactions only occurred in the gas cavities. However, the greatest reduction in hydrogen peroxide formation was not recorded for the addition of formic acid, the most volatile solute. Thus the radical reactions must also occur outside of the gas cavities, at the liquid interface (Weissler, 1959).

The concentration of a solute that decreases the hydrogen peroxide yield to 50 % of the yield observed in the absence of the solute is defined as the $C_{½}$ concentration (Henglein and Kormann, 1985). This concentration was found to be dependent on the hydrophobicity of the solute and not on the rate constant for the reaction between the solute and hydroxyl radicals. Hydrophobicity is defined as the ratio of the number of hydrophobic groups (such as CH_3, CH_2 and CH) to hydrophilic groups (such as OH, COOH, CO and NH_2) in a solute molecule (Henglein and Kormann, 1985). Riesz and co-workers investigated the sonochemistry of volatile and non-volatile solutes, the interfacial region was found to have a low polarity and a high concentration of hydrophobic, non-volatile solutes (Riesz et al., 1990b; Riesz and Kondo, 1992).

Organic radicals were generated in the interfacial region from the thermal decomposition of non-volatile solutes. The formation of these radicals was dependent on the ability of the solutes to accumulate at the cavity interface and on the activation energy (determining ease of bond scission); the higher the solute concentration and the lower the activation energy, the higher the yield of thermal decomposition products (Krishna et al., 1989). Products from reactions between solute molecules and hydrogen and hydroxyl radicals predominate when only low concentrations of non-volatile solutes are present at the interface (Kondo et al., 1993; Riesz et al., 1990b).

The formation of supercritical water has been proposed to occur in the interfacial region since temperatures and pressures greater than the critical temperature (647 K) and critical pressure (22,4 MPa) of water are reached (Hua et al., 1995b; Riesz and Kondo, 1992). The physicochemical properties of supercritical water, such as viscosity, density and heat capacity, are different to that of water; supercritical water acts as a more non-polar solvent because of its lower dielectic constant (Franck, 1987). This explanation has been used to account for the preferential accumulation of hydrophobic solutes in the interfacial region (Riesz and Kondo, 1992). Hua and co-workers investigated the formation of supercritical water during sonication by measuring the ultrasonic hydrolysis of *p*-nitrophenyl acetate (Hua et al., 1995b). The reaction was accelerated by ultrasound by two orders of magnitude over the pH range of 3 to 8 (Hua et al., 1995b). It was proposed that the reaction took place in a supercritical region at the interface because *p*-nitrophenyl acetate is non-volatile and relatively hydrophobic; hydroxyl radicals are not involved in the reaction mechanism. The changes in the thermodynamic activation parameters ($\Delta S^{\ddagger}$, $\Delta G^{\ddagger}$ and $\Delta H^{\ddagger}$) of the *p*-nitrophenyl acetate hydrolysis in sonicated and unsonicated solutions were explained in terms of the physical properties of supercritical water (Hua et al., 1995b). A heat transfer model was used to estimate that after 10 ms, the radius of the supercritical region around a collapsed cavity extended about 40 % further into the bulk solution than the original cavity; also, approximately 0,15 % of the water would be in the supercritical state at any time during sonication (Hua et al., 1995b).

The third region where sonochemical reactions take place, as shown in Figure 2.6, is in the bulk liquid at ambient temperature (Riesz et al., 1990b). Radicals produced in the collapsing cavities and at the cavity interface diffuse into this region and react with non-volatile solutes with kinetics analogous to that observed

in aqueous radiation chemistry (Riesz et al., 1990b; Sehgal et al., 1982). Gutiérrez and co-workers estimated that less than 10 % of the hydroxyl and hydrogen radicals formed in the gas cavity reach the bulk solution (Gutiérrez et al., 1991). Products, such as hydrogen peroxide, from radical reactions occurring in the first two regions (as listed in Scheme 2.2) also diffuse into this region and undergo secondary reactions. Anbar and Pecht showed that the radical reactions producing hydrogen peroxide do not occur in the bulk liquid (Anbar and Pecht, 1964a). Shock waves are generated in the bulk liquid when the liquid moves back into the volume occupied by the collapsing cavities. These shock waves generate shear forces that fragment polymers dissolved in the liquid (Webster, 1963).

The relative contributions of reactions in the collapsing cavities, interfacial region and in the bulk liquid depend on the volatility and hydrophobicity of solutes (Riesz et al., 1990b).

2.3.1.2 Effects of dissolved gas

Early ultrasonic investigations showed that the nature of a gas present during sonication affected the sonochemical reactions. Weissler and co-workers found that the amount of iodine liberated from a potassium iodide solution was dependent on the gas (air, oxygen, nitrogen, helium or carbon dioxide) that was present during sonication (Weissler et al., 1950). Parke and Taylor found that hydrogen peroxide formation differed when different gases (oxygen, argon or nitrogen) were present during sonication (Parke and Taylor, 1956).

The investigation by Weissler into the effect of volatile solutes (allylthiourea, formic acid or acrylamide) on the yield of hydrogen peroxide found that it decreased in the presence of the solutes, however, for each solute, the yield was higher when the water was saturated with oxygen than with argon (Weissler, 1959). This was attributed to the formation of additional hydrogen peroxide from the reactions listed in Scheme 2.3. Hydrogen radicals, in the presence of oxygen, react with the oxygen molecules, as shown in reaction [a] of Scheme 2.3, to form perhydroxyl radicals ($^{\bullet}HO_2$). Hydrogen peroxide is formed from the reaction between a hydrogen radical and perhydroxyl radical (reaction [b] of Scheme 2.3) and from the reaction (reaction [c] of Scheme 2.3) between two perhydroxyl radicals (Él'piner, 1959; Parke and Taylor, 1956; Weissler, 1959).

$$H^{\bullet} + O_2 \rightarrow HO_2^{\bullet} \quad [a]$$

$$HO_2^{\bullet} + H^{\bullet} \rightarrow H_2O_2 \quad [b]$$

$$HO_2^{\bullet} + HO_2^{\bullet} \rightarrow H_2O_2 + O_2 \quad [c]$$

Scheme 2.3

The investigation of the sonochemical formation of hydrogen peroxide by Del Duca and co-workers using isotopic techniques estimated that one third of hydrogen peroxide in oxygen-saturated water was produced via the perhydroxyl radical reactions listed in Scheme 2.3 and the remaining hydrogen peroxide from the hydroxyl radical reactions listed in Scheme 2.2 (Del Duca et al., 1958). It was found that the O-O bond in an oxygen molecule (O_2) was not broken and that the molecule was incorporated as a unit into a peroxide

molecule (H_2O_2). Other radical reactions that Del Duca and co-workers proposed may occur during sonolysis, based on the standard free energy change in the gaseous state at 25 °C, are listed in Scheme 2.4 (Del Duca et al., 1958).

$$HO^{\bullet} + HO_2^{\bullet} \rightarrow H_2O + O_2 \quad [a]$$

$$HO^{\bullet} + HO^{\bullet} \rightarrow H_2O + O^{\bullet} \quad [b]$$

$$O^{\bullet} + H_2O \rightarrow H_2O_2 \quad [c]$$

$$HO^{\bullet} + HO^{\bullet} \rightarrow H_2 + O_2 \quad [d]$$

Scheme 2.4

Mead and co-workers compared the formation of hydrogen peroxide in water saturated with different gases (Mead et al., 1976). It was found that the hydrogen peroxide yield was a maximum for oxygen saturation and decreased in the order for air, argon and nitrogen saturation. Hydrogen peroxide formation does not occur in water saturated with carbon dioxide (Henglein, 1985) or hydrogen (Gutiérrez et al., 1987; Hart and Henglein, 1987). Hydroxyl radicals are scavenged, during hydrogen saturation, according to the reaction listed in Scheme 2.5 and are thus unable to react with other radicals to produce hydrogen peroxide (Gutiérrez et al., 1987; Hart and Henglein, 1987).

$$HO^{\bullet} + H_2 \rightarrow H_2O + H^{\bullet}$$

Scheme 2.5

Although the yield of hydrogen peroxide in water saturated with pure gases is a maximum for oxygen, higher yields have been observed for mixtures of oxygen with argon (Fischer et al., 1986b; Hart and Henglein, 1985) and with hydrogen (Hart and Henglein, 1987). The maximum hydrogen peroxide yield for gas mixtures of oxygen and argon occurs at a 30 to 70 % oxygen to argon ratio. An increasing oxygen concentration initially increases the formation of hydrogen peroxide because of perhydroxyl radical formation (according to Scheme 2.3). The temperature in the gas cavities decreases with increasing oxygen concentration (oxygen has a lower specific heat ratio than argon) causing fewer hydrogen and hydroxyl radicals to be formed. The formation of hydrogen peroxide thus reaches a maximum and then decreases (Fischer et al., 1986b; Hart and Henglein, 1985). The investigation by Fischer and co-workers using $^{18,18}O_2$ showed that oxygen molecules dissociate in the gas cavities and are not included in a peroxide molecule as a whole unit as proposed by Del Duca in 1958 (Fischer et al., 1986b).

The maximum hydrogen peroxide yield for gas mixtures of oxygen and hydrogen occurs at a 80 to 20 % oxygen to hydrogen ratio (Hart and Henglein, 1987). The hydrogen molecules dissociate into hydrogen radicals, as shown in Scheme 2.6.

$$H_2 \rightarrow H^{\bullet} + H^{\bullet}$$

Scheme 2.6

The yield of hydrogen peroxide is initially increased by the reaction of hydrogen radicals with oxygen to form perhydroxyl radicals (Scheme 2.3). Hydrogen peroxide formation decreased at higher hydrogen concentrations because the cavity temperature was lowered by the higher heat conductivity of hydrogen (Hart and Henglein, 1987). No hydrogen peroxide is formed in water saturated with gas mixtures of hydrogen and argon if the proportion of hydrogen is greater than 20 % (Gutiérrez et al., 1987). This is due to the scavenging of hydroxyl radicals by hydrogen, as shown in Scheme 2.5 (Gutiérrez et al., 1987).

Hydrogen peroxide is the major product formed during the sonication of water (Mead et al., 1976). Other products, such as nitrous and nitric acid, are formed when a nitrogen-containing gas (N_2 or N_2O) is present during sonication (Hart et al., 1986; Hart and Henglein, 1986). Mead and co-workers found that the pH of water saturated with oxygen, air or argon decreased during sonication whereas pH during nitrogen-saturation decreased initially before remaining constant (Mead et al., 1976).

2.3.2 Physical effects

Sonochemical applications, such as catalysis, cleaning, emulsification and depolymerization, are possible because of the physical effects of ultrasound. These effects, like the chemical effects of ultrasound, are caused by the collapse of cavities in a liquid under the action of a sound wave. The two mechanisms responsible for the effects of cavitation in solid-liquid mixtures, as shown in Figure 2.7, are microjet impact and shock wave damage (Suslick, 1990).

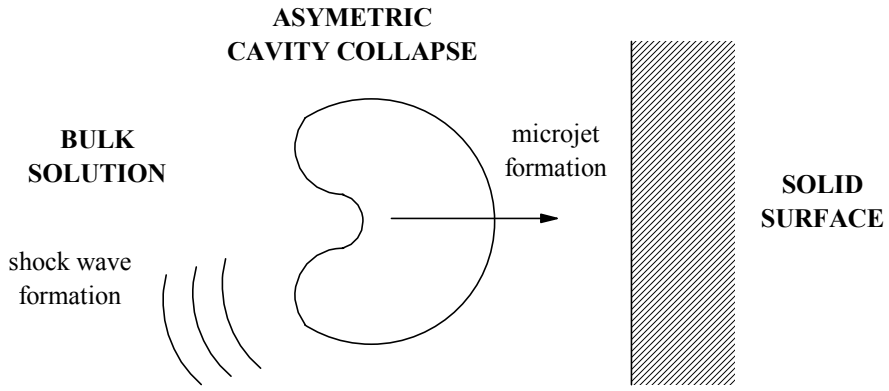

Figure 2.7 : Schematic diagram of the origin of cavitational physical effects

The changes in a sound field near a solid-liquid interface lead to asymmetric cavity collapse. The cavity deformation occurring during the collapse is self-reinforcing and a stream of fast-moving liquid directed towards the solid surface, called a microjet, is generated (Olson and Hammitt, 1969; Suslick et al., 1990). The velocities of the microjets are estimated as being as high as 100 m s^{-1} (Suslick et al., 1990). The impact of microjets on a solid surface causes localised erosion or pitting. Ultrasonic pitting has been recorded

photographically (Numachi, 1965; Olson and Hammitt, 1969). The surface area of a solid is increased and new surface material is exposed through pitting. Ultrasound can thus be used to activate solid catalysts (Mason and Cordemans, 1996). Cavity collapse is only distorted by a solid surface if the surface is considerably larger than the resonance size of the cavity, for example, microjet formation does not occur for particles smaller than 200 μm in an ultrasonic field with frequency of 20 kHz (Suslick et al., 1990). Alex and co-workers also found that microjet formation was dependent on the size of solid particles. Reaction yields were greater for copper turnings than copper powder (< 0,63 μm), and similarly for lead foil pieces and lead powder (Alex et al., 1995).

Shock wave formation also occurs during cavity collapse (Boudjouk, 1986). Shock waves break apart loosely aggregated particles along existing cracks (increasing the surface area) and remove loosely adhering particles to a solid surface (Crawford, 1963). Reaction products are thus removed from a solid surface, leaving the surface clean and available for further reaction (Mason, 1990). The turbulent flow and the shock waves produced by intense ultrasound cause small metal particles to collide with sufficiently high speed so as to induce melting at the point of collision (Suslick et al., 1990). Suslick and co-workers published scanning electron micrographs of zinc powders, before and after sonication, to show the fusion of particles due to interparticle collisions (Suslick et al., 1990).

Shock wave formation also results in high micromixing in the bulk liquid surrounding solid particles (Contamine et al., 1994). Davidson and co-workers reported that ultrasonic mixing increases the product yield for the reaction of an amine with an alkyl halide in toluene solution in the presence of potassium hydroxide and a phase transfer catalyst (Davidson et al., 1987). An 80 % yield was obtained for the reaction between indole and benzyl bromide with stirring at 20 °C for 8 h, the yield was increased to 95 % for 2 h of sonication without any external stirring (Davidson et al., 1987). Ultrasonic mixing increases heat and mass transfer as well as the diffusion of chemical species inside the pores of the solid particles (Contamine et al., 1994).

The rapid collapse of cavities also produces shear forces in the surrounding bulk liquid (Mason and Cordemans, 1996; Webster, 1963). This causes the breakage of chemical bonds in any polymeric materials dissolved in the liquid. A pair of macromolecular radicals is formed from the break in the polymer-chain, these radicals recombine randomly and reduce the molecular weight of the polymer (Mason and Cordemans, 1996).

In a solution of two immiscible liquids, ultrasonic cavitation leads to the formation of an emulsion. An emulsion occurs when microscopic droplets of one liquid are suspended in another liquid (Suslick, 1989). The cohesive forces that hold a droplet together are overcome by the conditions created during cavity collapse, this causes a droplet to burst into smaller droplets and the liquids become emulsified (Suslick, 1989). Ultrasonic reaction enhancement between immiscible liquids is due to the large increase in the interfacial contact area during emulsification (Pestman et al., 1994).

2.4 APPLICATIONS OF ULTRASOUND

The different applications of ultrasound are reviewed in the following sections, physical applications in Section 2.4.1, chemical applications in Section 2.4.2, medical applications in Section 2.4.3 and industrial applications in Section 2.4.4.

2.4.1 Physical applications

The first application of ultrasound, underwater depth determination, was made possible by Paul Langevin building the first underwater sound transducer (based on the piezoelectric effect in quartz crystals). The underwater transducer was initially developed for detection of submarines during World War I, however, it was not completed in time and was used for depth determination after the war (Mason, 1976). During World War II, ultrasound was used for both the detection and destruction of submarines. Ultrasonic listening devices mounted on torpedoes allowed the sound from the target submarine or ship to control the direction of the torpedo (Mason, 1976).

The ultrasonic flaw detection system to detect flaws in materials and to measure the thickness of materials with only one surface exposed developed independently in America and Britain between 1939 and 1945 (Mason, 1976). In 1945, ferroelectric materials such as barium titanate became available in ceramic form (Mason, 1976). These ceramics behave as piezoelectric crystals when polarised by means of a high voltage applied at a high temperature. Ferroelectric materials have a natural polarisation, yet in the unpolarized state the polarisation occurs in a random direction. The availability of ferroelectric ceramics increased the production of ultrasonic transducers and allowed for the diversification of ultrasonic applications (Mason, 1976).

Ultrasound is widely used in industry for non-destructive testing and fluid flow measurement (Hoyle and Luke, 1994). Application in fluid flow measurement has lead to ultrasound being used in chemical analysis (Asher, 1987). The measurement of ultrasonic velocity can be used for liquid identification (for example, the grade of petrol passing along a pipeline has been identified using ultrasound), determination of solution concentration and composition of liquid mixtures (Asher, 1987). Advantages of ultrasonic meters are that the response is rapid, radioactivity is not used, *moving parts* (that could lead to mechanical failure) are not employed and the system is non-invasive (Asher, 1987).

2.4.2 Chemical applications

The earliest chemical application of ultrasound was performed by Richards and Loomis in 1927. Reactions such as the hydrolysis of dimethyl sulfate and the iodine clock reaction were enhanced by ultrasound (Richards and Loomis, 1927). Early application of ultrasound in organic chemistry was demonstrated by Zechmeister and co-workers in the 1950's. Ring cleavage in compounds containing aromatic or heterocyclic rings, such as bromobenzene, phenol and pyridine, occurred during sonication (Currell and Zechmeister, 1958; Zechmeister and Wallcave, 1955).

Ultrasound has the following benefits when applied to chemical reactions (Mason, 1990).

- Ultrasound can be used to accelerate reaction rates. Mason and co-workers found that the homogeneous solvolysis of 2-chloro-2-methylpropane in aqueous ethanolic mixtures showed a 20-fold rate increase at 10 °C in 50 % ethanol (Mason et al., 1985). Kristol and co-workers found that ultrasound increased the rate of hydrolysis of a series of nitrophenyl esters by up to 15 % (Kristol et al., 1981).
- Ultrasound can be used to avoid forcing conditions. The production of transition metal carbonyl anions from the metal halide, sodium and tetrahydrofuran requires a high temperature and pressure. Suslick and Johnson found that the use of ultrasound for the reaction listed in Scheme 2.7 decreased the required temperature from 160 to 10 °C, and the required pressure from 20,3 to 0,45 MPa, while still giving a comparable yield of the end product (Suslick and Johnson, 1984).

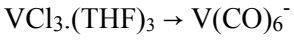

Scheme 2.7

- Ultrasound can allow for the use of simpler and safer procedures. The preparation of highly reactive *Rieke* metal powders involves refluxing the metal halide with potassium (the reducing agent) in tetrahydrofuran for extended periods of time (Rieke and Rhyne, 1979). Metal powders with similar reactivity can be prepared using a less hazardous procedure if the potassium is replaced by lithium and the reaction mixture is sonicated. For example, the formation of *Rieke* copper powder, that usually requires refluxing the metal halide ($CuBr_2$ or CuI_2) in tetrahydrofuran for 8 h, was complete within 40 min (as shown in Scheme 2.8) if the reaction was sonicated in an ultrasonic bath (Boudjouk et al., 1986). Similarly, zinc powder was produced from $ZnBr_2$ within 40 min with sonication instead of refluxing in tetrahydrofuran for 4 h (Boudjouk et al., 1986).

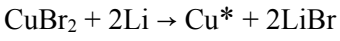

Scheme 2.8

- The use of ultrasound reduces particle size and allows for the continuous activation of surfaces. The rate of reaction of the Ullmann coupling reaction of 2-iodonitrobenzene, in the presence of a 4-fold excess of copper powder (as shown in Scheme 2.9), increased over 50-fold with ultrasound (Lindley et al., 1986; Lindley et al., 1987). Scanning electron micrographs showed that ultrasonic pretreatment increased the reaction rate because of a reduction in size of the copper particles (Lindley et al., 1987). The reaction rate was further increased if ultrasound was applied continually through the reaction. The ultrasonic-induced over 50-fold increase in reaction rate was thus not only

due to a reduction in particle size but also due to the continual activation of the copper surface (Lindley et al., 1986; Lindley et al., 1987).

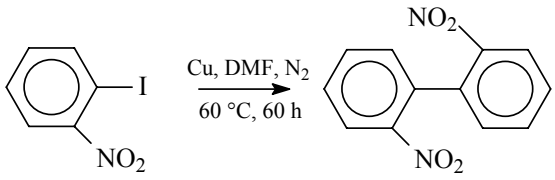

Scheme 2.9

- Ultrasound can be used to accelerate phase transfer catalyst reactions. Phase transfer catalysts act as a bridge between aqueous and organic phases in a reaction; reactants are carried one way and products returned the other way (Bremner, 1986). The addition of diethylmalonate to chalcone in toluene, using potassium hydroxide as a solid catalyst and trimethylbenzylammonium chloride as a phase transfer catalyst has been used as a model reaction to investigate the effect of ultrasound on a phase transfer catalyst reaction (Contamine et al., 1994; Ratoarinoro et al., 1995). The reaction does not occur (with stirring) in the absence of the phase transfer catalyst within a reaction time of 2 min. Without the phase transfer catalyst but with sonication, the yield increased to 40 % after a 2 min period. In the presence of the phase transfer catalyst, the yield was 5 % after stirring for 2 min and 91 % for sonication (Contamine et al., 1994; Ratoarinoro et al., 1995).
- Ultrasound can be used to change a reaction pathway. Ando and Kimura have proposed that ultrasound switches the pathway for the reaction of benzyl bromide, potassium cyanide and alumina stirred in toluene from the Friedel-Crafts reaction to nucleophilic substitution (Ando and Kimura, 1990). A mixture of *o*- and *p*-benzyltoluene (75 %) was produced in the absence of ultrasound but benzyl cyanide (71 %) was formed when the reaction mixture was sonicated (Ando et al., 1984). The change in pathway was caused by the ultrasonic acceleration of the poisoning of the acidic sites on the alumina surface by the potassium cyanide so that the reaction was catalysed instead by the basic sites on the alumina surface (Ando and Kimura, 1990). Sonochemical switching has also been observed in the Kornblum-Russell reaction (Luche, 1992). The alkylation of nitronate anions by 4-nitrobenzyl bromide follow either a polar two-electron pathway leading to the *O*-alkylation product, or a single electron transfer leading to the *C*-alkylation product. Luche used the reaction of an ethanolic solution of 4-nitrobenzyl bromide and 2-lithio-2-nitropropane to show that the ratio of the *C*/*O* alkylated products was almost reversed with the application of ultrasound. The single electron transfer pathway was the dominant mechanism during sonication (Luche, 1992).

The benefits as described above indicate that ultrasound enhances both homogeneous and heterogeneous reactions. The chemical and physical effects of ultrasound that causes such reaction enhancement are described in Section 2.3.1 and Section 2.3.2. Ultrasonic reaction enhancement is greater in heterogeneous

reactions and the industrial application of ultrasonic chemical reactions is more feasible for reactions incorporating a solid phase or catalyst (Bremner, 1986). Liquid-liquid reactions, another heterogeneous application, are also enhanced by ultrasound because of the formation of emulsions. Davidson and co-workers investigated the saponification of naturally occurring and commercially important waxes, such as wool waxes (Davidson et al., 1987). Sonication led to the formation of an emulsion of the wool wax dissolved in ethanol and the aqueous sodium hydroxide, this decreased the reaction time and temperature at which saponification occurred. Another advantage of ultrasound was that the products formed during sonication exhibited less colour than that produced in the absence of ultrasound (Davidson et al., 1987).

Ultrasound has also been used to improve the liquid-liquid extraction of acetic acid with water from a methyl isobutyl ketone-acetic acid mixture (Flisak and Perna, 1977). An increase of 11 % in the rate of acetic acid extraction was observed when an ultrasonic transducer, operating at 60 W, was attached to the side of the extraction column so as to cause the ultrasonic energy to be propagated at right angles to the direction of liquid flow (Flisak and Perna, 1977).

The following chemical applications of ultrasound have been reviewed separately, organic synthesis in Section 2.4.2.1, sonocatalysis in Section 2.4.2.2, polymer chemistry in Section 2.4.2.3, sonoelectrochemistry in Section 2.4.2.4 and sonocrystallization in Section 2.4.2.5.

2.4.2.1 Organic synthesis

In organic synthesis, the use of ultrasound can reduce reaction time and by-product formation, and increase the reaction yield (Henglein, 1987). Luche and Damiano investigated the application of ultrasound in the formation of organometallic compounds, frequently-used chemical reagents (Luche and Damiano, 1980). Activating agents are used to shorten the induction period, during which no reaction between the organic halide and the metal occurs. Ultrasound caused the reaction to occur almost immediately without requiring an activating agent. Reaction yields of 90; 61 and 95 % were obtained, respectively, in the preparation of *n*-propyl-, *n*-butyl- and phenyllithium from the bromide compounds with a sonication period of 1 h (Luche and Damiano, 1980).

The Barbier reaction, a one-step coupling of an organic halide with a carbonyl compound in the presence of lithium or magnesium, was also found to be enhanced by ultrasound (Luche and Damiano, 1980). The use of ultrasound allows for such reactions to be performed in wet technical grade tetrahydrofuran instead of in dry tetrahydrofuran. The use of wet solvents, at room temperature, has potential for large-scale production (Luche and Damiano, 1980). Under ultrasonic conditions, yields of between 76 and 100 % were obtained for the reaction of organic halides (alkyl, aryl, benzyl, allyl and vinyl halides) with ketones and aldehydes (Luche and Damiano, 1980). A 100 % yield was obtained after a reaction time of 10 min for the reaction, in the presence of lithium wire, shown in Scheme 2.10 (Luche and Damiano, 1980).

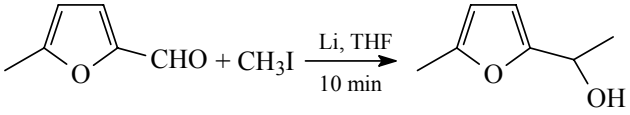

Scheme 2.10

Scanning electron microscopy has been used to show that the ultrasonic enhancement of these organometallic reactions is at least partly due to the effect of ultrasound on the lithium surface [de Souza-Barboza et al., 1988). Electron micrographs show the significant corrosion pits (thus increasing surface area) that formed in the lithium during sonication (de Souza-Barboza et al., 1988). Luche and co-workers, however, showed that ultrasound also has a direct chemical effect on the Barbier reaction (Luche et al., 1990). The lithium metal was preactivated under highly energetic conditions (in the absence of the reagents) so that the mechanical effects of ultrasound would not be dominant. The reaction was carried out at both a low and high ultrasonic intensity; the product concentration was found to be greater at the higher intensity (Luche et al., 1990). The difference in product concentration was attributed to the direct effect of ultrasound on the rate determining step of the reaction sequence. This step is the electron transfer from the metal to the carbon-halogen bond producing the radical anion, the first reactive species of the Barbier reaction (Luche et al., 1990).

Boudjouk and co-workers investigated the use of ultrasound in the preparation of symmetrical organic and bimetallic compounds (Boudjouk, 1986). The Wurtz-type coupling reactions of organic halides (shown in Scheme 2.11) and organometallic chlorides (shown in Scheme 2.12) using lithium wire and dry tetrahydrofuran at room temperature takes place only in the presence of ultrasound. The yield of the reaction shown in Scheme 2.11 is 70 % for a reaction of 10 h (Han and Boudjouk, 1981). The yield of the reaction shown in Scheme 2.12 is 68 % for a reaction time of 10 h (Boudjouk and Han, 1981).

$$2C_6H_5Br \rightarrow H_5C_6\text{-}C_6H_5 + Br_2$$

Scheme 2.11

$$2Ph_2HSiCl \rightarrow Ph_2HSi\text{-}SiHPh_2 + Cl_2$$

Scheme 2.12

The coupling reaction to produce tetramesityldisilene, a compound discovered by West and co-workers where the silicon-silicon double bond is stabilised by four mesityl groups (West et al., 1981), was prepared ultrasonically by Boudjouk and co-workers (Boudjouk et al., 1982). The reaction was carried out with lithium wire in tetrahydrofuran. Tetramesityldisilene was prepared ultrasonically in one step, as shown in Scheme 2.13; the yield of the reaction is 90 % for a reaction time of 20 min (Boudjouk et al., 1982). The symbol))) denotes ultrasonic radiation.

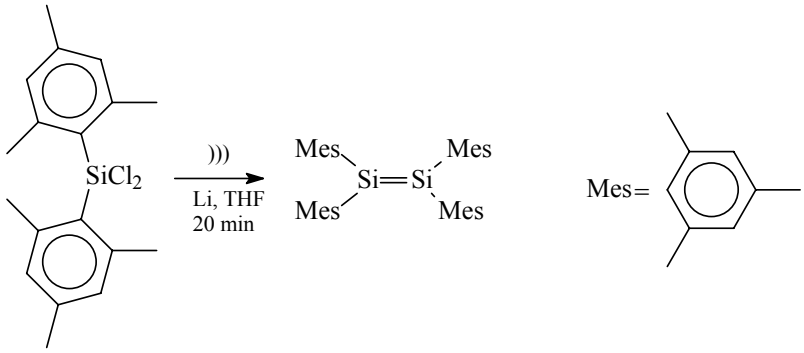

Scheme 2.13

Boudjouk and co-workers also investigated other metal reactions such as the Reformatsky reaction (Han and Boudjouk, 1982b) and the generation of *o*-xylylene (Han and Boudjouk, 1982a). The Reformatsky reaction is the reaction of ethyl bromoacetate with activated zinc dust and aldehydes or ketones to give the β-hydroxyl ester (Han and Boudjouk, 1982b). The yield of the reaction of cyclopentanone (as shown in Scheme 2.14) in the presence of ultrasound is 98 % after 30 min at a reaction temperature of 25 to 30 °C. The yield in the absence of ultrasound is 50 % after 12 h at a reaction temperature of 80 °C (Han and Boudjouk, 1982b).

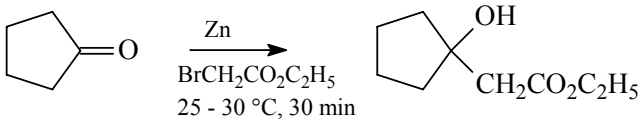

Scheme 2.14

The reaction of α,α'-dibromo-*o*-xylene, zinc and a dienophile does not proceed in the absence of ultrasound (Han and Boudjouk, 1982a). A high yield of cycloaddition products is obtained with ultrasound; the reaction proceeds via the reactive intermediate, *o*-xylylene. The yield of the reaction shown in Scheme 2.15 is 89 % for a reaction time of 15 h at a reaction temperature of 20 to 25 °C (Han and Boudjouk, 1982a).

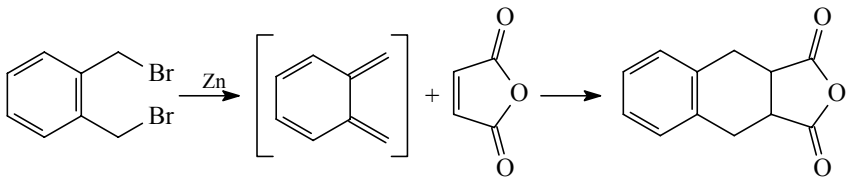

Scheme 2.15

Ultrasound can be used to accelerate the reduction of aromatic halides (Han and Boudjouk, 1982c). These compounds do not readily undergo nucleophilic substitution and electron-donating groups on the ring further impede the displacement of the halogen. The yield of the reduction of *p*-bromoanisole to anisole in the presence of lithium aluminium hydride (as shown in Scheme 2.16) is 70 % after 7 h of sonication (Han and

Boudjouk, 1982c). A yield of 35 % is obtained without sonication after refluxing with an excess of lithium aluminium hydride in diglyme for 24 h at 100 °C (Han and Boudjouk, 1982c).

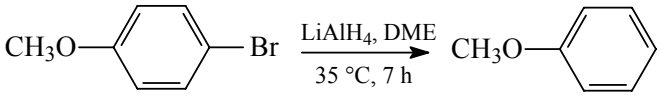

Scheme 2.16

2.4.2.2 Sonocatalysis

Catalysts are classified as either homogeneous or heterogeneous. A homogeneous system exists if the catalyst is a molecular or ionic species dissolved in a liquid; a heterogeneous system exists if the catalyst is a solid and the reactants are either in a percolating gas or liquid (Suslick, 1990). Both types of catalysts may be difficult to activate or to keep active (Suslick, 1990). The advantages of the application of ultrasound to catalysis are the use of ambient temperatures to preserve thermally-sensitive substrates and to enhance selectivity, the ability to generate high-energy species that are difficult to obtain from photolysis or pyrolysis, and the production of high temperatures and pressures during cavitation that generate autoclave reaction conditions on a microscale (Suslick, 1990).

Organometallic compounds are used as homogeneous catalysts, these compounds are often catalytically inactive until the loss of metal-bonded ligands such as carbon monoxide (Suslick, 1990). Suslick and co-workers investigated the sonolysis of iron carbonyl compounds for the catalysis of olefin isomerization reactions (Suslick et al., 1981; Suslick et al., 1983). Ultrasound induces ligand dissociation of iron carbonyl $Fe(CO)_5$ producing $Fe_3(CO)_{12}$ and finely divided iron in the absence of additional ligands (Suslick et al., 1981). The primary process $Fe(CO)_5$ undergoes during sonication is shown in reaction [a] of Scheme 2.17. The compound $Fe_2(CO)_9$ is formed from $Fe(CO)_4$ according to reaction [b] of Scheme 2.17; and $Fe_3(CO)_{12}$ is formed from $Fe(CO)_3$ according to reactions [c] and [d] of Scheme 2.17 (Suslick et al., 1981).

$$Fe(CO)_5 \rightarrow Fe(CO)_{5-n} + nCO \ (n = 1 \text{ to } 5) \quad [a]$$

$$Fe(CO)_4 + Fe(CO)_5 \rightarrow Fe_2(CO)_9 \quad [b]$$

$$Fe(CO)_3 + Fe(CO)_5 \rightarrow Fe_2(CO)_8 \quad [c]$$

$$Fe_2(CO)_8 + Fe(CO)_5 \rightarrow Fe_3(CO)_{12} + CO \quad [d]$$

Scheme 2.17

Sonication of 1-pentene in a decane solution with either $Fe(CO)_5$, $Fe_2(CO)_9$ or $Fe_3(CO)_{12}$ produces *trans*- and *cis*-2-pentene in approximately a 3:1 ratio, the thermodynamic ratio (Suslick et al., 1981). Sonolysis of

1-pentene with $Fe(CO)_5$, $Fe_2(CO)_9$ or $Fe_3(CO)_{12}$ enhances the rate of isomerization of 1-pentene by factors of approximately 10^5, 10^2 and 10^2, respectively (Suslick et al., 1981).

The sonolysis of $Fe(CO)_5$ in the presence of additional ligands (such as phosphine or phosphite compounds) produces $Fe(CO)_3L_2$ and $Fe(CO)_4L$, where L is a phosphine or phosphite compound (Suslick et al., 1983). Similar substitution patterns have been observed for other metal carbonyl compounds, such as $Fe_3(CO)_{12}$, $Mn_2(CO)_{10}$, $Cr(CO)_6$, $Mo(CO)_6$ and $W(CO)_6$ (Suslick et al., 1983). Similarities between the sonocatalysis and photocatalysis of metal carbonyl compounds exist, however, different relative efficiencies and selectivities are observed (Suslick et al., 1983).

Ultrasound also enhances the preparation of the transition-metal carbonyl complexes. Suslick and Johnson found that where high pressures of CO and high temperatures are usually required to produce the transition-metal carbonyl anions, the use of ultrasound allows for the reaction to be carried out at low temperatures and pressures (Suslick and Johnson, 1984). For the reaction listed in Scheme 2.7, sonication allowed for the required temperature to be decreased from 160 to 10 °C, and the required pressure from 20,3 to 0,45 MPa, while still giving a comparable yield of the end product (Suslick and Johnson, 1984).

Heterogeneous catalysts play an important role in industry, for example the bulk of the petroleum industry is based on a series of catalytic transformations (Suslick, 1990). These catalysts are often produced from rare and expensive metals, the use of ultrasound could allow for the activation of less reactive (and less expensive) metals (Suslick, 1990). Suslick and Casadonte found that the sonication of nickel powder increased its activity as a hydrogenation catalyst by a factor greater than 10^5 (Suslick and Casadonte, 1987). Nickel powder is usually an inactive catalyst for the hydrogenation of alkenes, ultrasonic pretreatment for 1 h activated the powder and caused the hydrogenation of 1-nonene to proceed with an initial rate of 1,5 mmol L^{-1} min^{-1} (Suslick and Casadonte, 1987). Sonication did not reduce the particle size of the powder, thus the surface area was not increased and the sonocatalytic activity was attributed to the changes in the particle aggregation, surface morphology and thickness of surface oxide coating. Electron micrographs revealed that sonication smoothed the initial highly crystalline structure of nickel and increased the aggregation of the powder. Auger electron spectra depth profiles showed that the initial oxide coat that extended for 25 x 10^{-9} m with a surface Ni/O ratio of 1 was decreased to a thickness of less than 5 x 10^{-9} m with a surface Ni/O ratio of 2. The changes in the nickel powder that led to the increased sonocatalytic activity were caused by interparticle collisions driven by the turbulent conditions and shock waves created by the ultrasonic field (Suslick and Casadonte, 1987; Suslick et al., 1989).

Suslick and co-workers investigated the ultrasonic-induced changes of copper powder (Suslick et al., 1989). Similar to nickel powder, ultrasound did not reduce the copper powder particle size (and hence increase the surface area); electron micrographs showed an increased aggregation and surface smoothing with sonication.

The partial oxide coating, approximately 30 x 10^{-9} m deep, was completely removed during sonication and was replaced by a thin, approximately 10 x 10^{-9} m, but heavy (greater than 60 % atomic composition) surface deposition of carbon. The origin of the carbon and its influence on the reactivity of the copper powder are not known (Suslick et al., 1989). The changes in the copper powder were also produced by the ultrasonic-induced interparticle collisions. Direct particle collisions produce agglomeration and collisions at an angle produce the surface smoothing and removal of the surface oxide coating (Suslick et al., 1989).

2.4.2.3 Polymer chemistry

Research into the effects of ultrasound on polymer chemistry began in the 1930's (Price and Smith, 1993). Most of the early work, such as the investigation by Thomas and de Vries of the heterolytic cleavage of polymethylsiloxane (Thomas and de Vries, 1959), focused on the degradation of polymer chains during sonication. Ultrasound, however, can also be used to initiate polymerisation (Kruus et al., 1988).

Bonds of polymers are broken because of the hydrodynamic shear forces produced in the liquid surrounding the vibrating and collapsing cavities (Henglein and Gutiérrez, 1988; Webster, 1963). The cleavage of a polymer does not occur randomly but statistically near the middle of the chain (Price and Smith, 1993). Polymer cleavage produces a pair of macromolecular radicals that react with other radicals and reduce the molecular weight of the polymer (Mason and Cordemans, 1996). A limiting molecular weight exists below which no further cleavage occurs. The sonication of a 1 % solution of polystyrene in toluene at 25 °C showed that polymer degradation was more efficient at higher molecular weights and that no further degradation occurred below the limiting value of approximately 30 000 for this system (Price, 1993).

Price and Smith investigated the role of parameters such as ultrasonic intensity, temperature and dissolved gas on the degradation of polystyrene in toluene (Price and Smith, 1993). The rate of degradation was found to increase, although not indefinitely, with increasing intensity and an optimum rate was reached at approximately 145 W cm^{-2}. Polymer degradation increased with decreasing temperature over the range of -10 to 61 °C (Price and Smith, 1993). Polymer degradation was also affected by the presence of a dissolved gas but because bond cleavage was caused by the hydrodynamic shear forces (and not of thermal origin) the degradation rate could not be directly correlated to gas properties such as thermal conductivity and specific heat ratio. Polymer degradation rate, however, tended to be greater for gases with a lower solubility (Henglein and Gutiérrez, 1988; Price and Smith, 1993). The rate of polymer degradation can also be enhanced by using a solvent with a low vapour pressure, reducing the ultrasonic frequency and decreasing the solution concentration (Lorimer, 1990).

The non-random nature of the polymer cleavage allows for the modelling of the process so that the polymer molecular weight during sonication can be predicted (Price, 1993). Manipulation of the experimental conditions allows for control of the limiting molecular weight. Price and Smith found that the limiting molecular weight increased linearly with increasing temperature, decreased linearly with increasing ultrasonic intensity and was lower for gases with a lower solubility (Price and Smith, 1993).

Macromolecular radicals produced from two polymers sonicated in a common solvent react with each other to produce the *cross product* called a block co-polymer (Price, 1993; Price and Smith, 1993). This process is not easily manageable since both the recovery of the co-polymer and the control of the co-polymer length are difficult. This technique, however, is of benefit if a polymer is sonicated together with a monomer such that the macromolecule radicals from the polymer initiate the polymerisation of the monomer (Price, 1993). The example shown in Figure 2.8 is of the formation of the block co-polymer, poly(styrene-*b*-methyl methacrylate), from the sonication of polystyrene and methyl methacrylate (Price, 1993).

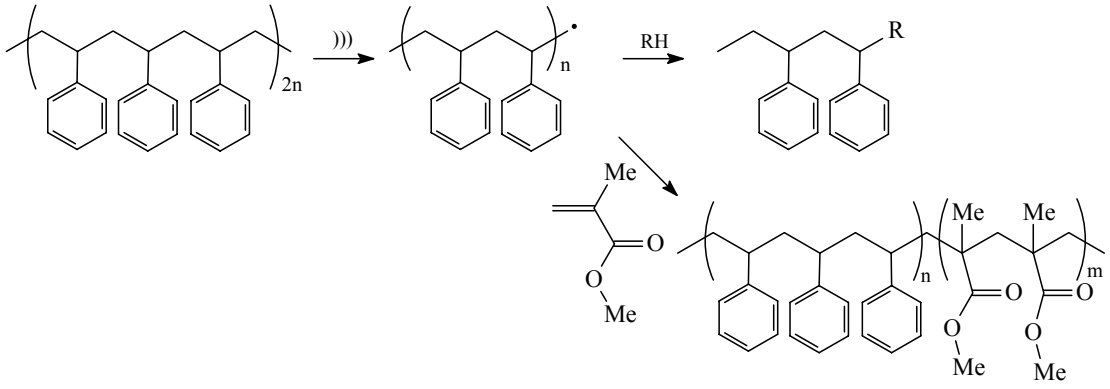

Figure 2.8 : Schematic diagram of the production of end capped polystyrene and poly(styrene-*b*-methyl methacrylate) block co-polymers (Price, 1993)

A radical initiator is required to start a polymerisation reaction. These compounds are usually activated by ultraviolet irradiation or by heating to above 60 °C (Price et al., 1991). Price and co-workers used the polymerisation of methyl methacrylate with azo-bis(isobutyronitrile), a common radical initiator, to show that ultrasound accelerates the formation of radicals from initiators (Price et al., 1991). Ultrasound has also been used to initiate polymerisation reactions in the absence of radical initiators. Kruus and co-workers showed that pure, dry, vinyl monomers (such as styrene) can be polymerised solely by the application of ultrasound (Kruus et al., 1988). Price and co-workers polymerised methyl methacrylate with ultrasound in the absence of a radical initiator (Price et al., 1991). The methyl methacrylate conversion (fraction of the monomer converted to polymer) after 4 h of sonication was 12 % for the solution containing azo-bis(iso butyronitrile) and 6 % without the radical initiator. The conversion did not proceed further than 12 % as the solution became viscous and cavitation was suppressed (Price et al., 1991). The suppression of cavitation with increasing viscosity has led to conversion rates of ultrasonic polymerisation reactions to not exceed 25 % (Price and Lenz, 1993).

Price and co-workers monitored the poly(methyl methacrylate) molecular weight and molecular weight distribution for 8 h of sonication; long polymer chains were initially formed but these were broken down after further sonication (Price et al., 1991). Polymerisation and polymer degradation were found to occur concurrently. In the investigation of the effect of argon on the polymerisation of styrene, Kruus and

co-workers found that polymerisation took place when argon was bubbled through the solution and that degradation occurred when the argon flow was turned off (Kruus et al., 1988). The molecular weight of a polymer produced from ultrasonic polymerisation is thus determined by parameters such as reaction time, ultrasonic intensity and gas present during sonication (Kruus et al., 1988; Price et al., 1991).

2.4.2.4 Sonoelectrochemistry

Electrochemical methods are used to produce reactive intermediates; organic electrosynthesis can generate compounds that may be difficult to prepare by other methods (Mason et al., 1990). The scale-up of laboratory electrolytic processes is hindered by restrictions to the maximum attainable current (such as the mass transfer to the electrode surface, fouling of the electrode surface and evolution of gases during reaction) and thus the maximum possible rate of reaction (Mason et al., 1990). Ultrasound produces the following benefits when applied to an electrochemical process (Mason et al., 1990; Reisse et al., 1994; Walton et al., 1996).

- Limited gas bubble accumulation at the electrode.
- Disturbance of the diffusion layer, thus the depletion of the electroactive species is stopped.
- More even transport of ions across the electrode double layer.
- Continual cleaning and activation of the electrode surface.

The potential for ultrasound to enhance electroplating by increasing the deposition rate has been investigated since the 1950's (Mason et al., 1990). Ultrasound is introduced into the electroplating process by sonicating the whole plating bath. Reisse and co-workers designed a sonoelectrochemical reactor in which the titanium ultrasonic horn acts as the working electrode (Reisse et al., 1994). The planar circular surface at the bottom of the horn acts as the electroactive part of the sonoelectrode and the immersed cylindrical part of the horn is covered by an isolating plastic jacket. The cathodic current during the investigation of the electrodeposition of copper (at -0,20 V relative to the standard hydrogen electrode) was found to be approximately 30 times greater with ultrasound than without (Reisse et al., 1994). Scanning electron micrographs showed that ultrasound also affected the morphology of the copper deposits, finer powders with a higher density of submicronic particles were produced. Nucleation of copper on the titanium sonoelectrode occurred at a higher overpotential than that occurring in the absence of ultrasound (Reisse et al., 1994).

The electrochemical synthesis of selenium and tellurium anions (Se_2^{2-}, Se^{2-}, Te_2^{2-} and Te^{2-}), intermediates in the formation of organoselenium and organotellurium compounds, have been enhanced by ultrasound (Gautheron et al., 1985). Mason and co-workers showed that ultrasound switches the reaction mechanism of the Kolbe reaction, the formation of alkanes from the electrodecarboxylation of carboxylate salts such as $RCOO^-Na^+$, from a single electron-transfer process to a process involving two electron transfers (Mason et al., 1990). The change in product distribution because of a change in reaction mechanism is shown in the sonoelectrolysis of cyclohexanecarboxylate (Chyla et al., 1989). Ultrasound decreased the yield of bicyclohexyl from 49 to 7,7 % and increased the yields of cyclohexene and cyclohexyl methyl ether

from 4,5 and 2,1 %, respectively, to 32,4 and 34,3 % (Chyla et al., 1989). The reaction efficiency was also increased by ultrasound, the average cell potential for the required current density of 2 000 A m^{-2} was 8,3 V in the absence and 7,3 V in the presence of ultrasound (Chyla et al., 1989). Walton and co-workers used ultrasound to enhance electrochemical reactions producing hydrogen and chlorine gas (Walton et al., 1996). The reactions are reversible and are limited by the removal of gaseous products from the electrode. Ultrasound did not enhance the oxygen-producing reaction for the experimental conditions used in the investigation (Walton et al., 1996). The application of ultrasound to such gas-producing reactions has implications for the operation of chloralkali cells (Walton et al., 1996).

2.4.2.5 Sonocrystallization

Ultrasound can be used to precipitate solids from a supersaturated solution because of the physical effects, such as particle fragmentation, produced by cavitation (Mason, 1990). Finely divided and uniform particles are produced by ultrasound because of the cycle of formation, growth and break-up of seed particles producing further seeding throughout the medium (Mason, 1990). Srinivasan and co-workers found that the application of ultrasound to the crystallisation of diphenyl oxide and dimethyl phenyl carbinol (compounds used to perfume soaps) improved crystal purity (Srinivasan et al., 1995). Ultrasound caused the crystal melting point for both diphenyl oxide and dimethyl phenyl carbinol to match, more closely, the melting point of the pure compounds. Ultrasound also improved the shape of the diphenyl oxide crystals, a higher proportion of needle-shaped crystals (the crystal structure of pure diphenyl oxide) was obtained under sonication (Srinivasan et al., 1995).

2.4.3 Medical applications

Ultrasound in medical applications is used for either interaction with a system producing a desired biological effect such as in physical therapy and surgery or for the purpose of extracting information without causing any biological effects such as in diagnosis (Dunn, 1991). Diagnostic applications of ultrasound are well established in medical fields such as obstetrics, cardiology, gynaecology, neurology and ophthalmology (Dunn, 1991). Medical applications are usually performed with pulsed ultrasound. The duration of the pulses is typically in the 1 ms range; intervals between the pulses are in the 1 ms range for diagnostic ultrasound and in the 1 s range for disintegration applications, such as the disintegration of kidney stones (Henglein et al., 1989). Continuous-wave ultrasound is used for physical therapy (ter Haar, 1988).

The mechanisms by which ultrasound can induce changes in biological systems are thermal, cavitation and mechanical effects such as particle movement (ter Haar, 1988). The energy of an ultrasonic wave moving through tissue is attenuated due to either absorption or scatter. The absorption of energy leads to tissue heating (ter Haar, 1988). The selective heating of tissue allows for ultrasound to be used in physical therapy for the relief of pain, reduction of soft tissue stiffness and the acceleration of healing (NCRP 74, 1983). Heating increases the blood flow to the area thus bringing metabolites needed for tissue repair and removing waste products; heating also increases the rate of many biochemical reactions and accelerates the diffusion rate across biologic membranes (NCRP 74, 1983).

The formation of free radicals could promote chemical reactivity *in vivo* if cavitation occurs during any medical application of ultrasound (Carmichael et al., 1986). Investigation of the chemical effects of pulsed ultrasound has shown that a *memory effect* exists, the shorter the time interval between pulses the more efficient the ultrasonic pulse is at producing a chemical effect. The memory for what has happened before fades as the length of interval increases (Henglein, 1987; Henglein et al., 1989). The low time ratio of pulse length to pulse interval used in ultrasonic diagnosis (over 1 to 1 000) indicates that the memory effect is unlikely to be evident and that the supplied time-averaged acoustic energy is low (Henglein et al., 1989). The high instantaneous intensity of the pulses, for example 150 W cm^{-2} for diagnosis and 10 000 W cm^{-2} for disintegration, could, however, induce cavitation to occur during a pulse (Henglein et al., 1989).

Theoretical studies of the cavitation threshold indicate that cavitation could possibly occur during pulsed ultrasound (Flynn, 1982; Flynn and Church, 1984). Pulsed ultrasound has been shown to produce free radicals in aqueous solution under conditions similar, although not identical, to diagnostic exposure conditions (Carmichael et al., 1986; Christman et al., 1987). The experimental conditions used in the investigation represented worst case values that would be more sensitive than typical diagnostic conditions (Carmichael et al., 1986; Christman et al., 1987). The extensive use of ultrasonic diagnosis has required that the safety of such techniques and instruments be continually investigated (Crum et al., 1992). There is little supporting evidence that diagnostic ultrasound instruments pose even a measurable risk to a patient (Crum et al., 1992; Dunn, 1991). Reports published by the World Health Organisation and the National Council on Radiation Protection and Measurements have also indicated that no adverse health effects in human beings exposed to diagnostic ultrasound have been reported (NCRP 74, 1983; EHC 22, 1982).

2.4.4 Industrial applications

The applications of ultrasound in industry include cleaning, drying, degassing, defoaming, soldering, drilling, plastic welding, extraction, filtration, sterilisation, emulsification, homogenisation, flotation, dissolution, deaggregation of powders, biological cell disruption, crystallisation and chemical reaction enhancement (Mason, 1991).

The application of ultrasound for cleaning is a long-established and efficient technology (Mason, 1993). Large cleaning systems are commercially available. An ultrasonic cleaner (volume, 7 500 L; power, 40 kW) has been used by the US Navy since 1968 to facilitate the disassembling of jet engines where heat and corrosion have made the unscrewing of fastening bolts difficult (Hunicke, 1990). The uniformity of the ultrasonic field, supplied by two banks of immersible transducers, was within 10 % throughout the tank (Hunicke, 1990).

Ultrasound can be applied in environmental remediation for the removal of airborne particles (Grinthal and Ondrey, 1992). Ultrasonic agglomeration was used to remove pollutant particles from air that were less than 5 μm in diameter and were too small to be removed by electrostatic precipitators. Airborne soot in a 15 m^3

chamber was reduced by three orders of magnitude with an ultrasonic transducer (frequency, 21 kHz) in experiments performed at the Institute of Transuranium Elements in Germany; experiments were also performed in a 170 m^3 chamber (Grinthal and Ondrey, 1992).

The recovery of precious metals from ore has been improved with the cleaning of 3 L s^{-1} water slurries of crushed ore in a reverbatory ultrasonic mixer of power 16 kW (Hunicke, 1990). An ultrasonic soldering pot (power, 14 kW) operating at 400 °C has been in operation for over 15 years with negligible ultrasonic equipment downtime (Hunicke, 1990). Ultrasonic defoaming has been used when the addition of chemical defoaming agents will contaminate the liquid to be defoamed (Chendke and Fogler, 1975). Ultrasonic defoaming has been used at a Coca-Cola bottling plant in Madrid to prevent overflow waste and rejections on a 72 000 bottle per hour line (Grinthal and Ondrey, 1992).

The application of ultrasound in various industries has been reviewed separately in the following sections, water and effluent treatment in Section 2.4.4.1, the food industry in Section 2.4.4.2, the textile industry in Section 2.4.4.3, the petroleum industry in Section 2.4.4.4 and membrane processes in Section 2.4.4.5

2.4.4.1 Water and effluent treatment

The combination of the physical effects (production of shear forces and shock waves) and chemical effects (radical formation) of cavitation allow for the application of ultrasound in water and effluent treatment (Mason et al., 1993). Ultrasound, however, is more effective when used in combination with other conventional treatment processes than as a stand-alone process (Mason et al., 1993; Mason et al., 1994).

The biocidal activity of chlorine is enhanced by ultrasound (Mason et al., 1994). The number of bacteria surviving a 5 min chlorine contact time was reduced by 30 % with 2 min of ultrasound. The break-up and dispersion of bacteria clumps, caused by ultrasound, allows for greater penetration of the biocide and renders bacteria more susceptible to chemical attack (Mason et al., 1994). Ultrasound could thus be used to reduce the biocide concentration required in water treatment (Mason et al., 1994).

The biological effects of ultrasound have been studied since the 1920's, ultrasound has been shown to disrupt cells (Alliger, 1975; Frizzell, 1988). Bacteria cells can be destroyed by ultrasound, however, high intensities are required for effective disinfection and a 100 % kill (Mason et al., 1994). Cellular disruption is due to the physical effects (such as shear forces and shock waves) of ultrasonic cavitation (Frizzell, 1988; Riesz and Kondo, 1992). Cells that are small and round in shape are more resistant to disruption by ultrasound (Alliger, 1975).

Ultrasound has been used to inactivate *Cryptosporidium parvum* oocysts that cause cryptosporidiosis (severe diarrhoea) in humans and domestic animals. (Anonymous, 1995). A 750 L h^{-1} pilot plant developed by Biwater and the University of Leeds has shown that complete destruction of the oocysts is achieved with 20 s of sonication, 99,8 % destruction is achieved with 15 s of sonication (Anonymous, 1995).

Ultrasound has also been used to ensure that no bacterial species are present after water treatment (Clasen and Sobotta, 1994). Rapid sand filters and flocculants are used to remove the bulk of planktonic organisms during water treatment, however, species such as *Notholca caudata* can persist through these processes. Bacterial regrowth can occur in water distribution networks if all bacterial species are not inactivated during water treatment. Clasen and Sobotta have shown that 99 % inactivation rates were achieved for the two plankton species *Artemia salina* and *Cyclops* nauplii within 30 s of sonication at an ultrasonic intensity of 0,8 W cm^{-2} and a frequency between 20 and 40 kHz (Clasen and Sobotta, 1994). A 95 % inactivation rate was achieved in an investigation of a pilot flow reactor (volume, 80 L) with a water throughput of 8 000 L h^{-1} and a specific output of 12 W L^{-1} (Clasen and Sobotta, 1994). The 1994 estimation of capital spending and operating costs were DM 0,026 per m^3, this compared favourably with the savings in flocculant chemicals and the reduction in sludge (Clasen and Sobotta, 1994).

Ultrasound has been used in combination with technologies such as ozone and electrostatics to improve water and effluent treatment. The use of ultrasound in combination with ozone enhances effluent treatment by producing an emulsion from suspended particles and dispersed microorganisms and by preventing the coalescence of ozone bubbles that ensures maximum bubble surface area is available for oxidation (Chendke and Fogler, 1975). An investigation of a pilot plant processing 76 kL of sewage per day indicated that 60 s of treatment with ultrasound and ozone destroyed 100 % of the faecal bacteria and viruses (Chendke and Fogler, 1975). Dahi found that ultrasonic treatment (2 min) of effluent from a biological sewage plant reduced the sterilization dose of ozone by 50 % (Dahi, 1976). Ultrasound combined with ozone has been used to enhance the degradation of natural organic matter (Olson and Barbier, 1994), cyclohexene (Weavers and Hoffmann, 1998) and 4-nitrophenol (Barbier and Pétrier, 1996). The 4-nitrophenol degradation increased with increasing ultrasonic frequency, (20 versus 500 kHz) because of the greater quantity of hydroxyl radicals escaping from the cavitation bubbles (Barbier and Pétrier, 1996).

Reimers and co-workers investigated the combination of ultrasound and electrostatics as a method to reduce the addition of chemicals during water treatment (Reimers et al., 1979). Benefits of ultrasound were the increased agitation and mixing of water, minerals and organics and the generation of kinetic energy to excite atoms and molecules. Application of this method in the soft drink bottling industry was found to reduce operation and maintenance problems and to reduce possible noxious effluents (Reimers et al., 1979).

Industrial effluent can also be treated with biological methods such as the activated sludge process (Balasubramaniam et al., 1995). Ultrasound has been used in conjuction with conventional techniques to enhance sludge processing. Bien investigated the use of ultrasound as a non-chemical method for the preparation of sludge for dewatering (Bien, 1988). Sludge is usually dewatered by filtration with the addition of polyelectrolytes as flocculants. The initial hydration of 92,8 % of a mineral sludge was reduced to 84,2 % after vacuum filtration, 77,7 % with the use of ultrasound, 69,2 % with the addition of a

polyelectrolyte and 61,2 % with the combination of ultrasound and polyelectrolyte addition (Bien, 1988). The required polyelectrolyte concentration was halved with the simultaneous application of ultrasound. A similar pattern in final hydration values was also found for an organic sludge. The effect of ultrasound was greater on sludges of higher hydration and rigid structure than on amorphous sludges of lower initial hydration (Bien, 1988). The investigation by Bien and Wolny of two digested and difficult dewatered sludges has also shown the advantageous use of ultrasound, in combination with polyelectrolyte addition, on sludge dewatering and reduction in sludge volume (Bien and Wolny, 1997).

Ultrasound was found to affect sludge and polyelectrolyte structure. In contrast to unprepared sludge, the addition of a polyelectrolyte produced compact but separate clusters of sludge flocs; the simultaneous application of ultrasound increased the spaces between the conglomerates (Bien and Wolny, 1997). The polymer chain shape and crystal outline of Zetag-50, the polyelectrolyte used in the investigation, was found to change during sonication (Bien and Wolny, 1997). It was concluded that the sonication time required to enhance sludge dewatering may depend on the type of polyelectrolyte used and should be determined experimentally (Bien and Wolny, 1997).

King and Foster investigated the effect of ultrasound on the settling properties of activated sludge (King and Foster, 1990). Ultrasound was found to improve the settleability of the sludge, however, the filterability of the solids deteriorated and the supernatant, after settlement, had a high concentration of suspended solids. Ultrasound degraded the sludge flocs and increased the number of small particles. Floc strength, which can vary widely in activated sludge flocs, determines the susceptibility of flocs to ultrasonic shear forces (King and Foster, 1990). Ultrasound also caused the release of extracellular polymeric material such as soluble carbohydrate and protein from the sludge (King and Foster, 1990).

Low intensities of ultrasound have been used to increase the activity of activated sludge microorganisms (Balasubramaniam et al., 1995; Tkachuk et al., 1990). The treatment of sludge with ultrasound with a frequency of 2,6 MHz and intensity between 2 and 6 W cm^{-2} caused the dehydrogenase, proteolytic and glycolytic activity to increase by a factor of 1,9; 1,1 and 4 respectively (Tkachuk et al., 1990). The increased biological activity was attributed to the partial loosening of the sludge structure, allowing greater contact between the bacterial cells and the substrate (Tkachuk et al., 1990). The investigation performed by Balasubramaniam and co-workers found that ultrasound increased substrate removal and oxygen uptake, thus indicating an increase in microorganism activity with ultrasound (Balasubramaniam et al., 1995). The suspended solid content in the effluent increased with ultrasound but decreased with refloculation of the floc particles. Ultrasound also improved the settleability of solid particles (such as Kaolin particles) in agglomeration experiments (Balasubramaniam et al., 1995).

Ultrasound has also been used to accelerate the anaerobic digestion of sewage sludge (Chiu et al., 1997; Tiehm et al., 1997). Sewage sludge is stabilised by anaerobic digestion, however, the slow degradation rate of the sludge (sludge hydrolysis) requires large digestors and long residence times of approximately 20 d

(Tiehm et al., 1997). Tiehm and co-workers used a flow-through ultrasonic reactor (frequency, 31 kHz; power, 3,6 kW; treatment time, 64 s) that was specially adapted for sludge treatment (Tiehm et al., 1997). The reduction in particle size and the increase in chemical oxygen demand of the supernatant (organic substances were transferred from the sludge solids into the aqueous phase) indicated that ultrasound caused the deagglomeration of aggregates and microbial cell disruption. Biogas production was greater during batch fermentation experiments (150 L fermenter vessels, 22 d residence time) in the fermentation vessel that had been fed with the ultrasonic-disintegrated sludge. This indicated that the organic compounds transferred from the sludge solids into the aqueous phase were readily biodegradable (Tiehm et al., 1997). The degree of sludge degradation in semi-continuous fermentation experiments was calculated with respect to the reduction of volatile solids. In fermentation vessels with a 22 d residence time, the reduction of volatile solids was 45,8 % for untreated sludge and 50,3 % for ultrasonic-disintegrated sludge. The reduction of volatile solids in a fermentation vessel with a 12 d residence time was 47,3 %. It was concluded that the ultrasonic pretreatment of sewage sludge was a potential method to increase the rate of fermentation and reduce the volume of sludge digestors (Tiehm et al., 1997).

Chiu and co-workers investigated the combination of alkaline (NaOH dosage) and ultrasonic pretreatment of sludge before anaerobic digestion (Chiu et al., 1997). Experiments were performed in 1 L fermentation vessels; an ultrasonic horn rated at 120 W with a frequency of 20 kHz was used for ultrasonic pretreatment of the sludge. The soluble chemical oxygen demand, soluble organic nitrogen release and production of total volatile fatty acids were monitored for alkaline treatment, alkaline treatment followed by ultrasound and the simultaneous application of alkaline treatment and ultrasound (Chiu et al., 1997). The highest initial rate of sludge hydrolysis (211,9 mg L^{-1} min^{-1}) and production of total volatile fatty acids (84 %) were recorded for the simultaneous application of ultrasound and alkaline treatment. It was concluded that alkaline and ultrasonic pretreatment of sludge could significantly reduce the treatment time of anaerobic digestion (Chiu et al., 1997). Chlorobenzene is not usually affected by conventional biological treatment due to the presence of other more readily metabolised organic compounds; ultrasonic pretreatment resulted in a significant reduction in chemical oxygen demand during biodegradation with activated sludge under aerobic conditions (Neis, 2000).

The removal or degradation of chemical pollutants, such as herbicides and pesticides of agricultural origin or hydrocarbons from industrial effluent and storm water run-off, is required during water treatment prior to the water being reused or discharged into the environment (Mason, 1993; Mason et al., 1994). Ultrasound has been used to enhance the degradation of various pollutants. Agricultural herbicides such as atrazine and alachlor degrade during sonication according to first-order kinetics with rate constants of 0,0021 and 0,0080 min^{-1}, respectively, degradation mechanisms were not investigated (Koskinen et al., 1994). Sonication of water saturated with the pesticide parathion indicated that parathion was totally degraded within 2 h of sonication at 30 °C with an ultrasonic horn operating at a frequency of 20 kHz and an intensity of 75 W cm^{-2} (Kotronarou et al., 1992a). The primary degradation mechanism of parathion was thermal

decomposition in the hot interfacial region of the collapsing cavities, reaction with hydroxyl radicals acted as a secondary mechanism. Degradation products such as *p*-nitrophenol and phosphate, sulfate, nitrite, nitrate and oxalate ions were identified (Kotronarou et al., 1992a).

Monochlorophenol compounds, water pollutants that exhibit moderate toxicity to mammalian and aquatic life, have been degraded with ultrasound (Gondrexon et al., 1993; Lin et al., 1996; Serpone et al., 1994). These compounds are formed during the degradation of chlorinated herbicides, the chlorination of phenolic compounds in industrial effluent and chlorine treatment of drinking water (Serpone et al., 1994). The application of ultrasound degraded 2-chlorophenol and 3-chlorophenol (initial concentration, 80 μmol L^{-1}) into dechlorinated intermediate products within 10 h; 4-chlorophenol degradation occurred within 15 h. Degradation followed first order kinetics, the disappearance rate constants were 0,0048; 0,0044 and 0,0033 min^{-1} respectively (Serpone et al., 1994). The ultrasonic degradation products were similar to those formed during ultraviolet radiation with TiO_2 semiconductor particles. Sonication was performed with an ultrasonic horn (power, 50 W; frequency, 20 kHz) in a glass sonication cell (Serpone et al., 1994). The degradation of 2-chlorophenol was greater with the addition of hydrogen peroxide (200 mg L^{-1}) during sonication than without the hydrogen peroxide (Lin et al., 1996). Lin and co-workers investigated how parameters such as pH, ionic strength, the presence of a catalyst and initial concentration affected the ultrasonic degradation of 2-chlorophenol in the presence of hydrogen peroxide (Lin et al., 1996). The degradation was found to follow pseudo first order reaction kinetics (Lin et al., 1996).

Ultrasound has been used to degrade chlorinated hydrocarbons that are typically the most common pollutants found at hazardous waste sites (Cheung et al., 1991; Cyr et al., 1998; Orzechowska et al., 1995). The use of these compounds in products such as solvents, dyes, pesticides and ink, have led to the contamination of water resources (Bhatnagar and Cheung, 1994). Cheung and co-workers found that the ultrasonic degradation of methylene chloride, carbon tetrachloride, 1,1,1-trichloroethane and trichloroethylene (for a concentration range of 100 to 1 000 mg L^{-1}) followed first order reaction kinetics (Cheung et al., 1991). The decrease in solution pH during sonication indicated that hydrochloric acid was produced, no other chlorinated products were identified (Cheung et al., 1991). The investigation by Bhatnagar and Cheung also recorded a decrease in solution pH, first order reaction kinetics and the formation of hydrochloric acid during the ultrasonic degradation of methylene chloride, 1,2-dichloroethane, carbon tetrachloride, chloroform, 1,1,1-trichloroethane, trichloroethylene and perchloroethylene (Bhatnagar and Cheung, 1994). Ultrasonic degradation varied between 72 and 99,9 % for solutions of initial concentration between 50 and 350 mg L^{-1} for a 40 min sonication period; the rate of degradation was not affected if mixtures of compounds were sonicated (Bhatnagar and Cheung, 1994).

Cyr and co-workers found that a 20 mg L^{-1} trichloroethylene solution degraded more than 90 % within a 10 min sonication period (Cyr et al., 1998). Sonication was performed with an ultrasonic horn (power, 120 W; frequency, 20 kHz) in a 50 mL reaction vessel. Parameters such as initial pH value of solution

(between 3 and 11), bicarbonate concentration (below 10 mmol L^{-1}), presence of a metal or metal oxide (0,01 to 100 g L^{-1} concentration) and the combination of a metal or metal oxide (0,01 to 0,1 g L^{-1} concentration) with 34 mg L^{-1} hydrogen peroxide did not affect the ultrasonic degradation of trichloroethylene (Cyr et al., 1998). Orzechowska and co-workers monitored chloride formation (Cl^-) to show the degradation of chloroform, carbon tetrachloride and trichloroethylene; chloride formation could be detected within 1 min of sonication of solutions with initial concentration between 3 and 80 mg L^{-1} (Orzechowska et al., 1995).

A range of other chlorinated compounds have been degraded with ultrasound. Cheung and Kurup investigated the sonochemical destruction of chlorofluorocarbon compounds (Cheung and Kurup, 1994). The degradation of fluorotrichloromethane and trifluorotrichloroethane followed first order reaction kinetics; 50 mg L^{-1} solutions were degraded within a 10 min sonication period. The decrease in solution pH during sonication was due to the formation of HCl and HF (Cheung and Kurup, 1994). The rate of ultrasonic degradation of chloral hydrate was found to depend on parameters such as initial concentration, oxygen concentration and the ultrasound frequency and intensity (Sakai et al., 1977). Degradation occurred through a radical mechanism producing hydrochloric acid (Sakai et al., 1977). Pétrier and co-workers investigated the effect of gases such as oxygen, air and argon on the ultrasonic degradation of pentachlorophenate (Pétrier et al., 1992). The reduction in toxicity of the solution during sonication (quickest for argon saturation) indicated that complete mineralization of pentachlorophenate occurred (Pétrier et al., 1992). The ultrasonic degradation of chlorobenzene and 1,4-dichorobenzene followed first order reaction kinetics; the rate of reaction depended linearly on the ultrasonic intensity (Price et al., 1994). Complete degradation of 1,4-dichlorobenzene occurred within 40 to 50 min with sonication at an intensity of 39 W cm^{-2}; the first step in the degradation was the removal of a chlorine atom from the aromatic ring and reduction to chloride (Price et al., 1994). Total degradation of polychlorinated biphenyl compounds in water treatment is not essential since the removal of chloride atoms reduces toxicity and accelerates biodegradation (Price et al., 1994). The investigation of effluent contaminated with benzene and toluene recommended that ultrasound be used as a pretreatment stage for relatively high target concentrations rather than as a polishing stage for meeting effluent guidelines (Thoma et al., 1998).

Ultrasound has been used to degrade a range of phenolic compounds. The rate of phenol degradation at different ultrasonic frequencies was directly related to the rate of hydrogen peroxide formation during sonication (Pétrier and Francony, 1997; Pétrier et al., 1994). The first step in the degradation mechanism of phenol was reaction with hydroxyl radicals; the primary intermediate products were hydroquinone, catechol and benzoquinone (Pétrier and Francony, 1997; Pétrier et al., 1994). The zero order reaction rate increased with increasing phenol concentration reaching a limit at a concentration of 188 mg L^{-1} for a frequency of 20 kHz and 470 mg L^{-1} at 487 kHz (Pétrier et al., 1994). The ultrasonic degradation of *p*-nitrophenol occurred primarily through thermal decomposition at the cavity interface and then due to reaction with

hydroxyl radicals (Kotronarou et al., 1991). Degradation followed first order reaction kinetics producing nitrate and nitrite ions, benzoquinone, hydroquinone, 4-nitrocatechol, formate and oxalate (Kotronarou et al., 1991). The rate of degradation of *p*-nitrophenol in solutions containing particulate matter, phosphate, bicarbonate and humic acid (to simulate natural waters) was the same as in pure water (Cost et al., 1993). Chemical components in natural waters that are radical scavengers thus do not affect the degradation of pollutants (such as *p*-nitrophenol) that degrade predominately due to high temperature reactions (Cost et al., 1993). Inhibition, however, occurs in waters containing high concentrations of bicarbonate and phosphate compounds (Cost et al., 1993).

Monocyclic aromatic compounds (such as benzene, ethylbenzene, styrene and *o*-chlorotoluene) and polyaromatic compounds (such as napthalene, anthracene and pyrene) have been degraded with ultrasound (de Visscher et al., 1996; Price et al., 1994). Degradation followed first order reaction kinetics; reaction products were not identified (de Visscher et al., 1996; Price et al., 1994). Hydrocarbon compounds such as methane, ethane, propane, butane, ethylene, acetylene, methanol, ethanol, *n*-propanol and isopropanol have also been degraded with ultrasound (Büttner et al., 1991; Hart et al., 1990a; Hart et al., 1990b; Koike, 1992).

Ultrasound has also been used to degrade inorganic compounds. Kotranarou and co-workers investigated the ultrasonic degradation of hydrogen sulfide dissolved in the effluent from fossil fuel refining processes (Kotronarou et al., 1992b). Degradation followed zero order reaction kinetics at a pH greater than 10 and was due to reaction with hydroxyl radicals; degradation at a pH less than 8,5 was due to thermal decomposition and followed first order reaction kinetics (Kotronarou et al., 1992b). De Visscher and co-workers concluded that mechanisms for ultrasonic degradation that are primarily due to reaction with hydroxyl radicals follow zero order reaction kinetics whereas degradation due to thermal decomposition (pyrolysis reactions) follow first order reaction kinetics (de Visscher et al., 1996).

Potential applications of ultrasound in water and effluent treatment have been summarised by Mason and co-workers and are listed in Table 2.3 (Mason et al., 1993).

Table 2.3 : Applications of ultrasound in water and effluent treatment (Mason et al., 1993)

Effect of ultrasound	Application
degassing	removal of excess chlorine
gasification	enhance oxygenation and ozonolysis
dispersion	homogenise mixtures before treatment and dispersal of chemicals in treatment
biocidal action	improve efficiency of biocide
filtration	improved dewatering
destruction of chemicals	removal of pollutants

2.4.4.2 Textile industry

Large quantities of water and energy are required in the wet processing of textiles (Thakore, 1990a). Conventional dyeing techniques could be enhanced by ultrasound because of the ultrasonic-induced dispersion and break-up of dye aggregates, the expulsion of entrapped air from fibre capillaries and the acceleration of the rate of diffusion of dye inside the fibre (Ahmad and Lomas, 1996). The effects of ultrasound are due to cavitation and heating, the temperature in the dye bath increases when ultrasonic waves pass through the liquid (Thakore, 1990a; Thakore, 1990b).

Shimizu and co-workers investigated the effect of ultrasound on the dyeing of nylon 6 films by dyeing amorphous, unoriented films with four dye types, disperse, reactive, acid and acid mordant at temperatures of 20, 40 and 60 °C (Shimizu et al., 1989). The uptake of the four dyes in nylon 6 increased (at all temperatures) with the application of ultrasound (Shimizu et al., 1989).

Shukla and Mathur investigated the low-temperature ultrasonic dyeing of silk (Shukla and Mathur, 1995). Silk was dyed with cationic, acid and metal-complex dyes at temperatures of 45 and 50 °C. The uptake of cationic dyes, in comparison with conventional dyeing for 60 min at 85 °C, increased by between 71 and 104 % when dyeing for 15 min at 45°C with ultrasound. Under similar ultrasonic conditions, dye uptake for acid and metal-complex dyes increased by 108 and 76 % respectively (Shukla and Mathur, 1995). Fibre degradation was not apparent and the level of wash fastness, for all the dyeings, was equivalent to that for samples dyed according to the conventional procedure (Shukla and Mathur, 1995).

Ahmad and Lomas investigated the low-temperature ultrasonic dyeing of polyester fabric with disperse dyes for possible application in batik printing (Ahmad and Lomas, 1996). Elevated dyeing temperatures would cause the wax used in batik printing to melt. The dye uptake was similar for both the conventional and ultrasonic dyeing processes at 50 °C and was lower than the dye uptake for the conventional dyeing process at 100 °C (Ahmad and Lomas, 1996). Shuklar and Mathur also found that the dye uptake in polyester fibres, even after pre-swelling, could not be enhanced by ultrasound (Shukla and Mathur, 1995). Polyester fibres are highly compact whereas fibres, such as silk, that have a less crystalline structure are more accessible for dyes and chemicals (Shukla and Mathur, 1995).

Öner and co-workers investigated the use of ultrasound in the dyeing of cotton fabrics with reactive dyes (Öner et al., 1995). Ultrasound was found to improve dye fixation and increase the colour yield without affecting the fastness properties (wash fastness and staining) of the dyed fabric (Öner et al., 1995). It was concluded that the shorter dyeing times and lower quantities of dye required to produce a particular colour, and the reduced water required to remove unfixed dye, would result in both energy and water savings with the use of ultrasound in reactive dyeing of cotton fabrics (Öner et al., 1995).

2.4.4.3 Food industry

Ultrasound is applied in both the analysis and processing of food (Floros and Liang, 1994). Ultrasound can be used for treating heat-sensitive materials such as in the extraction of apple juice from apple pulp and the decolouration of soyabean oil without causing a loss in flavour or other heat-related damage (Chendke and Fogler, 1975). Lillard investigated the application of ultrasound for the microbial decontamination of poultry skin (Lillard, 1994). A combination of ultrasound and chlorine, for application in the final processing stage of broilers, was more effective in reducing the *Salmonella* count in poultry skin than either ultrasound or chlorine alone (Lillard, 1994). Ultrasound can affect enzyme activity (Roberts, 1993). Ultrasound usually inactivates oxidase enzymes but only affects low concentrations of catalase enzymes. Reductase and amylase enzymes are resistant to sonication (Roberts, 1993). Ultrasound has been used to improve the rate of the hydrogenation reaction for converting unsaturated fatty acids (such as vegetable oil) to saturated fatty acids that are used as shortening agents in the baking industry (Roberts, 1993). Ultrasound has been used to induce nucleation in the crystallisation of aqueous salt solutions and sugar solutions (Roberts, 1993). Dehydration rates of products, such as gelatine, yeast cake and orange powder have been enhanced with the application of ultrasound (Floros and Liang, 1994). The use of ultrasound to measure animal back fat thickness is the major application of low-intensity ultrasound in the food industry (Povey, 1989).

2.4.4.4 Petroleum industry

An ultrasonic vibrating tray (power, 2 kW) has been used to treat ore slurries with a flow rate of 6 kg s^{-1} (Hunicke, 1990). Junk coal from waste-coal ponds, after screening and mixing with water to produce a slurry, can be cleaned on the vibrating tray to yield a coal with a low ash, sulphur and residual water content (Hunicke, 1990). The removal of sulphur from coal in which the sulphur is predominantly in the pyrite form improves the susceptibility of coal to spontaneous combustion (Zaidi, 1993). The sulphur content in a high sulphur Pakistani lignitic coal was reduced by 34 % with sonication at 30 °C in a 0,975 g L^{-1} sodium hydroxide solution (Zaidi, 1993). The ash content, during ultrasonic treatment, increased between 2 and 18 % for different coals; no enhancement of sulphur removal was achieved for sonication of coal in water (Zaidi, 1993).

Sadeghi and co-workers have developed an ultrasonic method to refine fossil fuel-containing materials (Sadeghi et al., 1994). Materials such as tar sand, asphalt, heavy oil, coal liquids and oil shales were sonicated in an alkaline solution at ambient temperature and pressure to recover upgraded lighter fuels. The recovered fuel was lower in heterocyclic elements. For the treatment of a coal liquid sample, the coal asphaltene content was reduced to 58 % within 30 min of sonication while the oil and resin content increased to 42 % (Sadeghi et al., 1994).

The characterisation of coal and coal tar pitches, performed by studying fractions extracted with organic solvents, is hindered by the insolubility of coal (Guillén et al., 1991; Matturro et al., 1990). Guillén and

co-workers studied 27 organic solvents to determine which was the most effective for the ultrasonic extraction of coal tar pitches (Guillén et al., 1991). Solvent extraction was performed at 25 °C for 2 h in an ultrasonic bath. Yields were more reproducible for solvents with a high density and low viscosity. Solvents such as carbon disulphide, pyridine, 1-methyl-2-pyrrolidinone, tetrahydrofuran, quinoline and nitrobenzene were the most effective in the extraction of six coal tar pitches (Guillén et al., 1991). Matturro and co-workers extracted coal with tetra-*n*-butylammonium hydroxide during sonication in a solvent mixture containing pyridine and methanol (Matturro et al., 1990). The sonication of an Illinois No. 6 coal for 3 h at 34 °C with an ultrasonic horn (frequency, 23 kHz; intensity, 85 W cm^{-2}) produced an extraction yield of 77 %, the yield for the stirred control was 27 % (Matturro et al., 1990).

Ultrasound can also be used to determine the concentration of coal extracts (Krzesinska and Pajak, 1988). The ultrasonic velocity in a tetrahydrofuran solution was found to be linearly dependent upon the concentration of coal in solution. Such a system would first have to be calibrated by measuring the ultrasonic velocity in solutions of known concentration for the specific coal to be monitored (Krzesinska and Pajak, 1988).

2.4.4.5 Membrane processes

Lenart and Ausländer investigated the effect of ultrasound on the diffusion of chloride compounds (sodium, potassium and calcium chloride) through cellophane membranes (Lenart and Ausländer, 1980). Ultrasound enhanced diffusion but the increase in the amount diffused was determined by the direction of diffusion flow. The greatest increase occurred when the ultrasonic field and diffusion flow where in the same direction. A lower increase occurred when the ultrasonic field was acting at 90° to the diffusion flow and the smallest increase occurred when the ultrasonic field and diffusion flow where acting in opposite directions (Lenart and Ausländer, 1980). The ultrasonic-enhanced diffusion was attributed to the acoustic microcurrents that increased the velocity of the particles in solution (Lenart and Ausländer, 1980). Howkins investigated the application of ultrasound to enhance dialysis in artificial kidney machines (Howkins, 1969). The enhanced rate of dialysis was attributed to the efficient stirring of fluid layers near the membrane surface (Howkins, 1969). Ultrasound also reduces the diffusion boundary layer and may increase the diffusion coefficient (Floros and Liang, 1994).

Wakeman and Tarleton investigated the effects of ultrasound on crossflow microfiltration (Wakeman and Tarleton, 1991). Crossflow filtration is used for slurry dewatering. Fouling of the membrane occurs if the shear rates generated by the crossflow velocities are not sufficiently high to prevent cake formation (Wakeman and Tarleton, 1991). Ultrasound reduced membrane fouling and increased the filtrate flux. Membrane fouling was further reduced and filtrate flux increased when ultrasound was used in conjunction with an electric field. It was concluded that lower crossflow velocities could be used when filtration is assisted by electric and ultrasonic fields (Wakeman and Tarleton, 1991).

2.5 SONOCHEMICAL EQUIPMENT

Sonochemical experiments are performed in equipment such as ultrasonic baths, horns and reactors. Equipment suitable for routine experiments only became available in the 1950's (Bremner, 1986).

Early ultrasonic research indicated that experimental conditions had to be carefully controlled to ensure reproducible results. Weissler and co-workers found that the tightness of clamping of a test-tube above an ultrasonic transducer affected the reaction yield of potassium iodide and carbon tetrachloride in the test-tube by 10 % (Weissler et al., 1950). Jennings and Townsend found that the deviation in reaction yield of carbon tetrachloride and chloroform in aqueous solution in an inert atmosphere was as large as 30 % (Jennings and Townsend, 1961). The large deviation in results was due to the ultrasonic equipment rather than the analysis procedure. Three possible sources of error were suggested: the ultrasonic intensity in the reaction solution would change unless the coupling of the transducer to the reaction vessel was identical for all experiments, the electrical output of the high frequency generator was not constant and thus caused variations in the ultrasonic intensity; and the amount of gas dissolved in the liquid at the start of reaction could be different for different experiments (Jennings and Townsend, 1961).

Recent literature also indicates the importance of careful control of experimental conditions in ultrasonic experiments. For example, a reaction vessel in an ultrasonic bath has to be placed in the exact position in the bath to ensure consistent and reproducible results (Goodwin, 1990). The range of parameters that have to be controlled in ultrasonic experiments lead to the results being specific to the particular piece of equipment and experimental setup (Mason, 1991).

Transducers used for ultrasonic equipment are described in Section 2.5.1. Ultrasonic equipment is reviewed in the following sections, ultrasonic baths in Section 2.5.2, ultrasonic horns in Section 2.5.3 and ultrasonic reactors in Section 2.5.4. Reactor modelling and equipment scale-up recommendations are reviewed in Section 2.5.5.

2.5.1 Transducers

Piezoelectric and magnetostrictive transducers are used in ultrasonic equipment; piezoelectric transducers are reviewed in Section 2.5.1.1 and magnetostrictive transducers in Section 2.5.1.2.

2.5.1.1 Piezoelectric transducers

Materials used as piezoelectric transducers undergo a change in dimension when an electrical potential is applied across the surface (Payne, 1994). Examples of such materials are quartz and ceramics such as barium titanate and lead zirconate titanate (a solid solution of lead zirconate and lead titanate). Lead zirconate titanate is the most commonly used material in piezoelectric transducers (Payne, 1994). The frequency at which a transducer operates is determined by the width of the piezoelectric material, typically, two or four layers of the material are used in a transducer. The piezoelectic material is prepolarised and

bolted between two metal blocks for protection, prevention of overheating and to improve the coupling of the ultrasonic vibrations to the liquid (Crawford, 1963; Mason, 1991; Payne, 1994).

Piezoelectric transducers are relatively small and inexpensive. Damage can be caused by impact, operation at temperatures above 150 to 200 °C or if operated without liquid (Hunicke, 1990). Generally, piezoelectric transducers are not suitable for industrial equipment if continuous usage at high temperatures is required since the polar orientation of the ceramic material changes gradually over time (Mason, 1991). These transducers have a relatively high gain but operate efficiently over a narrow band width. The narrow band width makes it difficult to operate a number of transducers in synchronism as required in large industrial applications (Hunicke, 1990).

Piezoelectric transducers have a potential efficiency of 98 % and can handle power transfers in the region of 500 to 1 000 W when used in continuous operation, the maximum amplitude of vibration at the radiating face of a transducer is between 15 and 20 μm for a frequency of 20 kHz (Perkins, 1990). Most ultrasonic baths and horns contain piezoelectric transducers (Mason, 1991).

2.5.1.2 Magnetostrictive transducers

A magnetostrictive transducer is based on the changes in dimension induced in a ferromagnetic material by an alternating magnetic field, such a transducer consists of a ferromagnetic rod or bar within a solenoid (Crawford, 1963; Mason, 1991). Nickel or a nickel alloy rod are used most commonly in magnetostrictive transducers. Such transducers are bigger and more expensive than piezoelectric transducers; operation over a larger temperature range (easily withstanding temperatures up to 180 °C) is also possible (Hunicke, 1990). A magnetostrictive transducer is resistant to mechanical damage because the nickel core is silver-brazed to a stainless steel plate to couple the ultrasonic vibrations to the liquid (Mason, 1991). No damage is caused to the transducer if operated without liquid (Hunicke, 1990). Since magnetostrictive transducers have no mode for degrading or failing, they are not only robust but are also suited for long-term continuous operation. Various large commercial systems have been recorded as operating successfully for over twenty years (Hunicke, 1990). Magnetostrictive transducers have a relatively low gain which can be an advantage in commercial applications requiring more than one transducer since all transducers will operate close to peak performance (Hunicke, 1990).

2.5.2 Ultrasonic baths

An ultrasonic bath or cleaner is the most readily available and inexpensive source of ultrasound for sonochemical experiments. An ultrasonic bath consists of a stainless steel tank of rectangular cross-section with transducers bonded externally to the base. The transducers are usually piezoelectric transducers and operate with an intensity of between 1 and 5 W cm^{-2} and within a frequency range of between 20 and 40 kHz (Goodwin, 1990). Intensity is defined as the ratio of the electrical power into a transducer to the radiating surface area of the transducer (Perkins, 1990). The intensity and frequency of an ultrasonic bath depends on the type and number of transducers the bath contains; operating power also varies between ultrasonic baths

produced by different manufacturers (Goodwin, 1990). Experimental results are thus characteristic to a particular model of ultrasonic bath. The volume of ultrasonic baths vary between 1,5 to approximately 50 000 L (Mason, 1991). Ultrasound is transmitted through a liquid medium, usually water, to a reaction vessel containing the reaction solution, as shown in Figure 2.9.

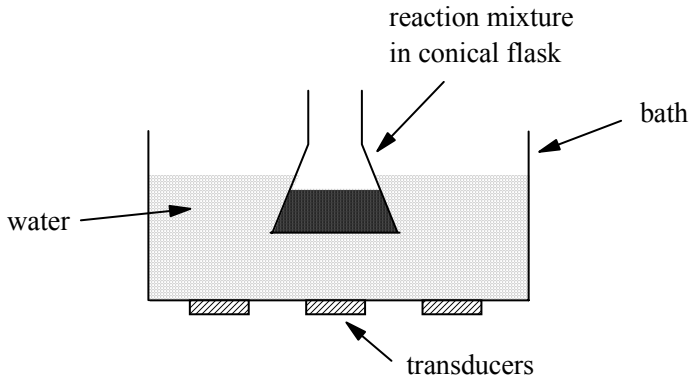

Figure 2.9 : Schematic diagram of an ultrasonic bath (Goodwin, 1990)

Ultrasound is attenuated at the water/glass interface of a reaction vessel. The decreased intensity within a reaction vessel may be below the cavitation threshold and cavitation will not occur (Goodwin, 1990). The amount of energy available in a reaction solution is also dependent on the size and shape of the reaction vessel (Mason and Berlan, 1992). Mason and Berlan defined the sonochemical yield as the ratio of a measured effect to the ultrasonic power entering the reaction vessel (Mason and Berlan, 1992). The sonochemical yield was calculated using iodine liberation as a model reaction. The amount of iodine liberated from a 4 % potassium iodide solution (containing 10 % carbon tetrachloride) was measured for a 5 min sonication period; the ultrasonic power entering the reaction vessel was determined by calorimetry. The sonochemical yields for reaction solutions (volume, 55 and 110 mL) in a 250 mL conical flask, a 100 mL conical flask and a 100 mL round bottomed flask are listed in Table 2.4.

Table 2.4 : Effect of reaction solution volume and size and shape of reaction vessel on sonochemical yield (Mason and Berlan, 1992)

Reaction vessel	Sonochemical yield (mg of I_2 per W of ultrasonic power)	
	55 mL reaction solution	**110 mL reaction solution**
100 mL round-bottomed flask	0.01	0.00
100 mL conical flask	0.02	0.02
250 mL conical flask	0.10	0.01

As shown in Table 2.4, the sonochemical yield was the highest for a 55 mL reaction solution in a 250 mL conical flask. The larger flat base area of the 250 mL conical flask allowed for a greater transfer of energy

(Mason and Berlan, 1992). Pugin also measured a greater ultrasonic intensity in a reaction vessel with a flat base, a 100 mL conical flask, than a round base, a 100 mL round-bottomed flask (Pugin, 1987). Less energy is lost through attenuation at a flat water/glass interface than at a rounded interface.

A non-uniform ultrasonic field is produced within the water in an ultrasonic bath, ultrasonic intensity varies with distance from a transducer (Goodwin, 1990). Maximum intensity occurs vertically at levels equal to multiples of the half-wavelength of sound in water (Niemczewski, 1980; Pugin, 1987); and horizontally directly above a transducer if an ultrasonic bath is fitted with a single transducer or midway between two transducers (Pugin, 1987). A reaction vessel has thus to be placed in the identical position in an ultrasonic bath for consistent and reproducible results to be obtained (Goodwin, 1990).

The ultrasonic power available for reaction enhancement is lower than the electrical power consumed by an ultrasonic device because energy is lost as heat or sound in the conversion of electrical to ultrasonic energy (Martin, 1992). The steps in the conversion of energy from electrical power to sonochemical benefit are presented in Figure 2.10.

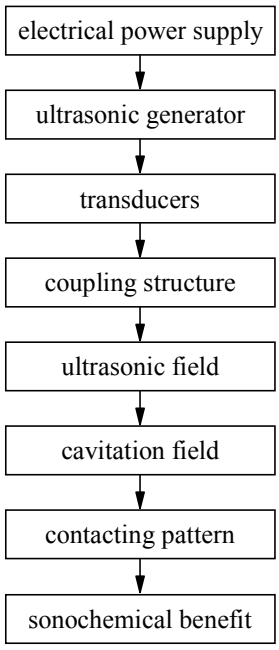

Figure 2.10 : Energy conversion steps in industrial sonochemistry (Martin, 1992)

The temperature of the water in an ultrasonic bath increases during sonication (Niemczewski, 1980). A calorimetric method can thus be used to measure the power of an ultrasonic bath; calorimetry is based on the transformation of an ultrasonic wave absorbed in water into thermal energy (Goswami et al., 1988).

The solution temperature in a reaction vessel in an ultrasonic bath is slightly higher than that of the ultrasonic bath water; temperature measurements for experiments monitoring the effect of temperature on a reaction must thus be taken within the reaction vessel (Goodwin, 1990).

2.5.3 Ultrasonic horns

Disadvantages of an ultrasonic bath, such as the low operating intensity and lack of control of energy input into a chemical reaction, are overcome with the use of an ultrasonic horn (Mason, 1991). The efficiency of energy transfer is increased with an ultrasonic horn because the horn is inserted directly into the reaction solution. Higher intensities (above 100 W cm^{-2}) are produced by ultrasonic horns. Reproducible operating conditions are obtained since the power input of an ultrasonic horn is controllable. Ultrasonic horns are more expensive than ultrasonic baths (Goodwin, 1990; Mason, 1991).

An ultrasonic horn system (shown in Figure 2.11) consists of a generator, transducer, upper fixed horn element, detachable horn and replaceable tip (Mason, 1991). The generator supplies the transducer (a piezoelectric transducer) with alternating electrical frequency (approximately 20 kHz). The low vibratory motion of the transducer (between 1 and 10 μm) is magnified by the upper fixed horn element and the detachable horn such that the horn tip vibrates with a peak-to-peak displacement of between 10 and 50 μm (Goodwin, 1990). The upper fixed horn element is attached to the transducer and is of such a length that the end face vibrates with maximum amplitude. The detachable horn, connected to the upper fixed horn, transfers the ultrasonic energy directly into the reaction vessel. Some ultrasonic horn systems include a replaceable horn tip so that the detachable horn does not have to be replaced when the tip of the horn becomes eroded (Goodwin, 1990).

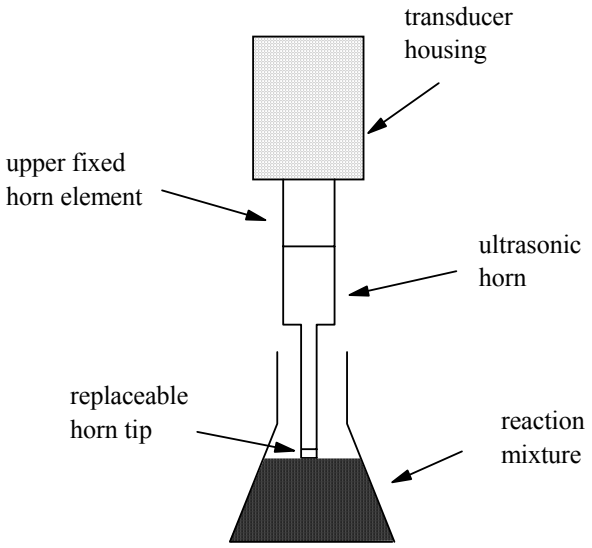

Figure 2.11 : Schematic diagram of an ultrasonic horn system (Goodwin, 1990)

The magnification of the vibratory motion of a transducer to a reaction solution is dependent on the length and shape of a horn. For maximum magnification, the length of a horn should be a half wavelength (or a multiple thereof) of the sound in the material from which the horn is manufactured (Mason, 1991). The following shapes (shown in Figure 2.12) are the most common designs of ultrasonic horns (Mason, 1991; Perkins, 1990).

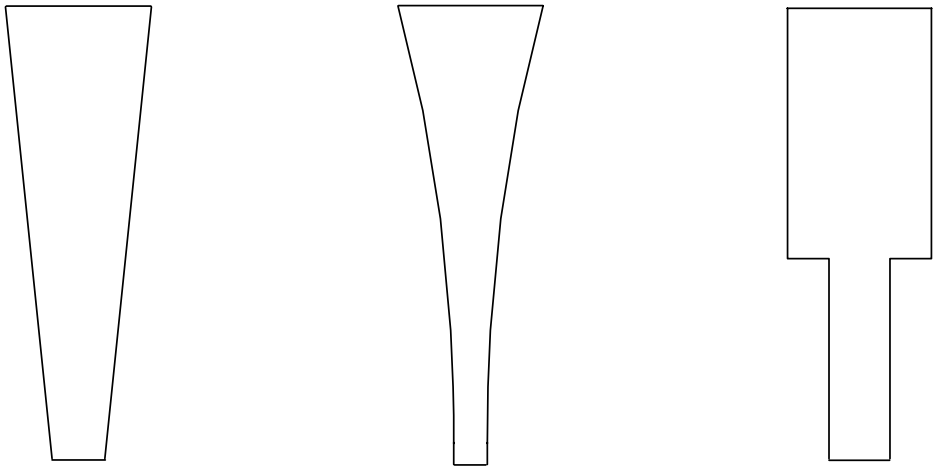

Figure 2.12 : Ultrasonic horn shapes (Perkins, 1990)

- The uniform cylinder acts as an extension of the working end of the transducer and does not change the amplitude of vibration.
- The linear taper or cone is simple to manufacture but potential magnification (the ratio of the upper to lower diameter) is limited to approximately 4-fold.
- The exponential taper produces a higher magnification than the linear taper because of the smaller tip diameter (magnification is also calculated from the ratio of the upper to lower diameter). This design is more difficult to manufacture. The narrow length and small tip area makes this type of horn suitable for the sonication of small samples.
- The amplitude magnification of a stepped horn is calculated from the square of the ratio of the upper to lower diameter and can be as high as 16-fold.

Ultrasonic horns are manufactured from materials that have a low acoustic loss, a high dynamic fatigue strength, are resistant to cavitation erosion and are chemically inert (Perkins, 1990). Titanium alloy is the most suitable material; other materials such as aluminium, aluminium bronze and stainless steel can also be used but the amplitude of vibration is dampened (Perkins, 1990).

Disadvantages of an ultrasonic horn system are that the erosion of the horn tip may contaminate the reaction solution and that a small zone of intense ultrasonic activity is created at the tip of the horn (Goodwin, 1990). Pugin used the chemical reaction of 1-bromopentane with lithium wire in tetrahydrofuran solution to show

the reduction of ultrasonic intensity with increasing distance from the tip of an ultrasonic horn (Pugin, 1987). It was found that the rate of decrease in 1-bromopentane concentration at 50 % conversion for a distance of 5 mm between the tip of the horn and the lithium wire was 2,70 % per min and for a distance of 15 mm was 0,85 % per min. It was concluded that the zone of high ultrasonic activity was relatively small and that only marginal ultrasonic activity occurred in the surrounding liquid (Pugin, 1987). The formation of a small zone of intense ultrasonic activity at the tip of a horn indicates that an ultrasonic horn is most suited to a flow system, as shown in Figure 2.13, where the reaction solution is pumped through a flow cell fitted to the horn (Goodwin, 1990).

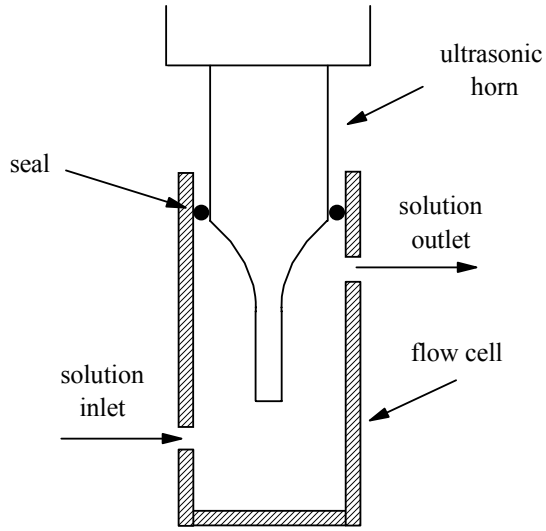

Figure 2.13 : Schematic diagram of a flow cell fitted to an ultrasonic horn (Goodwin, 1990)

For an ultrasonic horn system, parameters such as frequency and ultrasonic power must be known to ensure that daily working conditions are consistent, results are reproducible and are based on some absolute values to allow for comparison and scale-up for industrial systems (Perkins, 1990). The frequency of an ultrasonic horn is provided by the manufacturer, this value can be used for comparison since a 5 to 10 % change in frequency does not significantly affect experimental results (Perkins, 1990). The rated electrical power of an ultrasonic horn system does not give an indication of the ultrasonic power because of the power-by-demand characteristic of many ultrasonic systems. The ultrasonic power drawn in a particular experiment will depend on the load placed on the horn (which is determined by the magnification of the horn) and the depth of the horn immersed in the reaction solution (Perkins, 1990). Ultrasonic power can be determined by the following three methods (Perkins, 1990).

- Ultrasonic power can be calculated from calorimetry by recording the initial increase in temperature during sonication.
- The measurement of the vibrational amplitude at the tip of the horn (which is proportional to the ultrasonic power) will indicate any changes in the transmission of power.

- Ultrasonic power can be calculated if the overall ultrasonic transfer efficiency of the transducer is known and the real electrical power to the transducer is measured.

The temperature of a solution sonicated with an ultrasonic horn increases during sonication and must be controlled by circulating cooling water around the reaction vessel (Pugin, 1987). In experiments monitoring the effect of temperature on a reaction, the temperature within the reaction vessel should be recorded since it may be more than 10 C° higher than the surrounding cooling water (Pugin, 1987).

The performance of ultrasonic baths and horns have been compared by various researchers. The results are specific to the ultrasonic equipment and the model reactions used, however, an indication is obtained of the greater effectiveness with which ultrasonic horns operate (Mason and Berlan, 1992). Mason and Berlan measured the amount of iodine liberated from a 4 % potassium iodide solution (containing 10 % carbon tetrachloride) within a 5 min sonication period for an ultrasonic bath and horn (Mason and Berlan, 1992). A Kerry Pulsatron 55 cleaning bath (frequency, 35 kHz) filled with water containing 5 % detergent was used to sonicate a 55 mL reaction solution in a 250 mL conical flask; a Sonics and Materials VC600 ultrasonic horn system (frequency, 20 kHz) was used to sonicate a 27,5 mL reaction solution (horn tip diameter, 12 mm). The sonochemical yield was 100 ng of iodine per W for the ultrasonic bath and 350 ng of iodine per W for the ultrasonic horn (Mason and Berlan, 1992). Pugin compared the performance of an ultrasonic bath (Laborette 17; frequency, 35 kHz) and ultrasonic horn (Branson B30 Sonifier; frequency, 20 kHz) using the reaction of 1-bromopentane with lithium wire in tetrahydrofuran solution as a model reaction (Pugin, 1987). The rate of decrease in 1-bromopentane concentration, at 50 % conversion, was 1,90 % per min for the ultrasonic bath and 2,70 % per min for the ultrasonic horn (Pugin, 1987).

Ratoarinoro and co-workers compared the performance of an ultrasonic bath (Branson 2200E; frequency, 47 kHz) and ultrasonic horn (Sonics and Materials; frequency, 20 kHz) at constant power per unit volume (1,3 W cm^{-3}) using the Michaël addition reaction of ethyl malonate to chalcone in toluene under solid-liquid phase transfer conditions (Ratoarinoro et al., 1992). The reaction yield was 77 % for the ultrasonic bath and 98 % for the ultrasonic horn (Ratoarinoro et al., 1992). It was concluded that an ultrasonic horn was a more effective emitter of ultrasonic energy than an ultrasonic bath (Ratoarinoro et al., 1992).

2.5.4 Ultrasonic reactors

Industrial applications of ultrasound, because of the chemical and physical effects of ultrasonic cavitation, have the potential to be operated with cheaper reagants, shorter reaction cycles and less extreme physical conditions, possibly leading to less expensive and smaller plants (Martin and Ward, 1992).

An ultrasonic reactor is possibly not required if reaction enhancement is due to the physical effects of ultrasound, rather, a slurry could be pretreated with ultrasound before the reaction take place within a conventional reactor. Reaction enhancement due to the chemical effects of ultrasound will require the design

and development of an ultrasonic reactor since the presence of ultrasound affects the reaction chemistry (Mason, 1992).

Difficulties associated with the scale-up of sonochemical processes are the estimation of ultrasonic energy required to perform a particular chemical transformation and the method by which this amount of energy is to be transferred to a large-scale process (Mason and Berlan, 1992). Laboratory equipment such as an ultrasonic bath or horn are not suitable for direct scale-up of a sonochemical process (Martin and Ward, 1992). The transmitted intensity within an ultrasonic bath is too low and the ultrasonic field is non-uniform and would be localised in the vicinity of the reactor walls. Significant heating of the reaction solution would take place because of the large number of transducers required for such a reactor. The mounting of the transducers to the reactor walls may also be a problem since conventional reactors are often constructed with an outer layer of insulating material or a water jacket, these would have to be modified or removed to allow for the transducers to be mounted to the inner walls (Goodwin, 1990). An immersible bank of transducers offers greater flexibility than permanently-mounted transducers but a non-uniform ultrasonic field is produced and problems could be experienced with erosion of the metallic transducer cover and sealing of transducers and electrical cables from chemical reagants that may be corrosive or highly inflammable (Goodwin, 1990). An ultrasonic horn generates a small zone of high intensity near the tip of the horn, a multiple array of ultrasonic horns would be required for the sonication of a large volume of solution. Other problems associated with an ultrasonic horn would be the erosion of the horn tip and the shielding of transducers and associated electrical supply from the reaction solution (Goodwin, 1990).

The range of ultrasound penetration in liquids is limited because intensity decreases with distance from the radiating surface; the presence of solid particles and cavitation bubbles cause further attenuation of the sound waves. Cavitation thus only occurs within a distance of a few tens of centimetres from the radiating source (Martin and Ward, 1992). The limited range of cavitation indicates that the design of large-scale ultrasonic equipment should rather be based on a flow system in which a small volume, of limited diameter, is sonicated and the reaction solution be pumped through this sonicated zone (Martin and Ward, 1992; Mason, 1992). An ultrasonic reactor, based on a flow system, generally consists of a flow loop outside a conventional batch reactor that acts as a reservoir or holding tank, as shown in Figure 2.14, or it can be configured as a cylindrical tube reactor that is included in an existing pipe network of a process (Martin and Ward, 1992; Mason, 1992).

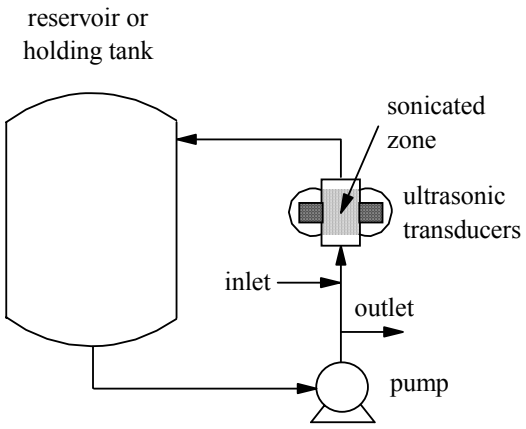

Figure 2.14 : Ultrasonic reactor for use in batch, semi-batch or continuous-flow operation (Martin and Ward, 1992)

The flow system shown in Figure 2.14 can be used for batch, semi-batch or continuous-flow operation (Martin and Ward, 1992). Advantages of such a system are the easy control of residence time in the sonicated zone (by controlling the solution flow rate), simplicity of retrofit to conventional reactors and less uncertainty about scale-up since the same type of ultrasonic module is used in a pilot-plant and large-scale reactor (Martin and Ward, 1992). Temperature is controlled by heat exchange in the circulating reaction solution (Mason, 1992). Scale-up may be made more favourable if the limiting reagent of a reaction is retained in the sonicated zone or if the reagants exhibit a *memory* effect and remain activated after passing through the sonicated zone (Martin and Ward, 1992). The following issues have to be considered in the design of an ultrasonic module for a flow system as shown in Figure 2.14 (Martin, 1992).

- method of mounting transducers to a circular duct,
- coupling of transducers to the liquid load,
- controlling the interaction through the hardware and in the reaction solution between multiple transducers,
- ensuring reasonable transducer life, and
- providing for the selective removal of transducers for maintenance.

Various designs of ultrasonic reactors are commercially available. The *Harwell* sonochemical reactor was designed at the Harwell laboratory of the Atomic Energy Authority in the United Kingdom (Grinthal and Ondrey, 1992). This reactor consists of a pumped loop as shown in Figure 2.14; the volume of the sonicated zone is 4 L. The ultrasonic module, shown in Figure 2.15, consists of three transducers set around a cylindrical duct, 13 cm in diameter and 30 cm long (Martin, 1992; Martin and Ward, 1992).

Figure 2.15 : Ultrasonic module of the *Harwell* sonochemical reactor (Martin, 1992)

The transducers operate with a frequency of 20 kHz and a combined power rating of 1 500 W. Each transducer can be removed separately for maintenance; transducers are coupled to the reaction medium through a buffer fluid with a high cavitation threshold (Martin and Ward, 1992). The ultrasonic module can be incorporated in a flow system to handle flow rates up to 230 L h^{-1} (Pandit and Moholkar, 1996). The *Harwell* sonochemical reactor has been used to achieve a 50-fold increase in the rate of formation of 1-phenyl-1-butanol from the reaction of *n*-bromopropane and benzaldehyde (catalysed by lithium in tetrahydrofuran solution) and a 5 to 10-fold increase in the rate of formation of methanol and sodium benzoate from the hydrolysis of methyl benzoate (Grinthal and Ondrey, 1992; Martin and Ward, 1992). The *Harwell* sonochemical reactor has also been used in crystallisation to improve crystal purity (Martin, 1993).

Ultrasonic tube reactors are not only circular in dimension; hexagonal and pentagonal shaped pipes allow for easier attachment of transducers to a planar wall rather than a curved surface (Mason, 1992). Different cross sections of ultrasonic tube reactors are shown in Figure 2.16 (Mason, 1992).

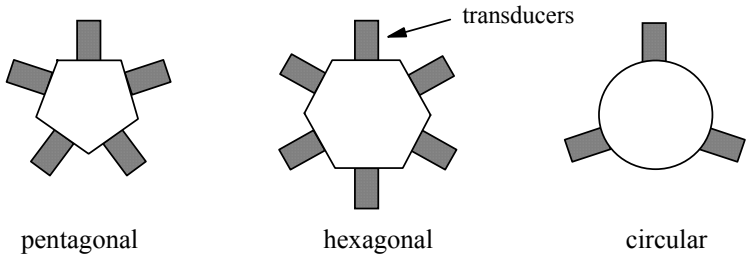

Figure 2.16 : Cross sections of ultrasonic tube reactors (Mason, 1992)

A tube reactor can be retrofitted in an existing pipe network if the length of the reactor is designed so that a null point exists at each end (Mason, 1992). Tube reactors are able to handle high flow rates and can be used for the treatment of viscous materials. The pentagonal pipe designed by Branson Ultrasonics (Danbury, Connecticut, USA) provides a fairly uniform low-power ultrasonic field; the energy irradiated from each tube wall is reflected at an angle by the two opposite tube walls (Mason, 1992). The hexagonal pipe designed by Sonic Services (Paris, France) provides a high power focus in the centre of the tube, this is where the direct energy irradiated from each tube wall meets the reflected energy from the opposite wall (Mason, 1992).

A cylindrical tube reactor also provides a focus of energy in the centre of the tube (Mason, 1992). Cylindrical tube reactors have been designed by a number of research groups and manufacturers. The resonating pipe designed by Battelle (Columbus, Ohio, USA) is 15,3 cm in diameter, operates at a frequency of 25 kHz and has been used for the degassing of oils (Mason, 1992). The cylindrical reactor designed at the University of Milan (Italy) has a central pipe that carries cooling liquid, as shown in Figure 2.17. The ultrasonic energy field is made more uniform by the coaxial reflection of the sound waves by the cooling pipe. The reactor volume is the annular space between the resonating pipe walls and the cooling core (Mason, 1992; Pandit and Moholkar, 1996).

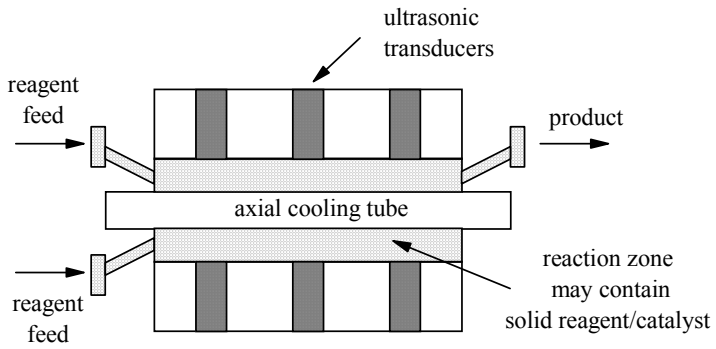

Figure 2.17 : Schematic diagram of the cylindrical reactor (with core cooling) designed at the University of Milan (Mason, 1992)

The *Sonitube* reactor designed by Sodeva (Bonnesur-Menoge, France) consists of a transducer system coupled directly to an annular collar that acts as a cylindrical resonator, as shown in Figure 2.18. The radial collar is screw-fitted to a stainless steel pipe of specific length such that a null point exists at each end. This allows for the inclusion of the reactor in an existing pipe network without causing vibration of the pipe work. A *Sonitube* with an operating length of 1,2 m and internal tube diameter of 42 mm was driven at 2 kW with an 80 % efficiency (Mason, 1992).

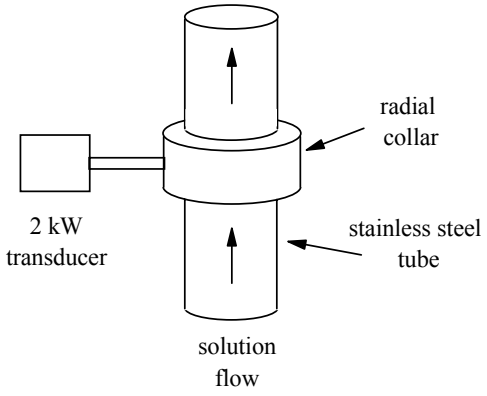

Figure 2.18 : Schematic diagram of a Sodeva *Sonitube* (Mason, 1992)

Ultrasonic flow systems are not only designed as tube reactors. The *Nearfield acoustic processor* designed by the Lewis Corporation (Oxford, Connecticut, USA) consists of two sonicated metal plates that operate at different frequencies; the reaction solution flows between the plates (Mason and Berlan, 1992). The ultrasonic intensity in the solution between the plates (operating at frequencies of 16 and 20 kHz) is greater than the sum of single plate intensities. The *Nearfield acoustic processor*, shown in Figure 2.19, is driven by magnetostrictive transducers and can be used to sonicate high flow rates of material (Berlan and Mason, 1992; Mason and Berlan, 1992).

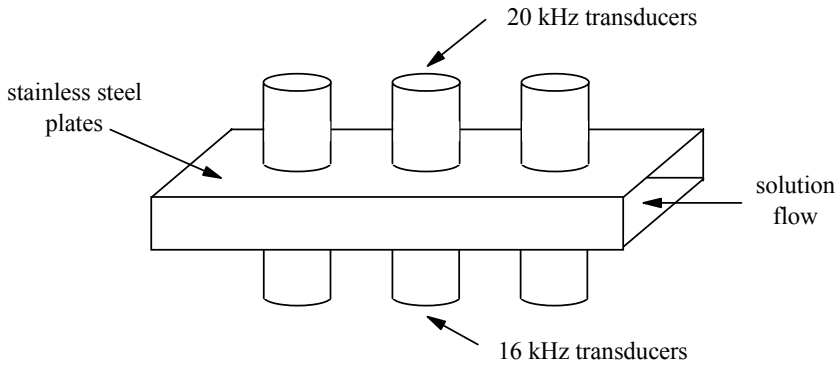

Figure 2.19 : Schematic diagram of a *Nearfield acoustic processor* (Mason, 1992)

The *Nearfield acoustic processor* has been used to degrade low concentrations of water pollutants such as *p*-nitrophenol, benzene and toluene (Hua et al., 1995a; Thoma et al., 1998). The degradation of *p*-nitrophenol increased proportionally with increasing power-to-volume ratio over the range of 0,98 to 7,27 W cm^{-2}. Degradation was greatest when a 4:1 (v/v) mixture of argon and oxygen gas was bubbled through the solution. A comparison of the energy efficiency of an *Nearfield acoustic processor* and an ultrasonic horn system (Sonics and Materials VCX-400; power, 130 W; sample volume, 25 mL) indicated that the G-value, defined as the number of molecules degraded per unit of energy input into the system, was 64 x 10^{15} and 2,3 x 10^{15} molecules kJ^{-1}, respectively (Hua et al., 1995a). The investigation of effluent containing benzene and toluene concluded that for scale-up, ultrasound would be most effective as a

pretreatment for relatively high target concentrations rather than as a polishing stage to meet effluent guidelines (Thoma et al., 1998).

The Lewis Corporation have also produced an ultrasonic vibrating tray (Mason, 1992). The vibrating tray was originally designed for the processing of coal and metal ores at flow rates of up to 20 ton h^{-1}. The vibrating tray could be used for the ultrasonic pretreatment of reaction slurries (Mason, 1992).

The ultrasonic *push-pull* system designed by Martin-Walter (Straubenhardt, Germany) consists of a cylindrical bar of titanium, cut to a length equal to a multiple of half-wavelengths of sound, with opposing piezoelectric transducers bonded to each end (Mason, 1992). The combined oscillations of the transducers (connected electrically through a central hole in the cylinder) sets up a *concertina* effect down the length of the cylinder. The push-pull system can be easily retrofitted co-axially in the centre of an existing pipe network. However, this system is susceptible to erosion and there is a lack of information relating to scale-up and industrial implementation (Mason, 1992; Pandit and Moholkar, 1996).

The 250 mL *ortho reactor* designed by Undatim Ultrasonics S.A. (Louvain la Neuve, Belgium) has two transducers (with frequencies of 20 kHz and 1,7 MHz) operating at right angles to each other (Grinthal and Ondrey, 1992). The interaction between the two ultrasonic fields is not completely understood, however, the different frequencies ensure efficient mass transfer and sonochemical reactions occur during sonication (Grinthal and Ondrey, 1992).

The Branson sonochemical reactor consists of a 200 mL module with a pair of 20 kHz horn-type sonicators mounted on either side of a pipe containing the reaction solution (Pandit and Moholkar, 1996). Each sonicator operates with a power rating of 1 800 W; the ultrasonic energy from the transducers is coupled to the pipe by means of a coupling fluid. The modules may be connected together for continuous-flow operation. This system is susceptible to erosion of the horn tips (Pandit and Moholkar, 1996).

The liquid whistle reactor designed by Dawe Ultrasonics (Hayes, UK) is one of the oldest commercial ultrasonic devices (Mason, 1992). The liquid whistle, shown in Figure 2.20, operates in a similar way as a gas whistle; cavitation occurs in a liquid as it passes across a vibrating blade. The vibrations are caused by the high flow rate of the liquid. The liquid whistle provides efficient mixing, homogenisation and dispersion in a flow system. Scale-up is easily achieved since a pump and blade are the only moving parts in the system. Erosion of the vibrating blade may be caused by particulate matter in the reaction solution (Mason, 1992; Pandit and Moholkar, 1996).

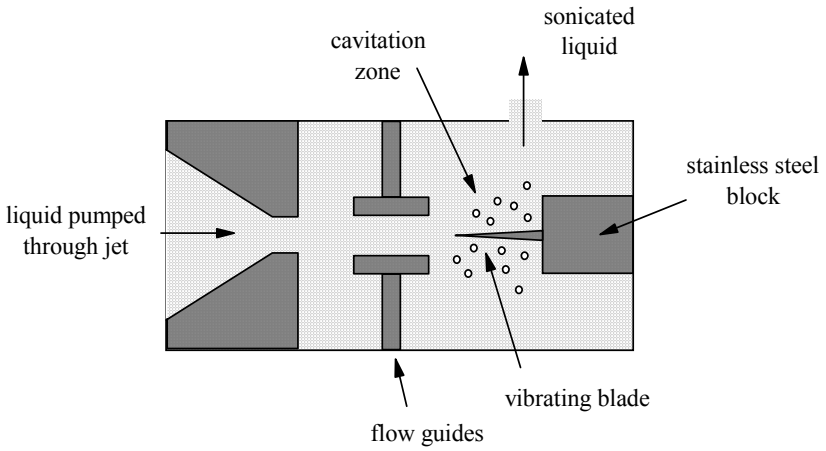

Figure 2.20 : Schematic diagram of an ultrasonic liquid whistle (Mason, 1992)

2.5.5 Equipment design and reactor modelling

Cavitation chemistry and thus the design of ultrasonic equipment is influenced by a variety of parameters that should be optimised for the sonication of a chemical process. Some examples of such parameters are listed in Table 2.5 (Berlan and Mason, 1992; Mason, 1992; Shah et al., 1999c; Thompson and Doraiswamy, 1999).

Table 2.5 : Parameters that affect cavitation (Mason, 1992)

Parameter	Examples
reaction medium	viscosity
	vapour pressure
	presence of solid particles
reaction conditions	pressure
	temperature
	presence of dissolved gas
type of ultrasonic system	power
	frequency
	size and geometry of chemical reactor

Ultrasonic effects are determined primarily by the amount of acoustic power delivered to a system. Power, for comparison between different experimental setups, is reported in literature as intensity, either, in terms of the surface radiating area of the ultrasonic source or the volume of liquid sonicated. Methods of reporting ultrasonic intensity (also referred to as power density) are summarised in Table 2.6. Perkins defined intensity as the electrical power supplied to the transducer divided by the radiating surface area of the ultrasonic horn (Perkins, 1990).

Table 2.6 : Methods of reporting ultrasonic intensity (Perkins, 1990)

	Units	Calculation
area-dependant quantity	W cm^{-2}	acoustic power divided by the radiating surface area of the ultrasonic source
volume-dependant quantity	W cm^{-3}	acoustic power divided by the volume of the liquid being sonicated

Ultrasonic effects increase with increasing intensity, the rate of degradation of chloral hydrate increased linearly with increasing intensity from 0 to 1,5 W cm^{-2} (Sakai et al., 1977). The rate constant for the Fricke dosimeter (conversion of Fe^{2+} to Fe^{3+}) increased linearly with increasing intensity from 5 to 30 W cm^{-2} (Price and Lenz, 1993). Acoustic power cannot, however, be increased indefinitely. The cavities formed by the sound waves become to big to implode within a single rarefaction stage and the formation of a large number of bubbles at the surface of the ultrasonic source act as a shield that diffuses and disperses the acoustic energy (Mason, 1990; Pestman et al., 1994). Sehgal and Wang found that the sonochemical reaction of thymine (15 mL reaction sample; 12,6 mg L^{-1} solution) reached a maximum at an intensity of 3,5 W cm^{-2} and decreased at higher intensities (Sehgal and Wang, 1981). Henglein and Gutiérrez found that the yield of iodide oxidation also reached a maximum and decreased at higher acoustic powers, the power at which the yield was a maximum increased as the reaction volume increased from 5 to 40 mL (Henglein and Gutiérrez, 1993).

Acoustic power can be measured calorimetrically or from the difference in electrical power consumed by a transducer when the ultrasonic horn is loaded and without load. The calorimetric method to calculate acoustic power is based on the measurement of the rate of temperature increase in a system, taking into account its thermal capacity (Delchar and Melvin, 1994; Perkins, 1990). Calorimetry was used to calculate acoustic power in an investigation of the degradation of benzene and styrene (de Visscher et al., 1996); in the degradation of thymine (Mead et al., 1975); in a sonochemical investigation of aqueous methanol (Rassokhin et al., 1995) and in an investigation of the formation of hydrogen peroxide under an argon atmosphere (Rassokhin et al., 1994). Calorimetry has been used to measure a range of intensities, from 1,06 W cm^{-2} in the investigation of pentachlorophenate degradation (Pétrier et al., 1992) to 37,6 W cm^{-2} in the polymerisation of methyl methacrylate (Price et al., 1991). Acoustic power was measured using the difference in electrical power method during an investigation of the chemical and physical effects of ultrasound (Contamine et al., 1994; Ratoarinoro et al., 1995).

The effect of frequency on sonochemical reactions is determined by two opposing phenomena. The compression and rarefaction cycles of ultrasonic waves are shortened as frequency increases, this leads to a reduction in size of cavitation bubbles and hence a lower cavitation intensity and radical formation. The smaller bubbles, however, lead to a greater number of radicals escaping from the bubbles and reacting with

solutes in the water (Mason, 1993; Pétrier et al., 1992; Pétrier and Francony, 1997). Pétrier and co-workers investigated the effect of frequency (20; 200; 500 and 800 kHz) on the initial rate of sonochemical degradation of a 94 mg L^{-1} phenol solution, the rate of degradation was greatest at 200 kHz and decreased in the order for 500, 800 and 20 kHz (Pétrier and Francony, 1997). The rate of sonochemical degradation of chloral hydrate in aqueous solution was 1,8 times greater at a frequency of 400 kHz than at 29 kHz (Sakai et al., 1977). Intensity and emission spectra of sonoluminescence are also dependant upon frequency (Mason, 1993; Sehgal et al, 1980a). Didenko and co-workers found that sonoluminescence intensity was greatest at a frequency of 337 kHz and decreased at frequencies of 1 100 and 22 kHz (Didenko et al., 1994).

The design of ultrasonic equipment should allow for the option of sparging with a gas during sonication. The investigation of the degradation of hydantoin compounds in an ultrasonic bath demonstrated that oxygen concentration of an oxygen-saturated solution was reduced, within 3 h, to that of an unsaturated solution due to the degassing nature of ultrasound (Schwikkard, 1995). Dissolved oxygen concentration is an important parameter to quantify and control in an ultrasonic system to ensure optimal performance and reproducible results.

Mason and Cordemans de Meulenaer made the following 10 recommendations in the optimisation of an ultrasonic process (Mason and Cordemans de Meulenaer, 1998):

- Make cavitation easier by the addition of solids or gas bubbles to act as nuclei.
- Try entraining different gases or mixtures of gases.
- Try different solvents for different temperature ranges and cavitation energies.
- Optimise the power required for the reaction.
- When using a solid-liquid system do not charge all the components in the reactor at once.
- If possible, try to homogenise two-phase systems as much as possible.
- Try different shapes (diameters and volumes) for the reactor.
- It can be better (but not always) to avoid standing wave conditions by performing sonochemical reactions under high-power conditions with mechanical stirring.
- Where possible, try to transform a batch system into a continuous one.
- Choose conditions which allow comparisons between different sonochemical reactions.

The choice of a continuous or batch system is dependent on the ultrasonic system. Shah and co-workers recommended the use of continuous processes when a high throughput is required and the use of batch processes when (Shah et al., 1999d):

- residence time is relatively long
- there is a need for more precise control of ingredients
- backmixing is not desirable
- several different products are made in essentially the same setup

- production volume is relatively small and a continuous process is not economic.

A model for gas-liquid cavitation reactors must take into account the different mechanistic sub-processes (Shah et al., 1999e). The sub-processes of ultrasonic cavitation are the formation of reactive intermediates and pyrolysis products due to the high temperatures and pressures in the collapsing cavities; the rate at which the reaction products and other intermediates are released into the bulk solution; and the rate of heat and mass transfer from the collapsed cavity into the bulk solution and the reactions between the transferred intermediates and other species present in solution (Shah et al., 1999e).

Proper characterisation of the nature and distribution of gas cavities in a reaction vessel (size, number and location) is important in a cavitation reactor model since the cavities are the initiation sites of chemical reactions (Shah et al., 1999e). Formulation of mathematical models of the location and distribution of the collapsing cavities is difficult due to the random nature of the process and the lack of knowledge about the relationship between cavitation energy imparted to a reaction solution and the size, number and distribution of cavities generated from the energy. Process scale-up is thus usually done on a qualitative or empirical basis (Shah et al., 1999e).

Cavitation reactor models have been reported in literature (Gogate and Pandit, 2000; Prasad Naidu et al., 1994; Shah et al., 1999d). Models start with the Rayleigh-Plesset equation for bubble dynamics (equation 2.3) which is altered to take into account different assumptions. Prasad Naidu and co-workers derived a model to predict the number of free radicals generated during cavity collapse for use in a kinetic model of the sonication of aqueous potassium iodide solutions (Prasad Naidu et al., 1994). The growth phase and initial cavity collapse were assumed to be isothermal, cavity collapse become adiabatic once the pressure of the gas within the cavity equalled the saturation vapour pressure of the liquid. The model predicted the rate of iodine liberation in potassium iodide solutions under an oxygen atmosphere but less so under a nitrogen atmosphere (Prasad Naidu et al., 1994).

Gogate and Pandit solved the Rayleigh-Plesset equation numerically (assuming complete adiabatic cavity collapse, with and without the assumption of liquid-phase incompressibility) to develop an empirical correlation of the pressure generated during cavity collapse as a function of intensity, frequency and initial nuclei size (Gogate and Pandit, 2000). The correlation is

$$P_{collapse} = 114(R_0)^{-1,88}(I)^{-0,17}(f)^{0,11} \qquad [2.13]$$

where initial cavity size R_0 is measured in mm, ultrasonic intensity I in W cm^{-2}, frequency f in kHz and the generated pressure $P_{collapse}$ in atm. This correlation can be used in the design of sonochemical reactors to indicate the magnitude of pressure generated during cavity collapse, irrespective, of the process for which

the reactor is being used (Gogate and Pandit, 2000). The sonochemical yield of a process is related to pressure generated during cavity collapse according to equation 2.14

$$Sonochemical\ yield\ =\ K(P_{collapse})^{c} \qquad [2.14]$$

where the constant K and exponent c are determined by reactor geometry, operating parameters and type of reaction being performed. These sort of correlations can be used by engineers in the design procedures for sonochemical processes where rigorous numerical solutions may not be feasible (Gogate and Pandit, 2000).

2.6 CONCLUDING REMARKS

Ultrasonic cavitation results in both chemical and physical effects. The chemical effects of ultrasound are due to the free radicals formed because of the high temperatures and pressures in the collapsing gas cavities. Radical reactions occur within the gas cavity, radical species and products diffuse into the bulk solution and react with solutes in the water. The presence of a gas influences the radical reactions occurring during sonication. Thermal dissociation processes (pyrolysis reactions) dominate within the gas cavities whereas reaction kinetics analogous to radiation chemistry occur in the bulk solution. The physical effects of ultrasound are due to shockwave formation and microject formation during asymmetric cavity collapse.

The potential application of ultrasound in water treatment is indicated in literature. Ultrasound enhances the biocidal activity of chlorine due to break-up and dispersion of bacteria clumps. Anaerobic digestion of sewage sludge is accelerated and sludge dewatering is enhanced. Low intensity ultrasound also increases the activity of activated sludge microorganisms. Various organic pollutants are degraded during sonication. Ultrasound, however, is best used in conjunction with other technologies as a pretreatment step.

Parameters such as acoustic power, ultrasonic frequency and the dissolved concentration of a gas must be quantified to characterise reaction conditions for comparative and scale-up purposes. The direct scale-up from ultrasonic baths and horns is not suitable for industrial applications. Larger-scale equipment such as the *Harwell* sonochemical reactor and the *Nearfield acoustic processor* are based on a flow system in which the reaction solution is pumped through a small sonicated zone, either being recirculated or on a once-through basis.

3

OZONE AND HYDROGEN PEROXIDE CHEMISTRY

Advanced oxidation processes are defined as processes (such as ozone) that generate sufficient quantities of hydroxyl radicals to affect water treatment (Glaze et al., 1987). The formation of hydroxyl radicals is enhanced by the simultaneous addition of hydrogen peroxide. Advanced oxidation processes may totally mineralise organic compounds, such as herbicides and pesticides, that are difficult to degrade during conventional water treatment. Partial oxidation, where conditions required for total mineralisation are not practical, may produce less recalcitrant compounds for microbial processes; under such conditions advanced oxidation processes are beneficial as pretreatment steps to other processes (Yue, 1992).

Ozone chemistry and the kinetics of ozone decomposition are reviewed in Section 3.1, the application of ozone in water treatment in Section 3.2 and hydrogen peroxide chemistry and application in water treatment in Section 3.3.

3.1 OZONE FUNDAMENTALS

Ozone is a triatomic allotrope of oxygen and is an unstable, blue, diamagnetic gas with a characteristic pungent odour (Greenwood and Earnshaw, 1984b). The bond angle of the triangular-shaped molecule was determined in microwave studies to be 116,8 ± 0,5° and the bond lengths 0,1278 nm (Greenwood and Earnshaw, 1984b). The structure of ozone is a hybrid of the resonance structures shown in Figure 3.1.

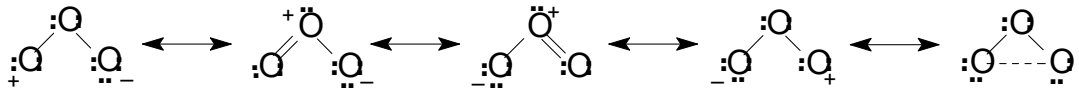

(a)(b) **(c)** **(d)** **(e)**

Figure 3.1 : Resonance structures of the ozone molecule (Harcourt et al., 1986; Nebel, 1981)

The bonding of structures (a) to (d) in Figure 3.1 consist of two σ bonds and one delocalised π bond in which the orbital is stretched over the three oxygen atoms (Greenwood and Earnshaw, 1984b; Nebel, 1981). The strong electrophilic or electron-deficient nature of ozone is indicated by structures (a) and (d) that are characterised by a terminal atom with only six electrons (Nebel, 1981). Structure (e) in Figure 3.1 has also been proposed for the ground-state resonance of the ozone molecule. This structure consists of two σ bonds

and a third *long bond* or π bond between the two terminal oxygen atoms (Harcourt and Rosa, 1978; Harcourt et al., 1986).

Ozone was initially detected by means of its smell. Van Mauren, in 1785, first recorded the distinct odour accompanying an electrical spark discharge in oxygen gas (Greenwood and Earnshaw, 1984b; Nebel, 1981). Ozone was named (from the Greek word *ozein* meaning *to smell*) by Schönbein, in 1840, who recognised it as a new compound (Greenwood and Earnshaw, 1984b; Rocke, 1994). The chemical structure of ozone was shown by Soret, in 1866, to be that of triatomic oxygen (Streng, 1961).

The chemical and physical properties of ozone are reviewed in Section 3.1.1, the kinetics of decomposition in Section 3.1.2 and rate constants of radical reactions in Section 3.1.3.

3.1.1 Chemical and physical properties

Some physical properties of ozone are listed in Table 3.1.

Table 3.1 : Physical properties of ozone (Greenwood and Earnshaw, 1984b; Streng, 1961)

Parameter	Value
molecular weight	47.998
molecular formula	O_3
form	blue gas at room temperature
melting point	-192,5 °C
boiling point	-111,9 °C
density (liquid)	1 354 kg m^{-3} at -119,4 °C
density (solid)	1 728 kg m^{-3} at -195,8 °C
viscosity (liquid)	1,57 cp at -183 °C
viscosity (gaseous)	1,33 x 10^{-2} cp at 25 °C

Ozone condenses to a deep blue liquid and to a violet-black solid (Greenwood and Earnshaw, 1984b). Liquid and solid forms of ozone are explosive due to rapid decomposition to gaseous oxygen. Gaseous ozone is also thermodynamically unstable with respect to decomposition to oxygen gas, though the decomposition is slow in the absence of catalysts or ultraviolet radiation (Greenwood and Earnshaw, 1984b).

$$\tfrac{3}{2}O_2(g) \rightarrow O_3(g) \quad \Delta H_f^\circ = 142{,}7 \text{ kJ mol}^{-1}; \quad \Delta G_f^\circ = 163{,}2 \text{ kJ mol}^{-1}$$

Scheme 3.1

Although ozone is a powerful oxidant, it is selective in its action (Bablon et al., 1991b; Nebel, 1981). The ozone oxidation of potassium iodide, shown in Scheme 3.2, indicates the strongly oxidising nature of ozone

and the tendency of ozone to transfer an oxygen atom during reaction to produce oxygen gas (Greenwood and Earnshaw, 1984b).

$$O_3 + 2I^- + H_2O \rightarrow O_2 + I_2 + 2OH^-$$

Scheme 3.2

3.1.2 Classification of ozone reactions

Oxidation of organic solutes in water by ozone is due either to direct reaction with ozone molecules or reaction with free radicals formed from ozone decomposition (Beltrán, 1995; Hoigné, 1975; Hoigné and Bader, 1976). Ozonation is a gas-liquid reaction and the influence of mass transfer (gas absorption) has to be considered in determining whether both direct and decomposition reactions occur (Beltrán, 1995). Beltrán and co-workers investigated the competition between direct and decomposition reactions using film and surface-renewal models for gas absorption (Beltrán, 1995). The film model was based on the concept of a stagnant film at the surface of a liquid next to a gas; convection does not occur within the film and the dissolved gas moves through the film by molecular diffusion alone (Charpentier, 1981; Danckwerts, 1970). A schematic diagram of ozone concentration in the gas bubble, film layer and bulk solution is presented in Figure 3.2.

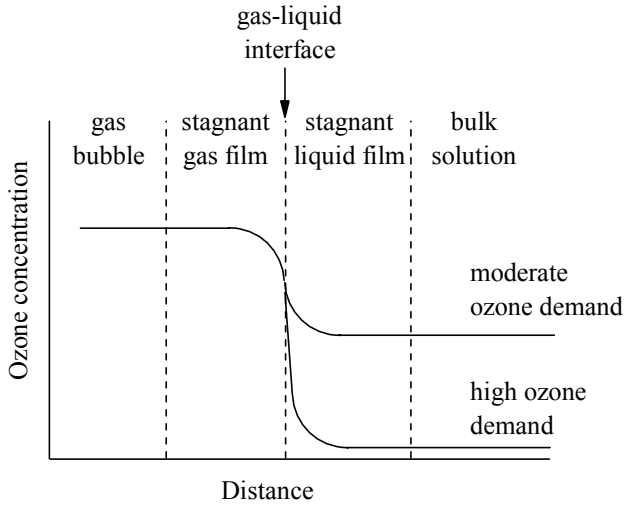

Figure 3.2 : Schematic diagram of ozone concentration in the gas bubble, film layer and bulk solution as described by the two-film theory (Adams and Randtke, 1992a)

Ozone, as shown in Figure 3.2, can be depleted in the film layer by a fast chemical reaction (high ozone demand) resulting in a negligible amount of ozone in the bulk solution whereas a slow chemical reaction results in the bulk solution being saturated with ozone. The kinetic regime of a gas absorbing into a liquid and then undergoing chemical reaction is determined in film theory by the value of the dimensionless Hatta number. The Hatta number is defined in equation 3.1 for an irreversible first-order reaction and in equation 3.2 for an irreversible second-order reaction (Charpentier, 1981; Danckwerts, 1970).

$$\text{Ha} = \frac{(k D_{O_3})^{0,5}}{k_L} \quad [3.1]$$

$$\text{Ha} = \frac{(k_d C_B D_{O_3})^{0,5}}{k_L} \quad [3.2]$$

where k is the first-order rate constant, D_{O_3} the ozone diffusivity in water, k_L the liquid-phase mass transfer coefficient, k_d the rate constant for the direct reaction between ozone and compound B in solution and C_B the concentration of compound B. The classification of the kinetic regime of gas absorption reaction according to the Hatta number is presented in Table 3.2.

Table 3.2 : Classification of kinetic regime of gas absorption reactions according to the Hatta number (Charpentier, 1981)

Ha	Kinetic regime	Description
< 0,02	very slow reaction in bulk solution	Reaction does not occur in the film; mass transfer keeps the concentration of the absorbed gas (ozone) in the bulk solution close to saturation level.
0,02 to 0,3	slow reaction in bulk solution	The process is that of physical absorption followed by reaction in the bulk solution; a negligible proportion of ozone reacts in the diffusion film.
0,3 to 3	moderately fast reaction	A substantial amount of ozone reacts in the film; ozone concentration in the bulk solution is very low.
> 3	fast reaction in film layer	Reaction is fast and occurs completely in the film layer; ozone concentration in the bulk solution is negligible.

The Hatta number indicates whether the overall reaction rate is controlled by reaction kinetics or by the mass-transfer coefficient, and thus whether a large liquid hold-up or large specific interfacial area is required in the design of a reactor for a specific reaction (Charpentier, 1981). As shown in Table 3.2, a Hatta number below 0,3 indicates that the reaction occurs completely in the bulk solution and that the reaction rate is controlled by the bulk volume; necessitating a large volume of liquid for the reaction. Conversely, a Hatta number greater than 3 indicates that the reaction occurs completely within the boundary layer and that the reaction rate is controlled by the interfacial surface area; necessitating a contacting device that creates a large interfacial area. A large liquid volume and interfacial area are required for a reaction that occurs within both the film layer and the bulk solution (Charpentier, 1981).

The surface-renewal model is based on the concept of periodic replacement of elements of liquid at the interface by liquid from the bulk solution; the rate of gas absorption is a function of the exposure time of the liquid element, initially being rapid and decreasing with time (Charpentier, 1981; Danckwerts, 1970). The

diffusion time (t_D) is defined as the time between two consecutive renovations of liquid elements, it is the available time for ozone to diffuse into the liquid elements; reaction time (t_R) is defined as that required for the reaction to proceed at an appreciable rate (Astarita, 1967 in Beltrán, 1995). The expressions for the diffusion and reaction times are presented in equations [3.3], [3.4] and [3.5].

$$t_D = \frac{D_{O_3}}{k_L^2} \quad [3.3]$$

$$t_R = \frac{1}{k_d C_B} \text{ (for a second-order reaction)} \quad [3.4]$$

$$t_R = \frac{1}{k} \text{ (for a first-order reaction)} \quad [3.5]$$

where k is the first-order rate constant, D_{O_3} the ozone diffusivity in water, k_L the liquid-phase mass transfer coefficient, k_d the rate constant for the direct reaction between ozone and compound B in solution and C_B the concentration of compound B in solution. The ratio of the diffusion time to the reaction time as defined according to the surface-renewal model is equal to the square of the Hatta number as defined according to the film layer model (Beltrán, 1995). The classification of kinetic regime of gas absorption reactions according to diffusion and reaction times is presented in Table 3.3.

Table 3.3 : Classification of kinetic regime of gas absorption reactions according to diffusion and reaction times (Beltrán, 1995)

	Kinetic regime	Description
$t_D << t_R$	slow reaction	Reaction is slow since the surface liquid elements are renewed before the reaction can develop appreciably.
$t_D >> t_R$	fast reaction	Reaction is fast since the dissolved gas is completely depleted between renovations of surface liquid.

where t_D is the diffusion time, the time between two consecutive renovations of liquid elements

t_R is the reaction time, the time required for a reaction to proceed at an appreciable rate

A kinetic regime of moderate reactions is defined to occur when t_R is between 0,1 and 10 times that of t_D (Beltrán, 1997). The limit between slow and moderate reactions ($t_R = 10t_D$) is called the diffusional regime, ozone diffusion controls absorption rate in this region (Beltrán, 1997).

The presence of dissolved ozone in the bulk solution, according to Table 3.2, indicates that reactions are slow and take place in the bulk solution whereas the absence of dissolved ozone in the solution indicates that reactions are fast and take place in the proximity of the interface (Beltrán, 1995). Beltrán investigated the effect of pH on the ozone decomposition reaction and found that at a pH of 2 and 7 the bulk solution was

saturated with ozone, thus, decomposition was slow and took place in the bulk solution whereas at a pH of 12 the dissolved ozone in the bulk solution was negligible and ozone disappeared due to a fast reaction while diffusing through the film layer (Beltrán, 1995).

Ozone decomposition and the direct ozone reaction with a generic compound *B* takes place in the same reaction zone during ozonation when $k_d < 10^6$ M^{-1} s^{-1} and $C_B < 10^{-4}$ M or when pH ≥ 10 and $k_d \geq 10^6$ M^{-1} s^{-1} with $C_B < 10^{-6}$ M (Beltrán, 1995). Beltrán concluded that the ozone decomposition reaction would not be able to compete with the direct ozone reaction when the rate constant for the direct reaction between ozone and a surface water pollutant (concentration typically below 10^{-6} M) was significantly greater than 10^6 M^{-1} s^{-1} (Beltrán, 1995).

3.1.3 Kinetics of ozone decomposition

Ozone decomposition occurs through a series of radical reactions that in pure water are initiated by the reaction of ozone with hydroxide ions, HO^- (Hoigné, 1975; Staehelin and Hoigné, 1982). Decomposition increases with increasing alkalinity (Hoigné and Bader, 1976; Sotelo et al., 1987; Staehelin and Hoigné, 1982). Staehelin and Hoigné found that the decomposition of ozone was slow but measurable at a pH below 8, easily measurable at a pH between 8 and 10 and too rapid to be measured at a pH above 10, decomposition was pH dependant because it was determined by HO^- concentration (Staehelin and Hoigné, 1982). Ozone decomposition is also temperature dependant, at a pH of 7 decomposition increased with increasing temperature from 10 to 40 °C; decomposition was extremely fast in experiments performed at a temperature above 30 °C and a pH above 8 (Sotelo et al., 1987).

Various reaction mechanisms have been proposed for the decomposition of ozone. The reaction mechanism proposed by Hoigné and co-workers for ozone decomposition in pure water at a neutral pH is presented in Scheme 3.3 (Bablon et al., 1991b; Staehelin et al., 1984).

Initiation step

$$O_3 + HO^- \xrightarrow{k_i} O_2^{\bullet -} + HO_2^{\bullet} \qquad k_i = 70\ M^{-1}\ s^{-1} \qquad [a]$$

Propagation steps

$$HO_2^{\bullet} \rightleftharpoons O_2^{\bullet -} + H^+ \qquad pK_a = 4{,}8 \qquad [b]$$

$$O_3 + O_2^{\bullet -} \xrightarrow{k_1} O_3^{\bullet -} + O_2 \qquad k_1 = 1{,}6 \times 10^9\ M^{-1}\ s^{-1} \qquad [c]$$

$$O_3^{\bullet -} + H^+ \overset{k_2}{\rightleftharpoons} HO_3^{\bullet} \qquad k_2 = 5{,}2 \times 10^{10}\ M^{-1}\ s^{-1} \qquad [d]$$

$$HO_3^{\bullet} \xrightarrow{k_3} HO^{\bullet} + O_2 \qquad k_3 = 1{,}1 \times 10^5\ M^{-1}\ s^{-1} \qquad [e]$$

$$O_3 + HO^{\bullet} \xrightarrow{k_4} HO_4^{\bullet} \qquad k_4 = 2 \times 10^9\ M^{-1}\ s^{-1} \qquad [f]$$

$$HO_4^{\bullet} \xrightarrow{k_5} HO_2^{\bullet} + O_2 \qquad k_5 = 2{,}8 \times 10^4\ M^{-1}\ s^{-1} \qquad [g]$$

Termination steps

$$HO_4^{\bullet} + HO_4^{\bullet} \rightarrow H_2O_2 + 2O_3 \quad [h]$$

$$HO_4^{\bullet} + HO_3^{\bullet} \rightarrow H_2O_2 + O_3 + O_2 \quad [i]$$

Scheme 3.3

The mechanism for ozone decomposition shown in Scheme 3.3 includes, as intermediate compounds, the species $HO_3^{\bullet}$ and $HO_4^{\bullet}$ that have not been measured directly (Bablon et al., 1991b; Westerhoff et al., 1997). Computer simulation was used by Staehelin and co-workers to prove that $HO_4^{\bullet}$ must be formed, most likely as a charge-transfer complex ($HO^{\bullet}O_3$) that decays into $HO_2^{\bullet}$ (Staehelin et al., 1984). Bahnemann and Hart also proposed the formation of $HO_4^{\bullet}$ radicals from the reaction of ozone and hydroxyl radicals, as in reaction [f] of Scheme 3.3, with subsequent decay into $HO_2^{\bullet}$ and oxygen, as in reaction [g] of Scheme 3.3 (Bahnemann and Hart, 1982). The chain reactions occurring during ozone decomposition (Scheme 3.3) are presented in Figure 3.3. The reaction numbers of Scheme 3.3 are included in Figure 3.3.

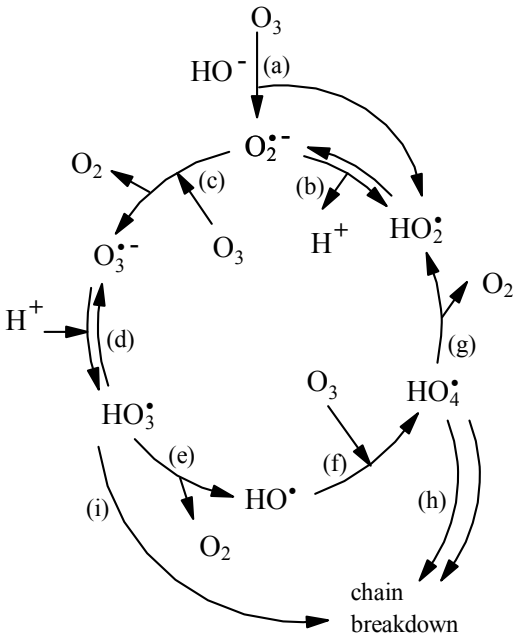

Figure 3.3 : Reaction diagram for the ozone decomposition process (Staehelin et al., 1984)

A mechanism for ozone decomposition has also been proposed by Tomiyasu and co-workers; the mechanism does not include the formation of $HO_3^{\bullet}$ and $HO_4^{\bullet}$ compounds but has only been verified with pulse radiolysis data at pH values above 10 (Bablon et al., 1991b; Westerhoff et al., 1997). Ozone decomposition according to the mechanisms proposed by Hoigné and co-workers, and Tomiyasu and co-workers was modelled by Westerhoff and co-workers using ACUCHEM, a kinetic-modelling computer package (Westerhoff et al., 1997). The objective was to demonstrate the use of computer models to generate profiles of radical species during ozonation. Both simulation models predicted similar ratios of ozone to hydroxyl radicals in the pH range 6,5 to 8,5; ozone to hydroxyl radical ratio decreased by a factor of ten for each

increase in pH of one unit. Predicted ozone consumption according to the Hoigné model was faster and matched the measured rate of ozone depletion more closely for conditions of 5,76 mg L^{-1} initial ozone concentration, pH of 7,5 and 30 min reaction time (Westerhoff et al., 1997). The Hoigné model was used to show the formation profiles of hydrogen peroxide, hydroxyl radicals, superoxide radicals ($O_2^{\bullet -}$) and ozonide radicals ($O_3^{\bullet -}$) during ozone decomposition; formation of hydrogen peroxide and the subsequent reaction between ozone and perhydroxyl radicals become dominant with increasing pH. Ozone consumption in the presence of natural organic matter was also simulated with the model (Westerhoff et al., 1997).

The rate-determining step in the reaction mechanism of ozone decomposition in water is the formation of superoxide radical anions ($O_2^{\bullet -}$), shown in reaction [a] of Scheme 3.3 and Figure 3.3 (Bablon et al., 1991b; Sotelo et al., 1987; Staehelin and Hoigné, 1982). Ozone decomposition occurs in a chain reaction (shown in Figure 3.3) since the formation of perhydroxyl radicals in reaction [a] and [g] of Scheme 3.3 lead to the formation of superoxide radical anions via reaction [b] and further reaction with ozone according to reaction [c] (Staehelin and Hoigné, 1982).

In non pure water, ozone decomposition is initiated, promoted or inhibited by solutes present in the water (Staehelin and Hoigné, 1985). Decomposition is accelerated by organic solutes that convert hydroxyl ($HO^{\bullet}$) radicals into superoxide radical anions ($O_2^{\bullet -}$) since superoxide radical anions react fast and selectively with ozone while hydroxyl radicals react with a variety of compounds (Bablon et al., 1991b; Staehelin and Hoigné, 1985). The reaction rate for reaction between superoxide radical anions and ozone (reaction [c] of Scheme 3.3) is significantly greater than that for the reaction of superoxide radical anions with other solutes present in water. The chain reaction of ozone decomposition in non pure water (shown in Figure 3.4) consists of reactions [a] to [e] of Scheme 3.3 followed by reactions [a] to [c] of Scheme 3.4 (Staehelin and Hoigné, 1985). Perhydroxyl radicals, that continue the cycle of ozone decomposition via reaction [b] of Scheme 3.3, are formed as shown in Scheme 3.4 from the reaction of hydroxyl radicals and an organic solute *B* (Staehelin and Hoigné, 1985).

$$B + HO^{\bullet} \rightarrow B^{\bullet} \qquad [a]$$

$$O_2 + B^{\bullet} \rightarrow BOO^{\bullet} \qquad [b]$$

$$BOO^{\bullet} \rightarrow HO_2^{\bullet} + B_{oxid} \qquad [c]$$

Scheme 3.4

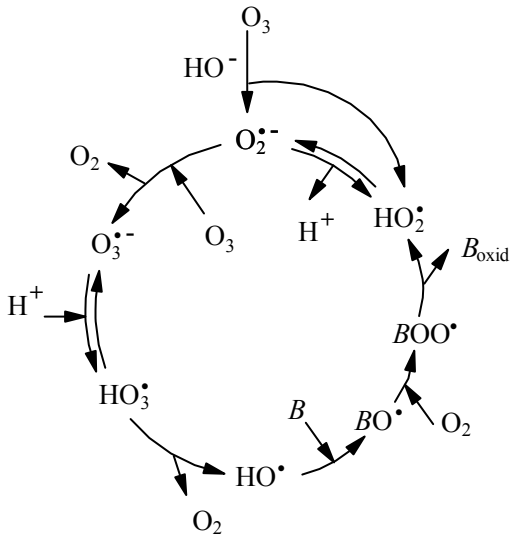

Figure 3.4 : Reaction diagram for the ozone decomposition process in the presence of a solute *B* (Staehelin and Hoigné, 1985)

Oxidation of solutes in water during ozonation takes place, under an acidic pH, predominantly through direct reaction with ozone and, under an alkaline pH predominantly through reaction as shown in Scheme 3.4 with hydroxyl radicals formed from ozone decomposition according to reactions [a] to [e] of Scheme 3.3 (Hoigné and Bader, 1976; Sotelo et al., 1987).

Initiators of ozone decomposition are compounds that generate superoxide radical anions from ozone molecules (Bablon et al., 1991b). Examples of initiators are inorganic compounds, such as perhydroxyl ions, hydroxide ions and some cations (such as Fe^{2+}); and organic compounds, such as glyoxylic acid, formic acid and humic substances (Bablon et al., 1991b; Sotelo et al., 1987; Staehelin and Hoigné, 1982; von Sonntag, 1996). Humic substances are complex macromolecular structures (containing a mixture of predominantly carboxylic and phenolic aromatic or aliphatic carbon functional groups) that are able to act as initiators, promoters and inhibitors of radical reactions (Bablon et al., 1991b; Westerhoff et al., 1997). Ozone decomposition is also initiated by ultraviolet radiation at 253,7 nm (Bablon et al., 1991b; Yue, 1992). Promoters of ozone decomposition are compounds that generate superoxide radical anions from hydroxyl radicals. Examples of promoters are inorganic compounds such as phosphates; and organic compounds such as aryl groups, formic acid, glyoxylic acid, primary alcohols and humic acids (Bablon et al., 1991b).

Radical scavengers are compounds that react with hydroxyl radicals but do not produce species (such as superoxide radical anions) that propagate the chain reaction of ozone decomposition. Common radical scavengers (and hence inhibitors of ozone decomposition) are carbonate (CO_3^{2-}) and bicarbonate (HCO_3^-) ions, alkyl groups, tertiary alcohols (such as *tert*-butyl alcohol) and humic substances (Bablon et al., 1991b; Glaze et al., 1992; Hoigné and Bader, 1976). Carbonate and bicarbonate ions are typically the principle

radical scavengers in natural waters but do not, however, always lead to the full inhibition of ozone decomposition (Glaze et al., 1992; Staehelin and Hoigné, 1985).

Different rate equations, as shown in Table 3.4, have been proposed for the decomposition of ozone. Typically, the reaction order varies, with respect to ozone concentration, from 1,5 at acidic pH to 1 at alkaline pH; and from 0 to 1 with respect to hydroxide ion concentration (Nadezhdin, 1988). Second order reaction kinetics, with respect to ozone concentration, may be observed in the presence of hydroxyl radical scavengers (Nadezhdin, 1988).

Table 3.4 : Some kinetic studies of ozone decomposition in water (Sotelo et al., 1987)

Reference	pH	Temperature (°C)	Reaction order with respect to	
			ozone	hydroxide ion
(Kilpatrick et al., 1956)	0 to 7	25	1.5	-
(Morooka et al., 1979)	2 to 9	10 to 30	1,5 to 1	0,28 to 1
(Staehelin and Hoigné, 1982)	8 to 10	20	1	1

The reaction kinetics of ozone decomposition proposed by Staehelin and co-workers, as shown in Table 3.4, are first order with respect to both ozone and hydroxide ion concentration (Staehelin and Hoigné, 1982; Staehelin and Hoigné, 1985). The expression derived by Staehelin and co-workers for the steady state concentration of hydroxyl radicals during ozonation of water containing an organic solute *B* is presented in equation 3.6 (Staehelin and Hoigné, 1985).

$$[HO^{\bullet}]_{SS} = \frac{2k_{HO,O_3}[HO^-] + k_I[B]}{k_S[B]}[O_3] \qquad [3.6]$$

where k_{HO,O_3} is the rate constant for the reaction between ozone and hydroxide ions, k_I the rate constant for the initiation reaction between solute *B* and hydroxide ions, k_S the rate constant for the scavenging reaction between solute *B* and hydroxyl radicals, and [*B*] the solute concentration (Staehelin and Hoigné, 1985).

Staehelin and co-workers estimated the steady-state concentration of hydroxyl radicals to be $\leqslant 10^{-9}$ M based on an ozone decomposition rate of 10^{-5} M s^{-1} producing hydroxyl radicals that are consumed by solutes of concentration 10^{-4} M with typical rate constants $\geqslant 10^{8}$ M^{-1} s^{-1} (Staehelin and Hoigné, 1985). Superoxide radical anions also exist as short-lived intermediates, the steady-state concentration was estimated to be $\leqslant 10^{-9}$ M assuming a formation rate of $\leqslant 10^{-5}$ M s^{-1} and an ozone concentration of 10^{-5} M controlling its consumption (Staehelin and Hoigné, 1985).

The number of hydroxyl radicals formed per mol of ozone decomposed has been estimated to be between 0,5 and 1 mol (Hoigné, 1975; Hoigné and Bader, 1976; Westerhoff et al., 1997). The theoretical number of

hydroxyl radicals formed, according to reactions [a] to [e] of Scheme 3.3 and the dissociation reaction of water, is 2 mol per 3 mol of ozone decomposed. The overall reaction of hydroxyl radical formation is shown in Scheme 3.5 (Westerhoff et al., 1997).

$$3O_3 + H_2O \rightarrow 2HO^{\bullet} + 4O_2$$

Scheme 3.5

The presence of hydrogen peroxide or the application of other advanced oxidation processes during ozonation initiates additional radical reactions in solution (Bablon et al., 1991b). Perhydroxyl ions, as shown in reaction [c] of Scheme 3.6, are formed from the dissociation of hydrogen peroxide in water. The direct reaction between ozone and hydrogen peroxide is slow whereas the reaction between ozone and perhydroxyl ions is rapid (Bablon et al., 1991b; Taube and Bray, 1940). Low concentrations of perhydroxyl ions are kinetically effective in initiating ozone decomposition (Bablon et al., 1991b). The radical reactions initiated by hydrogen peroxide during ozonation are listed in Scheme 3.6 (Beltrán et al., 1998; Glaze and Kang, 1989a; Glaze and Kang, 1989b).

Initiation steps

$O_3 + HO^- \xrightarrow{k_i} O_2^{\bullet -} + HO_2^{\bullet}$	$k_i = 70\ M^{-1}\ s^{-1}$	[a]
$HO_2^{\bullet} \rightleftharpoons O_2^{\bullet -} + H^+$	$pK_a = 4,8$	[b]
$H_2O_2 \rightleftharpoons HO_2^- + H^+$	$pK = 11,8$	[c]
$O_3 + HO_2^- \xrightarrow{k'_i} O_3^{\bullet -} + HO_2^{\bullet}$	$k'_i = 2,8 \times 10^6\ M^{-1}\ s^{-1}$	[d]

Propagation steps

$O_3 + O_2^{\bullet -} \xrightarrow{k_1} O_3^{\bullet -} + O_2$	$k_1 = 1,6 \times 10^9\ M^{-1}\ s^{-1}$	[e]
$O_3^{\bullet -} + H^+ \overset{k_2}{\rightleftharpoons} HO_3^{\bullet}$	$k_2 = 5,2 \times 10^{10}\ M^{-1}\ s^{-1}$	[f]
$HO_3^{\bullet} \xrightarrow{k_3} HO^{\bullet} + O_2$	$k_3 = 1,1 \times 10^5\ M^{-1}\ s^{-1}$	[g]
$O_3 + HO^{\bullet} \xrightarrow{k_4} O_2 + HO_2^{\bullet}$	$k_4 = 2,0 \times 10^9\ M^{-1}\ s^{-1}$	[h]
$HO^{\bullet} + H_2O_2 \xrightarrow{k_5} O_2^{\bullet -} + H_2O + H^+$	$k_5 = 2,7 \times 10^7\ M^{-1}\ s^{-1}$	[i]
$HO^{\bullet} + HO_2^- \xrightarrow{k_6} O_2^{\bullet -} + H_2O$	$k_6 = 7,5 \times 10^9\ M^{-1}\ s^{-1}$	[j]

Termination steps

$HO^{\bullet} + B \xrightarrow{k_{HO,B}} B'_{oxid}$	[k]
$O_3 + B \xrightarrow{k_d} B_{oxid}$	[l]

Scheme 3.6

The termination steps of Scheme 3.6 are the reaction of a solute *B* with hydroxyl radicals, reaction [k], and the direct reaction of *B* with ozone, reaction [l]. The reactions listed in Scheme 3.6 are presented in Figure 3.5. The reaction numbers of Scheme 3.6 are included in Figure 3.5.

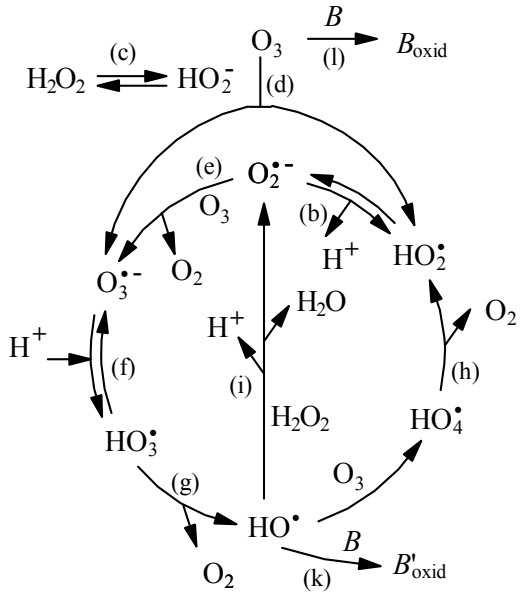

Figure 3.5 : Reaction diagram for the ozone decomposition process in the presence of hydrogen peroxide and a solute *B* (Glaze and Kang, 1989a; Glaze and Kang, 1989b)

The overall stoichiometry for the reaction between ozone and hydrogen peroxide, as summarised from the reactions listed in Scheme 3.6, is shown in Scheme 3.7; a total of 2 mol of ozone are consumed per mol of hydrogen peroxide (Beltrán et al., 1998; von Sonntag, 1996).

$$H_2O_2 + 2O_3 \rightarrow 2HO^{\bullet} + 3O_2$$

Scheme 3.7

Hydrogen peroxide is formed during ozonation from reactions such as [h] and [i] of Scheme 3.3, however, it exists as a short-lived intermediate since upon dissociation the perhydroxyl ions formed initiate further ozone decomposition (Hoigné and Bader, 1976; Staehelin and Hoigné, 1982; Staehelin and Hoigné, 1985; Westerhoff et al., 1997). Perhydroxyl ions consumed by ozone are replaced from the dissolved hydrogen peroxide by an equilibrium shift in reaction [c] of Scheme 3.6 (Bablon et al., 1991b).

Hoigné and Bader measured the concentration of hydrogen peroxide during ozonation (with and without prior addition of hydrogen peroxide) at different pH levels (Hoigné and Bader, 1976). Hydrogen peroxide concentration (for an approximate ozone addition of 2,88 mg L^{-1}) was between 0,34 and 0,51 mg L^{-1} at pH 2 and below the detection limit (0,10 mg L^{-1}) at pH values 6 and 10,5. Hydrogen peroxide concentration at a pH of 2 was equal to the sum of that added (6,80 mg L^{-1}) and that formed during ozonation whereas at a pH of 10,5 less hydrogen peroxide was present (0,14 mg L^{-1}) than what was initially added (Hoigné and Bader, 1976). Hydrogen peroxide is not observed as a significant intermediate in ozonated water, unless the pH is low (below 6), because of the high reactivity of perhydroxyl ions (Staehelin and Hoigné, 1982).

Hydrogen peroxide initiated decomposition of ozone, as shown in Scheme 3.6, increases with increasing pH (Bablon et al., 1991b; Hoigné and Bader, 1976; Staehelin and Hoigné, 1982). The reaction between ozone and perhydroxyl radicals, reaction [b] of Scheme 3.6, is classified (according to calculation of the reaction time, t_R, and diffusion time, t_D, for an ozone mass transfer coefficient of 2 x 10^{-4} m s^{-1}) as a slow reaction at pH 4 for an hydrogen peroxide concentration $\leqslant$ 340 mg L^{-1} and as a moderate to fast reaction at pH $\geqslant$ 10 for a hydrogen peroxide concentration $\geqslant$ 3,4 mg L^{-1} (Beltrán, 1997). Computer simulation also indicated that the reaction between ozone and perhydroxyl ions becomes more dominant with increasing pH (Westerhoff et al., 1997).

Staehelin and Hoigné determined the relative contribution of perhydroxyl and hydroxyl ions to the decomposition of ozone in aqueous solution (Staehelin and Hoigné, 1982). Perhydroxyl ions had a greater effect than hydroxyl ions on ozone decomposition in solutions with a hydrogen peroxide concentration greater than 3,4 x 10^{-3} mg L^{-1} and a pH below 12 (Staehelin and Hoigné, 1982). Beltrán calculated that the rate of ozone decomposition due to reaction with perhydroxyl ions in a 0,34 mg L^{-1} hydrogen peroxide solution at pH 7 and 12 was approximately 63 and 24 times greater, respectively, than that due to reaction with hydroxyl ions (Beltrán, 1997).

3.2 OZONE IN WATER TREATMENT

Ozone is used in potable water treatment for disinfection, degradation of organic compounds and control of taste and odour (Glaze, 1987; Masten and Davies, 1994; Nebel, 1981). Pre-ozonation has been found to enhance flocculation of suspended particles in surface waters (Glaze, 1987). By-product formation during chlorination (trihalomethane compounds are potentially harmful to humans) has increased the application of ozone in water treatment (Bowers et al., 1973; Brink et al., 1991; Rachwal et al., 1992). The limitations associated with ozone are the lack of residual disinfectant capacity and the potential biological growth that can occur in a distribution network (Glaze, 1987). The lack of residual disinfectant is due to the instability of ozone and subsequent decomposition to oxygen, the half-life of ozone at pH 8 is less than 1 h. Ozonation of natural organic matter produces more readily biodegradable compounds that if not removed through filtration can lead to biological growth in a distribution network. Improved performance is obtained when ozone is combined with other disinfectants that maintain an active residual for longer periods and a method of filtration for the removal of biodegradable material (Glaze, 1987).

Ozone is used in the treatment of industrial wastewaters to improve water quality for recycling or discharge (Masten and Davies, 1994; Nebel, 1981; Rice, 1997). Ozonation can improve the biodegradability of non-biodegradable compounds since the oxygenated functional groups introduced during ozonation are potential starting points for metabolic processes (Nebel, 1981). Compounds associated with odour problems contain functional groups possessing a high electron density such as sulfides, amines and olefins. These

functional groups are oxidised by ozone to produce oxygenated groups that are not odoriferous, for example, dimethyl sulfoxide is formed from the oxidation of dimethyl sulfide (Nebel, 1981).

The history of ozone use in water treatment is detailed in Section 3.2.1, the equipment for ozone generation and transfer in Section 3.2.2 and the applications of ozone in water treatment in Section 3.2.3.

3.2.1 History of ozone use

The first full-scale ozonation plants for water treatment were constructed at the turn of the century in Western Europe, the majority were located in France, a plant was built in Paris in 1898 and Nice in 1906 (Brink et al., 1991; Gomella, 1972). Other early plants were located at Oudshoorn, Netherlands (1893), Niagara Falls, New York (1903), Wiesbaden, Germany (1901), and Madrid, Spain (1910). The initial expansion in ozone usage was halted by World War I, research conducted during the war into poisonous gases led to the development of inexpensive chlorine (Brink et al., 1991). Water treatment was performed by chlorination, chloramination and the application of chlorine dioxide (Gomella, 1972).

The initial application of ozone in water treatment was for disinfection. Other early applications of ozone were for taste and odour control (Brink et al., 1991). Ozonation was generally implemented during the final stage of water treatment; during the 1960s applications such as colour removal and oxidation of iron and manganese that required ozone addition early during treatment (hence the term pre-ozonation) were developed. The coagulating effects of ozone and the oxidation of specific micropollutants (such as phenolic compounds and various pesticides) were also first exploited during the 1960s (Brink et al., 1991). The ability of ozone to control algal growth was utilised in France during the 1970s. Further applications of ozone include the control of disinfection by-products and the minimisation of microbiological growth potential of water by ozonation prior to granular activated carbon filtration (Brink et al., 1991).

Ozone application, post World War II, increased more rapidly in Europe than in America. By 1976, approximately 1 000 installations world-wide used ozone in water treatment; the treatment plants were situated predominantly in Europe, however, 20 were in operation in Canada. The largest (that treated water flow rates of up to 910 ML d^{-1}) supplied drinking water to the City of Quebec (Peleg, 1976). By 1984, the number of ozone facilities grew to 20 in the United States and 50 in Canada; the largest at Los Angeles treated approximately 2 360 ML d^{-1} of water (Glaze, 1987). By 1994, 40 effluent treatment plants using ozone were situated in the United States (Masten and Davies, 1994). Three installations using ozone in water treatment were operating in South Africa during 1991 (Brink et al., 1991).

3.2.2 Ozone generation and transfer

The instability of ozone requires that it is generated on-site (Brink et al., 1991; Glaze, 1987; Rosen, 1973). Ozone is formed according to the reactions listed in Scheme 3.8. Cleavage of the double bond of an oxygen

molecule produces two short-lived oxygen atoms, these atoms react rapidly with oxygen molecules to produce ozone (Brink et al., 1991; Glaze, 1987; Nebel, 1981).

$$O_2 \rightarrow O^{\bullet} + O^{\bullet} \quad [a]$$

$$O^{\bullet} + O_2 \rightarrow O_3 \quad [b]$$

Scheme 3.8

Ozone generation in water treatment is performed by the corona discharge method (Brink et al., 1991; Glaze, 1987; Nebel, 1981; Rosen, 1973). This method consists of an electrical discharge maintained between two charged electrodes of a double-tube ozone generator (shown in Figure 3.6). The electrical discharge (lasting up to 10 ns) accelerates electrons so that they possess sufficient kinetic energy to, upon impact, split the double bond of an oxygen molecule (Brink et al., 1991; Glaze, 1987).

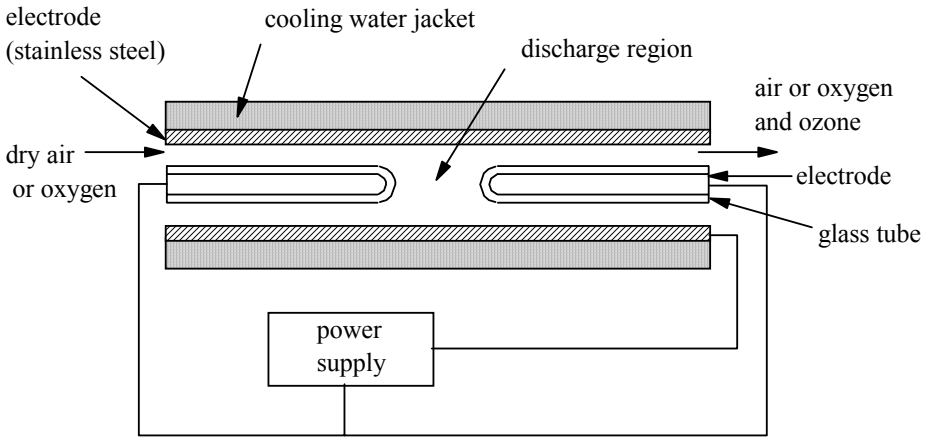

Figure 3.6 : Double-tube ozone generator (Glaze, 1987)

The outer (grounded) electrode, as shown in Figure 3.6, consists of a stainless steel tube surrounded by cooling water (Rosen, 1973). The high potential electrode is centred inside the stainless steel tube within a tubular glass or ceramic dielectric material; the electrode is usually a conductor coated on the inner surface of the dielectric material. The feed gas (dry oxygen or air) passes through the discharge area around the sealed glass tube (Rosen, 1973). An alternating current induces electrons entering the discharge area to vibrate between the electrodes in accordance with the frequency of the current. The higher the frequency the longer the period electrons remain within the discharge area to interact with oxygen molecules (Nebel, 1981). Ozone generators using oxygen as a feed gas are designed with a discharge gap thickness of 1 to 1,5 mm (Brink et al., 1991). Ozone formation is approximately 1,7 to 2,5 times greater in oxygen than in air; typical concentrations of ozone are 1 to 3 % in air and 3 to 7 % in oxygen (Brink et al., 1991; Glaze, 1987). Generators can contain as many as 400 of the double tubes shown in Figure 3.6 and can generate 600 kg of ozone per day with dry oxygen as feed gas (Glaze, 1987). The maximum concentration of ozone produced in air and oxygen is approximately 4 and 8 %, respectively; reaction of ozone with oxygen atoms within a

generator prevents concentrations forming (greater than 20 wt%) at which spontaneous detonation may take place (Nebel, 1981).

Ozone production is an inefficient process, only 5 to 10 % of the applied electrical energy is used in the generation of ozone; an insignificant amount is liberated as light energy and the bulk is converted to heat (Glaze, 1987; Rosen, 1973). Ozone generators have to be cooled to prevent heat build-up and the thermal decomposition of ozone. Ozone formation is also decreased with increasing moisture and oil content of the feed gas. Oxygen and air feed gas must be dry with a low dew point of approximately -52 to -58 °C (Glaze, 1987; Rosen, 1973). The moisture content in air leads to the formation of nitrous and nitric acids that are deposited in the ozone generator and decrease the life of the glass or ceramic dielectric material (Brink et al., 1991; Nebel, 1981). Oxygen atoms are not always produced during the impact of electrons with oxygen molecules; the addition or removal of an electron from a molecule produces a negatively (O_2^-) or positively (O_2^+) charged ion (Nebel, 1981). Approximately 50 % of electrical power (or electrons) in a double-tube ozone generator can be lost (because of conduction) as the electrons move through the field of charged ions (Nebel, 1981).

Ozone production is a direct function of electrical frequency and is doubled when the frequency is doubled (Nebel, 1981). The frequency at which generators are designed to operate varies between 50 and 2 000 Hz; practical limitations such as heat removal and current saturation vary for different ozone generators. The rate of ozone production is usually controlled with the voltage applied to the high voltage electrode since ozone generation varies exponentially with the voltage (Nebel, 1981). Factors such as the width of the corona discharge gap and the thickness of the dielectric material influence the power efficiency of an ozone generator. The smaller the corona discharge gap, the greater the power efficiency. The thickness of the glass (or ceramic) dielectric material is inversely proportional to the ozone production. The glass electrode, however, has to be sufficiently thick to withstand some mechanical impact and the voltage stress under which it is placed. The higher the applied voltage, the thicker the electrode has to be to prevent failure by electrical arcing (Nebel, 1981). Although ozone production increases with increasing voltage and frequency, the power efficiency of ozone generators does not necessarily increase (Nebel, 1981). Both ozone production and power efficiency vary indirectly with gas pressure. Ozone production decreases whereas operating efficiency increases with an increase in flow of the ozone-generating gas (Nebel, 1981).

The solubility of ozone in water is a function of the pressure at which the gas is applied and the temperature of the water (Nebel, 1981). Ozone solubility increases with increasing pressure and decreasing water temperature. The residual ozone in water decreases with increasing temperature due to the faster rate of decomposition and faster reaction rates in the water. The partial pressure of ozone in the gas phase is related to the solubility of ozone in water by Henry's Law. Henry's Law is defined in equation 3.7

$$C^* = \frac{P_{O_3}}{H} \qquad [3.7]$$

where C^* is the liquid-phase ozone concentration in equilibrium with the gas-phase concentration, H the Henry's law constant for ozone (0,082 atm m^3 $gmol^{-1}$ at 25 °C) and P_{O_3} the partial pressure of ozone in the gas phase (Glaze, 1987). Ozone solubility is expressed in terms of an absorption coefficient (β) or as the ratio of the ozone concentration in water to that in the gas (Brink et al., 1991).

A number of devices are used to transfer ozone from gas to water. Ozone transfer is increased by maximising the surface area between the water and the ozonated gas; smaller bubbles are characterised by a larger surface area for a given volume of dispersed gas (Nebel, 1981). Bubble size is controlled by the pore size of an ozone diffuser. Transfer efficiency also increases with increasing contact time between gas and water; the slower the rise time of the bubbles, the greater the contact time (Nebel, 1981). Contact time increases with increased water depth in an ozone contactor (optimal depths vary between 3,7 and 5,5 m). Mixing increases the transfer of ozone but also increases the rate of destruction of residual ozone. The volume of an ozone contact chamber should also minimise contact between ozone bubbles so as to prevent bubble coalescence and the reduction of contact surface area (Nebel, 1981). The speed of ozone transfer is usually limited by the ratio of gas volume to water volume in the contactor (Nebel, 1981).

Devices used for ozone transfer include packed and plate columns, static mixers, jet reactors and agitated vessels (Brink et al., 1991; Martin and Galey, 1994; Munter et al., 1993). One of the most commonly used devices (shown in Figure 3.7) is the counter-current bubble column (Glaze, 1987).

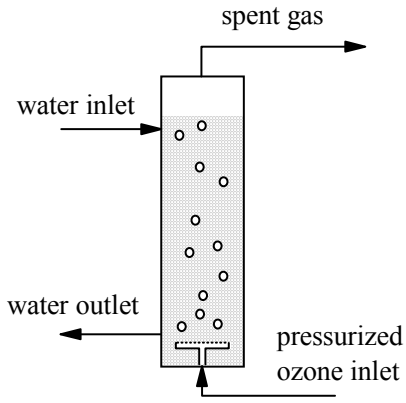

Figure 3.7 : Counter-current bubble column for ozone transfer (Glaze, 1987)

The efficiency of an ozone contactor is important because of the low partial pressure of ozone in the process gas. An ozone contactor should maximise mass transfer efficiency, gas/liquid mixing and contact time (Schulz and Prendiville, 1993). Both contact time and bubble surface area are determined by pore size in dispersion systems using porous disks or rods (Bowers et al., 1973). A smaller pore size leads to an increase in bubble surface area but also an increase in fouling and gas pressure drop across the diffuser (Bowers et al., 1973). Ozone contacting systems using porous disks usually consist of alternating diffusion and reaction

chambers (Schulz and Prendiville, 1993). Water flows downward in the ozone diffusion chamber, counter-current to the rising gas bubbles, and upward in the reaction chamber. Multi-chamber systems satisfy the ozone demand for both fast- and slow-reacting chemicals while maintaining a required ozone residual at the outlet of the reaction chamber for disinfection. Mass transfer efficiency is determined by gas-phase ozone concentration, the ratio of gas flow rate to liquid flow rate, water depth and bubble size (Schulz and Prendiville, 1993). Transfer efficiency may be reduced at higher gas flow rates due to bubble coalescence and at very low gas flow rates due to channelling of gas bubbles. The actual contact time in counter-current ozone diffusion contactors is approximately 50 % of the theoretical hydraulic retention time (Schulz and Prendiville, 1993).

Static mixers (shown in Figure 3.8) are systems using fixed internal mixing elements to rapidly transfer ozone into water (Martin and Galey, 1994). Mixing occurs due to the division of the main water flow by the mixing elements into partial flows that are continually recombined and again divided; ozone loss occurs because of the intense mixing. Static mixers require low maintenance and are robust due to the lack of moving parts (Martin and Galey, 1994).

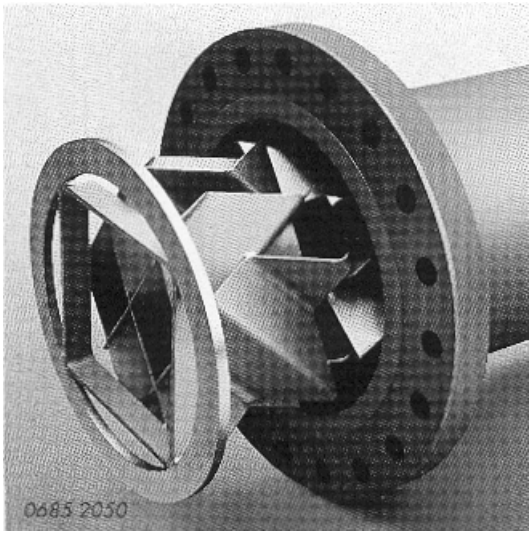

Figure 3.8 : A static mixer (Martin and Galey, 1994)

A pilot-scale study (8 to 12 $m^3 h^{-1}$) at the Méry-sur-Oise water treatment plant showed that ozone could be dissolved in water within 15 s with the use of a static mixer. Ozone transfer increased with decreasing water flow rate and increasing gas flow rate (Martin and Galey, 1994).

Inline injection contactors either introduce ozone directly into the mainstream of water flow or into a side stream that has been diverted and pressurised by a booster pump (Bowers et al., 1973; Schulz and Prendiville, 1993). Static mixing elements are used in a side stream to generate fine gas bubbles that enhance mass transfer and mixing of the ozone in the side stream back into the main stream of water. Advantages of side stream injection contactors over diffusion contactors include operation at a higher ratio of

gas flow rate to liquid flow rate and thorough mixing without bubble channelling problems (Schulz and Prendiville, 1993). Injection contactors are inexpensive but are subject to bumping and corrosion (Brink et al., 1991). Contact time is minimal unless a secondary reactor is installed downstream for the oxidation of slow-reacting chemicals and for settling and removal of oxidised precipitates. Inline injectors are not designed for the disinfection of water because of the difficulty in maintaining a minimum ozone residual for a specific contact time in such a secondary reactor (Schulz and Prendiville, 1993). A two-stage ozone water treatment plant in Henrico County, Virginia (USA) uses inline injection for pre-ozonation and fine-bubble diffusers for intermediate ozonation. Inline injection was used in the pre-ozonation stage in order to avoid maintenance problems associated with plugging of fine-bubble diffusers by suspended solids and oxidised precipitates in the raw water (Schulz and Prendiville, 1993).

3.2.3 Application

Ozone is used in water treatment for disinfection, colour removal, taste and odour removal, oxidation of organic compounds and for the enhancement of flocculation (Koga et al., 1992). Trihalomethane formation is also lowered by the use of ozone instead of chlorine. Ozone has traditionally been used for water treatment in only North America and Europe; facilities are being installed in other countries, such as that in Nizhny Novgorod, Russia, that treats 280 ML d^{-1} of water (Brink et al., 1991; Haglund, 1997).

The application of ozone in water potable treatment is reviewed in Section 3.2.3.1 and in industrial effluent treatment in Section 3.2.3.2.

3.2.3.1 Potable water treatment

Ozone is used in potable water treatment as a biocide, an oxidant and a pretreatment to improve the performance of processes such as coagulation (Martin and Galey, 1994; Nebel, 1981; Schulz and Prendiville, 1993). Ozone disinfection is limited by the lack of residual disinfectant capacity and the potential for biological regrowth in a distribution network. Ozone disinfection is thus usually combined with another disinfectant to maintain a longer active residual and a method of filtration for removal of biodegradable material (Glaze, 1987). The two-stage ozone water treatment plant in Henrico County, Virginia (USA) included ozone disinfection ahead of granular activated carbon filters so as to maintain biological growth on the filters; filter bed life was extended by a factor of between 4 and 10 before reactivation was required (Schulz and Prendiville, 1993).

Ozone is a strong biocide with disinfection occurring due to cell wall rupture (Nebel, 1981). Inactivation of bacteria by ozone varies from that of *Escherichia coli*, the most sensitive to inactivation, to bacteria such as the Gram-positive cocci (*Staphylococcus* and *Streptococcus*), the Gram-positive bacillae (*Bacillus*) and *Mycobacteria* that are more resistant (Bablon et al., 1991a). Viruses are typically more resistant to ozone inactivation than vegetative bacteria but not more so than the sporular forms of *Mycobacteria*. The resistance of parasites (protozoan cysts such as *Giardia lamblia*) to ozone inactivation is greater than that of viruses (Bablon et al., 1991a). Ozone is more effective than chlorine for the removal of *Escherichia coli*,

Giardia, viruses and certain forms of algae (Glaze, 1987; Nebel, 1981). Disinfection with a static mixer to enhance ozone transfer achieved the required 1-log reduction in colony forming units for *Giardia lamblia* and 3-log reduction for viruses (required by the US Environmental Protection Agency) with a 90 s contact time and 2 mg L^{-1} ozone transfer (Martin and Galey, 1994). Disinfection under ideal laboratory conditions occurs when an ozone residual of 0,4 mg L^{-1} is maintained for a 4 min contact time (Martin and Galey, 1994). Ozone dosage required for disinfection is dependant on pH and water temperature; the decay rate of ozone increases with increasing pH and water temperature (Meijers et al., 1995). The rate of ozone disinfection was improved with the simultaneous application of ultrasound but unaffected by the addition of hydrogen peroxide (Dahi, 1976; Martin and Galey, 1994). Dahi found that the rate of ozone decomposition was significantly greater during sonication than without sonication, k = 0,207 min^{-1} versus k = 0,032 min^{-1} (Dahi, 1976). Ozone disinfection has also been used in the recycling of marine aquaria wastewaters such as that at Sea World in Orlando, Florida (Rice, 1997).

Taste and odour are associated with various types of organic compounds including polysulfides, aldehydes and alicyclic alcohols such as geosmin (1,10-*trans*-dimethyl-*trans*-(9)-decalol) and 2-methylisoborneol (Bablon et al., 1991a; Glaze et al., 1990). Taste- and odour-producing compounds are present in raw water or are produced during water treatment itself. Such compounds are formed from the decomposition of plant matter and by the activity of organisms such as actinomycetes and blue-green algae and occasionally by organisms such as zooplankton and nematodes (Bablon et al., 1991a). Taste and odour problems occur more frequently when raw water is distributed from impoundments, especially in summer when water demand is high and water levels are low. Taste and odour problems may be of industrial origin such as from chlorinated solvents, hydrocarbons and pesticides (Bablon et al., 1991a). Formation of taste and odour compounds may take place in a distribution network if conditions lead to the growth of microorganisms or if products used for the lining of pipes and reservoirs contain chemicals that are released into the water (Bablon et al., 1991a).

Glaze and co-workers evaluated various oxidising agents for the removal of six model taste and odour compounds from a municipal water supply (Glaze et al., 1990). The model compounds were geosmin, 2-methylisoborneol, 2,4-decadienal, dimethyltrisulfide, 1-heptanal and 1-hexanal. Effective oxidation of geosmin and 2-methylisoborneol (100 ng L^{-1} concentration) by potassium permanganate, chlorine dioxide, chlorine, chloramine or hydrogen peroxide did not take place; percentage removals were less than 31 % for a 3 mg L^{-1} oxidant dose and a 120 min contact time. Ozone oxidation of geosmin and 2-methylisoborneol were 35 and 40 %, respectively, for a 2 mg L^{-1} ozone dose and a 20 min contact time; oxidation increased to 86 and 73 %, respectively, for a 4 mg L^{-1} ozone dose. The simultaneous application of hydrogen peroxide (2 mg L^{-1}) and ozone (4 mg L^{-1}) over 20 min lead to 95 and 89 % oxidation, respectively, of geosmin and 2-methylisoborneol (Glaze et al., 1990). The five-year pilot-plant investigation by Weng and co-workers at

Hackensack Water Company, New Jersey (USA) found that ozone transferred the *musty* or *grassy* odour of the raw water into a *sweet* odour in the pilot-plant finished water (Weng et al., 1986).

Ozone is used as an oxidant in water treatment to oxidise synthetic organic compounds and compounds produced by natural processes (Bablon et al., 1991a). Naturally occurring organic matter such as humic acids, fulvic acids and proteins are characterised by non-specific measurements such as chemical oxygen demand, UV absorbance (at 254 nm) and total organic carbon. Synthetic organic chemicals in raw water (such as biocides, hydrocarbons, phenols, plasticizers, dyes, amines and solvents) are often toxic; these pollutants are present in concentrations in the 1 ng L^{-1} to 1 mg L^{-1} range (Bablon et al., 1991a).

Pesticides are regularly detected in the raw water of potable water treatment plants (Kang et al., 1997; Lambert et al., 1996; Xiong and Graham, 1992). Koga and co-workers detected 18 pesticides in river water used as a water source for the City of Kitakyushu in China; 11 of the pesticides were still present after treatment with pre-chlorination, flocculation, sedimentation, rapid sand filtration and post-chlorination (Koga et al., 1992). Triazines (such as atrazine and simazine) and phenoxyalkyl acid derivatives (such as Mecoprop) are two groups of herbicides detected in water supplies in England and Wales at concentrations above 0,1 μg L^{-1}, the maximum admissible concentration stipulated by the EC Drinking Water Directive (Xiong and Graham, 1992). Ozone is used as an oxidant for the degradation of pesticides that are not readily degraded in conventional water treatment processes. Kang and co-workers found that the concentration of pesticides in most raw waters was reduced by 90 % during ozonation (Kang et al., 1997). Triazine pesticides are more resistant to oxidation by ozone than phenolic pesticides and other organonitrogen pesticides (Masten and Davies, 1994). The complete degradation of chlorophenoxy acid herbicides required 4 to 5 moles of ozone per mole of solute while atrazine required 25 moles of ozone (Xiong and Graham, 1992). Pesticide degradation by ozone is dependant on ozone dose and contact time; atrazine degradation increased from 45 to 65 % with an increase in ozone dose from 2 to 5 mg L^{-1} for a 10 min contact time, and increased from 60 to 90 % for an increase in contact time from 10 to 60 min for a 3 mg L^{-1} ozone dose (Roche, 1994; Roche and Prados, 1995). Pesticide degradation is also influenced by pH and temperature; the degradation of diuron by ozone increased with increasing pH, in the range 7,2 to 8,3, and increasing temperature, 5 to 20 °C (Meijers et al., 1995).

Ozone is a selective oxidant and the degradation of pesticides is hindered by oxidation of compounds that have higher oxidation rates or are present in greater quantities, for example, natural organic matter and bicarbonate ions (Orlandini et al., 1996; Roche and Prados, 1995). Pesticide degradation is enhanced when ozone is used in combination with hydrogen peroxide or ultraviolet light (Kang et al., 1997; Koga et al., 1992; Prados et al., 1995). Atrazine degradation (1,42 μg L^{-1} initial concentration) for a 10 min contact time was 40, 65 and 70 %, respectively, for treatment with ozone, ozone with ultraviolet light and ozone with hydrogen peroxide where the ozone dose was 3 mg L^{-1} and the hydrogen peroxide to ozone mass ratio was 0,4 (Prados et al., 1995). Roche and co-workers found that atrazine degradation (835 ng L^{-1} initial

concentration) for a 10 min contact time was 40 and 90 %, respectively, for ozone and ozone with hydrogen peroxide for a 3 mg L^{-1} ozone dose and a hydrogen peroxide to ozone mass ratio of 0,4 (Roche, 1994). Lambert and co-workers investigated the degradation of five pesticides for ozone doses of 1; 2 and 3 mg L^{-1} and mass ratios of hydrogen peroxide to ozone of between 0 and 1 for each of the ozone doses (Lambert et al., 1996). Pesticide degradation increased with increasing ozone consumption and applied hydrogen peroxide concentration. Ozone transfer was independent of hydrogen peroxide concentration. Hydrogen peroxide was not totally consumed during ozonation and the residual increased with the increasing applied concentration (Lambert et al., 1996).

Aromatic compounds (such as the chlorinated derivatives of phenol and benzene) have been detected in potable water supplies (Boncz et al., 1997; Masten et al., 1997; Trapido et al., 1997). Chlorinated phenols are oxidised effectively by ozone at a high pH; the toxicity of the degradation products, as tested by *Daphnia magna* 24 h tests, was less that that of the parent compounds (Boncz et al., 1997; Trapido et al., 1997). Fewer disinfection by-products that may induce the formation of trihalomethane compounds were produced during the ozonation of phenolic and benzene compounds than during chlorination (Kim et al., 1997). The degradation of *p*-nitrophenol increased with increasing pH; the kinetic regime of the reaction between ozone and *p*-nitrophenol changed from slow to fast to instantaneous as the pH increased from 2 to 6,5 to greater than 8,4 (Beltrán et al., 1992). Degradation of 1,3,5-trichlorobenzene by ozone and ozone with hydrogen peroxide was greatest in the pH range 7 to 8,5 (Masten et al., 1997). Hydrogen peroxide and ultraviolet light enhanced the ozone oxidation of volatile organic compounds such as trichloroethylene and carbon tetrachloride (Bellamy et al., 1991; Peyton et al., 1982).

Oxidation of organic compounds by ozone in potable water treatment is also enhanced with the addition of a catalyst or with the simultaneous application of ultrasound (Olson and Barbier, 1994; Volk et al., 1997). Ozone, ozone with hydrogen peroxide and ozone with titanium dioxide catalyst mineralised 15, 18 and 24 %, respectively, of the initial dissolved organic carbon (2,84 mg L^{-1}) of a synthetic solution of fulvic acids (Volk et al., 1997). The rate of removal of total organic carbon (TOC) in a 10 mg L^{-1} fulvic acid solution was increased from 40 to 91 % with the simultaneous application of ultrasound with ozone (60 min; power, 55 W; frequency, 20 kHz); the amount of original carbon removed as carbon dioxide increased from 28 to 87 %, respectively (Olson and Barbier, 1994). Ozonation may increase the biodegradability of non-biodegradable material (Nebel, 1981). The partial oxidation of naturally occurring organic matter (humic and fulvic acids) produce compounds such as aldehydes and ketones that are more biodegradable than the parent compounds (Foster et al., 1992). Van Leeuwen demonstrated the improved biodegradability of South African water sources and industrial effluents such as Rietvlei Dam water, a Sasol effluent and industrially-polluted Ngagane River water; the water samples were inoculated with *Pseudomonas fluorescens* and the growth of the microorganisms was studied by measuring adenosine triphosphate concentration and UV absorption at 400 nm (van Leeuwen, 1987). The formation of trihalomethane compounds during chlorination of naturally occurring organic matter is reduced with pre-ozonation

(Rachwal et al., 1992). Simultaneous application of hydrogen peroxide or ultraviolet light with ozone enhances the removal of trihalomethane precursors (Duguet et al., 1985; Glaze et al., 1982).

3.2.3.2 Industrial effluent treatment

Ozone is a strong oxidising agent and is thus used in the treatment of various industrial effluents. Effluents from the textile industry are highly coloured, contain dyes and ancillary chemicals such as sizing agents and surfactants (Perkowski et al., 1996; Rice, 1997). Textile effluents are toxic and tend to be non-biodegradable due to the complex chemical structure of organic compounds in the effluent. The source of colour, biological oxygen demand (BOD) and chemical oxygen demand (COD) changes since textile plants use different organic dyes depending upon the season (Rice, 1997). Ozone decolourises textile effluent, however, the large organic load (represented by high COD and total organic carbon (TOC) residues) are not completely converted to carbon dioxide and water. Treatment of textile effluent is performed more effectively by a combined method of ozone pretreatment and subsequent biodegradation; the removal of COD and non-ionic surfactants by biodegradation increased, respectively, from 10 and 9 % without pre-ozonation to 65 and 87 % with pre-ozonation (Perkowski et al., 1996). Textile effluent treatment with ozone is practised in Japan, Germany, Italy, Taiwan, the USA, the UK and Spain (Rice, 1997).

Ruppert and Bauer found that a red-coloured wastewater with an initial TOC of 275 mg L^{-1} and pH of 10,06 was completely decolourised by ozone within 20 min (Ruppert et al., 1994). The TOC reduction was 20 % and pH decreased from 10,06 to 8,08. The first step in colour removal, the cleavage of double bonds in aromatic rings or azo groups, followed by hydroxylation, did not lead to the elimination of carbon resulting in a low reduction in TOC (Ruppert et al., 1994). Liakou and co-workers used Orange II (CI 15510), 4-(2-hydroxy-1-naphthylazobenzenesulfonic acid), as a model dye to demonstrate ozone decolourisation (Liakou et al., 1997). Oxalate, formate and benzenesulfonate were identified as intermediate compounds of Orange II oxidation. The chemical structure of Orange II is shown in Figure 3.9.

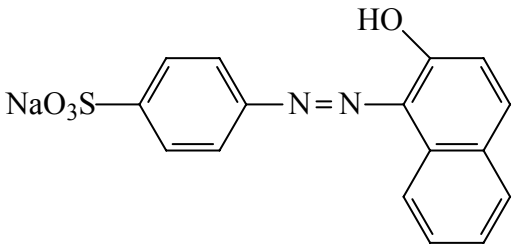

Figure 3.9 : Chemical structure of Orange II dye (Liakou et al., 1997)

Ozonation can be used to convert cyanide ions into the less toxic cyanate ions in electroplating effluents (Rice, 1997). Chlorination is less expensive than ozonation but cyanide ion conversion is also lower. An ozone treatment facility was installed at the Cadillac Motor Car Division of General Motors Corporation in

Detroit, Michigan, in 1978; the ozone to cyanide ratio ranged from 2 to 3, ozone utilisation was greater than 99 % and total cyanide levels have been consistently reduced to below 1 mg L^{-1} (Rice, 1997).

Effluents from petroleum refineries are saturated with hydrocarbon compounds. Ozonation followed by granular activated carbon (GAC) adsorption has been used to reduce concentrations of petroleum-derived organic material in effluent at five USA petroleum product storage and transportation facilities to below 0,1 mg L^{-1} (Rice, 1997). Pre-ozonation increased the lifetime of the GAC adsorbent by between 10 and 50 %. Ozone is used in the treatment of effluent (predominantly phenolic compounds) from the oil shale industry in Estonia; approximately 2 000 tons of effluent is produced annually (Rice, 1997).

Ozone has also been used to degrade protocatechuic acid (a phenolic compound) in the effluent from an olive oil manufacturing plant (Benítez et al., 1996) and for colour removal in the effluent from a molasses processing plant (Gehringer et al., 1997).

3.3 HYDROGEN PEROXIDE

Hydrogen peroxide was first made by J.L. Thenard in 1818; relatively pure hydrogen peroxide was produced from the acidification of barium peroxide and the removal of the barium precipitate that formed (Greenwood and Earnshaw, 1984c; Manly, 1962). A hydrogen peroxide molecule consists of two hydrogen and two oxygen atoms covalently bonded in a non-polar H-O-O-H structure (Kirchener, 1981; Pakiari and Linnett, 1975). The molecular structure of hydrogen peroxide is shown in Figure 3.10.

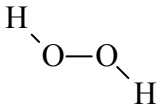

Figure 3.10 : Molecular structure of hydrogen peroxide (Greenwood and Earnshaw, 1984c)

The bond lengths and bond angles of liquid and crystalline hydrogen peroxide are different to the dimensions of gaseous hydrogen peroxide because of hydrogen bonding between neighbouring molecules. The O-O bond length of crystalline hydrogen peroxide (at -163 °C) is 145,8 pm (145,8 x 10^{-12} m); the O-H bond length is 98,8 pm; the OOH angle is 101,9° and the dihedral angle between the planes of O-H bonds is 90,2° (Busing and Levy, 1963; Greenwood and Earnshaw, 1984c). The O-O bond length of gaseous hydrogen peroxide is 147,5 pm; the O-H bond length is 95,0 pm; the OOH angle is 94,8° and the dihedral angle between the planes of O-H bonds is 111,5° (Busing and Levy, 1963; Greenwood and Earnshaw, 1984c). Hydrogen peroxide is the smallest molecule that shows hindered rotation about a single bond, the rotational barriers for the *trans* and *cis* conformations are 4,62 and 29,45 kJ mol^{-1}, respectively (Giguére and Srinivasan, 1977; Greenwood and Earnshaw, 1984c).

Hydrogen peroxide is manufactured commercially from the auto-oxidation of an anthraquinone compound (Greenwood and Earnshaw, 1984c; Kirchener, 1981; Manly, 1962). The process developed by I.G. Farbenindustrie in Germany during World War II (shown in Figure 3.11) consists of dissolving 2-ethylanthraquinone in a mixed ester/hydrocarbon or alcohol/hydrocarbon solvent and reducing it to the corresponding quinol by a Raney nickel or supported palladium catalyst. The quinol is oxidised non-catalytically in a stream of air to produce hydrogen peroxide and 2-ethylanthraquinone. The catalyst is separated and the hydrogen peroxide extracted by water and concentrated to 30 wt% by distillation under reduced pressure. Higher concentrations of hydrogen peroxide are produced by further distillation (Greenwood and Earnshaw, 1984c; Kirchener, 1981).

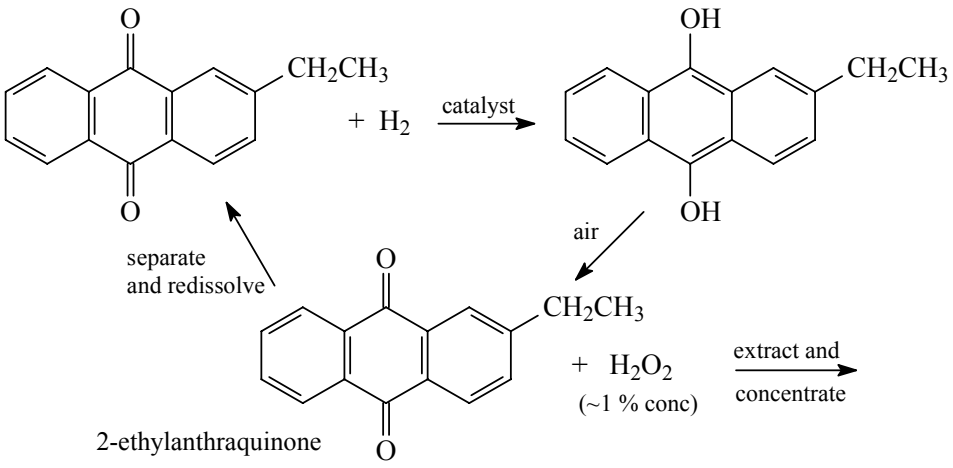

Figure 3.11 : Commercial production of hydrogen peroxide via the auto-oxidation of an anthraquinone compound (Greenwood and Earnshaw, 1984c)

Hydrogen peroxide is miscible in water in all proportions and is sold in concentrations from 3 to 98 % (Kirchener, 1981). Hydrogen peroxide is used industrially as a bleach for textiles and paper, in the manufacture of chemicals, for pollution control, in hydrometallurgy and for minor purposes such as in personal care products, food processing and furniture manufacture (Greenwood and Earnshaw, 1984c).

Chemical reagents are added to stabilize commercial hydrogen peroxide solutions. Stabilizers deactivate catalytic impurities by complex formation or by adsorption (Kirchener, 1981). Sodium pyrophosphate acts in acidic solutions as a complexing agent whereas sodium stannate forms a protective colloid. Alkaline solutions can be stabilized with alkali metal silicates. Various stabilizing systems have been developed, combinations of tin salts and phosphates are frequently used. Some stabilizers contain organic compounds that are effective in dilute solutions but cannot be used in concentrated solutions. The required quantity of stabilizer decreases with increasing peroxide concentration. Container corrosion is also a source of catalytic impurities, nitrate salts are frequently added to inhibit corrosion (Kirchener, 1981).

The chemical and physical properties of hydrogen peroxide are reviewed in Section 3.3.1 and the application of hydrogen peroxide in water treatment in Section 3.3.2.

3.3.1 Chemical and physical properties

Some physical properties of hydrogen peroxide are listed in Table 3.5.

Table 3.5 : Physical properties of hydrogen peroxide (Greenwood and Earnshaw, 1984c; Kirchener, 1981)

Parameter	Value
molecular weight	34.016
molecular formula	H_2O_2
form	colourless liquid at room temperature
melting point	-0,43 °C
boiling point	150,2 °C
density (liquid)	1 442 kg m^{-3} at 25 °C
density (solid)	1 643 kg m^{-3} at -4,5 °C
viscosity	1,249 cp at 20 °C
heat of dissociation	34,3 kJ mol^{-1}

Hydrogen peroxide is a weak acid and may react directly or after dissociation into free radicals. Free radicals, shown in Scheme 3.9, are formed from the homolytic cleavage of either an O-H or O-O bond (Bablon et al., 1991b; Kirchener, 1981; Manly, 1962).

$$H_2O_2 \rightarrow H^{\bullet} + HO_2^{\bullet} \qquad \Delta H = 380 \text{ kJ mol}^{-1} \qquad [a]$$

$$H_2O_2 \rightarrow 2HO^{\bullet} \qquad \Delta H = 210 \text{ kJ mol}^{-1} \qquad [b]$$

Scheme 3.9

The formation of hydroxyl radicals, reaction [b] of Scheme 3.9, is the dominant reaction during uncatalysed decomposition and photochemically initiated reactions (Kirchener, 1981). Hydrogen peroxide reactions are listed in Scheme 3.10.

decomposition $2H_2O_2 \rightarrow 2H_2O + O_2$ [a]

molecular addition $H_2O_2 + Y \rightarrow Y.H_2O_2$ [b]

substitution $H_2O_2 + RX \rightarrow ROOH + HX$ [c]

$H_2O_2 + 2RX \rightarrow ROOR + 2HX$ [d]

oxidation $H_2O_2 + W \rightarrow WO + H_2O$ [e]

reduction $H_2O_2 + Z \rightarrow ZH_2 + O_2$ [f]

Scheme 3.10

Hydrogen peroxide is stable in the absence of catalysts, however, decomposition is strongly catalysed by metal surfaces (metal ions or metal oxides), MnO_2 or traces of alkali dissolved from glass (Kirchener, 1981; Koubek et al., 1963). Peroxyhydrates are formed from molecular addition reactions with hydrogen peroxide; peroxyhydrates such as that formed from sodium carbonate or urea are commercially available. Peroxygen compounds prepared by substitution reactions of hydrogen peroxide with organic reagents are used commercially as polymerisation catalysts or as oxidising agents for a number of special reactions. Hydrogen peroxide is a strong oxidising agent and is capable of oxidising a wide variety of organic and inorganic compounds. Reduction reactions occur when hydrogen peroxide reacts with a stronger oxidising agent than itself, for example chlorine, sodium hypochlorite, potassium permanganate or ceric sulfate (Kirchener, 1981).

3.3.2 Application in water treatment

Hydrogen peroxide is applied in water treatment because it is a strong oxidant. Hydroxyl radicals, formed from the decomposition of hydrogen peroxide, react with organic matter by either adding to a C=C double bond, as shown in reaction [a] of Scheme 3.11, or by abstracting a carbon-bound H atom, as shown in reaction [b] of Scheme 3.11 (Clarke and Knowles, 1982; von Sonntag et al., 1997). Radical cations are formed from molecules containing heteroatoms such as nitrogen or sulfur.

$$HO^{\bullet} + R_2C{=}CR_2 \rightarrow R_2(HO)C{-}CR_2^{\bullet} \quad [a]$$

$$HO^{\bullet} + RH \rightarrow H_2O + R^{\bullet} \quad [b]$$

Scheme 3.11

The addition to a double bond, reaction [a] of Scheme 3.11, is generally faster than hydrogen abstraction, reaction [b] of Scheme 3.11. Hydroxyl radicals react non-selectively with most organic and inorganic solutes with reaction rates (typically of the order of 10^5 s^{-1}) that approach diffusion-controlled limits (Hoigné, 1997; von Sonntag et al., 1997). Hydroxyl radicals are scavenged in water by bicarbonate and carbonate ions (von Sonntag et al., 1997).

Hydrogen peroxide is used in both municipal and industrial effluent treatment. Hydrogen peroxide is used in municipal effluent treatment for the abatement of odours (such as hydrogen sulfide) and as an oxygen source (Cole et al., 1974; Eul et al., 1991). Hydrogen sulfide is formed from bacterial action and leads to the corrosion of sewer systems as well as odour problems. A supplemental oxygen source is required when overloaded activated sludge aeration systems, denitrification in secondary clarifiers and stale or septic wastewaters result in low dissolved oxygen concentrations (Ayling and Castrantas, 1981; Cole et al., 1974).

Hydrogen peroxide is used in industrial effluent treatment for the detoxification of cyanide, nitrite and hypochlorite; for the destruction of phenol aromatics and formaldehyde and for the removal of sulfite,

thiosulfate and sulfide compounds (Bull and Zeff, 1991; Eul et al., 1991). Hydrogen peroxide is also used as a pre-oxidation technology to enhance biodegradation of persistent and recalcitrant organic compounds such as trichloroethylene and pentachlorophenol (Carberry and Benzing, 1991; Marco et al., 1997).

Environmental disasters such as accidental chemical spills and offensive odours can be treated with hydrogen peroxide. A broken tanker spilt 900 ton of fermented molasses into a marine dock along the River Mersey in England contaminating approximately 3 million m^3 of water. The water turned black and began to evolve hydrogen sulfide as the dissolved oxygen was depleted and a sulfate-reducing bacteria began to grow. Hydrogen peroxide was dosed in a 1,5 to 1 ratio of hydrogen peroxide to hydrogen sulfide. The water was mixed with tug boats and normal boating and recreational activities were allowed to resume after 48 h (Robinson and Monsen, 1991). An industrial landfill operation in England experienced problems with offensive odours emanating from four leachate lagoons. Drums of hydrogen peroxide (35 %) were placed every 20 m along the upwind bank of the lagoons and allowed to drip at a rate of 100 mL min^{-1} into the water. Hydrogen peroxide was dosed in a 3 to 1 ratio of hydrogen peroxide to hydrogen sulfide and was followed by jetting for aeration and mixing. The concentration of hydrogen sulfide in the lagoons (3 mg L^{-1} in two lagoons and greater than 10 mg L^{-1} in the other lagoons) was reduced to below the limits of detection after treatment with hydrogen peroxide (Robinson and Monsen, 1991).

Hydrogen peroxide is used in conjunction with advanced oxidation technologies such as in UV/H_2O_2; O_3/H_2O_2 and $UV/O_3/H_2O_2$ to enhance the degradation of stable organic compounds (Bull and Zeff, 1991; Clarke and Knowles, 1982; Glaze et al., 1987). Compounds typically destroyed are highly substituted aromatics, chlorinated aromatics, chlorinated aliphatics, furans and dioxins (Eul et al., 1991).

3.4 CONCLUDING REMARKS

Ozone is used in water treatment for disinfection, colour removal, taste and odour removal, oxidation of organic compounds and for the enhancement of flocculation. Ozone is a power but selective oxidant. Oxidation of compounds takes place through the direct reaction with ozone molecules but also via reaction with hydroxyl radicals formed from the decomposition of ozone. Hydroxyl radicals are not only a stronger oxidant than ozone but are also less selective, hydroxyl radicals react with most organic and many inorganic solutes with high rate constants that approach diffusion-controlled limits.

Ozonation is a gas-liquid reaction and is dependant upon the diffusion of ozone into solution. The kinetic regime of ozone absorption is calculated from the Hatta number. Dissolved ozone concentration in the bulk solution is negligible when all the ozone is consumed in fast reactions ($Ha > 3$) in the film layer. Conversely, slow reactions ($Ha < 0,02$) take place in the bulk solution and ozone mass transfer maintains the dissolved ozone concentration in solution close to saturation.

The decomposition of ozone in solution is initiated by the reaction with hydroxide ions, decomposition is thus pH dependant and increases with increasing pH. Oxidation of organic compounds is dominated by the direct reaction with ozone under acidic conditions and by the reaction with hydroxyl radicals under alkaline conditions. Hydrogen peroxide is formed from the free radical reactions initiated by the decomposition of ozone, however, it is not produced as a significant intermediate because of the fast reaction of perhydroxyl ions with ozone. Perhydroxyl ions are formed from the dissociation of hydrogen peroxide.

The oxidation of organic compounds during ozonation is enhanced during the combination with technologies such as hydrogen peroxide, UV radiation and ultrasound that enhance the decomposition of ozone. Ozone decomposition is enhanced during the combination with hydrogen peroxide or ultrasound by the reaction with perhydroxyl ions. The rate constant for the reaction of ozone with perhydroxyl ions is a factor of more than 10^4-fold greater than the rate constant for the reaction of ozone with hydroxyl ions.

Ozone disinfection is improved when ozone is combined with other disinfectants that maintain an active residual for longer periods and with a method of filtration for the removal of biodegradable material. Ozonation of natural organic matter produces more readily biodegradable compounds that if not removed through filtration can lead to biological growth in a distribution network. The biodegradability of non-biodegradable compounds is improved during ozonation since the oxygenated functional groups introduced during ozonation are potential starting points for metabolic processes.

4

ATRAZINE CHEMISTRY

Atrazine is a herbicide that is used world-wide, it is one of the most commonly used herbicides in the United States. Runoff into surface waters and seepage into groundwater has resulted in the contamination of potable water resources. Atrazine is the most frequently detected herbicide in groundwater in countries of the European Community. Concern for the environmental impact and potential effects it may have on humans has resulted in the use of atrazine being banned or regulated in many countries. Water treatment processes to degrade atrazine are being investigated by various organisations and university research groups.

The general chemistry, physical properties and toxicity data for atrazine are presented in Section 4.1. The role of atrazine in soil and in aquatic systems in the environment are reviewed in Section 4.2. Atrazine degradation kinetics and different methods used to degrade atrazine in water treatment are reviewed in Section 4.3.

4.1 CHARACTERISTICS OF ATRAZINE

The Chemical Abstracts name of atrazine is 6-chloro-*N*-ethyl-*N*'-(1-methylethyl)-1,3,5-triazine-2,4-diamine and the IUPAC name is 6-chloro-N^2-ethyl-N^4-isopropyl-1,3,5-triazine-2,4-diamine (Tomlin, 1997). It is also referred to in earlier literature as 2-chloro-4-ethylamino-6-isopropylamino-*s*-triazine. Atrazine is a six-membered heterocyclic ring, the chemical structure of atrazine is shown in Figure 4.1.

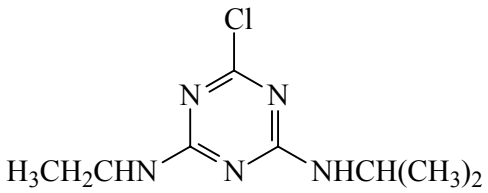

Figure 4.1 : Chemical structure of atrazine (Tomlin, 1997)

The discovery of atrazine is reviewed in Section 4.1.1, chemical and physical properties in Section 4.1.2 and toxicity data in Section 4.1.3.

4.1.1 Discovery

Atrazine was developed by the Geigy Chemical Company in Basel, Switzerland, from research begun in 1952 into derivatives of symmetrical triazines. It was patented in Switzerland in 1958 and in the United States in 1959 (Solomon et al., 1996). Atrazine has been produced by other companies since the early 1970s when the patent protection of Ciba-Geigy expired. Ciba-Geigy in 1989/1990 supplied approximately 60 % of the market (Seiler et al., 1992). In 1992, atrazine was produced by over 10 different companies marketing it alone or in mixtures with their own active ingredients (Seiler et al., 1992).

Atrazine is prepared, in the presence of an acid-binding agent, by the reaction of cyanuric chloride with one equivalent of ethylamine followed by one equivalent of isopropylamine (Sittig, 1980). The reaction pathway for the preparation of atrazine is shown in Figure 4.2.

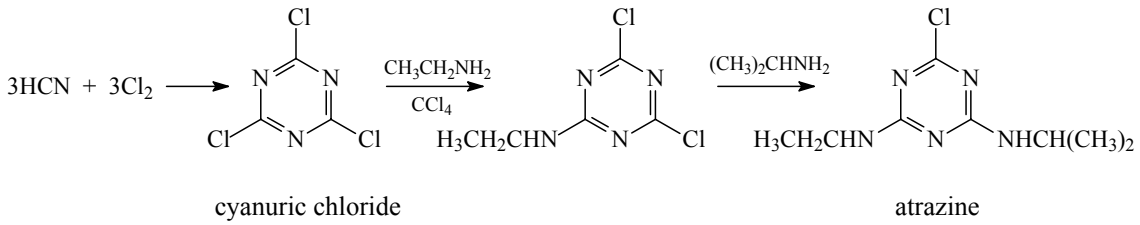

Figure 4.2 : Reaction pathway of the industrial preparation of atrazine (Sittig, 1980)

4.1.2 Chemical and physical properties

Chemical and physical properties of atrazine are listed in Table 4.1.

Table 4.1 : Chemical and physical properties of atrazine (Tomlin, 1997)

Parameter	Value
molecular weight	215.687
molecular formula	$C_8H_{14}ClN_5$
form	colourless powder
melting point	175,8 °C
boiling point	205,0 °C at 101 kPa
vapour pressure	0,0385 mPa at 25 °C
K_{ow}	Log P = 2,5 at 25 °C
Henry's law constant	1,5 x 10^{-4} Pa m^3 mol^{-1}
standard gravity (density)	1,23 at 22 °C
water solubility	33 mg L^{-1} at pH 7 and 22 °C
pKa	1,7 (very weak base)

Atrazine is relatively stable in neutral, weakly acidic or weakly alkaline media; it is rapidly hydrolysed to the hydroxy derivative in strong acids or alkalis, and at 70 °C in neutral media (Tomlin, 1997). Pure atrazine may be stored for several years, decomposition begins immediately after application in soil (Huber, 1993). The stability of the *s*-triazine ring is due to the electronic configuration of the heterocyclic ring with the π electrons being delocalized over the six ring atoms. The π electrons are not evenly distributed over the whole ring and are localized in the vicinity of the nitrogen atoms. The strong electronegativity of the nitrogen atoms causes the *s*-triazine ring to display few of the characteristics of a compound containing an aromatic nucleus (Esser et al., 1975; Weber, 1970).

Properties of *s*-triazine derivatives are determined by the substituents on the ring (primarily by the substituent in position 6), the ring itself does not contribute except for its effect on the charge distribution (Leclercq and Pacáková, 1979; Weber, 1970). Substituents in position 6 are usually chlorine, methoxy (OCH_3) or thiomethyl (SCH_3) groups, various alkylamino groups are substituted in positions 4 and 6 (Leclercq and Pacáková, 1979). The dissociation constant is strongly affected by the substituent in position 6, basicity increases in the order $Cl < SCH_3 < OCH_3$. The effect of the groups in positions 2 and 4 are smaller but still pronounced, the greater the number of ethyl groups replacing hydrogen atoms, the more basic the compound (Leclercq and Pacáková, 1979).

4.1.3 Toxicity

Atrazine acts as a herbicide because of its inhibition of photosynthesis, it is thus less toxic to animals than to plants (Solomon et al., 1996). The toxicity of atrazine to different animal species is listed in Table 4.2. The terms LD_{50} and LC_{50} refer to the dosage and concentration of a chemical that kills 50 % of the group of animals to which it is administered. Acute LD_{50} values indicate that the chemical administration was by a single dose; dosage is expressed in mg active ingredient per kilogram of animal bodyweight (Jones et al., 1968).

Table 4.2 : Acute toxicity of atrazine (Seiler et al., 1992)

Parameter	Species	Concentration ($mg\ kg^{-1}$)
acute oral LD_{50}	rat	1 869 to 3 080
acute oral LD_{50}	mouse	1 750 to 3 992
acute dermal LD_{50}	rat	> 3 100
acute inhalation LC_{50}	rat	> 710 mg m^{-3}
skin irritation	rabbit	slight irritant
eye irritation	rabbit	no irritant
sensitisation	guinea pig	sensitising

The evaluation performed by Ciba-Geigy indicated that atrazine had no mutagenic effects on mammals (Seiler et al., 1992). Atrazine was also found not to be mutagenic in the Ames *Salmonella*/microsome assay (Simmon et al., 1979). Long term experiments indicated a slight impairment in weight development following high doses of atrazine in rats, mice and dogs; dogs fed for a year with 1 000 mg kg^{-1} of atrazine in their food showed changes in heart and circulation. No carcinogenic effects, independent of the dose administered, were found in mouse trials (Seiler et al., 1992).

Exposure to atrazine under factory conditions did not adversely affect the health of workers or increase the incidence of benign or malignant disease attributable to atrazine (Loosli, 1995; Seiler et al., 1992). Weighted evidence of studies of farming populations in the United States support no causal association of malignant changes with atrazine (Loosli, 1995). Two studies of a rural Italian population suggested an increase in ovarian tumours in exposed women; statistical review suggested the increase could be by chance, exposure data was unsatisfactory and no supporting evidence has been presented in other studies (Loosli, 1995). High doses of atrazine (500 and 1 000 g) were ingested in two medically documented cases of intended suicide. No signs of poisoning due to atrazine were reported, therapeutic measures were required to control the adverse effects due to the co-formulants (Loosli, 1995).

4.2 ATRAZINE IN THE ENVIRONMENT

Atrazine is a herbicide and is introduced into the environment for weed control during crop cultivation or on railway tracks (Huber, 1993). Point-source contamination arises from accidents, inadequately cleaned tools, spillage during pesticide mixing and from disposal of waste pesticide and empty containers (Gan et al., 1996; Huber, 1993). Atrazine contaminates water sources by seeping into groundwater or from runoff processes into surface water (Huber, 1993).

Atrazine persists longer in soils than other herbicides and has been the most frequently detected herbicide in groundwater in Europe (Chopra et al., 1973; Galassi et al., 1996). The half-life of atrazine in soil (the time for 50 % dissipation) varies between 14 and 109 d; degradation is usually biphasic in that initial rapid degradation occurs during the first 2 months after application and slower degradation occurs during the drier summer and cold winter months (Koskinen and Clay, 1997). Atrazine concentrations of between 0 and 10 μg L^{-1}, 0,4 and 10 μg L^{-1} and 0 and 26 μg L^{-1} have been detected in rivers in France, Austria and Germany, respectively; concentrations in rivers in the United States are usually between 0 and 20 μg L^{-1} (Huber, 1993; Solomon et al., 1996). Atrazine residues in rivers in agricultural regions are usually episodic with major peaks in spring and early summer following application (Solomon et al., 1996). The presence and persistence of atrazine in potable water sources has resulted in the regulation or banning of atrazine use in many European countries. Health standards have been set in the United States by the Environmental Protection Agency for atrazine at 3,0 μg L^{-1} and in the European Community the health advisory standard for

each triazine herbicide and metabolite is 0,1 μg L^{-1}, the total triazine concentration is not to exceed 0,5 μg L^{-1} in groundwater (Thurman et al., 1991; Thurman et al., 1994).

The role of atrazine in the environment has been reviewed in the following sections, application and usage in Section 4.2.1, persistence and degradation in soil in Section 4.2.2, persistence and degradation in aquatic systems in Section 4.2.3 and metabolism in plants in Section 4.2.4.

4.2.1 Application and usage

Atrazine is used for the control of broadleaf and some grassy weeds in maize, sorghum and sugarcane cultivation (Koskinen and Clay, 1997; Solomon et al., 1996). It can be applied before or after the emergence of weeds and generally provides season-long weed control, typically, the herbicide is applied pre-emergence as a water-dispersed spray or in liquid fertiliser (Koskinen and Clay, 1997; Solomon et al., 1996). It is sold as the active ingredient in various wettable powders or in granular formulations and is marketed under trade names such as Gesaprim® and Aatrex® (Huber, 1993). Atrazine is also used as a non-selective herbicide for weed control on railway tracks (Huber, 1993).

Atrazine is one of the most heavily used herbicides in the United States, approximately 29 000 t active ingredient was applied annually between 1987 and 1989 to about 84 % of the maize crop (Koskinen and Clay, 1997). The estimated use in 1993 was between 32 000 and 34 000 t active ingredient and in 1995 between 31 000 and 33 000 t active ingredient (Koskinen and Clay, 1997; Solomon et al., 1996).

The detection of atrazine in ground and surface water resulted in the reduction of the maximum allowable application rate of atrazine. The *Good farming practice programme* for atrazine, presented in Table 4.3, was proposed by Ciba-Geigy in 1991, it was implemented in 1992 in European Community countries that did not already have more stringent atrazine restrictions in place (Seiler et al., 1992).

Table 4.3 : *Good farming practice programme* for atrazine (Seiler et al., 1992)

Parameter	
target crops :	maize and sorghum only
maximum use rate :	1,5 kg active ingredient per hectare per year
timing of application :	pre-emergence and early post-emergence, no autumn applications
product offer :	prepack mixtures favoured compared to straight atrazine formulations

The registered application rate (as recommended on the label) of atrazine in the United States was reduced from 5,6 to 3,4 kg active ingredient per ha in 1990 and further, in 1993, to a maximum total pre- and post-emergent use rate of 2,2 to 2,8 kg active ingredient per hectare (Solomon et al., 1996).

4.2.2 Atrazine in soil

The applied atrazine tends to remain in the surface soil as it degrades, however, off-site movement has been documented (Koskinen and Clay, 1997). Movement of atrazine through soil into groundwater is affected by soil processes that vary throughout the soil profile. The two major processes that affect the amount of atrazine present in soil and the movement thereof are transformation and retention (Koskinen and Clay, 1997). Transformation processes (by partial or complete degradation) reduce or eliminate the amount of atrazine present in soil and retention processes (by adsorption) decrease or eliminate the amount of atrazine available for transport to groundwater (Koskinen and Clay, 1997).

4.2.2.1 Transformation

Atrazine is transformed in soil by chemical and microbial processes such as hydrolysis, *N*-dealkylation, deamination and ring cleavage (Kaufman and Kearney, 1970; Koskinen and Clay, 1997). The primary metabolites in the transformation of atrazine, as shown in Figure 4.3, are hydroxyatrazine (6-hydroxy-*N*-ethyl-*N*'-(1-methylethyl)-1,3,5-triazine-2,4-diamine), deethylatrazine (6-chloro-*N*-(1-methyl-ethyl)-1,3,5-triazine-2,4-diamine) and deisopropylatrazine (6-chloro-*N*-ethyl-1,3,5-triazine-2,4-diamine). These are further degraded to deethyldeisopropylatrazine (6-chloro-1,3,5-triazine-2,4-diamine), deethyl-hydroxyatrazine, deisopropylhydroxyatrazine and ammeline (Koskinen and Clay, 1997; Winkelmann and Klaine, 1991a).

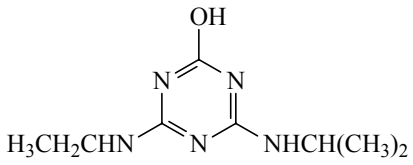

hydroxyatrazine

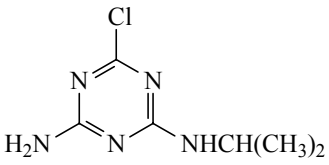

deethylatrazine

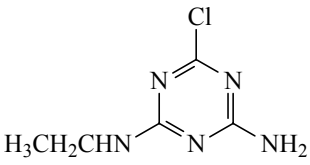

deisopropylatrazine

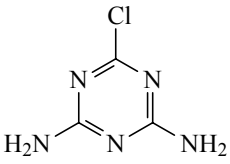

deethyldeisopropylatrazine

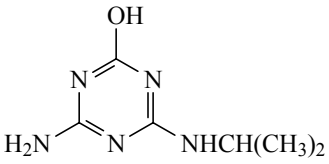

deethylhydroxyatrazine

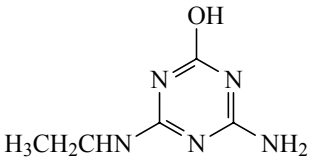

deisopropylhydroxyatrazine

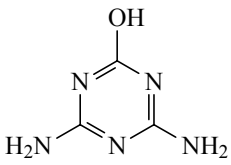

ammeline

Figure 4.3 : Primary and secondary metabolites of atrazine (Koskinen and Clay, 1997)

Atrazine is transformed in soil by adsorption-catalyzed chemical hydrolysis to hydroxyatrazine (Burkhard and Guth, 1981; Skipper et al., 1967; Skipper and Volk, 1972). The reaction follows first order reaction kinetics (Burkhard and Guth, 1981) and is dependant on factors such as pH, temperature and concentration of dissolved organic carbon (Koskinen and Clay, 1997). Burkhard and Guth found that the formation of hydroxyatrazine was greater at a lower pH, the half-life of atrazine (at 22 °C) in two German standard soils of pH 4,8 and 6,5 was 53 and 113 d, respectively (Burkhard and Guth, 1981). The hydrolysis half-life of atrazine (at 25 °C) in aqueous buffered solutions of pH 5, 7 and 9 was 64, > 200 and > 200 d, respectively (Burkhard and Guth, 1981). The degradation of atrazine is dominated by chemical transformation to hydroxyatrazine in acidic soil and by microbial transformation to *N*-dealkylation metabolites in alkaline soil (Blumhorst and Weber, 1994; Qiao et al., 1996).

The metabolites, deethylatrazine and deisopropylatrazine, are formed by microbial degradation through *N*-dealkylation of atrazine (Blumhorst and Weber, 1994; Kaufman and Kearney, 1970). The presence of both alkyl groups on the triazine ring inhibits the microbial dechlorination of atrazine, however, elimination of one or both of the alkyl groups allows for the microbial dechlorination of the metabolites producing the hydroxylated derivatives, as shown in Figure 4.3 (Behki and Khan, 1986).

Greater amounts of deethylatrazine than deisopropylatrazine are produced from the *N*-dealkylation of atrazine (Gan et al., 1996; Shapir and Mandelbaum, 1997; Winkelmann and Klaine, 1991a). Deethyl-atrazine, deisopropylatrazine and hydroxyatrazine are all formed in surface soil, however, with increasing soil depth atrazine is transformed mainly through *N*-dealkylation rather than through chemical hydrolysis (Rodriguez and Harkin, 1997; Sorenson et al., 1995). The major metabolite produced in the top 10 cm of soil is hydroxyatrazine whereas deethylatrazine is the most common metabolite produced at greater depths (Sorenson et al., 1994; Sorenson et al., 1995). Constant levels of hydroxyatrazine and deisopropylatrazine throughout the soil profile indicate that the rates of formation and degradation are relatively equal, the increasing concentration of deethylatrazine with depth indicates that it is more resistant to degradation and can accumulate over time (Sorenson et al., 1994; Sorenson et al., 1995).

The rate of atrazine degradation depends on soil and environmental factors that influence the presence and activity of atrazine-degrading microorganisms (Koskinen and Clay, 1997). These factors include atrazine, water and oxygen concentration, soil temperature, soil type, pH and organic matter content and previous soil management and crop practices (Koskinen and Clay, 1997; Skipper and Volk, 1972; Stojanovic et al., 1972). Atrazine is degraded faster at a soil temperature of 25 °C than at 10 °C, atrazine half-life is 28,4 d at 25 °C and 102,9 d 10 °C (Qiao et al., 1996). Atrazine concentration (5 to 5 000 mg kg^{-1} of soil) did not influence the rate of biodegradation in a clay loam soil (half-life < 56 d), however, degradation decreased with increasing concentration in a sandy loam soil, the half-life was 56 d at 5 mg kg^{-1} and 91 d at 5 000 mg kg^{-1} of soil (Gan et al., 1996). Atrazine is degraded more rapidly in silt loam than in clay loam or sandy loam soil, atrazine concentration after 4 months decreased to 64, 75 and 80 %, respectively, of the initial concentration in silt loam, clay loam and sandy loam soils (Sorenson et al., 1993; Sorenson et al., 1994; Sorenson et al.,

1995). Atrazine degradation is reduced during unsaturated moisture conditions, 22 % of initial atrazine remained after 60 d under saturated conditions whereas 34 % remained under unsaturated conditions (Kruger et al., 1997).

Atrazine degradation is slower in subsurface soil (Lavy et al., 1973; Miller et al., 1997; Shapir and Mandelbaum, 1997). Lavy and co-workers found that the phytotoxicity of atrazine in a silty clay loam soil dissipated within 5 months at a depth of 15 cm, within 17 months at a depth of 40 cm and no dissipation occurred after 41 months at a depth of 90 cm (Lavy et al., 1973). Shapir and Mandelbaum found that after 30 d of incubation more than 50 % of atrazine in surface soil had degraded whereas less than 33 % had degraded in soil from a depth below 50 cm (Shapir and Mandelbaum, 1997). Atrazine degradation is greater in soil that has a history of atrazine treatment. Vanderheyden and co-workers found that the half-life of atrazine in soil, typically between 35 and 50 d, was reduced to between 5 and 10 d in maize fields that had been treated annually with atrazine for more than five years (Vanderheyden et al., 1997).

The factors that affect the degradation of atrazine also affect the degradation of the primary metabolites of atrazine. Deethylatrazine degrades slower in subsoil than surface soil and is also lower under saturated than unsaturated moisture conditions (Kruger et al., 1997). The degradation of deethylatrazine, deisopropyl-atrazine, deethyldeisopropylatrazine and hydroxyatrazine follow first order reaction kinetics, 2 % of the deethylatrazine and 2 % of the deisopropylatrazine, 33 % of the hydroxyatrazine and no deethyldeisopropyl-atrazine was found to remain in soil 180 d after application (Winkelmann and Klaine, 1991b). The soil half-lives of atrazine, deethylatrazine, deisopropylatrazine, deethyldeisopropylatrazine and hydroxyatrazine were 21, 26, 17, 19 and 121 d, respectively, under similar conditions (Winkelmann and Klaine, 1991b).

Mineralisation of atrazine to carbon dioxide involves cleavage of the triazine ring. Early investigations found that the triazine ring was not readily broken by soil microorganisms and the formation of $^{14}CO_2$ from ring-labeled atrazine in soil was generally low. Skipper and co-workers found that approximately 0,4 to 0,5 % $^{14}CO_2$ evolved from ring-labeled atrazine in a sandy loam and silty clay loam soil after a 14 d incubation period (Skipper et al., 1967). Kruger and co-workers found that less than 1 % of the applied ^{14}C had mineralised after a 120 d period (Kruger et al., 1997). Skipper and Volk measured a 0,1 % formation of $^{14}CO_2$ from ring-labeled atrazine after a 14 d incubation period and Dao and co-workers found that the formation of $^{14}CO_2$ was less than 0,5 % after an 8 month incubation period (Dao et al., 1979; Skipper and Volk, 1972). Amounts of carbon dioxide evolved in the mineralisation of atrazine range from 0,05 % within 3 months to 1 % per month (Geller, 1980). Higher rates of atrazine mineralisation have been reported for soils that have a history of atrazine application (Vanderheyden et al., 1997; Winkelmann and Klaine, 1991a). Gan and co-workers found that an average of 64 % mineralisation occurred after 140 d for atrazine concentrations of between 5 and 500 mg kg^{-1} of soil (Gan et al., 1996). The degradation products of atrazine are more easily biodegradable than the parent compound (Geller, 1980). Mineralisation of ring-labeled ^{14}C

deethylatrazine, deisopropylatrazine and hydroxyatrazine yielded 25, 16 and 21 %, respectively, of $^{14}CO_2$ after 180 d (Winkelmann and Klaine, 1991b).

The atrazine-ring carbon atoms are in the same oxidation state as in carbon dioxide and cannot be used by microorganisms as a source of carbon or energy for growth, however, energy can be obtained from the oxidation of the carbon atoms in the side chains substituted on the *s*-triazine ring (Cook, 1987). Atrazine is usually utilised as a nitrogen source for microbial growth when carbon and energy are supplied by other substrates (Cook, 1987).

Microbial strains that can mineralise atrazine, especially in soils with a prolonged history of annual atrazine application, have been identified (Behki and Khan, 1986). Mirgain and co-workers identified three bacterial species (*Sphingomonas paucimobilis*, *Sphingobacterium multivorum* and *Agrobacterium radiobacter*) that together, but not individually, could degrade atrazine (Mirgain et al., 1995). Behki and Khan identified three strains of *Pseudomonas* (*Pseudomonas putida*, *Pseudomonas fluorescens* and *Pseudomonas stutzeri*) that degraded atrazine via *N*-dealkylation to deethylatrazine and deisopropylatrazine (Behki and Khan, 1986). Two of the species could dechlorinate deethylatrazine and deisopropylatrazine (but not atrazine) following incubation in glucose-supplemented mineral salts medium (Behki and Khan, 1986). Shapir and Mandelbaum demonstrated that a *Pseudomonas* strain completely degraded atrazine, between 90 and 100 % mineralisation occurred in soil within 15 d after inoculation with the *Pseudomonas* strain (Shapir and Mandelbaum, 1997). The first step in the mineralisation was dechlorination to hydroxyatrazine (Shapir and Mandelbaum, 1997).

Mirgain and co-workers, in an investigation in north-eastern France, isolated several aerobic gram-negative bacteria that were capable of metabolising atrazine in association with other species or in pure culture (Mirgain et al., 1993). The degradation curves consisted of three phases, an adaptive period in which degradation was slow or absent, a rapid degradation phase in which 80 % of the pesticide was consumed over a few days and the final stage in which the degradation of the remaining atrazine was again slow (Mirgain et al., 1993). Isolates from agricultural soil samples indicated that atrazine was degraded by *Acinetobacter calcoaceticus* in pure culture and by a combination of *Pseudomonas alcaligenes* and an *Agrobacterium* species. Atrazine was also degraded by a consortium of microorganisms from a garden soil sample (*Pseudomonas fluorescens*, *Pseudomonas putida*, *Flavobacterium multivorum*, *Enterobacter cloacae* and an *Acinetobacter* species). No microbial species in a groundwater sample were found that degraded atrazine whereas two species (*Pseudomonas putida* and *Xanthomonas maltophilia*) were identified in a surface water sample (Mirgain et al., 1993). Giardi and co-workers demonstrated that a *Nocardia* 10strain was capable of degrading atrazine, degradation (as shown in Figure 4.4) was through *N*-dealkylation and deamination yielding dicyanodiamidine (Giardi et al., 1985).

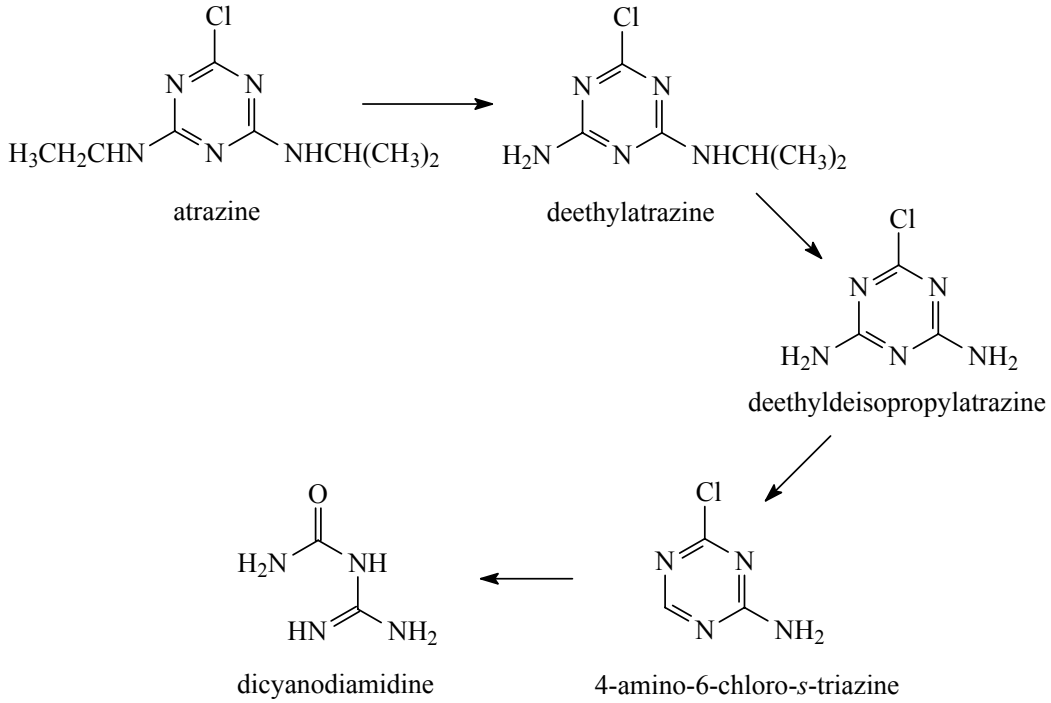

Figure 4.4 : Microbial degradation of atrazine by a *Nocardia* strain (Giardi et al., 1985)

The biodegradation pathway of atrazine is presented in Figure 4.5. Biodegradation is predominantly through *N*-dealkylation to deethylatrazine and deisopropylatrazine even though Shapir and Mandelbaum showed that atrazine can be dechlorinated to hydroxyatrazine by a *Pseudomonas* strain (Erickson and Lee, 1989; Shapir and Mandelbaum, 1997). Several pathways exist for subsequent degradation of deethylatrazine and deisopropylatrazine, as shown in Figure 4.5, these depend on the order in which dechlorination, deamination and further dealkylation take place. Behki and Khan found that dechlorination occurred first in the degradation by two *Pseudomonas* bacterial strains whereas Giardi and co-workers found, as shown in Figure 4.4, that dealkylation and deamination occurred before dechlorination in the degradation by a *Nocardia* bacterial strain (Behki and Khan, 1986; Giardi et al., 1985). Degradation through ammeline, ammelide and cyanuric acid was caused by a *Pseudomonas* species strain A (Jutzi et al., 1982). The different degradation pathways, as shown in Figure 4.5, converge with the formation of cyanuric acid (Cook et al., 1985; Cook, 1987). Two soil fungi (*Stachybotrys chartarum* and *Hendersonula toruloidea*), a *Pseudomonas* species strain D and a facultative anaerobic bacterium have been shown to degrade cyanuric acid (Cook et al., 1985; Jessee et al., 1983; Wolf and Martin, 1975). Ring cleavage of cyanuric acid, as shown in Figure 4.5, produces biuret that is further degraded to urea and then to carbon dioxide and ammonia (Cook et al., 1985). Three moles of CO_2 and three moles of NH_4^+ are produced per mol of cyanuric acid (Cook et al., 1985).

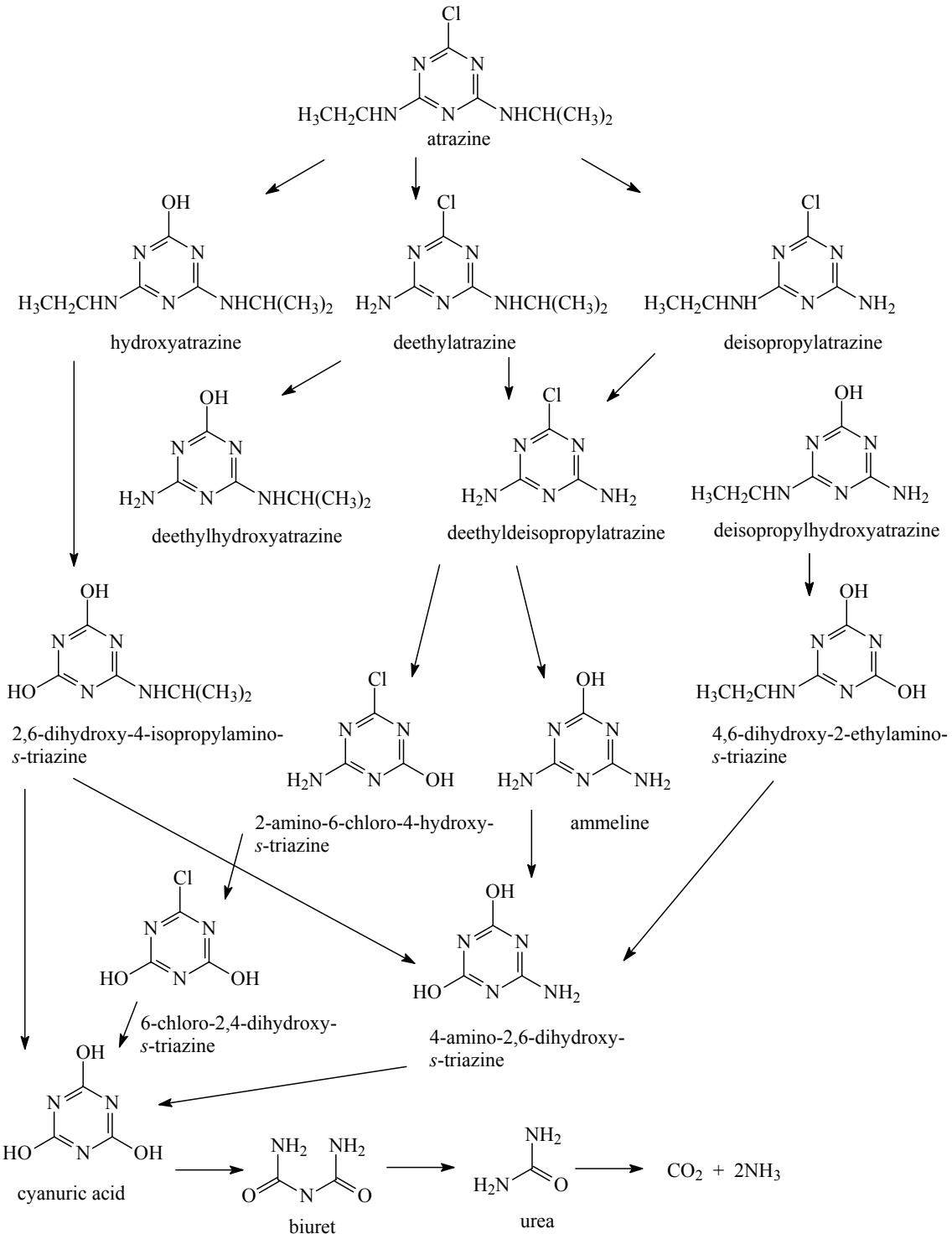

Figure 4.5 : Mineralisation pathway of atrazine (Erickson and Lee, 1989; Koskinen and Clay, 1997)

4.2.2.2 Retention

Retention is defined as the restriction or retardation of mobility of a chemical in soil because of the interaction of the chemical with the surface of a soil particle (Cheng, 1990). Retention of atrazine in soil

decreases the amount available for weed control, microbial transformation and the amount that can move to greater soil depths leading to groundwater contamination (Koskinen and Clay, 1997). Typically between 50 and 80 % of atrazine under slurry conditions is retained in silt loam, loam or clay loam surface soils (Koskinen and Clay, 1997). The energy required and available for desorption determines whether the retention process is reversible or irreversible (Cheng, 1990).

Different binding mechanisms are involved in the retention of atrazine and its metabolites in soil, the binding mechanisms or binding strengths change with time, more atrazine was extracted from soil after 35 d than after 138 d using methanol or supercritical fluid extraction (Koskinen et al., 1995). Mechanisms such as ion exchange, metal complexation, covalent bonding, hydrogen bonding, van der Waals forces and physical trapping have been postulated for the retention of atrazine in soil (Bailey and White, 1970; Cheng, 1990; Chopra et al., 1973). Cheng proposed that hydrogen bonding (the partial transfer of charge between an electron donor and acceptor) could be a major force in the binding of atrazine to soil (Cheng, 1990). Welhouse and Bleam evaluated the hydrogen-bonding potential of atrazine by measuring formation constants for hydrogen-bond complexation with hydrogen-bond donors and acceptors typically found in organic matter in soil (Welhouse and Bleam, 1993a; Welhouse and Bleam, 1993b). Atrazine was found to form strong co-operative hydrogen bonds with compounds such as pyrrolidinone and acetic acid because of the favourable geometry for orbital overlap and the ability of both molecules to redistribute electronic charge and reinforce complexation (Welhouse and Bleam, 1993b). The most stable bound residues of atrazine in soil are associated with humified organic matter (Koskinen and Clay, 1997).

Atrazine adsorption is dependant upon factors such as organic carbon content, soil clay content, soil type, pH, atrazine concentration and atrazine-soil contact time (Bailey and White, 1970; Koskinen and Clay, 1997). The formation of soil-bound residues of atrazine decreases in subsoil. Kruger and co-workers found that after 120 d soil-bound residues in the surface soil accounted for between 62 and 73 % of the applied atrazine and in the subsoil for between 13 and 22 % of the applied atrazine (Kruger et al., 1997). Miller and co-workers found that more than 50 % of the applied atrazine after 6 months at a depth of 45 cm was still unbound and untransformed and at a depth of 75 cm almost 80 % was unbound and untransformed (Miller et al., 1997). Atrazine adsorption increases with contact time with soil (Dao et al., 1979; Miller et al., 1997) and with increasing soil organic matter and clay content (Burkhard and Guth, 1981; Chopra et al., 1973; Koskinen and Rochette, 1996). Atrazine adsorption is greater at lower pH values, more atrazine was adsorbed to soil in the pH range 4 to 6 than to soil of pH 7 or greater (Clay and Koskinen, 1990; Koskinen and Clay, 1997). Atrazine adsorption increased in sand as moisture content increased from 4 to 16 % and in silt loam as moisture increased from 9,6 to 27 % (Koskinen and Rochette, 1996).

The adsorption characteristics of atrazine metabolites are different to those of atrazine. Hydroxyatrazine was more strongly adsorbed to soil than atrazine (Clay and Koskinen, 1990; Dao et al., 1979). Seybold and Mersie found that the adsorption of atrazine and its major metabolites decreased in the order hydroxyatrazine > atrazine > deisopropylatrazine > deethylatrazine (Seybold and Mersie, 1996). The desorption process

decreased in the order deethylatrazine > atrazine and deisopropylatrazine > hydroxyatrazine (Seybold and Mersie, 1996). Both adsorption and desorption influence the mobility of a chemical in soil, high adsorption and low desorption restrict the mobility and the potential of a chemical to leach through the soil column. Seybold and Mersie ranked the overall order of decreasing mobility as deethylatrazine > deisopropylatrazine > atrazine > hydroxyatrazine (Seybold and Mersie, 1996). Kruger and co-workers, in an investigation of five Iowa soils, identified three mobility groups for atrazine and selected metabolites: most mobile - deethylatrazine; intermediate mobility - atrazine, deisopropylatrazine and deethyldeisopropylatrazine; nearly immobile - hydroxyatrazine and ammeline (Kruger et al., 1996).

4.2.3 Atrazine in aquatic systems

Atrazine has been detected in both groundwater and surface water systems (Huber, 1993; Koskinen and Clay, 1997; Solomon et al., 1996). Atrazine contamination of aquatic systems is particularly widespread where maize is the dominant crop such as in the Midwestern United States (Solomon et al., 1996). The persistence and mobility of atrazine and metabolites such as deethylatrazine in soil allow for leaching into groundwater (Sorenson et al., 1994). Atrazine contamination of surface water systems is caused by runoff following precipitation or irrigation of agricultural fields (Huber, 1993).

4.2.3.1 Groundwater

Atrazine has the potential to contaminate groundwater because of its persistence and mobility in soil. Measurements of atrazine half life in soil range between 14 and 109 d (Koskinen and Clay, 1997). Sorenson and co-workers found that the amount of atrazine persisting 16 months after treatment was 32, 24 and 22 %, respectively, in clay loam, silt loam and a sandy loam soil (Sorenson et al., 1993; Sorenson et al., 1994; Sorenson et al., 1995). Gan and co-workers and Sorenson and co-workers found that atrazine moved to a depth of 70 to 80 cm within the first month after application (Gan et al., 1996; Sorenson et al., 1994). Atrazine movement to this depth in clay loam was due to macroporous water flow (macropores are caused by roots and earthworm burrows); insufficient water from precipitation (2,3 cm in 4 increments) and irrigation (5 cm in 2 increments) was available to move the atrazine to such a depth unless macroporous flow occurred (Sorenson et al., 1994). The rate of atrazine leaching is soil dependent, the greater water holding capacity of silt loam and clay loam allows for greater atrazine movement (Sorenson et al., 1995). Leachate collected from an 80 cm clay loam column 16 months after treatment contained 0,04 % of the applied atrazine (Sorenson et al., 1994). The metabolites most likely to leach into groundwater because of their lower retention in soil are deethylatrazine, the dominant metabolite in subsoil, and deisopropylatrazine (Koskinen and Clay, 1997; Kruger et al., 1996).

A representative survey of the groundwater of the United States by the US Environmental Protection Agency recorded atrazine concentrations of between 0,18 and 1,04 $\mu g\ L^{-1}$; half of the tested wells showed concentrations below 0,28 $\mu g\ L^{-1}$ (Huber, 1993). The maximum concentration recorded in wells in the Netherlands, Switzerland and Germany was 0,58; 1,34 and 3,1 $\mu g\ L^{-1}$, respectively; the higher values were found in shallow wells in the vicinity of intensive agricultural production (Huber, 1993). The concentrations

of atrazine, deethylatrazine and deisopropylatrazine measured in groundwater at Dalmine, Italy, in June 1995 were 0,232; 0,045 and 0,058 μg L^{-1}, respectively (Galassi et al., 1996).

Significant degradation of atrazine and its metabolites does not occur in groundwater because of the low microbial populations, low amount of dissolved organic carbon (below 1 mg of carbon L^{-1}) and temperatures below 10 °C (Mirgain et al., 1993). Rodríguez and Harkin found that more than 85 % of atrazine in groundwater was still present after 270 d (Rodríguez and Harkin, 1997). The atrazine concentration in a well in the Lombardy area in Italy (where atrazine use has been banned since 1986) was in the range of 0,25 to 0,46 μg L^{-1} between February and December 1987 (monitored monthly) and between 0,147 and 0,232 μg L^{-1} between May and July 1995 (Galassi et al., 1996). The resistance of deethylatrazine to degradation in subsoil indicates that it is just as persistent as atrazine in groundwater (Rodríguez and Harkin, 1997).

4.2.3.2 Surface water

Atrazine contamination of surface water is caused by runoff following precipitation and irrigation of agricultural fields (Huber, 1993). Losses due to runoff range between 0,1 and 7,7 % of the applied atrazine, the loss in a year with average rainfall is typically 1,2 % (Gaynor et al., 1992; Gaynor et al., 1995). Atrazine transport in runoff occurs throughout the year but losses are higher during the growing season when runoff occurs soon after herbicide application (Gaynor et al., 1992).

Atrazine concentrations of between 0 and 87 μg L^{-1} have been detected in rivers in the United States, concentrations, however, rarely exceeded 20 μg L^{-1} (Huber, 1993; Solomon et al., 1996). Atrazine concentration in rivers in France ranges between 0 and 10 μg L^{-1}, in Austria between 0,4 and 10 μg L^{-1} and in Germany between 0 and 26 μg L^{-1}, the mean concentration levels are significantly lower than the upper peak values (Huber, 1993). The atrazine concentration in standing freshwater systems (ponds, natural lakes and reservoirs) is lower than that in flowing water; for example, in Germany, most of the detected atrazine concentration in standing freshwater systems is below 0,1 μg L^{-1} (Huber, 1993). Atrazine concentration in surface water in the United States is highest in the first two months after application in early summer (late spring and early summer rainfall flushes atrazine from croplands) and decreases during autumn and winter months (Thurman et al., 1991; Thurman et al., 1992). Atrazine is also found to persist from year to year in both soil and water (Thurman et al., 1991).

Atrazine metabolites such as deethylatrazine and deisopropylatrazine have been detected in surface runoff and surface water systems (Gaynor et al., 1995; Thurman et al., 1991). Metabolite concentrations in surface water is dependant on the hydrologic conditions of the basin and timing of runoff; early rains and a dry summer leads to an peak of metabolites in surface water, a wet summer delays but increases the maximum metabolite concentration (Thurman et al., 1994). The deethylatrazine peak concentration occurs later in the season than the atrazine peak concentration (Gaynor et al., 1992). The investigation by Thurman and co-workers of the surface water systems in the Midwestern maizebelt of the US found that the ratio of

deisopropylatrazine to deethylatrazine was approximately 0,6 and that the ratio of deethylatrazine to atrazine, 2 months after application, varied between 0,5 and 0,7 (Thurman et al., 1994). The persistence of atrazine and its metabolites in surface water in the United States decreases in the order of atrazine, deethylatrazine and deisopropylatrazine (Thurman et al., 1991; Thurman et al., 1992). The concentration of metabolites is greater in standing water than in flowing water; hydroxyatrazine, although not detected in flowing water, has been detected in Midwestern reservoirs in the United States (Solomon et al., 1996).

Deethylatrazine and deisopropylatrazine are also formed, as shown in Figure 4.6, from the degradation of other triazine herbicides such as simazine, cyanazine and propazine (Thurman et al., 1994). The investigation by Thurman and co-workers of the surface water systems in the Midwestern maizebelt of the United States found that deethylatrazine was formed predominantly from atrazine (98 %) with trace levels derived from propazine; deisopropylatrazine was formed from atrazine (75 %), cyanazine (25 %) and trace levels from simazine (Thurman et al., 1994). Atrazine is the most widely used triazine herbicide, over 2,5 times more atrazine than cyanazine was found by Thurman and co-workers to be applied on a regional scale, propazine had already been removed from the US market (Thurman et al., 1994).

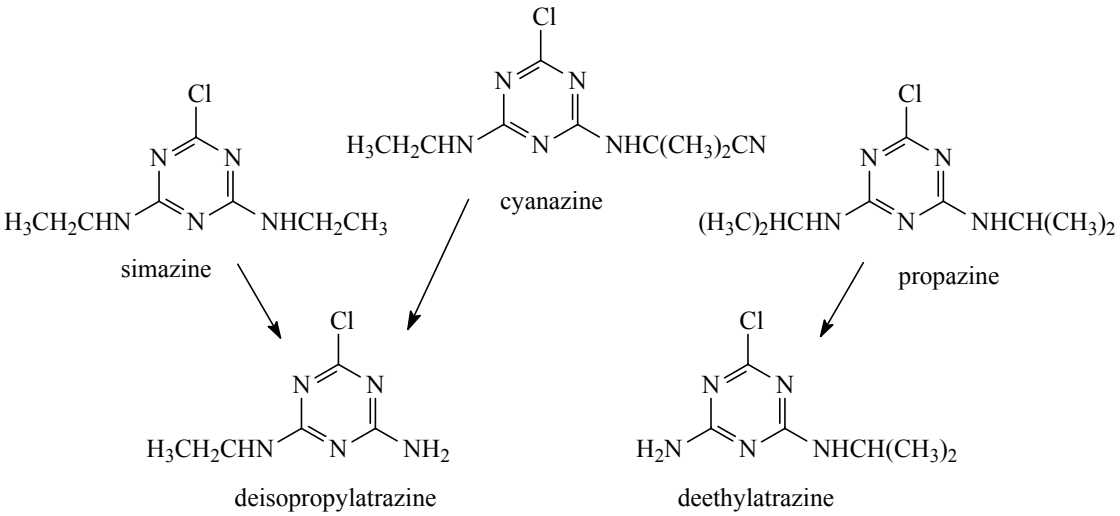

Figure 4.6 : Formation of deethylatrazine and deisopropylatrazine from simazine, cyanazine and propazine (Thurman et al., 1994)

Surface water ecosystems may be affected by the long term presence of atrazine and its metabolites. The two mechanisms by which atrazine is taken up by aquatic organisms are adsorption from water or uptake via the food chain (Huber, 1993). The investigation by Ellgehausen and co-workers of a model aquatic food chain consisting of an algae (*Scenedesmus acutus*), daphnid (*Daphnia magna*) and catfish (*Ictalurus melas*) species found that direct uptake from water was significantly more important than transfer of atrazine residues via the food chain (Ellgehausen et al., 1980). Atrazine is taken up by nearly all aquatic organisms, however, a large portion of the adsorbed atrazine is eliminated quickly by the organisms (Huber, 1993). Ellgehausen

and co-workers found that the degradation of atrazine in the investigated algae, daphnid and catfish species followed second order reaction kinetics (Ellgehausen et al., 1980).

Phytoplanktons are the most sensitive organisms to atrazine in aquatic ecosystems (freshwater and saltwater), followed in decreasing order of sensitivity by macrophytes, benthic invertebrates, zooplankton and fish (Solomon et al., 1996). Phytoplankton biomass and production rates are unaffected by exposure to atrazine concentrations below 20 μg L^{-1}, ecologically important effects occur only with exposure to concentrations above 50 μg L^{-1} (Solomon et al., 1996). The investigation, initiated by the Environmental Protection Agency, of the ecological risk of atrazine in North American surface waters concluded that atrazine did not pose a significant risk to the aquatic environment (Solomon et al., 1996). It was recommended that site-specific assessments be performed of the inhibitory effects of atrazine on algae, phytoplankton or macrophyte production in small streams that are vulnerable to agricultural runoff (Solomon et al., 1996). The review by Huber on the ecotoxicological relevance of atrazine in aquatic systems concluded that the potential hazard of atrazine in the environment depended on the concentration and degree of exposure, atrazine concentrations of up to 20 μg L^{-1} would not cause any permanent damage to aquatic ecosystems (Huber, 1993).

4.2.4 Mode of action in plants

Atrazine is readily taken up by all plants, take up is primarily through roots and foliage (Esser et al., 1975; Solomon et al., 1996). Plant uptake of atrazine increases with increasing atrazine concentration, time of exposure, higher temperatures and low relative humidity (Esser et al., 1975). Atrazine take-up in maize plants 2 months after treatment was found to be greater in sandy loam (3,6 % of applied atrazine) than in clay loam (2,9 % of applied atrazine) even though organic content levels in the soil were similar and soil pH in the sandy loam was lower than in the clay loam (Sorenson et al., 1993; Sorenson et al., 1994). Atrazine take-up in maize plants is also greater in silty loam that in clay loam (Sorenson et al., 1995).

Atrazine is not toxic to plants in the dark, it thus interferes with the photosynthesis process in plants (Esser et al., 1975). Atrazine inhibits photosynthesis by interrupting the light-driven flow of electrons from water to NADP, nicotinamide adenine dinucleotide phosphate (Esser et al., 1975). Chlorophyll molecules are oxidized by light energy during photosynthesis. Replacement electrons for the oxidized chlorophyll molecules (as shown in Figure 4.7) are obtained from the cleavage of water with oxygen being produced as a by-product, the reaction is known as the *Hill reaction* (Ebert and Dumford, 1976; Solomon et al., 1996). Atrazine inhibits the *Hill reaction* and competes with plastoquinone at its binding site thus blocking the transport of electrons from photosystem II (Ebert and Dumford, 1976; Solomon et al., 1996).

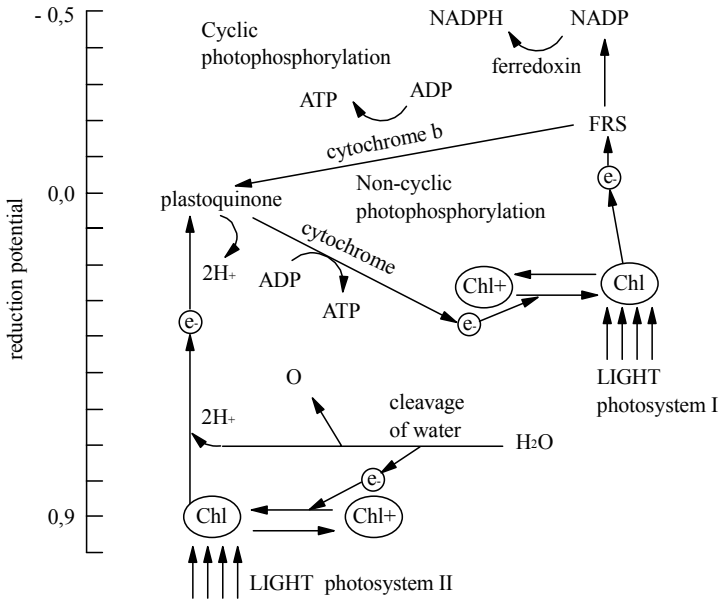

Figure 4.7 : Photophosphorylation (Solomon et al., 1996)

Inhibition of the *Hill reaction* leads to the destruction of the chlorophyll molecules in photosystem II since, without replacement electrons from water, the light-induced electron flow occurs until all of the chlorophyll molecules are oxidized (Solomon et al., 1996). The blockage of electron flow from photosystem II causes photophosphorylation (the production of ATP), reduction of photosystem I chlorophyll molecules, cyclic photophosphorylation and the production of NADPH to cease (Solomon et al., 1996). The binding of atrazine to the plastoquinone II binding site is reversible since photosynthetic activity increased in plants removed from atrazine-contaminated growing medium (Solomon et al., 1996).

The phytotoxicity of atrazine is reduced by degradation, dechlorination metabolites are non-toxic and *N*-dealkylation metabolites are less toxic than atrazine (Harris, 1967; Kaufman and Kearney, 1970). Stratton found that atrazine was more inhibitory to growth and photosynthesis in two species of green algae and three species of cyanobacteria than hydroxyatrazine, deethylatrazine, deisopropylatrazine and deethyldeisopropylatrazine (Stratton, 1984). Deethylatrazine and deisopropylatrazine are the most toxic transformation products for plants. Atrazine is between 7 to 10 and 20 to 50 times more inhibitory to cyanobacteria, respectively, than deethylatrazine and deisopropylatrazine, similarly, atrazine is between 4 to 6 and 7 to 13 times more inhibitory to green algae than these metabolites (Stratton, 1984). Hydroxyatrazine and deethyldeisopropylatrazine are relatively non-toxic, atrazine is between 200 and 1 000 times more toxic than either of these metabolites (Stratton, 1984).

Plants such as maize possess efficient detoxification mechanisms for atrazine (Ebert and Dumford, 1976). Three possibly pathways for atrazine detoxification in maize are hydroxylation, *N*-dealkylation and glutathione conjugation (Ebert and Dumford, 1976; Shimabukuro, 1967; Shimabukuro et al., 1970). The

presence of benzoxazinone (2,4-dihydroxy-7-methoxy-1,4-benzoxazin-3-one) in maize leads to the hydroxylation of atrazine producing hydroxyatrazine (Esser et al., 1975; Shimabukuro, 1967). Raveton and co-workers found that the reaction followed first order reaction kinetics and proposed the reaction pathway shown in Figure 4.8 (Raveton et al., 1997a).

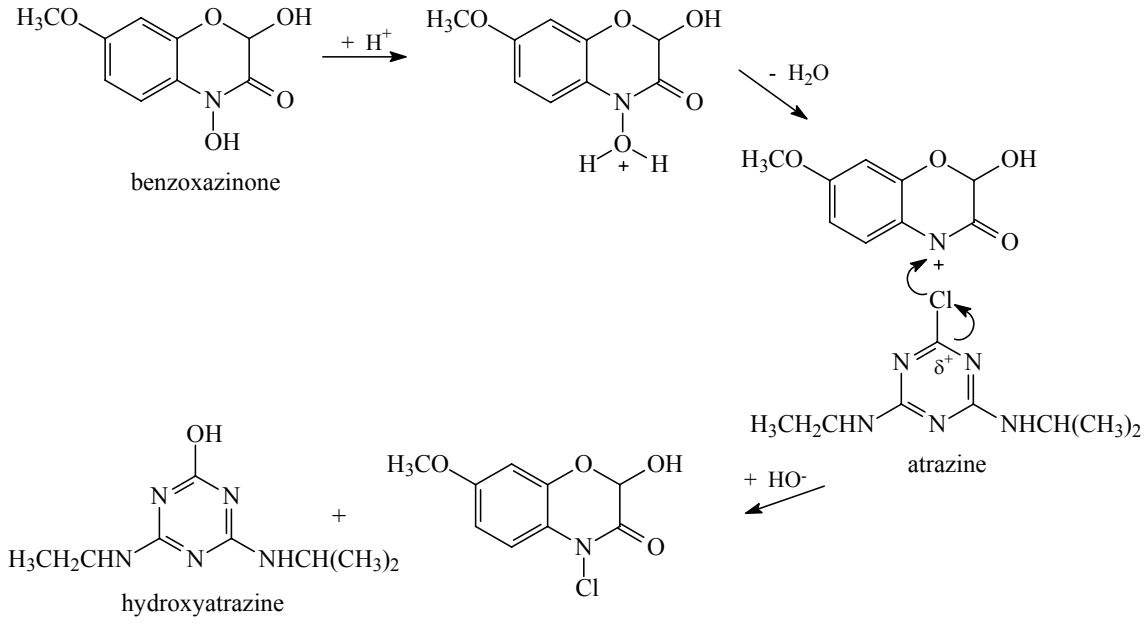

Figure 4.8 : Reaction pathway of atrazine hydroxylation in maize (Raveton et al., 1997a)

Raveton and co-workers found that after 72 h less than 5 % of applied atrazine was still present as atrazine in extracts of roots and shoots of maize seedlings, most atrazine had been transformed to hydroxyatrazine and small quantities of deethylhydroxyatrazine and deisopropylhydroxyatrazine (Raveton et al., 1997b).

The displacement of the 6-chloro group in atrazine with glutathione also reduces the toxicity of atrazine (Lamoureux et al., 1972). The glutathione conjugate of atrazine, shown in Figure 4.9, has been identified in maize and sorghum leaves (Lamoureux et al., 1972; Shimabukuro et al., 1970). It is formed by an enzymatic reaction catalysed by glutathione *s*-transferase (Shimabukuro et al., 1971). Shimabukuro and co-workers found that within 24 h between 60 and 80 % of applied atrazine to leaf blades of six maize varieties was converted to the glutathione conjugate of atrazine (Shimabukuro et al., 1971).

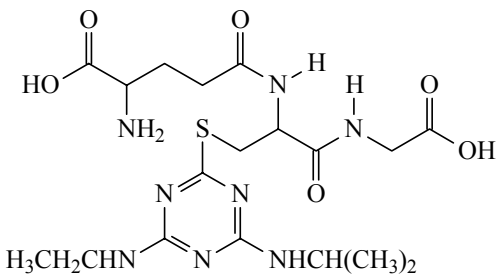

Figure 4.9 : Glutathione conjugate of atrazine in maize leaves (Lamoureux et al., 1972)

Atrazine hydroxylation (which occurs mainly in the roots) and glutathione conjugation (which occurs only in the leaves) are independent processes (Raveton et al., 1997a; Raveton et al., 1997b). Hydroxylation is the dominant atrazine detoxification process in maize plants, the relative importance of glutathione conjugation is greater with post-emergence herbicide treatment (Raveton et al., 1997a; Raveton et al., 1997b).

4.3 ATRAZINE IN WATER TREATMENT

A comparative study of four disinfection methods (chlorine, monochloramine, chlorine dioxide and ozone) and an evaluation of the effectiveness of granular activated carbon versus sand filtration for chemical contaminant removal was performed over a year at Jefferson Parish, on the mouth of the Mississippi river, in the United States (Lykins and Koffskey, 1986; Lykins et al., 1986). The raw water, after clarification and filtration, was split into five process streams, one for each of the disinfection methods and a control without any disinfection. The disinfection process streams consisted of a contact chamber, the contact time was approximately 30 min, followed by parallel filtration through a sand column, a granular activated carbon column and a duplicate granular activated carbon column. The control non-disinfection stream did not have a contact chamber but was also split into three parallel filtration streams. The influent concentration of atrazine ranged from 23 to 249 ng L^{-1} and was not affected by chlorine dioxide, chloramine or chlorine disinfection whereas ozone disinfection reduced the atrazine concentration, on average, by 83 %. Atrazine concentration was unchanged after sand filtration, however, filtration through the granular activated carbon column removed between 95 and 97 % of the atrazine throughout the 1 year operational period (Lykins and Koffskey, 1986; Lykins et al., 1986).

A South African study investigated the fate of organic micropollutants in a pilot-scale integrated effluent treatment/water reclamation system consisting of a denitrification reactor, a chemical clarifier, a combined nitrification pond and biological clarifier, prechlorination, dual media filtration, granular activated carbon adsorption and final chlorination (van Rensburg et al., 1981). The atrazine concentration through the system, relative to the feedwater, was 81 % after denitrification, 64 % after the chemical clarifier, 60 % after the biological clarifier, 53 % after prechlorination, 62 % after dual media filtration and 0 % after adsorption with granular activated carbon (van Rensburg et al., 1981). An investigation of a pilot plant consisting of a clarifier, rapid sand filter, ozonation tank and slow sand filter indicated that the atrazine concentration was not reduced by flocculation and coagulation in the clarifier but was partly reduced (by between 30 and 45 %) after the ozonation tank (Montiel and Welté, 1992). Atrazine concentration in the effluent from an agrochemical formulation plant has been reduced from 6 300 mg L^{-1} to below 0,1 mg L^{-1} in an integrated chemical/biological oxidation system consisting of an aerobic fluidised bed, an aerobic trickling filter, a chemical oxidation reactor for ozonation and catalysed hydrogen peroxide oxidation, an anaerobic fixed bed filter, ultrafiltration modules and reverse osmosis and nanofiltration membranes (Haverhoek et al., 1997). An investigation of a nanofiltration pilot plant at the Méry-sur-Oise water treatment plant in France indicated

that nanofiltration, for initial atrazine concentrations of between 0 and 900 ng L^{-1}, reduced the concentration by between 80 and 90 % (Agbekodo et al., 1996).

Activated carbon and advanced oxidation processes, such as ozone, are some of the most effective processes for reducing atrazine concentration in water treatment (Adams and Randtke, 1992b). Atrazine is strongly adsorbed by activated carbon, however, naturally occurring organic matter competes with atrazine and lowers the adsorptive capacity (Adams et al., 1990). Breakthrough of granular activated carbon filters can occur rapidly (Duguet et al., 1990). Advanced oxidation technologies involve the generation of highly reactive radical intermediates, particularly hydroxyl radicals (Beltrán et al., 1998). The reaction pathway proposed by Chan and co-workers for the acid and alkaline hydrolysis of atrazine is shown in Figure 4.10 (Chan et al., 1992).

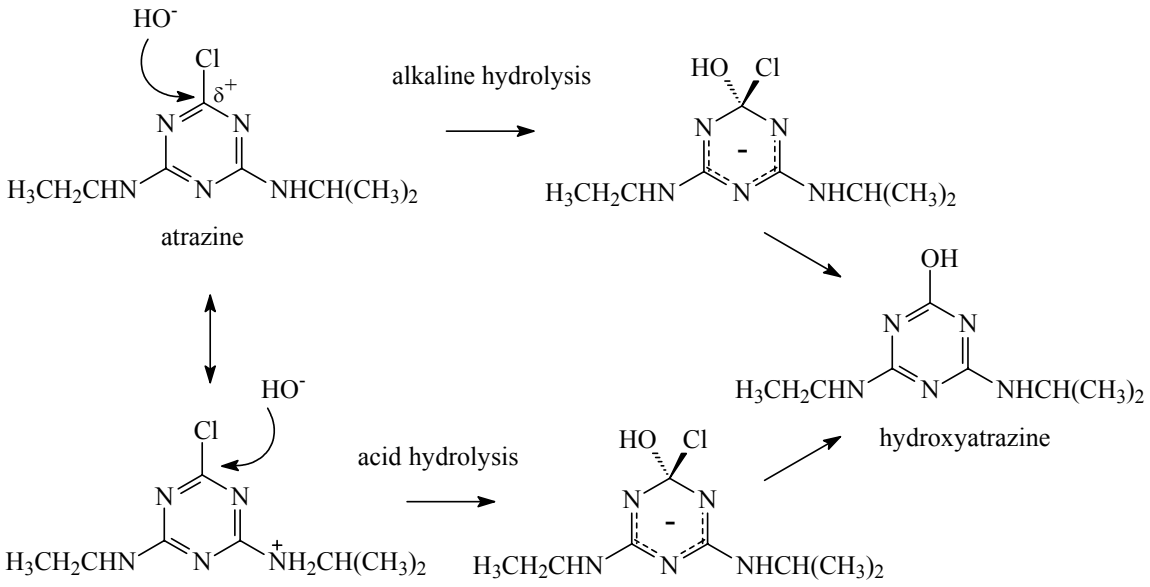

Figure 4.10 : Acid and alkaline hydrolysis of atrazine (Chan et al., 1992)

Chan and co-workers proposed that alkaline hydrolysis was a two-step nucleophilic displacement of chlorine by hydroxyl ions and that the acid hydrolysis proceeded via protonation at one of the side-chain nitrogen atoms (Chan et al., 1992). The C-Cl bond is readily broken (45,2 kJ mol^{-1}) because of the electron deficiency of the ring carbon atoms and the electron withdrawing nature of the chlorine atom. The carbon atoms in a triazine ring are slightly positively charged because the π-electrons are not evenly distributed over the ring but are localised in the vicinity of the nitrogen atoms (Esser et al., 1975; Paris and Lewis, 1973).

Atrazine reaction with hydroxyl radicals also occurs at the site of the side chains producing dealkylated products. The mechanism proposed by Hapeman and co-workers for the formation of dealkylated products from the reaction of atrazine with hydroxyl radicals in the presence of oxygen is shown in Figure 4.11 (Hapeman et al., 1995).

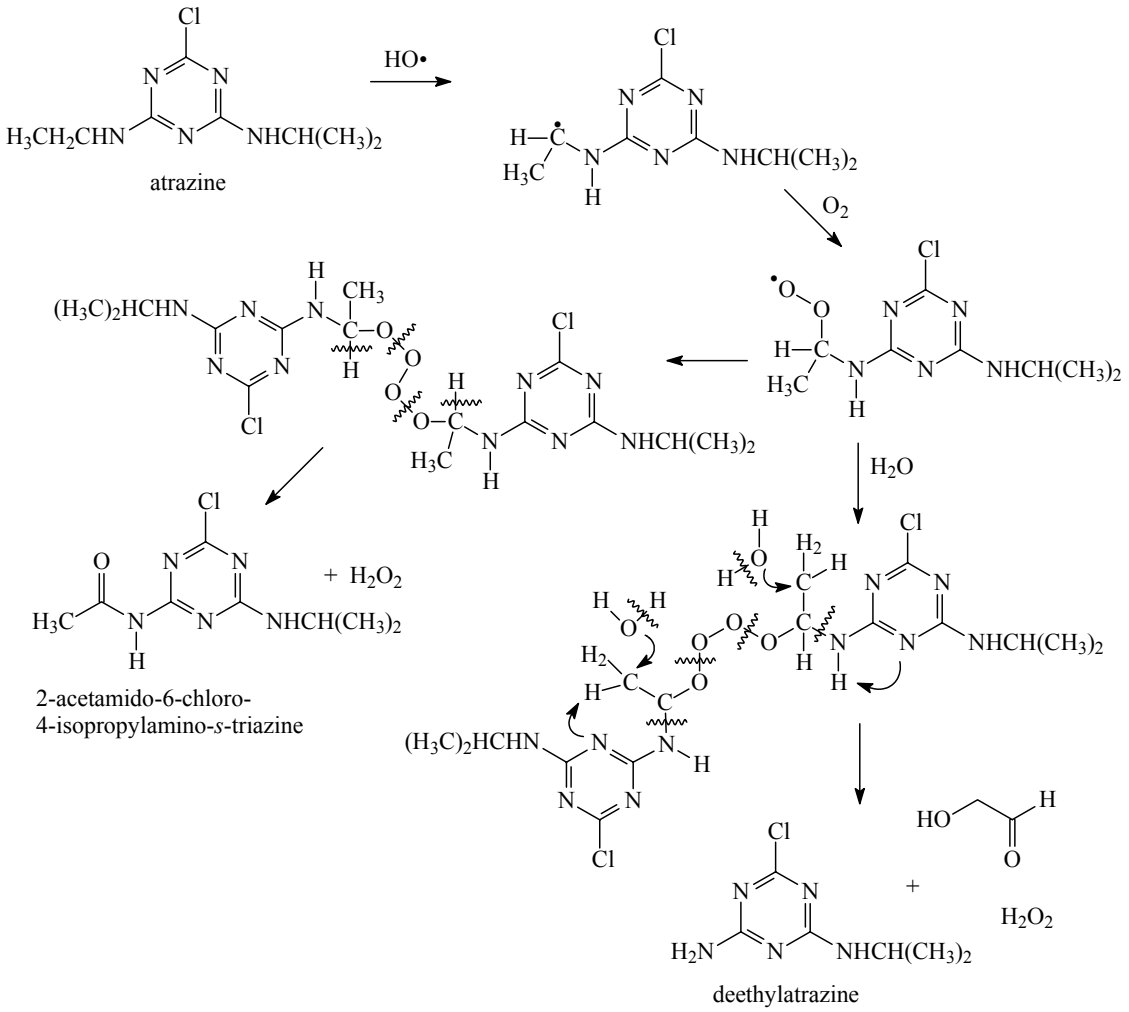

Figure 4.11 : Reaction mechanism for the formation of dealkylated degradation products from the reaction of atrazine with hydroxyl radicals (Hapeman et al., 1995)

Hydroxyl radical attack, shown in Figure 4.11, occurs at the side-chain carbon α to the amine nitrogen (Hapeman et al., 1995). The carbon is relatively electron-rich since the amine nitrogen provides additional electron density. The formation of deethylatrazine is favoured above that of deispropylatrazine as the reaction is sterically controlled, hydroxyl radical attack thus occurs more readily on the ethyl side chain than on the isopropyl side chain. Oxygen is required in the degradation of atrazine to form the perhydroxy radical (step 2 of the reaction mechanism presented in Figure 4.11) that reacts with an identical molecule to yield the final products. Hydrogen peroxide, shown in Figure 4.11, is formed during atrazine degradation (Hapeman et al., 1995).

Second order rate constants for the reaction between atrazine and hydroxyl radicals, measured at different temperatures and pH values, are listed in Table 4.4.

Table 4.4 : Second order rate constants for the reaction of atrazine and hydroxyl radicals

Reference	Temperature (°C)	pH	Rate constant (M^{-1} s^{-1})
(Beltrán et al., 1993a)	20	7	$1{,}8 \times 10^{10}$
(Chramosta et al., 1993)	20	7.5	$1{,}7 \times 10^{9}$
(De Laat et al., 1994)	20	7.5	$2{,}4 \times 10^{9}$
(Haag and Yao, 1992)	24	3.6	$2{,}6 \pm 0{,}4 \times 10^{9}$

The second order rate constants for the reaction, at 20 °C and a pH ≈ 7,5 to 8,1, of hydroxyl radicals with various atrazine degradation products are listed in Table 4.5. The lower rate constants for the reactions of deethyldeisopropylatrazine and cyanuric acid with hydroxyl radicals indicate that these compounds are not readily oxidised by hydroxyl radicals (De Laat et al., 1994).

Table 4.5 : Rate constants for the reaction of hydroxyl radicals with atrazine degradation products at 20 °C and pH ≈ 7,5 to 8,1 (De Laat et al., 1994)

Compound	Rate constant (M^{-1} s^{-1})
deethylatrazine	$1{,}2 \times 10^{9}$
deisopropylatrazine	$1{,}9 \times 10^{9}$
hydroxyatrazine	$2{,}6 \times 10^{9}$
deethyldeisopropylatrazine	$< 5 \times 10^{7}$
cyanuric acid	$\ll 2 \times 10^{7}$

The following advanced oxidation technologies for atrazine degradation in water treatment have been reviewed, ozone in Section 4.3.1, ultraviolet radiation in Section 4.3.2 and ultrasound in Section 4.3.3. The biological degradation of atrazine in water treatment is reviewed in Section 4.3.4.

4.3.1 Ozonation

Trihalomethane formation in disinfection with chlorine in water treatment has lead to an increase in the use of ozone for disinfection (Adams and Randtke, 1992b). Ozone also significantly reduces the concentration of micropollutants (such as atrazine) in water (Lykins and Koffskey, 1986; Lykins et al., 1986). Atrazine degradation products are formed during ozonation since complete degradation involving ring cleavage does not occur (Hapeman, 1994; Legube et al., 1987; Nélieu et al., 1996). The ozonation products of atrazine are shown in Figure 4.12.

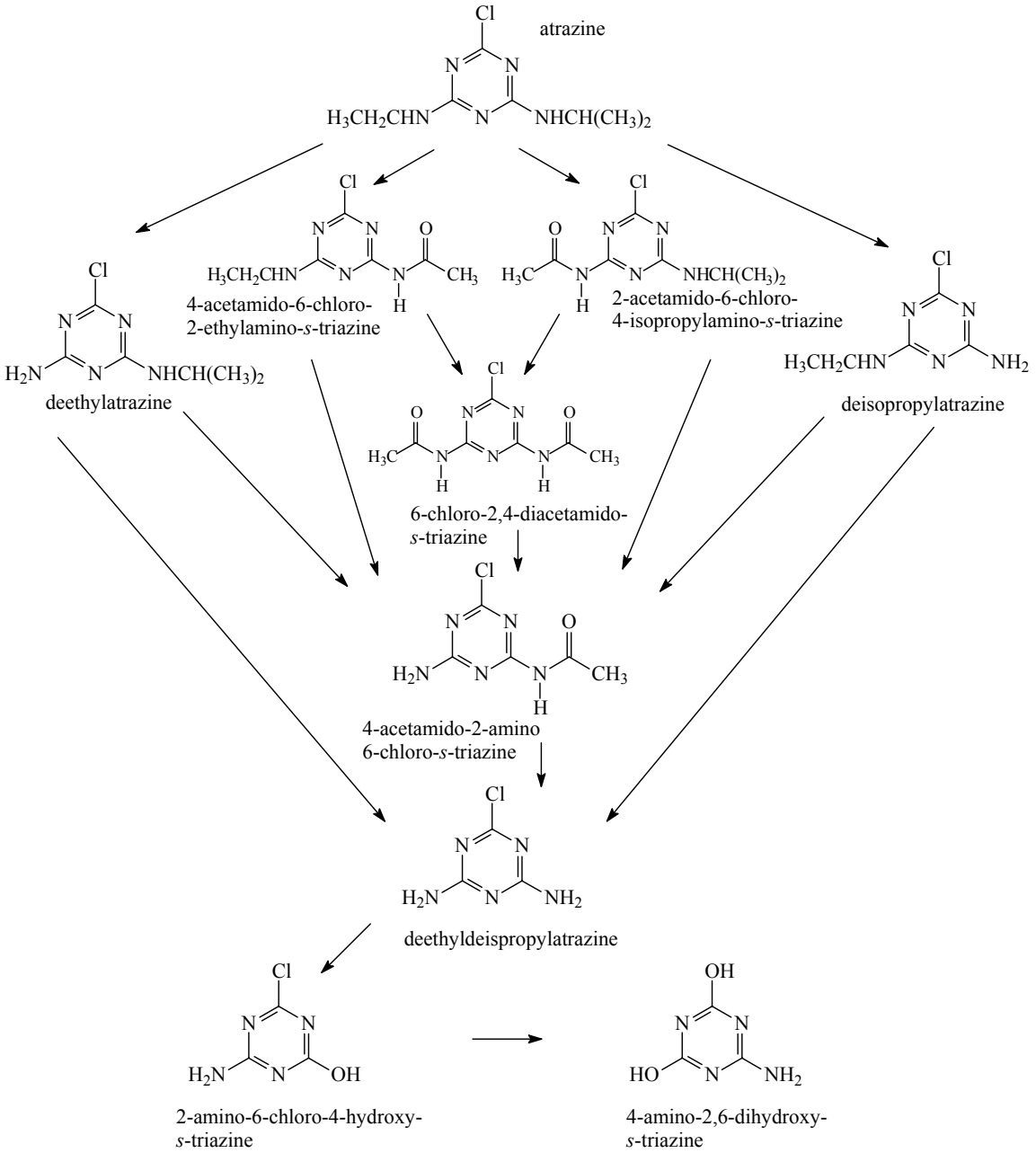

Figure 4.12 : Degradation pathway of the ozonation of atrazine (Hapeman, 1994)

The four primary ozonation products of atrazine, shown in Figure 4.12, are deethylatrazine, 2-acetamido-6-chloro-4-isopropylamino-*s*-triazine, deisopropylatrazine and 4-acetamido-6-chloro-2-ethylamino-*s*-triazine (Hapeman, 1994; Hapeman-Somich et al., 1992). The three secondary products formed are 6-chloro-2,4-diacetamido-*s*-triazine, 4-amino-2-acetamido-6-chloro-*s*-triazine and deethyldeisopropyl-atrazine. Extended ozonation of deethyldeisopropylatrazine leads to the stepwise formation of 2-amino-6-chloro-4-hydroxy-*s*-triazine and 2-amino-4,6-dihydroxy-*s*-triazine (Hapeman, 1994; Hapeman-Somich et al., 1992).

Deethylatrazine and deisopropylatrazine are in the same oxidation state as atrazine and are not oxidized by-products of atrazine despite the strong oxidizing power of ozone, the leaving side-chain alkyl group is oxidised and not the portion of the molecule containing the *s*-triazine ring (Adams and Randtke, 1992a). The amino alkyl groups are the first site of attack during ozonation. The alkyl group is either removed or converted to the *N*-acetyl, according to the degradation pathway shown in Figure 4.12, with the *s*-triazine ring remaining intact (Hapeman, 1994).

Atrazine degradation during ozonation is due to both reaction with hydroxyl radicals and the direct reaction with ozone. The reaction mechanisms illustrating the formation of hydrolysed and dealkylated degradation products due to reaction with hydroxyl radicals are presented, respectively, in Figure 4.10 and Figure 4.11. The mechanism for the direct reaction of atrazine with ozone is shown in Figure 4.13.

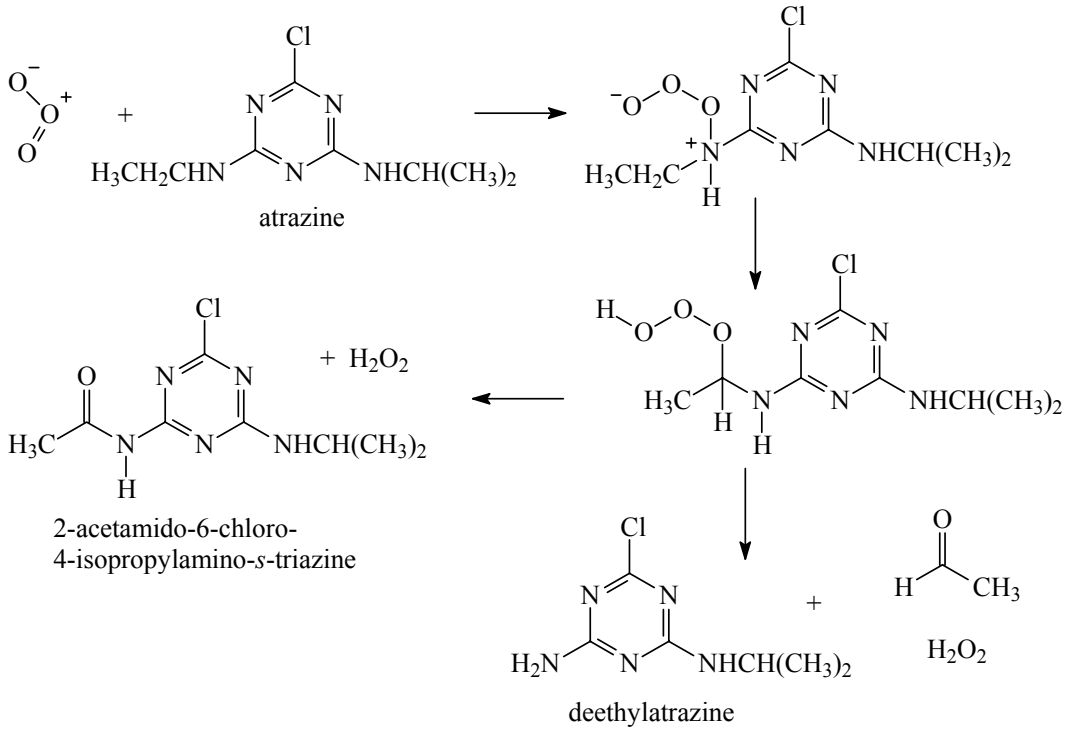

Figure 4.13 : Reaction mechanism for the formation of dealkylated degradation products from the direct reaction of atrazine with ozone at acidic pH (Bolzacchini et al., 1994)

The reaction of atrazine and ozone at acidic pH, as shown in Figure 4.13, is initiated with the formation of a complex from the coordination of ozone to a side chain nitrogen. Transfer of the hydride from carbon to oxygen gives the hydrotrioxide which either undergoes *N*-dealkylation to form deethylatrazine, acetaldehyde and hydrogen peroxide or rearranges to form 2-acetamido-6-chloro-4-isopropylamino-*s*-triazine and hydrogen peroxide (Bolzacchini et al., 1994). Steric hindrance causes the formation of deethylatrazine to be 5-fold greater that that of deisopropylatrazine (Bolzacchini et al., 1994; Hapeman, 1994).

The mixture of degradation products obtained from the ozonation of atrazine was dependant on reaction conditions, particularly pH, ozone concentration and contact time (Adams et al., 1990). All the products identified in the investigation by Hapeman and co-workers contained a chlorine atom (Hapeman, 1994; Hapeman-Somich et al., 1992). Hydrolysed degradation products from the ozonation of atrazine have been identified under certain reaction conditions (Adams and Randtke, 1992b; Legube et al., 1987; Nélieu et al., 1996). Adams and Randtke found that under conditions that prevented the autodecomposition of ozone to hydroxyl radicals, only dealkylated products were formed and that under conditions that favoured the formation of hydroxyl radicals (such as high pH values), minor quantities of hydrolysed products were formed in addition to the dealkylated products (Adams, 1990; Adams and Randtke, 1992a). It was proposed that the hydrolysis of the Cl-C bond was due only to reaction with hydroxyl radicals and not due to direct reaction with ozone (Adams and Randtke, 1992a). The formation pathway of hydrolysed products during the ozonation of atrazine is shown in Figure 4.14.

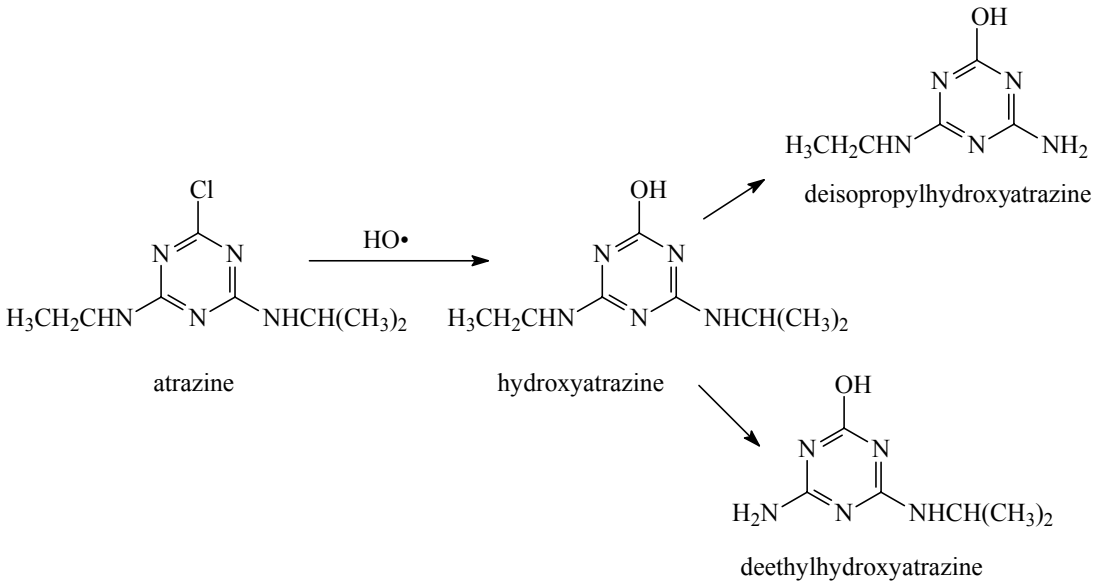

Figure 4.14 : Formation pathway of hydrolysed products during atrazine ozonation (Adams and Randtke, 1992a)

Atrazine, during ozonation, reacts either directly with ozone or with hydroxyl radicals formed from the decomposition of ozone. Rate constants, measured at different temperatures and pH values, for the reaction of atrazine with hydroxyl radicals are listed in Table 4.4. Rate constants for the direct reaction between ozone and atrazine, at pH values of 2, 7 and 12 are listed in Table 4.6.

Table 4.6 : Rate constants for the direct reaction between ozone and atrazine at pH 2, 7 and 12 (Beltrán et al., 1993b)

pH	Rate constant (M^{-1} s^{-1})
2	4.5

7	6.3
12	6.3

Atrazine degradation increases with increasing pH (Adams, 1990; Beltrán et al., 1993b; Beltrán et al., 1994a). Hydroxyl ions at high pH values catalyse the decomposition of ozone, atrazine is degraded through reaction with the radicals formed from the ozone decomposition (Beltrán et al., 1993b). The presence of hydroxyl radical scavengers, *t*-butanol and carbonate/bicarbonate ions, decreased the degradation of atrazine at pH values of 2, 7 and 12 (Beltrán et al., 1994a). Atrazine is thus degraded by radical reactions even at low pH values. The direct reaction between atrazine and ozone at 20 °C and a pH of 2 represented 24 and 81 %, respectively, of the total degradation in the absence and presence of 0,74 g L^{-1} *t*-butanol (Beltrán et al., 1994a). The higher rate constant for the reaction between atrazine and hydroxyl radicals (Table 4.4) than that of atrazine and ozone (Table 4.6) indicates that atrazine degradation is more likely to occur via free radical reactions than by direct ozonation. Atrazine degradation during ozonation at a pH below 12 occurs due to both direct reaction with ozone and free radical reactions whereas atrazine degradation at a pH above 12 is due only to radical reactions (Beltrán, 1995).

The reactions for the degradation of atrazine are

$$A + O_3 \xrightarrow{k_d} products$$
$$A + HO^{\bullet} \xrightarrow{k_{HO,A}} products$$

Scheme 4.1

where k_d and $k_{HO,A}$ are the rate constants for the reactions of atrazine with ozone and atrazine with hydroxyl radicals (Beltrán et al., 1994a).

Hydroxyl radicals are generated from the decomposition of ozone according to the mechanism shown in Scheme 3.3 in Section 3.1.3. Beltrán and co-workers modelled the rate of atrazine degradation using equation 4.1 (Beltrán et al., 1993b; Beltrán et al., 1994a).

$$\frac{-dC_A}{dt} = k_d C_{O_3} C_A + k_{HO,A} C_A C_{HO} \qquad [4.1]$$

where C_A, C_{O_3} and C_{HO} represent, respectively, the concentrations of atrazine, dissolved ozone and hydroxyl radicals. The first term on the right hand side of the equation represents the contribution of atrazine degradation from direct ozone reaction and the second term the contribution from reaction with hydroxyl radicals. Equation 4.1 is only valid if the decomposition of ozone is slow relative to the ozone mass transfer rate (Beltrán et al., 1994a). The kinetic regime of ozone absorption is determined from the dimensionless Hatta number for the reaction between ozone and atrazine; the Hatta number, as detailed in Section 3.1.2,

relates the chemical reaction rate to the physical absorption rate of ozone (Beltrán et al., 1993b; Beltrán et al., 1994a). Reactions undergone by gases dissolving in solution develop in the proximity of the gas-liquid interface (fast reactions), in the bulk liquid (slow or very slow reactions) or in between both zones (moderate reactions); the kinetic regime is classified as slow when the Ha number is less than 0,3 (Beltrán et al., 1993b; Beltrán et al., 1994a). The Hatta number for an irreversible second-order reaction is defined as

$$\mathrm{Ha} = \frac{(k_d C_A D_{O_3})^{0,5}}{k_L} \qquad [4.2]$$

where k_d is the rate constant of the direct reaction between ozone and atrazine, C_A the concentration of atrazine, D_{O_3} the ozone diffusivity in water and k_L the liquid-phase mass transfer coefficient (Beltrán et al., 1993b). The Hatta numbers for the direct reaction between ozone and atrazine at pH 2, 7 and 12 are listed in Table 4.7.

Table 4.7 : Hatta numbers and kinetic regimes of ozone absorption for the direct reaction between ozone and atrazine at pH 2, 7 and 12 (Beltrán et al., 1993b)

pH	Ha	Kinetic regime
2	0	very slow
7	0	very slow
12	0	very slow

The direct reaction between ozone and atrazine at any pH value is a very slow reaction, thus, the degradation rate of atrazine is determined only by chemical reaction and is not limited by ozone mass transfer nor the ozone decomposition rate (Beltrán et al., 1993b; Beltrán et al., 1994a). Saturation of the bulk solution with ozone during ozonation also indicates that the ozonation of atrazine occurs by a set of slow gas-liquid reactions (Beltrán et al., 1994a). Both the direct reaction with ozone and the free radical reactions develop in the bulk solution (Beltrán et al., 1993b).

Atrazine degradation was not significantly affected by temperature (3, 10 and 20 °C) for ozonation at a partial pressure of 1,1 kPa (Beltrán et al., 1994a). Atrazine degradation increased with increasing temperature when ozonation was performed at partial pressures of 0,67; 0,84 and 1,1 kPa for temperatures of 3, 10 and 20 °C, respectively; the partial pressure was adjusted since ozone solubility, and thus the amount of ozone available in solution, decreased with increasing temperature (Beltrán et al., 1994a).

Duguet and co-workers found that an applied ozone dose of 5,1 mg L^{-1} caused a 46 % reduction in atrazine concentration from 0,35 to 0,19 μg L^{-1} (Duguet et al., 1990). The addition of 2,8 mg L^{-1} hydrogen peroxide increased the degradation to 84 % (Duguet et al., 1990). Atrazine degradation is enhanced by the addition of hydrogen peroxide because of the increase in hydroxyl radicals (Paillard et al., 1991). Typical conditions applied during ozonation in water treatment plants are a maximum dosage of 5 to 6 g of ozone per m^3 of

water (equivalent to a concentration of 5 to 6 mg L^{-1}) and a maximum contact time of 20 min. Atrazine is not completely degraded under such conditions and the oxidation potential of ozone towards pesticides is improved with the addition of hydrogen peroxide (Paillard et al., 1991). The combination of ozone and hydrogen peroxide in comparison with other advanced oxidation technologies (UV/O_3 and UV/H_2O_2) is more efficient, costs less and is simple in application (Beltrán et al., 1998; Paillard et al., 1991). The reactions occurring during the oxidation of atrazine by ozone and hydrogen peroxide, Scheme 3.6 in Section 3.1.3, are repeated in Scheme 4.2.

Initiation steps

$O_3 + HO^- \xrightarrow{k_i} O_2^{\bullet -} + HO_2^{\bullet}$	$k_i = 70\ M^{-1}\ s^{-1}$	[a]
$HO_2^{\bullet} \rightleftharpoons O_2^{\bullet -} + H^+$	$pK_a = 4,8$	[b]
$H_2O_2 \rightleftharpoons HO_2^- + H^+$	$pK = 11,8$	[c]
$O_3 + HO_2^- \xrightarrow{k'_i} O_3^{\bullet -} + HO_2^{\bullet}$	$k'_i = 2,8 \times 10^6\ M^{-1}\ s^{-1}$	[d]

Propagation steps

$O_3 + O_2^{\bullet -} \xrightarrow{k_1} O_3^{\bullet -} + O_2$	$k_1 = 1,6 \times 10^9\ M^{-1}\ s^{-1}$	[e]
$O_3^{\bullet -} + H^+ \overset{k_2}{\rightleftharpoons} HO_3^{\bullet}$	$k_2 = 5,2 \times 10^{10}\ M^{-1}\ s^{-1}$	[f]
$HO_3^{\bullet} \xrightarrow{k_3} HO^{\bullet} + O_2$	$k_3 = 1,1 \times 10^5\ M^{-1}\ s^{-1}$	[g]
$O_3 + HO^{\bullet} \xrightarrow{k_4} O_2 + HO_2^{\bullet}$	$k_4 = 2,0 \times 10^9\ M^{-1}\ s^{-1}$	[h]
$HO^{\bullet} + H_2O_2 \xrightarrow{k_5} O_2^{\bullet -} + H_2O + H^+$	$k_5 = 2,7 \times 10^7\ M^{-1}\ s^{-1}$	[i]
$HO^{\bullet} + HO_2^- \xrightarrow{k_6} O_2^{\bullet -} + H_2O$	$k_6 = 7,5 \times 10^9\ M^{-1}\ s^{-1}$	[j]

Termination steps

$HO^{\bullet} + B \xrightarrow{k_{HO,B}} B_{oxid}$	[k]
$O_3 + B \xrightarrow{k_d} B_{oxid}$	[l]

Scheme 4.2

The main initiation step in the oxidation of atrazine by ozone and hydrogen peroxide is reaction [d] of Scheme 4.2, the reaction between ozone and perhydroxyl ions (HO_2^-), the ionic form of hydrogen peroxide (Beltrán et al., 1998). Hydrogen peroxide does not act as an overall scavenging agent of hydroxyl radicals during ozonation, despite reactions [i] and [j] of Scheme 4.2, since the superoxide radical anions produced in reactions [i] and [j] promote the further decomposition of ozone, regenerating hydroxyl radicals via reactions [e], [f] and [g] of Scheme 4.2. Reactions between hydroxyl radicals and atrazine intermediates also act as termination steps in the reaction mechanism shown in Scheme 4.2 (Beltrán et al., 1998). Beltrán and co-workers modelled the degradation of atrazine, based on the mechanism in Scheme 4.2, using equation 4.3.

$$\frac{-dC_A}{dt} = k_d C_{O_3} C_A + k_{HO,A} C_A C_{HO} \qquad [4.3]$$

where C_A, C_{O_3} and C_{HO} represent, respectively, the concentrations of atrazine, dissolved ozone and hydroxyl radicals (Beltrán et al., 1998). Beltrán and co-workers calculated, using equation 4.3, the contributions to atrazine degradation from hydroxyl radical reaction (reaction [k] of Scheme 4.2) and direct ozone reaction (reaction [l] of Scheme 4.2). Hydroxyl radical reactions accounted for 76,6 % of the total atrazine degradation for an atrazine concentration of 10,8 mg L^{-1} and an ozone concentration of 3,3 mg L^{-1}. The addition of 0,34 mg L^{-1} hydrogen peroxide increased the degradation due to radical reactions to 86 %; degradation was due only to radical reactions (90 to 100 %) for hydrogen peroxide concentrations above 34 mg L^{-1} (Beltrán et al., 1998). The deviation in data for the modelled degradation of atrazine and intermediates, deethylatrazine and deisopropylatrazine, was within 15 % of the experimental results. The kinetic model also predicted that the removal of atrazine, deethylatrazine and deisopropylatrazine (of similar concentrations to that found in natural waters) would occur in less than 7 min for oxidation with ozone and hydrogen peroxide even in the presence of bicarbonates or other hydroxyl radical scavengers (Beltrán et al., 1998).

Paillard and co-workers found that the optimum pH for atrazine degradation in pure water was between 8 and 9 for ozone and between 7 and 8 for ozone combined with hydrogen peroxide (Paillard et al., 1991). Ozonation contact time (usually between 5 and 20 min) is determined by the required disinfection that has to be achieved during water treatment (Meijers et al., 1993). Contact time for advanced oxidation processes depend on the rate of formation of hydroxyl radicals since, once formed, the radicals react with organic compounds in the water within 1 μs to 10 ms time period. The estimated contact times for advanced oxidation with ozone and hydrogen peroxide at different pH values and ratios of ozone to hydrogen peroxide are listed in Table 4.8 (Meijers et al., 1993).

Table 4.8 : Estimated contact times for advanced oxidation with ozone and hydrogen peroxide (Meijers et al., 1993)

pH	O_3 dosage (mg L^{-1})	H_2O_2 dosage (mg L^{-1})	Estimated contact time for 95 % $HO^{\bullet}$ formation (min)	
			bubble column	contact chamber
7.8	3	1	1.5	4
7.8	3	2	1.5	2
7.8	3	4	1.5	1
7.8	3	1	1.5	15
8.3	3	1	1.5	0.5

Radical formation for advanced oxidation at a pH of 7,8 or greater (as indicated in Table 4.8) occurs within minutes. Contact time for oxidation at a pH below 7,8 is longer since the rate of hydroxyl radical formation decreases by a factor of 10 for each pH unit decrease (Meijers et al., 1993). The estimated contact time for 95 % hydroxyl radical formation in a contact chamber (as indicated in Table 4.8) decreases with increasing hydrogen peroxide concentration. The overall stoichiometry of the reaction of ozone with hydrogen

peroxide, shown in Scheme 3.7 in Section 3.1.3, indicates that 2 mol of ozone are consumed per mol of hydrogen peroxide (Beltrán et al., 1998; Meijers et al., 1993).

Paillard and co-workers found that atrazine degradation in pure water was a maximum at the molar ratio of ozone to hydrogen peroxide of 2:1 for a 10 min contact time, 1,75 mg L^{-1} initial atrazine concentration, 1,58 mg L^{-1} ozone concentration and pH of 7,5 (Paillard et al., 1991). Meijers and co-workers proposed that an excess of ozone (ratio ≤ 0,4 mol of hydrogen peroxide per mol of ozone) would be required if disinfection was the primary objective during water treatment whereas an excess of hydrogen peroxide (ratio between 0,7 and 1 mol of hydrogen peroxide per mol of ozone) would be required for the degradation of pesticides by reaction with hydroxyl radicals. Higher concentrations of hydrogen peroxide lead to the scavenging of hydroxyl radicals by hydrogen peroxide (Meijers et al., 1993).

A ratio of 2,6 mol of ozone consumed per mol of hydrogen peroxide was found to be optimal for the degradation of atrazine, deethylatrazine and deisopropylatrazine for the experimental conditions used by Beltrán and co-workers (Beltrán et al., 1998). Hydrogen peroxide concentrations below 0,34 mg L^{-1} did not significantly influence the degradation of atrazine for an initial atrazine concentration of 1,70 mg L^{-1}, ozone concentration of 16 mg L^{-1}, pH of 7 and temperature of 20 °C. The 2,6 molar ratio of ozone to hydrogen peroxide corresponded to a hydrogen peroxide concentration in the range of 3,4 to 34 mg L^{-1}; atrazine degradation decreased at higher concentrations of hydrogen peroxide (>340 mg L^{-1}) since the kinetic regime of ozone absorption changes and is controlled by the mass transfer of ozone, the rate of atrazine oxidation becomes inversely proportional to hydrogen peroxide concentration (Beltrán et al., 1998).

The degradation products generated from the oxidation of atrazine by ozone and hydrogen peroxide are the same as those (shown in Figure 4.11) produced from the ozonation of atrazine (Paillard et al., 1991). The rate constants (at 20 °C and pH 7) for the direct reaction between ozone and the primary intermediates, deethylatrazine and deisopropylatrazine, are 0,19 and 7,51 M^{-1} s^{-1}, respectively (Beltrán et al., 1998). Degradation of these compounds is due only to radical reactions (90 to 100 %) for hydrogen peroxide concentrations above 340 mg L^{-1} (Beltrán et al., 1998).

Paillard and co-workers investigated a pilot plant treating water from the river Seine in France with ozone and hydrogen peroxide (Paillard et al., 1991). The addition of hydrogen peroxide, under continuous flow conditions, reduced the time to achieve maximum atrazine degradation from 8 min for ozonation to 4 min for oxidation with ozone and hydrogen peroxide. An ozone dose of 4 mg L^{-1} was required to reduce the atrazine concentration from 1,1 to below 0,1 μg L^{-1} in the outlet water (the required EEC threshold); the optimal ratio of ozone to hydrogen peroxide was shown to be between 0,5 and 0,64 mole of ozone per mol of hydrogen peroxide. Atrazine degradation decreased with increasing water alkalinity, degradation was 76 % with 150 mg L^{-1} of calcium carbonate ($CaCO_3$) and 55 % with 300 mg L^{-1} of $CaCO_3$ for an initial atrazine

concentration of 2 μg L^{-1}, 2 mg L^{-1} ozone concentration, ozone to hydrogen peroxide ratio of 0,35 mol mol^{-1} and pH of 8 (Paillard et al., 1991). Ozone dosage used on an industrial scale (maximum of 5 mg L^{-1}) does not result in complete degradation of atrazine concentrations above 0,25 μg L^{-1} (Meijers et al., 1993; Paillard et al., 1991). The combination of ozone and hydrogen peroxide is an effective and easy implemented method for the degradation of atrazine at higher concentrations (Paillard et al., 1991).

Treatment of Thames river water in the United Kingdom (alkalinity between 200 and 300 mg L^{-1} as $CaCO_3$; total organic carbon of 3 to 6 mg L^{-1}) has indicated that between 30 and 60 % of atrazine is removed with ozone doses of 2 to 4 mg L^{-1} and a contact time of 5 to 15 min (Foster et al., 1992; Rachwal et al., 1992). Addition of hydrogen peroxide increased the atrazine removal by a further 20 to 30 %; the improvement was not consistent or predictable and depended on the presence of natural organics and free radical scavengers (bicarbonates) in the Thames river source water (Foster et al., 1992; Rachwal et al., 1992). Pesticides, such as atrazine, and natural organic carbon compounds, such as humic and fulvic acids, are not completely oxidised by ozone or ozone and hydrogen peroxide during water treatment. Intermediate oxidation and hydrolysis by-products tend to be more biodegradable than the original compounds, a biological process is required after ozonation to prevent the increased assimilable organic carbon levels from supporting growth of biofilms and microorganisms in the distribution system (Foster et al., 1992). Activated carbon has been used to remove ozonation by-products (Foster et al., 1992).

Activated carbon is a porous material (used in either the powder or granulated form) with a large surface area and a high affinity for organic compounds (Foster et al., 1992). It is produced by controlled combustion of coal, peat, coconut shells or wood and can be regenerated thermally when the adsorption capacity fills. Regeneration is usually performed for only high value activated carbon. Disposal of spent activated carbon can be a problem since it is laden with pesticides and can be a potentially hazardous material for landfill purposes (Foster et al., 1992). Activated carbon is used primarily in water treatment for the removal of taste, odour, colour, organic micropollutants (such as pesticides) and biodegradable organic matter. Activated carbon adsorbs most compounds from water that are not strongly hydrophillic in nature (Orlandini et al., 1996).

The dosage of granular activated carbon (GAC) required to achieve a given treatment objective is determined by capacity, adsorption kinetics (the rate of adsorption), competitive and displacement adsorption and the pre-adsorption of naturally occurring organic matter (Orlandini et al., 1996). Natural organic matter (NOM) in surface water consists mostly of substances that are less adsorbable and are of lower diffusivity than target micropollutants such as atrazine. The zone in the filter bed in which the natural organic matter adsorbs is larger and moves faster through the bed than the zone in which the micropollutants adsorb. Natural organic matter thus tends to adsorp onto granular activated carbon ahead of micropollutants and reduces the adsorptive capacity of the GAC bed for micropollutants (Huang and Banks, 1996; Orlandini et al., 1997). Biodegradation also occurs within granular activated carbon filters and contributes to the removal of organic

compounds. Microbial activity is supported by the biodegradable portion of the natural organic matter in the GAC filter influent (Orlandini et al., 1996).

The pilot-plant study by Foster and co-workers found that the breakthrough for atrazine of a GAC bed with an empty bed contact time of 6 min was extended from 3,5 months, without pre-ozonation, to 5 months with pre-ozonation with an ozone concentration of 2 to 3 mg L^{-1} and a contact time of 5 min (Foster et al., 1992). Orlandini and co-workers also demonstrated the extension of the lifetime of a GAC bed with pre-ozonation (Orlandini et al., 1996; Orlandini et al., 1997). Atrazine breakthrough at a bed depth of 0,35 m in a GAC filter that had treated 51 000 bed volumes of water was 66 % when receiving non-ozonated influent and 39 % when receiving ozonated influent. The GAC filter had a bed depth of 1,1 m and an empty bed contact time of 20 min, ozone concentration was 0,7 mg L^{-1} and atrazine concentration was 2 μg L^{-1}. Similarly, atrazine breakthrough, at a bed depth of 1,1 m, after 17 000 bed volumes of water had been treated, was 6 and 3 %, respectively, for filters receiving non-ozonated and ozonated influent (Orlandini et al., 1996).

Rachwal and co-workers found that atrazine was still being removed to less than 0,1 μg L^{-1} after 2 yr of operation of a pilot plant consisting of pre-ozonation, chemical dosage, flocculation, filtration, main ozonation and GAC filtration. Atrazine removal (initial concentration between 0,2 and 0,4 μg L^{-1}) was low in the pre-ozonation stage, between 30 and 60 % occurring during main ozonation and the final reduction to below 0,1 μg L^{-1} was due to adsorption in the GAC filter (Rachwal et al., 1992). Pre-ozonation increased the mineralisation of ring-labelled atrazine in GAC filters (Huang and Banks, 1996). Approximately 62 % of the ring-UL-^{14}C atrazine was converted to $^{14}CO_2$ in the GAC filter receiving ozonated atrazine and ozonated surface water, a 50 % conversion occurred in the filter receiving ozonated surface water and untreated atrazine and only 38 % conversion occurred in the filter receiving untreated water and untreated atrazine (Huang and Banks, 1996).

The increased atrazine removal in GAC filters receiving ozonated influent rather than non-ozonated influent is due to increased biodegradation of atrazine, decreased competitive adsorption of atrazine and natural organic matter and lower natural organic matter pre-adsorption (Orlandini et al., 1997). Ozonation lowers the adsorbability of natural organic matter with respect to activated carbon and increases the portion of biodegradable natural organic matter that is removed in the filter via biodegradation rather than by adsorption (Orlandini et al., 1997). The combination of ozone and granular activated carbon effectively removes pesticides from surface water since compounds that are not fully oxidised by the ozone are readily removed by the granular activated carbon (Rachwal et al., 1992).

4.3.2 Ultraviolet radiation

The degradation of a substrate during UV radiation can be due to both direct and indirect photolysis (Torrents et al., 1997). Direct photolysis is the adsorption of UV-visible light by a substrate which then undergoes transformation. Indirect photolysis is the adsorption of light by a species other than the substrate

which then either transfers the energy directly to the substrate (called photosensitization), undergoes electron transfer with the substrate or causes a series of reactions producing oxidants such as singlet oxygen, hydroxyl radicals and alkylperoxy radicals (Torrents et al., 1997). Direct photolysis of atrazine proceeds via excitation of the molecule followed by dechlorination and hydroxylation to produce hydroxyatrazine (Khan and Schnitzer, 1978; Nick et al., 1992; Pape and Zabik, 1970; Torrents et al., 1997). Between 0,95 and 1 mol of hydroxyatrazine is produced per mole of atrazine photolysed (De Laat et al., 1995). The mechanism for the direct photolysis of atrazine, shown in Scheme 4.3, proceeds via the homolytic scission of the C-Cl bond, reaction [b], followed by electron transfer, within the solvent cage, of the two resulting radicals, reaction [c], and reaction of the carbocation with water, reaction [d] (Nick et al., 1992). The term, *A*Cl, in Scheme 4.3, represents the atrazine molecule, it indicates the bond between the Cl atom in position 6 and the rest of the molecule.

$$A\mathrm{Cl} + h\nu \rightarrow A\mathrm{Cl}^{\star} \quad [a]$$

$$A\mathrm{Cl}^{\star} \rightarrow A^{\bullet} + \mathrm{Cl}^{\bullet} \quad [b]$$

$$A^{\bullet} + \mathrm{Cl}^{\bullet} \rightarrow A^{+} + \mathrm{Cl}^{-} \quad [c]$$

$$A^{+} + \mathrm{H_2O} \rightarrow A\mathrm{OH} + \mathrm{H}^{+} \quad [d]$$

$$A\mathrm{Cl}^{\star} \rightarrow A^{+} + \mathrm{Cl}^{-} \quad [e]$$

$$A^{+} + \mathrm{Cl}^{-} \rightarrow A\mathrm{Cl} \quad [f]$$

Scheme 4.3

Nick and co-workers proposed that the heterolytic scission of atrazine in the excited state, reaction [e], could occur as an alternative to reaction [b] (Nick et al., 1992). The carbocation may react with the chloride ion within the solvent cage, reaction [f], in competition with reaction [d] to reform atrazine and reduce the quantum yield of product formation (Nick et al., 1992). The quantum yield of a photochemical reaction is defined as the amount of reactant degraded or product formed per amount of photons absorbed by the system (Braslavsky and Houk, 1988).

Beltrán and co-workers detected low concentrations of hydrogen peroxide during the photolysis of atrazine (Beltrán et al., 1993a). Hydroxyl radicals are formed from the photolysis of hydrogen peroxide, as shown in Scheme 4.4, and the formation of hydrogen peroxide could indicate that atrazine degradation was also due to radical reactions (Beltrán et al., 1993a; De Laat et al., 1997). The quantum yield of hydrogen peroxide ($\Phi_{H_2O_2}$) at 254 nm was 0,5 mol per photon (Beltrán et al., 1993a).

$$\mathrm{H_2O_2} + 2h\nu \rightarrow 2\mathrm{HO}^{\bullet}$$

Scheme 4.4

The degradation of atrazine was unaffected by the presence of hydroxyl radical scavengers such as bicarbonate and carbonate ions. Beltrán and co-workers concluded that the concentration of hydrogen

peroxide formed during the direct photolysis of atrazine was too low to compete with atrazine for the incident UV radiation (Beltrán et al., 1993a). Atrazine degradation decreased when humic substances were present in the water and competed for the incident radiation (Beltrán et al., 1993a).

Atrazine concentration was unaffected at UV radiation levels that are sufficient for water disinfection (Nick et al., 1992). Atrazine was degraded 2,4 % at a UV fluence of 250 J m^{-2} which reduces *E. coli* count by four orders of magnitude where fluence is defined as the total radiant energy per cross sectional area of target (Braslavsky and Houk, 1988; Nick et al., 1992). A UV fluence of 24 kJ m^{-2} was required to reduce atrazine concentration by one order of magnitude (Nick et al., 1992).

The presence of other species such as hydrogen peroxide or nitrates at sufficient concentration to absorb the incident radiation and produce hydroxyl radicals increases atrazine degradation (Arántegui et al., 1995; Beltrán et al., 1993a; De Laat et al., 1997; Torrents et al., 1997). The UV degradation of atrazine in the presence of hydrogen peroxide follows first order reaction kinetics (Arántegui et al., 1995; Burkhard and Guth, 1976; Khan and Schnitzer, 1978). Atrazine degradation does not occur with hydrogen peroxide in the absence of light or UV radiation (Arántegui et al., 1995; Beltrán et al., 1993a). The reactions De Laat and co-workers used to model the degradation of atrazine with hydrogen peroxide are listed in Scheme 4.5 (De Laat et al., 1997).

Photodecomposition of hydrogen peroxide and production of hydroxyl radicals

$H_2O_2 + H_2O \rightleftharpoons HO_2^- + H_3O^+$	pKa = 11,7	[a]
$H_2O_2 + 2hv \rightarrow 2HO^\bullet$	$\Phi_{H_2O_2} = 0,5$	[b]
$HO^\bullet + H_2O_2 \rightleftharpoons HO_2^\bullet + H_2O$	$k_{H_2O_2} = 2,7 \times 10^7\ M^{-1}\ s^{-1}$	[c]
$HO^\bullet + HO_2^- \rightleftharpoons HO_2^\bullet + HO^-$	$k_{HO_2^-} = 7,5 \times 10^9\ M^{-1}\ s^{-1}$	[d]
$[PER] = [H_2O_2] + [HO_2^-]$	k_{PER} ($M^{-1}\ s^{-1}$)	[e]
$HO_2^\bullet + HO_2^\bullet \rightarrow H_2O_2 + O_2$		[f]
$2H_2O_2 + 2hv \rightarrow 2H_2O + O_2$	overall reaction	[g]

Reactions with hydroxyl radicals

$HO^\bullet + A \rightarrow products$	k_A ($M^{-1}\ s^{-1}$)	[h]
$HO^\bullet + S_i \rightarrow products$	k_i ($M^{-1}\ s^{-1}$)	[i]
$CO_3^- + H_3O^+ \rightleftharpoons HCO_3^\bullet + H_2O$	pKa_1 = 10,38 at 20 °C	[j]
$HCO_3^{2-} + H_3O^+ \rightleftharpoons H_2CO_3 + H_2O$	pKa_2 = 6,39 at 20 °C	[k]
$HO^\bullet + HCO_3^\bullet \rightarrow CO_3^{\bullet -} + H_2O$	$k_{HCO_3^-} = 8,5 \times 10^6\ M^{-1}\ s^{-1}$	[l]
$HO^\bullet + CO_3^{2-} \rightarrow CO_3^{\bullet -} +$	$k_{CO_3^{2-}} = 3,9 \times 10^8\ M^{-1}\ s^{-1}$	[m]
$[C_{inorg}] = [HCO_3^-] + [CO_3^{2-}]$	k_{Cinorg} ($M^{-1}\ s^{-1}$)	[n]

Photodecomposition of atrazine

$A + hv \rightarrow products$	(Φ_A)	[o]

Scheme 4.5

The photodecomposition of hydrogen peroxide, reaction [b] of Scheme 4.5, produces two hydroxyl radicals per molecule of hydrogen peroxide decomposed. Hydroxyl radicals, as shown in Scheme 4.5, initiate a radical chain decomposition of hydrogen peroxide and react with atrazine, bicarbonate or carbonate ions and other inorganic and organic solutes (S_i) in the water (De Laat et al., 1997).

De Laat and co-workers used equation 4.4 to represent the degradation of atrazine by hydrogen peroxide and UV radiation in a batch reactor (De Laat et al., 1997).

$$\frac{-d[A]}{dt} = \frac{-\Phi_A(I_a)A}{V} + k_{HO,A}[A][HO^\bullet]_{SS} \qquad [4.4]$$

where $[A]$ is atrazine concentration, $[HO^\bullet]_{SS}$ the steady state concentration of hydroxyl radicals, Φ_A the quantum yield of atrazine at 253,7 nm, V the volume of irradiated solution, I_a the intensity of absorbed radiation and $k_{HO,A}$ the rate constant for the reaction of atrazine with hydroxyl radicals (De Laat et al., 1997). The first term on the right hand side of the equation in equation 4.4 represents the decomposition of atrazine due to direct photolysis and the second term the decomposition by reaction with hydroxyl radicals generated from the photodecomposition of hydrogen peroxide (De Laat et al., 1997). De Laat and co-workers used the

model to estimate the value of the quantum yield of the photolysis of atrazine and to predict the effects of variable such as hydrogen peroxide dose, pH and bicarbonate alkalinity on the degradation of atrazine (De Laat et al., 1997). The quantum yield of atrazine, as calculated by different authors, is listed in Table 4.9.

Table 4.9 : Quantum yield of atrazine

Reference	Wavelength (nm)	Φ_A
Beltrán et al., 1993a	254	0.05
De Laat et al., 1997	253.7	0.04
Nick et al., 1992	254	0.05

Hydrogen peroxide increases the degradation of atrazine because of radical reactions and the formation of hydroxyl radicals (Beltrán et al., 1993a). However, at high concentrations of hydrogen peroxide, hydroxyl radicals are scavenged by the hydrogen peroxide; for an atrazine concentration of 10,4 mg L^{-1}, hydroxyl radicals are scavenged by concentrations of hydrogen peroxide above 340 mg L^{-1} (Beltrán et al., 1993a). The oxidation of atrazine, even at high concentrations of hydrogen peroxide, is due to hydroxyl radical attack since the relative concentration of hydrogen peroxide to atrazine indicates that most of the incident light is absorbed by the hydrogen peroxide which produces hydroxyl radicals (Beltrán et al., 1993a). Photo-oxidation of atrazine, in the presence of hydrogen peroxide, leads to the formation of hydroxyatrazine, deethylatrazine, deisopropylatrazine and deethyldeisopropylatrazine (De Laat et al., 1997). The degradation pathway of the photolysis of atrazine in the presence of hydrogen peroxide (indirect photolysis) is the same as that for the ozonation of atrazine as shown in Figure 4.11. Products such as 2-acetamido-6-chloro-4-isopropylamino-*s*-triazine and 2-acetamido-6-chloro-4-ethylamino-*s*-triazine have been detected; 3 % hydroxyatrazine, 6 % 2-acetamido-6-chloro-4-isopropylamino-*s*-triazine, 20 % deethyl-atrazine, 3 % 2-acetamido-6-chloro-4-ethylamino-*s*-triazine, 10 % deisopropylatrazine, 1 % 4-amino-2-acetamido-6-chloro-*s*-triazine and 16 % deethyldeisopropylatrazine were detected for an 87 % conversion of atrazine (Torrents et al., 1997).

The UV degradation of atrazine has also been investigated with photosensitizers such as acetone and photocatalysts such as titanium dioxide and zinc oxide (Burkhard and Guth, 1976; Hustert et al., 1991; Pelizzetti et al., 1990). The use of acetone as a photosensitizer increases the photodegradation of atrazine. Degradation follows first order reaction kinetics. Burkhard and Guth found that after a 6 h exposure period 30 % of the initial atrazine remained unreacted and 16 % deethylatrazine, 5 % deisopropylatrazine, 15 % deethyldeisopropylatrazine and 10 % hydroxyatrazine had formed (Burkhard and Guth, 1976). The degradation of atrazine during UV radiation ($\lambda > 290$ nm) in an aqueous titanium dioxide suspension (250 mg L^{-1}) was found to follow first order reaction kinetics, the atrazine half-life was less than 10 min (Hustert et al., 1991). The degradation rate of deethylatrazine, the primary metabolite of atrazine in soil, is similar to that of atrazine. The photocatalytic degradation pathway of atrazine passes through

deethyldeisopropylatrazine which degrades slowly to cyanuric acid. Atrazine is degraded faster by UV radiation in the presence of titanium dioxide than in the presence of hydrogen peroxide. The atrazine half-life was approximately 6 min in the presence of titanium dioxide and 180 min in the presence of hydrogen peroxide under comparable conditions, 20 mg L^{-1} atrazine concentration, 55 mg L^{-1} hydrogen peroxide concentration and $\lambda > 290$ nm (Hustert et al., 1991). Pelizzetti and co-workers investigated the photocatalytic degradation of atrazine under simulated solar-irradiation conditions (Pelizzetti et al., 1987; Pelizzetti et al., 1990). The spectral distribution of a 1 500 W Xenon lamp above 340 nm simulates solar radiation (Pelizzetti et al., 1987). The half-life of atrazine was approximately 5 and 80 min, respectively, in the presence of titanium dioxide and zinc oxide for an atrazine concentration of 25 mg L^{-1} and a semiconductor concentration of 500 mg L^{-1}. Atrazine degradation in 4 different soil slurries (2 000 mg L^{-1}) with titanium dioxide (5 000 mg L^{-1}) had a half-life, depending on the nature of the soil, of between 10 and 40 min (Pelizzetti et al., 1990). Degradation in the soils was slow in the absence of titanium dioxide; in one soil, atrazine concentration was reduced to approximately 40 % of the initial concentration after 7 d of irradiation (Pelizzetti et al., 1990). Complete degradation of an aqueous solution of atrazine (5 mg L^{-1}) with titanium dioxide (100 mg L^{-1}) occurred within 1 h (Pelizzetti et al., 1987).

Kearney and co-workers found that ozone together with UV radiation decreased the concentration of a 10 and 100 mg L^{-1} atrazine solution by 90 % in 1 h and a 1 000 mg L^{-1} within 4 h (Kearney et al., 1987). Beltrán and co-workers investigated the effects of parameters such as pH, temperature and the presence of radical scavengers on the oxidation of atrazine by UV/ozonation (Beltrán et al., 1994b). Atrazine degradation increased with decreasing pH and increasing temperature (3, 10 and 20 °C). The ozone partial pressure was adjusted so that the ozone solubility in water was the same at the three temperatures. Atrazine degradation also decreased in the presence of bicarbonate and carbonate ions because of the scavenging of hydroxyl radicals (Beltrán et al., 1994b).

The degradation of atrazine during UV/ozonation is determined by three processes, the direct photolysis of ozone, atrazine and hydrogen peroxide; direct reactions of ozone with atrazine and hydrogen peroxide; and reactions between atrazine and radicals generated from the decomposition of ozone and hydrogen peroxide (Beltrán et al., 1994b). The mechanism of the oxidation of atrazine by UV/ozonation consists of the reactions listed in Scheme 4.2 and the reactions listed in Scheme 4.6 (Beltrán et al., 1994b; Zwiener et al., 1995).

$O_3 + H_2O + h\nu \rightarrow H_2O_2 + O_2$		[a]
$H_2O_2 + h\nu \rightarrow 2HO^{\bullet}$		[b]
$A + h\nu \rightarrow products$		[c]
$H_2O_2 \rightleftharpoons HO_2^- + H^+$	pK = 11,7	[d]
$HO_2^- + O_3 \xrightarrow{k_1} HO_2 + O_3^{\bullet -}$	$k_1 = 2{,}8 \times 10^6\ M^{-1}\ s^{-1}$	[e]
$O_3^- + H^+ \rightarrow HO^{\bullet} + O_2$		[f]
$H_2O_2 + HO^{\bullet} \xrightarrow{k_2} HO_2^{\bullet} + H_2O$	$k_2 = 2{,}7 \times 10^7\ M^{-1}\ s^{-1}$	[g]
$HO_2^- + HO^{\bullet} \xrightarrow{k_3} HO_2^{\bullet} + HO^-$	$k_3 = 7{,}5 \times 10^9\ M^{-1}\ s^{-1}$	[h]

Scheme 4.6

The direct photolysis reactions are listed in reactions [a] to [c] of Scheme 4.6. Hydrogen peroxide in neutral solution dissociates to the hydroperoxide ion, reaction [d] of Scheme 4.6. The reaction initiates further decomposition of ozone to produce hydroxyl radicals, reactions [e] and [f]. Reactions of hydrogen peroxide with hydroxyl radicals, reactions [g] and [h], are of low importance because of the low concentration of hydrogen peroxide and high pK value (Beltrán et al., 1994b).

The primary quantum yields of ozone, hydrogen peroxide and atrazine, reactions [a], [b] and [c] of Scheme 4.6, are 0,62; 0,5 and 0,05 mol per photon, respectively (Beltrán et al., 1994b). The extinction coefficients at 254 nm of hydrogen peroxide and ozone, 18,6 and 2 900 L mol^{-1} cm^{-1}, respectively, indicate that since hydrogen peroxide is the least light absorbing species (lowest extinction coefficient) the formation of hydroxyl radicals from reaction [b] of Scheme 4.6 would be significantly lower than that formed through reactions [d] to [f] (Beltrán et al., 1994b; Zwiener et al., 1995). Atrazine degradation is due mainly to reaction with hydroxyl radicals, followed by direct photolysis and the lowest contribution due to direct ozonation (Beltrán et al., 1994b).

Both Beltrán and co-workers and Zwiener and co-workers represented the degradation of atrazine by a first order differential equation with three terms representing each of the contributing processes, ozonation, photolysis and photolytic oxidation (Beltrán et al., 1994b; Zwiener et al., 1995). The equation proposed by Beltrán and co-workers is listed in equation 4.5.

$$\frac{-dC_A}{dt} = k_d C_A C_{O_3} - I_A + k_{HO,A} C_A C_{HO} \qquad [4.5]$$

The first term on the right hand side of the equation represents degradation due to direct reaction with ozone in the liquid phase, the third term the photolytic oxidation due to reaction with hydroxyl radicals. The second term I_A represents degradation due to direct photolysis and is calculated using equation 4.6.

$$I_A = -\Phi_A I_0 f_A [1 - \exp(-2{,}3 L \Sigma \varepsilon_i C_i)] \qquad [4.6]$$

where Φ_A is the quantum yield of atrazine, I_0 the effective intensity of the incident radiation in water, L the effective path of radiation, ε_i and C_i the extinction coefficient and concentration of a species i present in the water and f_A the fraction of radiation absorbed by atrazine (Beltrán et al., 1994b).

Beltrán and co-workers compared various oxidation technologies for the degradation of atrazine, the degradation rate increased in the order: direct photolysis < ozonation < UV radiation with hydrogen peroxide < UV radiation with ozonation (Beltrán et al., 1994b). Atrazine degradation in the presence of hydroxyl radical scavengers, such as bicarbonate or carbonate ions, is the same for direct photolysis, ozonation and UV radiation with hydrogen peroxide and is greatest for UV radiation with ozone (Beltrán et al., 1994b).

Zwiener and co-workers investigated the degradation of atrazine and deethylatrazine by UV radiation with ozone (ozone doses of 0; 2,2; 4,4; 6,7; and 8,9 mg L^{-1} and a UV radiant power of 42,5; 54,6; 72,25 and 85 W L^{-1}) in a large-scale water treatment plant (Zwiener et al., 1995). Atrazine of concentration 0,28 μg L^{-1} was degraded in a 70 m^3 h^{-1} flowrate of raw water to below the EEC threshold limit for pesticides (0,1 μg L^{-1}) at ozone doses of 4,4; 6,9 and 8,9 mg L^{-1} in combination with a radiant power of between 42,5 and 85 W L^{-1}. A radiant power greater than 72,25 W L^{-1} was required to reduce the ozone concentration in the outlet water to the allowed threshold limit for ozone (0,05 mg L^{-1}) in drinking water. The concentration of deethylatrazine, at a flow rate of 70 m^3 h^{-1}, was reduced from 0,6 to 0,25 μg L^{-1} for an ozone dose of 8,9 mg L^{-1} and a UV radiant power of 85 W L^{-1}. The outlet concentration of deethylatrazine was only reduced to the EEC limit of 0,1 μg L^{-1} at an ozone dose of 16 mg L^{-1} and a radiant power of 85 W L^{-1} when the hydraulic residence time in the UV radiation unit was increased by decreasing the water flow from 70 to 30 m^3 h^{-1} (Zwiener et al., 1995).

4.3.3 Ultrasonic degradation

The advanced oxidation technology, ultrasound, has also been investigated for application in water treatment. Investigations by Koskinen and co-workers and Pétrier and co-workers have indicated that atrazine is degraded by ultrasound (Koskinen et al., 1994; Pétrier et al., 1996).

Atrazine degradation followed first order reaction kinetics with a rate constant of 2,10 x 10^{-3} min^{-1} for sonication of a 0,67 mg L^{-1} atrazine solution, at 30 ° C, with a Heat-Systems Ultrasonics model W-225R sonicator operating at a power of between 70 and 80 W and a frequency of 20 kHz (Koskinen et al., 1994). A 200 mL sample volume was sonicated in a 250 mL beaker. The solution pH did not change significantly during sonication, after 120 min, pH had changed from 7,64 to 7,45 (Koskinen et al., 1994). The rate of atrazine degradation increased with increasing frequency; the initial degradation rate was 7,8 times greater at 500 kHz than at 20 kHz for sonication at 20 °C with an acoustical power of 18,5 W (Pétrier et al., 1996).

Hydrogen peroxide formation was also greater at 500 kHz than at 20 kHz. The concentration of an atrazine solution (22 mg L^{-1} initial concentration) was reduced within 80 min, during sonication of a 100 mL sample at an acoustical power of 18 W and frequency of 500 kHz, to below the detection limit (0,02 mg L^{-1}) of the system (Pétrier et al., 1996).

Sonochemical degradation products (deethylatrazine, deisopropylatrazine and deethyldeisopropylatrazine) resulted from dealkylation of atrazine similarly to that occurring during the oxidation of atrazine by ozone or photocatalysis with titanium dioxide (Pétrier et al., 1996). The intermediate, 2,4-diamino-6-chloro-N-aceto-N'-(1-methylethyl)-1,3,5-triazine, was also detected. This intermediate precedes the formation of deethylatrazine and characterises the reaction of hydroxyl radicals with the carbon atom adjacent to a secondary amine (De Laat et al., 1995). Sonochemical degradation of atrazine is due to reaction with hydroxyl radicals, the presence of *n*-pentanol (a radical scavenger) during sonication totally inhibited the degradation of atrazine (Pétrier et al., 1996). The higher hydrogen peroxide formation at an ultrasonic frequency of 500 kHz accounted for the greater atrazine degradation at that frequency since more hydroxyl radicals would be present (Pétrier et al., 1996). The reactions reported by Pétrier and co-workers to occur during the ultrasonic degradation of atrazine are listed in Scheme 4.7.

Initiation step

$$H_2O \overset{)))}{\rightarrow} H^{\bullet} + HO^{\bullet} \quad [a]$$

$$O_2 \overset{)))}{\rightarrow} 2O^{\bullet} \quad [b]$$

Reactions in the cavitation bubble

$$H^{\bullet} + O_2 \rightarrow HO_2^{\bullet} \quad [c]$$

$$O + H_2O \rightarrow 2HO^{\bullet} \quad [d]$$

$$2HO^{\bullet} \rightarrow H_2O + O \quad [e]$$

$$2O^{\bullet} \rightarrow O_2 \quad [f]$$

$$HO_2^{\bullet} + HO^{\bullet} \rightarrow H_2O + O_2 \quad [g]$$

Reactions in the interfacial area of a cavitation bubble

$$2HO_2^{\bullet} \rightarrow H_2O_2 + O_2 \quad [h]$$

$$2HO^{\bullet} \rightarrow H_2O_2 \quad [i]$$

$$A + HO^{\bullet} \rightarrow products \quad [j]$$

Scheme 4.7

The degradation of atrazine is initiated by the homolytic scission of water and oxygen, reactions [a] and [b] of Scheme 4.7. Water and oxygen are reformed from the radical reactions (reactions [c] to [g]) occurring in the cavitation bubble. Hydrogen peroxide and products from the reaction of hydroxyl radicals and atrazine are produced in the interfacial area of a cavitation bubble and in the bulk solution. Atrazine degradation is related to the availability of hydroxyl radicals escaping the cavitation bubble (Pétrier et al., 1996).

4.3.4 Biological treatment

Atrazine is not readily degraded in activated sludge systems during water treatment (Dries et al., 1987; Hogrefe et al., 1986; Meakins et al., 1994; Nsabimana et al, 1996). Meakins and co-workers investigated the behaviour of atrazine and its primary degradation products, deethylatrazine and deisopropylatrazine, during bench-scale primary and secondary wastewater treatment (Meakins et al., 1994). The triazine compounds remained in solution and were not removed during primary sedimentation by adsorption onto settleable solids. Secondary treatment with biologically active mixed liquor (of different suspended solids concentration) removed between 9 and 39 % of the triazine compounds. The reduction in concentration was not a biological process since similar results were achieved with mixed liquor in which the microbial activity had been suppressed by the addition of a 1 % (w/v) sodium azide solution and reduction in temperature to 4 °C. The percentage removal of triazine herbicides with mixed liquor, as shown in Table 4.10, increased with increasing suspended solids concentration (Meakins et al., 1994). Reduction in triazine concentration during secondary wastewater treatment was thus due to physical adsorption onto suspended solids (Meakins et al., 1994).

Table 4.10 : Removal of triazine herbicides with mixed liquor with different concentrations of suspended solids (Meakins et al., 1994)

	Triazine herbicide removal (%)			
Suspended solids (mg L^{-1})	**0**	**1,900**	**2,200**	**2,700**
atrazine	-0.9	12.5	18.6	35.5
deethylatrazine	4.9	9.5	16.5	21.0
deisopropylatrazine	-6.5	15.4	17.2	39.1

The maximum removal of deisopropylatrazine (39 %) indicated that the bulk of triazine compounds would pass through a sewage treatment process and be discharged in the effluent into the environment. A conventional two-stage sewage treatment process is thus ineffective in substantially reducing the concentration of triazine compounds (Meakins et al., 1994).

Nsabimana and co-workers investigated the effects of atrazine on the microbiology of the activated sludge process since atrazine is toxic to organisms such as bacteria and fungi in soil and algaes and shrimps in aquatic ecosystems (Nsabimana et al., 1996). Six bacterial strains were isolated from a sludge sample as representative of activated sludge microflora. Growth of the bacterial strains was unaffected by atrazine concentrations of 1 and 10 mg L^{-1}; an atrazine concentration of 100 mg L^{-1} retarded the growth of one of the bacterial strains. The total bacterial count and biomass (measured as mixed liquor volatile suspended solids) were reduced in a laboratory pilot plant that was fed continuously with an atrazine concentration of either 1 mg L^{-1} for 6 d or 20 mg L^{-1} for 7 d. Chemical oxygen demand (COD) was increased after 22 h for an

atrazine concentration of 20 mg L^{-1}. Sludge metabolic activities such as dehydrogenation, proteolyis, nitrification and denitrification were unaffected by atrazine (Nsabimana et al., 1996).

Volskay and co-workers investigated the toxicity of various organic compounds (including atrazine) to activated sludge microorganisms by measuring the concentration that reduced the oxygen consumption of the organisms by 50 % in comparison to a control (Volskay and Grady, 1988; Volskay et al., 1990). Oxygen consumption was reduced by 5 % for an atrazine concentration (33 mg L^{-1}) equal to its solubility limit (Volskay and Grady, 1988; Volskay et al., 1990).

Hogrefe and co-workers developed a small-scale system that was capable of degrading 80 % of triazine compounds in real wastes (Hogrefe et al., 1985). The process consisted of a mixed bacterial culture (aerobic) maintained at 37 °C in an open, unsterilised system. An added source of carbon, such as glucose, in a molar ratio of carbon to nitrogen of 10 was required for microbial growth. Microbial growth and thus atrazine degradation was retarded by salt concentrations above 3 %. A residence time of 40 h (i.e. a dilution rate of 0,025 h^{-1}) was necessary to prevent washout. The dilution rate was too low for industrial applications and a fluidised bed reactor, in which the organisms were immobilised on a layer of sand, was developed (Hogrefe et al., 1986). The biomass concentration, of between 12 and 18 g L^{-1} volatile suspended solids, in the reactor was 10-fold higher than that in the continuous culture system; a lower residence time (25 h versus 40 h) was also achieved. The system recovered readily from process perturbations. Aerobic conditions and an added carbon source were required to achieve maximal removal (approximately 80 %) of triazine compounds (Hogrefe et al., 1986).

A mixed microbial culture has also been used to degrade atrazine in soil and water systems (Grigg et al., 1997). Degradation in soil, after 100 d, was 78 and 21 %, respectively, for atrazine concentrations of 10 and 50 g L^{-1}; degradation in water, after 80 d, was 90 and 56 %, respectively. Lower degradation of the 50 g L^{-1} atrazine concentration was attributed to phosphorous depletion. Degradation of these atrazine concentrations indicated that mixed microbial cultures could be used for atrazine bioremediation at contamination concentrations, typically between 0,02 and 410 mg L^{-1}, reported at agrochemical mixing and loading facilities (Grigg et al., 1997).

Microorganisms, in the biological transformation of pesticides and other compounds in natural waters, use a variety of electron acceptors such as oxygen, nitrate, sulfate and carbon dioxide (Wilber and Parkin, 1995). The dominant electron acceptor condition can affect the rate of transformation of compounds. Wilber and Parkin investigated the biotransformation of atrazine under aerobic, nitrate-reducing, sulfate-reducing and methanogenic conditions (Wilber and Parkin, 1995). Biotransformation occurred under all electron acceptor conditions. The relative rates of transformation decreased in the order methanogenic > sulfate-reducing > aerobic > nitrate-reducing conditions, however, the differences in rates were not statistically significant at a 95 % confidence limit. Atrazine was transformed as a secondary co-metabolic substrate; acetate was fed as a

primary substrate and transformation, under aerobic and nitrate-reducing conditions, stopped once the acetate had been depleted (Wilber and Parkin, 1995).

Ozonation has been used as a pretreatment for soil biodegradation of atrazine because of the enhanced biodegradability of the oxidation by-products (Kearney et al., 1988). Kearney and co-workers developed a two-chamber unit consisting of ozonation and subsequent circulation through a biologically active soil column for on-site treatment of herbicide wastewater (Kearney et al., 1988; Somich et al., 1990). Degradation of atrazine in the soil column after 50 d, as shown in Table 4.11, increased with increasing pH of ozonation.

Table 4.11 : Effect of ozone pretreatment on atrazine biodegradation in soil columns after 50 d (Kearney et al., 1988)

	Percentage atrazine degradation (%)
without ozonation	< 20
ozonation at pH 6,5 (unbuffered)	55
ozonation at pH 8	65
ozonation at pH 10	75

Atrazine solutions, after ozonation at pH 10, were neutralised before being added to the soil column of the unit developed by Kearney and co-workers. The microbial population of the soil column was fortified with *Pseudomonas* strain A since different strains of *Pseudomonas* have been identified that degrade atrazine (Behki and Khan, 1986; Shapir and Mandelbaum, 1997). Atrazine metabolism was rapid in the first 3 d, slower over the following 7 d and levelled off at approximately 60 % after 15 d of treatment. Indigenous soil microorganisms, without the addition of *Pseudomonas* strain A, degraded atrazine more slowly, a 40 % degradation was achieved after 15 d (Kearney et al., 1988).

Ozonation and metabolism in a biologically active soil column were used to treat the pesticide waste and rinsate, a mixture of several pesticides, from a small farm (Somich et al., 1990). Degradation kinetics of atrazine in solution with other pesticides did not follow first order reaction kinetics as did degradation in pure solution. The lag in degradation was attributed to preferential reaction of ozone with other compounds such as formulating agents (Somich et al., 1990). Atrazine concentration, in 114 L batch experiments, decreased from 17,2 mg L^{-1} in the untreated pesticide waste to 8,8 mg L^{-1} after ozonation and 5,1 mg L^{-1} after ozonation and circulation through the soil column (Somich et al., 1990).

Bioassays were conducted to determine the toxicity of by-products produced from treatment of the pesticide waste and rinsate (Somich et al., 1990). Wheat, a monocotoyledon, and soybean, a dicotyledon, were treated 2 wk post-emergence with either distilled water, untreated pesticide waste, ozonated pesticide waste or

pesticide waste that had been ozonated and circulated through the soil column. Leaves of the soybean plants that had received untreated pesticide waste were withered and discoloured after 1 wk; all other plants appeared normal. Wheat plants showed no visible differences after 3 wk; soybean plants that had received untreated pesticide waste were stunted relative to the control, while the plants that had received either of the treated solutions were larger and healthier. This was attributed to the bioavailable nitrogen in the oxidation by-products. Toxic effects were not observed in wheat or soybean plants that received untreated or treated pesticide waste (Somich et al., 1990). Ames tests using several strains of *Salmonella typhimurium* and one strain of *Escherichia coli*, with and without metabolic activity, showed no evidence of mutagenic activity in untreated pesticide waste, ozonated pesticide waste or pesticide waste that had been ozonated and circulated through the soil column (Somich et al., 1990).

Oxidation of atrazine in the binary treatment system consisting of ozonation and biomineralisation produced chlorodiamino-*s*-triazine as the final ozonation product (Leeson et al., 1993). This compound is used as a nitrogen source by the microbial species in the soil column, however, agricultural wastes usually contain other nitrogen sources such as ammonia fertilisers. An ammonia concentration of 0,14 g L^{-1} inhibited the biodegradation of atrazine by *Pseudomonas* strain A. The microbial strain *Klebsiella terragena* (strain DRX-I) which preferred an organic nitrogen source and was able to tolerate high ammonia concentrations was isolated from a sewage sludge (Hapeman et al., 1995; Leeson et al., 1993). Degradation of chlorodiamino-*s*-triazine by *Klebsiella terragena* required an added carbon source (corn syrup) and occurred regardless of the presence of ammonia. Complete mineralisation of chlorodiamino-*s*-triazine occurred within 3 d in the presence of either a 0,07 or 0,14 g L^{-1} ammonia concentration; 40 % degradation occurred within 10 d in the presence of a 14 g L^{-1} ammonia concentration. The complete utilisation of chlorodiamino-*s*-triazine in the presence of ammonia concentrations of 0,07 and 0,14 g L^{-1} indicated that *Klebsiella terragena* had a strong preference for chlorodiamino-*s*-triazine as a nitrogen source and that both the nitrogen atoms of the amino groups and the triazine ring structure were being utilised as nitrogen sources (Leeson et al., 1993). Degradation of chlorodiamino-s-triazine occurred via the intermediate aminochlorohydroxy-*s*-triazine (Hapeman et al., 1995). Pilot-scale trials of the ozonation and biomineralisation process of pesticide wastes were performed in a 200 L system (Hapeman et al., 1995). Formulated atrazine was mineralised by *Klebsiella terragena* with and without ammonium nitrate (NH_4NO_3), a fertiliser often found in agricultural waste, with respective ozonation efficiencies of 0,0088 and 0,0108 mol of atrazine per mol of ozone (Hapeman et al., 1995).

4.4 CONCLUDING REMARKS

Atrazine is a herbicide that acts due to the inhibition of photosynthesis and is thus less toxic to animals than to plants. The effect of atrazine on humans has not been fully investigated though it appears to be minimally toxic during inhalation, eye and skin contact and for ingestion in small quantities.

The major concern with atrazine is its persistence in the environment, its half-life in soil varies between 14 and 109 d, it has been found to persist from year to year in soil and water. It is the most frequently detected herbicide in ground and surface waters in Europe and the United States. The presence and persistence of atrazine in potable water sources has resulted in various countries regulating or banning the use of atrazine. Health standards in the US have been set for atrazine at 0,3 $\mu g\ L^{-1}$ and in Europe at 0,1 $\mu g\ L^{-1}$.

Atrazine in soil is degraded or adsorped into soil particles. Degradation is through hydrolysis to form hydroxyatrazine or via *N*-dealkylation to form deethylatrazine and deisopropylatrazine. Dealkylation is usually due to microbial action whereas hydrolysis is an adsorption-catalysed chemical reaction. Further degradation is via deamination and ring cleavage. The degradation products are more biodegradable than atrazine.

Groundwater contamination occurs due to atrazine leaching through the soil. Deethylatrazine and deisopropylatrazine are the main degradation products that leach because of their lower retention in soil. Further degradation does not continue in groundwater due to the lower temperatures and microbial populations. Atrazine accumulation in surface water is due to runoff from agricultural fields during rainfall and irrigation. Deethylatrazine and deisopropylatrazine are also formed from the degradation of other triazine herbicides such as simazine, cyanazine and propazine.

Chlorine, chlorine dioxide and chloramine have no effect on atrazine during water treatment. Atrazine is also not readily degraded in an activated sludge system or affected by flocculation and coagulation in a clarifier. Nanofiltration removes between 80 and 90 % of atrazine. Atrazine concentration is reduced by about 83 % during ozonation and between 95 and 97 % with the use of granular activated carbon. Pretreatment with ozone improves atrazine degradation in an activated sludge system (due to the enhanced biodegradability of the degradation products) as well as the length of time before atrazine breakthrough occurs in activated carbon filters. Atrazine degradation during ozonation is improved with the addition of hydrogen peroxide. Atrazine is also degraded by ultrasound.

The nature of the ozonation degradation products depends upon reaction conditions, although, ring cleavage does not occur. Degradation is due to both reaction with ozone and hydroxyl radicals. The direct reaction with ozone produces only dealkylated products whereas dealkylated and hydrolysed products are formed from the reaction with hydroxyl radicals. Hydrogen peroxide is formed during the production of dealkylated products. The higher rate constant indicates that the reaction with hydroxyl radicals is faster than the direct reaction with ozone. Both reactions occur in the bulk solution and are not limited by mass transfer.

5

EXPERIMENTAL DESIGN

The advanced oxidation processes, ultrasound and ozone, have been investigated. The equipment designed and used during the investigation, as well as, the analytical procedures followed are described in this chapter. The ultrasonic equipment is detailed in Section 5.1, ozonation equipment in Section 5.2, experimental procedures in Section 5.3, analytical procedures in Section 5.4 and the statistical software program in Section 5.5.

5.1 ULTRASOUND EQUIPMENT

The investigation of the sub-processes occurring during sonication and the degradation of atrazine was performed in an ultrasonic laboratory reactor (ultrasonic cell). The cell was designed and operated using an ultrasonic horn for an energy source. The ultrasonic horn is described in Section 5.1.1 and the ultrasonic cell in Section 5.1.2.

5.1.1 Ultrasonic horn

A 20 kHz Ultrasonic process system, model P100/2-20, was obtained from Sonic Systems (postal address: Unit 3, Monks Dairy, Isle Brewers, Taunton, Somerset, TA3 6QL, UK). The system, shown in Figure 5.1, consists of a generator (model P100-20), transducer assembly (model 23820-AS) and an high intensity ultrasonic horn (part no. A93655) with replaceable tip (part no. A93656-2).

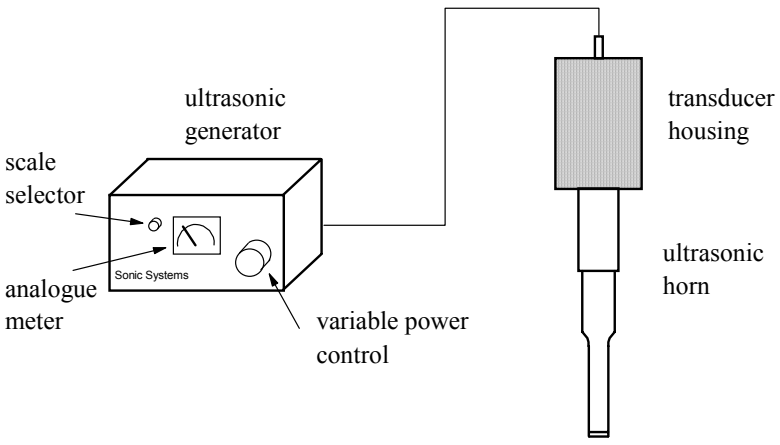

Figure 5.1 : Ultrasonic process system

The system operates at a nominal frequency of 20 kHz. The vibration amplitude of the transducer and the electrical power to the transducer are determined by means of a variable control mounted on the front panel of the generator assembly. Amplitude and electrical output by means of a selector switch are read from an analogue meter, amplitude off the green scale and electrical power off the red scale. The amplitude of the peak to peak transducer displacement is calibrated in micrometres, the meter range is 0 to 15 μm. Electrical power is measured in Watts, the meter range is 0 to 100 W. The mass of the generator assembly is 4,5 kg, the width, depth and height dimensions are 321, 175 and 110 mm, respectively. The generator assembly is designed for continuous operation without forced air cooling (Sonic Systems, 1994).

The pre-stressed piezoelectric transducer is mounted in a sealed housing and is designed for continuous operation at ambient temperature (5 to 40 °C). The mass of the transducer assembly is 0,332 kg. A schematic diagram and a picture of the transducer assembly and ultrasonic horn are presented in Figure 5.2.

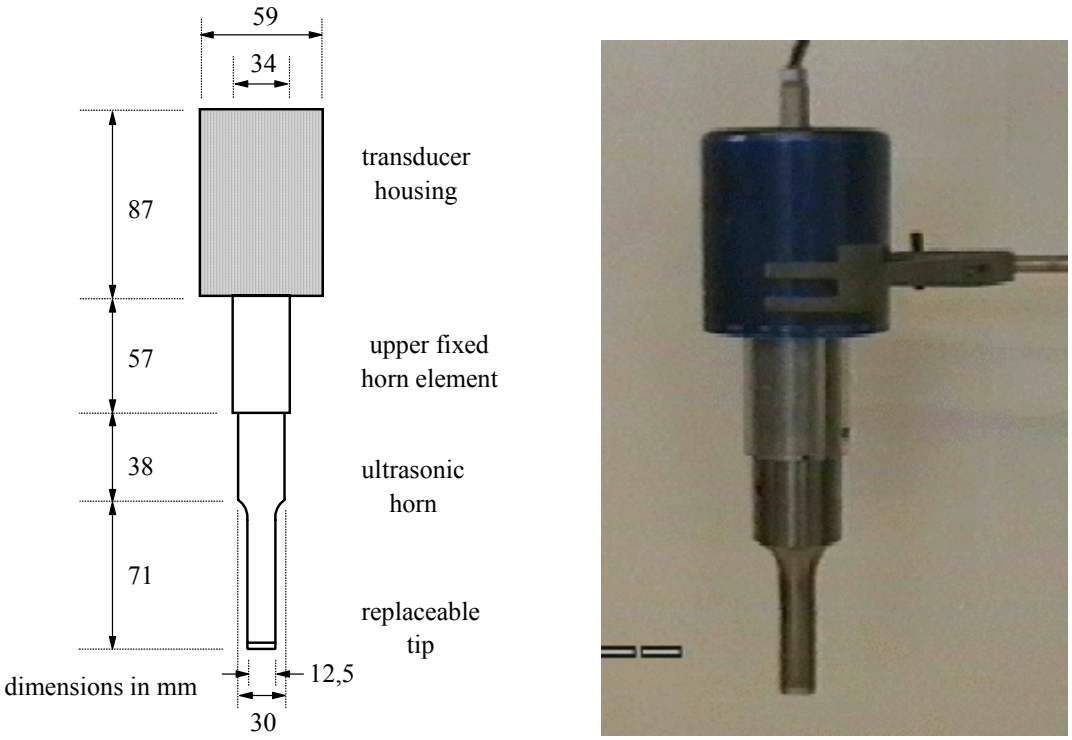

Figure 5.2 : Ultrasonic horn

The horn and replaceable tip are manufactured from a titanium alloy (Ti-64) containing 6 % of an aluminium alloy and 4 % vanadium (Perkins, 1997b). The horn is coupled to the transducer assembly by a stud that is screwed into the transducer. The working surface of the horn is eroded during sonication. Erosion of the horn is prevented with the use of a replaceable tip screwed into the end of the horn. Replacement of a tip due to erosion is less expensive than replacement of the entire horn. Approximately 1 mm of the tip can be machined without significantly changing the total length of the horn and thus affecting the resonant

frequency of the system (Perkins, 1997a). The surface of the tips used during the investigation were machined once the electrical power drawn by the transducer for a preset vibrational amplitude began to fluctuate. A tip was replaced when the machined surface had also eroded. The effect of machining the surface of a horn tip on the performance of the ultrasonic system was evaluated by measuring the formation of hydrogen peroxide generated by a new tip and comparing it to that generated after machining (Section A.1.1 of Appendix A). The data presented in Figure A.1 indicates that machining the surface of a horn tip does not affect the performance of the system.

The Ultrasonic process system supplied by Sonic Systems has a *power-by-demand* characteristic, the generator automatically delivers the required electrical power to maintain a preset transducer displacement amplitude irrespective of the load conditions (Sonic Systems, 1994). The acoustic power transferred to a sample is calculated (equation 5.1) from the difference between the electrical power supplied to the transducer when the horn is placed in a sample and the electrical power supplied to the transducer when the horn is without load (Sonic Systems, 1994). The horn is defined as being without load when the tip rests in air and is not submersed in any sample.

$$\text{Acoustic power (W)} = \left(\begin{array}{l}\text{electrical power supplied to}\\ \text{transducer when loaded}\end{array}\right) - \left(\begin{array}{l}\text{electrical power supplied to}\\ \text{transducer when unloaded}\end{array}\right) \qquad [5.1]$$

The calculation of acoustic power is based on the assumption that the losses in the system are only mechanical and displacement-related, electrical losses are low and can be ignored (Perkins, 1997a). The losses in the system are mechanical hysteresis losses in the transducer stack (both in the piezoceramic and at the interface joints), dynamic frictional losses in the transducer compression bolt threads and mechanical losses in the transducer and horn materials (Perkins, 1997a). The total electrical power (as indicated on the power meter) supplied to the transducer when it is unloaded is used to overcome these mechanical losses at a set transducer displacement amplitude. The mechanical losses are unchanged when the transducer is loaded and operated at the same displacement amplitude, the measurement indicated on the power meter is thus the sum of the acoustic mechanical losses and the acoustic power supplied to the reaction solution. It follows that the acoustic power supplied to a treatment sample is the difference between the loaded transducer power and the unloaded transducer power (Perkins, 1997a).

The efficiency of the energy transformation of the ultrasonic horn was determined by comparison of acoustic power with electrical power. Acoustic power is the energy delivered into a reaction solution, electrical power is the energy drawn at the wall. The electrical power supplied to the transducer of the ultrasonic horn was read from the meter on the face of the ultrasonic generator when the transducer was loaded. The acoustic power was calculated from the difference in electrical power supplied to the transducer when loaded and without load (Sonic Systems, 1994). The calculation of acoustic power was confirmed using calorimetry (described in Section A.1.2). The average acoustic power measured during sonication at each transducer displacement amplitude is compared in Table 5.1 with the average electrical power.

Table 5.1 : Conversion of electrical power to acoustic power

Transducer displacement (μm)	Average acoustic power (W)	Average electrical power (W)	Energy conversion (%)
5	24.2	28.2	86
8	39.3	46.3	85
11	56.7	68.7	83

Acoustic powers generated during sonication with the ultrasonic horn at different transducer displacement amplitudes are recorded in Table 5.1. The conversion of electrical to acoustic power by the ultrasonic horn is approximately 85 %.

5.1.2 Ultrasonic cell

An ultrasonic laboratory reactor (ultrasonic cell) was designed and constructed to investigate the free radical reactions occurring during sonication and to apply in a case study of the ultrasonic degradation of a model organic compound. The ultrasonic cell is shown in Figure 5.3.

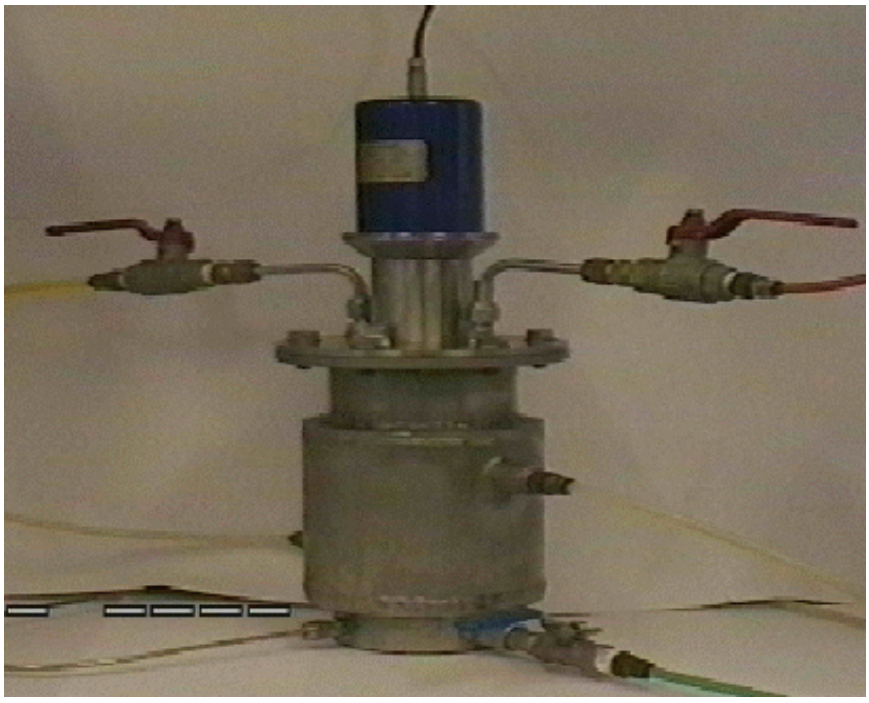

Figure 5.3 : Ultrasonic cell

The ultrasonic cell (manufactured from 316 stainless steel) is 195 mm high (from the base to the top of the lid) and the external diameter of the water jacket is 114 mm. Other dimensions of the cell are presented in

Figure 5.4. A 500 mL sample can be sonicated in the cell. Temperature is measured by a thermocouple in a well centred at the bottom of the cell and is regulated by the circulation of cooling water in the water jacket. A schematic diagram of the cell is shown in Figure 5.4.

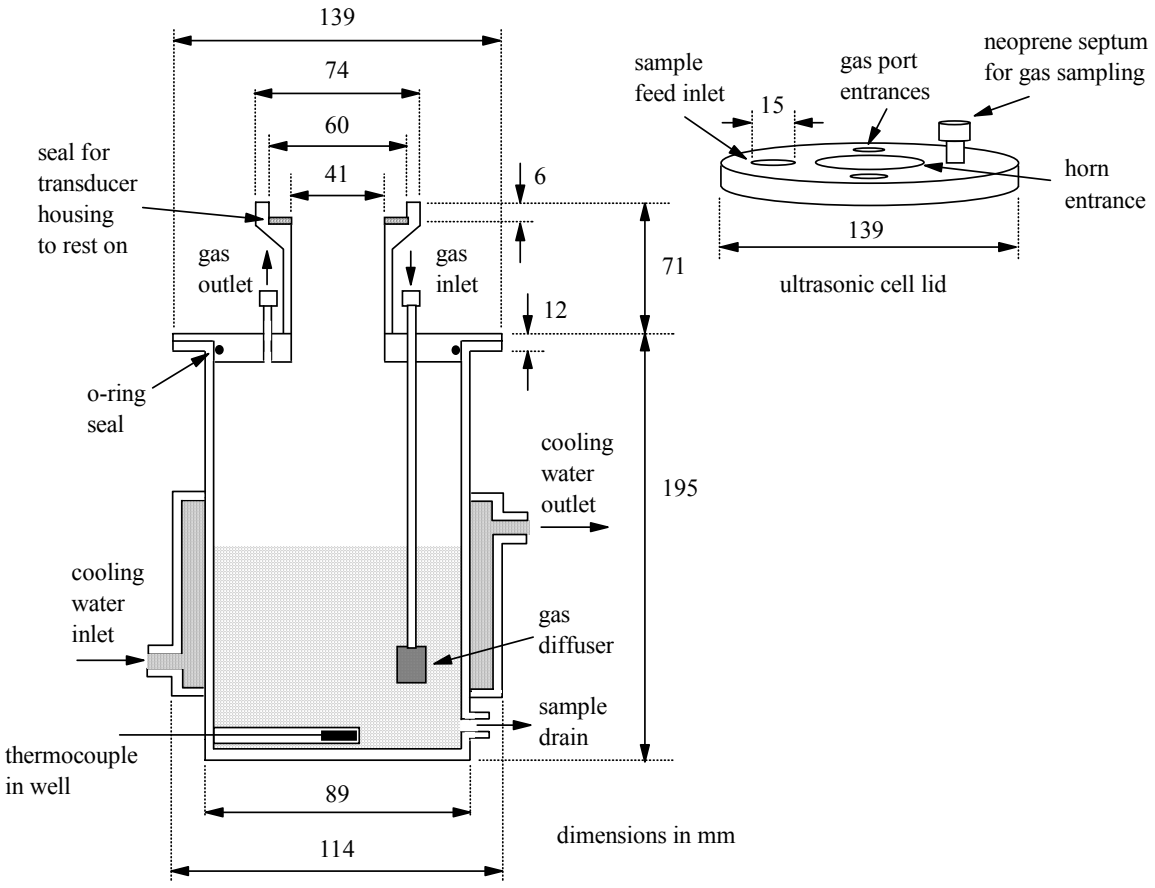

Figure 5.4 : Schematic diagram of ultrasonic cell

The sample inlet port, gas inlet and outlet ports and a neoprene septum for gas sampling are positioned, as shown in Figure 5.4, in the lid of the cell. A liquid sample can be saturated with gas during sonication by bubbling the gas through the stainless steel diffuser in the cell.

The parameters that affect cavitation and thus the outcome of a sonochemical experiment are listed in Table 2.5 in Section 2.5.5. These parameters include the characteristics of the reaction medium (viscosity, vapour pressure, presence of solid particles), reaction conditions (pressure, temperature, gas sparging) and the type of ultrasonic system (power, frequency, reactor size and geometry). These parameters were taken into account during the design of the ultrasonic cell and are discussed in the following subsections.

5.1.2.1 Frequency

Ultrasonic experiments are usually performed at frequencies of between 20 and 100 kHz, the frequencies used in different ultrasonic investigations are reported in Section 2.5.5. The ultrasonic intensity required to

initiate cavitation increases as frequency increases (Mason, 1993; Pestman et al., 1994). Commercial ultrasonic equipment operate at a fixed frequency (determined by the transducer) and optimisation in regards to frequency cannot be performed. The frequency of the Ultrasonic process system supplied by Sonic Systems is 20 kHz (Sonic Systems, 1994).

5.1.2.2 Acoustic power

Ultrasonic effects are determined primarily by the amount of acoustic power delivered to a system. Acoustic power is also reported in literature as intensity (or power density), either, in terms of the surface radiating area of the ultrasonic source or the volume of liquid sonicated (Table 2.6 in Section 2.5.5). Perkins defined intensity as the electrical power supplied to the transducer divided by the radiating surface area of the ultrasonic horn (Perkins, 1990).

The acoustic power delivered by the Ultrasonic process system from Sonic Systems was varied by changing the displacement amplitude of the transducer from 0 to 12 μm. The ultrasonic effects, in 500 mL of water, increased with increasing power. Experiments were performed at a transducer displacement of 11 μm and not at 12 μm because the maximum displacement vibration began to decrease as the horn tip eroded. Experiments were also performed at displacement amplitudes of 5 and 8 μm when the effect of acoustic power was being investigated. Typically, 69 W of electrical power was required by the transducer to generate a displacement of 11 μm when the ultrasonic horn was loaded with 500 mL of water. An electrical power of 12 W was required by the transducer to generate a displacement of 11 μm when the horn was without load. Hence, the acoustic power delivered to 500 mL of water for a transducer displacement of amplitude of 11 μm was 57 W. Ultrasonic intensity calculated in terms of the radiating surface area of the horn (1,25 cm diameter; 1,23 cm^2 radiating surface area) was 46,1 W cm^{-2}. The radiating surface area was calculated from π x $(radius)^2$. Ultrasonic intensity calculated in terms of the volume of liquid sonicated (500 mL) was 0,114 W cm^{-3}. Acoustic power and ultrasonic intensity (in terms of both area and volume) of the Ultrasonic process system for sonication of a 500 mL sample at transducer displacement amplitudes of 5, 8 and 11 μm are reported in Table 5.2.

Table 5.2 : Acoustic power and intensity of the Ultrasonic process system

Transducer displacement (μm)	Acoustic power (W)	Ultrasonic intensity (W cm^{-2})	Ultrasonic intensity (W cm^{-3})
5	24.2	19.7	0.048
8	39.3	32.0	0.079
11	56.7	46.1	0.114

The ultrasonic intensity at the radiating horn surface of the Ultrasonic process system, shown in Table 5.3, is comparable with that of other investigations using an ultrasonic horn.

Table 5.3 : Comparison of the ultrasonic intensity of the Ultrasonic process system with that of other sonochemical investigations using an ultrasonic horn

Reference	Investigation	Frequency (kHz)	Ultrasonic intensity (W cm^{-2})
(Pugin, 1987)	enhancement of reaction between lithium and 1-bromopentane	20	24
(Donaldson et al., 1979)	polymerisation of nitrobenzene	20	25
(Price et al., 1994)	degradation of aromatic compounds	22	39
this investigation	**degradation of atrazine**	**20**	**46**
(Suslick et al., 1989)	effect of ultrasound on nickel and copper powders	20	50
(Serpone et al., 1994)	degradation of chlorophenol compounds	20	52
(Ratoarinoro et al., 1992)	enhancement of reaction between ethyl malonate and chalcone	20	57
(Kotronarou et al., 1992b)	degradation of hydrogen sulfide	20	75

5.1.2.3 Horn shape

The vibrating motion generated by a transducer is magnified by the horn (Goodwin, 1990; Perkins, 1990). Different shapes of ultrasonic horns and the magnification obtained with each shape is discussed in Section 2.5.3. Materials of construction are also discussed in Section 2.5.3. Two stepped ultrasonic horns manufactured from a titanium alloy were obtained with the Ultrasonic process system. The low intensity horn had an upper and lower diameter of 3,0 and 2,0 cm, respectively, and the high intensity horn an upper and lower diameter of 3,0 and 1,25 cm, respectively. The magnification of transducer displacement calculated for the low and high intensity ultrasonic horns was 2,25 and 5,76, respectively. Magnification for stepped horns is calculated from the square of the ratio of upper to lower horn diameter (Perkins, 1990).

The low intensity horn was only used during preliminary experiments (reported in Section A.1.3) to determine acoustic intensity in sample volumes from 100 to 1 000 mL. The high intensity horn was incorporated in the design of the ultrasonic cell all experiments in the cell were performed with the high intensity horn.

5.1.2.4 Volume

Preliminary experiments using the low intensity ultrasonic horn (Section A.1.3 of Appendix A) indicated that the initial rate of hydrogen peroxide formation increased with increasing ultrasonic intensity and hence decreasing sample volume for a range of water volumes from 100 to 1 000 mL. Gondrexon and co-workers, in an investigation of the sonochemical degradation of chlorophenol, found that the rate of degradation decreased with increasing sample volume for the range of 100 to 400 mL when the acoustic power input was 60 W (Gondrexon et al., 1993). Sonochemical effects decrease with increasing sample volume for a set acoustic power input. The volume of a sample to be sonicated in the ultrasonic cell was fixed at 500 mL. The volume had to be large enough so that the kinetic information would be applicable for process scale-up but also small enough so that the ultrasonic intensity would be sufficient to cause sonochemical effects. The sample volume could also not be too big since as discussed in Section 2.5.3 a small zone of high intensity is created around the tip of an ultrasonic horn and intensity decreases with increasing distance from the horn tip (Goodwin, 1990; Pugin, 1987; Suslick et al., 1984). The internal diameter of the cell is 8,1 cm and the height of a 500 mL sample in the cell is thus 9,7 cm. The diameter was chosen so that the sample volume would not be flat and wide which would have created deadspots in the liquid on either side of the horn tip. The height of the cell was calculated such that the tip of the horn would be approximately 1 cm below the surface of the liquid and would not be exposed even with the vigorous liquid movement and splashing that occurs during sonication. The total volume of the ultrasonic cell is approximately 900 mL.

The volume of a sample (500 mL) that can be sonicated in the ultrasonic cell is compared in Table 5.4 with sample volumes used in other sonochemical investigations. The comparison of ultrasonic intensity in Table 5.3 indicates that the Ultrasonic process system operates with a comparable intensity at the radiating surface area of the horn with that of other sonochemical investigations, however, as shown in Table 5.4 the greater sample volume in the ultrasonic cell results in a lower volume-based intensity.

Table 5.4 : Comparison of the sample volume that can be sonicated in the ultrasonic cell with sample volumes of other sonochemical investigations

Reference	Investigation	Sample volume (mL)	Ultrasonic intensity (W cm^{-3})
(Cost et al., 1993)	degradation of *p*-nitrophenol	25	2
(Kotronarou et al., 1992b)	degradation of hydrogen sulfide	25	1.7
(Ratoarinoro et al., 1992)	enhancement of reaction between ethyl malonate and chalcone	57	1.3
(Serpone et al., 1994)	degradation of chlorophenol compounds	100	0.5
(Pugin, 1987)	enhancement of reaction between lithium and 1-bromopentane	100	0.3
(Price et al., 1994)	degradation of aromatic compounds	120	0.25
(de Visscher et al., 1996)	degradation of monocyclic aromatic compounds	150	0.097
(Pétrier et al., 1994)	degradation of phenol	200	0.15
(Donaldson et al., 1979)	polymerization of nitrobenzene	250	0.28
this investigation	**degradation of atrazine**	**500**	**0.11**
(Lorimer et al., 1991)	decomposition of potassium persulphate	1,200	0.025
(Bhatnagar and Cheung, 1994)	degradation of chlorinated C1 and C2 volatile organic compounds	2,000	0.1

5.1.2.5 Vessel type

Ultrasonic horns are used to sonicate samples, described in Section 2.5.3, in beakers, cuphorns or flow cells. Sample volumes sonicated by ultrasonic horns, indicated in Table 5.5, typically range from 25 to 1 400 mL. Flow cells incorporating an ultrasonic horn as the source of ultrasonic energy allow for sonication in both batch and continuous mode, the sonicated zone of the system used by Cheung and Kurup to study the degradation of chlorofluorocarbon compounds was 35 mL when used in batch mode and 250 mL when used in continuous mode (Cheung and Kurup, 1994). Lin and co-workers used a circulating system in the study of the degradation of 2-chlorophenol, the 1 L sample volume was circulated at a flow rate of 0,5 L min^{-1} through the sonication cell (Lin et al., 1996). Flow cells are manufactured, indicated in Table 5.5, from either glass or 316 stainless steel. The ultrasonic cell was designed as a closed batch system (to allow for saturation with different gases) that could be modified later to be used in continuous mode. It was manufactured from stainless steel so that the material of construction in a scale-up exercise would be the same to that used in a pilot-plant system. The ultrasonic cell is compared in Table 5.5 with vessel types and volumes of other sonochemical investigations using an ultrasonic horn.

Table 5.5 : Comparison of the ultrasonic cell with vessel types and volumes of other sonochemical investigations using an ultrasonic horn

Reference	Investigation	Sample volume (mL)	Vessel volume (mL)	Vessel type
(Kotronarou et al., 1992a)	degradation of parathion	25	50	stainless steel cell with water jacket
(Serpone et al., 1994)	degradation of chlorophenol compounds	100	150	glass cell with water jacket
(Price et al., 1994)	degradation of aromatic compounds	120	500	centrifuge tube immersed in cooling bath
(de Visscher et al., 1996)	degradation of monocyclic aromatic compounds	150	200	glass vessel with water jacket
this investigation	**degradation of atrazine**	**500**	**900**	**stainless steel cell with water jacket**
(Lorimer et al., 1991)	decomposition of potassium persulphate	1,200	1,400	flange top, round-bottomed glass flask

The connection between an ultrasonic horn and the wall of a flow cell (Figure 2.13 in Section 2.5.3) can be sealed with either an *O-ring* or by screwing the cell onto an external thread at the nodal point on the horn (Goodwin, 1990). Suslick and co-workers used flow cells that were sealed with a Teflon collar and gas-tight *O-rings* in various sonochemical investigations (Suslick et al., 1983; Suslick, 1990). The flow cell used by Cheung and Kurup in the investigation of the degradation of chlorofluorocarbon compounds was sealed by threading the reactor body onto an external thread on the transducer housing of the ultrasonic horn (Cheung and Kurup, 1994).

The ultrasonic horn was initially inserted through a hole in the lid of the ultrasonic cell that was sealed with an *O-ring*. The contact between the horn and the lid of the cell dampened the movement of the horn and reduced the transfer of acoustic power to a sample in the cell. Acoustic power transferred to a water sample in the cell was calculated to be approximately 17 % of that transferred to a 500 mL water sample in a beaker (detailed in Section A.1.4).

The cell lid was changed such that the transducer housing fitted into a raised support, shown in Figure 5.4, to prevent contact between the horn and the lid. A rubber seal coated with Vaseline® was used to ensure a gastight fit between the transducer housing and the cell support. Elastic bands were also used to hold the transducer housing down and exert a slight pressure on the seal. The connection between the transducer

housing and cell support was checked using soapy water for leakage when gas experiments were performed in the cell.

5.1.2.6 Pressure

External applied pressure is one of the parameters that determines the level of cavitation in a system (Section 2.2.1). Henglein and Gutiérrez found that the yield of iodide oxidation decreased with increasing pressure from 100 to 300 kPa at acoustic powers of 30 and 50 W and reached a maximum before decreasing at powers of 80 to 150 W (Henglein and Gutiérrez, 1993). Chendke and Fogler found that the intensity of sonoluminescence from an aqueous carbon tetrachloride solution varied non-linearly with pressure, local maxima occurred at 608 and 1 216 kPa (Chendke and Fogler, 1983a).

The connection between the transducer housing of the horn and the lid of the ultrasonic cell, as described in Section 5.1.2.5, did not allow for pressure control in the cell. Pressure is not usually controlled in flow cells. Kotronarou and co-workers during the investigation of the ultrasonic oxidation of hydrogen sulfide noted that pressure was not controlled in the flow cell and that initial headspace pressure was atmospheric (Kotronarou et al., 1992b).

5.1.2.7 Mixing

Shock wave formation during sonication, (discussed in Section 2.3.2), results in efficient mixing. Goodwin noted that high-intensity ultrasound delivered by ultrasonic horns may provide sufficient agitation so as to eliminate the need for stirring (Goodwin, 1990).

The agitation induced in 500 mL of water by the ultrasonic horn was investigated (described in Section A.1.5) using potassium permanganate crystals. A comparison of the mixing in the water after 5 s of sonication and after 10 min of the control without sonication is shown in Figure 5.5. The efficient mixing shown in Figure 5.5 indicated that additional facilities for stirring in the ultrasonic cell did not have to be included.

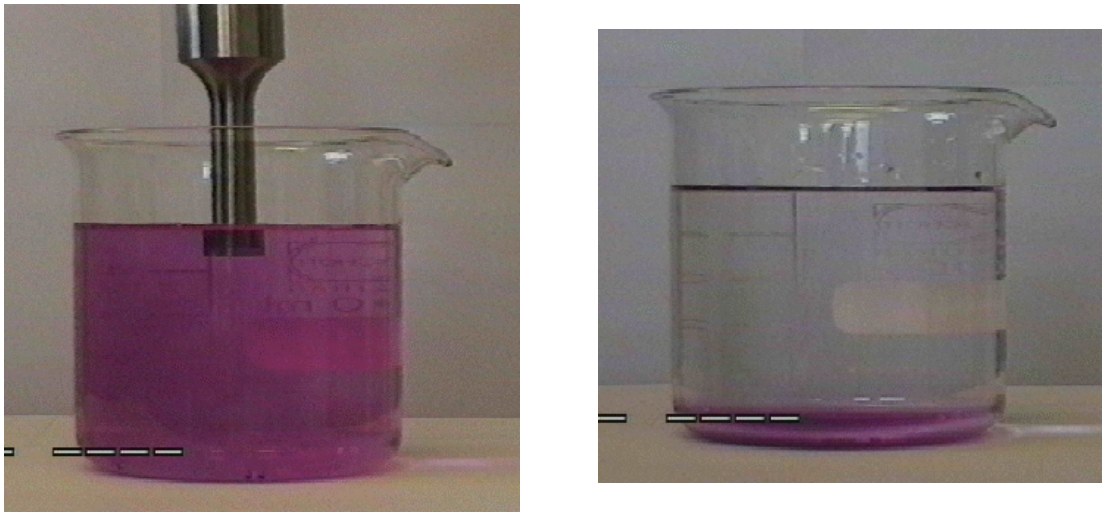

(a) (b)

Figure 5.5 : Mixing of potassium permanganate crystals in 500 mL of water during sonication and in the control without sonication; (a) after 5 s of sonication and (b) the control after 10 min

5.1.2.8 Temperature

Ultrasonic experiments are affected by temperature, generally, the lower the temperature the greater the sonochemical effect (Mason et al., 1992). The temperature of a sample also increases during sonication and must be controlled for repeatable and consistent results. The intensity of ultrasonic cavitation in water is a maximum at 35 °C, cavitation intensity is within 70 to 100 % of the maximum in the temperature range 20 to 50 °C (Niemczewski, 1980). Sonication in the ultrasonic cell was performed at 25 ± 1 °C. Ultrasonic experiments are typically performed at 25 °C (Kotronarou et al., 1992b; Lin et al., 1996; Mead et al., 1975; Sehgal et al., 1982), other temperatures reported in literature include 15°C (Suslick et al., 1989), 20°C (Donaldson et al., 1979; Price et al., 1994) and 30 °C (Kotronarou et al., 1991; Kotronarou et al., 1992a).

Temperature was regulated in the ultrasonic cell by circulating cooling water through a water jacket. Flow cells used in ultrasonic experiments, as noted in Table 5.5, usually incorporate water jackets for the control of temperature. The cold water bath from which the cooling water was circulated was maintained below 17 °C (usually between 10 and 15 °C) by a Labotec refrigeration unit (model no. FTC 300). The cooling water had to be cooler than 17 °C for the temperature in the cell to be maintained at 25 °C. The refrigeration unit and pump (Little Giant pump, catalogue no. 582013) that circulated the water through the refrigeration unit were set on a timer (National TB 179) that typically switched the unit on for 2 h and off for 3 h when overnight experiments were being performed. A schematic diagram of the cooling system is shown in Figure 5.6.

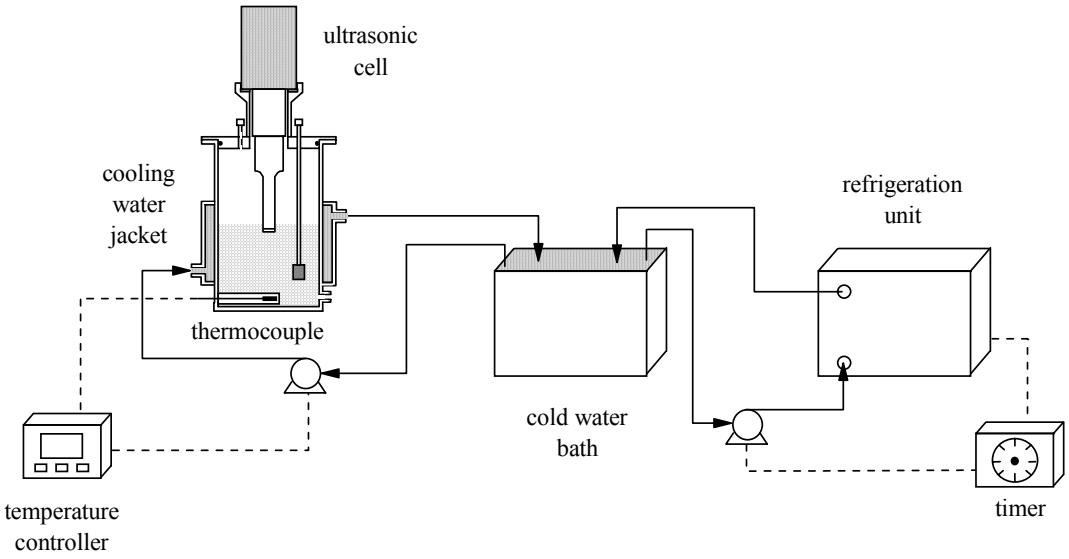

Figure 5.6 : Schematic diagram of the cooling system of the ultrasonic cell

The temperature in the ultrasonic cell was measured by a thermocouple positioned in the centre, just above the base of the cell. The pump (Gormann Rupp Industries) that circulated the cooling water through the water jacket was controlled by a Fuji PYZ 7 digital controller. The pump was automatically switched on if the temperature in the cell rose above 25 °C and switched off if the temperature fell below 25 °C.

5.1.2.9 Gas saturation

The presence of a gas during sonication, as discussed in Section 2.2.1, provides additional nucleation sites for cavitation. The nature of the gas, as discussed in Section 2.3.1.2, influences the radical reactions that occur during sonication. A diffuser was included in the ultrasonic cell to allow for saturation of liquid samples with different gases. The gas inlet pipe, as shown in Figure 5.4, entered through the lid of the cell. The diffuser was screwed into the bottom of the gas inlet pipe and was positioned in the lower half of the liquid sample. The diffuser was made from an approximate 1,5 cm piece of porous steel pipe. Gas was sparged continually through the liquid samples in the ultrasonic cell during sonication since liquids are degassed by ultrasound (Mason, 1990). To ensure saturation, gas was also sparged for 10 min prior to sonication through the liquid samples. Saturation periods reported in literature are 5 min (Misík et al., 1995; Young, 1976), 10 min (Donaldson et al., 1979; Mead et al., 1976; Sehgal and Wang, 1981), 15 min (Hart and Henglein, 1985) and 20 min (Gutiérrez et al., 1987; Rassokhin et al., 1995). A schematic diagram of the gas lines is shown in Figure 5.7.

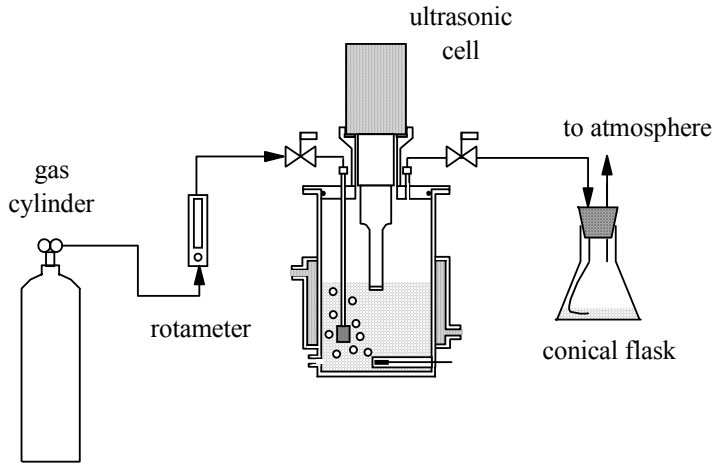

Figure 5.7 : Schematic diagram of the gas lines

Gas flow rate was controlled by the rotameter shown in Figure 5.7. The calibration of the rotameter is described in Section A.1.6. A flow rate of 6,0 mL s^{-1} was used to ensure gas saturation in the liquid samples but without excessive splashing. Gas flowrates reported in literature vary between 0,25 and 31,7 mL s^{-1} depending on the volume of sample (Hua et al., 1995a; Hua et al., 1995b; Rassokhin et al., 1995; Weissler, 1959).

5.1.2.10 Sampling

The ultrasonic cell was designed such that samples could be taken for analysis in three ways. A neoprene septum, as shown in Figure 5.4, allowed for gas sampling during the sonication of volatile compounds. Liquid samples (up to 5 mL) were also taken through the septum using a syringe with a long needle. This allowed for continuous sampling during an experiment without disturbing the gas atmosphere in the cell. Liquid samples (up to 10 mL) were sucked up using a pipette through the sample inlet port in the lid of the cell. Larger samples (50 to 200 mL) were collected through the outlet drainage port at the bottom of the cell. The final two methods of sampling could not be performed continuously but only once an experiment had been completed and the ultrasonic cell was opened.

5.2 OZONE EQUIPMENT

Ozone was generated using a Sorbios generator model GSG 001.2 that was loaned by Umgeni Water. The generator produces ozone according to the corona discharge method, described in Section 3.2.2, and is air cooled. The ozone-generating element consists of an AL_2O_3-ceramic tube with an outergrounded electrode and an inner net-like counter electrode (Sorbios, 1993). The oxygen used as feed gas has to be free of hydrocarbon compounds and have a dew point below -40 °C (Sorbios, 1993).

The mass of the generator assembly is 8 kg, the width, height and depth dimensions are 360, 200 and 360 mm, respectively. A rotameter with regulating valve for gas flow adjustment and a variable dial to

regulate power input are mounted in the front panel of the generator assembly. Analogue meters to record current and pressure are also mounted in the front panel of the generator assembly. Ozone production is determined by gas flow (production increases with decreasing flow) and by power input that can be varied between 0 and 220 V. The generator produces ozone at a nominal rate of 1 g h^{-1} with a concentration of 50 g m^{-3} for an oxygen flow rate of 1 L h^{-1} (Sorbios, 1993).

Ozone experiments were performed in a fumehood due to ozone toxicity. The ultrasonic cell was used as the ozonation chamber and was moved into the fumehood. Ozone was bubbled through a sample using the existing gas diffuser in the cell. Typical volumes of ozonation chambers recorded in literature are 200 mL (Andreozzi et al., 1989), 250 mL (Upham et al., 1997), 500 mL (Siddiqui, 1996; Sotelo et al., 1987) and 1 000 mL (Beltrán, 1995; Perkowski et al., 1996).

The gas lines, shown in Figure 5.7, were modified to allow for both ozonation and non-ozonation gas experiments. A schematic diagram of the complete experimental setup is shown in Figure 5.8.

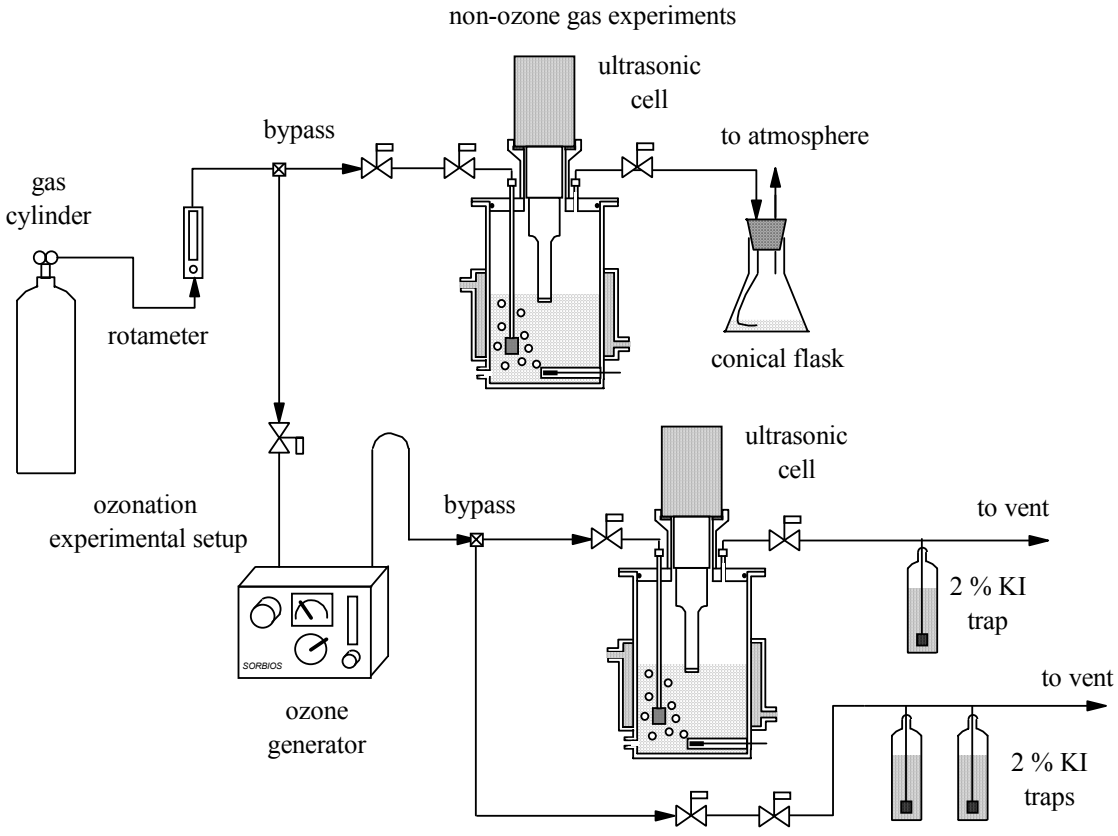

Figure 5.8 : Schematic diagram of the ozonation experimental setup

The experimental setup, shown in Figure 5.8, is similar to that used in the investigation by Singer and Zilli of the ozonation of ammonia (Singer and Zilli, 1975) and in the disinfection investigation by Upham and co-workers (Upham et al., 1997). A bypass line allowed for the ozone-containing gas to be diverted when

the ultrasonic cell was opened for a sample to be taken. The bypass line and the exhaust gas line from the ultrasonic cell were passed through 500 mL gas washing bottles containing a 2 % (20 000 mg L^{-1}) potassium iodide solution. The potassium iodide reacted with any remaining ozone before the gas lines ended near the top of the fumehood. The solutions changed from colourless to yellow with the iodine that was liberated during the reaction with ozone. A 2 % potassium iodide solution was used to degrade unreacted ozone in the investigations by Smith and co-workers (Smith et al., 1992) and Volk and co-workers (Volk et al., 1997).

The flow rate of oxygen (medical grade; 99,5 %) was controlled by the rotameter in the gas-line and the rotameter in the ozone generator. Oxygen flow rate was maintained at 2,4 mL s^{-1}, oxygen flowrates recorded in literature vary between 1,7 and 17 mL s^{-1} (Andreozzi et al., 1989; Koga et al., 1992; Singer and Zilli, 1975; Sotelo et al., 1987; Trapido et al., 1997). Oxygen flow was always started prior to the generator being switched on at the start of a day and stopped after the generator had been switched off at the end of a day. The generator was switched on and allowed to run for over an hour to warm up and stabilise before experiments were started.

The ozone generator was characterised, described in Section A.2, by measuring ozone production at different voltages (voltage could be adjusted between 0 and 220 V). A voltage setting of 130 V was used as a standard voltage for ozone experiments. The concentration of ozone generated in the oxygen stream at voltages between 100 and 200 V is shown in Figure 5.9.

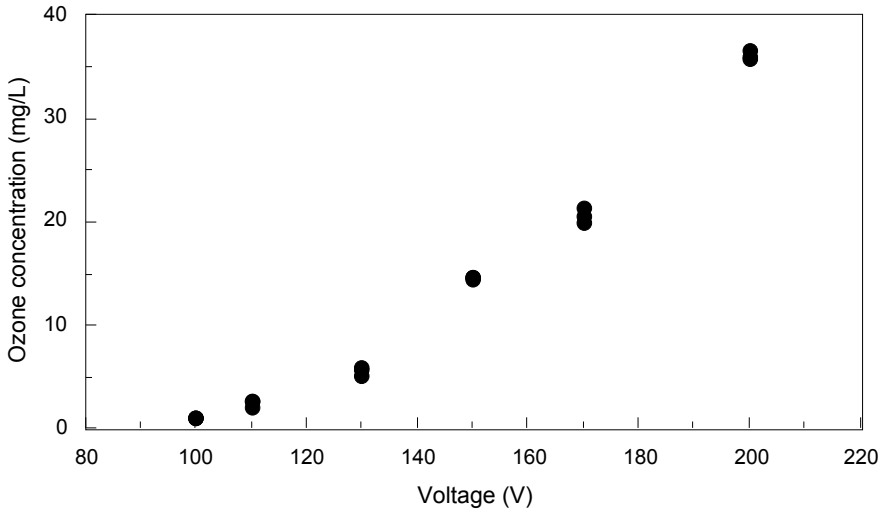

Figure 5.9 : Ozone concentration in a 2,4 mL s^{-1} oxygen gas stream generated by a Sorbios ozone generator at voltages between 100 and 200 V (*n* = 3 per voltage)

The average ozone concentration, the weight percentage of ozone in the oxygen/ozone gas stream and the ozone production rate generated by the Sorbios ozone generator at voltages of 100, 130, 150 and 170 V for an oxygen flow rate of 2,4 mL s^{-1} are presented in Table 5.6.

Table 5.6 : Average ozone concentration and weight percentage of ozone in a 2,4 mL s^{-1} oxygen gas stream generated by the Sorbios ozone generator at voltages of 100, 130, 150 and 170 V

Voltage (V)	Ozone concentration (mg L^{-1})	Ozone weight percentage (%)	Ozone production rate (mg s^{-1})
100	1.2	0.1	0.003
130	5.7	0.4	0.014
150	14.6	1.1	0.030
170	20.7	1.6	0.047

The % error in the daily rate of ozone production during experimentation (at 130 V) was calculated from the ozone mass balances reported in Section D.4 to be 7,5%.

5.3 EXPERIMENTAL PROCEDURES

Hydrogen peroxide, dissolved oxygen, ozone and atrazine concentrations were measured during the investigation. Hydrogen peroxide and dissolved oxygen concentrations were measured in the characterisation of the ultrasonic cell. Hydrogen peroxide is formed during sonication and was thus used as a qualitative measure of the free radical reactions initiated by ultrasound. Dissolved oxygen concentration was determined since the presence of oxygen enhances free radical reactions. Hydrogen peroxide and ozone concentrations were measured in the characterisation of the ozone system. Atrazine concentration was measured in the atrazine degradation experiments. The analytical procedures used to perform each of the measurements are detailed in Section 5.4.

An 8 mL sample was required for the hydrogen peroxide determination. Samples were sucked up using a pipette through the sample inlet port in the lid of the ultrasonic cell. Each data point in an experiment was thus measured in a separate experiment since the ultrasonic cell had to be opened to take the measurement, thus altering the gas atmosphere in the cell. Separate experiments were also performed for each data point in the measurement of dissolved oxygen and ozone concentrations. Dissolved oxygen concentration was measured by lifting the ultrasonic horn out of the ultrasonic cell and inserting the oxygen electrode into the reaction solution immediately after sonication was stopped. Larger sample volumes were required in the determination of ozone concentration, volumes of between 15 and 90 mL were used in the indigo method and 50 mL in the potassium iodide method. Samples were collected through the outlet sample drain at the bottom of the ultrasonic cell. The ozone gas was diverted through the bypass line to the potassium iodide traps so the ultrasonic cell could be opened for a sample to be taken.

Atrazine samples for determination were withdrawn continually during an experiment since samples of only up to 2 mL were required for HPLC analysis (25 μL sample injection volume). Atrazine samples were taken through a syringe with a long needle through the neoprene septum in the ultrasonic cell lid. The total reaction volume (500 mL) was not significantly affected by the three samples (< 10 mL in total) that were taken during the experiment.

Experiments were performed in either duplicate or triplicate to ensure data reproducibility. The standard deviation in data was calculated at each time period of an experiment though only the maximum value is reported where the data is presented in a figure or table. Statistical analysis (mean, 95 % confidence limits, standard deviation) is reported in Appendix F.

5.4 ANALYTICAL PROCEDURES

The analytical procedure used to measure hydrogen peroxide concentration is described in Section 5.3.1, to measure ozone concentration in Section 5.3.2, dissolved oxygen in Section 5.3.3 and atrazine concentration in Section 5.3.4.

5.4.1 Hydrogen peroxide measurement

A method based on the reduction of copper(II) ions by hydrogen peroxide in the presence of an excess of 2,9-dimethyl-1,10-phenanthroline (DMP) was used to measure the concentration of hydrogen peroxide in solution (Baga et al., 1988). A copper(I)-DMP complex, $Cu(DMP)_2^+$, is formed according to the reaction presented in Scheme 5.1.

$$2Cu^{2+} + 4DMP + H_2O_2 \rightarrow 2Cu(DMP)_2^+ + O_2 + 2H^+$$

Scheme 5.1

The product is stable in air- and oxygen-saturated solutions and is measured spectrophotometrically at a wavelength of 454 nm. The method is accurate to measure hydrogen peroxide concentrations in the range 0,030 to 4,08 mg L^{-1} (Baga et al., 1988).

A sample mixture consisting of 1 mL of a copper(II) sulphate solution, 1 mL of an ethanolic DMP solution and 8 mL of the solution of which the hydrogen peroxide concentration was to be determined was prepared in a 10 mL volumetric flask. Absorbance of the sample mixture was measured at a wavelength of 454 nm in a 10 mm glass cuvette with a Pharmacia Biotech Ultrospec 2000 (model 30-2106-00) spectrophotometer. Absorbance was measured for solutions of known hydrogen peroxide concentration and a calibration curve was drawn by plotting absorbance at 454 nm versus hydrogen peroxide concentration. The concentration of a hydrogen peroxide solution of unknown concentration could thus be determined using the calibration curve and the measured absorbance value of the solution.

The experimental procedure used to construct a calibration curve and the calibration curve drawn for each batch of chemical reagents used during the investigation are presented in Section B.1 of Appendix B. The error associated with determining hydrogen peroxide concentration using the three calibration curves reported in Appendix B were 11, 14 and 13 %, respectively.

5.4.2 Ozone measurement

Aqueous ozone concentration was determined using an iodometric (Eaton et al., 1995a) and indigo colorimetric method (Bader and Hoigné, 1981; Eaton et al., 1995b). The iodometric method could detect concentrations greater than 1 mg L^{-1} whereas the indigo colorimetric method could measure ozone concentrations down to 2 μg L^{-1} (Eaton et al., 1995a; Eaton et al., 1995b). The iodometric method was used for the daily characterisation to determine the rate of ozone generation as well as to determine the amount of ozone that had passed through the ultrasonic cell and reacted with the potassium iodide in the gas traps. The indigo colorimetric method was used to measure residual ozone in solution in the ultrasonic cell after an experiment had been completed. Both methods are reported in literature for ozone determination, the iodometric method was used in the investigations by Caprio and co-workers (Caprio et al., 1982), Smith and co-workers (Smith et al., 1992) and Singer and Zilli (Singer and Zilli, 1975) and the indigo method in investigations by Roche and co-workers (Roche et al., 1994; Roche and Prados, 1995), Volk and co-workers (Volk et al., 1997) and Hoigné and Bader (Hoigné and Bader, 1983).

5.4.2.1 Iodometric method

The iodometric method is based on the liberation of free iodine from potassium iodide (KI) solutions by reaction with ozone (Eaton et al., 1995a). The liberated iodine is titrated with a standard solution of sodium thiosulfate ($Na_2S_2O_3$) using starch as an indicator. The titration is performed at a pH of 3 to 4 since the reaction is not stoichiometric at a neutral pH due to the partial oxidation of thiosulfate to sulfate. The chemical reactions of the iodometric method are shown in Scheme 5.2 (Hargis, 1988).

$$O_3 + 2I^- + H_2O \rightarrow 2OH^- + O_2 + I_2 \quad [a]$$

$$2S_2O_3^{2-} + I_2 \rightleftharpoons S_4O_6^{2-} + 2I^- \quad [b]$$

Scheme 5.2

The iodometric method can be used to determine ozone concentrations above 1 mg L^{-1}. The procedure of the potassium iodide reaction and titration with sodium thiosulphate was performed as recorded in Standard Methods (Eaton et al., 1995a). The daily characterisation to determine the rate of ozone generation is described in Section B.2.

5.4.2.2 Indigo colorimetric method

The indigo colorimetric method is based on the decolourisation of indigo in acidic solution by ozone (Bader and Hoigné, 1981; Eaton et al., 1995b). Potassium indigo trisulfonate is used to prepare the indigo stock solution. Indigo trisulfonate absorbs light strongly at a wavelength of 600 nm and has a molar absorptivity

of $\in_{600}$ = 23 800 M^{-1} cm^{-1} (Bader and Hoigné, 1981). A potassium indigo trisulfonate molecule contains one carbon-carbon double bond that will react with ozone. Thus, as shown in Scheme 5.3, one mole of ozone reacts with one mole of sulfonated indigo. The reaction produces sulfonated isatin and similar products that do not absorb light at a wavelength of 600 nm (Bader and Hoigné, 1981).

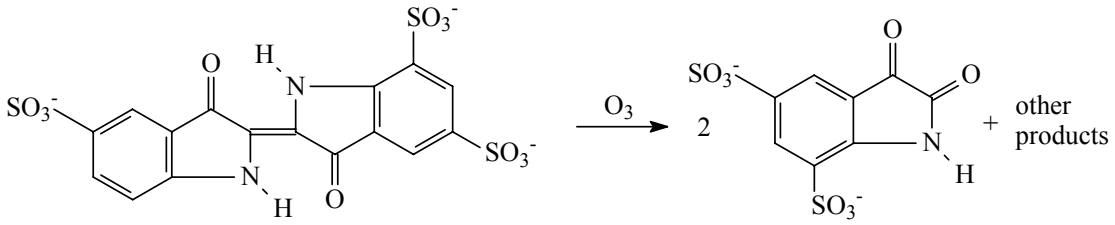

indigo trisulfonic acid isatin sulfonic acid

Scheme 5.3

The indigo colorimetric method can be used to detect ozone concentrations down to 2 μg L^{-1} (Eaton et al., 1995b). The relative error is less than 5 % without special sampling setups and in laboratory testing may be reduced to 1 % (Eaton et al., 1995b). Hydrogen peroxide and organic peroxides decolourize the indigo reagent very slowly; no interference is recorded for hydrogen peroxide if the absorbance at 600 nm is measured within 6 h of adding the reagents. The indigo method cannot be used to determine ozone concentration in the presence of bromine, the interference of chlorine can be masked by malonic acid (Eaton et al., 1995b). The procedure of the indigo colorimetric method (Section B.2) was performed as recorded in Standard Methods (Eaton et al., 1995b).

5.4.3 Dissolved oxygen measurement

The dissolved oxygen concentration of water samples was measured using a WTW 90 oxygen electrode with a WTW OXI 91 controller. Dissolved oxygen concentration was measured immediately after sonication and care was taken so as to not trap oxygen bubbles below the electrode. The controller was adjusted daily for changes in atmospheric pressure. Atmospheric pressure was read from a Negretti & Zambra barometer (model number MM 4 188/43). The controller was calibrated daily by submersing the oxygen electrode in oxygen-saturated water at 25 °C and setting the standard measurement to 40,32 mg L^{-1}, the solubility concentration of dissolved oxygen in water at 25 °C (International Critical Tables, 1928). The solubility concentration of oxygen in water at temperatures between 0 and 40 °C is recorded in Section B.3.

5.4.4 Atrazine measurement

Atrazine concentration during sonication and ozonation was measured using high performance liquid chromatography (HPLC). The HPLC system consisted of a Waters TM 600 controller, a Waters 486 tunable absorbance detector, a Waters U6K injector system, a Demark Technology computer system and a Seikosha SL-75 printer. The solvent was a 70:30 (v/v) mixture of methanol to water and was pumped at a flow rate of 0,6 mL min^{-1} through a reverse phase column, LiChrospher® RP-Select B (250 x 4 mm, 5 μm particles). The

sample injection volume was 25 μL. Absorbance was measured at a wavelength of 230 nm. A calibration curve relating atrazine concentration to absorbance measured with the HPLC at a wavelength of 230 nm is presented in Section B.4. The error in the atrazine concentrations calculated using the atrazine calibration curve is 7 %. HPLC methods, as reported in literature, have been used to detect atrazine concentrations from 0,4 to over 50 mg L^{-1} (Brambilla et al., 1995; Chan et al., 1992; Pétrier et al., 1996; Stucki et al., 1995). Solvents are usually 50:50 to 80:20 (v/v) mixtures of methanol and water (Hustert et al., 1991; Pétrier et al., 1996) or 30:70 to 55:45 (v/v) mixtures of acetonitrile and water (Beltrán et al., 1993a; Beltrán et al., 1998; Mirgain et al., 1993). Columns are typically reverse phase C18 columns (Arántegui et al., 1995; Chan et al., 1992; Grigg et al., 1997) and absorbance is measured at a wavelength between 214 and 235 nm (Arántegui et al., 1995; Beltrán et al., 1998; Mirgain et al., 1993).

An atrazine stock solution was prepared in a 1 L volumetric flask by dissolving 100 mg of atrazine (97 %; Sanachem) in 60 mL methanol and diluting with ultrapure water to total volume. Methanol was used to dissolve the atrazine since atrazine solubility in water is 33 mg L^{-1} at 22 °C (Tomlin, 1997). The ultrasonic cell was rinsed between experiments with both acetone and water due to the low solubility of atrazine in water. Waste atrazine solution was collected in buckets and as recommended in the Material Safety Data Sheet (MSDS) was reacted with a 10 000 mg L^{-1} sodium hydroxide solution before dilution and disposal to drain (Bradfield, 1997).

The methods used to measure ozone and hydrogen peroxide concentration were tested using controls for interference due to atrazine. Atrazine was shown not to interfere with the methods.

5.5 STATISTICAL MODELLING

Statistical analysis of the data was performed using the software programme *STATISTICA* that was developed by Statsoft, Inc (Statsoft, Inc., 2000). *STASTICA* is a comprehensive statistical data analysis, graphics, data base management and custom application development system. *STATISTICA* consists of modules in which the different types of analyses are performed (Statsoft, Inc., 2000). Statistical analysis used in the investigation included descriptive analysis to calculate means and standard deviations, regression analysis, analysis of variance, non-linear estimation and experimental design to generate surface response diagrams.

6

ULTRASOUND PROCESS INVESTIGATION

The implementation of a new industrial process, as shown in Figure 1.1, progresses from the discovery or demonstration of a process to a laboratory reactor so that reaction rate and yield data can be measured and a mathematical reactor model be formulated, to a pilot plant reactor for the evaluation of the reactor model and investigation of process control and hence to the design and construction of a large-scale reactor. A sound fundamental knowledge of the process should be obtained during the investigation in the ultrasonic laboratory reactor. An ultrasonic laboratory reactor (the ultrasonic cell) was designed (Chapter 5) for laboratory experimentation to demonstrate and evaluate the potential application of ultrasound to degrade organic pollutants during water treatment and to investigate the implications for scale-up.

This chapter details the process investigation to characterise the ultrasonic cell and to investigate the mechanistic sub-processes occurring during sonication. Experiments investigating dissolved oxygen concentration are reported in Section 6.1, hydrogen peroxide formation in Section 6.2, hydrogen peroxide degradation in Section 6.3, interval experiments in Section 6.4 and commercial hydrogen peroxide experiments in Section 6.5. A summary of the experimental programme of the ultrasonic process investigation is presented in Table 6.1.

Table 6.1 : Experimental programme of the ultrasonic process investigation

Section	Title	Measured parameters	Variables	Data Appendix	Statistics Appendix
6.1	Dissolved oxygen concentration	$[O_2]$	O_2 concentration gas (N_2; air; O_2)	C.1	F.3.1
6.2	Hydrogen peroxide formation	$[H_2O_2]$	O_2 concentration acoustic power	C.2	F.3.2
6.3	Hydrogen peroxide degradation	$[H_2O_2]$	gas (N_2; air; O_2)	C.3	F.3.3
6.4	Interval experiments	$[H_2O_2]$	sonication intervals gas intervals	C.4	F.3.4
6.5	Commercial hydrogen peroxide experiments	$[H_2O_2]$	H_2O_2 concentration gas (N_2; air; O_2)	C.5	F.3.5

The experimental data discussed in this chapter is reported (as indicated in Table 6.1) in Appendix C. The statistical analysis (mean, 95 % confidence limits, standard deviation) is reported in Appendix F. Standard deviation was calculated for each time period of an experiment though only the maximum value is reported in this chapter. Each data point in experiments measuring hydrogen peroxide or dissolved oxygen concentration was measured in a separate experiment since the ultrasonic cell had to be opened during sampling (described in Section 5.3), thus altering the gas atmosphere in the cell.

6.1 DISSOLVED OXYGEN CONCENTRATION

The chemical reactions that take place during sonication are reported in Section 2.3. The reaction schemes are summarised in Appendix H on A3 paper that can be folded out. Free radicals react to produce hydrogen peroxide and to oxidise organic compounds in water. The reactions that take place during sonication are affected by the presence of a gas since certain reactions may be inhibited or other reactions initiated depending on the nature of the gas. The presence of carbon dioxide or hydrogen, explained in Section 2.3.1.2, inhibits the sonochemical formation of hydrogen peroxide whereas the presence of oxygen enhances oxidation taking place during sonication since perhydroxyl radicals ($^{\bullet}HO_2$) are produced from the additional reactions shown in Scheme 2.3 and Scheme 2.4 (see Appendix H). Cavitation intensity is also enhanced, explained in Section 2.2.1, when a gas is present during sonication since additional nucleation sites are available for cavity formation.

A gas-saturated liquid, however, is degassed during sonication. Schwikkard demonstrated that the oxygen concentration of an oxygen-saturated solution was reduced to that of an unsaturated solution within 3 h of sonication in a ultrasonic bath (Schwikkard, 1995). Dissolved oxygen concentration is an important parameter to quantify and control in an ultrasonic system in order to obtain reproducible results.

The dissolved oxygen concentration in oxygen-saturated water was measured during sonication over 3 h. The water was saturated with oxygen by sparging medical grade oxygen through the water at a flow rate of 6 mL s^{-1} for 10 min prior to sonication; oxygen sparging was stopped as the ultrasonic horn was switched on. Oxygen concentration was measured at time periods of 0; 5; 10; 20; 30; 45; 60; 90; 120; 150 and 180 min. Triplicate experiments were performed for each time period. The dissolved oxygen concentration in water with no sonication, once oxygen sparging was stopped, was measured as a control. The reduction in dissolved oxygen concentration during nitrogen sparging of oxygen-saturated water (without sonication) is also shown in Figure 6.1; nitrogen sparging was started as the oxygen sparging was stopped.

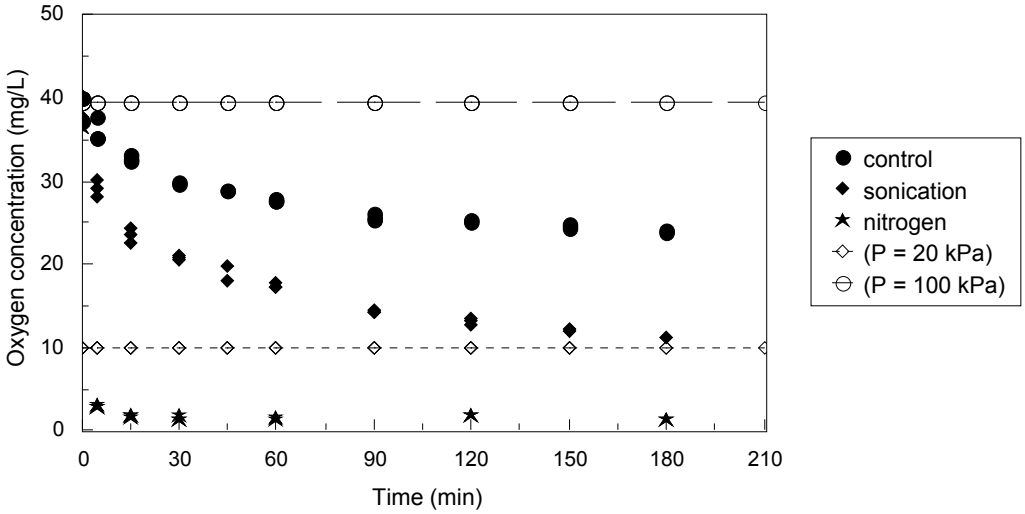

Figure 6.1 : Reduction in dissolved oxygen concentration in oxygen-saturated water during sonication, without sonication (control) and during nitrogen sparging without sonication; the dissolved oxygen concentrations in water saturated with oxygen at partial pressures of 20 and 100 kPa are also shown (*n* = 3 per time period)

Sonication, shown in Figure 6.1, reduces the oxygen concentration of oxygen-saturated water faster than the reduction in concentration in the absence of ultrasound, demonstrated by the control. The maximum standard deviation in the oxygen concentrations measured for the control and during sonication are 1,65 and 1,85 mg L^{-1}, respectively. Oxygen concentration decreased during sonication from that of saturation at a partial pressure of 100 kPa (approximately 40 mg L^{-1} at 25 °C, the long dashed line in Figure 6.1 denoting water saturated with pure oxygen) to that of water saturated with oxygen at a partial pressure of 20 kPa (the short dashed line in Figure 6.1 denoting water saturated with air). The oxygen concentration of water saturated with air was measured in all samples before experimentation, oxygen concentration varied between 8,3 and 12,3 mg L^{-1}, the average was 10,0 mg L^{-1} (Table C.2 in Appendix C).

The rapid decrease in oxygen concentration in water saturated with pure oxygen during nitrogen sparging, shown in Figure 6.1, is a convenient method to de-oxygenate a solution so as to investigate chemical reactions occurring in the absence of oxygen. Oxygen concentration decreased within 5 min from 40 mg L^{-1} to below 3 mg L^{-1} and remained below 2 mg L^{-1} from 15 min onwards. The maximum standard deviation in oxygen concentrations measured during nitrogen sparging is 2,15 mg L^{-1}, the standard deviation in data at each time period is recorded in Table F.11 in Appendix F. It is thus possible to operate the ultrasonic cell as an anaerobic environment by sparging nitrogen through the system.

The degassing characteristic of ultrasound resulted in the oxygen concentration of oxygen-saturated water to decrease during sonication, as shown in Figure 6.1, however, the dissolved oxygen concentration must be kept constant during sonication if the effect of oxygen on radical reactions is to be investigated. A constant

oxygen concentration, shown in Figure 6.2, was obtained by continuing the oxygen sparging during sonication. Pure oxygen was sparged through water at a flow rate of 6 mL s^{-1} for 10 min prior to and during sonication. Oxygen concentration was measured at time periods of 0; 5; 10; 20 and 40 min. Duplicate experiments were performed for each time period. Oxygen concentration was also measured over 40 min in water saturated with air and nitrogen; saturation was achieved by sparging air or nitrogen through the water for 10 min prior to and during sonication at a flow rate of 6 mL s^{-1}. A control was performed by measuring dissolved oxygen concentration during sonication in water that had been saturated with air and subsequently had no gas sparging through it.

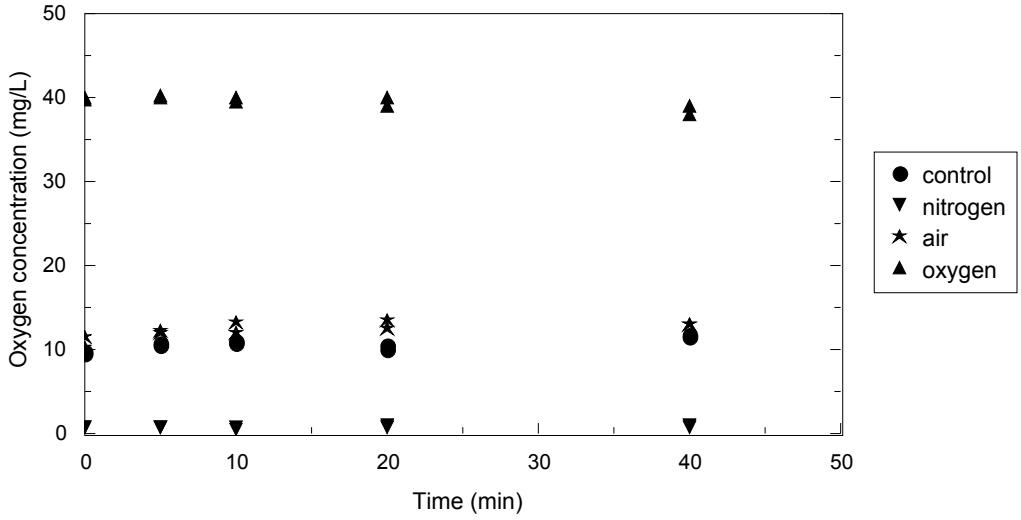

Figure 6.2 : Dissolved oxygen concentration in nitrogen-, air- and oxygen-saturated water during sonication in the ultrasonic cell (*n* = 2 per time period)

The dissolved oxygen concentration in water during sparging with nitrogen, air or oxygen, as shown in Figure 6.2, remained constant during the 40 min experiment. Dissolved oxygen concentration in the control and during air and oxygen sparging was approximately 10,7; 12,5 and 39,6 mg L^{-1}, respectively. The saturation concentration of pure oxygen (at 100 kPa partial pressure) in water is approximately 40 mg L^{-1}. Oxygen concentration during sonication with nitrogen sparging was below 1,2 mg L^{-1} throughout the experiment. The maximum standard deviation in oxygen concentrations measured for the control and during nitrogen, air and oxygen saturation are 0,28; 0,21; 0,71 and 0,96 mg L^{-1}, respectively. There is not a significant difference between air sparging and the control with out air sparging.

The ultrasonic cell is thus able to be used to investigate the effect of oxygen concentration on reactions occurring during sonication. Oxygen concentration is kept constant by continuing the gas sparging through the water during sonication. Different oxygen concentrations can be maintained during sonication by sparging gases such as nitrogen, air and oxygen or no gas through the solution in the ultrasonic cell.

6.2 HYDROGEN PEROXIDE FORMATION

Free radicals are highly reactive chemical species and have a very short lifespan. Radical concentrations can be measured using spin trapping compounds and electron spin resonance techniques. The chemistry of free radicals is summarised in Appendix G. The radical reactions occurring during sonication, as shown in Scheme 2.2 in Section 2.3.1.1 and Scheme 2.3 in Section 2.3.1.2, lead to the production of hydrogen peroxide (summarised in Appendix H). Various routine methods are available to measure hydrogen peroxide concentration in water. Thus the detection of hydrogen peroxide can be used as a qualitative measure of the radical reactions occurring during sonication. A higher hydrogen peroxide concentration indicating process conditions that enhance the occurrence of the radical reactions. The effect of ultrasound on a system is indirect, as discussed in Section 2.3.1.1, in that it is due to the formation of highly reactive radical species and not due to direct attack on solutes present in solution. The measurement of hydrogen peroxide was used in this investigation as an indirect *surrogate* measure of the degree of radical reactions occurring during sonication and as a tool to judge under which process conditions the most radical reactions occurred in the ultrasonic cell.

6.2.1 Effect of dissolved gas

The formation of hydrogen peroxide in water in the ultrasonic cell was measured using the DMP method detailed in Section 5.4.1. The effect of dissolved oxygen concentration on hydrogen peroxide formation (and hence on the occurrence of radical reactions) during sonication was investigated by measuring hydrogen peroxide concentration in nitrogen-, air- and oxygen-saturated water. The gases were sparged through the water at a flow rate of 6 mL s^{-1} for 10 min prior to and during sonication to maintain saturation. The rate of formation of hydrogen peroxide under saturation with each gas was calculated from the measurement of hydrogen peroxide concentration at time periods of 0; 4; 8; 12; 16; 20; 30; 60; 120; 240; 480 and 960 min (16 h). Triplicate experiments were performed for each time period for each gas. A control was performed by measuring hydrogen peroxide concentration during sonication of water with no gas sparging. The formation of hydrogen peroxide in nitrogen-, air- and oxygen-saturated water is presented in Figure 6.3.

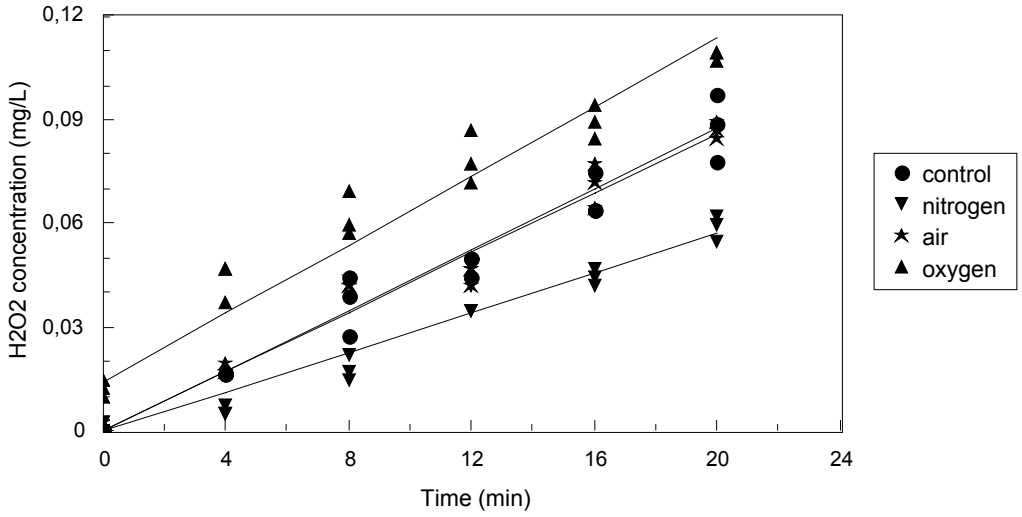

(a) 20 min

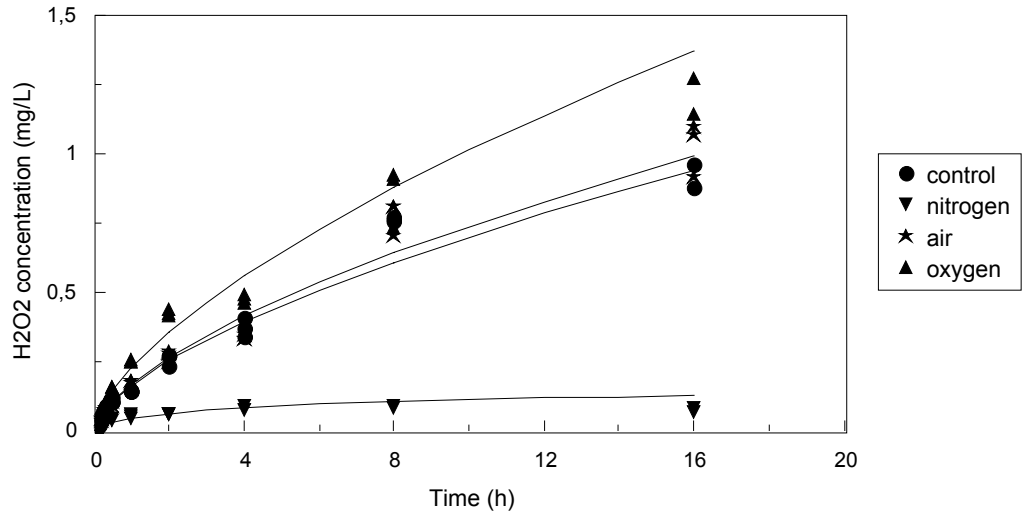

(b) 16 h

Figure 6.3 : Hydrogen peroxide formation in nitrogen-, air- and oxygen-saturated water during sonication in the ultrasonic cell at an acoustic power of 57 W (*n* = 3 per time period)

The formation of hydrogen peroxide over 20 min is shown in Figure 6.3(a) and over 16 h in Figure 6.3(b). The type of gas present during sonication is shown to influence the concentration of hydrogen peroxide in solution, Figure 6.3(a). Hydrogen peroxide concentration was the greatest during oxygen saturation, the least during nitrogen saturation and similar in the control and during air saturation. The maximum standard deviation in the hydrogen peroxide concentrations measured over 0 to 20 min for the control and during nitrogen, air and oxygen saturation are 0,010; 0,004; 0,006 and 0,008 mg L^{-1}, respectively (the maximum standard deviation for the experiment is quoted, though, the standard deviations calculated for each of the time periods are listed in Appendix F). The initial offset in Figure 6.3(a) in the hydrogen peroxide concentration during oxygen sparging after the 10 min saturation period is unexplained but was present

during the 3 replicate experiments. The very low concentrations, however, lie at the minimum detection limit of the DMP method and the offset could be due to experimental error. Hydrogen peroxide concentration (and hence the occurrence of radical reactions) during sonication is directly determined by the dissolved oxygen concentration which, as reported in Section 6.1, is greatest for oxygen saturation, the least during nitrogen saturation and similar in the control and air saturation.

The rate of hydrogen peroxide formation for the different gases was calculated over the initial 20 min period from the regression of the data using the linear regression model

$$y = a + bx \qquad [6.1]$$

where the coefficient *b*, the gradient of the regression line, represents the rate of hydrogen peroxide formation. The calculated rates of hydrogen peroxide formation in nitrogen-, air- and oxygen-saturated water during sonication (and the standard error of the calculated values) are recorded in Table 6.2.

Table 6.2 : Rate of hydrogen peroxide formation in nitrogen-, air- and oxygen-saturated water during sonication in the ultrasonic cell for 20 min at an acoustic power of 57 W

Gas	Rate of H_2O_2 formation ($mg\ L^{-1}\ min^{-1}$)	R^2
control	0,0043 ± 0,0001	0.968
nitrogen	0,0028 ± 0,0001	0.962
air	0,0044 ± 0,0001	0.971
oxygen	0,0050 ± 0,0003	0.928

The statistical *F*-test at a 95 % confidence level indicated that there was a significant difference in the gradients of the regression model for the different gases. Multiple comparison using the Bonferroni method (Coetzer, 2000) indicated that the significant difference was between the gradient of the nitrogen regression line and the other regression lines, there was no significant difference between the gradients of the control, air and oxygen regression lines. Thus, although the increased dissolved oxygen concentration during oxygen saturation increased hydrogen peroxide concentration in solution, as shown in Figure 6.3(a), the rate of formation was not significantly greater than that of the control and during air saturation. The significant difference between nitrogen saturation and air or oxygen saturation indicates the importance of the presence of oxygen to enhance radical reactions and thus the performance of an ultrasonic process. Ultrasonic systems should not be run under anaerobic conditions if the primary goal is chemical oxidation of solutes.

The difference in hydrogen peroxide formation over longer time periods (16 h), as shown in Figure 6.3(b), between the control and oxygen and air saturation was not as significant as during the shorter periods of sonication although hydrogen peroxide concentrations were still greater during oxygen sparging. The data is

more scattered after the longer sonication periods and has a greater standard deviation than that measured at shorter periods of sonication. The regression lines in Figure 6.3(b) are plotted from the correlation (equation 6.3) of hydrogen peroxide as a function of time, acoustic power and oxygen concentration. The maximum standard deviation in the hydrogen peroxide concentrations measured over 0 to 16 h for the control and during nitrogen, air and oxygen saturation are 0,060; 0,012; 0,097 and 0,108 mg L^{-1}, respectively. The lack of oxygen present during sonication with nitrogen saturation, shown in Figure 6.3(b), caused the hydrogen peroxide concentration after 20 min of sonication to remain relatively constant and to fluctuate between 0,06 and 0,09 mg L^{-1}. Whereas hydrogen peroxide concentration under nitrogen saturation reached steady state after 20 min, the hydrogen peroxide concentrations during air and oxygen saturation only started to level off and approach steady state conditions after 16 h.

6.2.2 Acoustic power

Hydrogen peroxide formation is not only dependent on the presence of oxygen during sonication but also on acoustic power. A lower acoustic power results in fewer water molecules being split into hydroxyl and hydrogen radicals (as shown in Scheme 2.1 in Section 2.3.1.1) and thus fewer radical reactions taking place during sonication. Hydrogen peroxide was again used as an indicator of the radical reactions occurring during sonication at a lower acoustic power. A lower acoustic power in the ultrasonic cell was achieved by sonicating at a transducer displacement amplitude of 5 μm whereas the previous experiments investigating the formation of hydrogen peroxide under saturation with different gases during sonication had been performed at a transducer displacement amplitude of 11 μm. Transducer displacement amplitudes of 5 and 11 μm, as recorded in Table 5.2 in Section 5.1.2.2, correspond to acoustic powers of 24 and 57 W, respectively, and ultrasonic intensities of 0,048 and 0,114 W cm^{-3}, respectively.

The effect of dissolved oxygen concentration was also investigated during sonication at a lower acoustic power. Hydrogen peroxide formation during the sonication of water saturated with nitrogen (an oxygen-free atmosphere) was compared with that in a control (water without any gas sparging through it). The oxygen concentration in a control, as reported in Section 6.1, is 10,7 mg L^{-1}. Water saturated with nitrogen was prepared by sparging nitrogen through the water for 10 min prior to and during sonication at a flow rate of 6 mL s^{-1}. A control was performed by measuring hydrogen peroxide concentration in water with no gas sparging. Hydrogen peroxide was measured at time periods of 0; 4; 8; 12; 16; 20; 30; 60; 120; 240; 480 and 960 min (16 h). Triplicate experiments were performed for each time period. A comparison of the hydrogen peroxide formation during sonication at acoustic powers of 24 and 57 W for the control is presented in Figure 6.4 and for the nitrogen-saturated water in Figure 6.5.

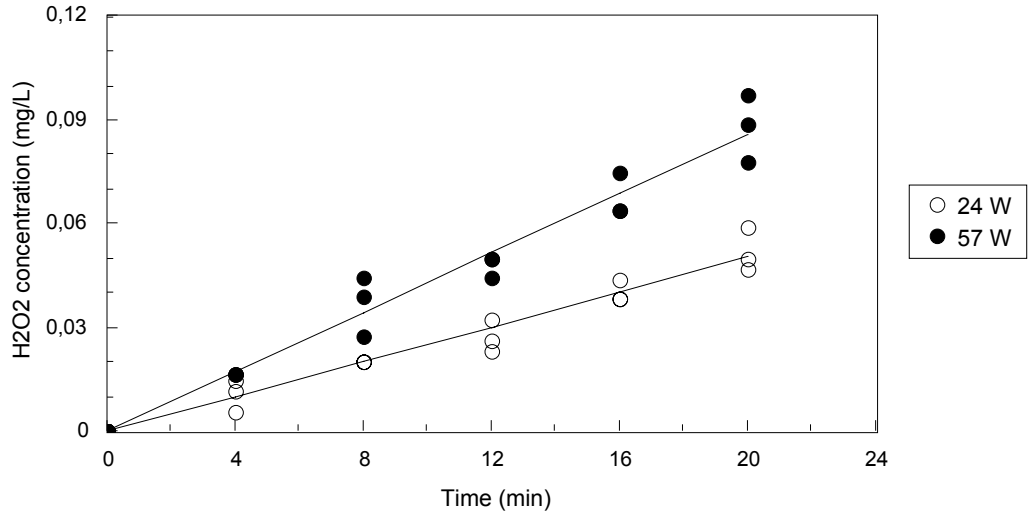

(a) 20 min

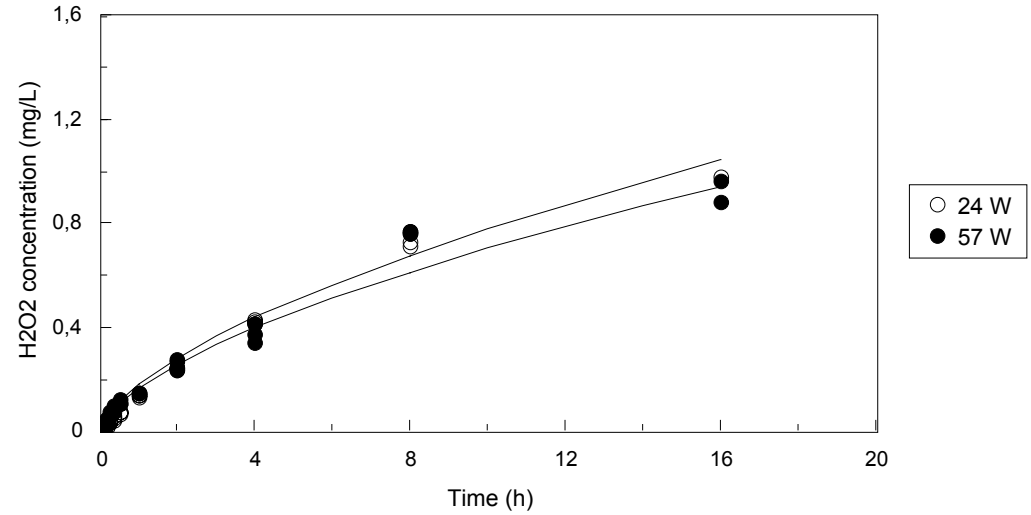

(b) 16 h

Figure 6.4 : Hydrogen peroxide formation in the control during sonication in the ultrasonic cell at acoustic powers of 24 and 57 W (*n* = 3 per time period)

The rate of hydrogen peroxide formation in the control, as shown in Figure 6.4(a), was lower when sonication was performed at an acoustic power of 24 W than at 57 W. The maximum standard deviation in the hydrogen peroxide concentrations measured over 20 min at acoustic powers of 24 and 57 W for the control are 0,006 and 0,010 mg L^{-1}, respectively. A lower acoustic power results in fewer water molecules being degraded into hydroxyl and hydrogen radicals and thus fewer radical reactions occurring in solution during sonication.

The difference in hydrogen peroxide formation in the control due to acoustic power input, as shown in Figure 6.4(b), became insignificant after 1 h. The regression lines in Figure 6.4(b) are plotted from the

correlation (equation 6.3) of hydrogen peroxide as a function of time, acoustic power and oxygen concentration. The maximum standard deviation in the hydrogen peroxide concentrations measured during sonication at acoustic powers of 24 and 57 W for the control over 16 h are 0,026 and 0,060 mg L^{-1}, respectively.

The hydrogen peroxide formation in nitrogen-saturated water during sonication at acoustic powers of 24 and 57 W is presented in Figure 6.5.

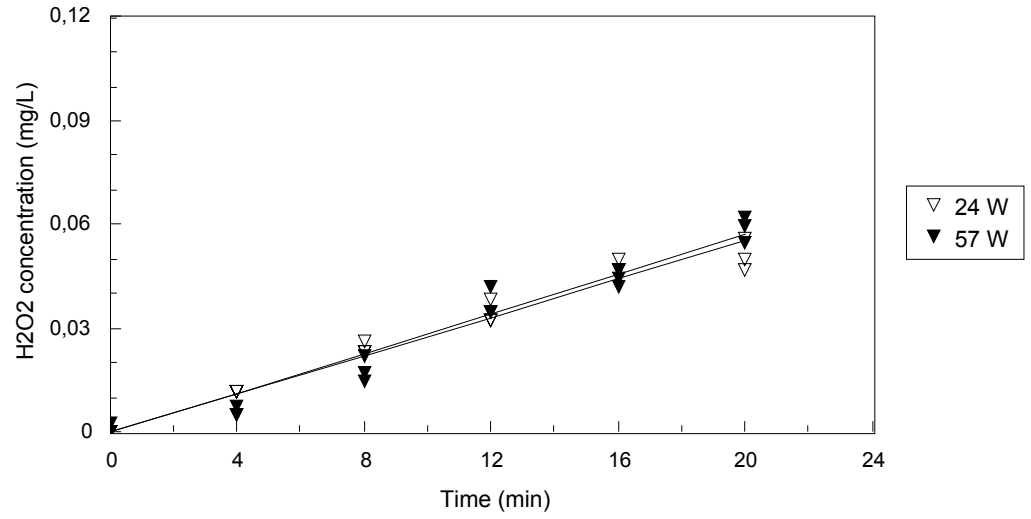

(a) 20 min

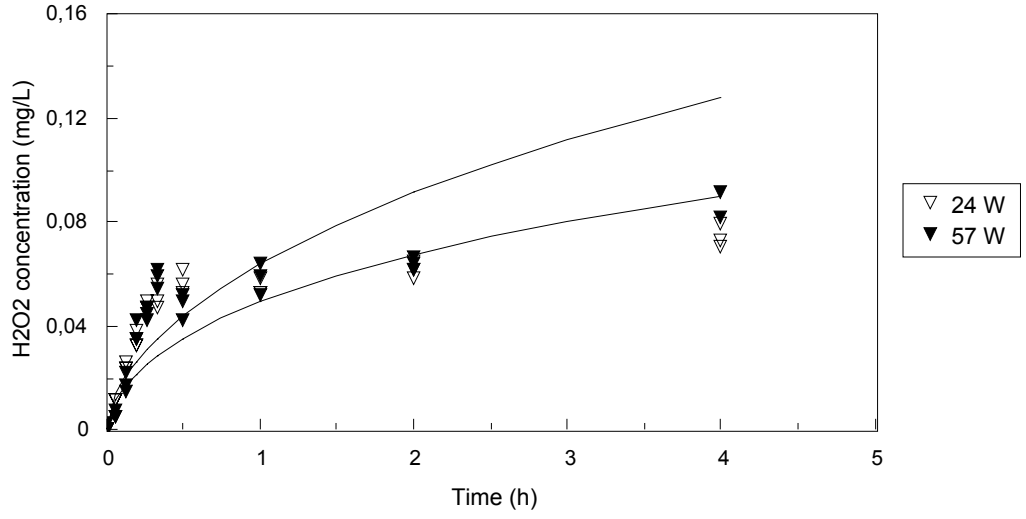

(b) 4 h

Figure 6.5 : Hydrogen peroxide formation in nitrogen-saturated water during sonication in the ultrasonic cell at acoustic powers of 24 and 57 W (*n* = 3 per time period)

Hydrogen peroxide formation in a nitrogen-saturated solution, as shown in Figure 6.5(a), was the same irrespective of the acoustic power input. The maximum standard deviation in the hydrogen peroxide concentrations measured at acoustic powers of 24 and 57 W during nitrogen saturation are 0,004 and 0,004 mg L^{-1}, respectively. Whereas in Figure 6.5(a) acoustic power was shown not to affect hydrogen peroxide formation in nitrogen-saturated water during 20 min of sonication, Figure 6.5(b) indicates that acoustic power did not influence hydrogen peroxide formation for up to 4 h of sonication. The regression lines in Figure 6.5(b) are plotted from the correlation (equation 6.3) of hydrogen peroxide as a function of time, acoustic power and oxygen concentration. The maximum standard deviation in the hydrogen peroxide concentrations measured during nitrogen saturation over 16 h at acoustic powers of 24 and 57 W are 0,004 and 0,007 mg L^{-1}, respectively.

The rates of hydrogen peroxide formation for the control and nitrogen-saturated water were calculated from the regression of the data presented in Figure 6.4(a) and Figure 6.5(a) using the linear regression model

$$y = bx \qquad [6.2]$$

where the coefficient b, the gradient of the regression line, represents the rate of hydrogen peroxide formation. The calculated rates of hydrogen peroxide formation at acoustic powers of 24 and 57 W for the control and during nitrogen saturation (and the standard error of the calculated values) are recorded in Table 6.3.

Table 6.3 : Rate of hydrogen peroxide formation in nitrogen-saturated water and the control during sonication in the ultrasonic cell at acoustic powers of 24 and 57 W for 20 min

Gas	Acoustic power (W)	Rate of H_2O_2 formation (mg L^{-1} min^{-1})	R^2
control	24	0,0025 ± 0,0001	0.962
control	57	0,0043 ± 0,0001	0.968
nitrogen	24	0,0028 ± 0,0001	0.968
nitrogen	57	0,0028 ± 0,0001	0.962

The statistical F-test at a 95 % confidence level indicated that there was a significant difference in the gradients of the regression model for sonication at acoustic powers of 24 and 57 W for the control but no significant difference in the gradients of the 24 and 57 W regression model for nitrogen saturation.

Hydrogen peroxide formation was shown to be affected by acoustic power in the presence of oxygen (as during the control) but not in the absence thereof (as during nitrogen saturation). Thus, under these experimental conditions, the presence or absence of oxygen had a greater effect on the rate of hydrogen peroxide formation than the change in acoustic power from 24 to 57 W. The formation of hydrogen

peroxide during sonication at both acoustic powers is an indication that the acoustic powers are greater than the threshold power value, as discussed in Section 2.2.1 of Chapter 2, required to initiate cavitation.

Oxygen sparging can thus be replaced with air sparging in ultrasonic systems of similar design and power that require the presence of oxygen and have a long sonication period without sacrificing performance as demonstrated in Figure 6.3(b). A lower acoustic power energy source can also be used under both oxygenated and de-oxygenated process conditions in ultrasonic systems with an extended sonication period as demonstrated in Figure 6.4(b) and Figure 6.5(b). Maximum performance in ultrasonic systems with a short sonication period is obtained with oxygen sparging and a high acoustic power input as demonstrated in Figure 6.3(a) and Figure 6.4(a). The most appropriate mode of operation should be investigated for potential ultrasonic applications, however, as a guide, short experiments should be performed with oxygen sparging and a high acoustic input and extended sonication experiments with air sparging and a lower acoustic energy source.

6.2.3 Regression analysis

The measurement of hydrogen peroxide concentration has been used as a tool to investigate process conditions (dissolved oxygen concentration and acoustic power) that enhance radical reactions occurring during sonication. A statistical software package *STATISTICA*, detailed in Section 5.5 of Chapter 5, was used to model hydrogen peroxide concentration, the dependent variable, as a function of dissolved oxygen concentration and acoustic power, the independent variables. Surface response diagrams, gradient profiles of hydrogen peroxide concentration as a function of the two independent variables, were generated for time periods of 20, 120 and 960 min. The gradient profiles presented in Figure 6.6 indicate the conditions of oxygen concentration and acoustic power that lead to the highest (dark grey) and lowest (light grey) hydrogen peroxide concentrations. The circular symbols indicate the experimental data points.

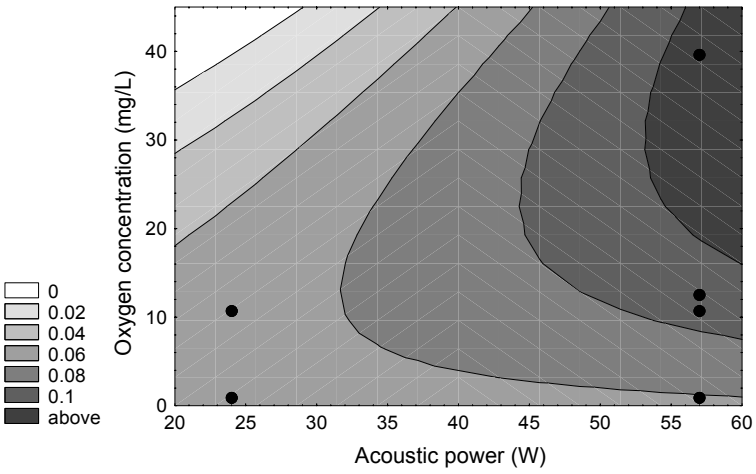

(a) 20 min

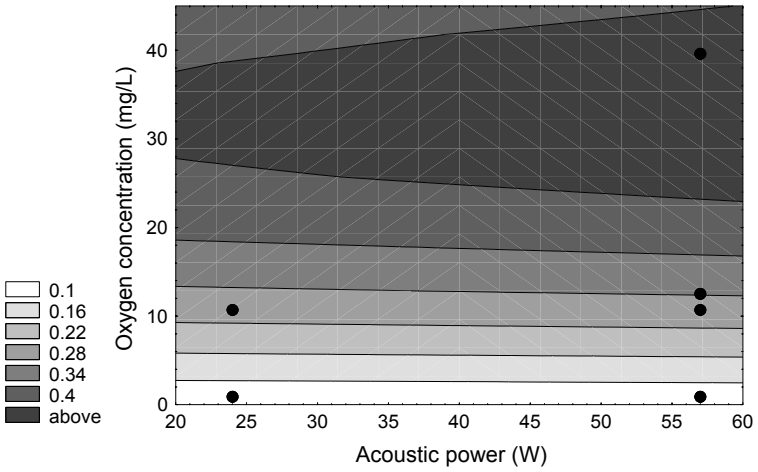

(b) 120 min

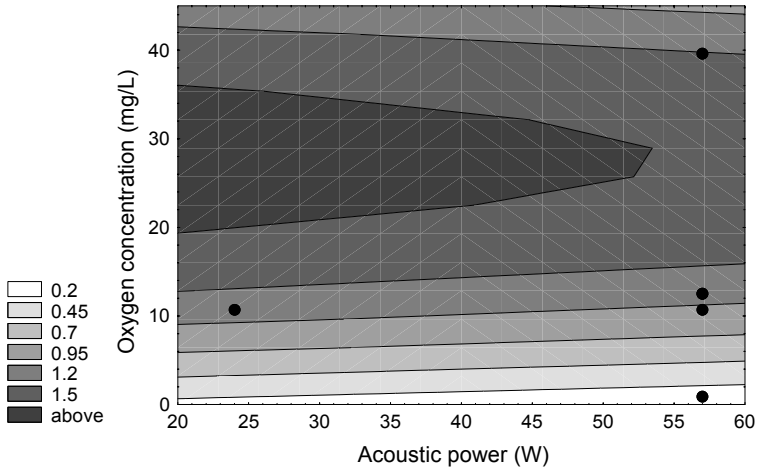

(c) 960 min

Figure 6.6 : Surface response diagrams of hydrogen peroxide concentration as a function of acoustic power and dissolved oxygen concentration during sonication of water in the ultrasonic cell

Surface response diagrams, as in Figure 6.6, indicate under which conditions a maximum response of the dependent variable is obtained or under what conditions future experiments should be performed to improve the response. Hydrogen peroxide concentration was not measured at a low acoustic power and high oxygen concentration (top left co-ordinate in the diagrams presented in Figure 6.6), measurement of hydrogen peroxide concentration under these conditions would improve the accuracy of the predicted gradient profiles as the 4 corners of the experimental programme would be mapped out. The trends of hydrogen peroxide concentration as a function of acoustic power and oxygen concentration are still illustrated. Hydrogen peroxide concentration during short sonication experiments is shown in Figure 6.6(a) to be a maximum with oxygen sparging and a high acoustic power input and during long sonication experiments, as in

Figure 6.6(c), is independent of acoustic power input and that air sparging can be used in place of oxygen sparging.

Oxygen concentration, shown in Figure 6.6, was varied from a de-oxygenated concentration to that of water saturated with pure oxygen, similarly, an acoustic power of 57 W is the maximum output of the ultrasonic horn in the ultrasonic cell. Oxygen concentration and acoustic power can thus not be increased in the present equipment to increase hydrogen peroxide concentration during short sonication experiments as recommended in Figure 6.6(a). The trends in hydrogen peroxide concentration (and hence radical reactions occurring during sonication), however, have been demonstrated and can be used to guide the choice of process conditions in larger-scale ultrasonic systems that deliver a wider range of acoustic powers.

The change in the surface response profiles of hydrogen peroxide at 20, 120 and 960 min, as shown in Figure 6.6, indicates that the dependence of hydrogen peroxide concentration on the independent variables, oxygen concentration and acoustic power, change with time. There is thus a significant interaction between the variables time and oxygen concentration, and time and acoustic power. The independent variable time should thus be included in a regression model of hydrogen peroxide formation in water during sonication in the ultrasonic cell. Possible non-linear relationships between the dependent and independent variables should also be taken into account, a non-linear response of hydrogen peroxide as a function of dissolved oxygen concentration is shown in Figure 6.6 by the curved gradient lines in the surface response profiles of hydrogen peroxide.

A correlation was generated for the prediction of hydrogen peroxide concentration as a function of oxygen concentration, acoustic power and time using the non-linear estimation module of the software *STATISTICA*. The correlation equation is

$$[H_2O_2] = -0,5420[time]^{0,6995} + 0,5516[time]^{0,6984}[uls]^{-0,001761}[O_2]^{0,004917} \qquad [6.3]$$

where $[H_2O_2]$ is measured in mg L^{-1}, $[uls]$ in W, $[O_2]$ in mg L^{-1} and $[time]$ in min. The coefficient of variance (R^2) of the correlation is 0,973. This indicates that approximately 97 % of the variance in the data is explained by the model. The correlation has been used to plot the solid regression lines in Figures 6.3(b), Figure 6.4(b) and Figure 6.5(b). The fit with experimental data is good for water saturated with oxygen and air and with no gas bubbling (control) but not that good for water saturated with nitrogen. This correlation can be used in the design of ultrasonic equipment, operating at the same frequency of 20 kHz, to predict changes in hydrogen peroxide concentration so as to guide the selection of appropriate process conditions. Batch operation mode is recommended for processes with a relatively long residence time (Shah et al., 1999d), this correlation by predicting the hydrogen peroxide concentration over time can indicate whether a long or short residence time is of greater benefit and thus whether a process should be operated in a batch or in a continuous mode.

6.3 HYDROGEN PEROXIDE DEGRADATION

Hydrogen peroxide, as demonstrated in Section 6.2, is produced by radical reactions occurring during sonication. The hydrogen peroxide that is formed can react further with the radical species in solution, can dissociate to form ions or due to bond cleavage break down to hydroxyl and perhydroxyl radicals. The concentration of hydrogen peroxide measured in solution is thus the combined effect of the formation and degradation of hydrogen peroxide.

The overall rate of hydrogen peroxide formation, as shown in Figure 6.3, was greatest during the initial period of sonication and decreased over time until hydrogen peroxide concentration levelled off and approached a constant value. The initial rate of degradation is significantly lower than the rate of formation as the amount of hydrogen peroxide in solution is still small, the rate of degradation increases as hydrogen peroxide concentration builds up. The overall concentration of hydrogen peroxide in solution begins to reach an equilibrium as the rate of degradation approaches that of the rate of formation. Equilibrium is established when the rates of formation and degradation are equal and the overall measured hydrogen peroxide concentration in solution remains constant. The equilibrium in hydrogen peroxide formation and degradation, as reported in Section 6.2, was established within 30 min during sonication in a de-oxygenated atmosphere and only after 16 h in the presence of oxygen.

The rate of hydrogen peroxide degradation was determined by sonicating water for 16 h at an acoustic power of 57 W (to produce hydrogen peroxide) and measuring peroxide concentration over 3 h after sonication was stopped. Hydrogen peroxide concentration was measured at time periods of 0; 5; 10; 20; 30; 60; 90; 120; 150 and 180 min. Nitrogen, air and oxygen were sparged through the water during the 3 h degradation period to investigate their effect upon the rate of hydrogen peroxide degradation. A control was performed by measuring hydrogen peroxide degradation in water with no gas sparging. Triplicate experiments were performed for each time period. Different hydrogen peroxide concentrations were produced during the 16 h period of sonication thus resulting in different initial concentrations for the degradation experiments. The average initial concentrations of the control and during nitrogen, air and oxygen saturation were 0,43; 0,99; 0,95 and 0,37 mg L^{-1}, respectively. The variation in initial concentration was removed, for comparison purposes, by normalising the data and dividing each concentration by the initial concentration for that particular experiment. The degradation of hydrogen peroxide in nitrogen-, air- and oxygen-saturated water after sonication in the ultrasonic cell for 16 h is shown in Figure 6.7.

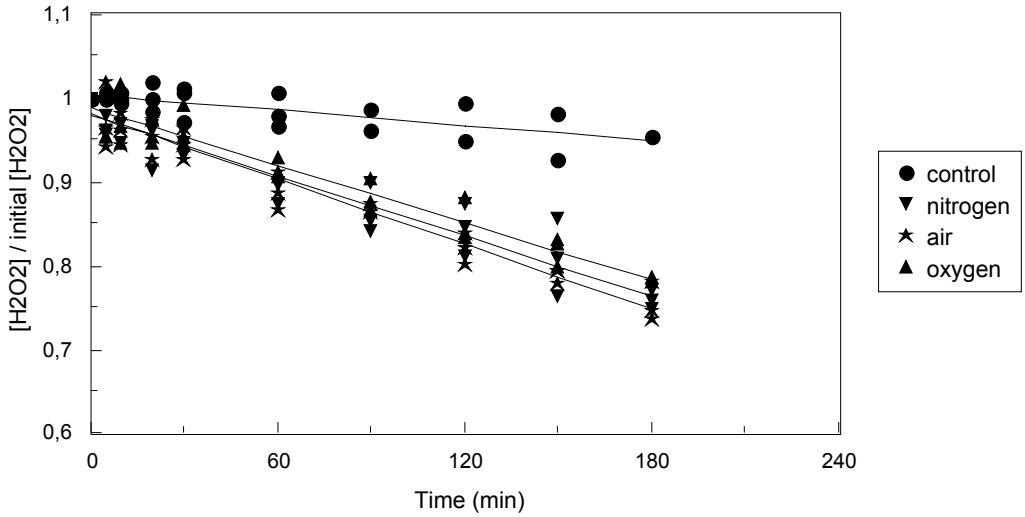

Figure 6.7 : Hydrogen peroxide degradation in nitrogen-, air- and oxygen-saturated water after sonication in the ultrasonic cell for 16 h (*n* = 3 per time period)

The maximum standard deviation in the normalised hydrogen peroxide concentrations, as shown in Figure 6.7, for the control and during nitrogen, air and oxygen saturation are 0,038; 0,046; 0,049 and 0,036 (mg L^{-1})/(mg L^{-1}) respectively. The rate of degradation over 3 h for each of the gases and the control was calculated from the regression of the data presented in Figure 6.7 using the linear regression model

$$y = a + bx \qquad [6.4]$$

where the coefficient *b*, the gradient of the regression line, represents the rate of hydrogen peroxide degradation. The calculated rates of hydrogen peroxide degradation after sonication for 16 h for a control and during nitrogen, air and oxygen saturation (and the standard errors of the calculated values) are recorded in Table 6.4.

Table 6.4 : Rate of hydrogen peroxide degradation over 3 h in nitrogen-, air- and oxygen-saturated water after sonication in the ultrasonic cell for 16 h

Gas	Rate of H_2O_2 degradation (min^{-1})	R^2
control	- 0,0003 ± 0,0001	0.543
nitrogen	- 0,0012 ± 0,0001	0.913
air	- 0,0013 ± 0,0001	0.945
oxygen	- 0,0011 ± 0,0001	0.933

Hydrogen peroxide degradation, as shown in Figure 6.7, in nitrogen-, air and oxygen-saturated water followed the same trend with almost identical rates within experimental standard deviation. The statistical

F-test at a 95 % confidence level with multiple comparison using the Bonferroni method (Coetzer, 2000) indicated that there was no significant difference between the gradients of the nitrogen, air and oxygen regression lines whereas the slope of the control regression line was significantly different from the other regression lines.

The significantly lower rate of degradation for the control than that measured during saturation with any of the gases indicates that hydrogen peroxide degradation is increased by the presence of a gas but unaffected by the type of gas. Degradation is thus increased due to the physical phenomena such as agitation and mixing provided by a sparging gas but not influenced according to any chemical mechanism dependent on the dissolved oxygen concentration in solution.

The formation of hydroxyl and hydrogen radicals in collapsing cavities and the formation of hydrogen peroxide from the radicals are stopped when sonication is ended. The remaining hydrogen peroxide in solution either decomposes to water and oxygen or is available to react with solutes in the water according to the reactions listed in Section 3.3.1. Decomposition to water and oxygen is slow as demonstrated by the control in Figure 6.7, hydrogen peroxide is thus available to react with organic compounds in solution. The implications for an industrial ultrasonic system is that equipment based on a flow system allows for ultrasonic degradation of organic pollutants and hydrogen peroxide formation to occur within the sonicated zone and further oxidation of pollutants by hydrogen peroxide to occur outside the sonicated zone. A gas such as oxygen may be used in a sonicated zone to increase dissolved oxygen concentration to enhance free radical formation, however, gas sparging beyond the sonicated zone has a negative impact leading to the decomposition of the available hydrogen peroxide.

6.4 INTERVAL EXPERIMENTS

The design of some ultrasonic reactors, as discussed in Section 2.5.4 of Chapter 2, is based on a flow system in which a small volume, of limited diameter, is sonicated and the reaction solution is pumped through the sonicated zone. Some systems include a flow loop that consists of a sonicated zone and a holding tank or reservoir so that the reaction solution is circulated through the system. An example of a flow loop system is the *Harwell* sonochemical reactor shown in Figure 2.14 and Figure 2.15 in Section 2.5.4. Scale-up of a flow loop system is favourable if the limiting reagent of a reaction is retained in the sonicated zone or if the reagents exhibit a *memory* effect and remains activated after passing through the sonicated zone.

The interval experiments performed to monitor hydrogen peroxide concentration when sonication was stopped for a certain time period and then restarted are reported in Section 6.4.1. The interval experiments performed to monitor the effect of a change in gas during sonication are reported in Section 6.4.2.

6.4.1 Sonication period intervals

Interval experiments were performed to monitor hydrogen peroxide concentration when sonication was stopped for a certain time period and then restarted so as to simulate a flow loop system with the solution moving in and out of a sonicated zone. Hydrogen peroxide concentration was measured in an oxygen-saturated solution at time periods of 0; 5; 10; 15; 20; 25; 30; 35; 40 and 45 min. Triplicate experiments were performed for each time period. Saturation was achieved by sparging pure oxygen (at a 100 kPa partial pressure) through the water for 10 min prior to and during the 45 min experiment at a flow rate of 6 mL s^{-1}. The experiment was structured so that the water was sonicated for 15 min; sonication was stopped for the following 15 min and then restarted for a further 15 min. Sonication in the ultrasonic cell was performed at an acoustic power of 57 W. A control was performed in water with no gas sparging. Hydrogen peroxide formation during a 15 min period of sonication followed by a 15 min period without sonication and a further 15 min period with sonication is presented in Figure 6.8.

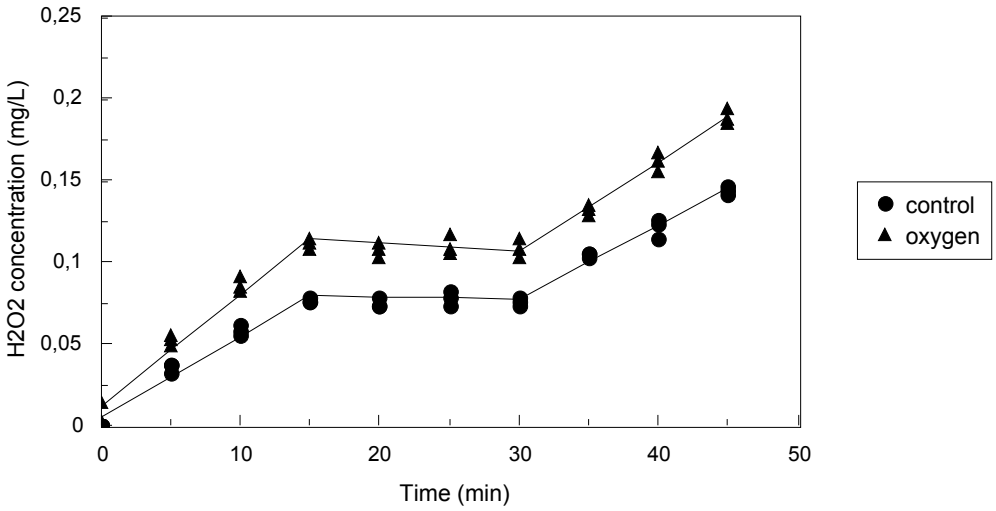

Figure 6.8 : Hydrogen peroxide formation in oxygen-saturated water in the ultrasonic cell during 15 min of sonication at an acoustic power of 57 W, 15 min without sonication and a further 15 min with sonication (n = 3 per time period)

The maximum standard deviation in the hydrogen peroxide concentrations measured in the control and oxygen-saturated water, as shown in Figure 6.8, are 0,006 and 0,008 mg L^{-1}, respectively. The rate of hydrogen peroxide formation in the control and oxygen-saturation solution during each of the 15 min periods was determined from the regression of each set of 15 min data using the linear regression model

$$y = a + bx \qquad [6.5]$$

where the coefficient *b*, the gradient of the regression line, represents the rate of hydrogen peroxide formation. The calculated rates of hydrogen peroxide formation in the control and oxygen-saturated water during interval experiments (and the standard error of the calculated values) are recorded in Table 6.5.

Table 6.5 : Rate of hydrogen peroxide formation in oxygen-saturated water and a control in the ultrasonic cell during 15 min of sonication at an acoustic power of 57 W, 15 min without sonication and a further 15 min with sonication

Gas	Time (min)	Ultrasound	Rate of H_2O_2 formation ($mg\ L^{-1}\ min^{-1}$)	R^2
control	0 to 15	on	0,0051 ± 0,0003	0.971
	15 to 30	off	0,0000 ± 0,0000	0.000
	30 to 45	on	0,0044 ± 0,0002	0.975
oxygen	0 to 15	on	0,0070 ± 0,0004	0.971
	15 to 30	off	- 0,0001 ± 0,0002	0.022
	30 to 45	on	0,0054 ± 0,0002	0.981

The rates of hydrogen peroxide formation presented in Table 6.5, as discussed in Section 6.2, were greater in an oxygen-saturated solution than in the control. Hydrogen peroxide concentration for both the oxygen-saturated solution and control increased during the periods of sonication and remained constant or decreased slightly during the period without sonication. The rates of hydrogen peroxide formation for both the control and oxygen-saturated solution were lower in the second period of sonication than in the first period.

The statistical *F*-test at a 95 % confidence level indicated that the rates of hydrogen peroxide formation in the control between 0 to 15 min and 30 to 45 min (determined from the regression model) were not significantly different whereas the peroxide formation rates in the oxygen-saturated solution between 0 to 15 min and 30 to 45 min were significantly different. The lower peroxide formation during the second sonication period of oxygen-saturated water could be due to the increasing hydrogen peroxide degradation relative to formation, as discussed in Section 6.2 and Section 6.3, because of the greater peroxide concentration in solution.

The peroxide concentration profiles presented in Figure 6.8 show that ultrasound initiates radical reactions to produce hydrogen peroxide, hydrogen peroxide concentration remains constant in the absence of ultrasound and then increases again with further sonication. The slow degradation of hydrogen peroxide, as discussed in Section 6.3, indicates that in a flow loop system hydrogen peroxide formed in a sonicated zone remains available for the oxidation of organic compounds even as the reaction solution moves through the holding tank or reservoir.

The solid lines shown in Figure 6.8 were obtained using the regression model (equation 6.4) that accounts for step changes in hydrogen peroxide concentration

$$[H_2O_2] = a + b[time] + c[time - 15][time > 15] + d[time - 30][time > 30] \qquad [6.4]$$

where $[H_2O_2]$ is measured in mg L^{-1} and time in min. Estimates of the coefficients for the regression model of the control and oxygen-saturated solution data and the calculated standard errors of the coefficients are recorded in Table 6.6. The terms of the regression model are significant at a confidence level of 95 %. The coefficient of variance (R^2) for the oxygen and control regression models were both 0,987. The regression models thus account for 99 % of the variance in the data.

Table 6.6 : Regression coefficients for the model of hydrogen peroxide formation in oxygen-saturated water and a control during 15 min of sonication at an acoustic power of 57 W, 15 min without sonication and a further 15 min with sonication

	Control				**Oxygen-saturated solution**			
	a	***b***	***c***	***d***	***a***	***b***	***c***	***d***
estimate	0.00539	0.00495	-0.00506	0.00458	0.01208	0.00686	-0.00740	0.00599
standard error	0.00230	0.00023	0.00039	0.00039	0.00291	0.00029	0.00050	0.00050

An empirical model for hydrogen peroxide formation of the type presented in equation 6.4 can be used in the study of an ultrasonic loop reactor where the reaction solution is circulated through a small sonicated zone. Equipment parameters such as the optimal time length between sonication periods and the presence of gas can be incorporated during sonication but not beyond require further investigation.

6.4.2 Gas intervals

Interval experiments were also performed to monitor the effect of a change in gas during sonication at an acoustic power of 57 W. An oxygen-saturated solution was prepared by sparging pure oxygen through the solution for 10 min prior to and during sonication at a flow rate of 6 mL s^{-1}. Sonication was performed with a 15 min period of oxygen saturation followed by a 15 min period with nitrogen saturation and a further 15 min period with oxygen saturation. Hydrogen peroxide concentration was measured at time periods of 0; 5; 10; 15; 20; 25; 30; 35; 40 and 45 min. Triplicate experiments were performed for each time period. Hydrogen peroxide formation during sonication with a 15 min period of oxygen saturation followed by a 15 min period with nitrogen saturation and a further 15 min period with oxygen saturation is presented in Figure 6.9.

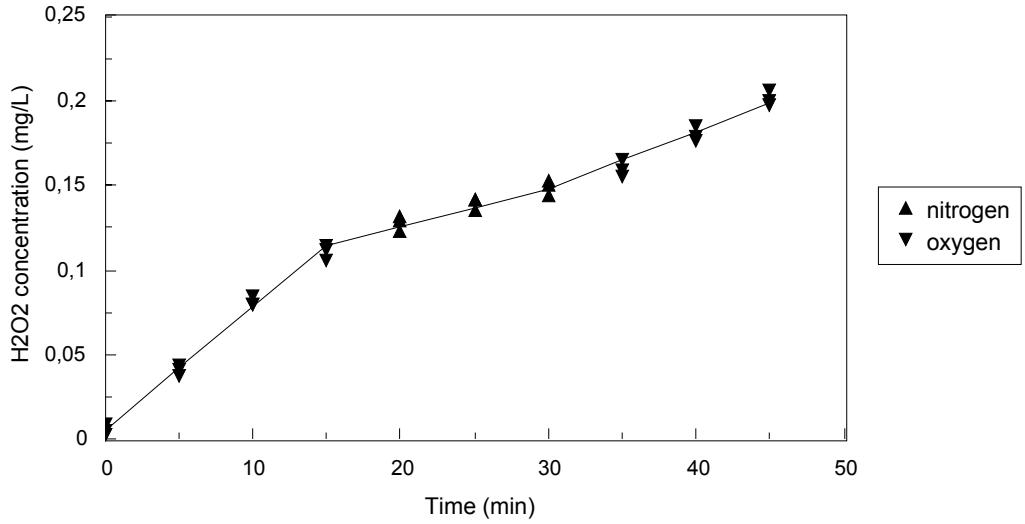

Figure 6.9 : Hydrogen peroxide formation in water during sonication in the ultrasonic cell at an acoustic power of 57 W with 15 min of oxygen saturation, 15 min of nitrogen saturation and a further 15 min of oxygen saturation (*n* = 3 per time period)

The maximum standard deviation in the hydrogen peroxide concentrations measured in water saturated alternately with oxygen and nitrogen, as shown in Figure 6.9, is 0,004 mg L^{-1}. The rate of hydrogen peroxide formation during the different 15 min periods (0 to 15 min; 15 to 30 min; 30 to 45 min) was determined from the regression of each set of 15 min data using the linear regression model

$$y = a + bx \qquad [6.7]$$

where the coefficient *b*, the gradient of the regression line, represents the rate of hydrogen peroxide formation. The calculated rates of hydrogen peroxide formation during 15 min periods of oxygen and nitrogen saturation (and the standard error of the calculated values) are recorded in Table 6.7.

Table 6.7 : Rate of hydrogen peroxide formation in water during sonication in the ultrasonic cell at an acoustic power of 57 W with 15 min of oxygen saturation, 15 min of nitrogen saturation and a further 15 min of oxygen saturation

Time (min)	Gas	Rate of H_2O_2 formation (mg L^{-1} min^{-1})	R^2
0 to 15	oxygen	0,0071 ± 0,0002	0.992
15 to 30	nitrogen	0,0025 ± 0,0002	0.924
30 to 45	oxygen	0,0035 ± 0,0003	0.950

The rates of hydrogen peroxide formation recorded in Table 6.7 indicate that peroxide formation decreased significantly when the gas was changed during sonication from oxygen to nitrogen. The rate of peroxide

formation during the period with nitrogen sparging was comparable, within the standard deviation, to the formation rate, as recorded in Table 6.1 in Section 6.2, in a nitrogen-saturated solution. The rapid depletion of dissolved oxygen due to nitrogen sparging prevented the formation of peroxide being enhanced by the earlier saturation with oxygen. The rate of peroxide formation during the second period of oxygen saturation, as shown in Figure 6.9, was lower than that during the first period due to the overall rate of peroxide formation decreasing with increasing concentration. The statistical *F*-test at a 95 % confidence level indicated that the rates of hydrogen peroxide formation during oxygen saturation between 0 to 15 min and 30 to 45 min (determined from the regression model) were significantly different.

A regression line (using the model in equation 6.4) was fitted to the data presented in Figure 6.9 (the solid line in Figure 6.9) to account for step changes in the data. The coefficients for the model are recorded in Table 6.8. Each term is significant at a confidence level of 95 % and the coefficient of variance (R^2) for the regression model is 0,995.

Table 6.8 : Regression coefficients for the model of hydrogen peroxide formation in water during sonication in the ultrasonic cell at an acoustic power of 57 W with 15 min of oxygen saturation, 15 min of nitrogen saturation and a further 15 min of oxygen saturation

	a	***b***	***c***	***d***
estimate	0.00606	0.00725	-0.00505	0.00118
standard error	0.00217	0.00022	0.00037	0.00037

6.5 COMMERCIAL HYDROGEN PEROXIDE EXPERIMENTS

Hydrogen peroxide is used commercially for oxidation. Examples of hydrogen peroxide oxidation in water treatment are given in Section 3.3.2 of Chapter 3. Hydrogen peroxide, as reported in Section 6.2, is formed during sonication, however, peroxide concentration in the ultrasonic cell was only approximately 1 mg L^{-1} after 16 h of sonication. The low sonochemical formation of hydrogen peroxide can be supplemented with a commercial source of hydrogen peroxide. Ultrasound acts as a promoter for the formation of hydroxyl radicals from hydrogen peroxide. The use of hydrogen peroxide to enhance the ultrasonic degradation of pollutants, such as 2-chlorophenol, is reported in Section 2.4.4.1 of Chapter 2. Ultrasound is described as being more effective when used in combination with other conventional water treatment processes than as a a stand-alone process.

Hydrogen peroxide concentration was monitored during sonication of solutions prepared from a commercial hydrogen peroxide source (AR grade; Saarchem). Hydrogen peroxide formation was measured in accurately prepared hydrogen peroxide solutions of approximate 0,25; 0,50 and 0,75 mg L^{-1} concentration during sonication in the ultrasonic cell for 1 h at an acoustic power of 57 W. The effect of gas on hydrogen

peroxide formation was investigated by sparging nitrogen, air or oxygen through the solutions for 10 min prior to and during sonication at a flow rate of 6 mL s^{-1}. A control was performed in water with no gas sparging. Hydrogen peroxide concentration was measured at time periods of 0; 5; 10; 20; 30 and 60 min. Triplicate experiments were performed for each time period for each gas. The hydrogen peroxide concentrations measured during the sonication of a 0,28 mg L^{-1} hydrogen peroxide solution is presented in Figure 6.10.

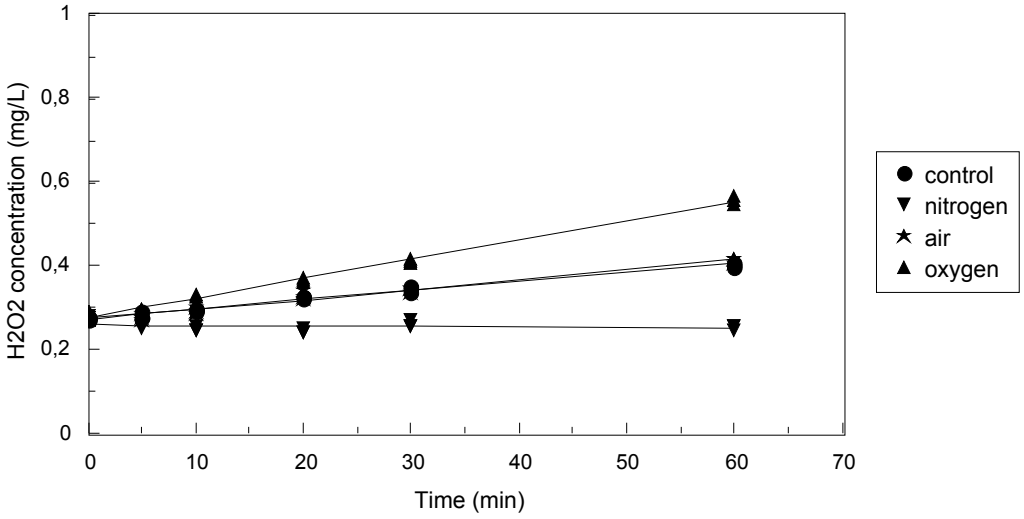

Figure 6.10 : Hydrogen peroxide formation in nitrogen-, air- and oxygen-saturated 0,28 mg L^{-1} hydrogen peroxide solutions during sonication in the ultrasonic cell for 1 h at an acoustic power of 57 W (*n* = 3 per time period)

The maximum standard deviation in the hydrogen peroxide concentrations measured during sonication of a 0,28 mg L^{-1} peroxide solution for the control and during nitrogen, air and oxygen saturation are 0,009; 0,008; 0,009 and 0,009 mg L^{-1}, respectively.

The hydrogen peroxide concentrations measured during the sonication of a 0,43 mg L^{-1} hydrogen peroxide solution is presented in Figure 6.11.

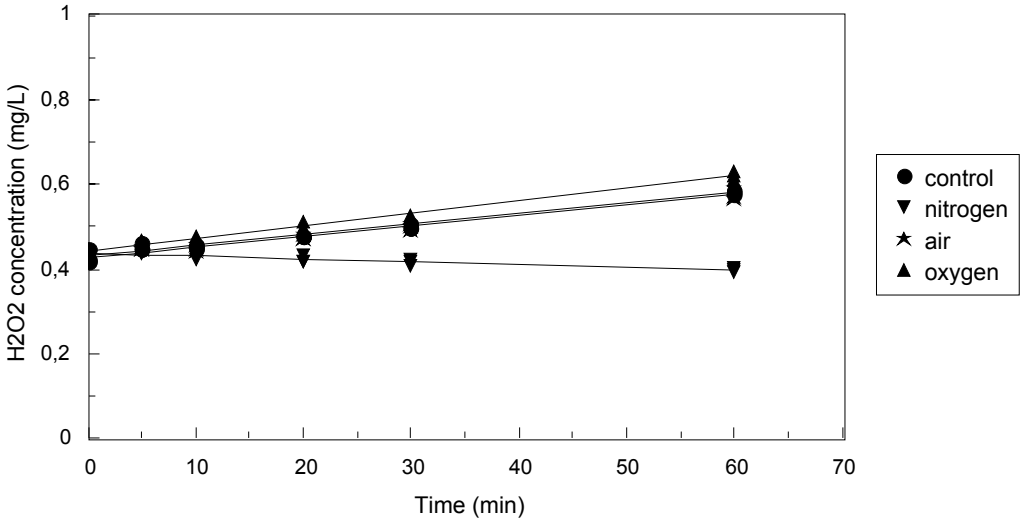

Figure 6.11 : Hydrogen peroxide formation in nitrogen-, air- and oxygen-saturated 0,43 mg L^{-1} hydrogen peroxide solutions during sonication in the ultrasonic cell for 1 h at an acoustic power of 57 W (*n* = 3 per time period)

The maximum standard deviation in the hydrogen peroxide concentrations measured during sonication of a 0,43 mg L^{-1} peroxide solution for the control and during nitrogen, air and oxygen saturation are 0,017; 0,010; 0,014 and 0,010 mg L^{-1}, respectively. The hydrogen peroxide concentrations measured during the sonication of a 0,72 mg L^{-1} hydrogen peroxide solution is presented in Figure 6.12.

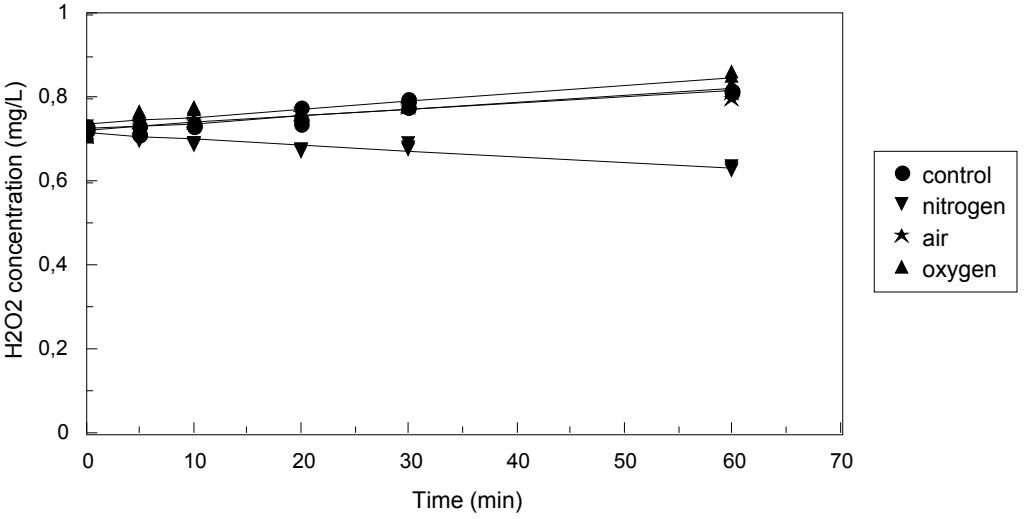

Figure 6.12 : Hydrogen peroxide formation in nitrogen-, air- and oxygen-saturated 0,72 mg L^{-1} hydrogen peroxide solutions during sonication in the ultrasonic cell for 1 h at an acoustic power of 57 W (*n* = 3 per time period)

The maximum standard deviation in the hydrogen peroxide concentrations measured during sonication of a 0,72 mg L^{-1} peroxide solution for the control and during nitrogen, air and oxygen saturation are 0,020; 0,009;

0,009 and 0,015 mg L^{-1}, respectively. The rates of hydrogen peroxide formation during sonication of hydrogen peroxide solutions were calculated from the regression of the data presented in Figure 6.10, Figure 6.11 and Figure 6.12 using the linear regression model

$$y = a + bx \qquad [6.8]$$

where the coefficient *b*, the gradient of the regression line, represents the rate of hydrogen peroxide formation. The calculated rates of hydrogen peroxide formation in peroxide solutions during sonication with nitrogen, air and oxygen saturation (and the standard error of the calculated values) are recorded in Table 6.9.

Table 6.9 : Rate of hydrogen peroxide formation in 0,28; 0,43 and 0,72 mg L^{-1} hydrogen peroxide solutions saturated with nitrogen, air and oxygen during sonication in the ultrasonic cell at an acoustic power of 57 W

Gas	Rate of H_2O_2 formation (mg L^{-1} min^{-1})					
	0,28 mg L^{-1}	R^2	0,43 mg L^{-1}	R^2	0,72 mg L^{-1}	R^2
control	0,0022 ± 0,0001	0.980	0,0024 ± 0,0001	0.972	0,0017 ± 0,0002	0.866
nitrogen	- 0,0001 ± 0,0001	0.073	- 0,0007 ± 0,0001	0.787	- 0,0014 ± 0,0001	0.871
air	0,0024 ± 0,0001	0.977	0,0025 ± 0,0001	0.979	0,0015 ± 0,0001	0.906
oxygen	0,0046 ± 0,0001	0.993	0,0029 ± 0,0001	0.986	0,0018 ± 0,0001	0.837

The trends of hydrogen peroxide formation were similar in all of the hydrogen peroxide solutions, formation was greatest during oxygen saturation, the lowest during nitrogen saturation and similar during air saturation and the control. The negative rate of formation shown in Table 6.9 for nitrogen saturation indicates that hydrogen peroxide was being degraded since the initial concentrations of the commercial hydrogen peroxide solutions were all greater than the equilibrium concentration (0,09 mg L^{-1}) of hydrogen peroxide during nitrogen sparging as shown in Figure 6.3(b) in Section 6.2.1. Hydrogen peroxide is both formed and degraded during sonication from chain radical reactions such as that shown in Scheme 6.1.

$$H_2O_2 \rightarrow HO^{\bullet} + HO^{\bullet} \qquad [a]$$

$$HO^{\bullet} + HO^{\bullet} \rightarrow H_2O + O^{\bullet} \qquad [b]$$

$$O^{\bullet} + H_2O \rightarrow H_2O_2 \qquad [c]$$

Scheme 6.1

Hydrogen peroxide is degraded, as shown in reaction [a] of Scheme 6.1, to form hydroxyl radicals that react to produce an oxygen radical. Hydrogen peroxide is reformed from the oxygen radical reaction with water,

reaction [c] of Scheme 6.1. The reactions presented in Scheme 6.1 are drawn from those presented in Scheme 2.4 in Section 2.3.1.2 and Scheme 3.9 in Section 3.3.1.

Oxygen radicals and molecules are formed, as shown in Scheme 2.3 and Scheme 2.4, from the radical reactions taking place during sonication (summarised in Appendix H). The radicals and molecules react further to continue the cycle of reactions. This was demonstrated with the oxygen radical formed in reaction [b] in Scheme 6.1. However, as described in Section 6.1, oxygen is removed from solution during nitrogen saturation. Oxygen radicals thus formed from the degradation of hydrogen peroxide, such as in reaction [a] and [b] of Scheme 6.1, are scavenged by the nitrogen. The cycle of hydrogen peroxide degradation and reformation is broken in that peroxide degrades but does not reform since the intermediate oxygen species have been scavenged by the nitrogen. Peroxide concentration was thus found to decrease, as recorded in Table 6.9, during the sonication of nitrogen-saturated hydrogen peroxide solutions.

The rate of hydrogen peroxide degradation during nitrogen saturation was found to be related to the initial hydrogen peroxide concentration of the solution. The rate of degradation increased from 0,0001 to 0,0014 mg L^{-1} min^{-1} as the concentration of the solution increased from 0,28 to 0,72 mg L^{-1}. The number of peroxide degradation and reformation reactions taking place is determined directly by the peroxide concentration, more reactions take place in more concentrated solutions. Thus during nitrogen saturation when all reformation reactions, are prevented from taking place, hydrogen peroxide concentration decreases quicker in a more concentrated solution since more degradation reactions are taking place. The increasing rate of hydrogen peroxide degradation is shown in Figure 6.13 to be linear as the initial concentration of the peroxide solution increases.

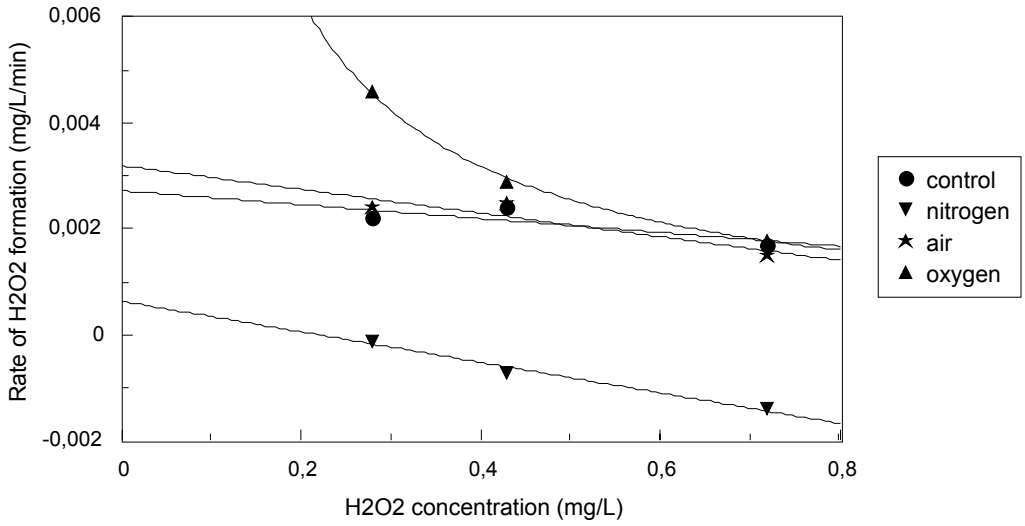

Figure 6.13 : Rates of hydrogen peroxide formation in 0,28; 0,43 and 0,72 mg L^{-1} commercial hydrogen peroxide solutions saturated with nitrogen, air and oxygen during sonication in the ultrasonic cell for 1 h at an acoustic power of 57 W

The hydrogen peroxide concentrations of the commercial peroxide solutions (0,28; 0,43 and 0,72 mg L^{-1}) were lower than the equilibrium peroxide concentrations in the control and for air and oxygen saturation (1 to 1,5 mg L^{-1} as shown in Figure 6.3(b) in Section 6.2.1). The concentration of hydrogen peroxide in the commercial peroxide solutions thus increased during sonication although the rate of peroxide formation (shown in Figure 6.13) decreased with increasing hydrogen peroxide concentration. The decreasing rate of hydrogen peroxide formation during oxygen saturation with increasing concentration of the peroxide solution (a power law relationship) is shown in Table 6.9 and Figure 6.13. The rate of hydrogen peroxide formation decreased from 0,0046 to 0,0018 mg L^{-1} min^{-1} as the concentration of the peroxide solution increased from 0,28 to 0,72 mg L^{-1}.

The rate of hydrogen peroxide formation in the 0,28 mg L^{-1} hydrogen peroxide solution was significantly greater during oxygen saturation than in the control and during air saturation. Whereas the rate of hydrogen peroxide formation in the 0,72 mg L^{-1} hydrogen peroxide solution was the same (within standard deviation) in the control and during air and oxygen saturation. Thus the enhancing effect due to oxygen saturation, shown in Figure 6.13, decreases with increasing concentration of a hydrogen peroxide solution.

The implications for an industrial ultrasonic system are that oxygen or air sparging do not significantly enhance free radical reactions when hydrogen peroxide is added during sonication and that the appropriate hydrogen peroxide concentration should be investigated for a particular process.

6.6 PROCESS CHEMISTRY

The sonochemical benefits of ultrasound are not derived as in UV radiation due to the direct effect of energy on solutes in solution but rather due to highly reactive radical species generated in the cavitation cavities. The high temperatures and pressures created in the collapsing gas cavities cause the thermal dissociation of water vapour to produce hydroxyl and hydrogen radicals. Radial recombination reactions lead to the formation of hydrogen peroxide, hydrogen and water. Volatile pollutants are degraded by pyrolytic reactions that occur in the gas cavity. The processes occurring in and around a collapsing gas cavity are illustrated in Figure 2.6 in Section 2.3.1.1. A comparison of bond dissociation energies is presented in Table 6.10.

Table 6.10 : Bond dissociation energies (Greenwood and Earnshaw, 1984a; Huang et al., 1974; Kirchener, 1981)

Reaction	Bond dissociation energy ($kJ\ mol^{-1}$)
$HO\text{-}H \rightarrow HO^{\bullet} + H^{\bullet}$	497.9
$HO\text{-}OH \rightarrow 2HO^{\bullet}$	209.2
$HOO\text{-}H \rightarrow HO_2^{\bullet} + H^{\bullet}$	376.6
$O\text{-}O \rightarrow 2O^{\bullet}$	493.4
$H\text{-}H \rightarrow 2H^{\bullet}$	435.1

The bond dissociation energies listed in Table 6.10 indicate that if the water molecule is split under the conditions in the collapsing gas cavities to initiate all sonochemical reactions, the other molecules with lower bond dissociation energies will also be split if present in the gas cavities. Thus, hydrogen peroxide formed from the reaction between two hydroxyl radicals can be split back to the radical species. Reactions also take place with volatile solutes in the collapsing gas cavity.

The radical recombination reactions producing hydrogen, water and hydrogen peroxide from hydroxyl and hydrogen radicals also take place at the gas/liquid interface when the species diffuse out of the cavity. The species may diffuse out of the cavity as they are formed or be released into the surrounding liquid on cavity collapse (Shah et al., 1999e). Hydrophobic pollutants accumulate and react at the gas/liquid interface, degradation at the interface is due to both pyrolysis and radical reactions. The concentration of hydroxyl radicals and hydrogen peroxide at the interface is significantly higher than in the bulk solution (Neis, 2000).

Hydrophilic pollutants in the bulk solution are degraded by reaction with free radicals or hydrogen peroxide molecules that have diffused from the gas cavities. It is estimated that approximately 10 % of the hydroxyl and hydrogen radicals generated in the gas cavities escape to the bulk solution (Thompson and Doraiswamy, 1999). Reaction kinetics in the bulk solution are analogous to that of radiation chemistry. In addition to the radical reactions, macromolecules and solid particles are degraded in the bulk solution due to the shock wave and microjet formation triggered by the collapse of the gas cavities (Neis, 2000).

The concentration of hydrogen peroxide and hydrogen in the bulk solution increase linearly at first, and then approach a limiting concentration due to further reaction or degradation in the gas cavities back to radical species (Chatterjee et al., 1983). The concentration of radical species in solution rapidly approaches a stationary value due to their high reactivity. The steady state approximation states that the concentration of free radicals will be very low at all times, essentially remaining constant, since they act as intermediates in a chain reaction (Chatterjee et al., 1983; Huang et al., 1974).

The radical species and products in solution can also dissociate to form ions that take part in further radical reactions. Perhydroxyl radicals dissociate at a pH greater than 4 (Scheme 6.2), hydrogen peroxide and hydroxyl radicals dissociate in basic solutions at a pH greater than 11 (Spinks and Woods, 1976).

$HO_2^{\bullet} \rightleftharpoons O_2^- + H^+$ pK = 4,88 [a]

$H_2O_2 \rightleftharpoons HO_2^- + H^+$ pK = 11,6 [b]

$HO^{\bullet} \rightleftharpoons O^- + H^+$ pK = 11,9 [c]

Scheme 6.2

A detailed list of radical reactions (from radiolysis and photolysis chemistry) that may potentially take place during sonication (due to similar reaction conditions) are listed in Appendix G.

6.7 CONCLUDING REMARKS

An ultrasonic laboratory reactor was designed and constructed to investigate the sub-processes occurring during sonication and to make recommendations for the scale-up of ultrasound processes.

The formation of hydrogen peroxide during sonication indicated that the ultrasonic source in the ultrasonic cell was sufficiently powerful to induce cavitation in solution. The collapsing gas cavities being the sites of sonochemistry initiation. Hydrogen peroxide concentration was used as a measure of the degree of radical reactions occurring during sonication and as a tool to judge under which process conditions the most radical reactions occurred in the ultrasonic cell.

The effects of dissolved oxygen concentration and acoustic power on hydrogen peroxide formation were investigated. De-oxygenation was achieved by sparging nitrogen through a solution. The gases (oxygen, air and nitrogen) were sparged continuously during sonication to keep the dissolved oxygen concentration constant. Hydrogen peroxide formation increased with increasing dissolved oxygen concentration due to the additional radical reactions being initiated. As hydrogen peroxide concentration in solution built up the rate of degradation increased until an equilibrium was established and the rate of degradation equalled the rate of formation. Equilibrium was reached during sonication in the absence of oxygen within 30 min and in the presence of oxygen after 16 h. Changes in the rate of hydrogen peroxide formation with changes in acoustic power were only observed during the first 30 min of sonication, and only in the presence of oxygen. Ultrasonic processes with a short reaction time, should thus, as a guide, be performed with oxygen sparging and a high acoustic power for optimum effectiveness whereas long ultrasonic processes should be operated with air sparging and a lower acoustic energy source.

A correlation was developed for hydrogen peroxide as a function of time, acoustic power and dissolved oxygen concentration to guide the choice of process conditions and mode of operation of an ultrasonic process.

The rate of degradation of hydrogen peroxide after sonication was slow in the absence of any gas sparging. A sparging gas, irrespective of the type, significantly enhanced peroxide degradation due to mixing and agitation. The post-sonication presence of hydrogen peroxide indicated the availability of peroxide in an ultrasonic loop system to oxidise organic compounds beyond the sonicated zone. Gas sparging with oxygen and air may be used in an ultrasonic reactor to enhance free radical formation, however, beyond the reactor in a flow loop system gas sparging has a negative effect and leads to the decomposition of hydrogen peroxide. Interval experiments demonstrated the formation of hydrogen peroxide during sonication, the constant peroxide concentration in the absence of sonication and a further increase in peroxide concentration with renewed sonication.

Sonication of commercial hydrogen peroxide solutions indicated that the enhancement in hydrogen peroxide formation, due to oxygen and air sparging, decreased with increasing concentration of the added commercial hydrogen peroxide. Thus the occurrence of free radical reactions during sonication should either be enhanced with added hydrogen peroxide or gas sparging but not with both.

To summarise, guidelines for the scale-up of ultrasonic processes:

- A gas (oxygen and air) or added hydrogen peroxide should be used to enhance radical reactions during sonication. If a gas, sparging should be continued throughout sonication.
- Oxygen sparging and a high acoustic power should be used for processes with a short retention time, air sparging and a lower acoustic energy source for longer processes.
- The measurement of hydrogen peroxide concentration is a convenient tool to investigate parameters that enhance process operation and reactor performance.
- A flow loop system should be considered to maximise the oxidation of organic compounds both in and out of a sonicated zone. However, gas sparging beyond the sonicated zone should be avoided.

7

OZONE PROCESS INVESTIGATION

Ozone is widely used in water treatment for colour, taste and odour removal, disinfection, oxidation of pollutants and flocculation enhancement. The oxidation of pollutants during ozonation is enhanced by the addition of hydrogen peroxide. Other advanced oxidation processes, such as ultrasound, when used in conjunction with ozone may also enhance the performance of ozone in water treatment. This chapter details the investigation of ozone chemistry and the effects of combining ultrasound and hydrogen peroxide with ozone. The implications of including ozone in the scale-up an ultrasound process are also discussed.

Ozonation experiments were performed in the ultrasonic cell (with and without ultrasound). Ozone was generated from oxygen in a Sorbios ozone generator and sparged through a solution in the ultrasonic cell similar to the gas experiments reported in Chapter 6. The measurement of dissolved ozone concentration is reported in Section 7.1, ozone decomposition in Section 7.2, the formation of hydrogen peroxide during ozonation in Section 7.3 and ozone mass balances in Section 7.4. A summary of the experimental programme of the ozone process investigation is presented in Table 7.1.

Table 7.1 : Experimental programme of the ozone process investigation

Section	Title	Measured parameters	Variables	Data Appendix	Statistics Appendix
7.1	Dissolved ozone concentration	$[O_3]$	ultrasound hydrogen peroxide	D.1	F.4.1
7.2	Ozone decomposition	$[O_3]$ $[H_2O_2]$	ozone ultrasound	D.2	F.4.2
7.3	Hydrogen peroxide formation	$[H_2O_2]$	ozone ultrasound	D.3	F.4.3
7.4	Mass balances	$[O_3]$ $[H_2O_2]$	ozone ultrasound hydrogen peroxide	D.4	F.4.4

The experimental data discussed in this chapter is reported (as indicated in Table 7.1) in Appendix D. The statistical analysis (mean, 95 % confidence limits, standard deviation) is reported in Appendix F. Standard deviation was calculated for each time period of an experiment though only the maximum value is reported

in this chapter. Each data point in experiments measuring hydrogen peroxide or dissolved ozone concentration was measured in a separate experiment since the ultrasonic cell had to be opened during sampling (described in Section 5.3), thus altering the gas atmosphere in the cell.

7.1 DISSOLVED OZONE CONCENTRATION

Oxidation of organic pollutants by ozone during water treatment can take place due to direct reaction with ozone molecules or by reaction with free radicals formed from the decomposition of ozone. The reaction scheme proposed by Hoigné and co-workers for the decomposition of ozone is presented in Scheme 3.3 in Section 3.1.2, the reaction scheme for the combination of ozone and hydrogen peroxide is presented in Scheme 3.6 in Section 3.1.2. These reaction schemes are summarised in Appendix H on A3 paper that can be folded out. Pollutant oxidation is enhanced with the addition of hydrogen peroxide during ozonation. Hydrogen peroxide, as shown in Scheme 2.3 in Section 2.3.1.1 (repeated in Appendix H), is formed during sonication. The combination of ultrasound with ozone may thus also enhance pollutant oxidation during ozonation. The amount of ozone available in solution for either direct reaction with pollutants or for the formation of free radicals is determined by the transfer of ozone into solution. Parameters that affect ozone transfer are discussed in Section 3.1.2 and Section 3.2.2.

Ozone chemistry was investigated by sparging the oxygen/ozone gas through water in the ultrasonic cell and measuring the dissolved ozone concentration in solution. The ozone concentration in the 2,4 mL s^{-1} gas stream was 5,7 mg L^{-1} and the ozone production rate was 0,014 mg s^{-1} (Table 5.6 in Section 5.2). Dissolved ozone concentration in water was measured during ozonation at time periods of 0; 1; 2,5; 5; 10; 20; 40 and 60 min. Experiments were performed in duplicate for each time period. Dissolved ozone concentration was also measured during ozonation when the water was sonicated at an acoustic power of 57 W, when 40 mg L^{-1} hydrogen peroxide was added prior to ozonation and when ozonation was combined with both hydrogen peroxide and sonication. Selection of the hydrogen peroxide concentration is described in Section E.2.3 of Appendix E, atrazine degradation was used as the selection criterion. Atrazine degradation was greatest over a 45 min period during ozonation with a hydrogen peroxide concentration of 10 mg L^{-1}, hydrogen peroxide concentration was thus increased 4-fold for a 3 h ozonation period. Dissolved ozone concentration in water during ozonation, ozonation combined with sonication, ozonation combined with hydrogen peroxide and ozonation combined with both sonication and hydrogen peroxide are presented in Figure 7.1.

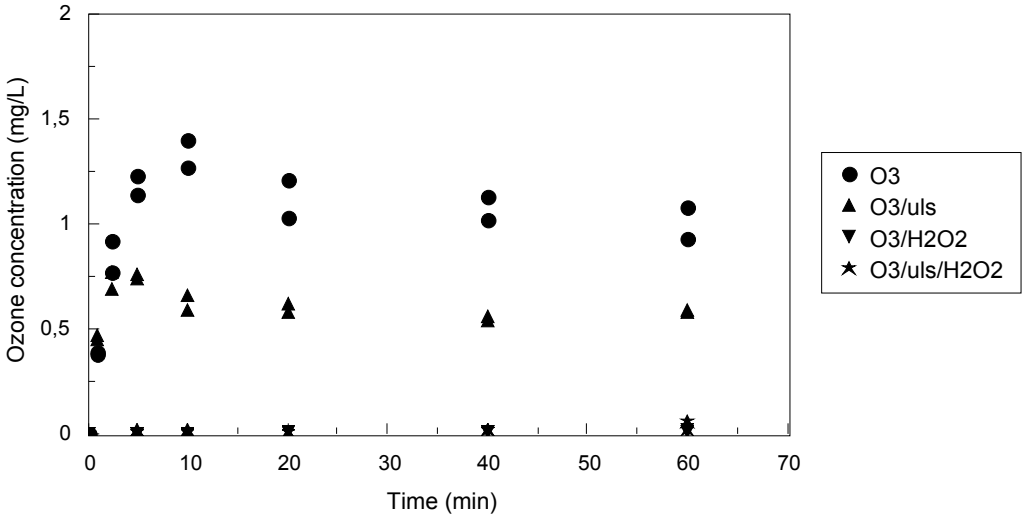

Figure 7.1 : Dissolved ozone concentration in water during ozonation (0,014 mg s^{-1}), ozonation combined with sonication (57 W), ozonation combined with hydrogen peroxide (40 mg L^{-1}) and ozonation combined with sonication and hydrogen peroxide (*n* = 2 per time period)

The maximum standard deviation in the measured dissolved ozone concentrations in water during ozonation, ozonation combined with sonication, ozonation combined with hydrogen peroxide and ozonation combined with sonication and hydrogen peroxide are 0,108; 0,054; 0,030 and 0,001 mg L^{-1}, respectively.

The concentration of dissolved ozone in water during ozonation, as shown in Figure 7.1, increased to a maximum after 10 min and remained relatively constant, within standard deviation, after 20 min. This trend in dissolved ozone concentration is similar to that reported by Beltrán and co-workers in which dissolved ozone concentration was found to increase rapidly during ozonation, reaching a stationary value after 10 min (Beltrán et al., 1994b; Beltrán et al., 1998). Dissolved ozone concentration after 10 min during ozonation combined with sonication was about 50 % (shown in Figure 7.1) of that during ozonation alone. Ultrasound thus reduces the amount of dissolved ozone in solution during ozonation.

The reduction in dissolved ozone concentration caused by sonication is due to reduced ozone transfer from the gas bubbles into the bulk solution as well as to the greater decomposition of ozone in solution. It is proposed that the ozone-containing bubbles act as nucleation sites for cavitation during the combination of ozonation with sonication. The ozone in the bubbles is thus subjected to the high temperatures and pressures created during bubble collapse in the compression stages of a sound wave. The slow decomposition of ozone in the gaseous phase to oxygen (at room temperature) is significantly enhanced by heat (Peleg, 1976). Ozone molecules under the conditions in the collapsing cavitation bubbles are destroyed by conversion to oxygen, reaction [a] of Scheme 7.1 (repeated from Scheme 3.1), and degradation to oxygen radicals, reaction [b] of Scheme 7.1. The decomposition of ozone to oxygen in the gas bubbles reduces the ozone that is available to diffuse into the bulk solution. Oxygen radicals are also formed according to reaction [c] of

Scheme 7.1 from molecular oxygen present in the cavitation bubbles because the bond dissociation energy of oxygen is lower than that of water which is dissociated during cavitation (discussed in Section 6.6). Oxygen is formed according to reactions [a] and [b] of Scheme 7.1 but it is present in the cavitation bubbles predominantly since it is the carrier gas in which ozone is generated.

$$2O_3 \rightarrow 3O_2 \quad [a]$$

$$O_3 \rightarrow O_2 + O^{\bullet} \quad [b]$$

$$O_2 \rightarrow O^{\bullet} + O^{\bullet} \quad [c]$$

Scheme 7.1

Weavers and Hoffmann proposed that ozone first dissolves into solution and then rediffuses into the gaseous cavitation bubbles where it undergoes thermolytic decomposition as shown in Scheme 7.1 (Weavers and Hoffmann, 1998). The reduction in dissolved ozone concentration below the saturation value during ozonation combined with sonication thus enhances the mass transfer effects and allows for more ozone to dissolve into solution as a function of time (Weavers and Hoffmann, 1998). The investigation of the degradation of 4-nitrophenol during ozonation combined with sonication by Barbier and Pétrier found that degradation increased with increasing ultrasonic frequency (20 versus 500 kHz) because of the greater quantity of hydroxyl radicals escaping from the cavitation bubbles (Barbier and Pétrier, 1996).

Ozone molecules inside the cavitation bubbles and at the gas/liquid interface also participate in the ultrasonic-initiated radical reactions listed in Scheme 2.1 to Scheme 2.4 (summarised in Appendix H) that occur in these regions. The reaction of ozone with hydroxyl radicals formed in the collapsing cavitation bubbles (reaction [f] of Scheme 3.3) initiates a chain of radical reactions that leads to the decomposition of ozone (Scheme 3.3 in Appendix H). The reaction sequence of the chain propagation steps is reaction [f] of Scheme 3.3 followed by reactions [g]; [b]; [c]; [d]; [e] and [f] which continues the reaction cycle.

Oxygen radicals generated from the decomposition of ozone (reactions [b] and [c] of Scheme 7.1) propagate further free radical reactions since hydrogen peroxide is generated according to reaction [a] of Scheme 7.2 (repeated from Scheme 2.4). The hydrogen peroxide is degraded under the conditions inside the cavitation bubbles (discussed in Section 6.6) to generate perhydroxyl and hydroxyl radicals according to reactions [b] and [c] of Scheme 7.2 (repeated from Scheme 3.9).

$$O^{\bullet} + H_2O \rightarrow H_2O_2 \quad [a]$$

$$H_2O_2 \rightarrow H^{\bullet} + HO_2^{\bullet} \quad [b]$$

$$H_2O_2 \rightarrow 2HO^{\bullet} \quad [c]$$

Scheme 7.2

Ozone decomposition due to conditions in the collapsing cavitation bubbles and due to participation in the ultrasonic-initiated free radical reactions occurs within the gas phase. Ultrasound, however, also initiates

ozone decomposition in the bulk solution. Hydrogen peroxide is formed during sonication (Scheme 2.2 and Scheme 2.3 in Appendix H); the hydrogen peroxide either reacts further inside the cavitation bubbles or diffuses into the bulk solution as summarised in Figure 2.6 in Section 2.3.1.1. Hydrogen peroxide in the bulk solution dissociates (discussed in Section 6.6) to form perhydroxyl ions as demonstrated in Scheme 7.3 (repeated from Scheme 6.2).

$$H_2O_2 \rightleftharpoons HO_2^- + H^+$$

Scheme 7.3

Ozone molecules in the bulk solution react with the perhydroxyl ions formed from the dissociation of hydrogen peroxide in solution; ozone reacts with perhydroxyl ions but not directly with hydrogen peroxide (Staehelin and Hoigné, 1982). The reaction of ozone and perhydroxyl ions (reaction [d] of Scheme 3.6 in Appendix H) initiates a chain of radical reactions that leads to the decomposition of ozone (Scheme 3.6 in Appendix H). Ozone decomposition initiated by the reaction of ozone with perhydroxyl ions HO_2^- is significantly greater than that initiated by reaction with hydroxyl ions HO^- since the reaction rate constant is over 4-fold greater. Staehelin and Hoigné calculated that ozone decomposition initiated by reaction with perhydroxyl ions was faster than that initiated by hydroxyl ions for aqueous solutions of hydrogen peroxide concentration above 0,0034 mg L^{-1} (Staehelin and Hoigné, 1982).

The reduction in dissolved ozone concentration caused by sonication, as shown in Figure 7.1, is thus due to processes inside the cavitation bubbles reducing ozone diffusion into the bulk solution as well as due to enhanced decomposition in the bulk solution because of the reaction with perhydroxyl ions.

The overshoot in dissolved ozone concentration during ozonation and when ozonation was combined with sonication before a stationary ozone concentration was reached, as shown in Figure 7.1, can be due to the formation of hydrogen peroxide during ozonation (reactions [h] and [i] of Scheme 3.3). Hydrogen peroxide starts to form as dissolved ozone concentration increases, however, the hydrogen peroxide dissociates to form perhydroxyl ions that reacts with the ozone. Thus, dissolved ozone concentration reaches a maximum once ozone decomposition (due to the reaction with perhydroxyl ions) becomes greater than the diffusion of ozone into solution, a correction in dissolved ozone concentration occurs and equilibrium is reached between the ozone diffusion into and ozone decomposition in solution. The maximum ozone concentration during ozonation combined with sonication is reached earlier than during ozonation alone (5 min versus 10 min) due to the enhanced formation of hydrogen peroxide. Hydrogen peroxide concentration increases faster because of the effect of ultrasound. Thus sufficient hydrogen peroxide to initiate ozone decomposition is formed in a shorter time period causing the maximum dissolved ozone concentration (as shown in Figure 7.1) to occur at an earlier time and at a lower ozone concentration. The equilibrium concentration of ozone in solution during ozonation combined with sonication is thus lower (approximately 50 %) than that during ozonation alone.

No significant dissolved ozone was measured as shown in Figure 7.1 during ozonation in the presence of the added 40 mg L^{-1} hydrogen peroxide. Similarly, no ozonation was measured during ozonation combined with sonication and hydrogen peroxide. The concentration of added hydrogen peroxide (40 mg L^{-1}) was significantly greater than that formed during sonication (shown in Figure 7.4 to be less than 0,5 mg L^{-1}) which caused a 50 % decrease in dissolved ozone concentration in solution. Ozone accumulation in solution during ozonation with added hydrogen peroxide is thus completely prevented since the ozone diffusing into the bulk solution reacts immediately with the perhydroxyl radicals formed from the dissociation of the added hydrogen peroxide. Beltrán and co-workers reported that dissolved ozone concentration decreases as the added hydrogen peroxide concentration is increased; a 34 mg L^{-1} hydrogen peroxide concentration was found to cause a 50 % decrease in the maximum dissolved ozone concentration (from approximately 3,4 to 1,7 mg L^{-1}) during ozonation (at an ozone production rate of 0,22 mg s^{-1}) and that a 340 mg L^{-1} hydrogen peroxide concentration completely prevented any accumulation of ozone in solution (Beltrán et al., 1998).

Although no dissolved ozone is present in solution during ozonation with added hydrogen peroxide, the decomposition of ozone initiates free radical reactions (as in Scheme 3.6 in Appendix H) in which highly reactive species are generated. Hydroxyl radicals are formed during ozone decomposition according to reaction [g] of Scheme 3.6, the high reactivity of hydroxyl radicals is discussed in Section 1.3. The oxidation of organic compounds during the combination of ozone with ultrasound or hydrogen peroxide is thus more likely due to reaction with free radicals (hydroxyl radicals) than direct reaction with ozone molecules.

The addition of hydrogen peroxide during ozonation only affects ozone chemistry in the bulk solution (the region of hydrogen peroxide dissociation) whereas ultrasound affects ozone chemistry both in the gas-phase of the ozone bubbles (because of the cavitation conditions and ultrasonic radical reactions) and in the bulk solution (because of the dissociation of hydrogen peroxide formed during sonication).

The statistical software package *STATISTICA* was used to model dissolved ozone concentration, the dependent variable, as a function of acoustic power and hydrogen peroxide concentration, the independent variables. Acoustic power values of 0 and 57 W represent the absence and presence of sonication during ozonation. Hydrogen peroxide concentrations of 0 and 40 mg L^{-1} represent the absence and presence of hydrogen peroxide during ozonation. Surface response diagrams of dissolved ozone concentration as a function of the two independent variables were generated for time periods of 10 and 60 min representing a short and an extended period of ozonation. The gradient profiles of dissolved ozone concentration presented in Figure 7.2 indicate the conditions of acoustic power and hydrogen peroxide concentration where dissolved ozone concentration (plotted on the z-axis) is highest (dark grey) and lowest (light grey). The circular symbols in Figure 7.2 indicate the experimental data points.

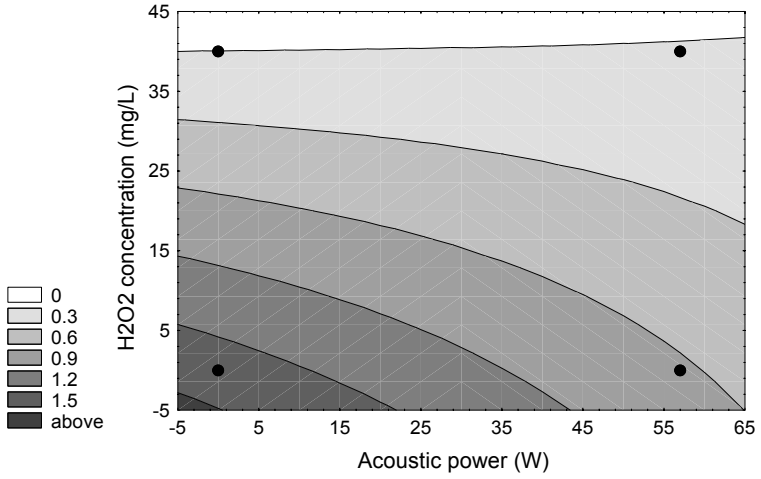

(a) 10 min

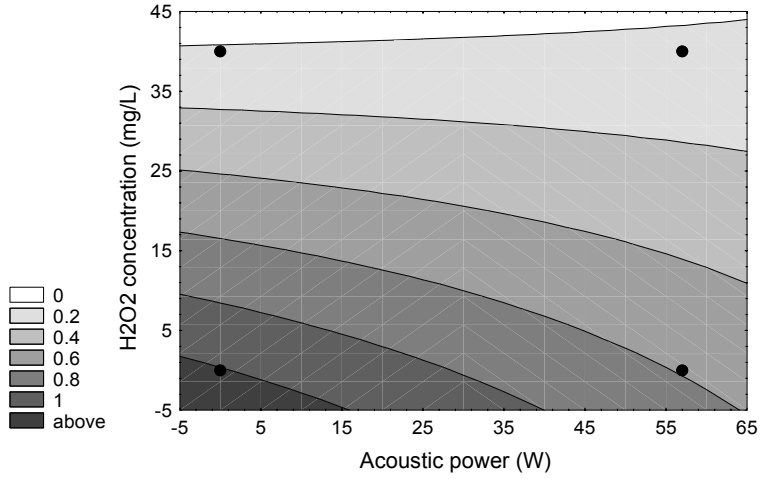

(b) 60 min

Figure 7.2 : Surface response diagrams of dissolved ozone concentration in water during ozonation as a function of acoustic power and hydrogen peroxide concentration

The similar gradient profiles of dissolved ozone concentration at 10 and 60 min during ozonation Figure 7.2(a) and Figure 7.2(b), indicates that the effects of ultrasound and hydrogen peroxide on dissolved ozone concentration do not change with time. Thus, the mechanism by which ozone concentration is reduced in solution by ultrasound and hydrogen peroxide is independent of time and will not change over an ozonation experiment.

The effect of hydrogen peroxide addition (40 mg L^{-1}) on the reduction of ozone concentration is greater than that of sonication at an acoustic power of 57 W, the addition of hydrogen peroxide in Figure 7.2(a) reduced dissolved ozone concentration from 1,35 to 0 mg L^{-1} whereas sonication only reduced ozone concentration from 1,35 to 0,65 mg L^{-1}. The effect of sonication is shown to decrease with increasing hydrogen peroxide concentration since the gradient profile lines become more horizontal as peroxide concentration increases.

The gradient profiles presented in Figure 7.2(a) and Figure 7.2(b) indicate that the reduction in dissolved ozone concentration obtained during sonication (without added hydrogen peroxide) is the same as that obtained during the addition of between 15 and 20 mg L^{-1} hydrogen peroxide (without sonication).

The gradient profiles presented in Figure 7.2(a) and Figure 7.2(b) also indicate the conditions where oxidation due to the direct reaction with ozone is favoured and where reaction with free radicals is favoured. Oxidation of organic compounds due to direct reaction with ozone molecules is favoured where dissolved ozone concentration in solution is highest, as during ozonation without sonication or added hydrogen peroxide. Conversely, oxidation of organic compounds due to reaction with free radicals is favoured where dissolved ozone concentration has been reduced by ozone decomposition, as during ozonation with sonication or added hydrogen peroxide. The total reduction of dissolved ozone in solution during ozonation with added hydrogen peroxide indicates that oxidation of organic compounds is due only to free radical reactions whereas the partial reduction in dissolved ozone concentration during ozonation combined with sonication indicates that both direct reaction with ozone and free radical reactions can take place. The combination of ozonation with sonication can thus be applied to treat a mixture of organic compounds since both reaction mechanisms take place, hence compounds that preferentially react with either ozone or hydroxyl radicals will be oxidised. Though, oxidation of organic compounds during ozonation is reported in literature to be predominantly due to free radical reactions (Beltrán et al., 1993b; Beltrán et al., 1994a).

7.2 OZONE DECOMPOSITION

The kinetics of the decomposition of ozone was investigated by monitoring the decrease in dissolved ozone concentration of a saturated solution under different experimental conditions. An ozone-saturated solution was prepared by sparging the oxygen/gas gas through water in the ultrasonic cell for 20 min. The ozone concentration in the 2,4 mL s^{-1} gas stream was 5,7 mg L^{-1} and the ozone production rate was 0,014 mg s^{-1} (Table 5.6 in Section 5.2). Dissolved ozone concentration was measured over 40 min (after the 20 min saturation period) during ozonation, during sonication and when ozonation was combined with sonication. A control was performed by measuring dissolved ozone concentration after the 20 min saturation period without ozonation or sonication. Duplicate experiments were performed for each time period. The dissolved ozone concentrations are presented in Figure 7.3.

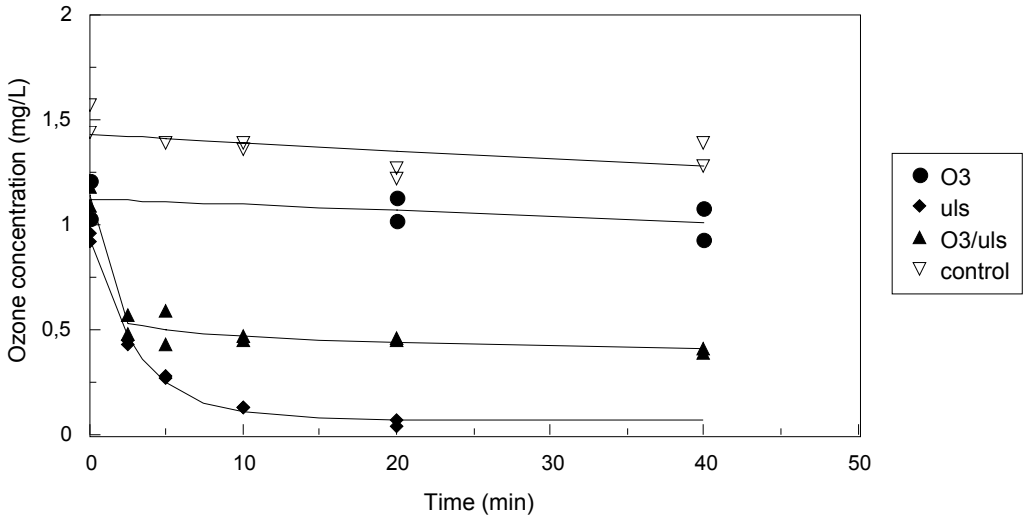

Figure 7.3 : Dissolved ozone concentration in water in the ultrasonic cell after a 20 min saturation period during ozonation (0,014 mg s^{-1}), sonication (57 W) and ozonation combined with sonication (*n* = 2 per time period)

The maximum standard deviation in the dissolved ozone concentrations measured in the control and during sonication, ozonation, and ozonation combined with sonication are 0,090; 0,033; 0,115 and 0,134 mg L^{-1}, respectively. The decrease in ozone concentration of an ozone-saturated solution once ozonation had been stopped, as shown by the control in Figure 7.3, indicates that ozone decomposition is relatively slow, ozone concentration decreased from approximately 1,50 to 1,35 mg L^{-1} over the 40 min period (a 10 % reduction). The degradation rate constant was calculated (from linear regression of the data) to be 0,004 mg L^{-1} min^{-1}. The higher initial concentration of the control was due to the daily fluctuation in experimental conditions, the % error in ozone generation (calculated during the ozone mass balances, Section D.4) is 7,5 %.

In comparison, the sonication of an ozone-saturated solution resulted in a rapid decrease in dissolved ozone concentration from 0,95 to 0,06 mg L^{-1} within 20 min (a 94 % reduction). The reduction in dissolved ozone concentration during sonication as discussed in Section 7.1 is due to the decomposition of ozone to oxygen and the reaction in solution with perhydroxyl ions. The degassing nature of ultrasound would also contribute to reducing the dissolved ozone concentration of an ozone-saturated solution.

The dissolved ozone concentration measured during ozonation combined with and without sonication is also compared in Figure 7.3. Dissolved ozone concentration remained relatively constant, decreasing slowly, during ozonation in the absence of ultrasound whereas ozonation combined with sonication led to the rapid decrease in ozone concentration (within 10 min) from the saturation value (1,50 mg L^{-1}) to approximately 0,5 mg L^{-1}. Dissolved ozone concentration is reduced during the combination of ozonation with sonication, however, radical reactions are initiated in solution. Thus the potential oxidation of organic compounds during ozonation is enhanced by combining ozonation with sonication.

The dissolved ozone concentration during ozonation combined with sonication in an ozone-saturated solution is shown in Figure 7.3 and in water with no pre-saturation in Figure 7.1. The dissolved ozone concentration in both experiments (either decreasing from saturation or increasing from zero) stabilised at 0,5 mg L^{-1}. This concentration is thus the equilibrium concentration of dissolved ozone during ozonation combined with sonication where the rate of ozone transfer into solution is equal to the rate of ozone decomposition initiated during sonication.

7.3 HYDROGEN PEROXIDE FORMATION

Hydroxyl radicals and hydrogen peroxide are formed in the free radical reactions, listed in Scheme 3.3 in Section 3.1.2 (summarised in Appendix H), occurring during ozonation. The combination of hydroxyl radicals, shown in Scheme 2.2 in Section 2.3.1.1 (Appendix H), may also lead to the formation of hydrogen peroxide. Hydrogen peroxide formation was investigated during ozonation, sonication and when ozonation was combined with sonication. Ozonation was performed at an ozone production rate of 0,014 mg s^{-1} and sonication at an acoustic power of 57 W. Hydrogen peroxide concentration was measured at time periods of 0; 5; 10; 20; 40 and 60 min. Duplicate experiments were performed for each time period. Hydrogen peroxide concentrations are presented in Figure 7.4.

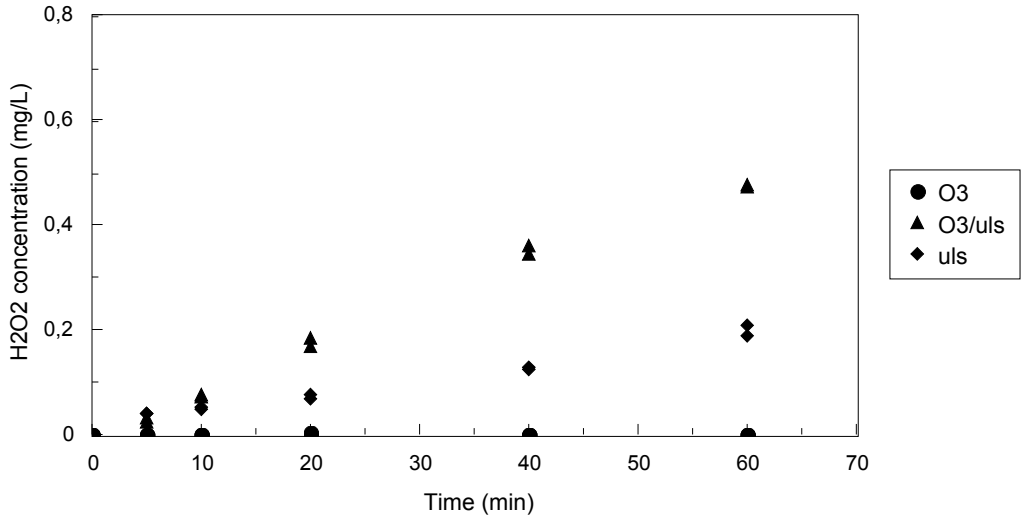

Figure 7.4 : Hydrogen peroxide concentration in water during ozonation (0,014 mg s^{-1}), sonication (57 W) and ozonation combined with sonication (n = 2 per time period)

The maximum standard deviation in the hydrogen peroxide concentrations measured during ozonation, sonication and ozonation combined with sonication are 0,002; 0,015 and 0,010 mg L^{-1}, respectively. The rates of hydrogen peroxide formation in water during ozonation, sonication and ozonation combined with sonication were calculated from the regression of the data presented in Figure 7.4 using the linear regression model

$$y = bx \qquad [7.1]$$

where the coefficient *b*, the gradient of the regression line, represents the rate of hydrogen peroxide formation. The calculated rates of hydrogen peroxide formation in water during ozonation, sonication and ozonation combined with sonication (and the standard error of the calculated values) are recorded in Table 7.2.

Table 7.2 : Rate of hydrogen peroxide formation in water in the ultrasonic cell during ozonation (0,014 mg s^{-1}), sonication (57 W) and ozonation combined with sonication

	Rate of H_2O_2 formation (mg L^{-1} min^{-1})	R^2
ozone	0,0000 ± 0,0000	0.000
ultrasound	0,0034 ± 0,0001	0.955
ozone/ultrasound	0,0082 ± 0,0001	0.992

Hydrogen peroxide was not detected in solution (shown in Figure 7.4) during ozonation alone. As discussed in Section 7.1 and 7.2, the hydrogen peroxide formed during ozonation according to reactions [h] and [i] of Scheme 3.3 would have dissociated and reacted with the ozone in solution (reactions [c] and [d] of Scheme 3.6). Thus preventing the accumulation of hydrogen peroxide in solution during ozonation. Staehelin and Hoigné reported that hydrogen peroxide would not be formed during ozonation at pH values greater than 6 due to the reaction of ozone with the highly reactive perhydroxyl ions formed from hydrogen peroxide dissociation (Staehelin and Hoigné, 1982). Distilled water with a neutral pH (around 7) was used in the ultrasonic cell. The pH of the solution was not measured during ozonation, although adsorption of carbon dioxide from the atmosphere may have made the water slightly acidic.

Hydrogen peroxide accumulated in solution during ozonation combined with sonication since the rate of formation was greater than the rate of dissociation and reaction with ozone molecules. A synergistic effect in the formation of hydrogen peroxide, shown in Figure 7.4 and Table 7.2, was obtained when ozonation was combined with sonication. The rate of hydrogen peroxide formation was greater during ozonation combined with sonication than the sum of that formed separately during ozonation and sonication. Water, hydrogen peroxide and hydrogen gas, as shown in Scheme 2.2 in Appendix H, are formed from the hydrogen and hydroxyl radicals produced in the collapsing gas cavities during sonication. Ultrasound, however, enhances the decomposition of ozone as shown in Figure 7.1 and discussed in Section 7.1. Thus more oxygen radicals and molecules are produced when ozonation is combined with sonication. Additional hydrogen peroxide is formed by the reaction of the oxygen radicals and molecules with the hydrogen radicals (formed from the sonication of water, Scheme 2.1) that usually recombine to produce hydrogen gas (reaction [c] of Scheme 2.2) in the absence of ozone. The concentration of hydrogen peroxide generated in solution is greater than 0,0034 mg L^{-1}, thus according to Staehelin and Hoigné (Staehelin and Hoigné, 1982) the reaction of ozone with perhydroxyl ions (reaction [d] of Scheme 3.6) has a greater effect on the

decomposition of ozone during ozonation combined with sonication than the reaction with hydroxyl ions (reaction [a] of Scheme 3.6).

The statistical software package *STATISTICA* was used to model hydrogen peroxide concentration as a function of acoustic power and ozone concentration. Acoustic power values of 0 and 57 W represent the absence and presence of sonication. Ozone concentrations of 0 and 5,7 mg L^{-1} represent the absence and presence of ozonation. Surface response diagrams of hydrogen peroxide concentration as a function of the two independent variables were generated for time periods of 10 and 60 min, a short and extended period of experimentation. The gradient profiles presented in Figure 7.5 indicate the conditions of sonication and ozonation where hydrogen peroxide concentration (plotted on the z-axis) is highest (dark grey) and lowest (light grey). The circular symbols in Figure 7.5 indicate the experimental data points.

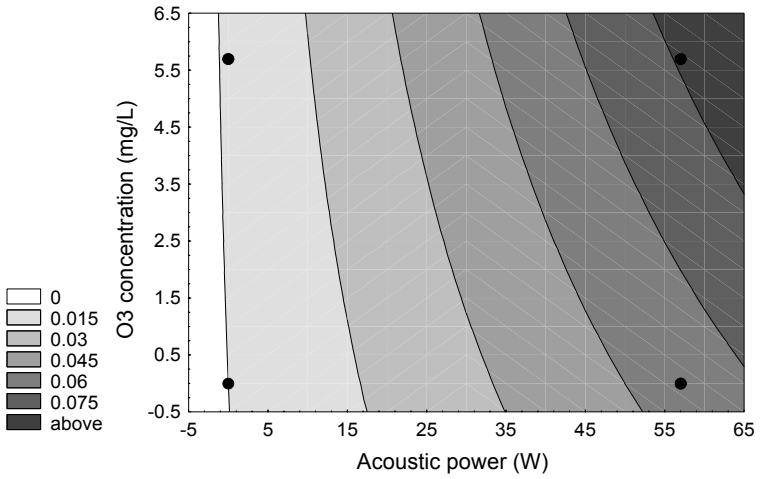

(a) 10 min

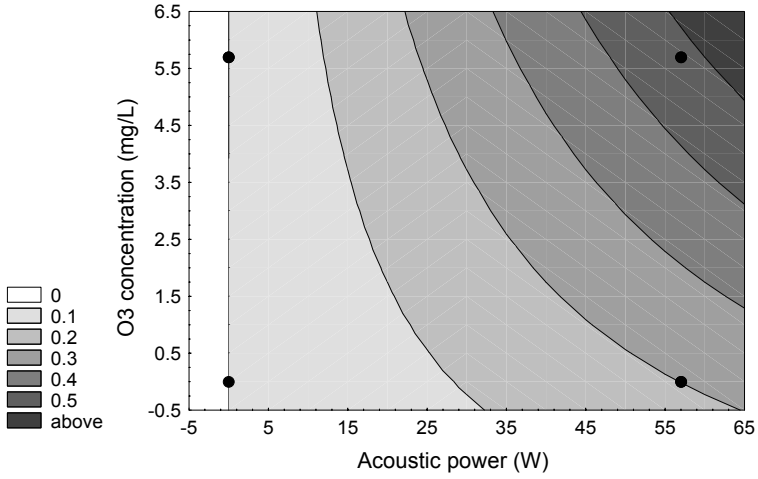

(b) 60 min

Figure 7.5 : Surface response diagrams of hydrogen peroxide concentration as a function of acoustic power and ozone concentration during ozonation of water in the ultrasonic cell

The similar gradient profiles of ozone concentration at 10 and 60 min, Figure 7.5(a) and Figure 7.5(b), indicates that the effect of sonication and ozonation on hydrogen peroxide concentration does not change with time. Thus, the mechanism by which hydrogen peroxide is formed during ozonation and sonication is independent of time and will not change during an experiment.

The gradient profiles presented in Figure 7.5(a) and Figure 7.5(b) indicate that the concentration of hydrogen peroxide in solution is greatest during ozonation combined with sonication. Ozone concentration, shown in Figure 7.1, is reduced by approximately 50 % during the combination of ozonation and sonication. Thus less ozone is available in solution for direct reaction with organic pollutants, however, the greater hydrogen peroxide concentration, shown in Figure 7.4, indicates that a greater degree of radical reactions occurs in solution. Thus, oxidation of organic compounds during ozonation combined with sonication is more likely to take place through radical reactions than the direct reaction with ozone molecules.

7.4 MASS BALANCES

The dissolved ozone concentration in solution as discussed in Section 7.1 is reduced when ozonation is combined with sonication or hydrogen peroxide. Ozone decomposition was investigated by performing 45 min mass balances to compare the amount of ozone generated in 45 min to the amount of unreacted ozone in the system at the termination of the 45 min experiment. The amount of ozone decomposed or consumed by reaction with solutes in the water is calculated from the difference between the amount of ozone generated over the time span of the experiment and the unreacted ozone in the system at the termination of the experiment. The total amount of unreacted ozone at the termination of an experiment consists of the dissolved ozone in solution in the ultrasonic cell, the ozone in the gas spaces of the system and the ozone that passed through the system and reacted with the potassium iodide in the gas traps.

Mass balances were performed over a 45 min period of ozonation, ozonation combined with sonication, ozonation combined with hydrogen peroxide and ozonation combined with sonication and hydrogen peroxide. Ozonation was performed at an ozone production rate of 0,014 mg s^{-1}, sonication at an acoustic power of 57 W and hydrogen peroxide was added so as to prepare a 40 mg L^{-1} solution. The experimental details of the mass balance experiments are reported in Section D.4. Ozone and hydrogen peroxide concentrations were measured after the 45 min ozonation period except in solutions with added hydrogen peroxide (40 mg L^{-1}) where only ozone concentration was measured. The upper limit of the hydrogen peroxide concentrations that can be measured using the DMP method (described in Section 5.4.1) is 4,08 mg L^{-1}. The average amounts of ozone generated in 45 min (Table D.4) and the amounts of unreacted ozone at the end of the 45 min mass balance experiments (Table D.6) are summarised in Table 7.3.

Table 7.3 : Ozone decomposition in water over 45 min during ozonation, ozonation combined with

sonication, ozonation combined with hydrogen peroxide and ozonation combined with sonication and hydrogen peroxide

	Average generated ozone (mg)	Unreacted ozone (mg)				% (unreacted)/ (generated)
		dissolved ozone	gas-phase ozone	ozone in KI traps	total	
ozone	54.6	0.64	4.18	47.09	51.91	95.1
		0.60	4.18	46.73	51.51	94.3
average		**0.62**	**4.18**	**46.91**	**51.71**	**94.7**
ozone/uls	49.2	0.21	3.36	35.56	39.13	79.5
		0.23	3.36	36.25	39.84	81.0
average		**0.22**	**3.36**	**35.91**	**39.49**	**80.3**
ozone/H_2O_2	49.0	0.00	3.30	35.25	38.55	78.7
		0.08	3.30	35.27	38.65	78.9
average		**0.04**	**3.30**	**35.26**	**38.60**	**78.8**
ozone/uls/H_2O_2	50.8	0.04	3.07	34.37	37.48	73.8
		0.05	3.07	33.84	36.96	72.8
average		**0.05**	**3.07**	**34.10**	**37.22**	**73.3**

The ozonation mass balance (shown in Table D.3) indicates that approximately 95 % of the ozone generated in 45 min was detected in the system at the termination of the experiment. The 5 % difference in ozone mass is in part due to decomposition of ozone to oxygen (Scheme 3.1 in Section 3.1.1) and reaction of ozone with perhydroxyl ions since no hydrogen peroxide accumulation (shown in Figure 7.4) occurred in solution during ozonation. The 5 % difference in ozone mass is also due to the variability in the amount of ozone generated in 45 min. The average amount is reported in Table 7.3 whereas the actual triplicate values are reported in Table D.4 in Appendix D. The error in the generated ozone in the ozonation mass balance is approximately 3,3 %; sample error is calculated from the standard deviation and sample mean recorded in Table F.26 in Appendix F.

The total mass of unreacted ozone in the different mass balances reported in Table 7.3 indicates that different amounts of unreacted ozone were measured at the termination of the 45 min experiments. The absolute values, however, cannot be compared as the rates of ozone generation were different. The % error in the rate of ozone generation throughout the mass balances was 7.5 %. Thus the amounts of unreacted ozone are converted to fractions of the ozone generated during the mass balance experiment. The unreacted ozone measured in the solution, gas-phase and KI traps are reported in Table 7.4 as fractions of the ozone generated during the different mass balance experiments.

Table 7.4 : Unreacted ozone in the solution, gas-phase and KI traps at the termination of the 45 min experiments as a fraction (%) of the generated ozone during the mass balance experiments

	Unreacted ozone (%)				decomposed or reacted ozone (%)
	dissolved ozone	**gas-phase ozone**	**ozone in KI traps**	**total**	
ozone	1.1	7.7	85.9	**94.7**	5.3
ozone/uls	0.4	6.8	73.0	**80.2**	19.8
ozone/H_2O_2	0.1	6.7	72.0	**78.8**	21.2
ozone/uls/H_2O_2	0.1	6.1	67.1	**73.3**	26.7

The amount of ozone remaining in the system at the termination of the 45 min mass balance experiments is shown in Table 7.4 to decrease from approximately 95 % to approximately 80 and 79 %, respectively, when ozonation is combined with either sonication or hydrogen peroxide. The increased ozone decomposition results in a lower dissolved ozone concentration in solution as shown in Figure 7.1. The mechanisms of ozone decomposition are discussed in Section 7.1. The increased ozone decomposition in the gas bubbles (during cavitation) and in solution reduces the dissolved ozone in solution and hence the ozone exiting the ultrasonic cell. Thus, as shown in Table 7.4 the gas-phase ozone and the ozone in the KI traps is reduced when ozonation in combined with either sonication or hydrogen peroxide.

The amount of ozone remaining in the system at the end of the ozonation combined with sonication mass balance (80 %) is similar, within experimental error, to that remaining at the end of the ozonation combined with hydrogen peroxide mass balance (79 %) although the ozone decomposition mechanisms are different. As discussed in Section 7.1 ozone decomposition during ozonation combined with hydrogen peroxide (40 mg L^{-1}) occurs in solution due to reaction with perhydroxyl ions formed from the hydrogen peroxide dissociation. Whereas ozone decomposition during ozonation combined with sonication occurs in the gas bubbles due to the cavitation conditions and radical reactions as well as in solution due to reaction with perhydroxyl ions formed from the hydrogen peroxide generated during sonication (less than 0,5 mg L^{-1}). The effect of ozonation combined with sonication on the dissolved ozone concentration in solution is shown in Figure 7.2 to be similar to that obtained during ozonation combined with between 15 and 20 mg L^{-1} hydrogen peroxide (without sonication). Hence the similar amount of ozone remaining in the system at the end of the mass balances in which ozonation is combined with either sonication or hydrogen peroxide.

The lowest amount of ozone remaining in the system (approximately 73 %, Table D.4) was measured at the end of the mass balance in which ozonation was combined with both sonication and hydrogen peroxide. Hydrogen peroxide is formed during sonication (shown in Figure 6.3 in Section 6.2.1), however, the rate of formation decreases as the concentration of peroxide increases (discussed in Section 6.5) until the equilibrium concentration is reached (discussed in Section 6.2). Hydrogen peroxide was shown to be degraded during sonication when the initial concentration of a hydrogen peroxide solution was greater than the equilibrium concentration (as during the nitrogen saturation experiments in Figure 6.10 to Figure 6.12 in Section 6.5). The equilibrium hydrogen peroxide concentration during sonication in the presence of oxygen

is shown in Figure 6.3(b) in Section 6.2.1 to be approximately 1 to 1,5 mg L^{-1}. The initial rate of hydrogen peroxide formation during sonication is shown in Figure 7.4 to be lower than that during sonication combined with ozonation. The equilibrium concentration of hydrogen peroxide during sonication combined with ozonation is thus greater, although it was not measured, than the equilibrium concentration during sonication without ozonation (1 to 1,5 mg L^{-1}). It is, however, unlikely to be as high as 40 mg L^{-1}. Hydrogen peroxide is thus degraded and the concentration is reduced from 40 mg L^{-1} during ozonation combined with both sonication and hydrogen peroxide as it changes towards the equilibrium concentration. Hydroxyl radicals are formed from the degradation of hydrogen peroxide according to reaction [a] of Scheme 6.1. The reaction of the hydroxyl radicals with ozone (reaction [h] of Scheme 3.6) results in the reduced ozone measured in the system when ozonation is combined with both sonication and hydrogen peroxide (Table 7.4).

An excess of ozone is evident in the system though less is available in solution for oxidation of organic compounds when ozonation is combined with either ultrasound or hydrogen peroxide. Oxidation is thus more likely to occur due to reaction with free radicals when ozonation is combined with either ultrasound or hydrogen peroxide.

7.5 PROCESS CHEMISTRY

Oxidation of organic solutes in water by ozone is due either to direct reaction with ozone molecules or reaction with free radicals formed from the decomposition of ozone. The radical reactions occurring during ozone decomposition are listed in Scheme 3.3 in Section 3.1.3. The combination of ozonation with sonication or hydrogen peroxide enhances ozone decomposition thus increasing the radical reactions occurring in solution and decreasing the dissolved ozone concentration. Hydrogen peroxide added to a solution or produced during sonication dissociates to form perhydroxyl ions. The reaction between ozone and the perhydroxyl ions, discussed in Section 7.1, causes the decrease in dissolved ozone concentration and the enhanced free radical reactions. The reduction in dissolved ozone concentration during ozonation combined with sonication is also due to the ozone-containing bubbles acting as nucleation sites for cavitation. Ozone is decomposed to oxygen within the bubbles due to the high temperatures and pressures created during bubble collapse. Ozone decomposition due to the reaction of ozone with the ultrasonic-initiated radical reactions occurs both within the gas bubbles and at the interface between the gas-phase and the bulk solution. The addition of hydrogen peroxide during ozonation only affects ozone chemistry in the bulk solution whereas ultrasound affects ozone chemistry both in the gas-phase of the ozone bubbles as well as in the bulk solution. Oxidation of organic compounds during the combination of ozonation with either ultrasound or hydrogen peroxide is thus more likely due to reaction with free radicals than to the direct reaction with ozone. Although the combination of ozonation combined with sonication allows for both reaction mechanisms to occur.

Ozonation is a gas-liquid reaction and is influenced by mass transfer. The presence of dissolved ozone in solution indicates that the free radical formation reactions are slow and take place in the bulk solution (as during ozonation and ozonation combined with sonication). Whereas a negligible ozone concentration in solution indicates that reactions are fast and take place in the film layer surrounding the ozone bubbles (as during ozonation combined with hydrogen peroxide and ozonation combined with both sonication and hydrogen peroxide).

7.6 CONCLUDING REMARKS

Ozone chemistry and the effects of combining ultrasound and hydrogen peroxide with ozone were investigated. Ozone is a powerful though selective oxidant. Oxidation during ozonation takes place either due to direct reaction with ozone molecules or reaction with free radicals formed from the decomposition of ozone.

The measurement of dissolved ozone concentration indicated that ultrasound reduced ozone concentration by approximately 50 % and added hydrogen peroxide (40 mg L^{-1}) totally depleted the ozone in solution. The decrease in dissolved ozone concentration during ozonation combined with sonication is equivalent to that obtained with between 15 and 20 mg L^{-1} of added hydrogen peroxide (without sonication). The decrease in dissolved ozone concentration, partial or total, was due to reaction between ozone and perhydroxyl ions formed from the dissociation of hydrogen peroxide. Ozone decomposition during sonication also occurred within and at the interface of the cavitation bubbles due to the cavitation conditions and free radical reactions. The addition of hydrogen peroxide during ozonation only affects ozone chemistry in the bulk solution whereas ultrasound affects ozone chemistry both in the gas-phase of the ozone bubbles as well as in the bulk solution.

The measurement of hydrogen peroxide concentration during ozonation, sonication and the combination of ozonation and sonication indicated that a synergistic effect occurred in the formation of hydrogen peroxide during the combination of ozonation and sonication. The enhanced rate of hydrogen peroxide formation is due to the reaction of ozone within the cavitation bubbles with hydrogen radicals that usually recombine to form hydrogen gas. The decreased dissolved ozone concentration in solution and the enhanced hydrogen peroxide formation during the combination of ozone with ultrasound indicates that the oxidation of organic compounds is more likely to take place due to the reaction with free radicals than the direct reaction with ozone. The oxidation of organic compounds is thus most effective when ozonation is combined with either ultrasound or hydrogen peroxide so as to enhance the degree of radical reactions occurring in solution.

Process conditions are altered depending on whether ozone is combined with ultrasound or hydrogen peroxide. The total reduction of dissolved ozone in solution during ozonation with added hydrogen peroxide indicates that oxidation of organic compounds is due only to free radical reactions whereas the partial reduction in dissolved ozone concentration during ozonation combined with sonication indicates that both

reaction mechanisms, direct reaction with ozone and free radical reactions, take place. The combination of ozonation with sonication thus allows for the oxidation of compounds that preferentially react with either ozone or hydroxyl radicals.

The equilibrium concentration of ozone in solution (0,5 mg L^{-1}) was measured when ozonation was combined with sonication in the ultrasonic cell. The implications for an ultrasonic system of sparging ozone through the sonicated zone is that ozone will be present to enhance the oxidation of organic pollutants, radical reactions will also be increased than during sonication alone. The slow degradation of ozone after ozonation has been terminated indicates that in a flow loop system ozone will also be available to react with organic pollutants once the reaction solution has moved out of the sonicated zone. Pollutant oxidation can thus be achieved both in and beyond the sonicated zone with the inclusion of ozone in an ultrasonic process.

8

ATRAZINE EXPERIMENTS

Atrazine is an effective and widely used herbicide. The stability of atrazine in the environment has lead to the contamination of potable water sources and is thus a potential health risk. The potential of using ultrasound to degrade organic pollutants during water treatment is demonstrated in the ultrasonic cell using atrazine as a model compound. This chapter details the atrazine investigation in the ultrasonic cell. The ultrasonic degradation of atrazine is compared with that achieved during oxidation with ozone and with hydrogen peroxide. Atrazine solution chemistry during ozonation and sonication is discussed, the enhancing effect of hydrogen peroxide is demonstrated. Potential degradation mechanisms are described to account for the degradation products identified using gas chromatography and mass spectroscopy. A summary of the experimental programme of the atrazine investigation is presented in Table 8.1.

Table 8.1 : Experimental programme of the atrazine investigation in the ultrasonic cell

Section	Title	Measured parameters	Variables	Data Appendix	Statistics Appendix
8.1	**Atrazine chemistry**	[atr]	gas (O_2)	0.100	F.5.1
8.1.1	Ultrasound	-	-	-	-
8.1.2	Ozone	[O_3]	ozone ultrasound hydrogen peroxide	E.1.1	F.5.1.1
8.1.3	Hydrogen peroxide	[H_2O_2]	ozone ultrasound	E.1.2	F.5.1.2
8.1.4	Mass balances	[O_3] [H_2O_2] [atr]	ozone ultrasound hydrogen peroxide	E.1.3	F.5.1.3
8.2	**Atrazine degradation**	-	-	-	-
8.2.1	Ultrasound	[atr]	atrazine concentration gas (N_2; O_2)	E.2.1	F.5.2.1
8.2.2	Ozone	[atr]	ozone ultrasound	E.2.2	F.5.2.2
8.2.3	Hydrogen peroxide	[atr]	ozone ultrasound	E.2.3	F.5.2.3
8.3	**Product identification**	-	-	0.300	-

Experimental data discussed in this chapter is reported in Appendix E as indicated in Table 8.1. Statistical analysis (mean, 95 % confidence limits, standard deviation) is reported in Appendix F. Standard deviation was calculated for each time period of an experiment though only the maximum value is reported in this chapter. Each data point in experiments measuring hydrogen peroxide or dissolved ozone concentration was measured in a separate experiment since the ultrasonic cell had to be opened during sampling (described in Section 5.3), thus altering the gas atmosphere in the cell. The ultrasonic cell did not have to be opened during atrazine sampling, atrazine concentration was thus measured continuously during an experiment. Atrazine was found not to interfere with the analytical methods used to measure ozone and hydrogen peroxide concentration (Section 5.4.4). Atrazine chemistry is discussed in Section 8.1. The atrazine degradation investigation is reported in Section 8.2 and the identification of degradation products is detailed in Section 8.3.

8.1 ATRAZINE CHEMISTRY

Atrazine concentration in the environment is typically in the range 0 to 20 μg L^{-1}. Starting concentrations in laboratory investigations of up to 50 mg L^{-1}, depending on the sensitivity and detection limit of the analytical method, have been reported in literature. The HPLC method used in this investigation, described in Section 5.3.4, measures atrazine concentrations in the 1 mg L^{-1} range. A concentration of 5 mg L^{-1} was thus used as an initial atrazine concentration. Atrazine concentration in a standing 5 mg L^{-1} solution was measured over 3 h as a degradation control at time periods of 0; 45; 90; 135 and 180 min. Atrazine concentration was also measured when oxygen was sparged through the solution at a flow rate of 6 mL s^{-1}. Experiments were performed in triplicate. The atrazine concentrations are presented in Figure 8.1.

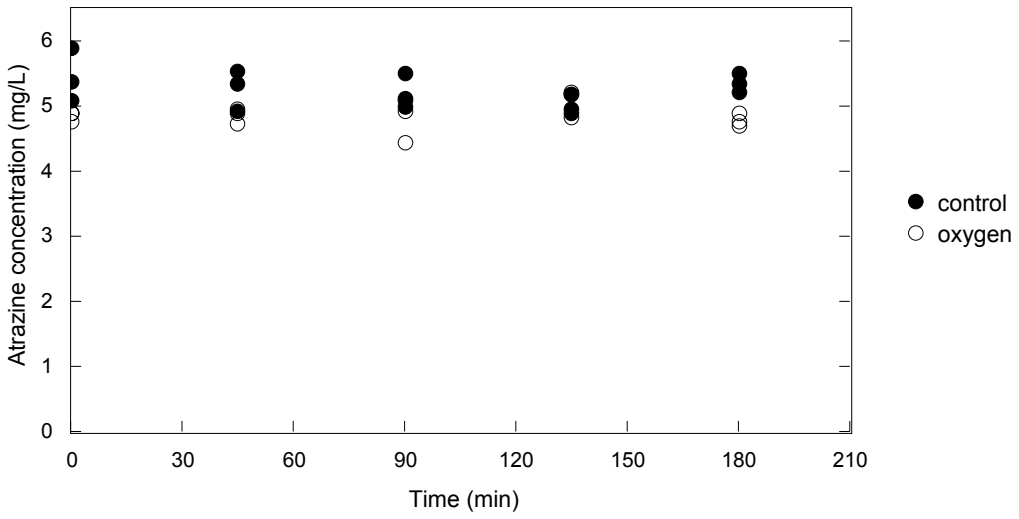

Figure 8.1 : Atrazine concentration in a 5 mg L^{-1} atrazine solution in the ultrasonic cell over 3 h in the absence of ultrasound without and with oxygen sparging (*n* = 3 per time period)

The maximum standard deviation in atrazine concentrations measured in the control, without and with oxygen sparging, are 0,34 and 0,42 mg L^{-1}, respectively. The rates of atrazine degradation were calculated from the regression of the data presented in Figure 8.1 using the linear regression model

$$y = a + bx \qquad [8.1]$$

where the coefficient *b*, the gradient of the regression line, represents the rate of atrazine degradation. The calculated rates of atrazine degradation in a control, without and with oxygen sparging (and the standard errors of the calculated values) are recorded in Table 8.2.

Table 8.2 : Rate of atrazine degradation in a 5 mg L^{-1} atrazine solution in the ultrasonic cell over 3 h in the absence of ultrasound without and with oxygen sparging

Gas	Rate of atrazine degradation (mg L^{-1} min^{-1})	R^2
control	- 0,00091 ± 0,00114	0.047
control with oxygen	- 0,00014 ± 0,00082	0.002

The low atrazine degradation rates reported in Table 8.2 and shown in Figure 8.1 indicate that atrazine does not degrade upon standing even with oxygen sparging. The statistical coefficient of variance (R^2) of the regression models (Table 8.1) are low as the regression lines are almost horizontal. The statistical *F*-test at a 95 % confidence level indicated that there was no significant difference in the gradients of the regression lines for the control and with oxygen sparging.

The chemistry of atrazine in solution during sonication is discussed in Section 8.1.1, during ozonation in Section 8.1.2 and in the presence of hydrogen peroxide in Section 8.1.3. Mass balances are reported in Section 8.1.4.

8.1.1 Ultrasound

Sonochemical benefits (discussed in Chapter 2) are caused by both physical and chemical effects of ultrasound. Physical effects are induced by shockwave and microjet formation, and usually impact only polymeric and heterogeneous systems. Atrazine degradation during sonication is thus not likely to occur due to the ultrasonic physical effects but rather to the chemical effects, the formation of free radicals in the collapsing gas cavities and their subsequent diffusion into the bulk solution. A diagram of the three reaction zones occurring during cavitation (gas cavity; gas/liquid interface; bulk solution) and the processes occurring in each zone is presented in Figure 2.6 in Section 2.3.1.1.

The low vapour pressure of atrazine (0,0385 mPa at 25 °C, Table 4.1 in Section 4.1.2) indicates that atrazine is relatively non-volatile and does not accumulate inside the collapsing gas cavities. Atrazine is also a

hydrophobic compound since it contains more hydrophobic groups (such as CH_3, CH_2 and CH) than hydrophilic groups (such as OH, COOH, CO and NH_2). Hydrophobicity is discussed in Section 2.3.1.1. The hydrophobicity of atrazine is demonstrated in that it is significantly more soluble in organic solvents than in water. The solubility of atrazine in water at 22 °C is 33 mg L^{-1} (Table 4.1) whereas the solubility in acetone is 31 000 mg L^{-1} (Tomlin, 1997). Atrazine thus accumulates in the gas/liquid interfacial region during sonication because of its non-volatility and hydrophobicity. Riesz and co-workers concluded that the gas/liquid interface was a region of low polarity with a high concentration of non-volatile hydrophobic compounds (Riesz et al., 1990b; Riesz and Kondo, 1992).

The gas/liquid interface, as shown in Figure 2.6 in Section 2.3.1.1, is a region where both free radical reactions (Scheme 2.3; Scheme 2.4; Scheme 2.5) and pyrolysis reactions take place. The gas/liquid interface is a region with a high concentration of free radicals since the radicals formed within the gas cavities as well as the products of the reactions taking place inside the cavities (such as hydrogen peroxide) diffuse through the interface into the bulk solution. Atrazine thus reacts with the hydroxyl radicals present at the gas/liquid interface.

The reaction of atrazine with hydroxyl radicals, as described in Chapter 4, leads to the formation of both dealkylated and hydrolysed degradation products. The mechanism by which dealkylated products are formed from the reaction of atrazine with hydroxyl radicals is shown in Figure 4.11 in Section 4.3. The formation of dealkylation products is summarised in Figure 8.2.

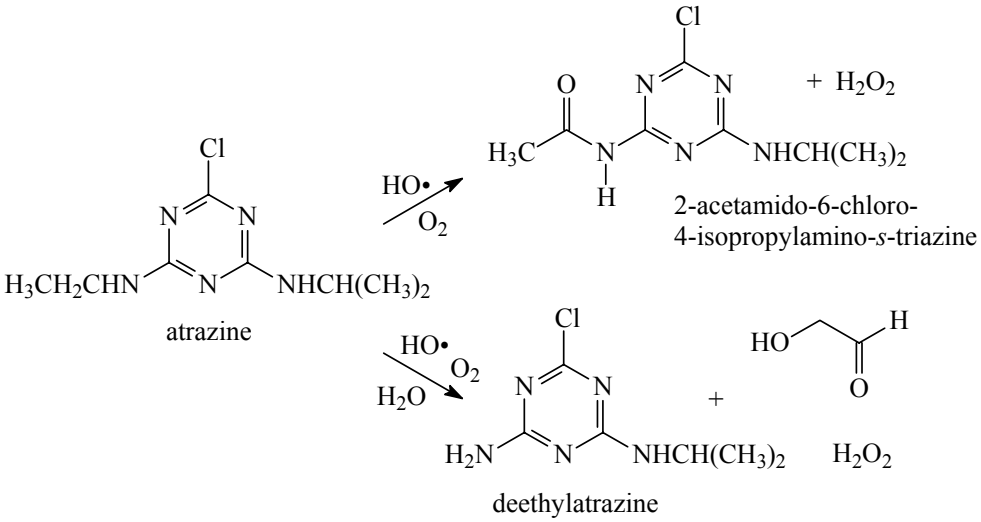

Figure 8.2 : Formation of dealkylated degradation products from the reaction of atrazine with hydroxyl radicals (Hapeman et al., 1995)

Dealkylation of atrazine by reaction with hydroxyl radicals, as discussed in Section 4.3, is initiated at the side-chain carbon α to the amine nitrogen (Hapeman et al., 1995). The carbon is relatively electron-rich

since the amine nitrogen provides additional electron density. Oxygen is required in the degradation pathway to form the intermediate radicals (shown in Figure 4.11) from which the acetamide and deethyl products are formed. Hydrogen peroxide is produced as a byproduct when both types of products are formed. The mechanism is sterically controlled, hence, the hydroxyl radical attack occurs preferentially on the ethyl side-chain producing deethylatrazine than on the isopropyl side-chain.

The mechanism by which hydrolysed products are formed from the reaction of atrazine with hydroxyl radicals is similar to the mechanism shown in Figure 4.10 in Section 4.3 for the reaction of atrazine with hydroxyl ions. The formation of hydrolysed products is summarised in Figure 8.3 (from Figure 4.14).

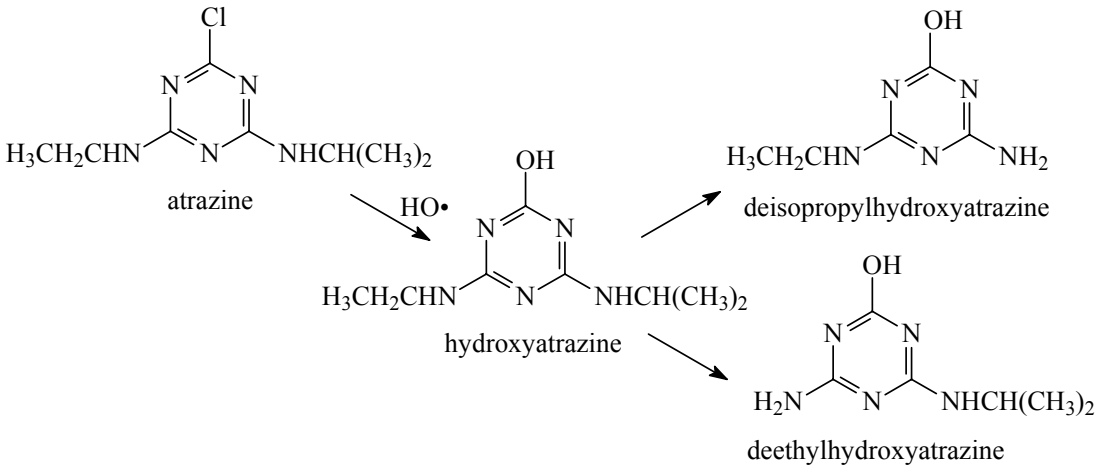

Figure 8.3 : Formation of hydrolysed degradation products from the reaction of atrazine with hydroxyl radicals (Adams and Randtke, 1992a)

The formation of hydrolysed products by the reaction of atrazine with hydroxyl ions, as discussed in Section 4.3, occurs by nucleophilic attack at the site of the C-Cl bond (Chan et al., 1992). Oxygen is not required for the reaction to occur and hydrogen peroxide is not formed as a byproduct during the reaction mechanism. Atrazine degradation due to reaction with hydroxyl radicals occurs more readily to produce dealkylated products according to the reaction mechanism presented in Figure 8.2 than to produce hydrolysis products according to the reaction mechanism presented in Figure 8.3 (Adams et al., 1990).

8.1.2 Ozone

Atrazine chemistry was investigated during ozonation to elucidate potential degradation mechanisms. The effect of atrazine on the dissolved ozone concentration during ozonation was investigated by sparging the oxygen/ozone gas through a 5 mg L^{-1} atrazine solution in the ultrasonic cell and measuring the dissolved ozone concentration in solution. The ozone concentration in the 2,4 mL s^{-1} gas stream was 5,7 mg L^{-1} and the ozone production rate was 0,014 mg s^{-1} (Table 5.6 in Section 5.2). Dissolved ozone concentration was measured in a 5 mg L^{-1} atrazine solution during ozonation at time periods of 0; 1; 2,5; 5; 10; 20; 40 and

60 min. Experiments were performed in duplicate for each time period. Dissolved ozone concentration was also measured during ozonation when the atrazine solution was sonicated at an acoustic power of 57 W, when 40 mg L^{-1} hydrogen peroxide was added prior to ozonation and when ozonation was combined with both hydrogen peroxide and sonication. Dissolved ozone concentration measured during the ozonation of water (Figure 7.1) is compared in Figure 8.4 to that measured in a 5 mg L^{-1} atrazine solution.

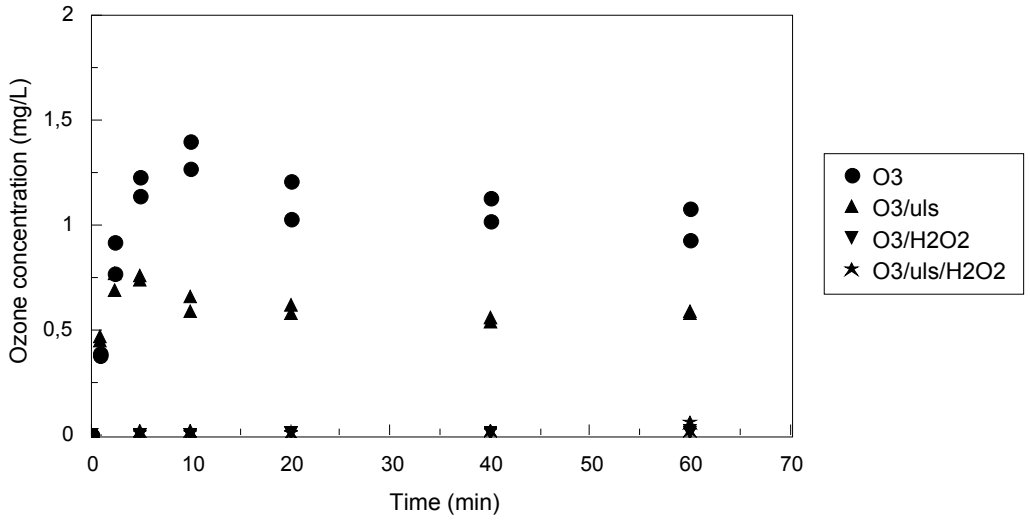

(a) water

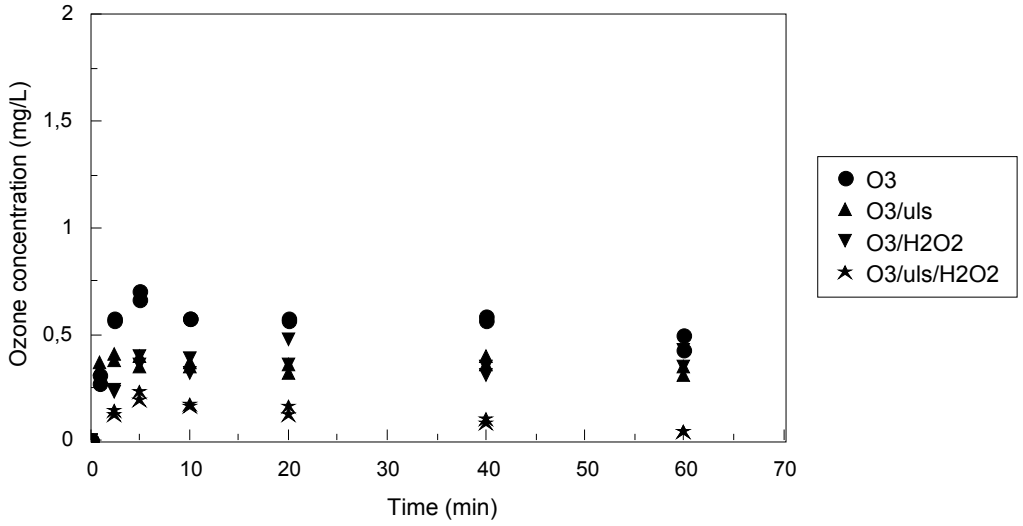

(b) 5 mg L^{-1} atrazine solution

Figure 8.4 : Dissolved ozone concentration in water and a 5 mg L^{-1} atrazine solution during ozonation (0,014 mg s^{-1}), ozonation combined with sonication (57 W), ozonation combined with hydrogen peroxide (40 mg L^{-1}) and ozonation combined with sonication and hydrogen peroxide (*n* = 2 per time period)

The maximum standard deviation in the dissolved ozone concentrations measured in a 5 mg L^{-1} atrazine solution during ozonation, ozonation combined with sonication, ozonation combined with hydrogen peroxide

and ozonation combined with both sonication and hydrogen peroxide are 0,047; 0,037; 0,084 and 0,030 mg L^{-1}, respectively.

The dissolved ozone concentration after 20 min during ozonation was reduced from approximately 1,1 mg L^{-1} in water, Figure 8.4(a), to 0,55 mg L^{-1} in the atrazine solution, Figure 8.4(b). The reduction in dissolved ozone concentration is due to the ozone consumed in the oxidation of atrazine (mass transfer limitation). Atrazine oxidation during ozonation, as discussed in Section 4.3.1, occurs via two mechanisms, the direct reaction with ozone and the reaction with free radicals formed during ozone decomposition. Both dealkylated and hydrolysed degradation products are formed from the reaction with free radicals whereas only dealkylated products are formed from the direct reaction with ozone (Adams et al., 1990; Adams and Randtke, 1992a). The formation of dealkylated degradation products from the direct reaction with ozone (summarised from Figure 4.13) is presented in Figure 8.5.

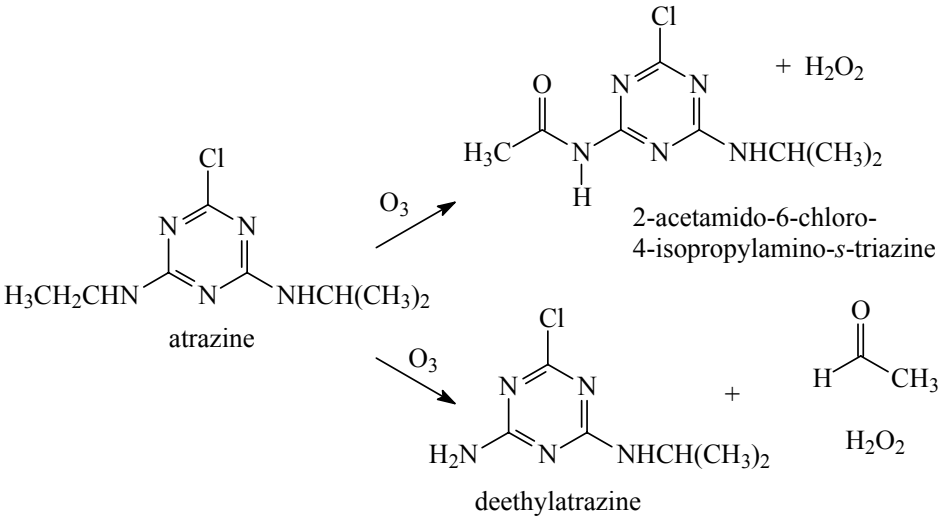

Figure 8.5 : Formation of dealkylated degradation products from the direct reaction of atrazine with ozone (Bolzacchini et al., 1994)

The direct reaction of ozone with atrazine, as shown in Figure 8.5, produces both the acetamide and deethyl degradation products. The mechanism is sterically controlled because of the crowded transition state during the coordination of the ozone to the side-chain nitrogen atom. Hence, the reaction occurs preferentially on the ethyl side-chain producing deethylatrazine than on the isopropyl side-chain. Hydrogen peroxide, as shown in Figure 8.5, is produced as a byproduct during the direct reaction of ozone with atrazine.

The reaction of atrazine with hydroxyl radicals generated from the decomposition of ozone produces dealkylated and hydrolysed degradation products according to the reaction mechanisms presented in Figure 8.2 and Figure 8.3. The radical reactions occurring in water during ozonation are listed in Scheme 3.3 (Appendix H) and presented graphically in Figure 3.3 in Section 3.1.3. Ozone decomposition is initiated by

reaction with HO^- ions, reaction [a] of Scheme 3.3, generated from the dissociation of water. Atrazine reacts with the hydroxyl radicals formed in reaction [e] of Scheme 3.3. The investigation by Beltrán and co-workers, described in Section 3.1.2, reported that atrazine oxidation during ozonation is pH dependent (Beltrán, 1995). Degradation at a pH less than 12 occurs due to both the direct reaction with ozone and the reaction with free radicals whereas oxidation at a pH greater than 12 is due only to reaction with free radicals. The pH of the atrazine solution during ozonation, Figure 8.4(b), was not measured, however, the initial neutral pH may have become slightly acidic due to carbon dioxide absorption from the atmosphere. The solution pH was below 12 and thus both atrazine degradation mechanisms could have occurred. Atrazine degradation increases with increasing pH due to the higher concentration of hydroxyl ions in solution. Hydroxyl ions enhance the decomposition of ozone (according to Scheme 3.3) and thus the generation of hydroxyl radicals.

Ozonation is a gas-liquid reaction, the degradation of organic compounds during ozonation is thus determined by both mass transfer and chemical reaction. The kinetic regime of the absorption of ozone in solution according to the dimensionless Hatta number (ratio of chemical reaction rate to physical absorption rate) is discussed in Section 3.1.2. The change in ozone concentration from within the gas bubbles, through the interfacial region to the bulk solution is presented in Figure 3.2 in Section 3.1.2.

Ozone diffuses from the gas bubbles through the interfacial region into the bulk solution. As discussed in Section 3.1.2 a fast reaction of a solute with ozone takes place in the proximity of the bubble interface resulting in a negligible amount, shown in Figure 3.2, of dissolved ozone in solution (Beltrán, 1995). Conversely, dissolved ozone in solution indicates that oxidation reactions are slow and take place in the bulk solution. The presence of dissolved ozone in solution during the ozonation of atrazine, shown in Figure 8.4(b), indicates that the degradation of atrazine is due to slow reactions taking place in the bulk solution despite the higher concentration of atrazine at the gas-liquid interface. Atrazine is a hydrophobic compound (discussed in Section 8.1.1) and thus gathers at the interface of the ozone bubbles. Beltrán and co-workers calculated the Hatta numbers to determine the kinetic regime of the direct reaction of atrazine with ozone and with free radicals, the Hatta numbers indicated that the reactions are very slow and take place in the bulk solution (Beltrán et al., 1993b).

The dissolved ozone concentration after 20 min in a 5 mg L^{-1} atrazine solution, as shown in Figure 8.4(b), was reduced from 0,55 mg L^{-1} during ozonation alone to 0,35 mg L^{-1} during ozonation combined with sonication. The reduction in dissolved ozone concentration caused by sonication is discussed in Section 7.1. The ozone-containing bubbles act as nucleation sites for cavitation. Ozone decomposition occurs because of the conditions within the collapsing cavitation bubbles as well as due to participation in the ultrasonic-initiated free radical reactions taking place within the bubbles and at the gas/liquid interface. The enhanced ozone decomposition in the gas-phase reduces the transfer of ozone into the bulk solution. Ozone

decomposition also takes place in the bulk solution because of the ultrasonic formation of hydrogen peroxide and the subsequent reaction of ozone with hydroxyl ions formed from the dissociation of hydrogen peroxide.

Dissolved ozone concentration in the atrazine solution during ozonation combined with sonication, Figure 8.4(b), is lower than that in water during ozonation combined with sonication, Figure 8.4(a). Ozone is thus consumed in the oxidation of atrazine either via the direct reaction between ozone and atrazine or due to the reaction of atrazine with hydroxyl radicals generated during ozone decomposition. The presence of dissolved ozone in solution indicates that atrazine oxidation takes place in the bulk solution. However, the reduced amount of ozone in the atrazine solution during ozonation combined with sonication compared to during ozonation alone indicates that either atrazine oxidation is increasingly occurring at the gas/liquid interface (a high ozone demand at the gas/liquid interface is shown in Figure 3.2 to reduce the dissolved ozone in solution, hence a change in kinetic regime from slow reactions in the bulk solution to moderately fast reactions at the interface) or that atrazine oxidation in the bulk solution is just significantly enhanced (a greater amount of ozone in solution is thus consumed and the dissolved ozone concentration decreases). Both changes in atrazine oxidation could possibly occur since ozone decomposition is enhanced both in the gas-phase and in the bulk solution as discussed in Section 7.1 when ozonation is combined with sonication.

Ozone decomposition, Figure 8.4(a) and Figure 8.4(b), is enhanced by the formation of hydrogen peroxide during sonication. A commercial source of hydrogen peroxide can be added during ozonation in place of that generated during sonication to obtain a more direct and controllable effect. The reactions initiated in water during ozonation with hydrogen peroxide are listed in Scheme 3.6 (Appendix H), the cycle of reaction species is presented graphically in Figure 3.5 in Section 3.1.3. An insignificant amount of dissolved ozone was measured in water during ozonation with 40 mg L^{-1} added hydrogen peroxide, Figure 8.4(a), whereas dissolved ozone was present in solution during the ozonation of a 5 mg L^{-1} atrazine solution in the presence of hydrogen peroxide, Figure 8.4(b). The concentration profile of dissolved ozone in the atrazine solution during ozonation in combination with hydrogen peroxide is similar to that measured during ozonation in combination with sonication. The lack of dissolved ozone in water during ozonation was due to the fast reaction of ozone with the perhydroxyl ions formed from the dissociation of hydrogen peroxide, as discussed in Section 7.1. The presence of dissolved ozone in the atrazine solution indicates that atrazine must have disrupted this mechanism by taking part in the free radical reactions occurring in solution creating a preferential reaction pathway involving the perhydroxyl ions, preventing the ions from reacting with all the ozone in solution. Similarly, dissolved ozone in solution during ozonation combined with both hydrogen peroxide and sonication was prevented from accumulating in water, Figure 8.4(a), but not in the atrazine solution, Figure 8.4(b). Dissolved ozone concentration in the atrazine solution increased to approximately 0,2 mg L^{-1} at 5 min and then decreased steadily to zero over the 60 min experiment.

8.1.3 Hydrogen peroxide

Hydrogen peroxide formation in a 5 mg L^{-1} atrazine solution was investigated during ozonation, sonication and when ozonation was combined with sonication. Ozonation was performed at an ozone production rate of 0,014 mg s^{-1} and sonication at an acoustic power of 57 W. Hydrogen peroxide concentration was measured at time periods of 0; 5; 10; 20; 40 and 60 min. Duplicate experiments were performed for each time period. Hydrogen peroxide concentration measured during the ozonation of water (Figure 7.4) is compared in Figure 8.6 to the hydrogen peroxide concentration measured in a 5 mg L^{-1} atrazine solution.

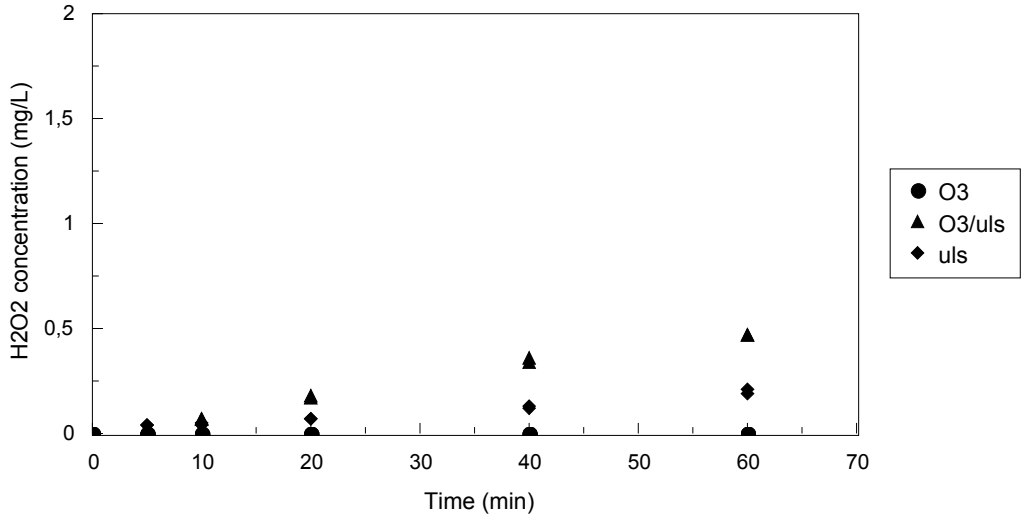

(a) water

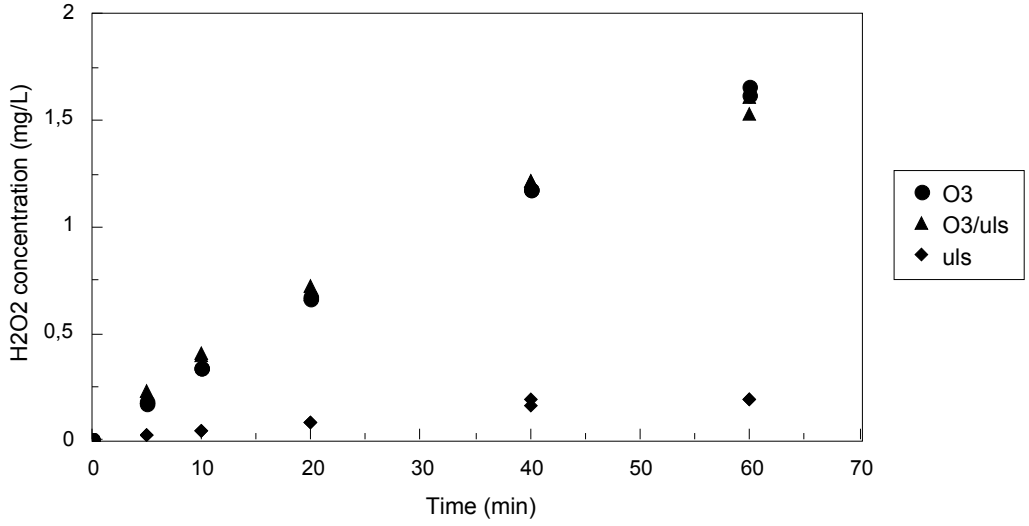

(b) 5 mg L^{-1} atrazine solution

Figure 8.6 : Hydrogen peroxide concentration in water and a 5 mg L^{-1} atrazine solution in the ultrasonic cell during ozonation (0,014 mg s^{-1}), sonication (57 W) and ozonation combined with sonication (n = 2 per time period)

The maximum standard deviation in the hydrogen peroxide concentrations measured in an atrazine solution during ozonation, sonication and ozonation combined with sonication are 0,029; 0,023; and 0,054 mg L^{-1}, respectively. The rates of hydrogen peroxide formation in a 5 mg L^{-1} atrazine solution during ozonation, sonication and ozonation combined with sonication were calculated from the regression of the data presented in Figure 8.6 using the linear regression model

$$y = bx \qquad [8.2]$$

where the coefficient *b*, the gradient of the regression line, represents the rate of hydrogen peroxide formation. The calculated rates of hydrogen peroxide formation in a 5 mg L^{-1} atrazine solution during ozonation, sonication and ozonation combined with sonication (and the standard error of the calculated values) are recorded in Table 8.3. The rates of hydrogen peroxide formation in water (Table 7.2) are also included in Table 8.3.

Table 8.3 : Rate of hydrogen peroxide formation in water and a 5 mg L^{-1} atrazine solution during ozonation (0,014 mg s^{-1}), sonication (57 W) and ozonation combined with sonication

	water		atrazine solution	
	Rate of H_2O_2 formation (mg L^{-1} min^{-1})	R^2	Rate of H_2O_2 formation (mg L^{-1} min^{-1})	R^2
ozone	0,0000 ± 0,0000	0.000	0,0285 ± 0,0006	0.989
ultrasound	0,0034 ± 0,0001	0.955	0,0036 ± 0,0002	0.934
ozone/ultrasound	0,0082 ± 0,0001	0.992	0,0283 ± 0,0010	0.965

The rate of hydrogen peroxide formation in water during sonication, shown in Table 8.3, was the same, within standard deviation, as that measured in a 5 mg L^{-1} atrazine solution. Atrazine is not present inside the cavitation bubbles due to its low volatility and hence does not affect the mechanism by which hydroxyl radicals are formed. Hydrogen peroxide is produced from the reaction of two hydroxyl radicals (reaction [b] of Scheme 2.2) that occurs within the cavitation bubbles as well as at the gas/liquid interface (discussed in Section 2.3.1.1) where atrazine collects due to its hydrophobicity (discussed in Section 8.1.1). Atrazine oxidation during sonication occurs by reaction with hydroxyl radicals which reduces the quantity of radicals recombining to form hydrogen peroxide. The oxidation of atrazine should thus result in a decreased rate of hydrogen peroxide formation in an atrazine solution in comparison with that in water. The similar rates of hydrogen peroxide formation in water and the atrazine solution as shown in Table 8.3 indicates that very few hydroxyl radicals are consumed in the oxidation of atrazine. The rate of atrazine oxidation during sonication in the ultrasonic cell is thus expected to be low. The similar rates of hydrogen peroxide formation in water and in the atrazine solution during sonication may also be a result of the hydrogen peroxide that is formed as

a byproduct during atrazine oxidation. Hydrogen peroxide, as shown in Figure 8.2, is formed as a byproduct when dealkylated degradation products are produced from the reaction of atrazine with hydroxyl radicals.

The formation of hydrogen peroxide during ozonation was significantly affected by the presence of atrazine. Hydrogen peroxide was not formed during ozonation in water (shown in Table 8.3) whereas the rate of formation in the atrazine solution was 0,0285 mg L^{-1} min^{-1}. The lack of hydrogen peroxide formation in water during ozonation is due to the fast reaction of ozone with perhydroxyl ions formed from the dissociation of hydrogen peroxide. The significantly greater rate of hydrogen peroxide formation in the atrazine solution is due to the oxidation of atrazine since hydrogen peroxide is formed as a byproduct in the reaction mechanisms producing the dealkylated degradation products. Hydrogen peroxide is generated when dealkylated atrazine products are formed from both the direct reaction with ozone (Figure 8.5) and the reaction with hydroxyl radicals (Figure 8.2). Thus more hydrogen peroxide is generated from the oxidation of atrazine than what is depleted through the reaction of ozone with perhydroxyl ions, the dissociated form of hydrogen peroxide.

The rate of hydrogen peroxide formation in an atrazine solution when ozonation was combined with sonication is also shown in Figure 8.6(b) to be significantly greater than that in water, Figure 8.6(a). Hydrogen peroxide, as described earlier, is produced as a byproduct during the oxidation of atrazine by the direct reaction with ozone and the reaction with hydroxyl radicals to produce dealkylated degradation products. Hence the greater rate of hydrogen peroxide formation in the atrazine solution. Hydrogen peroxide formation in water when ozonation was combined with sonication in comparison with ozonation alone, as shown in Figure 8.6(a), was enhanced due to the ultrasonic-initiated decomposition of ozone generating more radical reactions and an increased rate of hydrogen peroxide formation. Similarly, the hydrogen peroxide formation in the atrazine solution is expected to be greater during ozonation combined with sonication in comparison with ozonation alone because of the ultrasonic-initiated decomposition of ozone as well as the greater atrazine oxidation producing more hydrogen peroxide as a byproduct. The rates of hydrogen peroxide formation during ozonation alone and during ozonation combined with sonication, however, are shown in Table 8.3 to be the same within standard deviation. Hydrogen peroxide formation is greater during ozonation combined with sonication, however as described in Section 6.5, hydrogen peroxide decomposition via radical reactions increases with increasing peroxide concentration in solution resulting in similar overall rates of hydrogen peroxide formation during ozonation combined with sonication and during ozonation alone.

8.1.4 Mass balances

Atrazine chemistry during sonication, ozonation and hydrogen peroxide has been investigated through the measurement of dissolved ozone and hydrogen peroxide concentrations in a 5 mg L^{-1} atrazine solution, as reported in Section 8.1.2 and Section 8.1.3. Atrazine oxidation during ozonation, sonication and hydrogen peroxide addition was investigated by performing mass balances over 45 min to relate atrazine degradation to ozone decomposition. The amount of ozone decomposed or consumed in the oxidation of atrazine is

calculated from the difference between the amount of ozone generated in 45 min and the unreacted ozone in the system at the termination of the experiment. The total amount of unreacted ozone consists of the dissolved ozone in solution in the ultrasonic cell, the ozone in the gas spaces of the system and the ozone that passed through the system and reacted with the potassium iodide in the gas traps.

Mass balances in a 5 mg L^{-1} atrazine solution were performed over a 45 min period of ozonation, ozonation combined with sonication, ozonation combined with hydrogen peroxide and ozonation combined with sonication and hydrogen peroxide. Ozonation was performed at an ozone production rate of 0,014 mg s^{-1}, sonication at an acoustic power of 57 W and hydrogen peroxide was added so as to prepare a 40 mg L^{-1} solution. The experimental details of the mass balance experiments are reported in Section E.1.3. Ozone and hydrogen peroxide concentrations were measured after the 45 min ozonation period except in solutions with added hydrogen peroxide (40 mg L^{-1}) where only ozone concentration was measured (detailed in Section 7.4). The average amounts of ozone generated in 45 min (Table D.4) and the amounts of unreacted ozone at the end of the 45 min mass balance experiments in an atrazine solution (Table E.4) are summarised in Table 8.4. The mass balances in water are presented in Table 7.3 in Section 7.4.

Table 8.4 : Ozone decomposition and atrazine oxidation in a 5 mg L^{-1} atrazine solution over 45 min during ozonation, ozonation combined with sonication, ozonation combined with hydrogen peroxide and ozonation combined with sonication and hydrogen peroxide

	Average generated ozone (mg)	Unreacted ozone (mg)				% (unreacted)/ (generated)	% atrazine degraded
		dissolved ozone	gas-phase ozone	ozone in KI traps	total		
ozone	54.6	0.16	3.82	43.42	47.40	86.8	26.0
		0.23	3.82	45.56	49.61	90.9	25.4
average		**0.20**	**3.82**	**44.48**	**48.50**	**88.9**	**25.7**
ozone/uls	49.2	0.12	2.89	30.65	33.66	68.4	36.3
		0.11	2.89	30.34	33.34	67.8	30.2
average		**0.11**	**2.89**	**30.50**	**33.50**	**68.1**	**33.3**
ozone/H_2O_2	49.0	0.14	3.18	33.61	36.93	75.4	41.9
		0.22	3.18	34.39	37.79	77.1	46.9
		0.20	3.18	33.68	37.06	75.6	37.6
average		**0.19**	**3.18**	**33.89**	**37.26**	**76.0**	**42.1**
ozone/uls/H_2O_2	50.8	0.02	2.67	29.42	32.11	63.2	34.5
		0.01	2.67	29.64	32.32	63.6	35.3
average		**0.02**	**2.67**	**29.53**	**32.22**	**63.4**	**34.9**

The amounts of unreacted ozone presented in Table 8.4 are converted to fractions of the ozone generated because of the different rates of ozone generation in the mass balance experiments. The unreacted ozone

measured in the solution, gas-phase and KI traps are reported in Table 8.5 as fractions of the ozone generated during the different atrazine mass balance experiments.

Table 8.5 : Unreacted ozone in solution, gas-phase and KI traps at the termination of the 45 min experiments as a fraction (%) of the generated ozone during the atrazine mass balance experiments

	Unreacted ozone (%)				decomposed or reacted ozone (%)
	dissolved ozone	gas-phase ozone	ozone in KI traps	total	
ozone	0.4	7.0	81.5	**88.9**	11.1
ozone/uls	0.2	5.9	62.0	**68.1**	31.9
ozone/H_2O_2	0.4	6.5	69.2	**76.1**	23.9
ozone/uls/H_2O_2	0.0	5.3	58.1	**63.4**	36.6

The total unreacted amount of ozone in all experiments in an atrazine solution (Table 8.5) decreased in comparison with that measured in water (Table 7.4) due to the ozone consumed in the oxidation of atrazine. Atrazine oxidation during the ozonation experiment reduced the final mass of ozone from 95 % to 89 %. Dissolved ozone concentration in solution, Figure 8.4(a), and total unreacted ozone, Table 8.4, was the highest (89 %) during the ozonation experiment yet the lowest atrazine degradation (26 %) was measured. The direct reaction of atrazine with ozone (mechanism presented in Figure 8.5) is thus less important in the oxidation of atrazine than the reaction with hydroxyl radicals (mechanism presented in Figure 8.2 and Figure 8.3). Atrazine degradation was greater in the ozone combination technologies (with ultrasound or hydrogen peroxide) that promoted free radical reactions. The implications for an ozone process system in water treatment is that ozone should be used in combination with technologies that promote free radical reactions for enhanced oxidation of organic pollutants.

Atrazine degradation over 45 min was the greatest during ozonation combined with hydrogen peroxide (approximately 42 %) although the amount of unreacted ozone only decreased from approximately 79 % in water to approximately 76 % in the atrazine solution (Table 8.4). Enhanced ozone decomposition in the presence of hydrogen peroxide has been described in Section 7.1 to be due to the reaction of ozone with perhydroxyl radicals formed from the dissociation of hydrogen peroxide. However, the small decrease in ozone decomposition (3 %) indicates that the bulk of the hydroxyl radicals produced that reacted with the atrazine originated from the hydrogen peroxide molecules (reaction [b] of Scheme 3.9).

The oxidation of atrazine due to the direct reaction between ozone and atrazine is not influenced by ultrasound. A similar degree of oxidation according to this reaction occurs during ozonation alone and during ozonation combined with sonication. Thus the enhanced oxidation of atrazine during ozonation combined with sonication (33 % versus 26 %) is due to the alternate mechanism of atrazine oxidation, the reaction of atrazine with hydroxyl radicals. Hydroxyl radical formation during ozonation alone is enhanced

during ozonation combined with sonication, as described in Section 7.1, due to the greater ozone decomposition and the radicals formed during sonication.

The dissolved ozone concentration in an atrazine solution during ozonation combined with sonication was the same as that during ozonation combined with hydrogen peroxide, Figure 8.4(b), however, atrazine degradation was lower (33 % versus 42 %) since less hydrogen peroxide is formed in solution during ozonation combined with sonication, Figure 8.7(b), than what was added (40 mg L^{-1}) during ozonation combined with hydrogen peroxide. The mechanism of atrazine oxidation when ozonation is combined with sonication or hydrogen peroxide is the same, in that it is due to the reaction with hydroxyl radicals. However, less atrazine degradation is observed during sonication since a lower amount of hydrogen peroxide is generated in solution.

The total amount of ozone remaining in the system after the 45 min experiment was lower (shown in Table 8.4) during ozonation combined with sonication (72 %) than with added hydrogen peroxide (79 %). Ozone is degraded during sonication, described in Section 8.1.2, since the ozone bubbles act as nucleation sites and the ozone molecules are subjected to the high temperatures and pressures inside the collapsing cavities. Ozone is destroyed in the collapsing cavities, however, additional oxygen radicals, shown in Scheme 8.1, are formed.

The highest decomposition of ozone (approximately 37 %) occurred when ozonation was combined with both sonication and hydrogen peroxide although atrazine degradation was not the greatest, atrazine degradation was similar to that achieved when ozonation was combined with only sonication. Thus more ozone is completely decomposed to oxygen (reaction [a] of Scheme 7.1) and does not contribute to the degradation of atrazine. The investigation by Beltrán and co-workers found that atrazine oxidation during ozonation was dependant upon hydrogen peroxide concentration (Beltrán et al., 1998). Atrazine oxidation increased with increasing hydrogen peroxide concentration up until between 3,4 and 34 mg L^{-1}, after which, atrazine degradation decreased with increasing hydrogen peroxide concentration. Atrazine oxidation in the presence of a peroxide concentration greater than 3 400 mg L^{-1} is less than in the absence of hydrogen peroxide. The negative relationship between atrazine degradation and peroxide concentration is related to the kinetic regime of ozone absorption which at high peroxide concentrations is mass transfer limited, the rate of oxidation of solutes in solution becomes inversely proportional to the hydrogen peroxide concentration (Beltrán et al., 1998). Atrazine degradation at high hydrogen peroxide concentrations occurs only due to reaction with hydroxyl radicals, the concentration of hydroxyl radicals is a function of the maximum physical rate of ozone absorption (Beltrán et al., 1998). Similarly, the lower atrazine oxidation in the ultrasonic cell during ozonation combined with both sonication and hydrogen peroxide can be due to the peroxide in solution because of the interaction of the ultrasound and the added hydrogen peroxide being greater than the optimal peroxide concentration for atrazine degradation.

8.2 ATRAZINE DEGRADATION

Atrazine chemistry in solution during ozonation, sonication and with hydrogen peroxide is discussed in Section 8.1 as a foundation for the investigation of the degradation of atrazine. Atrazine degradation during sonication is reported in Section 8.2.1, during ozonation in Section 8.2.2 and with hydrogen peroxide in Section 8.2.3.

8.2.1 Ultrasound

The ultrasonic degradation of atrazine was investigated by sonicating 5, 10 and 20 mg L^{-1} atrazine solutions in the ultrasonic cell for 3 h at an acoustic power of 57 W. Atrazine concentration was measured at time periods of 0; 45; 90; 135 and 180 min. Experiments were performed in triplicate. The ultrasonic degradation of atrazine is presented in Figure 8.7.

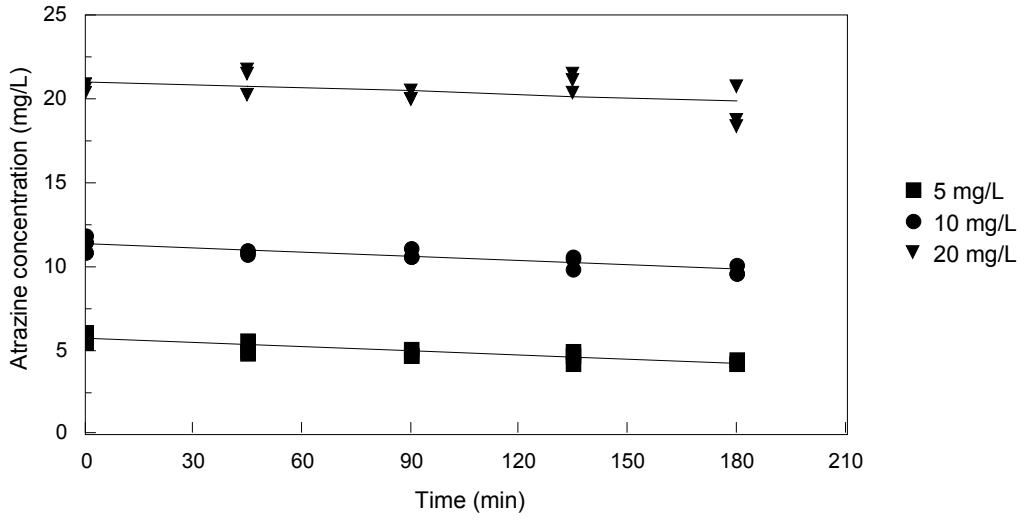

Figure 8.7 : Atrazine concentration in a nominal 5, 10 and 20 mg L^{-1} atrazine solution during sonication in the ultrasonic cell at an acoustic power of 57 W for 3 h (n = 3 per time period)

Atrazine is degraded (as shown in Figure 8.7) during sonication in the ultrasonic cell. The maximum standard deviation in the measured atrazine concentrations during the sonication of nominal 5, 10 and 20 mg L^{-1} atrazine solutions are 0,44; 0,48 and 1,27 mg L^{-1}, respectively. The rates of atrazine degradation in the different solutions were calculated from the regression of the data presented in Figure 8.7 using the linear regression model

$$y = a + bx \qquad [8.3]$$

where the coefficient *b*, the gradient of the regression line, represents the rate of atrazine degradation. The calculated rates of atrazine degradation in different atrazine solutions during sonication (and the standard errors of the calculated values) are recorded in Table 8.6.

Table 8.6 : Rate of atrazine degradation in a nominal 5, 10 and 20 mg L^{-1} atrazine solution during sonication in the ultrasonic cell at an acoustic power of 57 W over 3 h

Atrazine concentration ($mg\ L^{-1}$)	Rate of atrazine degradation ($mg\ L^{-1}\ min^{-1}$)	R^2
5	0,0082 ± 0,0013	0.759
10	0,0085 ± 0,0014	0.750
20	0,0061 ± 0,0036	0.185

The rate of atrazine degradation in solutions of initial concentration between 5 and 20 mg L^{-1} was not significantly affected by concentration. The absolute reduction in atrazine concentration in the solutions varied between 1,3 and 1,7 mg L^{-1}. The slow degradation of atrazine during sonication, reported in Table 8.6, is as discussed in Section 8.1.3, in which, similar rates of hydrogen peroxide formation in water, Figure 8.6(a), and an atrazine solution, Figure 8.6(b), indicated that low quantities of hydroxyl radicals were consumed during atrazine oxidation. A concentration of 5 mg L^{-1} was used as the initial concentration for all further atrazine experiments. The mean of the initial atrazine solutions reported in the atrazine investigation of Chapter 8 is 5,2 mg L^{-1}, the standard deviation is 0,43 mg L^{-1} (Table F.33 in Appendix F).

The effect of acoustic power on atrazine degradation was not measured since the degradation rates listed in Table 8.6 were achieved during sonication at the maximum operating acoustic power of the ultrasonic horn (57 W). The rate of atrazine degradation is expected to decrease during sonication at a lower acoustic power since the formation of free radicals is dependent upon the intensity of cavitation.

The effect of a gas sparging through the solution during sonication was investigated as a means to enhance atrazine degradation. Atrazine is degraded by reaction with hydroxyl radicals and the presence of oxygen during sonication, as discussed in Section 6.1 and Section 6.2, enhances hydrogen peroxide formation and free radical reactions. Conversely, the presence of nitrogen during sonication decreases hydrogen peroxide formation. Oxygen, as demonstrated in Figure 8.2, is required in the oxidation of atrazine to yield dealkylated degradation products. Experiments were undertaken in which oxygen and nitrogen were sparged at a flow rate of 6 mL s^{-1} through a 5 mg L^{-1} atrazine solution during sonication for 3 h in the ultrasonic cell at an acoustic power of 57 W. Atrazine concentration was measured at time periods of 0; 45; 90; 135 and 180 min. Experiments were performed in triplicate. The effect of oxygen and nitrogen sparging on atrazine degradation in the ultrasonic cell is shown in Figure 8.8.

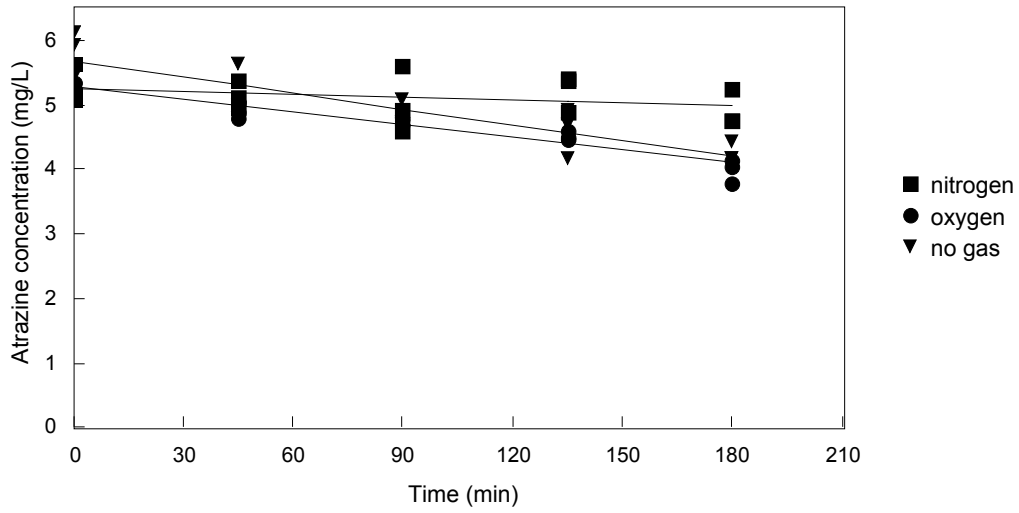

Figure 8.8 : Effect of oxygen and nitrogen sparging on the degradation of atrazine in a 5 mg L^{-1} atrazine solution during sonication in the ultrasonic cell at an acoustic power of 57 W over 3 h (*n* = 3 per time period)

The maximum standard deviation in the atrazine concentrations measured during sonication with nitrogen and oxygen sparging are 0,51 and 0,20 mg L^{-1}, respectively. The rates of atrazine degradation during sonication with nitrogen and oxygen sparging were calculated from the regression of the data presented in Figure 8.8 using the linear regression model

$$y = a + bx \qquad [8.4]$$

where the coefficient *b*, the gradient of the regression line, represents the rate of atrazine degradation. The calculated rates of atrazine degradation during sonication with nitrogen and oxygen sparging (and the standard errors of the calculated values) are recorded in Table 8.7.

Table 8.7 : Rate of atrazine degradation in a 5 mg L^{-1} atrazine solution during sonication with nitrogen and oxygen sparging in the ultrasonic cell for 3 h at an acoustic power of 57 W

Gas	Rate of atrazine degradation (mg L^{-1} min^{-1})	R^2
no gas	0,0082 ± 0,0013	0.759
nitrogen	0,0014 ± 0,0013	0.091
oxygen	0,0065 ± 0,0006	0.913

The atrazine degradation rates reported in Table 8.7 indicate that oxygen is required for the degradation of atrazine. The mechanism for the formation of dealkylated degradation products from the reaction of atrazine with hydroxyl radicals, shown in Figure 8.2, indicates the required presence of oxygen during atrazine oxidation. Atrazine degradation, shown in Figure 8.8, was significantly retarded in the absence of oxygen

(during nitrogen sparging) in contrast to that in a sample saturated with air (no gas sparging) and with oxygen sparging. Atrazine degradation in the presence of oxygen, however, was not enhanced with increasing dissolved oxygen concentration from 10,7 mg L^{-1} (no gas sparging) to 39,6 mg L^{-1} (oxygen sparging). The reaction mechanism of atrazine degradation thus requires the presence of oxygen whereas an increase in oxygen concentration is less significant. Enhanced degradation in the presence of oxygen confirms that atrazine degradation during sonication is due to the chemical effects of ultrasound (free radical reactions) and not due to the physical effects (shockwave formation) that would also be evident during nitrogen sparging.

8.2.2 Ozone

Ozone is used in water treatment for disinfection, however, other benefits include the oxidation of organic pollutants such as atrazine. Ozone is reported in literature to significantly reduce the concentration of atrazine during water treatment (Adams and Randtke, 1992b; Beltrán et al., 1994a). Atrazine is degraded as discussed in Section 8.1 by direct reaction with ozone and by reaction with hydroxyl radicals formed during ozone decomposition. The relative amount of degradation due to either mechanism is determined by pH and reaction conditions. Atrazine degradation during ozonation in the ultrasonic cell was investigated by measuring atrazine concentration over 3 h during ozonation at ozone production rates of 0,003; 0,014; 0,030 and 0,047 mg s^{-1}. Atrazine concentration was measured at time periods of 0; 15; 30; 45; 90; 135 and 180 min. Experiments were performed in duplicate. The degradation of atrazine during ozonation is presented in Figure 8.9.

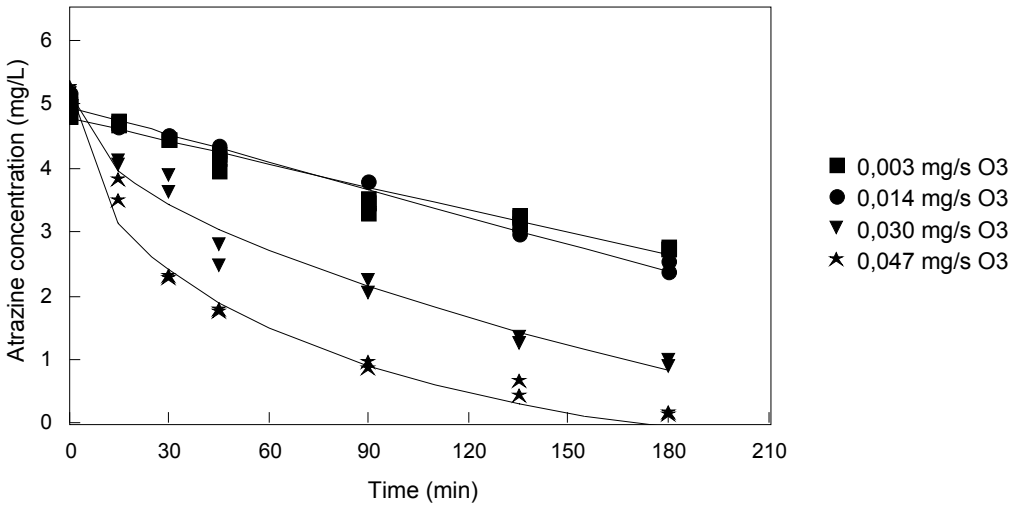

Figure 8.9 : Atrazine concentration in a 5 mg L^{-1} atrazine solution during ozonation over 3 h at ozone production rates of 0,003; 0,014; 0,030 and 0,047 mg s^{-1} (n = 2 per time period)

The maximum standard deviation in the atrazine concentrations measured during ozonation at ozone production rates of 0,003; 0,014; 0,030 and 0,047 mg s^{-1} are 0,18; 0,30; 0,22 and 0,25 mg L^{-1}, respectively.

The rates of atrazine degradation during the initial period of ozonation were calculated from the regression of the data presented in Figure 8.9 using the linear regression model

$$y = a + bx \qquad [8.5]$$

where the coefficient *b*, the gradient of the regression line, represents the rate of atrazine degradation. The calculated rates of atrazine degradation during the initial period of ozonation (and the standard errors of the calculated values) are recorded in Table 8.8.

Table 8.8 : Initial rate of atrazine degradation in a 5 mg L^{-1} atrazine solution during ozonation at ozone production rates of 0,003; 0,014; 0,030 and 0,047 mg s^{-1}

Ozone production rate (mg s^{-1})	Regression time period	Rate of atrazine degradation (mg L^{-1} min^{-1})	R^2
0.003	0 to 180 min	0,0120 ± 0,0006	0.957
0.014	0 to 180 min	0,0143 ± 0,0006	0.979
0.030	0 to 45 min	0,0506 ± 0,0048	0.949
0.047	0 to 30 min	0,0937 ± 0,0058	0.985

The rate of atrazine degradation is shown in Figure 8.9 and Table 8.8 to increase with increasing ozone production rate. Atrazine degradation was linear over the 3 h experiment (indicating a zero order process) during ozonation at ozone production rates of 0,003 and 0,014 mg s^{-1}. The rates of atrazine degradation during ozonation at ozone production rates of 0,030 and 0,047 mg s^{-1} were initially linear but decreased with decreasing atrazine concentration (shown in Figure 8.9). The linear regression lines of the 0,030 and 0,047 mg s^{-1} data in the plot of $-\ln(C/C_0)$ versus time presented in Figure 8.10 indicates that atrazine degradation during ozonation at ozone production rates of 0,030 and 0,047 mg s^{-1} is a first order process. Atrazine degradation during ozonation thus changed from a zero order process independent of atrazine concentration at ozone production rates of 0,003 and 0,014 mg s^{-1} to a first order process dependant on atrazine concentration at ozone production rates of 0,030 and 0,047 mg s^{-1}. An ozone production rate of 0,014 mg s^{-1}, as reported in Section 5.2, was used as the standard ozone production rate throughout the investigation.

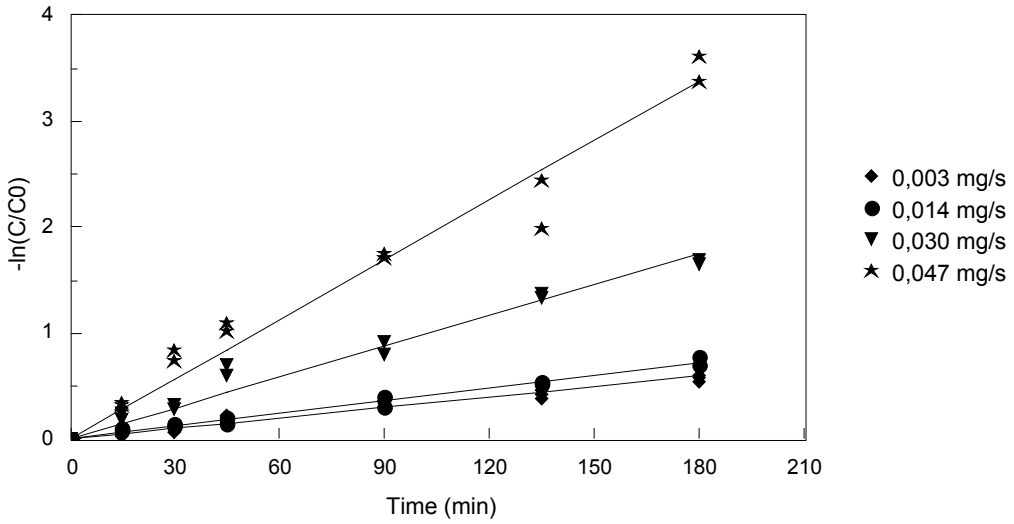

Figure 8.10 : First order atrazine degradation in a 5 mg L^{-1} atrazine solution during ozonation over 3 h at ozone production rates of 0,003; 0,014; 0,030 and 0,047 mg s^{-1}

Atrazine degradation during ozonation combined with sonication was investigated by measuring atrazine concentration in a 5 mg L^{-1} atrazine solution over 3 h during ozonation at ozone production rates of 0,003; 0,014; 0,030 and 0,047 mg s^{-1} combined with sonication at an acoustic power of 57 W. Atrazine concentration was measured at time periods of 0; 15; 30; 45; 90; 135 and 180 min. Experiments were performed in triplicate. Atrazine degradation during ozonation combined with sonication is presented in Figure 8.11.

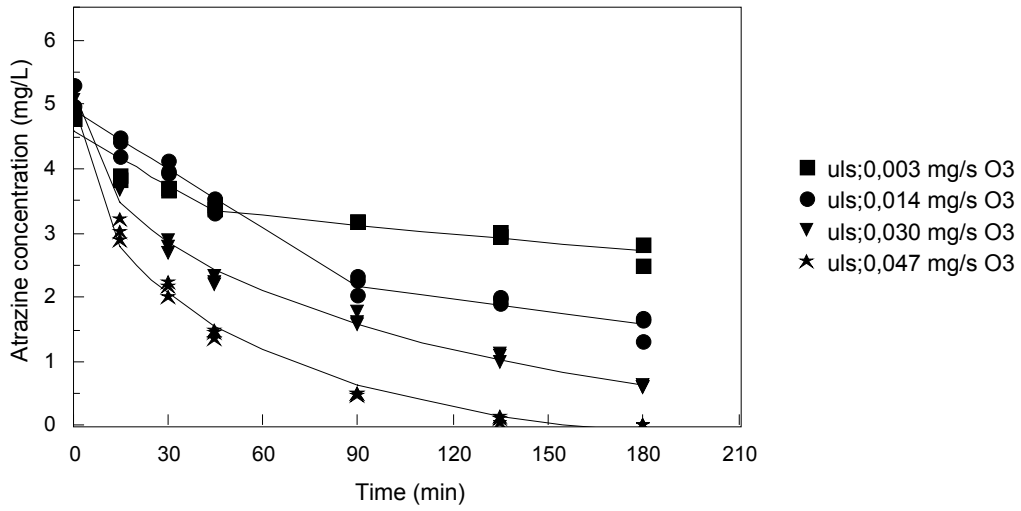

Figure 8.11 : Atrazine concentration in a 5 mg L^{-1} atrazine solution during ozonation over 3 h at ozone production rates of 0,003; 0,014; 0,030 and 0,047 mg s^{-1} combined with sonication at an acoustic power of 57 W (*n* = 3 per time period)

The maximum standard deviation in the atrazine concentrations measured during sonication combined with ozonation at ozone production rates of 0,003; 0,014; 0,030 and 0,047 mg s^{-1} are 0,25; 0,21; 0,11 and 0,06 mg L^{-1}, respectively. The rates of atrazine degradation during the initial period of ozonation were calculated from the regression of the data presented in Figure 8.11 using the linear regression model

$$y = a + bx \qquad [8.6]$$

where the coefficient *b*, the gradient of the regression line, represents the rate of atrazine degradation. The calculated rates of atrazine degradation during the initial period of ozonation combined with sonication (and the standard errors of the calculated values) are recorded in Table 8.9.

Table 8.9 : Initial rate of atrazine degradation in a 5 mg L^{-1} atrazine solution during ozonation over 3 h at ozone production rates of 0,003; 0,014; 0,030 and 0,047 mg s^{-1} combined with sonication at an acoustic power of 57 W

Ozone production rate (mg s^{-1})	Regression time period	Rate of atrazine degradation (mg L^{-1} min^{-1})	R^2
0.003	0 to 45 min	0,0287 ± 0,0045	0.871
0.014	0 to 45 min	0,0351 ± 0,0027	0.946
0.030	0 to 45 min	0,0644 ± 0,0045	0.953
0.047	0 to 30 min	0,0918 ± 0,0075	0.955

The rate of atrazine degradation during ozonation combined with sonication is shown in Figure 8.11 and Table 8.9 to increase with increasing ozone production rate. Atrazine degradation is only linear over the initial period and decreases, as shown in Figure 8.11, with decreasing atrazine concentration. The linear regression lines presented in Figure 8.12, a plot of $-\ln(C/C_0)$ versus time, indicates that atrazine degradation during ozonation combined with sonication is a first order process for any ozone production rate.

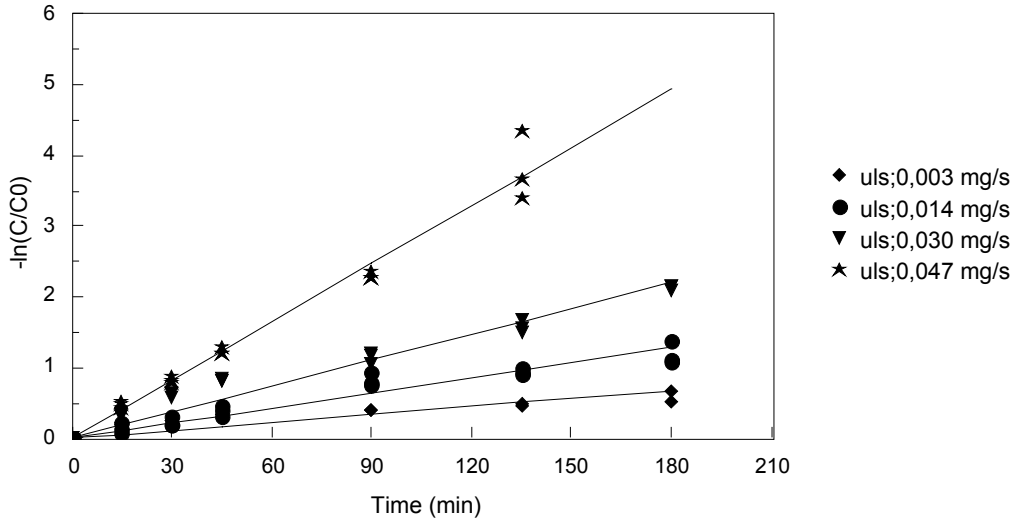

Figure 8.12 : First order atrazine degradation in a 5 mg L^{-1} atrazine solution during ozonation over 3 h at ozone production rates of 0,003; 0,014; 0,030 and 0,047 mg s^{-1} combined with sonication at an acoustic power of 57 W

The initial rate of atrazine degradation, as shown in Table 8.8 and Table 8.9, is enhanced when ozonation (at ozone production rates of 0,003; 0,014 and 0,030 mg s^{-1}) was combined with sonication. The atrazine degradation rates during ozonation (listed in Table 8.8) and during ozonation combined with sonication (listed in Table 8.9) are compared in Figure 8.13.

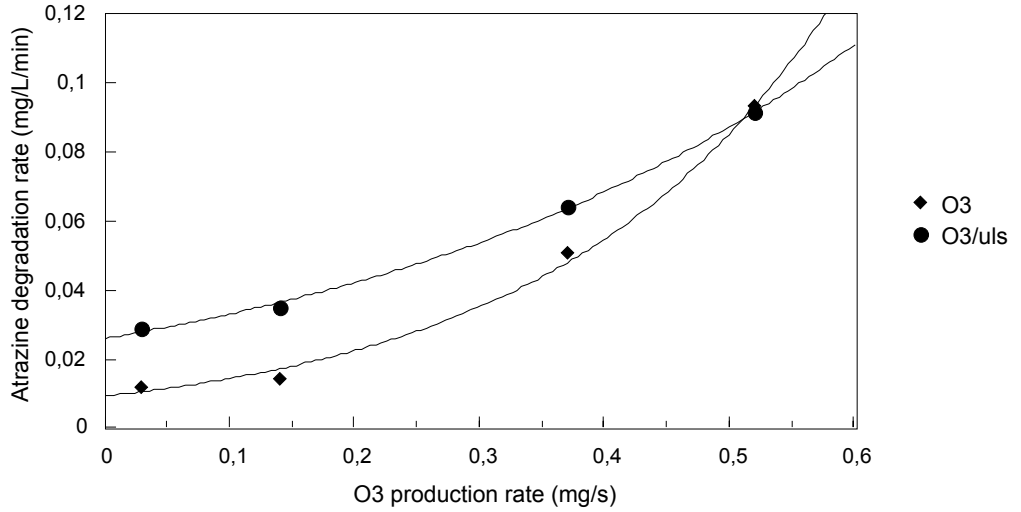

Figure 8.13 : Comparison of atrazine degradation rates in a 5 mg L^{-1} atrazine solution during ozonation and ozonation combined with sonication

The atrazine degradation rates presented in Figure 8.13 indicate the enhanced effect on atrazine degradation by combining ozone with ultrasound. The effect, however, decreases with increasing rate of ozone production. The effect of ultrasound during ozonation at the different ozone production rates is presented in

Figure E.1 to Figure E.4 in Appendix E. The enhanced initial degradation of atrazine due to ultrasound decreases with increasing rate of ozone production until no significant enhancement takes place during ozonation at an ozone production rate of 0,047 mg s^{-1} (Figure E.4). Ultrasound enhances the degradation of atrazine because of the increased decomposition of ozone and, hence, the increased formation of hydroxyl radicals (discussed in Section 8.1.2). Hydroxyl radicals are also formed during ozonation (in the absence of ultrasound). Thus the formation of hydroxyl radicals initiated by the ultrasound becomes insignificant in comparison with that generated during ozone decomposition (in the absence of ultrasound) at high ozone production rates. The production rates of ozone applied during ozonation in water treatment are low were the impact of ultrasound is highest, thus, a significant improvement in the degradation of organic compounds can be obtained by combining ozonation with sonication.

8.2.3 Hydrogen peroxide

The combination of hydrogen peroxide with advanced oxidation processes such as ultrasound or ozone enhances the oxidation of organic pollutants due to the generation of free radicals. Hydrogen peroxide, as shown in Scheme 3.9 in Section 3.3.1, is decomposed by ultrasound or ozone into perhydroxyl and hydroxyl radicals. The effect of hydrogen peroxide on atrazine degradation in the ultrasonic cell was investigated over 3 h with the addition of 40 mg L^{-1} hydrogen peroxide to a 5 mg L^{-1} atrazine solution during sonication at an acoustic power of 57 W and ozonation at an ozone production rate of 0,014 mg s^{-1}. The selection of the hydrogen peroxide concentration is detailed in Section E.2.3 in Appendix E. Atrazine concentration was measured at time periods of 0; 15; 30; 45; 90; 135 and 180 min. Experiments were performed in triplicate. The effect of hydrogen peroxide on atrazine degradation is shown in Figure 8.14.

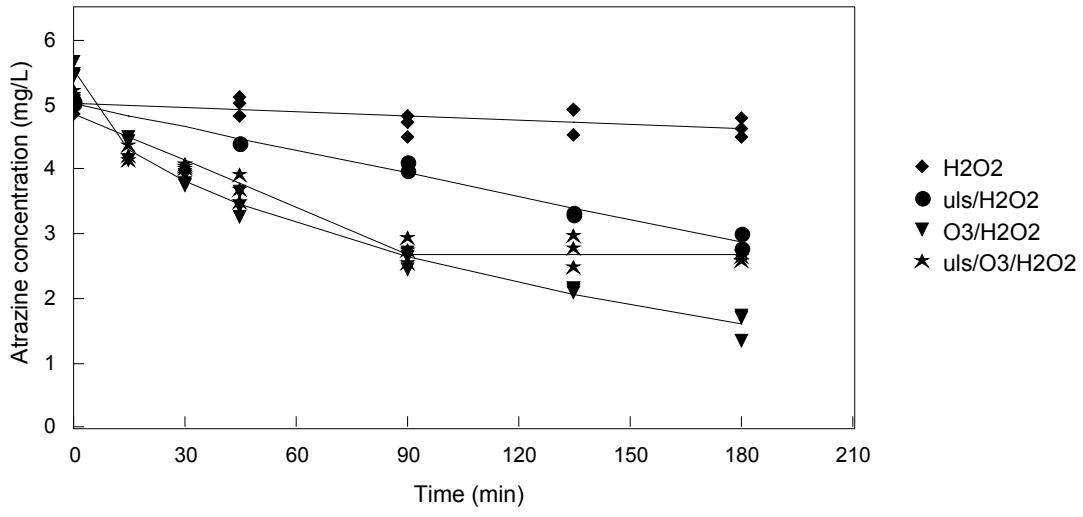

Figure 8.14 : Atrazine concentration in a 5 mg L^{-1} atrazine solution with 40 mg L^{-1} hydrogen peroxide, hydrogen peroxide combined with sonication (57 W), hydrogen peroxide combined with ozonation (0,014 mg s^{-1}) and hydrogen peroxide combined with sonication and ozonation

The maximum standard deviation in atrazine concentrations measured in a hydrogen peroxide solution, during sonication of the peroxide solution, during ozonation of the peroxide solution and during sonication combined with ozonation are 0,23; 0,19; 0,21 and 0,24 mg L^{-1}, respectively. The initial rates of atrazine degradation in a hydrogen peroxide solution during ozonation, sonication and the combination of ozonation and sonication were calculated from the regression of the data presented in Figure 8.14 using the linear regression model

$$y = a + bx \qquad [8.7]$$

where the coefficient *b*, the gradient of the regression line, represents the rate of atrazine degradation. The calculated rates of atrazine degradation in a hydrogen peroxide solution during the initial period of ozonation, sonication or ozonation combined with sonication (and the standard errors of the calculated values) are recorded in Table 8.10.

Table 8.10 : Initial rate of atrazine degradation in a 5 mg L^{-1} atrazine solution with 40 mg L^{-1} hydrogen peroxide, hydrogen peroxide combined with sonication (57 W), hydrogen peroxide combined with ozonation (0,14 mg s^{-1}) and hydrogen peroxide combined with sonication and ozonation

	Regression time period	Rate of atrazine degradation (mg L^{-1} min^{-1})	R^2
H_2O_2	0 to 180 min	0,0021 ± 0,0007	0.422
uls/H_2O_2	0 to 180 min	0,0120 ± 0,0005	0.984
O_3/H_2O_2	0 to 30 min	0,0568 ± 0,0058	0.932
uls/O_3/H_2O_2	0 to 30 min	0,0370 ± 0,0056	0.860

Atrazine degradation is relatively slow, as shown in Figure 8.14, in the presence of hydrogen peroxide alone whereas the degradation was significantly enhanced during the combination of hydrogen peroxide with ozone or ultrasound. The reaction mechanisms of atrazine degradation during sonication or ozonation combined with hydrogen peroxide are discussed in Section 8.1. The degradation rate of atrazine during sonication increased from 0,0082 mg L^{-1} min^{-1} (Table 8.6) to 0,0120 mg L^{-1} min^{-1} with the addition of hydrogen peroxide (Table 8.10). Similarly, the degradation rate of atrazine during ozonation increased from 0,0143 mg L^{-1} min^{-1} (Table 8.8) to 0,0568 mg L^{-1} min^{-1} with hydrogen peroxide (Table 8.10). The highest rate of atrazine degradation was measured when ozonation was combined with hydrogen peroxide. This was confirmed by the mass balance experiments (Section 8.1.4) in which the total atrazine degradation over 45 min was the greatest (42 %) during ozonation combined with hydrogen peroxide (Table 8.4).

Atrazine degradation in a 5 mg L^{-1} atrazine solution during sonication, ozonation and sonication combined with ozonation, all with and without hydrogen peroxide, are compared in Figure E.6 to Figure E.8 in Appendix E. Hydrogen peroxide is shown to enhance atrazine degradation during sonication and during ozonation but not to affect degradation during the combination of sonication with ozonation. The reduced atrazine degradation in the presence of high hydrogen peroxide concentrations, as discussed in Section 8.1.4, is due to the change in kinetic regime of ozone absorption and the scavenging of hydroxyl radicals by the hydrogen peroxide thus hindering the reaction of atrazine and hydroxyl radicals. The comparisons of atrazine degradation presented in Figure E.6 to Figure E.8 indicate that ultrasound should be combined in water treatment with either ozone or hydrogen peroxide but not both together since the peroxide concentration in solution may be greater than the optimal concentration required for the oxidation of organic pollutants.

8.3 PRODUCT IDENTIFICATION

Atrazine concentration in the degradation experiments discussed in Section 8.2 was measured using the HPLC method described in Section 5.4.4. The HPLC chromatogram of an unreacted 5 mg L^{-1} atrazine solution is presented in Figure E.9 in Appendix E. The retention time of atrazine on the chromatograms for the HPLC analysis system, as shown in Figure E.9, is approximately 6,5 min, although some variation occurred on a daily basis. The blimp at a retention time of 8 min that was present on all chromatograms was an impurity in the atrazine feedstock (97 %). The same peak was also present when new atrazine feedstock was obtained from Sanachem. Atrazine degradation products were detected with the HPLC system, the product peaks on the chromatograms increased in size as the atrazine peak decreased. Typically the degradation products appeared as a double peak ahead of the atrazine peak, at retention times of approximately 5,2 and 5,4 min. Prolonged oxidation of atrazine resulted in the product peaks increasing in size beyond that of the decreasing atrazine peak.

The size of the product peaks detected during the ozonation of atrazine increased with time over the 3 h experiment and with increasing ozone production rate (0,003 to 0,047 mg s^{-1}). Formation of degradation products occurred sooner during ozonation at higher ozone production rates. Degradation products were first evident at 90 min during ozonation at an ozone production rate of 0,003 mg s^{-1} whereas they were present from 15 min onwards for an ozone production rate of 0,047 mg s^{-1}. The decreasing atrazine peak and increasing product peaks on the HPLC chromatograms during the ozonation of atrazine at an ozone production rate of 0,047 mg s^{-1} are presented in Figure 8.15.

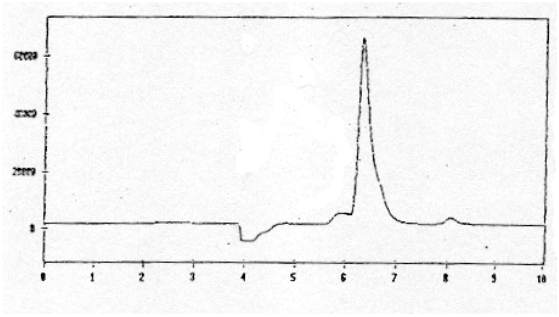

(a) 0 min

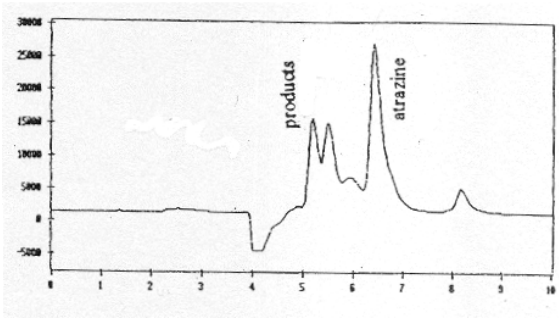

(b) 30 min

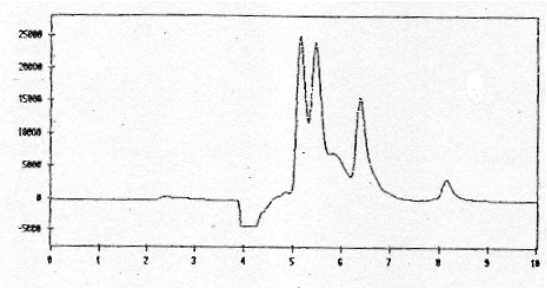

(c) 90 min

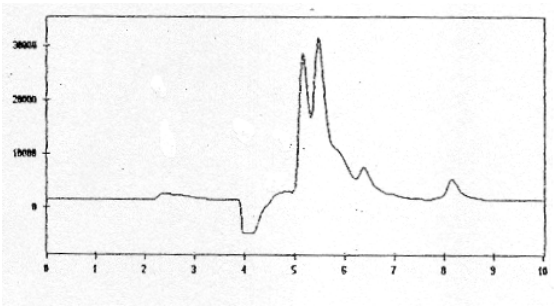

(d) 180 min

Figure 8.15 : HPLC chromatograms for the ozonation of a 5 mg L^{-1} atrazine solution at an ozone production rate of 0,047 mg L^{-1}

The oxidation of atrazine, as discussed in Section 8.1 and Section 8.2, was enhanced during ozonation (0,047 mg s^{-1}) combined with sonication (57 W). The HPLC chromatograms over the 3 h experiments showed the enhanced formation of degradation products during ozonation combined with sonication versus during ozonation alone. The decreasing atrazine peak and increasing product peaks on the HPLC chromatograms during ozonation combined with sonication are presented in Figure 8.16.

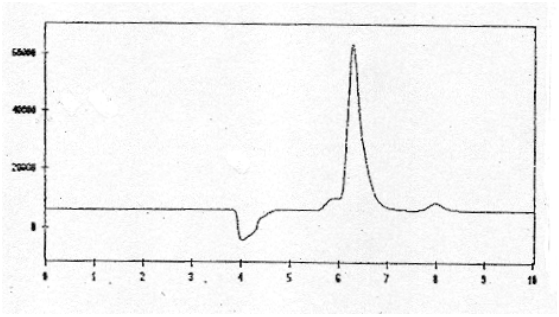

(a) 0 min

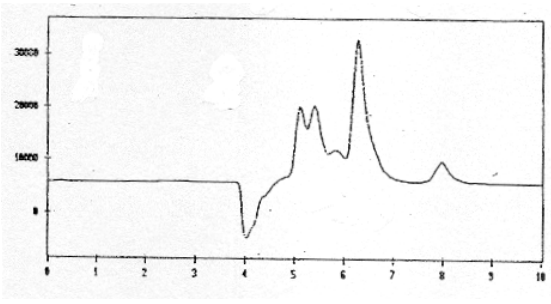

(b) 30 min

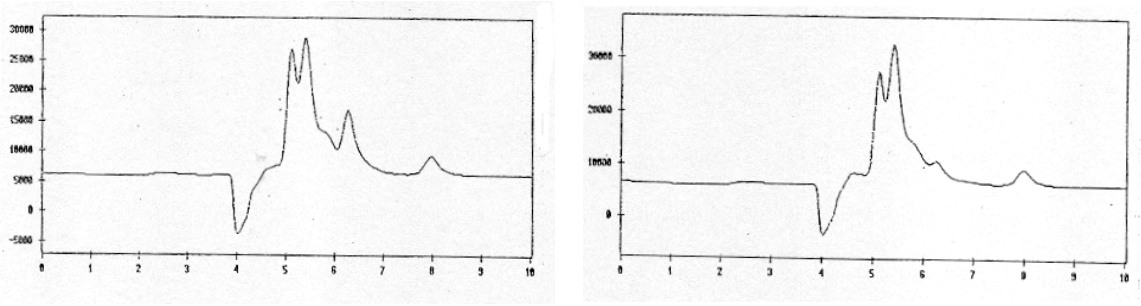

(c) 90 min **(d) 180 min**

Figure 8.16 : HPLC chromatograms for the ozonation of a 5 mg L^{-1} atrazine solution at an ozone production rate of 0,047 mg L^{-1} combined with sonication at an acoustic power of 57 W

The relatively slow degradation of atrazine in the presence of hydrogen peroxide alone (Figure 8.14) was confirmed since no product peaks were evident on the HPLC chromatograms. The degradation of atrazine, discussed in Section 8.14 and Section 8.2.3, during ozonation combined with hydrogen peroxide was greater than during ozonation combined with both sonication and hydrogen peroxide. Thus a greater quantity of degradation products, as shown in Figure 8.17, were formed during ozonation combined with hydrogen peroxide than during ozonation combined with both sonication and hydrogen peroxide.

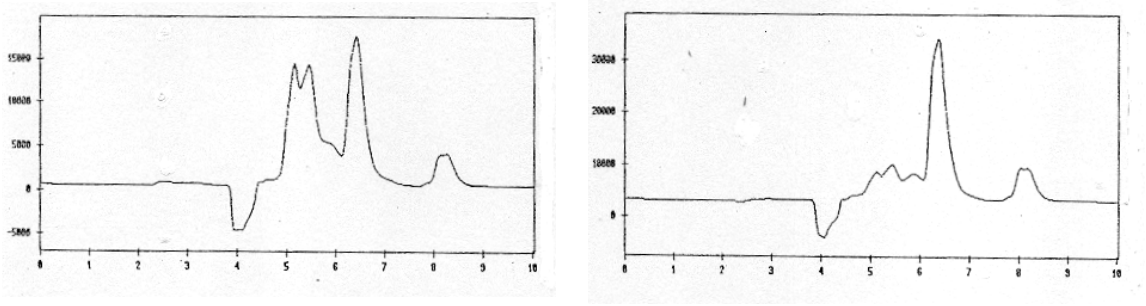

(a) ozone/H_2O_2 **(b) ozone/uls/H_2O_2**

Figure 8.17 : HPLC chromatograms at 180 min for a 5 mg L^{-1} atrazine solution during ozonation (0,014 mg L^{-1}) combined with hydrogen peroxide (40 mg L^{-1}) and ozonation combined with both sonication (57 W) and hydrogen peroxide

The double product peaks on the different chromatograms indicate that more than one product is being formed during the oxidation of atrazine. The same pattern of peaks indicates that the same products are being formed during ozonation, ozonation combined with sonication, ozonation combined with hydrogen peroxide and ozonation combined with sonication and hydrogen peroxide. The same mechanism of atrazine degradation is thus occurring. Minor products formed from further degradation of the primary degradation products or from other degradation mechanisms may be hidden on the chromatograms under the dominant

product peaks because of similar retention times. The overlap of the double product peaks on the chromatograms indicated that the products were co-eluting and could not be collected separately for identification. Gas chromatography- mass spectrometry (GC-MS) was thus used to identify degradation products. Samples at the end of an experiment (at 180 min) during ozonation (0,047 mg s^{-1}), sonication (57 W) and ozonation combined with sonication of a 5 mg L^{-1} atrazine solution were analysed. Product identification was the primary objective of the GC-MS analysis thus once-off samples for each experiment were analysed. Samples throughout the experiments would have to be analysed for the investigation of the trends in product formation and further degradation.

GC-MS analysis was performed at the CSIR and Rand Afrikaans University (RAU). Analytical procedures are detailed in Section E.3. A 5 mg L^{-1} atrazine solution was analysed to identify degradation products after 3 h of sonication, ozonation and sonication combined with ozonation in the ultrasonic cell. An unreacted atrazine sample (control) was analysed using the same method as that used to analyse the reaction samples. The mass spectrum of atrazine is presented in Figure 8.18.

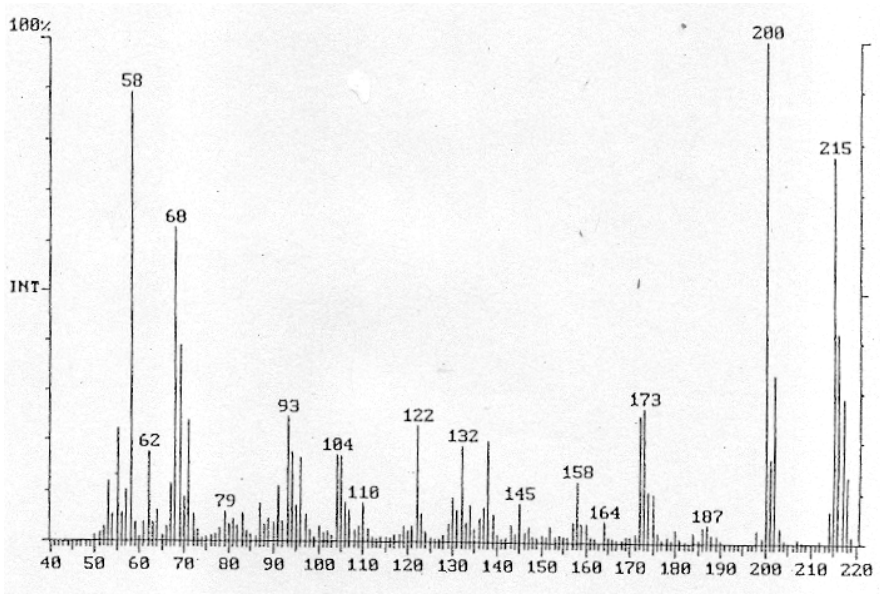

Figure 8.18 : Mass spectrum of a 5 mg L^{-1} atrazine solution

The molecular ion peak [M^+] at a *m/e* ratio of 215 for atrazine is evident in the mass spectrum presented in Figure 8.18. Chlorine-containing compounds reflect a $[M + 2]^+$ peak approximately a third of the intensity of the [M^+] peak because the natural abundance of the ^{37}Cl isotope is approximately 32,5 % of the ^{35}Cl isotope (Pavia et al., 1979). The $[M + 2]^+$ peak at *m/e* 217 for atrazine, a third of the size of the peak at 215, is evident in Figure 8.18. Structures of some of the molecular fragments generated during the ionisation of atrazine, as indicated on the mass spectrum in Figure 8.18, are presented in Figure 8.19.

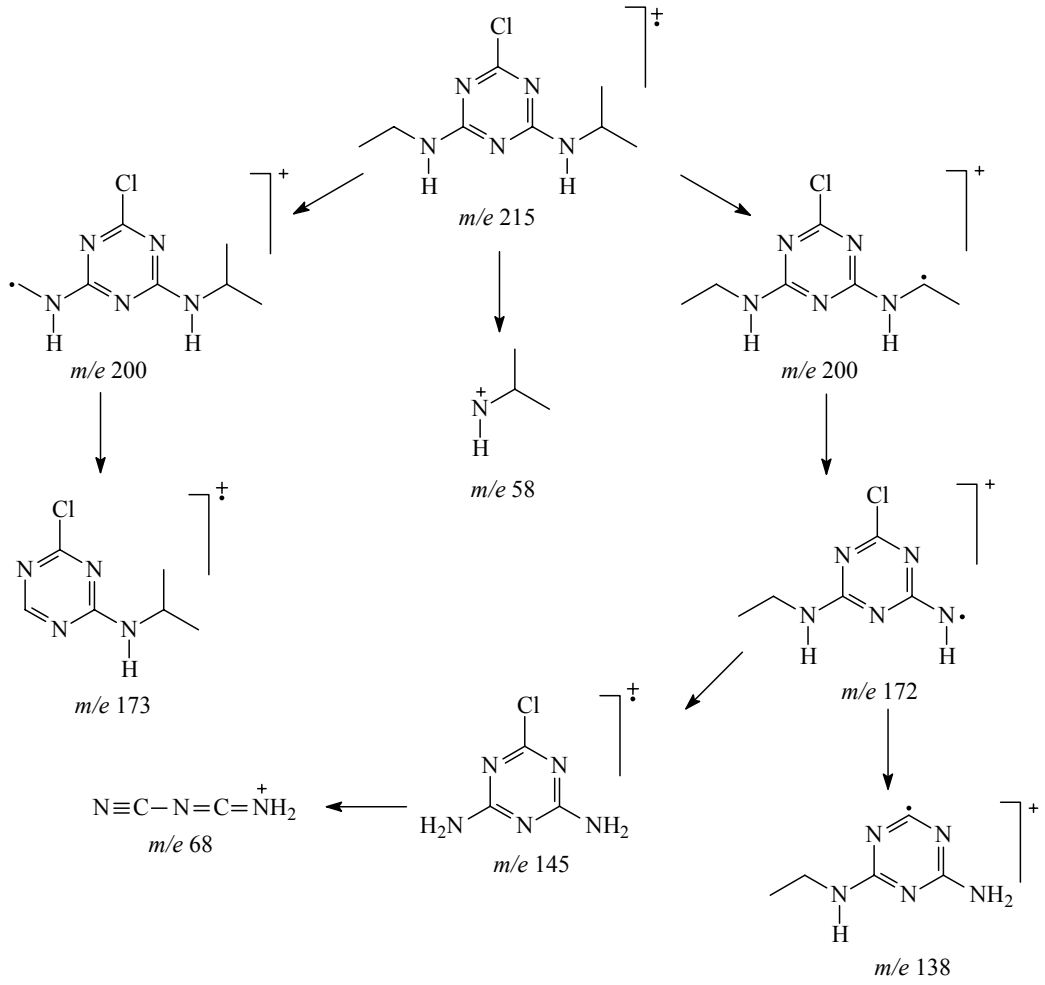

Figure 8.19 : Molecular fragments generated during the ionisation of atrazine

The molecular fragments of atrazine presented in Figure 8.19 indicate that the cleavage of the alkyl side chains occurs more readily during ionisation than that of the chlorine substituent, cleavage of the chlorine atom only takes place after the loss of part of the alkyl side chain groups. The peak at *m/e* 200 (202, ^{37}Cl) in Figure 8.18 indicates the loss of a methyl group ($^{\bullet}CH_3$) from either the ethylamino or isopropylamino side chains. Cleavage of the methyl group from the isopropylamino side chain produces a more stable radical because of the positive inductive effect of the other methyl group (Emslie, 2001). The peak at *m/e* 172 (174, ^{37}Cl) is due to the cleavage, as shown in Figure 8.19, of the isopropyl group ($^{\bullet}CH(CH_3)_2$) from the isopropylamino side chain. The ethyl group ($^{\bullet}CH_2CH_3$) in the ethylamino side chain is not directly cleaved since a significant peak is not present at *m/e* 186 (188, ^{37}Cl). Hapeman-Somich and co-workers also observed the lack of direct cleavage of the ethyl group (Hapeman-Somich et al., 1992). The peak at *m/e* 58 represents the cleavage of the complete isopropylamino side chain. The peak at *m/e* 68 is due to the fragment rearrangement shown in Scheme 8.1 that was proposed by Hapeman-Somich and co-workers (Hapeman-Somich et al., 1992).

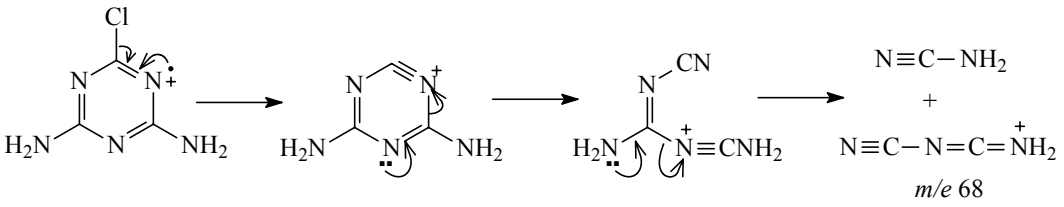

Scheme 8.1

The GC-MS spectra presented in Figure E.10 of a 5 mg L^{-1} atrazine solution after sonication, ozonation and sonication combined with ozonation indicate that a range of atrazine degradation products are formed. Deethylatrazine, deisopropylatrazine and hydroxyatrazine are shown in Figure 4.3 in Section 4.2.2.1 to be the primary metabolites of atrazine. Deethylatrazine was identified as a degradation product in the analysis performed at the CSIR of the sonication and ozonation atrazine samples by comparison of the $[M + H]^+$ peak at *m/e* 188 with the library of compounds (Naicker, 1999). Deethylatrazine was also identified in the ozonation sample analysed at RAU, shown in Figure E.10(b). The mass spectrum of deethylatrazine is presented in Figure 8.20.

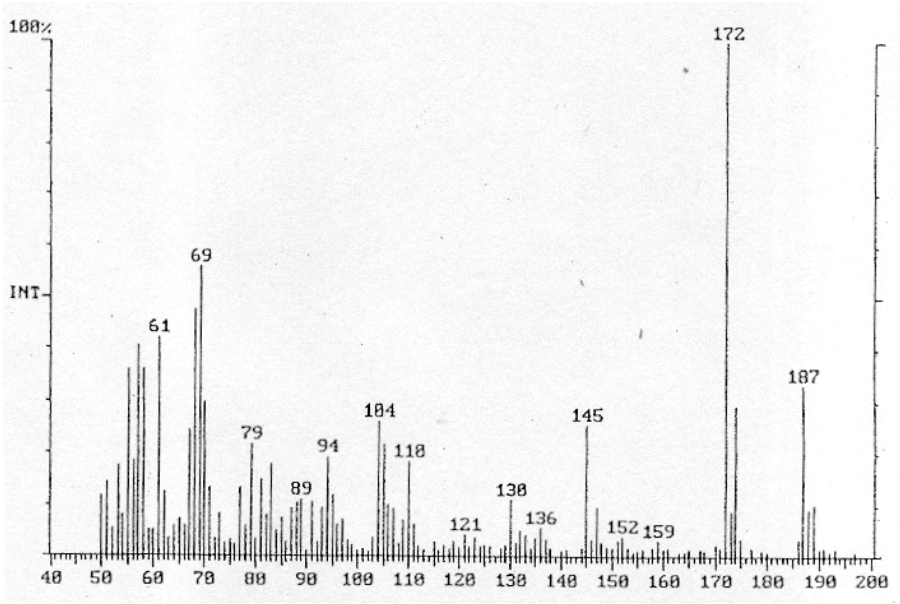

Figure 8.20 : Mass spectrum of deethylatrazine formed during the sonication and ozonation of a 5 mg L^{-1} atrazine solution for 3 h

The parent peak $[M]^+$ of deethylatrazine is evident in Figure 8.20 at *m/e* 187 (189, ^{37}Cl). The spectrum presented in Figure 8.20 is similar to that identified by Legube and co-workers as deethylatrazine with peaks at *m/e* 43, 58, 69, 83, 85, 104, 145, 172, 175, 187 and 189 (Legube et al., 1987). The base peak at *m/e* 172 (174, ^{37}Cl) indicates the loss of a methyl group ($^{\bullet}CH_3$) from the isopropylamino side chain. Also shown in Figure 8.20 is the lack of direct cleavage of chlorine from the parent compound to generate a peak at *m/e* 152. Structures of the molecular fragments generated during the ionisation of deethylatrazine, as indicated on the mass spectrum in Figure 8.20, are presented in Figure 8.21.

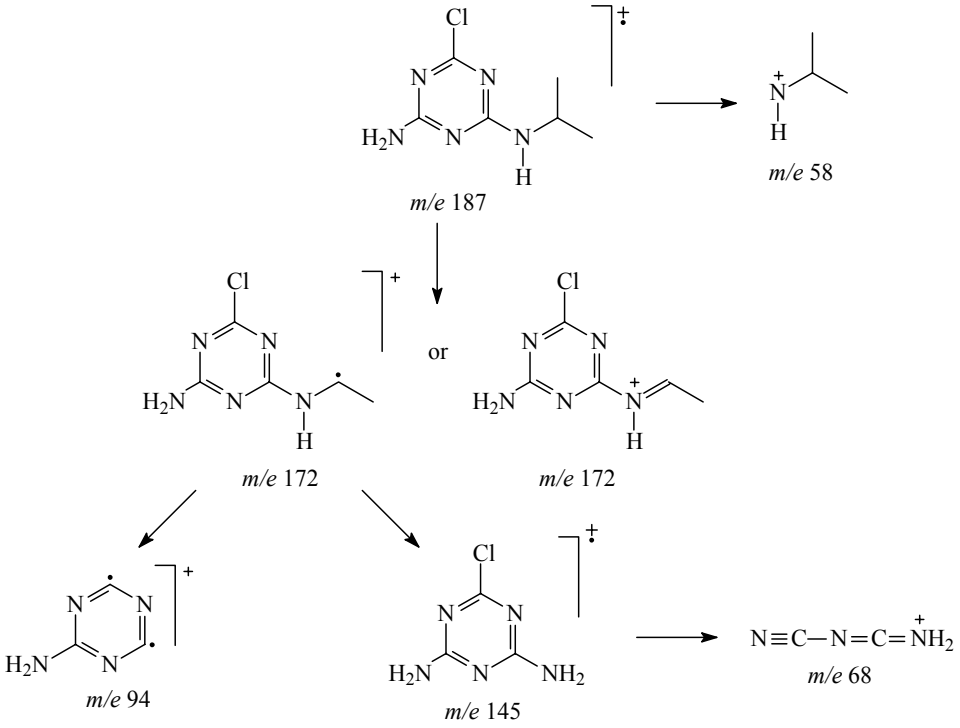

Figure 8.21 : Molecular fragments generated during the ionisation of deethylatrazine

Hydroxyatrazine was formed in a 5 mg L^{-1} atrazine solution during sonication, ozonation and sonication combined with ozonation for 3 h. The mass spectrum of hydroxyatrazine is presented in Figure 8.22.

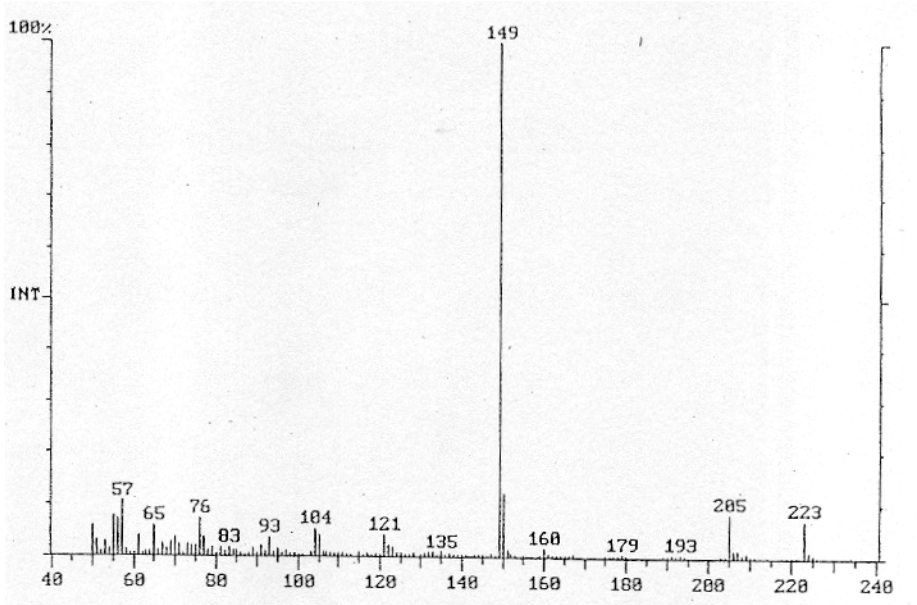

Figure 8.22 : Mass spectrum of hydroxyatrazine formed during the sonication, ozonation and sonication combined with ozonation of a 5 mg L^{-1} atrazine solution for 3 h

Hydroxyatrazine was identified by its principle fragmentation ion at *m/e* 149 as the $[M]^+$ peak was not evident in the mass spectrum presented in Figure 8.22. Hydroxyatrazine has two aliphatic amine side chains that undergo β-cleavage as shown in Scheme 8.2 (Pavia et al., 1979).

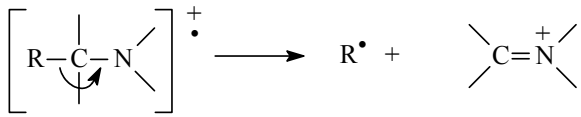

Scheme 8.2

The base peak at *m/e* 149 in Figure 8.22 is proposed to be due to either of the compounds presented in Figure 8.23 that are formed from the β-cleavage of the hydroxyatrazine side chains (Schwikkard, 2000). The OH group of hydroxyatrazine is readily lost during ionisation and the structures presented in Figure 8.22 are based on the prior loss of the OH group.

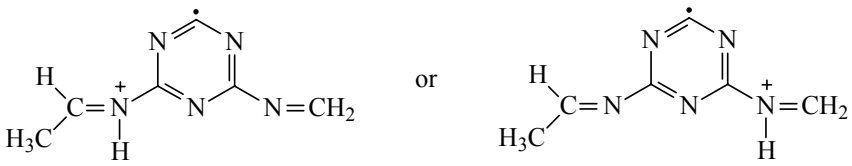

Figure 8.23 : Compounds formed during the ionisation of hydroxyatrazine due to the β-cleavage of the aliphatic amine side chains

Minor, unidentified products were also formed, as shown in Figure E.10, in a 5 mg L^{-1} atrazine solution during sonication, ozonation and sonication combined with ozonation for 3 h. The mass spectrum presented in Figure 8.24 of the product with a retention time of approximately 12 min in Figure E.10(b) and (c) is tentatively identified as deethyldeisopropylatrazine due to the characteristic $[M + 2H]^{2+}$ peak at *m/e* 147 (149, ^{37}Cl) although the peak at *m/e* 73 is unexplained. The peak at *m/e* 73 is not due to the direct cleavage of a fragment from the parent compound but possibly the rearrangement of such a fragment. Nélieu and co-workers found that deethyldeisopropylatrazine was formed in ozonation experiments longer than 60 min though the concentration was always less than 2 % of the initial atrazine (Nélieu et al., 1996). The small quantities of products formed in the investigation in the ultrasonic cell did not allow for nuclear magnetic resonance spectroscopy (NMR) of products to facilitate identification.

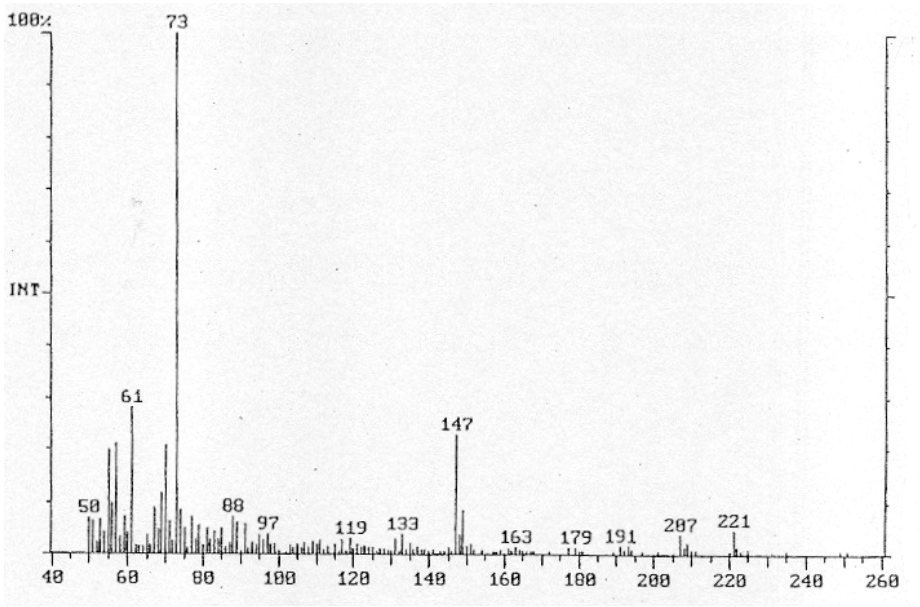

Figure 8.24 : Mass spectrum of deethyldeisopropylatrazine formed during the sonication, ozonation and sonication combined with ozonation of a 5 mg L^{-1} atrazine solution for 3 h

The formation of dealkylated products (deethylatrazine and possibly deethyldeisopropylatrazine) is due to both the reaction of atrazine with hydroxyl radicals (Figure 8.2 in Section 8.1.1) and the direct reaction with ozone (Figure 8.5 in Section 8.1.2). Hydrogen peroxide is produced as a byproduct in the formation of dealkylated degradation products. Enhanced hydrogen peroxide formation was measured in an atrazine solution (in comparison with that measured in water) during ozonation and ozonation combined with sonication (shown in Figure 8.6 in Section 8.1.3). Hydrolysed degradation products (hydroxyatrazine) are only formed due to the reaction of atrazine with hydroxyl radicals (Figure 8.3 in Section 8.1.1).

Both dealkylated and hydrolysed degradation products (shown in Figure E.10) were detected during the ozonation and sonication of atrazine. The degradation mechanism of atrazine during sonication is due to the reaction with hydroxyl radicals. The degradation mechanism during ozonation is due to both the direct reaction with ozone and the reaction with hydroxyl radicals, although, as concluded in Section 8.1, the reaction with hydroxyl radicals is the dominant degradation mechanism.

8.4 CONCLUDING REMARKS

Atrazine is not degraded upon standing even with oxygen sparging and only slightly in the presence of hydrogen peroxide whereas degradation occurs during sonication and ozonation. Atrazine accumulates in the gas/liquid interfacial region during sonication because of its non-volatility and hydrophobicity. Ultrasound enhances the degradation achieved during atrazine oxidation with either ozone or hydrogen peroxide. The influence of ultrasound is limited when ozonation is also combined with hydrogen peroxide or when the concentrations of ozone and hydrogen peroxide are very high, such concentrations though are not

appropriate for industrial application. Ultrasound initiates the decomposition of ozone and hydrogen peroxide to enhance the degree of free radical reactions occurring in solution.

Atrazine degradation during ozonation can be due to the direct reaction with ozone or to the reaction with free radicals in solution. Reaction with free radicals was found to be the dominant degradation mechanism. The greatest atrazine degradation was measured during ozonation combined with hydrogen peroxide where dissolved ozone and free radicals were available in solution. Enhanced hydrogen peroxide formation during ozonation or sonication of an atrazine solution, in comparison with that in water, is due to the peroxide generated as a byproduct during the formation of dealkylated degradation products.

Atrazine degradation products were identified used gas chromatography and mass spectrometry. The degradation products formed during the ozonation, sonication and ozonation combined with sonication of atrazine were deethylatrazine, hydroxyatrazine and deethyldeisopropylatrazine (tentatively identified). Dealkylated degradation products are formed due to both the direct reaction with ozone and the reaction with free radicals whereas hydrolysed products are only formed from the reaction with free radicals. The dominant degradation mechanism of atrazine was via the reaction with free radicals. Other minor degradation products were formed but could not be identified.

9

CONCLUDING REMARKS

The deteriorating water quality in South Africa and changing legislation requiring the implementation of waste minimisation and pollution prevention strategies has highlighted the need for the investigation of new effluent treatment technologies such as advanced oxidation processes. This study investigated the potential application of ultrasound in water treatment for the oxidation of organic pollutants using atrazine as a model compound. The objectives of the investigation are listed below with concluding remarks addressing each of the objectives.

a) Design and construct an ultrasonic cell to be used in the evaluation of ultrasound to degrade organic pollutants in water treatment

A 500 mL batch ultrasonic laboratory reactor, with an ultrasonic horn as an energy source, was designed and constructed. The reactor operates at atmospheric pressure and allows for the gas sparging of solutions during sonication. Different sample ports allow for both gas and liquid samples to be drawn, liquid samples can be taken continuously throughout an experiment if the volume required for analysis is small. The ultrasonic cell is thus a versatile system that can be used in screening experiments to investigate whether ultrasound enhances a particular reaction or be used to degrade a particular organic compound.

b) Use such equipment to investigate the process mechanism (the sequence of sub-processes whose overall result produces the observed effect) occurring during sonication.

Pollutant oxidation during sonication is due to free radical reactions occurring within the collapsing gas cavities, at the gas liquid interface and in the bulk solution. Hydrophobicity and volatility determine in which region a compound participates in the radical reactions. Hydrogen peroxide is formed during the ultrasonic-initiated free radical reactions. The measurement of hydrogen peroxide concentration was used as a measure of the degree of radical reactions occurring during sonication and is thus a tool that can be used to investigate under which process conditions reactor performance is enhanced.

The rate of hydrogen peroxide formation during sonication increases with increasing dissolved oxygen concentration due to the additional radical reactions initiated in solution. The rate of peroxide formation, however, decreases with increasing peroxide concentration as the equilibrium between peroxide formation and degradation is approached. Hydrogen peroxide concentration thus decreases during sonication in a solution with an initial concentration greater than the equilibrium value. Hydrogen peroxide degradation is

slow after sonication has been ended, thus oxidation of organic compounds can occur both during and after sonication. A correlation (accounting for approximately 97 % of the variation in the data) was developed for the prediction of hydrogen peroxide concentration as a function of dissolved oxygen concentration, acoustic power and time. The correlation equation is

$$[H_2O_2] = -0,5420[time]^{0,6995} + 0,5516[time]^{0,6984}[uls]^{-0,001761}[O_2]^{0,004917} \qquad [9.1]$$

where $[H_2O_2]$ is measured in mg L^{-1}, $[uls]$ in W, $[O_2]$ in mg L^{-1} and $[time]$ in min. This correlation can be used to guide the choice of process conditions and mode of operation of an ultrasound process so as to maximise hydrogen peroxide formation and hence free radical reactions.

c) Investigate the equipment operation and implications for scale-up.

This study (using the measurement of hydrogen peroxide concentration as an indication of the free radical reactions occurring during sonication) has resulted in the following guidelines being proposed for the scale-up of ultrasonic processes, these are:

- The continual sparging with a gas (oxygen or air) or added hydrogen peroxide should be used during sonication to enhance free radical reactions.
- Oxygen sparging and a high acoustic power input should be used in processes with a short retention time, conversely, air sparging and a lower acoustic energy source should be used in processes with a long retention time.
- A flow loop system should be considered to maximise oxidation of organic compounds both within and beyond the sonicated zone, gas sparging should only occur within the sonicated zone

d) Compare the performance of ultrasound, an emerging technology in water treatment, with that of ozone, an already established advanced oxidation process.

Ozone chemistry was investigated as a foundation for the comparison of ultrasound with ozone. Oxidation of organic compounds during ozonation takes place due to either direct reaction with ozone or reaction with free radicals formed from the decomposition of ozone. Ozone decomposition (and hence free radical reactions) is enhanced with the combination of ozone with ultrasound or hydrogen peroxide. A 40 mg L^{-1} hydrogen peroxide concentration totally depleted the dissolved ozone concentration in solution whereas ultrasound only partially reduced the ozone concentration. The partial reduction obtained with sonication in the ultrasonic cell is equivalent to that obtained with between 15 and 20 mg L^{-1} of hydrogen peroxide. Enhanced ozone decomposition occurs due to the conditions (high temperatures and pressures) as well as the free radical reactions occurring within the collapsing cavitation bubbles and at the gas-liquid interface.

Ozone is a powerful but selective oxidant and the performance of ozonation during water treatment for the oxidation of organic compounds is thus enhanced with the combination with either hydrogen peroxide or

ultrasound. Ozonation combined with hydrogen peroxide allows for oxidation primarily due to reaction with hydroxyl radicals whereas ozonation combined with sonication allows for oxidation of compounds that preferentially react with either ozone or hydroxyl radicals.

e) Use atrazine as a model organic compound and investigate degradation rates during sonication and ozonation.

Atrazine was used as a model compound in the evaluation of ultrasound to degrade organic compounds in water treatment as it is difficult to degrade and atrazine chemistry is well studied. Atrazine is used extensively in South Africa and is highly persistent in the environment. Atrazine is also relatively safe to handle and is readily available. Atrazine was degraded during sonication and during ozonation, degradation was enhanced with the addition of hydrogen peroxide. Atrazine degradation was greatest during ozonation combined with hydrogen peroxide and decreased in the order for ozonation combined with both sonication and hydrogen peroxide > ozonation combined with sonication > ozonation > sonication and hydrogen peroxide. The enhancing effect of ultrasound on atrazine degradation during ozonation was greatest at low ozone concentrations. Atrazine degradation during sonication and ozonation is via reaction with free radicals. Degradation during ozonation can also be due to direct reaction with ozone, though, this reaction is the less preferred mechanism.

Ultrasound is a viable technology to be used to enhance the decomposition of oxidants such as ozone or hydrogen peroxide thus generating highly reactive free radicals. Ultrasound is most effectively applied in water treatment, to degrade organic compounds, as a pretreatment stage in combination with other technologies and not as a stand-alone process.

f) Identify degradation products obtained during the sonication and ozonation of atrazine.

Gas chromatography and mass spectrometry were used to identify atrazine degradation products produced during sonication, ozonation and sonication combined with ozonation. Deethylatrazine, hydroxyatrazine and deethyldeisopropylatrazine (tentatively identified) were all formed during sonication, ozonation and sonication combined with ozonation. Dealkylated degradation products are formed due to the reaction of atrazine with both ozone and hydroxyl radicals whereas hydrolysed degradation products are only formed due to the reaction of atrazine with hydroxyl radicals.

Recommendations

This study has focused on the investigation of the fundamental processes occurring during sonication and ozonation. Atrazine chemistry was also investigated prior to degradation experiments. The fundamental understanding of the system can be used as a foundation for more application-focused investigations. The following work is recommended to be performed to continue with the investigation of advanced oxidation processes in water treatment.

- Process and kinetic modelling of the atrazine system to be performed, as a case study, to generate information for the modelling and design of large-scale ultrasonic reactors.

- The ultrasonic cell to be modified to allow for continuous as well as batch operation, thus enabling a greater versatility in process operation and scale-up studies.

- The degradation of other recalcitrant organic compounds in the ultrasonic cell to be investigated to establish the class of pollutants that are most suited for ultrasonic degradation.

- The use of ultrasound as a pretreatment technology for biodegradation to be investigated, especially for the treatment of concentrated and toxic effluents that will be generated as waste minimisation technologies are applied in industry.

- Different reactor configurations to be investigated to determine the most effective way of combining ultrasound with ozone. The investigation should not only focus on the simultaneous application of ultrasound and ozone but also on whether any benefit is obtained if sonication is applied before or after ozonation.

- The power efficiency of ultrasound should be investigated and compared with that of ozone and hydrogen peroxide.

REFERENCES

Adams, C.D. and Randtke, S.J. (1992a) **Ozonation byproducts of atrazine in synthetic and natural waters**, *Environmental Science and Technology,* **26**(11), 2218-2227.

Adams, C.D. and Randtke, S.J. (1992b) **Removal of atrazine from drinking water by ozonation**, *Journal of the American Water Works Association,* **84**(9), 91-102.

Adams, C.D., Randtke, S.J., Thurman, E.M. and Hulsey, R.A. (1990) **Occurrence and treatment of atrazine and its degradation products in drinking water**, *Proceedings of the American Water Works Association's Annual Conference,* Cincinnati, Ohio, USA, **1**, 871-894.

Agbekodo, K.M., Legube, B. and Dard, S. (1996) **Atrazine and simazine removal mechanisms by nanofiltration: influence of natural organic matter concentration**, *Water Research,* **30**(11), 2535-2542.

Ahmad, W.Y.W. and Lomas, M. (1996) **The low-temperature dyeing of polyester fabric using ultrasound**, *Journal of the Society of Dyers and Colourists,* **112**(9), 245-248.

Alex, C.-C.T., Goh, N.K. and Chia, L.S. (1995) **Effects of particle size morphology on ultrasonic-induced cavitational mechanisms in heterogeneous systems**, *Journal of the Chemical Society. Chemical Communications,* (2), 201.

Alliger, H. (1975) **Ultrasonic disruption**, *American Laboratory,* **7**(10), 75-85.

Anbar, M. and Pecht, I. (1964a) **On the sonochemical formation of hydrogen peroxide in water**, *Journal of Physical Chemistry,* **68**(2), 352-355.

Anbar, M. and Pecht, I. (1964b) **The sonolytic decomposition of organic solutes in dilute aqueous solutions. I. Hydrogen abstraction from sodium formate**, *Journal of Physical Chemistry,* **68**(6), 1460-1462.

Anbar, M. and Pecht, I. (1967) **The sonolytic decomposition of organic solutes in dilute aqueous solutions. III. Oxidative deamination of ethylenediamine by HO• radicals**, *Journal of Physical Chemistry,* **71**(5), 1246-1249.

Ando, T. and Kimura, T. (1990) **Reactivity and selectivity in organic sonochemical reactions involving inorganic solids**, *Ultrasonics,* **28**(5), 326-332.

Ando, T., Sumi, S., Kawate, T., Ichihara, J. and Hanafusa, T. (1984) **Sonochemical switching of reaction pathways in solid-liquid two-phase reactions**, *Journal of the Chemical Society. Chemical Communications,* (7), 439-440.

Andreozzi, R., Caprio, V., Insola, A., Marotta, R. and Sanchirico, R. (1989) **Advanced oxidation processes for the treatment of mineral oil-contaminated wastewaters**, *AWT98 - Advanced Wastewater Treatment, Recycling and Reuse,* Milan, Italy, 891-894.

Anonymous (1995) **Inactivating *Crypto* oocysts with ultrasound**, *Worldwater and Environmental Engineering,* **18**(7), 42.

Apfel, R.E. (1972) **The tensile strength of liquids**, *Scientific American,* **227**(6), 58-71.

Apfel, R.E. (1984) **Acoustic cavitation inception**, *Ultrasonics,* **22**(4), 167-173.

Arántegui, J., Prado, J., Chamarro, E. and Esplugas, S. (1995) **Kinetics of the UV degradation of atrazine in aqueous solution in the presence of hydrogen peroxide**, *Journal of Photochemistry and Photobiology. Part A. Chemistry,* **88**(1), 65-74.

Asher, R.C. (1987) **Ultrasonics in chemical analysis**, *Ultrasonics,* **25**(1), 17-19.

Ayling, G.W. and Castrantas, H.M. (1981) **Waste treatment with hydrogen peroxide**, *Chemical Engineering,* **88**(24), 79-82.

Bablon, G., Bellamy, W.D., Billen, G., Bourbigot, M.-M., Daniel, F.B., Erb, F., Gomella, C., Gordon, G., Hartemann, P., Joret, J.-C., et al. (1991a) **Chapter 3. Practical application of ozone: principles and case studies**. In *Ozone in Water Treatment: Application and Engineering,* B. Langlais, D.A. Reckhow and D.R. Brink, eds., Lewis Publishers, Chelsea, Michigan, ISBN 0-87371-474-1, 133-316.

Bablon, G., Bellamy, W.D., Bourbigot, M.-M., Daniel, F.B., Doré, M., Erb, F., Gordon, G., Langlais, B., Laplanche, A., Legube, B., et al. (1991b) **Chapter 2. Fundamental aspects**. In *Ozone in Water Treatment: Application and Engineering,* B. Langlais, D.A. Reckhow and D.R. Brink, eds., Lewis Publishers, Chelsea, Michigan, ISBN 0-87371-474-1, 11-132.

Bader, H. and Hoigné, J. (1981) **Determination of ozone in water by the indigo method**, *Water Research,* **15**(4), 449-456.

Baga, A.N., Johnson, G.R.A., Nazhat, N.B. and Saadalla-Nazhat, R.A. (1988) **A simple spectro-photometric determination of hydrogen peroxide at low concentrations in aqueous solution**, *Analytical Chimica Acta,* **204**, 349-353.

Bahnemann, D. and Hart, E.J. (1982) **Rate constants of the reaction of the hydrated electron and hydroxyl radical with ozone in aqueous solution**, *Journal of Physical Chemistry,* **86**(2), 252-255.

Bailey, G.W. and White, J.L. (1970) **Factors influencing the adsorption, desorption and movement of pesticides in soil**. In *Residue Reviews,* F.A. Gunther and J.D. Gunther, eds., Springer-Verlag, New York, Library of Congress Catalogue Card Number 62-18595, **32**, 30-92.

Balasubramaniam, K., Abesingha, C. and Kumar, S.B. (1995) **Potential for application of ultrasound in the wastewater treatment process**, *Proceedings of the 25th Mississippi Water Resources Conference,* B.J. Danial, ed., 281-287.

Barbier, P.F. and Pétrier, C. (1996) **Study at 20 kHz and 500 kHz of the ultrasound-ozone advanced oxidation system: 4-nitrophenol degradation**, *Journal of Advanced Oxidation Technology,* **1**(2), 154-159.

Behki, R.M. and Khan, S.U. (1986) **Degradation of atrazine by *Pseudomonas*: *N*-dealkylation and dehalogenation of atrazine and its metabolites**, *Journal of Agricultural and Food Chemistry,* **34**(4), 746-749.

Bellamy, W.D., Hickman, G.T., Mueller, P.A. and Ziemba, N. (1991) **Treatment of VOC-contaminated groundwater by hydrogen peroxide and ozone oxidation**, *Research Journal of the Water Pollution Control Federation,* **63**(2), 120-128.

Beltrán, F.J. (1995) **Theoretical aspects of the kinetics of competitive ozone reactions in water**, *Ozone Science & Engineering,* **17**(2), 163-181.

Beltrán, F.J. (1997) **Theoretical aspects of the kinetics of competitive first reactions of ozone in the O_3/H_2O_2 and O_3/UV oxidation processes**, *Ozone Science & Engineering,* **19**(1), 13-38.

Beltrán, F.J., García-Araya, J.F. and Acedo, B. (1994a) **Advanced oxidation of atrazine in water. Part I. Ozonation**, *Water Research,* **28**(10), 2153-2164.

Beltrán, F.J., García-Araya, J.F. and Acedo, B. (1994b) **Advanced oxidation of atrazine in water. Part II. Ozonation combined with ultraviolet radiation**, *Water Research,* **28**(10), 2165-2174.

Beltrán, F.J., García-Araya, J.F., Álvarez, P.M. and Rivas, J. (1998) **Aqueous degradation of atrazine and some of its main byproducts with ozone/hydrogen peroxide**, *Journal of Chemical Technology and Biotechnology,* **71**(4), 345-355.

Beltrán, F.J., Gómez-Serrano, V. and Durán, A. (1992) **Degradation kinetics of *p*-nitrophenol ozonation in water**, *Water Research,* **26**(1), 9-17.

Beltrán, F.J., Ovejero, G. and Acedo, B. (1993a) **Oxidation of atrazine in water by ultraviolet radiation combined with hydrogen peroxide**, *Water Research,* **27**(6), 1013-1021.

Beltrán, F.J., Rivas, F.J. and Acedo, B. (1993b) **Direct, radical and competitive reactions in the ozonation of water micropollutants**, *Journal of Environmental Science and Health. Part A. Environmental Science and Engineering and Toxic and Hazardous Substance Control,* **A28**(9), 1947-1976.

Benítez, F.J., Beltrán-Heredia, J., Acero, J.L. and Gonzalez, T. (1996) **Degradation of protocatechuic acid by two advanced oxidation processes: ozone/UV radiation and H_2O_2/UV radiation**, *Water Research,* **30**(7), 1597-1604.

Berlan, J. and Mason, T.J. (1992) **Sonochemistry: from research laboratories to industrial plants**, *Ultrasonics,* **30**(4), 203-212.

Bhatnagar, A. and Cheung, H.M. (1994) **Sonochemical destruction of chlorinated C1 and C2 volatile organic compounds in dilute aqueous solution**, *Environmental Science and Technology,* **28**(8), 1481-1486.

Bien, J. (1988) **Ultrasonic preparation of sludges to improve dewatering**, *Filtration and Separation,* **25**(6), 425-426.

Bien, J. and Wolny, L. (1997) **Changes of some sewage sludge parameters prepared with an ultrasonic field**, *Water Science and Technology,* **36**(11), 101-106.

Blumhorst, M.R. and Weber, J.B. (1994) **Chemical versus microbial degradation of cyanazine and atrazine in soils**, *Pesticide Science,* **42**(4), 79-84.

Bolzacchini, E., Brambilla, A., Orlandi, M., Polesello, S. and Rindone, B. (1994) **Oxidative pathways in the degradation of triazine herbicides: a mechanistic approach**, *Water Science and Technology,* **30**(7), 129-136.

Boncz, M.A., Bruning, H., Rulkens, W.H., Sudhölter, E.J.R., Harmsen, G.H. and Bijsterbosch, J.W. (1997) **Kinetic and mechanistic aspects of the oxidation of chlorophenols by ozone**, *Water Science and Technology,* **35**(4), 65-72.

Boudjouk, P. (1986) **Synthesis with ultrasonic waves**, *Journal of Chemical Education,* **63**(5), 427-429.

Boudjouk, P. and Han, B.-H. (1981) **Organic sonochemistry. Ultrasound-promoted coupling of chlorosilanes in the presence of lithium wire**, *Tetrahedron Letters,* **22**(39), 3813-3814.

Boudjouk, P., Han, B.-H. and Anderson, K.R. (1982) **Sonochemical and electrochemical synthesis of tetramesityldisilene**, *Journal of the American Chemical Society,* **104**(18), 4992-4993.

Boudjouk, P., Thompson, D.P., Ohrbom, W.H. and Han, B.-H. (1986) **Effects of ultrasonic waves on the generation and reactivities of some metal powders**, *Organometallics,* **5**(6), 1257-1260.

Bowers, A., Netzer, A. and Norman, J.D. (1973) **Ozonation of wastewater - some technical and economic aspects**, *Canadian Journal of Chemical Engineering,* **51**(3), 332-336.

Bradfield, E. (1997) **Atrazine technical (product code 34216)**, Material Safety Data Sheet no. PS 057, Sanachem.

Brambilla, A., Bolzacchini, E., Orlandi, M., Polesello, S. and Rindone, B. (1995) **Reactivity of organic micropollutants with ozone: a kinetic study**, *Life Chemistry Reports,* **13**(1-2), 79-84.

Braslavsky, S.E. and Houk, K.N. (1988) **Glossary of terms used in photochemistry**, *Pure and Applied Chemistry,* **60**(7), 1055-1106.

Bremner, D. (1986) **Chemical ultrasonics**, *Chemistry in Britain,* **22**(7), 633-638.

Brink, D.R., Langlais, B. and Reckhow, D.A. (1991) **Chapter 1. Introduction**. In *Ozone in Water Treatment: Application and Engineering,* B. Langlais, D.A. Reckhow and D.R. Brink, eds., Lewis Publishers, Chelsea, Michigan, ISBN 0-87371-474-1, 1-10.

Bull, R.A. and Zeff, J.D. (1991) **Hydrogen peroxide in advanced oxidation processes for treatment of industrial process and contaminated groundwater**, *First International Symposium: Chemical Oxidation, Technology for the 90s,* Nashville, Tennessee, W.W. Eckenfelder, A.R. Bowers and J.A. Roth, eds., 26-36.

Burkhard, N. and Guth, J.A. (1976) **Photodegradation of atrazine, atraton and ametryne in aqueous solution with acetone as a photosensitiser**, *Pesticide Science,* **7**(1), 65-71.

Burkhard, N. and Guth, J.A. (1981) **Chemical hydrolysis of 2-chloro-4,6-bis(alkylamino)-1,3,5-triazine herbicides and their breakdown in soil under the influence of adsorption**, *Pesticide Science,* **12**(1), 45-52.

Busing, W.R. and Levy, H.A. (1963) **Crystal and molecular structure of hydrogen peroxide: a neutron-diffraction study**, *Journal of Chemical Physics,* **42**(9), 3054-3059.

Büttner, J., Gutiérrez, M. and Henglein, A. (1991) **Sonolysis of water-methanol mixtures**, *Journal of Physical Chemistry,* **95**(4), 1528-1530.

Caprio, V., Insola, A., Lignola, P.G. and Volpicelli, G. (1982) **A new attempt for the evaluation of the absorption constant of ozone in water**, *Chemical Engineering Science,* **37**(1), 122-124.

Carberry, J.B. and Benzing, T.M. (1991) **Peroxide pre-oxidation of recalcitrant toxic waste to enhance biodegradation**, *Water Science and Technology,* **23**(1-3), 367-376.

Carmichael, A.J., Mossoba, M.M., Riesz, P. and Christman, C.L. (1986) **Free radical production in aqueous solutions exposed to simulated ultrasonic diagnostic conditions**, *IEEE Transactions on Ultrasonics, Ferroelectrics and Frequency Control,* **UFFC-33**(2), 148-155.

Central Statistical Service (2000) **RSA statistics in brief**, http://www.statssa.gov.za/stats_in_brief_2000.

Chan, G.Y.S., Hudson, M.J. and Isaacs, N.S. (1992) **Degradation of atrazine by hydrolysis and by hydroxyl radicals**, *Journal of Physical Organic Chemistry,* **5**, 600-608.

Charpentier, J.-C. (1981) **Mass-transfer rates in gas-liquid absorbers and reactors**. In *Advances in Chemical Engineering,* T.B. Drew, G.R. Cokelet, J.W. Hoopes and T. Vermeulen, eds., Academic Press, New York, ISBN 0-12-008511-9, **11**, 1-133.

Chatterjee, A., Magee, J.L. and Dey, S.K. (1983) **The role of homogeneous reactions in the radiolysis of water**, *Radiation Research,* **96**(1), 1-19.

Chendke, P.K. and Fogler, H.S. (1975) **Macrosonics in industry. 4. Chemical processing**, *Ultrasonics,* **13**(1), 31-37.

Chendke, P.K. and Fogler, H.S. (1983a) **Sonoluminescence and sonochemical reactions of aqueous carbon tetrachloride solutions**, *Journal of Physical Chemistry,* **87**(8), 1362-1369.

Chendke, P.K. and Fogler, H.S. (1983b) **Effect of static pressure on the intensity and spectral distribution of the sonoluminescence of water**, *Journal of Physical Chemistry,* **87**(9), 1644-1648.

Cheng, H.H. (1990) **Organic residues in soils: mechanisms of retention and extractability**, *International Journal of Environmental Analytical Chemistry,* **39**(2), 165-171.

Cheung, H.M., Bhatnagar, A. and Jansen, G. (1991) **Sonochemical destruction of chlorinated hydrocarbons in dilute aqueous solution**, *Environmental Science and Technology,* **25**(8), 1510-1512.

Cheung, H.M. and Kurup, S. (1994) **Sonochemical destruction of CFC 11 and CFC 113 in dilute aqueous solution**, *Environmental Science and Technology,* **28**(9), 1619-1622.

Chiu, Y.-C., Chang, C.-N., Line, J.-G. and Huang, S.-J. (1997) **Alkaline and ultrasonic pretreatment of sludge before anaerobic digestion**, *Water Science and Technology,* **36**(11), 155-162.

Chopra, S.L., Sethi, B.K. and Baweja, A.S. (1973) **Residues of atrazine (2-chloro-4-ethylamino-6-isopropyl-amino-*s*-triazine) in soils**, *Journal of the Indian Society of Soil Science,* **21**(3), 319-322.

Chramosta, N., De Laat, J., Doré, M., Suty, H. and Pouillot, M. (1993) **Rate constants for reaction of hydroxyl radicals with *s*-triazines**, *Environmental Technology,* **14**(3), 215-226.

Christman, C.L., Carmichael, A.J., Mossoba, M.M. and Riesz, P. (1987) **Evidence for free radicals produced in aqueous solutions by diagnostic ultrasound**, *Ultrasonics,* **25**(1), 31-34.

Chyla, A., Lorimer, J.P., Mason, T.J., Smith, G. and Walton, D.J. (1989) **Modifying effect of ultrasound upon the electrochemical oxidation of cyclohexanecarboxylate**, *Journal of the Chemical Society. Chemical Communications,* (9), 603-604.

Clarke, N. and Knowles, G. (1982) **High purity water using hydrogen peroxide and ultraviolet radiation**, *Effluent and Water Treatment Journal,* (September), 335-341.

Clasen, J. and Sobotta, R. (1994) **Inactivation of microorganisms by ultrasound**, *Water Supply,* **12**(3-4), 243-251.

Clay, S.A. and Koskinen, W.C. (1990) **Adsorption and desorption of atrazine, hydroxyatrazine and *S*-glutathione atrazine on two soils**, *Weed Science,* **38**(3), 262-266.

Coetzer, R. (2000) Personal communication, Sasolburg.

Cole, C.A., Ochs, L.D. and Funnell, F.C. (1974) **Hydrogen peroxide as a supplemental oxygen source**, *Journal of the Water Pollution Control Federation,* **46**(11), 2579-2592.

Contamine, F., Faid, F., Wilhelm, A.M., Berlan, J. and Delmas, H. (1994) **Chemical reactions under ultrasound: discrimination of chemical and physical effects**, *Chemical Engineering Science,* **49**(24B), 5865-5873.

Cook, A.M. (1987) **Biodegradation of *s*-triazine xenobiotics**, *FEMS Microbiology Reviews,* **46**(2), 93-116.

Cook, A.M., Beilstein, P., Grossenbacher, H. and Hütter, R. (1985) **Ring cleavage and degradative pathway of cyanuric acid in bacteria**, *Biochemical Journal,* **231**(1), 25-30.

Cost, M., Mills, G., Glisson, P. and Lakin, J. (1993) **Sonochemical degradation of *p*-nitrophenol in the presence of chemical components of natural waters**, *Chemosphere,* **27**(9), 1737-1743.

Crawford, A.E. (1963) **A practical introduction to ultrasonic cleaning**, *Ultrasonics,* **1**(2), 65-69.

Crum, L.A., Roy, R.A., Dinno, M.A. and Church, C.C. (1992) **Acoustic cavitation produced by microsecond pulses of ultrasound: a discussion of some selected results**, *Journal of the Acoustical Society of America,* **91**(2), 1113-1119.

Crum, L.S. and Reynolds, G.T. (1985) **Sonoluminescence produced by stable cavitation**, *Journal of the Acoustical Society of America,* **78**(1), 137-139.

Currell, D.L. and Zechmeister, L. (1958) **On the ultrasonic cleavage of some aromatic and heterocyclic rings**, *Journal of the American Chemical Society,* **80**(1), 205-208.

Cyr, P.J., Zhang, Q. and Suri, R.P.S. (1998) **Sonochemical destruction of trichloroethylene in water**, *AWT98 - Advanced Wastewater Treatment,* Milan, Italy, 173-179.

Dahi, E. (1976) **Physicochemical aspects of disinfection of water by means of ultrasound and ozone**, *Water Research,* **10**, 677-684.

Danckwerts, P.V. (1970) **Chapter 5. Absorption into agitated liquids**. In *Gas-liquid reactions,* McGraw-Hill, New York, Library of Congress Catalogue Card Number 75-91678, 96-151.

Dao, T.H., Lavy, T.L. and Sorensen, R.C. (1979) **Atrazine degradation and residue distribution in soil**, *Soil Science Society of America Journal,* **43**(6), 1129-1134.

Davidson, R.S., Safdar, A., Spencer, J.D. and Robinson, B. (1987) **Applications of ultrasound to organic chemistry**, *Ultrasonics,* **25**(1), 35-39.

De Laat, J., Berger, P., T Poinot, Karpel vel Leitner, N. and Doré, M. (1997) **Modelling the oxidation of atrazine by H_2O_2/UV. Estimation of kinetic parameters**, *Ozone Science & Engineering,* **19**(5), 395-408.

De Laat, J., Chramosta, N., Doré, M., Suty, H. and Pouillot, M. (1994) **Rate constants for reaction of hydroxyl radicals with some degradation byproducts of atrazine by O_3 or O_3/H_2O_2**, *Environmental Technology,* **15**(5), 419-428.

De Laat, J., Doré, M. and Suty, H. (1995) **Oxidation of *s*-triazines by advanced oxidation processes. Byproducts and kinetic rate constants**, *Revue des Sciences de L'Eau,* **8**(1), 23-42.

de Souza-Barboza, J.C., Pétrier, C. and Luche, J.-L. (1988) **Ultrasound in organic synthesis. 13. Some fundamental aspects of the sonochemical Barbier reaction**, *Journal of Organic Chemistry,* **53**(6), 1212-1218.

de Visscher, A., van Eenoo, P., Drijvers, D. and van Langenhove, H. (1996) **Kinetic model for the sonochemical degradation of monocyclic aromatic compounds in aqueous solution**, *Journal of Physical Chemistry,* **100**(28), 11636-11643.

Degrois, M. and Baldo, P. (1974) **A new electrical hypothesis explaining sonoluminescence, chemical actions and other effects produced in gaseous cavitation**, *Ultrasonics,* **12**(1), 25-28.

Del Duca, M., Yeager, E., Davies, M.O. and Hovorka, F. (1958) **Isotopic techniques in the study of the sonochemical formation of hydrogen peroxide**, *Journal of the Acoustical Society of America,* **30**(4), 301-307.

Delchar, T.A. and Melvin, R.J. (1994) **A calorimeter for ultrasound total power measurements**, *Measurement Science and Technology,* **5**(12), 1533-1537.

Didenko, Y.T., Nastich, D.N., Pugach, S.P., Polovinka, Y.A. and Kvochka, V.I. (1994) **The effect of bulk solution temperature on the intensity and spectra of water sonoluminescence**, *Ultrasonics,* **32**(1), 71-76.

Donaldson, D.J., Farrington, M.D. and Kruus, P. (1979) **Cavitation-induced polymerisation of nitrobenzene**, *Journal of Physical Chemistry,* **83**(24), 3130-3135.

Dries, D., de Corte, B., Liessens, J., Steurbaut, W., Dejonckheere, W. and Verstraete, W. (1987) **Recalcitrance of atrazine at low levels to aerobic and hydrogenotrophic microorganisms**, *Biotechnology Letters,* **9**(11), 811-816.

Duguet, J.P., Bernazeau, F. and Mallevialle, J. (1990) **Removal of atrazine by ozone and ozone-hydrogen peroxide combinations in surface water**, *Ozone Science & Engineering,* **12**(2), 195-197.

Duguet, J.P., Brodard, E., Dussert, B. and Mallevialle, J. (1985) **Improvement in the effectiveness of ozonation of drinking water through the use of hydrogen peroxide**, *Ozone Science & Engineering,* **7**, 21-258.

Dunn, F. (1991) **Ultrasound**, *IEEE Transactions on Education,* **34**(3), 266-268.

DWAF (1997) **National water policy for South Africa, White Paper**, Department of Water Affairs and Forestry, http://www-dwaf.pwv.gov.za/idwaf/Documents/.

DWAF (2000) **Water conservation strategy for the industry, mining and power generation user sector**, Department of Water Affairs and Forestry, http://www-dwaf.pwv.gov.za/idwaf/Documents/.

Eaton, A.D., Clesceri, L.S. and Greenberg, A.E., eds. (1995a) **Section 4500-Cl B. Iodometric method I**. In *Standard Methods for the Examination of Water and Wastewater,* 19th edition, American Public Health Association, Washington DC, ISBN 0-87553-223-3, 4/38-4/39.

Eaton, A.D., Clesceri, L.S. and Greenberg, A.E., eds. (1995b) **Section 4500-O_3 B. Indigo colorimetric method**. In *Standard Methods for the Examination of Water and Wastewater,* 19th edition, American Public Health Association, Washington DC, ISBN 0-87553-223-3, 4/104-4/106.

Ebert, E. and Dumford, S.W. (1976) **Effects of triazine herbicides on the physiology of plants**. In *Residue Reviews,* F.A. Gunther and J.D. Gunther, eds., Springer-Verlag, New York, ISBN 0 387 90222 8, **65**, 1-97.

EHC 22 (1982) **Environmental health criteria 22: ultrasound**, World Health Organisation, ISBN 92-4-154082-6.

Ellgehausen, H., Guth, J.A. and Esser, H.O. (1980) **Factors determining the bioaccumulation potential of pesticides in the individual compartments of aquatic food chains**, *Ecotoxicology and Environmental Safety,* **4**, 134-157.

Él'piner, I.E. (1959) **On the chemical action of ultrasonic waves**, *Soviet Physics - Acoustics,* **5**(2), 135-146.

Él'piner, I.E. (1960) **Ultrasonic luminescence: a survey**, *Soviet Physics - Acoustics,* **6**(1), 1-12.

Emslie, N. (2001) Personal communication, Sasolburg.

Erickson, L.E. and Lee, K.H. (1989) **Degradation of atrazine and related *s*-triazines**, *Critical Reviews in Environmental Control,* **19**(1), 1-14.

Esser, H.O., Dupuis, G., Ebert, E., Marco, G. and Vogel, C. (1975) **Chapter 2. *s*-Triazines**. In *Herbicides: chemistry, degradation and mode of action,* P.C. Kearney and D.D. Kaufman, eds., Marcel Dekker, Inc., New York, ISBN 0-8247-6175-8, **1**, 129-208.

Eul, W., Scherer, G. and Helmling, O. (1991) **Practical applications of hydrogen peroxide for wastewater treatment**, *First International Symposium: Chemical Oxidation, Technology for the 90s,* Nashville, Tennessee, W.W. Eckenfelder, A.R. Bowers and J.A. Roth, eds., 68-77.

Faul, C.F.J. (1996a) **Ultrasound for the treatment of water and industrial effluent**, ESKOM report no. TRR/DS96/ET016.

Faul, C.F.J. (1996b) **Ultrasound for the treatment of water and wastewater, Part 2**, ESKOM report no. TRR/DS96/ET028.

Fischer, C.-H., Hart, E.J. and Henglein, A. (1986a) **H/D isotope exchange in the D_2-H_2O system under the influence of ultrasound**, *Journal of Physical Chemistry,* **90**(2), 222-224.

Fischer, C.-H., Hart, E.J. and Henglein, A. (1986b) **Ultrasonic irradiation of water in the presence of $^{18,18}O_2$: isotope exchange and isotopic distribution of H_2O_2**, *Journal of Physical Chemistry,* **90**(9), 1954-1956.

Flint, E.B. and Suslick, K.S. (1989) **Sonoluminescence from non-aqueous liquids: emission from small molecules**, *Journal of the American Chemical Society,* **111**(18), 6987-6992.

Flint, E.B. and Suslick, K.S. (1991) **The temperature of cavitation**, *Science,* **253**(5026), 1397-1399.

Flisak, F. and Perna, A. (1977) **The influence of ultrasonics on liquid-liquid extraction**, *Ultrasonics,* **15**(1), 27-29.

Floros, J.D. and Liang, H. (1994) **Acoustically assisted diffusion through membranes and biomaterials**, *Food Technology,* **48**(12), 79-84.

Flosdorf, E.W., Chambers, L.A. and Malisoff, W.M. (1936) **Sonic activation in chemical systems: oxidations at audible frequencies**, *Journal of the American Chemical Society,* **58**(4), 1069-1076.

Flynn, H.G. (1982) **Generation of transient cavities in liquids by microsecond pulses of ultrasound**, *Journal of the Acoustical Society of America,* **72**(6), 1926-1932.

Flynn, H.G. and Church, C.C. (1984) **A mechanism for the generation of cavitation maxima by pulsed ultrasound**, *Journal of the Acoustical Society of America,* **76**(2), 505-512.

Foster, D.M., Rachwal, A.J. and White, S.L. (1992) **Advanced treatment for the removal of atrazine and other pesticides**, *Water Supply,* **10**(2), 133-146.

Franck, E.U. (1987) **Fluids at high pressures and temperatures**, *Journal of Chemical Thermodynamics,* **19**(3), 225-242.

Frizzell, L.A. (1988) **Chapter 7. Biological effects of acoustic cavitation**. In *Ultrasound: Its Chemical, Physical and Biological Effects,* K.S. Suslick, ed., VCH Publishers, Inc., New York, ISBN 0-89573-328-5, 287-303.

Galassi, S., Provini, A. and Halfon, E. (1996) **Risk assessment for pesticides and their metabolites in water**, *International Journal of Environmental Analytical Chemistry,* **65**(1-4), 331-344.

Gan, J., Becker, R.L., Koskinen, W.C. and Buhler, D.D. (1996) **Degradation of atrazine in two soils as a function of concentration**, *Journal of Environmental Quality,* **25**(5), 1064-1072.

Gautheron, B., Tainturier, G. and Degrand, C. (1985) **Ultrasound-induced electrochemical synthesis of the anions Se_2^{2-}, Se^{2-}, Te_2^{2-} and Te^{2-}**, *Journal of the American Chemical Society,* **107**(19), 5579-5581.

Gaynor, J.D., MacTavish, D.C. and Findlay, W.I. (1992) **Surface and subsurface transport of atrazine and alachlor from a Brookston clay loam under continuous corn production**, *Archives of Environmental Contamination and Toxicology,* **23**(2), 240-245.

Gaynor, J.D., MacTavish, D.C. and Findlay, W.I. (1995) **Atrazine and metolachlor loss in surface and subsurface runoff from three tillage treatments in corn**, *Journal of Environmental Quality,* **24**(2), 246-256.

GCIS (1999) **Water affairs and forestry**, South Africa Yearbook, http://www.gov.za/yearbook/water.

Gehringer, P., Szinovatz, W., Eschweiler, H. and Haberl, R. (1997) **Oxidative treatment of a wastewater stream from a molasses processing plant using ozone and advanced oxidation technologies**, *Ozone Science & Engineering,* **19**(2), 157-168.

Geller, A. (1980) **Studies on the degradation of atrazine by bacterial communities enriched from various biotopes**, *Archives of Environmental Contamination and Toxicology,* **9**(3), 289-305.

Gericke, G. (1999) **Advanced oxidation processes and the current ESKOM position with respect to the technology**, ESKOM report no. TRR/C99/102.

Giardi, M.T., Giardina, M.C. and Filacchioni, G. (1985) **Chemical and biological degradation of primary metabolites of atrazine by a *Nocardia* strain**, *Agricultural and Biological Chemistry,* **49**(6), 1551-1558.

Giguére, P.A. and Srinivasan, T.K.K. (1977) **The ground-state geometry of the H_2O_2 and D_2O_2 molecules**, *Journal of Molecular Spectroscopy,* **66**(1), 168-170.

Glaze, W.H. (1987) **Drinking-water treatment with ozone**, *Environmental Science and Technology,* **21**(3), 224-230.

Glaze, W.H., Beltrán, F., Tuhkanen, T. and Kang, J.-W. (1992) **Chemical models of advanced oxidation processes**, *Water Pollution Research Journal of Canada,* **27**(1), 23-42.

Glaze, W.H. and Kang, J.-W. (1989a) **Advanced oxidation processes. Description of a kinetic model for the oxidation of hazardous materials in aqueous media with ozone and hydrogen peroxide in a semibatch reactor**, *Industrial and Engineering Chemistry Research,* **28**(11), 1573-1580.

Glaze, W.H. and Kang, J.-W. (1989b) **Advanced oxidation processes. Test of a kinetic model for the oxidation of organic compounds with ozone and hydrogen peroxide in a semibatch reactor**, *Industrial and Engineering Chemistry Research,* **28**(11), 1580-1589.

Glaze, W.H., Kang, J.-W. and Chapin, D.H. (1987) **The chemistry of water treatment processes involving ozone, hydrogen peroxide and ultraviolet radiation**, *Ozone Science & Engineering,* **9**(4), 335-352.

Glaze, W.H., Peyton, G.R., Lin, S., Huang, R.Y. and Burleson, J.L. (1982) **Destruction of pollutants in water with ozone in combination with ultraviolet radiation. Part 2. Natural trihalomethane precursors**, *Environmental Science and Technology,* **16**(8), 454-458.

Glaze, W.H., Schep, R., Chauncey, W., Ruth, E.C., Zarnoch, J.J., Aieta, E.M., Tate, C.H. and McGuire, M.J. (1990) **Evaluating oxidants for the removal of model taste and odour compounds from a municipal water supply**, *Journal of the American Water Works Association,* **82**(5), 79-84.

Gogate, P.G. and Pandit, A.B. (2000) **Engineering design method for cavitational reactors: I. Sonochemical reactors**, *AIChE Journal,* **46**(2), 372-379.

Gomella, C. (1972) **Ozone practices in France**, *Journal of the American Water Works Association,* **64**(1), 39-45.

Gondrexon, N., Renaudinn, V., Bernis, A., Gonthier, Y. and Boldo, P. (1993) **Ultrasonic degradation kinetic study of chlorophenol aqueous solution**, *Environmental Technology,* **14**(6), 587-593.

Gonzalez, M.C. and Mártire, D.O. (1997) **Kinetics of O^- and O^{3-} in alkaline aqueous solutions**, *Water Science and Technology,* **35**(4), 49-55.

Goodwin, T.J. (1990) **Chapter 5. Equipment**. In *Critical Reports on Applied Chemistry: Chemistry with Ultrasound,* T.J. Mason, ed., Elsevier Applied Science, New York, ISBN 1-85166-422-X, **28**, 159-187.

Goswami, S., Ghosh, P.N. and Basumallick, S. (1988) **Measurement of ultrasonic power in liquids - a review**, *Journal of the Institution of Engineers (India). Part ET: Electronics and Telecommunications,* **69**(1), 12-27.

Greenwood, N.N. and Earnshaw, A. (1984a) **Section 14.1.4. Atomic and physical properties of oxygen**. In *Chemistry of the Elements,* Pergamon Press, Oxford, ISBN 0-08-022057-6, 704-707.

Greenwood, N.N. and Earnshaw, A. (1984b) **Section 14.1.5. Other forms of oxygen: ozone**. In *Chemistry of the Elements,* Pergamon Press, Oxford, ISBN 0-08-022057-6, 707-712.

Greenwood, N.N. and Earnshaw, A. (1984c) **Section 14.2.3. Hydrogen peroxide**. In *Chemistry of the Elements,* Pergamon Press, Oxford, ISBN 0-08-022057-6, 742-748.

Grigg, B.C., Assaf, N.A. and Turco, R.F. (1997) **Removal of atrazine contamination in soil and liquid systems using bioaugmentation**, *Pesticide Science,* **50**(3), 211-220.

Grinthal, W. and Ondrey, G. (1992) **Ultrasound seen but not heard**, *Chemical Engineering,* **99**(10), 37-41.

Guillén, M.D., Blanco, J., Canga, J.S. and Blanco, C.G. (1991) **Study of the effectiveness of 27 organic solvents in the extraction of coal tar pitches**, *Energy & Fuels,* **5**(1), 188-192.

Gutiérrez, M., Henglein, A. and Dohrmann, J.K. (1987) **H atom reactions in the sonolysis of aqueous solutions**, *Journal of Physical Chemistry,* **91**(27), 6687-6690.

Gutiérrez, M., Henglein, A. and Ibañez, F. (1991) **Radical scavenging in the sonolysis of aqueous solutions of I^-, Br^-, and N^{3-}**, *Journal of Physical Chemistry,* **95**(15), 6044-6047.

Haag, W.R. and Yao, C.C.D. (1992) **Rate constants for reaction of hydroxyl radicals with several drinking water contaminants**, *Environmental Science and Technology,* **26**(5), 1005-1013.

Haglund, P. (1997) **Advanced ozone technology improves water quality in Nizhny Novgorod, Russia**, *Water and Wastewater International,* **12**(1), 14-17.

Han, B.-H. and Boudjouk, P. (1981) **Organic sonochemistry. Ultrasound-promoted coupling of organic halides in the presence of lithium wire**, *Tetrahedron Letters,* **22**(29), 2757-2758.

Han, B.-H. and Boudjouk, P. (1982a) **Organic sonochemistry. Ultrasound-promoted reaction of zinc with α,α′-dibromo-*o*-xylene. Evidence for facile generation of *o*-xylylene**, *Journal of Organic Chemistry,* **47**(4), 751-752.

Han, B.-H. and Boudjouk, P. (1982b) **Organic sonochemistry. Sonic acceleration of the Reformatsky reaction**, *Journal of Organic Chemistry,* **47**(25), 5030-5032.

Han, B.-H. and Boudjouk, P. (1982c) **Organic sonochemistry. Ultrasonic acceleration of the reduction of simple and deactivated aryl halides using lithium aluminum hydride**, *Tetrahedron Letters,* **23**(16), 1643-1646.

Hapeman, C.J. (1994) **Chapter 14. Oxidation of *s*-triazine pesticides**. In *American Chemical Society Symposium Series: Emerging Technologies in Hazardous Waste Management IV,* D.W. Tedder and F.G. Pohland, eds., American Chemical Society, Washington, DC, ISBN 0-8412-2857-4, **554**, 223-233.

Hapeman, C.J., Karns, J.S. and Shelton, D.R. (1995) **Total mineralisation of aqueous atrazine in the presence of ammonium nitrate using ozone and *Klebsiella terragena* (strain DRS-I): mechanistic considerations for pilot scale disposal**, *Journal of Agricultural and Food Chemistry,* **43**(5), 1383-1391.

Hapeman-Somich, C.J., Gui-Ming, Z., Lusby, W.R., Muldoon, M.T. and Waters, R. (1992) **Aqueous ozonation of atrazine. Product identification and description of the degradation pathway**, *Journal of Agricultural and Food Chemistry,* **40**(11), 2294-2298.

Harcourt, R.D. and Roso, W. (1978) **Valence-bond studies of 4-electron 3-centre bonding units. I. The π-electrons of O_3, NO_2^- and CH_2N_2**, *Canadian Journal of Chemistry,* **56**(8), 1093-1101.

Harcourt, R.D., Skrezenek, F.L., Wilson, R.M. and Flegg, R.H. (1986) ***Ab initio* valence bond calculations for the ground state of ozone**, *Journal of the Chemical Society. Faraday Transactions II,* **82**(4), 495-509.

Hargis, L.G. (1988) **Chapter 11. Oxidation-reduction titrations**. In *Analytical Chemistry: Principles and Techniques,* Prentice-Hall, Inc., Englewood Cliffs, New Jersey, USA, ISBN 0-13-033507-X, 260-299.

Harris, C.I. (1967) **Fate of 2-chloro-*s*-triazine herbicides in soil**, *Journal of Agricultural and Food Chemistry,* **15**(1), 157-162.

Hart, E.J., Fischer, C.-H. and Henglein, A. (1986) **Isotopic exchange in the sonolysis of aqueous solutions containing $^{14,14}N_2$ and $^{15,15}N_2$**, *Journal of Physical Chemistry,* **90**(22), 5989-5991.

Hart, E.J., Fischer, C.-H. and Henglein, A. (1990a) **Pyrolysis of acetylene in sonolytic cavitation bubbles in aqueous solution**, *Journal of Physical Chemistry,* **94**(1), 284-290.

Hart, E.J., Fischer, C.-H. and Henglein, A. (1990b) **Sonolysis of hydrocarbons in aqueous solution**, *Radiation Physics and Chemistry,* **36**(4), 511-516.

Hart, E.J. and Henglein, A. (1985) **Free radical and free atom reactions in the sonolysis of aqueous iodide and formate solutions**, *Journal of Physical Chemistry,* **89**(20), 4342-4347.

Hart, E.J. and Henglein, A. (1986) **Sonolytic decomposition of nitrous oxide in aqueous solution**, *Journal of Physical Chemistry,* **90**(22), 5992-5995.

Hart, E.J. and Henglein, A. (1987) **Sonochemistry of aqueous solutions: H_2-O_2 combustion in cavitation bubbles**, *Journal of Physical Chemistry,* **91**(13), 3654-3656.

Harvey, E.N. (1939) **Sonoluminescence and sonic chemiluminescence**, *Journal of the American Chemical Society,* **61**(9), 2392-2398.

Haverhoek, S., Kroning, J., van Staveren, N.A. and de Ruyter, M.A. (1997) **Advanced treatment of effluents from an agrochemical formulation plant**, *Water Science and Technology,* **35**(10), 155-163.

Henglein, A. (1985) **Sonolysis of carbon dioxide, nitrous oxide and methane in aqueous solution**, *Zeitschrift für Naturforshung.,* **40B**(1), 102-107.

Henglein, A. (1987) **Sonochemistry: historical developments and modern aspects**, *Ultrasonics,* **25**(1), 6-16.

Henglein, A. and Gutiérrez, M. (1988) **Sonolysis of polymers in aqueous solution. New observations on pyrolysis and mechanical degradation**, *Journal of Physical Chemistry,* **92**(13), 3706-3707.

Henglein, A. and Gutiérrez, M. (1993) **Sonochemistry and sonoluminescence: effects of external pressure**, *Journal of Physical Chemistry,* **97**(1), 158-162.

Henglein, A. and Kormann, C. (1985) **Scavenging of HO• radicals produced in the sonolysis of water**, *International Journal of Radiation Biology,* **48**(2), 251-258.

Henglein, A., Ulrich, R. and Lilie, J. (1989) **Luminescence and chemical action by pulsed ultrasound**, *Journal of the American Chemical Society,* **111**(6), 1974-1979.

Hogrefe, W., Grossenbacher, H., Cook, A.M. and Hütter, R. (1985) **Biological treatment specific for an industrial wastewater containing *s*-triazines**, *Biotechnology and Bioengineering,* **27**(9), 1291-1296.

Hogrefe, W., Grossenbacher, H., Cook, A.M. and Hütter, R. (1986) **Biotreatment of *s*-triazine-containing wastewater in a fluidized bed reactor**, *Biotechnology and Bioengineering,* **28**(10), 1577-1581.

Hoigné, J. (1975) **Comparison of the chemical effects of ozone and of irradiation on organic impurities in water**, *Proceedings of the IAEA Symposium,* Munich, 297-305.

Hoigné, J. (1997) **Inter-calibration of HO• radical sources and water quality parameters**, *Water Science and Technology,* **35**(4), 1-8.

Hoigné, J. and Bader, H. (1976) **The role of hydroxyl radical reactions in ozonation processes in aqueous solutions**, *Water Research,* **10**(5), 377-386.

Hoigné, J. and Bader, H. (1983) **Rate constants of reactions of ozone with organic and inorganic compounds in water - Part I**, *Water Research,* **17**(2), 173-183.

Howkins, S.D. (1969) **Diffusion rates and the effect of ultrasound**, *Ultrasonics,* **8**(April), 129-130.

Hoyle, B.S. and Luke, S.P. (1994) **Ultrasound in the process industries**, *Journal of Engineering Science and Education,* **3**(3), 119-122.

Hua, I., Höchemer, R.H. and Hoffmann, M.R. (1995a) **Sonochemical degradation of *p*-nitrophenol in a parallel-plate near-field acoustical processor**, *Environmental Science and Technology,* **29**(11), 2790-2796.

Hua, I., Höchemer, R.H. and Hoffmann, M.R. (1995b) **Sonolytic hydrolysis of *p*-nitrophenyl acetate: the role of supercritical water**, *Journal of Physical Chemistry,* **99**(8), 2335-2342.

Huang, C.M. and Banks, M.K. (1996) **Effect of ozonation on the biodegradability of atrazine in GAC columns**, *Journal of Environmental Science and Health. Part B. Pesticides, Food Contaminants and Agricultural Wastes,* **B31**(6), 1253-1266.

Huang, C.P., Dong, C. and Tang, Z. (1993) **Advanced chemical oxidation: its present role and potential future in hazardous waste treatment**, *Waste Management,* **13**(5-7), 361-377.

Huang, R.L., Gog, S.H. and Ong, S.H. (1974) **Chapter 3. Characteristics of radical reactions**. In *The Chemistry of Free Radicals,* Edward Arnold (Publishers) Ltd., London, ISBN 0 7131 2418 0, 19-44.

Huber, W. (1993) **Ecotoxicological relevance of atrazine in aquatic systems**, *Environmental Toxicology and Chemistry,* **12**(10), 1865-1881.

Hunicke, R.L. (1990) **Industrial applications of high power ultrasound for chemical reactions**, *Ultrasonics,* **28**(5), 291-294.

Hustert, K., Moza, P.N. and Pouyet, B. (1991) **Photocatalytic degradation of *s*-triazine herbicides**, *Toxicological and Environmental Chemistry,* **31-32**, 97-102.

International Critical Tables (1928) Vol. III, McGraw-Hill, New York.

Jennings, B.H. and Townsend, S.N. (1961) **The sonochemical reactions of carbon tetrachloride and chloroform in aqueous suspension in an inert atmosphere**, *Journal of Physical Chemistry,* **65**(9), 1574-1579.

Jessee, J.A., Benoit, R.E., Hendricks, A.C., Allen, G.C. and Neal, J.L. (1983) **Anaerobic degradation of cyanuric acid, cysteine, and atrazine by a facultative anaerobic bacterium**, *Applied and Environmental Microbiology,* **45**(1), 97-102.

Jones, K.H., Sanderson, D.M. and Noakes, D.N. (1968) **Acute toxicity data for pesticides**, *World Review of Pest Control,* **7**(3), 135-143.

Jutzi, K., Cook, A.M. and Hütter, R. (1982) **The degradative pathway of the *s*-triazine melamine**, *Biochemical Journal,* **208**(3), 679-684.

Kang, J.-W., Park, H.-S., Wang, R.-Y., Koga, M., Kadokami, K., Kim, H.-Y., Lee, E.-T. and Oh, S.-M. (1997) **Effect of ozonation for treatment of micropollutants present in drinking water source**, *Water Science and Technology,* **36**(12), 299-307.

Kasrils, R. (2000) Address by the Minister of Water Affairs and Forestry at the National Water Week Celebrations.

Kaufman, D.D. and Kearney, P.C. (1970) **Microbial degradation of *s*-triazine herbicides**. In *Residue Reviews,* F.A. Gunther and J.D. Gunther, eds., Springer-Verlag, New York, Library of Congress Catalogue Card Number 62-18595, **32**, 235-265.

Kearney, P.C., Muldoon, M.T. and Somich, C.J. (1987) **UV-ozonation of eleven major pesticides as a waste disposal pretreatment**, *Chemosphere,* **16**(10-12), 2321-2330.

Kearney, P.C., Muldoon, M.T., Somich, C.J., Ruth, J.M. and Voaden, D.J. (1988) **Biodegradation of ozonated atrazine as a wastewater disposal system**, *Journal of Agricultural and Food Chemistry,* **36**(6), 1301-1306.

Khan, S.U. and Schnitzer, M. (1978) **UV irradiation of atrazine in aqueous fulvic acid solution**, *Journal of Environmental Science and Health. Part B. Pesticides, Food Contaminants and Agricultural Wastes,* **B13**(3), 299-310.

Kidd, M. (1997a) **Chapter 3. The environment and the constitution**. In *Environmental Law. A South African Guide,* Juta & Co, Kenwyn, South Africa, ISBN 0 7021 4204 2, 34-46.

Kidd, M. (1997b) **Chapter 6. Water law and the environment**. In *Environmental Law. A South African Guide,* Juta & Co, Kenwyn, South Africa, ISBN 0 7021 4204 2, 83-101.

Kilpatrick, M.L., Herrick, C.C. and Kilpatrick, M. (1956) **The decomposition of ozone in aqueous solution**, *Journal of the American Chemical Society,* **78**(9), 1784-1789.

Kim, S.J., Oh, K.H., Lee, S.H., Choi, S.S. and Lee, K.C. (1997) **Study on secondary reaction and fate of hazardous chemicals by oxidants**, *Water Science and Technology,* **36**(12), 325-331.

King, R.O. and Forster, C.F. (1990) **Effects of sonication on activated sludge**, *Enzyme and Microbial Technology,* **12**(2), 109-115.

Kirchener, J.R. (1981) **Hydrogen peroxide**. In *Kirk-Othmer Encyclopedia of Chemical Technology,* M. Grayson and D. Eckroth, eds., 3rd edition, John Wiley & Sons, New York, ISBN 0-471-02066-4, **13**, 12-38.

Koga, M., Kadokami, K. and Shinohara, R. (1992) **Laboratory-scale ozonation of water contaminated with trace pesticides**, *Water Science and Technology,* **25**(9-11), 2257-2260.

Koike, T. (1992) **Sonolysis studies of alcohols in aqueous solutions by gaseous products analysis**, *Bulletin of the Chemical Society of Japan,* **65**(11), 3215-3217.

Kondo, T., Kirschenbaum, L.J., Kim, H. and Riesz, P. (1993) **Sonolysis of dimethyl sulfoxide-water mixtures: a spin-trapping study**, *Journal of Physical Chemistry,* **97**(2), 522-527.

Koskinen, W.C., Cheng, H.H., Jarvis, L.J. and Sorenson, B.A. (1995) **Characterization of mechanisms of pesticide retention in soils using the supercritical fluid extraction technique**, *International Journal of Environmental Analytical Chemistry,* **58**(1-4), 379-385.

Koskinen, W.C. and Clay, S.A. (1997) **Factors affecting atrazine fate in North Central US soils**, *Reviews of Environmental Contamination and Toxicology,* **151**, 117-165.

Koskinen, W.C. and Rochette, E.A. (1996) **Atrazine sorption-desorption in field-moist soils**, *International Journal of Environmental Analytical Chemistry,* **65**(1-4), 223-230.

Koskinen, W.C., Sellung, K.E., Baker, J.M., Barber, B.L. and Dowdy, R.H. (1994) **Ultrasonic decomposition of atrazine and alachlor in water**, *Journal of Environmental Science and Health. Part B. Pesticides, Food Contaminants and Agricultural Wastes,* **B29**(3), 581-590.

Kotronarou, A., Mills, G. and Hoffmann, M.R. (1991) **Ultrasonic irradiation of *p*-nitrophenol in aqueous solution**, *Journal of Physical Chemistry,* **95**(9), 3630-3638.

Kotronarou, A., Mills, G. and Hoffmann, M.R. (1992a) **Decomposition of parathion in aqueous solution by ultrasonic irradiation**, *Environmental Science and Technology,* **26**(7), 1460-1462.

Kotronarou, A., Mills, G. and Hoffmann, M.R. (1992b) **Oxidation of hydrogen sulfide in aqueous solution by ultrasonic irradiation**, *Environmental Science and Technology,* **26**(12), 2420-2428.

Koubek, E., Hagget, M.L., Battaglia, C.J., Ibne-Rasa, K.M., Pyun, H.Y. and Edwards, J.O. (1963) **Kinetics and mechanism of the spontaneous decompositions of some peroxoacids, hydrogen peroxide and *t*-butyl hydroperoxide**, *Journal of the American Chemical Society,* **85**(15), 2263-2268.

Krishna, C.M., Kondo, T. and Riesz, P. (1989) **Sonochemistry of alcohol-water mixtures: spin-trapping evidence for thermal decomposition and isotope-exchange reactions**, *Journal of Physical Chemistry,* **93**(13), R66-5172.

Krishna, C.M., Lion, Y., Kondo, T. and Riesz, P. (1987) **Thermal decomposition of methanol in the sonolysis of methanol-water mixtures. Spin-trapping evidence for isotope exchange reactions**, *Journal of Physical Chemistry,* **91**(23), 5847-5850.

Kristol, D.S., Klotz, H. and Parker, R.C. (1981) **The effect of ultrasound on the alkaline hydrolysis of nitrophenyl esters**, *Tetrahedron Letters,* **22**(10), 907-908.

Kruger, E.L., Rice, P.J., Anhalt, J.C., Anderson, T.A. and Coats, J.R. (1997) **Comparative fates of atrazine and deethylatrazine in sterile and non-sterile soils**, *Journal of Environmental Quality,* **26**(1), 95-101.

Kruger, E.L., Zhu, B. and Coats, J.R. (1996) **Relative mobilities of atrazine, five atrazine degradates, metolachlor and simazine in soils of Iowa**, *Environmental Toxicology and Chemistry,* **15**(5), 691-695.

Kruus, P., Lawrie, J.A.G. and O'Neill, M.L. (1988) **Polymerisation and depolymerisation by ultrasound**, *Ultrasonics,* **26**(6), 352-355.

Krzesinska, M. and Pajak, J. (1988) **Application of ultrasonic measurements to the determination of concentration of coal extracts**, *Fuel Processing Technology,* **19**(3), 229-233.

Kuo, J.-F. and Mou, L. (1997) **Disinfection and antimicrobial processes**, *Water Environment Research,* **69**(4), 526-534.

Kyle, B. (1995) *Successful Industrial Experimentation,* VCH Publishers, New York, ISBN 1-56081-050-5.

Laburn, R.J. (1995) **Water supply in South Africa**, *Journal of Water Supply Research and Technology - Aqua,* **44**(4), 161-165.

Lambert, S.D., Graham, N.J.D. and Croll, B.T. (1996) **Degradation of selected herbicides in a lowland surface water by ozone and ozone-hydrogen peroxide**, *Ozone Science & Engineering,* **18**(3), 251-269.

Lamoureux, G.L., Stafford, L.E. and Shimabukuro, R.H. (1972) **Conjugation of 2-chloro-4,6-bis(alkylamino)-*s*-triazines in higher plants**, *Journal of Agricultural and Food Chemistry,* **20**(5), 1004-1010.

Lavy, T.L., Roeth, F.W. and Fenster, C.R. (1973) **Degradation of 2,4-D and atrazine at three soil depths in the field**, *Journal of Environmental Quality,* **2**(1), 132-137.

Leclercq, P.A. and Pacáková, V. (1979) **Gas chromatrography and mass spectrometry of bis(alkylamino)-*s*-triazines**, *Journal of Chromatography,* **178**(1), 193-207.

Leeman, S. and Vaughan, P.W. (1992) **Cavitation phenomena**. In *Current Trends in Sonochemistry,* G.J. Price, ed., Royal Society of Chemistry, Cambridge, ISBN 0-85186-365-5, .

Leeson, A., Hapeman, C.J. and Shelton, D.R. (1993) **Biomineralisation of atrazine ozonation products. Application to the development of a pesticide waste disposal system**, *Journal of Agricultural and Food Chemistry,* **41**(6), 983-987.

Legube, B., Guyon, S. and Doré, M. (1987) **Ozonation of aqueous solutions of nitrogen heterocyclic compounds: benzotriazoles, atrazine and amitrole**, *Ozone Science & Engineering,* **9**(3), 233-246.

Lenart, I. and Ausländer, D. (1980) **The effect of ultrasound on diffusion through membranes**, *Ultrasonics,* **18**(5), 216-218.

Liakou, S., Pavlou, S. and Lyberatos, G. (1997) **Ozonation of azo dyes**, *Water Science and Technology,* **35**(4), 279-286.

Lii, R.-R., Gorse, R.A., Sauer, M.C. and Gordon, S. (1980) **Rate constant for the reaction of $HO^{\bullet}$ with $HOO^{\bullet}$**, *Journal of Physical Chemistry,* **84**(8), 819-821.

Lillard, H.S. (1994) **Decontamination of poultry skin by sonication**, *Food Technology,* **48**(12), 72-73.

Lin, J.-G., Chang, C.-N., Wu, J.-R. and Ma, Y.-S. (1996) **Enhancement of decomposition of 2-chlorophenol with ultrasound/H_2O_2 process**, *Water Science and Technology,* **34**(9), 41-48.

Lindley, J., Lorimer, J.P. and Mason, T.J. (1986) **Enhancement of an Ullmann coupling reaction induced by ultrasound**, *Ultrasonics,* **24**(5), 292-293.

Lindley, J., Lorimer, J.P. and Mason, T.J. (1987) **Sonochemically enhanced Ullmann reactions**, *Ultrasonics,* **25**(1), 45-48.

Liu, S.-C. and Wu, H. (1934) **Mechanism of oxidation promoted by ultrasonic radiation**, *Journal of the American Chemical Society,* **56**(5), 1005-1007.

Loosli, R. (1995) **Epidemiology of atrazine**, *Reviews of Environmental Contamination and Toxicology,* **143**, 47-57.

Lorimer, J.P. (1990) **Chapter 4. Polymers**. In *Critical Reports on Applied Chemistry: Chemistry with Ultrasound,* T.J. Mason, ed., Elsevier Applied Science, New York, ISBN 1-85166-422-X, **28**, 115-157.

Lorimer, J.P., Mason, T.J. and Fiddy, K. (1991) **Enhancement of chemical reactivity by power ultrasound: an alternative interpretation of the hot spot**, *Ultrasonics,* **29**(4), 338-343.

Luche, J.L. (1992) **Developments of the new 'experimental theory' of sonochemistry initiated in Grenoble**, *Ultrasonics,* **30**(3), 156-162.

Luche, J.L. and Damiano, J.-C. (1980) **Ultrasound in organic synthesis. 1. Effect of the formation of lithium organometallic reagents**, *Journal of the American Chemical Society,* **102**(27), 7926-7927.

Luche, J.L., Einhorn, C., Einhorn, J., de Souza-Barboza, J.C., Pétrier, C., Dupuy, C., Delair, P., Allavena, C. and Tuschl, T. (1990) **Ultrasonic waves as promoters of radical processes in chemistry: the case of organometallic reactions**, *Ultrasonics,* **28**(5), 316-321.

Lykins, B.W. and Koffskey, W. (1986) **Products identified at an alternative disinfection pilot plant**, *Environmental Health Perspectives,* **69**, 119-127.

Lykins, B.W., Koffskey, W.E. and Miller, R.G. (1986) **Chemical products and toxicologic effects of disinfection**, *Journal of the American Water Works Association,* **78**(11), 66-75.

Makino, K., Mossoba, M.M. and Riesz, P. (1982) **Chemical effects of ultrasound on aqueous solutions. Evidence for HO$^{\bullet}$ and H$^{\bullet}$ by spin trapping**, *Journal of the American Chemical Society,* **104**(12), 3537-3539.

Makino, K., Mossoba, M.M. and Riesz, P. (1983) **Chemical effects of ultrasound on aqueous solutions. Formation of hydroxyl radicals and hydrogen atoms**, *Journal of Physical Chemistry,* **87**(8), 1369-1377.

Manly, T.D. (1962) **Hydrogen peroxide and other peroxides in chemical manufacture**, *Chemistry & Industry,* (1), 12-18.

Marco, A., Esplugas, S. and Saum, G. (1997) **How and why combine chemical and biological processes for wastewater treatment**, *Water Science and Technology,* **35**(4), 321-327.

Margulis, M.A. (1969) **Sonoluminescence and ultrasonic chemical reactions**, *Soviet Physics - Acoustics,* **15**(2), 135-151.

Margulis, M.A. (1985) **Sonoluminescence and sonochemical reactions in cavitation fields. A review**, *Ultrasonics,* **23**(4), 157-169.

Margulis, M.A. (1992) **Fundamental aspects of sonochemistry**, *Ultrasonics,* **30**(3), 152-255.

Martin, N. and Galey, C. (1994) **Use of static mixer for oxidation and disinfection by ozone**, *Ozone Science & Engineering,* **16**(6), 455-473.

Martin, P.D. (1992) **Sonochemistry: a chemical engineer's view**. In *Current Trends in Sonochemistry,* G.J. Price, ed., Royal Society of Chemistry, Cambridge, ISBN 0-85186-365-5, .

Martin, P.D. (1993) **Sonochemistry in industry: progress and prospects**, *Chemistry & Industry,* (7), 233-236.

Martin, P.D. and Ward, L.D. (1992) **Reactor design for sonochemical engineering**, *Transactions of the Institute of Chemical Engineering,* **70**(A), 296-303.

Mason, T.J. (1990) **Chapter 1. Introduction**. In *Critical Reports on Applied Chemistry: Chemistry with Ultrasound,* T.J. Mason, ed., Elsevier Applied Science, New York, ISBN 1-85166-422-X, **28**, 1-25.

Mason, T.J. (1991) **Chapter X**. In *Practical Sonochemistry: User's Guide to Applications in Chemistry and Chemical Engineering,* Ellis Horwood, New York, ISBN 0-13-682642-3.

Mason, T.J. (1992) **Industrial sonochemistry: potential and practicality**, *Ultrasonics,* **30**(3), 192-196.

Mason, T.J. (1993) **Sonochemistry: a technology for tomorrow**, *Chemistry & Industry,* (2), 47-50.

Mason, T.J. and Berlan, J. (1992) **Ultrasound in industrial processes. The problems of scale-up**. In *Current Trends in Sonochemistry,* G.J. Price, ed., Royal Society of Chemistry, Cambridge, ISBN 0-85186-365-5, 148-157.

Mason, T.J. and Cordemans de Meulenaer, E. (1998) **Chapter 8. Practical considerations for process optimization**. In *Synthetic Organic Sonochemistry,* J.-L. Luche, ed., Plenum Publishers, New York, , 301-329.

Mason, T.J. and Cordemans, E.D. (1996) **Ultrasonic intensification of chemical processing and related operations: a review**, *Transactions of the Institute of Chemical Engineering,* **74**(A), 511-516.

Mason, T.J., Lorimer, J.P. and Bates, D.M. (1992) **Quantifying sonochemistry: casting some light on a 'black art'**, *Ultrasonics,* **30**(1), 40-42.

Mason, T.J., Lorimer, J.P. and Mistry, B.P. (1985) **The effect of ultrasound on the solvolysis of 2-chloro-2-methylpropane in aqueous ethanol**, *Tetrahedron,* **41**(22), 5201-5204.

Mason, T.J., Lorimer, J.P. and Walton, D.J. (1990) **Sonoelectrochemistry**, *Ultrasonics,* **28**(5), 333-337.

Mason, T.J., Newman, A.P. and Phull, S.S. (1993) **Sonochemistry in water treatment**, *Proceedings of the 2nd International Conference on Advances in Water and Effluent Treatment,* M.J.D. White, ed., 243-250.

Mason, T.J., Newman, A.P., Phull, S.S., Pollet, B. and Hutt, K.R. (1994) **The use of ultrasound to enhance water treatment**, *Proceedings of Hydrotop '94,* Colloque Mieux Gere L'Eau, **2**, 508-515.

Mason, W.P. (1976) **Sonics and ultrasonics: early history and applications**, *IEEE Transactions on Sonics and Ultrasonics,* **SU-23**(4), 224-232.

Masten, S.J. and Davies, S.H.R. (1994) **The use of ozonation to degrade organic contaminants in wastewaters**, *Environmental Science and Technology,* **28**(4), 180-185.

Masten, S.J., Galbraith, M.J. and Davies, S.H.R. (1997) **Oxidation of 1,3,5-trichlorobenzene using advanced oxidation processes**, *Ozone Science & Engineering,* **18**(6), 535-547.

Matturro, M.G., Liotta, R. and Reynolds, R.P. (1990) **Ultrasonically enhanced coal extraction: use of base-solvent swollen coal slurries**, *Energy & Fuels,* **4**(4), 346-351.

Mead, E.L., Sutherland, R.G. and Verrall, R.E. (1975) **The ultrasonic degradation of thymine**, *Canadian Journal of Chemistry,* **53**(16), 2394-2399.

Mead, E.L., Sutherland, R.G. and Verrall, R.E. (1976) **The effect of ultrasound on water in the presence of dissolved gases**, *Canadian Journal of Chemistry,* **54**, 1114-1120.

Meakins, N.C., Bubb, J.M. and Lester, J.N. (1994) **The behaviour of the *s*-triazine herbicides, atrazine and simazine, during primary and secondary biological waste water treatment**, *Chemosphere,* **28**(9), 1611-1622.

Meijers, R.T., Oderwald-Muller, E.J., Nuhn, P.A.N.M. and Kruithof, J.C. (1995) **Degradation of pesticides by ozonation and advanced oxidation**, *Ozone Science & Engineering,* **17**(6), 673-686.

Meijers, R.T., van der Veer, A.J. and Kruithof, J.C. (1993) **Degradation of pesticides by ozonation and advanced oxidation**, *Water Supply,* **11**(3-4), 309-320.

Miller, J.L., Wollum, A.G. and Weber, J.B. (1997) **Degradation of carbon-14-atrazine and carbon-14-metolachlor in soil from four depths**, *Journal of Environmental Quality,* **26**(3), 633-638.

Miller, N. (1950) **Chemical action of sound waves on aqueous solutions**, *Transactions of the Faraday Society,* **45**, 546-550.

Mirgain, I., Green, G.A. and Monteil, H. (1993) **Degradation of atrazine in laboratory microcosms: isolation and identification of the biodegrading bacteria**, *Environmental Toxicology and Chemistry,* **12**(9), 1627-1634.

Mirgain, I., Green, G.A. and Monteil, H. (1995) **Biodegradation of the herbicide atrazine in groundwater under laboratory conditions**, *Environmental Technology,* **16**(10), 967-976.

Misík, V., Miyoshi, N. and Riesz, P. (1995) **EPR spin-trapping study of the sonolysis of H_2O/D_2O mixtures: probing the temperatures of cavitation regions**, *Journal of Physical Chemistry,* **99**(11), 3605-3611.

Montiel, A. and Welté, B. (1992) **Alternative options for atrazine: incidence on water treatment device**, *Water Science and Technology,* **25**(11), 103-110.

Morooka, S., Ikemizu, K. and Kato, Y. (1979) **The decomposition of ozone in aqueous solution**, *International Chemical Engineering,* **19**(4), 650-654.

Muller, M. (2000) **Inter-basin water sharing to achieve water security - a South African perspective**, *Proceedings of the World Water Forum*.

Munter, R., Preis, S., Kamenev, S. and Siirde, E. (1993) **Methodology of ozone introduction into water and wastewater treatment**, *Ozone Science & Engineering,* **15**(2), 149-165.

Nadezhdin, A.D. (1988) **Mechanism of ozone decomposition in water. The role of termination**, *Industrial and Engineering Chemistry Research,* **24**(4), 548-550.

Naicker, S. (1999) **The extraction and quantification of triazine herbicides using high performance liquid chromatography-ultra violet diode array detector**. B.Tech dissertation, ML Sultan Technikon, Durban.

NCRP 74 (1983) **Biological effects of ultrasound: mechanisms and clinical implications**, National Council on Radiation Protection and Measurements, ISBN 0-913392-64-2.

Nebel, C. (1981) **Ozone**. In *Kirk-Othmer Encyclopedia of Chemical Technology,* M. Grayson and D. Eckroth, eds., 3rd edition, John Wiley & Sons, New York, ISBN 0-471-02069-9, **16**, 683-713.

Neis, U. (2000) **Ultrasound in water, wastewater and sludge treatment**, *Water21,* (April), 36-39.

Nélieu, S., Kerhoas, L. and Einhorn, J. (1996) **Atrazine degradation by ozonation in the presence of methanol as scavenger**, *International Journal of Environmental Analytical Chemistry,* **65**(1-4), 297-311.

Neppiras, E.A. (1980) **Acoustic cavitation**, *Physics Reports,* **61**(3), 159-251.

Neppiras, E.A. (1984) **Acoustic cavitation: an introduction**, *Ultrasonics,* **22**(1), 25-28.

Neppiras, E.A. and Fill, E.E. (1969) **A cyclic cavitation process**, *Journal of the Acoustical Society of America,* **46**(5), 1264-1271.

Nick, K., Schöler, H.F., Mark, G., Söylemez, T., Akhlaq, M.S., Schuchmann, H.-P. and von Sonntag, C. (1992) **Degradation of some triazine herbicides by UV radiation such as used in the UV disinfection of drinking water**, *Journal of Water Supply Research and Technology - Aqua,* **41**(2), 82-87.

Niemczewski, B. (1980) **A comparison of ultrasonic cavitation intensity in liquids**, *Ultrasonics,* **18**(3), 107-110.

Noltingk, B.E. and Neppiras, E.A. (1950) **Cavitation produced by ultrasonics**, *Proceedings of the Physical Society of London,* Section B, **63**, 674-685.

Nsabimana, E., Bohatier, J., Belan, A., Pepin, D. and Charles, L. (1996) **Effects of the herbicide atrazine on the activated sludge process: microbiology and functional views**, *Chemosphere,* **33**(3), 479-494.

Numachi, F. (1965) **An experimental study of accelerated cavitation induced by ultrasonics**, *Journal of Basic Engineering,* (December), 967-976.

O'Keeffe, J.H., Uys, M. and Bruton, M.N. (1992) **Chapter 13. Freshwater systems**. In *Environmental Management in South Africa,* R.F. Fuggle and M.A. Rabie, eds., Juta and Company, Cape Town, ISBN 0-7021-2847-3, 277-315.

Olson, H.G. and Hammitt, F.G. (1969) **High-speed photographic studies of ultrasonically induced cavitation**, *Journal of the Acoustical Society of America,* **46**(5), 1272-1283.

Olson, T.M. and Barbier, P.F. (1994) **Oxidation kinetics of natural organic matter by sonolysis and ozone**, *Water Research,* **28**(6), 1383-1394.

Öner, E., Baser, I. and Acar, K. (1995) **Use of ultrasonic energy in reactive dyeing of cellulosic fabrics**, *Journal of the Society of Dyers and Colourists,* **111**(9), 279-281.

Orlandini, E., Gebereselassie, T.G., Kruithof, J.C. and Schippers, J.C. (1997) **Effect of ozonation on preloading of background organic matter in granular activated carbon filters**, *Water Science and Technology,* **35**(7), 295-302.

Orlandini, E., Siebel, M.A., Graveland, A. and Schippers, J.C. (1996) **Pesticide removal by combined ozonation and granular activated carbon filtration**, *Water Supply,* **14**(2), 99-108.

Orzechowska, G.E., Poziomek, E.J., Hodge, V.F. and Engelmann, W.H. (1995) **Use of sonochemistry in monitoring chlorinated hydrocarbons in water**, *Environmental Science and Technology,* **29**(5), 1373-1379.

Paillard, H., Legube, B., Allemane, E. and Doré, M. (1991) **Oxidation of atrazine and simazine by combined ozone/hydrogen peroxide process**, *Proceedings of the Water Quality Technology Conference,* Orlando, Florida, **1**, 609-622.

Pakiari, A.H. and Linnett, J.W. (1975) **Applications of a simple molecular wavefunction. Part 9. Floating spherical Gaussian orbital calculation for hydrogen peroxide**, *Journal of the Chemical Society. Faraday Transactions II,* **71**(9), 1590-1594.

Pandit, A.B. and Moholkar, V.S. (1996) **Harness cavitation to improve processing**, *Chemical Engineering Progress,* **92**(7), 57-69.

Pape, B.E. and Zabik, M.J. (1970) **Photochemistry of bioactive compounds. Photochemistry of selected 2-chloro- and 2-methylthio-4,6-di(alkylamino)-*s*-triazine herbicides**, *Journal of Agricultural and Food Chemistry,* **18**(2), 202-207.

Paris, D.F. and Lewis, D.L. (1973) **Chemical and microbial degradation of ten selected pesticides in aquatic systems**, *Residue Reviews,* **45**, 95-124.

Parke, A.V.M. and Taylor, D. (1956) **The chemical action of ultrasonic waves**, *Journal of the Chemical Society. Part IV,* (855), 4442-4450.

Pavia, D.L., Lampman, G.M. and Kriz, G.S. (1979) **Chapter 6. Mass spectrometry**. In *Introduction to Spectroscopy,* Saunders College Publishing, Philadelphia, ISBN 0-7216-7119-5, 225-299.

Payne, P.A. (1994) **Ultrasonic transducers: design, construction and applications**, *International Journal of Materials and Product Technology,* **9**(4-6), 403-427.

Peleg, M. (1976) **The chemistry of ozone in the treatment of water**, *Water Research,* **10**(5), 361-365.

Pelizzetti, E., Carlin, V., Maurino, V., Minero, C., Dolci, M. and Marchesini, A. (1990) **Degradation of atrazine in soil through induced photocatalytic processes**, *Soil Science,* **150**(2), 523-526.

Pelizzetti, E., Minero, C., Pramauro, E., Barbeni, M., Maurino, V. and Tosato, M. (1987) **Photocatalytic degradation of atrazine at ppb levels under solar light and in the presence of TiO_2 particles**, *Chimica e l'industria,* **69**(10), 88-89.

Perkins, J.P. (1990) **Chapter 4. Power ultrasound**. In *Sonochemistry: The Uses of Ultrasound in Chemistry,* T.J. Mason, ed., Royal Society of Chemistry, Cambridge, ISBN 0-85186-293-4.

Perkins, J.P. (1997a) Personal communication: fax dated 13 May 1997.

Perkins, J.P. (1997b) Personal communication: fax dated 30 June 1997.

Perkowski, J., Kos, L. and Ledakowicz, S. (1996) **Application of ozone in textile wastewater treatment**, *Ozone Science & Engineering,* **18**(1), 73-85.

Pestman, J.M., Engberts, J.B.F.N. and de Jong, F. (1994) **Sonochemistry: theory and applications**, *Journal of the Royal Netherlands Society,* **113**(12), 533-542.

Pétrier, C., David, B. and Laguian, S. (1996) **Ultrasonic degradation at 20 and 500 kHz of atrazine and pentachlorophenol in aqueous solution: preliminary results**, *Chemosphere,* **32**(9), 1709-1718.

Pétrier, C. and Francony, A. (1997) **Incidence of wave-frequency on the reaction rates during ultrasonic wastewater treatment**, *Water Science and Technology,* **35**(4), 175-180.

Pétrier, C., Jeunet, A., Luche, J.-L. and Reverdy, G. (1992) **Unexpected frequency effects on the rate of oxidative processes induced by ultrasound**, *Journal of the American Chemical Society,* **114**(8), 3148-3150.

Pétrier, C., Lamy, M.-F., Francony, A., Benahcene, A. and David, B. (1994) **Sonochemical degradation of phenol in dilute aqueous solutions: comparison of reaction rates at 20 and 487 kHz**, *Journal of Physical Chemistry,* **98**(41), 10514-10520.

Pétrier, C., Micolle, M., Merlin, G., Luche, J.-L. and Reverdy, G. (1992) **Characteristics of pentachlorophenate degradation in aqueous solution by means of ultrasound**, *Environmental Science and Technology,* **26**(6), 1639-1642.

Peyton, G.R. (1990) **Chapter 14. Oxidative treatment methods for removal of organic compounds from drinking water supplies**. In *Significance and Treatment of Volatile Organic Compounds in Water Supplies,* N.M. Ram, R.F. Christman and K.P. Cantor, eds., Lewis Publishers Inc., Chelsea, Michigan, ISBN 0-87371-123-8, 313-362.

Peyton, G.R., Huang, F.Y., Burleson, J.L. and Glaze, W.H. (1982) **Destruction of pollutants in water with ozone in combination with ultraviolet radiation. Part 1. General principles and oxidation of tetrachloroethylene**, *Environmental Science and Technology,* **16**(8), 448-453.

Podolske, J.R. and Johnston, H.S. (1983) **Rate of the resonant energy-transfer reaction between $O_2(^1\Delta_g)$ and $HOO^\bullet$**, *Journal of Physical Chemistry,* **87**(4), 628-634.

Povey, M.J.W. (1989) **Ultrasonics in Food Engineering. Part II. Applications**, *Journal of Food Engineering,* **9**(1), 1-20.

Prados, M., Paillard, H. and Roche, P. (1995) **Hydroxyl radical oxidation processes for the removal of triazine from natural water**, *Ozone Science & Engineering,* **17**(2), 183-194.

Prasad Naidu, D.V., Rajan, R., Kumar, R., Gandhi, K.S., Arakeri, V.H. and Chandrasekaran, S. (1994) **Modelling of a batch sonochemical reactor**, *Chemical Engineering Science,* **49**(6), 877-888.

Price, G.J. (1993) **Applications of high intensity ultrasound in polymer chemistry**, *Chemistry & Industry,* (3), 75-78.

Price, G.J. and Lenz, E.J. (1993) **The use of dosimeters to measure radical production in aqueous sonochemical systems**, *Ultrasonics,* **31**(6), 451-456.

Price, G.J., Matthias, P. and Lenz, E.J. (1994) **The use of high power ultrasound for the destruction of aromatic compounds in aqueous solution**, *Process Safety and Environmental Protection. Transactions of the Institution of Chemical Engineers,* **72**(B1), 27-31.

Price, G.J. and Smith, P.F. (1993) **Ultrasonic degradation of polymer solutions. 2. The effect of temperature, ultrasound intensity and dissolved gases on polystyrene in toluene**, *Ultrasonics,* **34**(9), 4111-4117.

Price, G.J., Smith, P.F. and West, P.J. (1991) **Ultrasonically initiated polymerisation of methyl methacrylate**, *Ultrasonics,* **29**(3), 166-170.

Pryor, M.J. and Freese, S.D. (2000) **The treatment of eutrophic water using pre- and intermediate ozonation, peroxone and pica carbon**, WRC report no. 694/1/00, ISBN 1 86845 588 2.

Pugin, B. (1987) **Qualitative characterization of ultrasound reactors for heterogeneous sonochemistry**, *Ultrasonics,* **25**(1), 49-55.

Qiao, X., Ma, L. and Hummel, H.E. (1996) **Persistence of atrazine and occurrence of its primary metabolites in three soils**, *Journal of Agricultural and Food Chemistry,* **44**(9), 2846-2848.

Quibell, G., van Vliet, H. and van der Merwe, W. (1997) **Characterising cause-and-effect relationships in support of catchment water quality management**, *Water SA,* **23**(3), 193-199.

Rabie, M.A. and Day, J.A. (1992) **Chapter 25. Rivers**. In *Environmental Management in South Africa,* R.F. Fuggle and M.A. Rabie, eds., Juta and Company, Cape Town, ISBN 0-7021-2847-3, 647-668.

Rachwal, A.J., Foster, D.M. and Holmes, M. (1992) **Combining ozone/advanced oxidation and biological filtration processes for organics removal from water**, *Proceedings of the Water Quality Technology Conference,* Toronto, Ontario, **1**, 542-560.

Rassokhin, D.N., Gokzhaev, M.B., Bugaenko, L.T. and Kovalev, G.V. (1994) **Sonolysis of aqueous solutions under argon: dependence of the rate of hydrogen peroxide formation on hydroxyl radical scavenger concentration**, *Mendeleev Communications*, 25-27.

Rassokhin, D.N., Kovalev, G.V. and Bugaenko, L.T. (1995) **Temperature effect on the sonolysis of methanol/water mixtures**, *Journal of the American Chemical Society,* **117**(1), 344-347.

Ratoarinoro, N., Contamine, F., Wilhelm, A.M., Berlan, J. and Delmas, H. (1995) **Activation of solid-liquid chemical reaction by ultrasound**, *Chemical Engineering Science,* **50**(3), 554-558.

Ratoarinoro, N., Wilhelm, A.M., Berlan, J. and Delmas, H. (1992) **Effects of ultrasound emitter type and power on a heterogeneous reaction**, *Chemical Engineering Journal,* **50**(1), 27-31.

Raveton, M., Ravanel, P., Kaouadji, M., Bastide, J. and Tissut, M. (1997a) **The chemical transformation of atrazine in corn seedlings**, *Pesticide Biochemistry and Physiology,* **58**(3), 199-208.

Raveton, M., Ravanel, P., Serre, A.M., Nurit, F. and Tissut, M. (1997b) **Kinetics of uptake and metabolism of atrazine in model plant systems**, *Pesticide Science,* **49**(2), 157-163.

Reimers, R.S., deKernion, P.S. and Leftwich, D.B. (1979) **Sonics and electrostatics - an innovative approach to water and waste treatment**, *Proceedings of the Water Reuse Symposium,* **2**, 1390-1416.

Reisse, J., Francois, H., Vandercammen, J., Fabre, O., Kirsch-de Mesmaeker, A., Maerschalk, C. and Delplancke, J.-L. (1994) **Sonoelectrochemistry in aqueous electrolyte: a new type of sonoelectroreactor**, *Electrochimica Acta,* **39**(1), 37-39.

Rice, R.G. (1997) **Applications of ozone for industrial wastewater treatment: a review**, *Ozone Science & Engineering,* **18**(6), 477-515.

Richards, W.T. and Loomis, A.L. (1927) **The chemical effects of high frequency sound waves. I. A preliminary survey**, *Journal of the American Chemical Society,* **49**(12), 3086-3100.

Rieke, R.D. and Rhyne, L.D. (1979) **Preparation of highly reactive metal powders. Activated copper and uranium. The Ullmann coupling and preparation of organometallic species**, *Journal of Organic Chemistry,* **44**(19), 3445-3446.

Riesz, P. and Kondo, T. (1992) **Free radical formation induced by ultrasound and its biological implications**, *Free Radical Biology and Medicine,* **13**(3), 247-270.

Riesz, P., Kondo, T. and Krishna, C.M. (1990a) **Free radical formation by ultrasound in aqueous solutions. A spin trapping study**, *Free Radical Research Communications,* **10**(1-2), 27-35.

Riesz, P., Kondo, T. and Krishna, C.M. (1990b) **Sonochemistry of volatile and non-volatile solutes in aqueous solutions: e.p.r. and spin trapping studies**, *Ultrasonics,* **28**(5), 295-303.

Roberts, R.T. (1993) **High intensity ultrasonics in food processing**, *Chemistry & Industry,* (4), 119-121.

Robinson, S.F. and Monsen, R.M. (1991) **Hydrogen peroxide and environmental immediate response**, *First International Symposium: Chemical Oxidation, Technology for the 90s,* Nashville, Tennessee, W.W. Eckenfelder, A.R. Bowers and J.A. Roth, eds., 51-67.

Roche, P. and Prados, M. (1995) **Removal of pesticides by use of ozone or hydrogen peroxide/ozone**, *Ozone Science & Engineering,* **17**(6), 657-672.

Roche, P., Volk, C., Carbonnier, F. and Paillard, H. (1994) **Water oxidation by ozone or ozone/hydrogen peroxide using the "ozotest" or "peroxotest" methods**, *Ozone Science & Engineering,* **16**(2), 135-155.

Rocke, A.J. (1994) **Schönbein's chemical goddess**, *Chemistry & Industry,* (21), 871.

Rodriguez, C.J. and Harkin, J.M. (1997) **Degradation of atrazine in subsoils, and groundwater mixed with aquifer sediments**, *Bulletin of Environmental Contamination and Toxicology,* **59**(5), 728-735.

Roi, N.A. (1957) **The initiation and development of ultrasonic cavitation**, *Soviet Physics - Acoustics,* **3**(1), 1-16.

Rooney, J.A. (1988) **Chapter 2. Other non-linear acoustic phenomena**. In *Ultrasound: Its Chemical, Physical and Biological Effects,* K.S. Suslick, ed., VCH Publishers, Inc., New York, ISBN 0-89573-328-5, 65-96.

Rosen, H.M. (1973) **Use of ozone and oxygen in advanced wastewater treatment**, *Journal of the Water Pollution Control Federation,* **45**(12), 2521-2536.

RSA (1996) **The Constitution of the Republic of South Africa**, ISBN 0-620-20214-9.

Ruppert, G., Bauer, R. and Heisler, G. (1994) **UV-O_3, UV-H_2O_2, UV-TiO_2 and the photo-Fenton reaction: comparison of advanced oxidation processes for wastewater treatment**, *Chemosphere,* **28**(8), 1447-1454.

Sadeghi, K.M., Lin, J.-R. and Yen, T.F. (1994) **Sonochemical treatment of fossil fuels**, *Energy Sources,* **16**(3), 439-449.

Sakai, Y., Sadaoka, Y. and Takamaru, Y. (1977) **Decomposition of chloral hydrate in aqueous solution by the action of ultrasound**, *Journal of Physical Chemistry,* **81**(6), 509-511.

Saksena, T.K. and Nyborg, W.L. (1970) **Sonoluminescence from stable cavitation**, *Journal of Chemical Physics,* **53**(5), 1722-1734.

Schmitt, F.O., Johnson, C.H. and Olson, A.R. (1929) **Oxidations promoted by ultrasonic radiation**, *Journal of the American Chemical Society,* **51**(2), 370-375.

Schulz, C.R. and Prendiville, P.W. (1993) **Designing high concentration ozone contactors for drinking water treatment plants**, *Ozone Science & Engineering,* **15**(3), 245-266.

Schwikkard, G.W. (1995) **An investigation of the sonochemical degradation of hydantoin compounds**, *School of Chemical Engineering,* MScEng thesis, University of Natal, Durban.

Schwikkard, S.L. (2000) Personal communication, Sasolburg.

Sehgal, C., Steer, R.P., Sutherland, R.G. and Verrall, R.E. (1979) **Sonoluminescence of argon saturated alkali metal salt solutions as a probe of acoustic cavitation**, *Journal of Chemical Physics,* **70**(5), 2242-2248.

Sehgal, C., Sutherland, R.G. and Verrall, R.E. (1980a) **Optical spectra of sonoluminescence from transient and stable cavitation in water saturated with various gases**, *Journal of Physical Chemistry,* **84**(4), 388-395.

Sehgal, C., Sutherland, R.G. and Verrall, R.E. (1980b) **Sonoluminescence of NO- and NO_2-saturated water as a probe of acoustic cavitation**, *Journal of Physical Chemistry,* **84**(4), 396-401.

Sehgal, C., Sutherland, R.G. and Verrall, R.E. (1980c) **Sonoluminescence intensity as a function of bulk solution temperature**, *Journal of Physical Chemistry,* **84**(5), 525-528.

Sehgal, C., Sutherland, R.G. and Verrall, R.E. (1980d) **Selective quenching of species that produce sonoluminescence**, *Journal of Physical Chemistry,* **84**(5), 529-531.

Sehgal, C., Yu, T.J., Sutherland, R.G. and Verrall, R.E. (1982) **Use of 2,2-diphenyl-1-picrylhydrazyl to investigate the chemical behaviour of free radicals induced by ultrasonic cavitation**, *Journal of Physical Chemistry,* **86**(15), 2982-2986.

Sehgal, C.H. and Verrall, R.E. (1982) **A review of the electrical hypothesis of sonoluminescence**, *Ultrasonics,* **20**(1), 37-38.

Sehgal, C.M. and Wang, S.Y. (1981) **Threshold intensities and kinetics of sonoreaction of thymine in aqueous solutions at low ultrasonic intensities**, *Journal of the American Chemical Society,* **103**(22), 6606-6611.

Seiler, A., Brenneisen, P. and Green, D.H. (1992) **Benefits and risks of plant protection products - possibilities of protecting drinking water: case atrazine**, *Water Supply,* **10**(2), 31-42.

Sen Gupta, S.K., Peori, R.G. and Wickware, S.L. (1995) **Destruction of organic contaminants in industrial wastewater**, *Industrial Water Treatment,* (September/October), 17-24, 35-37.

Serpone, N., Terzian, R., Hidaka, H. and Pelizzetti, E. (1994) **Ultrasonic induced dehalogenation and oxidation of 2-, 3- and 4-chlorophenol in air-equilibrated aqueous media. Similarities with irradiated semiconductor particulates**, *Journal of Physical Chemistry,* **98**(10), 2634-2640.

Seybold, C.A. and Mersie, W. (1996) **Adsorption and desorption of atrazine, deethylatrazine, deisopropylatrazine, hydroxyatrazine, and metolachlor in two soils from Virginia**, *Journal of Environmental Quality,* **25**(6), 1179-1185.

Shah, Y.T., Pandit, A.B. and Moholkar, V.S. (1999a) **Chapter 1. Sources and types of cavitation**. In *Cavitation Reaction Engineering,* Kluwer Academic/Plenum Publishers, New York, ISBN 0-306-46141-2, 1-14.

Shah, Y.T., Pandit, A.B. and Moholkar, V.S. (1999b) **Chapter 2. Cavitation bubble dynamics**. In *Cavitation Reaction Engineering,* Kluwer Academic/Plenum Publishers, New York, ISBN 0-306-46141-2, 15-54.

Shah, Y.T., Pandit, A.B. and Moholkar, V.S. (1999c) **Chapter 4. Gas-liquid cavitation chemistry**. In *Cavitation Reaction Engineering,* Kluwer Academic/Plenum Publishers, New York, ISBN 0-306-46141-2, 85-153.

Shah, Y.T., Pandit, A.B. and Moholkar, V.S. (1999d) **Chapter 6. Cavitation reactors**. In *Cavitation Reaction Engineering,* Kluwer Academic/Plenum Publishers, New York, ISBN 0-306-46141-2, 193-245.

Shah, Y.T., Pandit, A.B. and Moholkar, V.S. (1999e) **Chapter 7. Models for cavitation reactors**. In *Cavitation Reaction Engineering,* Kluwer Academic/Plenum Publishers, New York, ISBN 0-306-46141-2, 247-275.

Shah, Y.T., Pandit, A.B. and Moholkar, V.S. (1999f) **Chapter 9. CAV-OX® process**. In *Cavitation Reaction Engineering,* Kluwer Academic/Plenum Publishers, New York, ISBN 0-306-46141-2, 313-332.

Shapir, N. and Mandelbaum, R.T. (1997) **Atrazine degradation in subsurface soil by indigenous and introduced microorganisms**, *Journal of Agricultural and Food Chemistry,* **45**(11), 4481-4486.

Shimabukuro, R.H. (1967) **Atrazine metabolism and herbicidal selectivity**, *Plant Physiology,* **42**(9), 1269-1276.

Shimabukuro, R.H., Frear, D.S., Swanson, H.R. and Walsh, W.C. (1971) **Glutathione conjugation: an enzymatic basis for atrazine resistance in corn**, *Plant Physiology,* **47**(1), 10-14.

Shimabukuro, R.H., Swanson, H.R. and Walsh, W.C. (1970) **Glutathione conjugation: atrazine detoxication mechanism in corn**, *Plant Physiology,* **46**(1), 103-107.

Shimizu, Y., Yamamoto, R. and Shimizu, H. (1989) **Effects of ultrasound on dyeing of nylon 6**, *Textile Research Journal,* **59**(11), 684-687.

Shukla, S.R. and Mathur, M.R. (1995) **Low-temperature ultrasonic dyeing of silk**, *Journal of the Society of Dyers and Colourists,* **111**(11), 342-345.

Siddiqui, M.S. (1996) **Chlorine-ozone interactions: formation of chlorate**, *Water Research,* **30**(9), 2160-2170.

Simmon, V.F., Kauhanen, K. and Tardiff, R.G. (1979) **Mutagenic activity of chemicals identified in drinking water**, *Developments in Toxicology and Environmental Science,* **2**, 249-258.

Singer, P.C. and Zilli, W.B. (1975) **Ozonation of ammonia in wastewater**, *Water Research,* **9**(2), 127-134.

Sirotyuk, M.G. (1963) **Ultrasonic cavitation**, *Soviet Physics - Acoustics,* **8**(3), 201-213.

Sirotyuk, M.G. (1966) **Cavitation strength of water and its distribution of cavitation nuclei**, *Soviet Physics - Acoustics,* **11**(3), 318-322.

Sittig, M., ed. (1980) **Atrazine**. In *Pesticide Manufacturing and Toxic Materials Control,* Noyes Data Corporation, Park Ridge, New Jersey, ISBN 0-8155-0814-X, 62-67.

Skipper, H.D., Gilmour, C.M. and Furtick, W.R. (1967) **Microbial versus chemical degradation of atrazine in soils**, *Proceedings of the Soil Science Society of America,* **31**(5), 653-656.

Skipper, H.D. and Volk, V.V. (1972) **Biological and chemical degradation of atrazine in three Oregon soils**, *Weed Science,* **20**(4), 344-347.

Smith, D.W., Mohammed, A. and Finch, G.R. (1992) **A bench-scale, two-phase reactor of ozone treatment: feasibility studies for high strength wastes**, *Ozone Science & Engineering,* **14**(5), 381-389.

Smith, J.M. (1970) **Chapter 12. The global rate and laboratory reactors**. In *Chemical Engineering Kinetics,* 2nd edition, McGraw-Hill, New York, Library of Congress Catalogue Card Number 74-99204, 466-492.

Solomon, K.R., Baker, D.B., Richards, R.P., Dixon, K.R., Klaine, S.J., La Point, T.W., Kendall, R.J., Weisskopf, C.P., Giddings, J.M., Giesy, J.P., et al. (1996) **Ecological risk assessment of atrazine in North American surface waters**, *Environmental Toxicology and Chemistry,* **15**(1), 31-76.

Somich, C.J., Muldoon, M.T. and Kearney, P.C. (1990) **On-site treatment of pesticide waste and rinsate using ozone and biologically active soil**, *Environmental Science and Technology,* **24**(5), 745-749.

Sonic Systems (1994) **High intensity ultrasonic liquid process systems instruction manual**.

Sorbios (1993) **Ozone generator GSG instruction manual**.

Sorenson, B.A., Koskinen, W.C., Buhler, D.D., Wyse, D.L., Lueschen, W.E. and Jorgenson, M.D. (1994) **Formation and movement of ^{14}C-atrazine degradation products in a clay loam soil in the field**, *Weed Science,* **42**(2), 618-624.

Sorenson, B.A., Koskinen, W.C., Buhler, D.D., Wyse, D.L., Lueschen, W.E. and Jorgenson, M.D. (1995) **Fate of ^{14}C-atrazine in a silt loam soil**, *International Journal of Environmental Analytical Chemistry,* **61**(1), 1-10.

Sorenson, B.A., Wyse, D.L., Koskinen, W.C., Buhler, D.D., Lueschen, W.E. and Jorgenson, M.D. (1993) **Formation and movement of ^{14}C-atrazine degradation products in a sandy loam soil under field conditions**, *Weed Science,* **41**(2), 239-245.

Sotelo, J.L., Beltrán, F.J., Benítez, F.J. and Beltrán-Heredia, J. (1987) **Ozone decomposition in water: kinetic study**, *Industrial and Engineering Chemistry Research,* **26**(1), 39-43.

Spinks, J.W.T. and Woods, R.J. (1976) **Chapter 7. Water and aqueous solutions**. In *An Introduction to Radiation Chemistry,* 2nd edition, John Wiley & Sons, New York, ISBN 0-471-81670-1, 247-359.

Srinivasan, R., Shirgaonkar, I.Z. and Pandit, A.B. (1995) **Effect of sonication on crystal properties**, *Separation Science and Technology,* **30**(10), 2239-2243.

Staehelin, J., Bühler, R.E. and Hoigné, J. (1984) **Ozone decomposition in water studied by pulse radiolysis. 2. HO• and •HO_4 as chain intermediates**, *Journal of Physical Chemistry,* **88**(24), 5999-6004.

Staehelin, J. and Hoigné, J. (1982) **Decomposition of ozone in water: rate of initiation by hydroxide ions and hydrogen peroxide**, *Environmental Science and Technology,* **16**(10), 676-681.

Staehelin, J. and Hoigné, J. (1985) **Decomposition of ozone in water in the presence of organic solutes acting as promoters and inhibitors of radical chain reactions**, *Environmental Science and Technology,* **19**(12), 1206-1213.

Statsoft, Inc. (2000) ***STATISTICA***, http:\\www.statsoft.com.

Stojanovic, B.J., Kennedy, M.V. and Shuman, F.L. (1972) **Edaphic aspects of the disposal of unused pesticides, pesticide wastes, and pesticide containers**, *Journal of Environmental Quality,* **1**(1), 54-62.

Stratton, G.W. (1984) **Effects of the herbicide atrazine and its degradation products, alone and in combination, on phototrophic microorganisms**, *Archives of Environmental Contamination and Toxicology,* **13**(1), 35-42.

Streng, A.G. (1961) **Tables of ozone properties**, *Journal of Chemical and Engineering Data,* **6**(3), 431-436.

Stucki, G., Yu, C.W., Baumgartner, T. and Gonzalez-Valero, J.F. (1995) **Microbial atrazine mineralisation under carbon limited and denitrifying conditions**, *Water Research,* **29**(1), 291-296.

Suslick, K.S. (1989) **The chemical effects of ultrasound**, *Scientific American,* **260**(2), 62-68.

Suslick, K.S. (1990) **Sonochemistry**, *Science,* **247**(4949), 1439-1445.

Suslick, K.S. and Casadonte, D.J. (1987) **Heterogeneous sonocatalysis with nickel powder**, *Journal of the American Chemical Society,* **109**(11), 3459-3461.

Suslick, K.S., Casadonte, D.J. and Doktycz, S.J. (1989) **The effects of ultrasound on nickel and copper powders**, *Solid State Ionics,* **32-33**(1), 444-452.

Suslick, K.S., Doktycz, S.J. and Flint, E.B. (1990) **On the origin of sonoluminescence and sonochemistry**, *Ultrasonics,* **28**(5), 280-290.

Suslick, K.S., Gawienowski, J.J., Schubert, P.F. and Wang, H.H. (1983) **Alkane sonochemistry**, *Journal of Physical Chemistry,* **87**(13), 2299-2301.

Suslick, K.S., Gawienowski, J.J., Schubert, P.F. and Wang, H.H. (1984) **Sonochemistry in non-aqueous liquids**, *Ultrasonics,* **22**(1), 33-36.

Suslick, K.S., Goodale, J.W., Schubert, P.F. and Wang, H.H. (1983) **Sonochemistry and sonocatalysis of metal carbonyls**, *Journal of the American Chemical Society,* **105**(18), 5781-5785.

Suslick, K.S. and Hammerton, D.A. (1986) **The site of sonochemical reactions**, *IEEE Transactions on Ultrasonics, Ferroelectrics and Frequency Control,* **UFFC-33**(2), 143-147.

Suslick, K.S., Hammerton, D.A. and Cline, R.E. (1986) **The sonochemical hot spot**, *Journal of the American Chemical Society,* **108**(18), 5641-5642.

Suslick, K.S. and Johnson, R.E. (1984) **Sonochemical activation of transition metals**, *Journal of the American Chemical Society,* **106**(22), 6856-6858.

Suslick, K.S. and Kemper, K.A. (1993) **The effect of fluorocarbon gases on sonoluminescence: a failure of the electrical hypothesis**, *Ultrasonics,* **31**(6), 463-465.

Suslick, K.S., Schubert, P.F. and Goodale, J.W. (1981) **Sonochemistry and sonocatalysis of iron carbonyls**, *Journal of the American Chemical Society,* **103**(24), 7342-7344.

Taube, H. and Bray, W.C. (1940) **Chain reactions in aqueous solutions containing ozone, hydrogen peroxide and acid**, **62**, 3357-3373.

ter Haar, G.T. (1988) **Chapter 8. Biological effects of ultrasound in clinical applications**. In *Ultrasound: Its Chemical, Physical and Biological Effects,* K.S. Suslick, ed., VCH Publishers, New York, ISBN 0-89573-328-5, 305-320.

Thakore, K.A. (1990a) **Physico-chemical study on applying ultrasonics in textile dyeing. Part I**, *American Dyestuff Reporter,* **79**(5), 45-47.

Thakore, K.A. (1990b) **Physico-chemical study on applying ultrasonics in textile dyeing. Part II**, *American Dyestuff Reporter,* **79**(6), 38-43.

Thoma, G., Gleason, M. and Popov, V. (1998) **Sonochemical treatment of benzene/toluene contaminated wastewater**, *Environmental Progress,* **17**(3), 154-160.

Thomas, J.R. and de Vries, L. (1959) **Sonically induced heterolytic cleavage of polymethylsiloxane**, *Journal of Physical Chemistry,* **63**(2), 254-256.

Thompson, L.H. and Doraiswamy, L.K. (1999) **Sonochemistry: science and engineering**, *Industrial and Engineering Chemistry Research,* **38**(4), 1215-1249.

Thurman, E.M., Goolsby, D.A., Meyer, M.T. and Kolpin, D.W. (1991) **Herbicides in surface waters of the midwestern United States: the effect of spring flush**, *Environmental Science and Technology,* **25**(10), 1794-1796.

Thurman, E.M., Goolsby, D.A., Meyer, M.T., Mills, M.S., Pomes, M.L. and Kolpin, D.W. (1992) **A reconnaissance study of herbicides and their metabolites in surface water of the midwestern United States using immunoassay and gas chromatography/mass spectrometry**, *Environmental Science and Technology,* **26**(12), 2440-2447.

Thurman, E.M., Meyer, M.T., Mills, M.S., Zimmerman, L.R., Perry, C.A. and Goolsby, D.A. (1994) **Formation and transport of deethylatrazine and deisopropylatrazine in surface water**, *Environmental Science and Technology,* **28**(13), 2267-2277.

Tiehm, A., Nickel, K. and Neis, U. (1997) **The use of ultrasound to accelerate the anaerobic digestion of sewage sludge**, *Water Science and Technology,* **36**(11), 121-128.

Tkachuk, N.G., Kravets, V.V., Nikitin, G.A. and Semenova, E.I. (1990) **Intensification of the activity of activated sludge microorganisms with ultrasound**, *Soviet Journal of Water Chemistry and Technology,* **11**(6), 82-85.

Todd, J.H. (1970) **Measurement of chemical activity of ultrasonic cavitation in aqueous solutions**, *Ultrasonics,* **8**(4), 234-238.

Tomlin, C.D.S., ed. (1997) **Atrazine**. In *The Pesticide Manual,* 11th edition, British Crop Protection Council, Farnham, Surrey, ISBN 1 901396 11 8, 55-57.

Torrents, A., Anderson, B.G., Bilboulian, S., Johnson, W.E. and Hapeman, C.J. (1997) **Atrazine photolysis: mechanistic investigations of direct and nitrate-mediated hydroxyl radical processes and the influence of dissolved organic carbon from the Chesapeake Bay**, *Environmental Science and Technology,* **31**(5), 1476-1482.

Trapido, M., Hirvonen, A., Veressinina, Y., Hentunen, J. and Munter, R. (1997) **Ozonation, ozone/UV and UV/H_2O_2 degradation of chlorophenols**, *Ozone Science & Engineering,* **19**(1), 75-96.

Upham, B.L., Boddy, B., Xing, X., Trosko, J.E. and Masten, S.J. (1997) **Non-genotoxic effects of selected pesticides and their disinfection byproducts on gap junctional intercellular communication**, *Ozone Science & Engineering,* **19**(4), 351-369.

van der Merwe, S.W. (1995) **An overview of water supply management in South Africa**, *Journal of Water Supply Research and Technology - Aqua,* **44**(4), 151-160.

van Leeuwen, H.J. (1987) **Preliminary investigation into the improvement of the biodegradability of organic substances in surface waters and effluents through ozonation**, *Water Science and Technology,* **19**, 931-937.

van Rensburg, J.F.J., Hassett, A., Theron, S. and Wiechers, S.G. (1981) **The fate of organic micropollutants through an integrated wastewater treatment/water reclamation system**, *Water Science and Technology,* **13**(1), 537-552.

Vanderheyden, V., Debongnie, P. and Pussemier, L. (1997) **Accelerated degradation and mineralisation of atrazine in surface and subsurface soil materials**, *Pesticide Science,* **49**(3), 237-242.

Vanysek, P. (1998) **Electrochemical series**. In *CRC Handbook of Chemistry and Physics,* D.R. Lide, ed., 79th edition, CRC Press, ISBN 0-8493-0479-2, 8/21-8/34.

Vaughan, P.W. and Leeman, S. (1989) **Acoustic cavitation revisited**, *Acustica,* **69**(3), 109-119.

Verrall, R.E. and Sehgal, C.M. (1988) **Chapter 6. Sonoluminescence**. In *Ultrasound: Its Chemical, Physical and Biological Effects,* K.S. Suslick, ed., VCH Publishers, New York, ISBN 0-89573-328-5, 227-286.

Vining, G.G. (1998) *Statistical Methods for Engineers,* Brooks/Cole Publishing Company, Pacific Grove, Florida, USA, ISBN 0-534-23706-1.

Vogel, A.I. (1961) *A Text-book of Quantitative Inorganic Analysis,* 3rd edition, Longman Group Limited, London, ISBN 0-582-44247-8.

Volk, C., Roche, P., Joret, J.-C. and Paillard, H. (1997) **Comparison of the effect of ozone, ozone-hydrogen peroxide system and catalytic ozone on the biodegradable organic matter of a fulvic acid solution**, *Water Research,* **31**(3), 650-656.

Volskay, V.T. and Grady, C.P.L. (1988) **Toxicity of selected RCRA compounds to activated sludge microorganisms**, *Journal of the Water Pollution Control Federation,* **60**(10), 1850-1856.

Volskay, V.T., Grady, C.P.L. and Tabak, H.H. (1990) **Effect of selected RCRA compounds on activated sludge activity**, *Research Journal of the Water Pollution Control Federation,* **62**(5), 654-664.

von Sonntag, C. (1996) **Degradation of aromatics by advanced oxidation processes in water remediation: some basic considerations**, *Journal of Water Supply Research and Technology - Aqua,* **45**(2), 84-91.

von Sonntag, C., Dowideit, P., Fang, X., Mertens, R., Pan, X., Schuchmann, M.N. and Schuchmann, H.-P. (1997) **The fate of peroxyl radicals in aqueous solution**, *Water Science and Technology,* **35**(4), 9-15.

Vorster, I. (2001) Personal communication: email dated 2 February 2001.

Wakeman, R.J. and Tarleton, E.S. (1991) **An experimental study of electroacoustic crossflow microfiltration**, *Transactions of the Institute of Chemical Engineering,* **69**(A), 386-397.

Walmsley, J.J. (1995) **Market forces and the management of water for the environment**, *Water SA,* **21**(1), 43-50.

Walton, D.J., Burke, L.D. and Murphy, M.M. (1996) **Sonoelectrochemistry: chlorine, hydrogen and oxygen evolution at platinised platinum**, *Electrochimica Acta,* **41**(17), 2747-2751.

Weavers, L.K. and Hoffmann, M.R. (1998) **Sonolytic decomposition of ozone in aqueous solution: mass transfer effects**, *Environmental Science and Technology,* **32**(24), 3941-3947.

Weber, J.B. (1970) **Mechanisms of adsorption of *s*-triazines by clay colloids and factors affecting plant availability**. In *Residue Reviews,* F.A. Gunther and J.D. Gunther, eds., Springer-Verlag, New York, Library of Congress Catalogue Card Number 62-18595, **32**, 93-130.

Webster, E. (1963) **Cavitation**, *Ultrasonics,* **1**(1), 39-48.

Weissler, A. (1959) **Formation of hydrogen peroxide by ultrasonic waves: free radicals**, *Journal of the American Chemical Society,* **81**(5), 1077-1081.

Weissler, A., Cooper, H.W. and Snyder, S. (1950) **Chemical effect of ultrasonic waves: oxidation of potassium iodide solution by carbon tetrachloride**, *Journal of the American Chemical Society,* **74**(4), 1769-1775.

Welhouse, G.J. and Bleam, W.F. (1993a) **Atrazine hydrogen-bonding potentials**, *Environmental Science and Technology,* **27**(3), 494-500.

Welhouse, G.J. and Bleam, W.F. (1993b) **Cooperative hydrogen bonding of atrazine**, *Environmental Science and Technology,* **27**(3), 500-505.

Welty, J.R., Wicks, C.E. and Wilson, R.E. (1984) *Fundamentals of Momentum, Heat and Mass Transfer,* 3rd edition, John Wiley and Sons, New York, Library of Congress Catalogue Card Number 83-17065.

Weng, C.-N., Hoven, D.L. and Schwartz, B.J. (1986) **Ozonation: an economic choice for water treatment**, *Journal of the American Water Works Association,* **78**(11), 83-89.

West, R., Fink, M.J. and Michl, J. (1981) **Tetramesityldisilene, a stable compound containing a silicon-silicon double bond**, *Science,* **214**(4527), 1343-1344.

Westerhoff, P., Song, R., Amy, G. and Minear, R. (1997) **Applications of ozone decomposition models**, *Ozone Science & Engineering,* **19**(1), 55-73.

Wilber, G.G. and Parkin, G.F. (1995) **Kinetics of alachlor and atrazine biotransformation under various electron acceptor conditions**, *Environmental Toxicology and Chemistry,* **14**(2), 237-244.

Winkelmann, D.A. and Klaine, S.J. (1991a) **Degradation and bound residue formation of atrazine in a western Tennessee soil**, *Environmental Toxicology and Chemistry,* **10**(3), 335-345.

Winkelmann, D.A. and Klaine, S.J. (1991b) **Degradation and bound residue formation of four atrazine metabolites, deethylatrazine, deisopropylatrazine, dealkylatrazine and hydroxyatrazine, in a western Tennessee soil**, *Environmental Toxicology and Chemistry,* **10**(3), 347-354.

Winship, S. (1999) **Evaluation of different methods to produce free radicals for the oxidation of organic molecules in industrial effluents and potable water with special reference to CAV-OX®**. WRC report no. 388/1/99, ISBN 1 86845 484 3.

Wolf, D.C. and Martin, J.P. (1975) **Microbial decomposition of ring-^{14}C atrazine, cyanuric acid, and 2-chloro-4,5-diamino-*s*-triazine**, *Journal of Environmental Quality,* **4**(1), 134-139.

Xiong, F. and Graham, N.J.D. (1992) **Rate constants for herbicide degradation by ozone**, *Ozone Science & Engineering,* **14**(4), 283-301.

Young, F.R. (1976) **Sonoluminescence from water containing dissolved gases**, *Journal of the Acoustical Society of America,* **60**(1), 100-104.

Young, F.R. (1989) **Chapter 1. Introduction**. In *Cavitation,* McGraw-Hill, London, ISBN 0-07-707094-1, 1-7.

Yue, P.L. (1992) **Degradation of organic pollutants by advanced oxidation**, *Transactions of the Institute of Chemical Engineering,* **70**(B), 145-148.

Yue, P.L. (1997) **Oxidation reactors for water and wastewater treatment**, *Water Science and Technology,* **35**(4), 189-196.

Zaidi, S.A.H. (1993) **Ultrasonically enhanced coal desulphurisation**, *Fuel Processing Technology,* **33**(2), 95-100.

Zechmeister, L. and Wallcave, L. (1955) **On the cleavage of benzene, thiophene and furan rings by means of ultrasonic waves**, *Journal of the American Chemical Society,* **77**(10), 2853-2855.

Zwiener, C., Weil, L. and Niessner, R. (1995) **Atrazine and parathion-methyl removal by UV and UV/O_3 in drinking water treatment**, *International Journal of Environmental Analytical Chemistry,* **58**(1-4), 247-264.

APPENDICES

A

EQUIPMENT CHARACTERISATION

The experiments performed for equipment characterisation are described in this Appendix. Ultrasonic experiments are described in Section A.1 and ozone experiments in Section A.2.

A.1 ULTRASOUND EQUIPMENT

Experiments relating to the operation of the ultrasonic horn, the evaluation of machining the eroded surface of a horn tip and the measurement of acoustic power, are described, respectively, in Section A.1.1 and Section A.1.2. The investigation of the effect of volume on hydrogen peroxide formation with the low intensity ultrasonic horn is presented in Section A.1.3. Acoustic power reduction due to the original design of the ultrasonic cell lid is described in Section A.1.4. Diagrams illustrating the mixing in the ultrasonic cell are presented in Section A.1.5 and the calibration of the rotameter for gas experiments is presented in Section A.1.6.

A.1.1 Evaluation of machining the surface of a horn tip

The effect of machining the surface of a horn tip on the performance of the ultrasonic system was evaluated by measuring the formation of hydrogen peroxide generated by a new tip and comparing it to that generated after machining. Hydrogen peroxide concentration was measured after a 20 min sonication period at transducer displacement amplitudes of 2; 4; 6; 8; 10; 11 and 12 μm. Experiments were performed in triplicate. The comparison of hydrogen peroxide formation generated using a new and a machined horn tip is presented in Figure A.1.

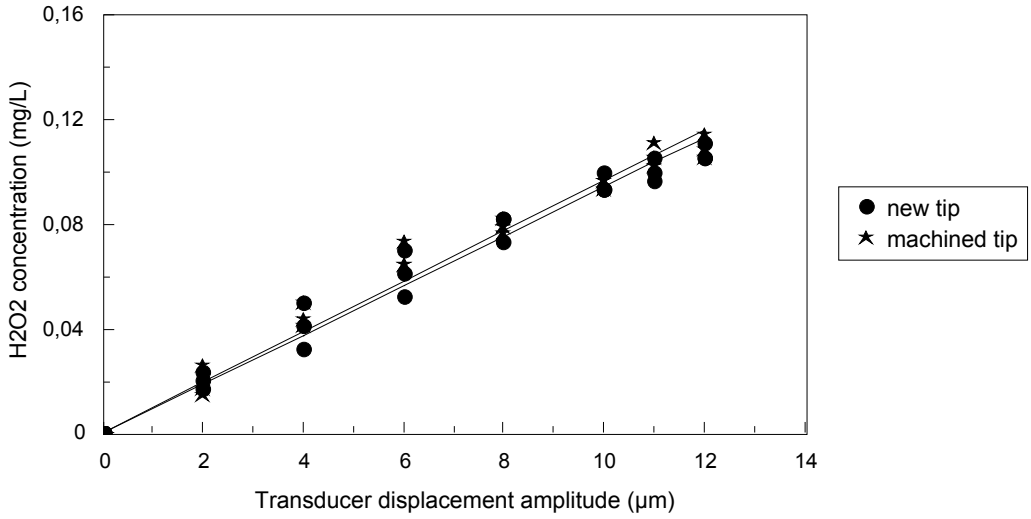

Figure A.1 : Hydrogen peroxide formation with a new and a machined horn tip (n = 3)

The data presented in Figure A.1 is recorded in Table A.1.

Table A.1 : Hydrogen peroxide formation with a new and a machined horn tip

Transducer vibration (µm)	Hydrogen peroxide concentration (mg L^{-1})					
	new horn tip			machined horn tip		
0	0.000	0.000	0.000	0.000	0.000	0.000
2	0.018	0.024	0.021	0.015	0.026	0.018
4	0.041	0.032	0.050	0.041	0.050	0.044
6	0.053	0.071	0.062	0.073	0.065	0.065
8	0.073	0.082	0.082	0.079	0.082	0.076
10	0.094	0.099	0.094	0.097	0.094	0.097
11	0.106	0.097	0.100	0.103	0.106	0.112
12	0.106	0.106	0.112	0.115	0.109	0.106

Statistical analysis of the data presented in Figure A.1 is reported in Table F.1 in Appendix F. The maximum standard deviation in the hydrogen peroxide concentrations measured during sonication with the new and machined horn tips are 0,009 and 0,006 mg L^{-1}, respectively. The rate of hydrogen peroxide formation during sonication with a new and a machined horn tip over 20 min were calculated from the regression of the data presented in Figure A.1 using the linear regression model

$$y = bx \qquad [A.1]$$

where the coefficient b, the gradient of the regression line, represents the rate of hydrogen peroxide formation. The calculated rates of hydrogen peroxide formation for the new and machined horn tips (and the standard errors of the calculated values) are recorded in Table A.2.

Table A.2 : Rate of hydrogen peroxide formation during sonication with a new and a machined horn tip over 20 min

	Rate of H_2O_2 formation ($mg\ L^{-1}\ min^{-1}$)	R^2
new horn tip	0,0094 ± 0,0002	0.978
machined horn tip	0,0097 ± 0,0002	0.977

The statistical *F*-test at a 95 % confidence level indicated that the rates of hydrogen peroxide formation during sonication with a new and a machined horn tip were not significantly different.

A.1.2 Acoustic power measurement

The efficiency of the energy transformation of the ultrasonic horn was determined by comparison of acoustic power with electrical power. Acoustic power is the energy delivered into a reaction solution, electrical power is the energy drawn at the wall. The electrical power supplied to the transducer of the ultrasonic horn was read from the meter on the face of the ultrasonic generator when the transducer was loaded. The acoustic power was calculated, as recommended by the manufacturer, from the difference in electrical power supplied to the transducer when loaded and without load (Sonic Systems, 1994). This method was also used to calculate acoustic power in the investigation of ultrasonic chemical and physical effects by Ratoarinoro and co-workers (Contamine et al., 1994; Ratoarinoro et al., 1995).

The calculated acoustic powers during sonication at transducer displacement amplitudes of 5, 8 and 11 μm are recorded in Table A.3. The electrical power drawn by the transducer when unloaded was 4, 7 and 12 W, respectively, for sonication at transducer displacement amplitudes of 5, 8 and 11 μm.

Table A.3 : Calculated acoustic power during the sonication of 500 mL of water at transducer displacement amplitudes of 5, 8 and 11 μm

Time (min)	Acoustic power (W)								
	5 μm			8 μm			11 μm		
0	24.5	24.3	25.0	40.0	40.0	39.5	59.5	57.0	56.5
1	24.5	24.2	24.5	39.5	39.5	39.2	59.3	57.0	56.5
2	24.5	24.2	24.5	39.5	39.5	39.0	59.0	57.0	56.3
3	24.3	24.0	24.5	39.5	39.3	39.0	59.0	57.0	56.0
4	24.3	24.0	24.5	39.5	39.2	39.0	58.8	56.5	56.0
5	24.3	24.0	24.5	39.5	39.2	39.0	58.5	56.5	55.5
6	24.2	24.0	24.3	39.5	39.0	39.0	58.3	56.2	55.0
7	24.2	24.0	24.3	39.5	39.0	39.0	58.2	56.0	54.5
8	24.2	24.0	24.2	39.3	39.0	39.0	58.0	56.0	54.5
9	24.0	23.8	24.1	39.5	39.0	39.0	57.8	55.0	54.0
10	24.0	23.6	24.0	39.3	39.0	38.8	57.5	55.0	54.0

Statistical analysis of the data recorded in Table A.3 is reported in Table F.2 in Appendix F. The maximum standard deviation in the measured acoustic powers at displacement amplitudes of 5, 8 and 11 μm are 0,36; 0,29 and 1,97 W, respectively.

The average acoustic power measured during sonication at each transducer displacement amplitude is compared in Table A.4 with the average electrical power. The energy conversion in the ultrasonic horn is approximately 85 % (Table 8.4).

Table A.4 : Conversion of electrical power to acoustic power

Transducer displacement (μm)	Average acoustic power (W)	Average electrical power (W)	Energy conversion (%)
5	24.2	28.2	86
8	39.3	46.3	85
11	56.7	68.7	83

Calorimetry was used to confirm the calculated acoustic powers. Calorimetry is based on the assumption that all the acoustic energy entering a system is converted into heat energy, the resulting temperature increase of the system being directly proportional to the amount of energy entering the system (Delchar and Melvin, 1994; Goswami et al., 1988). The acoustic power delivered to a reaction solution was calculated using equation A.2.

$$Q = m\,Cp\,\frac{dT}{dt} \qquad [A.2]$$

where Q is the acoustic power, m the mass of the water sonicated, Cp the heat capacity of the water and $\frac{dT}{dt}$ the rate of temperature increase of the water at time zero (Welty et al., 1984). The use of calorimetry to determine acoustic power has been demonstrated by Mason and co-workers in a review of parameters that affect sonochemistry and by Lorimer and co-workers in a investigation of the ultrasonic decomposition of potassium persulphate (Lorimer et al., 1991; Mason et al., 1992). Calorimetry is frequently used in ultrasonic investigations to calculate acoustic power (Section 2.5.5).

Temperature profiles were measured in 500 mL of water in an insulated plastic beaker during sonication with the ultrasonic horn at transducer displacement amplitudes of 5, 8 and 11 μm. A schematic diagram of the insulated vessel is shown in Figure A.2.

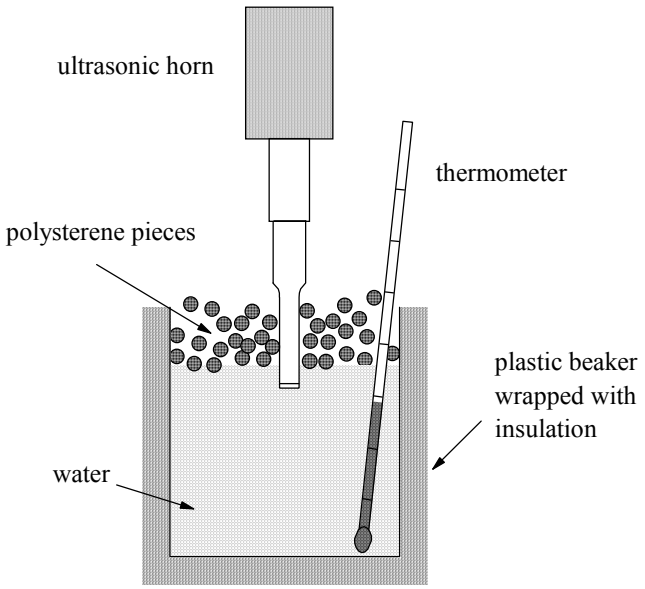

Figure A.2 : Schematic diagram of the insulated vessel used in calorimetric experiments

Temperature was measured during sonication with a spirit-filled 76 mm immersion thermometer every minute from 0 to 10 min, every 2 min from 10 to 20 min and every 5 min from 20 to 40 min. Temperature profiles recorded during sonication at transducer displacement amplitudes of 5, 8 and 11 μm are shown in Figure A.3. Experiments were performed in triplicate.

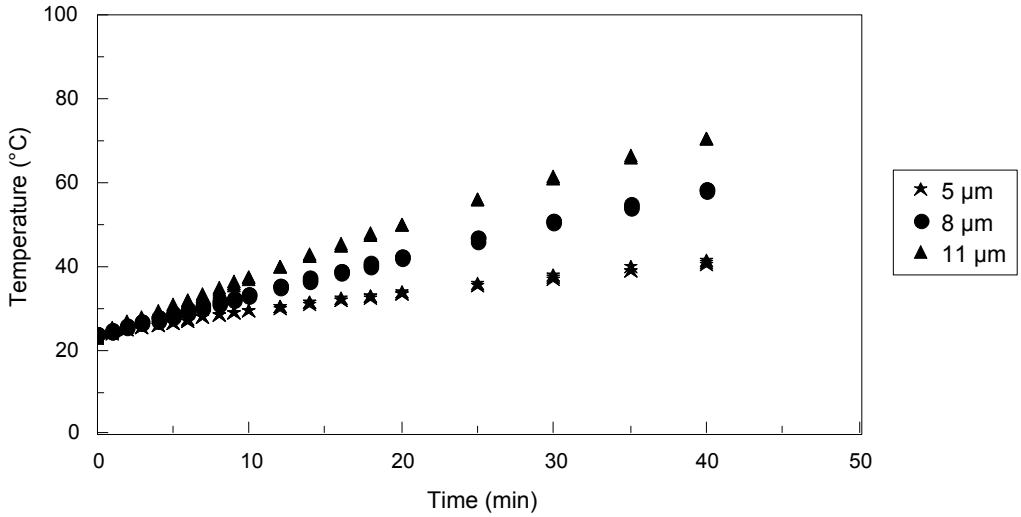

Figure A.3 : Temperature measurements in 500 mL of water in an insulated vessel during sonication over 40 min at transducer displacement amplitudes of 5, 8 and 11 μm (*n* = 3 time period)

The data presented in Figure A.3 is recorded in Table A.5.

Table A.5 : Temperature measurements in 500 mL of water in an insulated vessel during sonication over 40 min at transducer displacement amplitudes of 5, 8 and 11 μm

Time (min)	Temperature (°C)								
	5 μm			8 μm			11 μm		
0	23.7	23.7	23.8	23.8	24.0	23.8	23.0	23.4	24.0
1	24.3	24.2	24.0	24.6	24.9	24.3	24.3	24.7	25.2
2	24.9	24.8	24.7	25.7	25.9	25.2	25.6	26.0	26.7
3	25.5	25.5	25.3	26.7	26.9	26.2	27.0	27.4	28.0
4	26.0	25.9	26.0	27.7	27.9	27.1	28.4	28.8	29.5
5	26.6	26.6	26.6	28.6	28.8	28.1	29.9	30.2	30.8
6	27.2	27.1	27.1	29.5	29.8	29.0	31.3	31.7	32.1
7	27.8	27.7	27.8	30.4	30.8	30.0	32.7	33.0	33.5
8	28.4	28.2	28.3	31.3	31.7	31.0	34.1	34.4	34.8
9	29.0	28.9	28.9	32.3	32.6	32.0	35.5	35.8	36.2
10	29.6	29.4	29.3	33.2	33.5	32.8	36.8	37.2	37.6
12	30.6	30.3	30.1	35.2	35.4	34.7	39.7	39.9	40.2
14	31.6	31.2	31.0	37.0	37.2	36.5	42.3	42.5	42.9
16	32.4	32.0	31.8	38.9	39.0	38.3	44.9	45.1	45.4
18	33.1	32.7	32.6	40.7	40.9	40.2	47.4	47.7	47.8
20	33.8	33.3	33.3	42.5	42.7	42.0	50.0	50.1	50.2
25	36.1	35.2	35.3	46.8	46.8	46.2	55.8	56.0	56.0
30	38.1	37.1	37.2	50.8	50.9	50.3	61.3	61.5	61.3
35	39.9	38.9	39.1	54.7	54.8	54.1	66.3	66.5	66.3
40	41.6	40.5	40.8	58.3	58.3	58.2	70.8	70.8	70.8

Statistical analysis of the data presented in Figure A.3 is reported in Table F.3 in Appendix F. The maximum standard deviation in the temperatures measured during sonication at transducer displacement amplitudes of 5, 8 and 11 μm are 0,57; 0,41 and 0,56 °C, respectively.

Acoustic power was calculated using equation A.2 for sonication at transducer displacement amplitudes of 5, 8 and 11 μm. The rate of temperature increase $\left(\frac{dT}{dt}\right)$ was determined from regression over the 0 to 10 min temperature were the temperature increase was linear. Density and heat capacity were calculated at the average temperature of each experiment. The calculated acoustic power using calorimetry is compared in Table A.6 with the values calculated from the difference in electrical power supplied to the transducer when loaded and unloaded.

Table A.6 : Comparison of acoustic power calculated from calorimetry with acoustic power calculated from the power drawn by the transducer when loaded and unloaded

Transducer displacement (μm)	Acoustic power from calorimetry (W)	Acoustic power from electrical method (W)	Difference (%)
5	20.2	24.2	17
8	32.8	39.3	17
11	47.9	56.7	16

Acoustic power calculated from calorimetry was similar though lower (approximately 17 %) than the acoustic power calculated from the power drawn by the ultrasonic transducer when loaded and unloaded. The lower value calculated using calorimetry can be due to not all acoustic energy being converted into heat (some energy is lost due to sound) and that not all the energy converted to heat was measured. The energy used in heating the plastic beaker is not taken into account in equation A.2, also, energy may have been lost to the atmosphere despite the insulation cladding and polystyrene pieces.

Bhatnagar and Cheung noted during the investigation of the ultrasonic degradation of chlorinated volatile organic compounds that although the W-385 sonicator was capable of delivering 475 W, when set at the maximum output it delivered only 40 % (200 W) of the rated acoustic power, the ultrasonic energy was not all converted to heat energy and may also have been converted to sound (Bhatnagar and Cheung, 1994). Pétrier and co-workers noted during the investigation of the ultrasonic degradation of phenol that the acoustic power estimated by the calorimetric method was approximately 50 % of the electrical power supplied to the transducer (Pétrier et al., 1994).

A modification of equation A.2 to account for the heat absorbed by the reaction vessel has been reported in literature (Thompson and Doraiswamy, 1999). The modified equation is

$$Q = m\,Cp\,\frac{dT}{dt} + A_{ws}\,x_w\,\rho_{vessel}\,Cp_{vessel}\,\frac{dT_v}{dt} \qquad [A.3]$$

where A_{ws} is the area of the wetted surface of the vessel, x_w the thickness of the inner wall, Cp_{vessel} the heat capacity of the vessel and T_v the temperature of the inner vessel wall (Thompson and Doraiswamy, 1999).

Acoustic power reported in this investigation is calculated from the power drawn by the transducer when loaded and unloaded as there is a greater uncertainty in the value calculated using calorimetry.

A.1.3 Volume experiments with the low intensity ultrasonic horn

The low intensity ultrasonic horn was used to investigate the effect of sample volume on the formation of hydrogen peroxide during sonication. Hydrogen peroxide formation was measured in water volumes of 100;

200; 300; 400; 500; 600; 700; 800; 900 and 1 000 mL at time periods of 0; 2; 4; 6; 8; 10; 15 and 20 min. The transducer displacement amplitude was set at 11 μm and the experiments were performed in duplicate. The formation of hydrogen peroxide in different volumes of water is shown in Figure A.4.

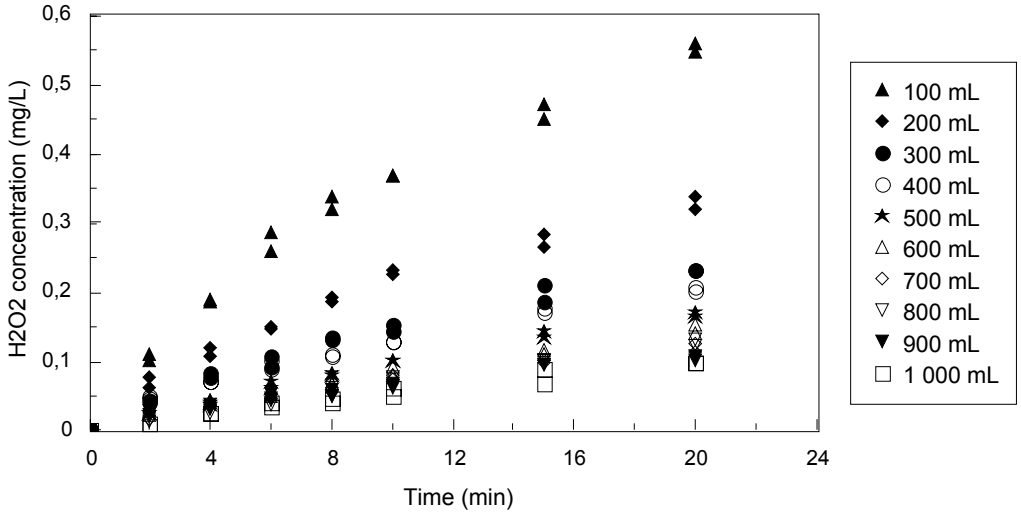

Figure A.4 : Hydrogen peroxide concentration in water volumes of 100 to 1 000 mL during sonication with the low intensity ultrasonic horn (*n* = 2 per time period)

Hydrogen peroxide concentration, shown in Figure A.4, increased with time and decreased with increasing water volume. The data presented in Figure A.4 is recorded in Table A.7.

Table A.7 : Hydrogen peroxide concentration in water volumes of 100 to 1 000 mL during sonication with the low intensity ultrasonic horn

Time (min)	Hydrogen peroxide concentration (mg L^{-1})									
	100 mL		200 mL		300 mL		400 mL		500 mL	
0	0.00	0.00	0.00	0.00	0.00	0.00	0.00	0.00	0.00	0.00
2	0.11	0.10	0.77	0.06	0.04	0.04	0.05	0.05	0.03	0.03
4	0.19	0.19	0.11	0.12	0.08	0.08	0.07	0.07	0.04	0.04
6	0.28	0.26	0.15	0.15	0.11	0.09	0.09	0.10	0.07	0.06
8	0.32	0.34	0.19	0.19	0.13	0.14	0.11	0.11	0.08	0.08
10	0.37	0.37	0.23	0.23	0.15	0.14	0.13	0.13	0.10	0.10
15	0.45	0.47	0.28	0.26	0.21	0.19	0.17	0.18	0.14	0.14
20	0.55	0.56	0.34	0.32	0.23	0.23	0.21	0.20	0.17	0.17

Table A.7 cont.

Time (min)	Hydrogen peroxide concentration (mg L^{-1})				
	600 mL	700 mL	800 mL	900 mL	1 000 mL

0	0.00	0.00	0.00	0.00	0.00	0.00	0.00	0.00	0.00	0.00
2	0.02	0.03	0.02	0.03	0.01	0.02	0.03	0.02	0.00	0.01
4	0.04	0.04	0.04	0.04	0.03	0.03	0.03	0.04	0.03	0.03
6	0.05	0.05	0.05	0.05	0.04	0.04	0.05	0.05	0.03	0.04
8	0.07	0.07	0.06	0.06	0.06	0.05	0.05	0.06	0.05	0.04
10	0.08	0.09	0.08	0.07	0.08	0.07	0.07	0.06	0.05	0.06
15	0.12	0.11	0.10	0.10	0.10	0.10	0.10	0.10	0.07	0.09
20	0.15	0.14	0.13	0.11	0.12	0.13	0.10	0.11	0.10	0.10

The mass of hydrogen peroxide generated in each water volume is reported in Table A.8.

Table A.8 : Mass of hydrogen peroxide generated in water volumes of 100 to 1 000 mL during sonication with the low intensity ultrasonic horn

Time	**Hydrogen peroxide mass (mg)**									
(min)	**100 mL**		**200 mL**		**300 mL**		**400 mL**		**500 mL**	
0	0.000	0.000	0.000	0.000	0.000	0.000	0.000	0.000	0.000	0.000
2	0.011	0.010	0.015	0.012	0.013	0.012	0.019	0.020	0.013	0.013
4	0.019	0.019	0.022	0.024	0.023	0.025	0.029	0.029	0.018	0.021
6	0.029	0.026	0.030	0.030	0.032	0.028	0.036	0.040	0.036	0.030
8	0.032	0.034	0.037	0.039	0.040	0.040	0.043	0.044	0.041	0.040
10	0.037	0.037	0.045	0.046	0.046	0.044	0.052	0.052	0.050	0.050
15	0.045	0.047	0.056	0.053	0.063	0.056	0.069	0.071	0.073	0.067
20	0.055	0.056	0.068	0.064	0.070	0.070	0.083	0.080	0.083	0.086
	600 mL		**700 mL**		**800 mL**		**900 mL**		**1 000 mL**	
0	0.000	0.000	0.000	0.000	0.000	0.000	0.000	0.000	0.000	0.000
2	0.014	0.017	0.011	0.019	0.011	0.015	0.026	0.021	0.008	0.011
4	0.027	0.027	0.028	0.026	0.021	0.025	0.029	0.033	0.026	0.026
6	0.032	0.030	0.037	0.033	0.030	0.036	0.048	0.043	0.034	0.040
8	0.041	0.041	0.042	0.039	0.051	0.040	0.045	0.052	0.048	0.040
10	0.048	0.055	0.055	0.052	0.061	0.053	0.062	0.057	0.050	0.063
15	0.070	0.067	0.068	0.070	0.080	0.080	0.086	0.086	0.069	0.090
20	0.092	0.084	0.089	0.079	0.099	0.106	0.093	0.097	0.098	0.098

Statistical analysis of the data presented in Figure A.4 is reported in Table F.4 in Appendix F. The maximum standard deviation in the hydrogen peroxide concentrations measured in water volumes of 100; 200; 300; 400; 500; 600; 700; 800; 900 and 1 000 mL are 0,013; 0,013; 0,017; 0,007; 0,007; 0,009; 0,009; 0,009; 0,006 and 0,014 mg L^{-1}, respectively. The initial rate of hydrogen peroxide formation was calculated for each

water volume from the regression of the data presented in Figure A.4 over 0 to 8 min using the linear regression model

$$y = bx \qquad [A.4]$$

where the coefficient *b*, the gradient of the regression line, represents the rate of hydrogen peroxide formation. The calculated rates of hydrogen peroxide formation in the different water volumes (and the standard errors of the calculated values) are recorded in Table A.9.

Table A.9 : Rate of hydrogen peroxide formation in water volumes of 100 to 1 000 mL during sonication with the low intensity ultrasonic horn

Water volume (mL)	Rate of H_2O_2 formation (mg L^{-1} min^{-1})	R^2
100	0,044 ± 0,0011	0.980
200	0,025 ± 0,0008	0.966
300	0,017 ± 0,0005	0.974
400	0,015 ± 0,0008	0.914
500	0,010 ± 0,0003	0.978
600	0,009 ± 0,0004	0.937
700	0,008 ± 0,0004	0.933
800	0,007 ± 0,0003	0.961
900	0,007 ± 0,0005	0.874
1,000	0,006 ± 0,0002	0.981

The temperature profiles in the different water volumes during sonication was recorded by measuring temperature every 2 min for a 10 min sonication period. The temperature profiles were performed in triplicate, the temperature measurements are recorded in Table A.10.

Table A.10 : Temperature profiles over 10 min in water volumes of 100 to 1 000 mL during sonication with the low intensity ultrasonic horn

Time	Temperature (°C)											
(min)	100 mL			200 mL			300 mL			400 mL		
0	25.3	24.5	24.7	24.4	23.7	24.5	23.8	24.0	24.3	25.2	26.0	25.7
2	37.1	36.4	36.2	31.0	29.6	31.0	27.5	28.1	28.4	28.0	28.9	28.3
4	45.4	44.8	44.8	35.8	34.2	35.9	30.7	31.5	32.1	30.9	31.5	31.0
6	53.0	51.9	51.3	40.4	38.9	40.1	33.9	35.0	35.2	33.5	34.0	33.6
8	59.2	57.6	57.0	44.9	43.7	44.9	37.5	38.1	38.7	35.8	36.3	35.9
10	65.9	63.1	63.5	49.1	47.7	49.0	40.0	41.1	41.9	38.0	38.6	38.0
	500 mL			600 mL			700 mL			800 mL		
0	25.9	26.2	26.5	26.2	26.8	26.0	26.3	26.7	26.5	24.2	24.5	24.8
2	28.0	29.0	29.0	28.8	28.8	28.0	28.0	28.4	28.3	25.6	25.8	25.8
4	30.5	31.2	31.2	30.5	30.5	30.0	29.8	29.0	29.7	27.2	27.5	27.1
6	32.5	33.2	33.1	32.4	32.5	31.8	31.0	31.1	31.3	28.6	28.6	28.8
8	34.8	35.4	35.3	34.0	34.1	33.2	32.8	32.4	32.8	29.8	30.0	30.0
10	36.8	37.1	37.5	36.0	36.0	35.1	34.1	34.0	34.1	31.0	31.3	31.1
	900 mL			1 000 mL								
0	24.0	24.4	24.7	26.0	25.9	25.8						
2	25.3	25.8	25.9	27.0	27.1	26.9						
4	26.4	26.1	27.0	28.4	28.1	28.0						
6	27.8	28.2	28.5	29.5	29.2	29.0						
8	28.8	29.6	29.8	30.6	30.2	30.0						
10	30.0	30.7	30.8	31.6	31.2	31.0						

Statistical analysis of the data recorded in Table A.10 is reported in Table F.5 in Appendix F. The maximum standard deviation in the temperatures measured during sonication in water volumes of 100; 200; 300; 400; 500; 600; 700; 800; 900 and 1 000 mL are 1,51; 0,95; 0,95; 0,46; 0,58; 0,49; 0,44; 0,30; 0,53 and 0,25 °C, respectively.

Acoustic power was calculated for each water volume using equation A.2 and ultrasonic intensity was calculated by dividing the acoustic power by the water volume. The rate of temperature increase $\left(\frac{dT}{dt}\right)$ for equation A.2 was determined from regression over the 0 to 4 min temperature data. Density (for mass calculation) and heat capacity were calculated at the average temperature of each experiment. The calculated values of acoustic power and ultrasonic intensity for each of the water volumes are recorded in Table A.11.

Table A.11 : Acoustic power and ultrasonic intensity in water volumes of 100 to 1 000 mL during sonication with the low intensity ultrasonic horn

Water volume (mL)	Acoustic power (W)	Ultrasonic intensity (W cm^{-3})
100	34.9	0.349
200	38.5	0.192
300	38.5	0.128
400	38.1	0.095
500	41.3	0.083
600	41.6	0.069
700	36.4	0.052
800	38.4	0.048
900	33.3	0.037
1,000	39.3	0.039

The relationship between ultrasonic intensity and water volume is presented in Figure A.5.

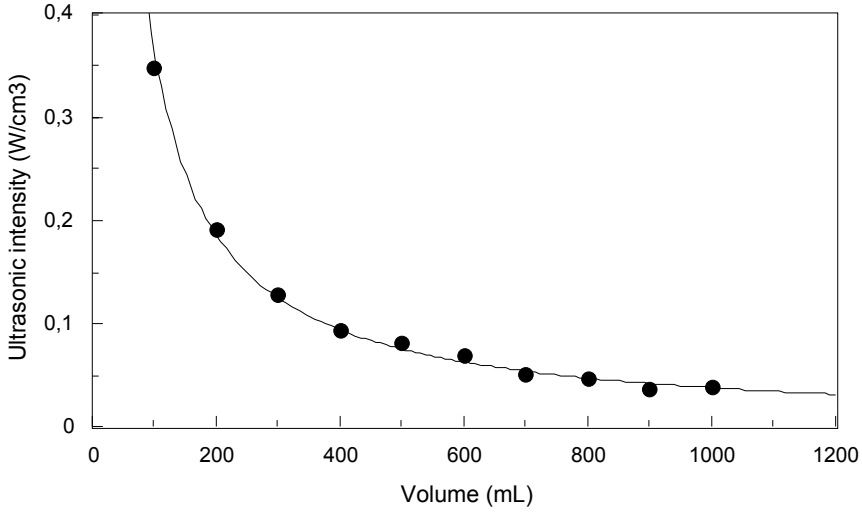

Figure A.5 : Relationship between ultrasonic intensity and water volume during sonication with the low intensity ultrasonic horn

Ultrasonic intensity, shown in Figure A.5, decreases with increasing water volume according to a power relationship. The formula of the regression line (R^2 = 0,997) in Figure A.5 is

$$y = 25{,}6x^{-0.931} \qquad [A.5]$$

The relationship between the initial rate of hydrogen peroxide formation and ultrasonic intensity is presented in Figure A.6.

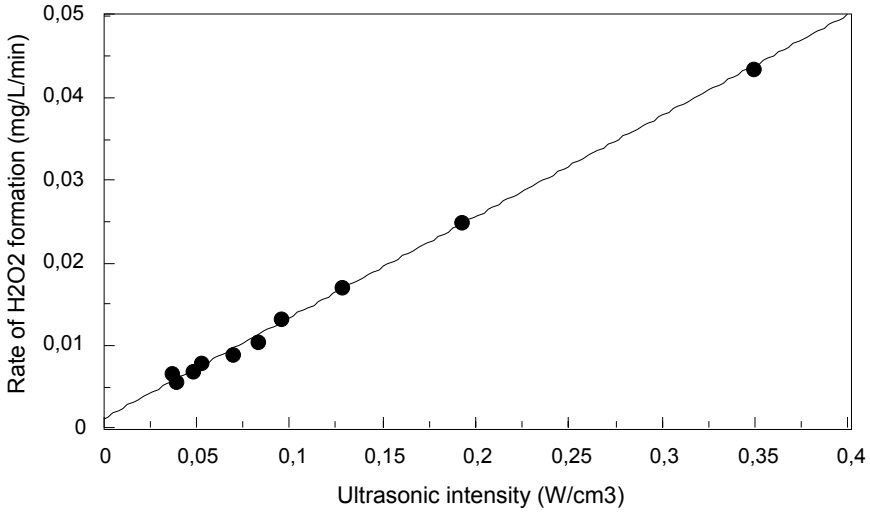

Figure A.6 : Relationship between initial rate of hydrogen peroxide formation and ultrasonic intensity during sonication with the low intensity ultrasonic horn

The initial rate of hydrogen peroxide formation, shown in Figure A.6, increased linearly with increasing ultrasonic intensity. The formula of the regression line (R^2 = 0,998) in Figure A.6 is

$$y = 0,001 + 0,122x \qquad [A.6]$$

The direct relationship between the initial rate of hydrogen peroxide formation and ultrasonic intensity and between intensity and water volume indicates that a sonochemical effect such as hydrogen peroxide formation is dependant (with all other parameters kept constant) upon the sample volume being sonicated.

A.1.4 Acoustic power reduction due to the ultrasonic cell lid design

The point of contact between the ultrasonic horn and lid of the ultrasonic cell was initially sealed with an *O-ring*. The contact between the horn and the lid of the cell dampened the movement of the horn and reduced the transfer of acoustic power to a sample in the cell. The acoustic power transferred to a water sample in the cell was calculated by measuring the temperature profile during sonication. The temperature profile during the sonication of 500 mL of water in a beaker was also measured. Temperature was recorded every 2 min for a 10 min sonication period, experiments were performed in triplicate. The temperature profiles measured during sonication of water with the low intensity horn in the ultrasonic cell and in a beaker are compared in Figure A.7.

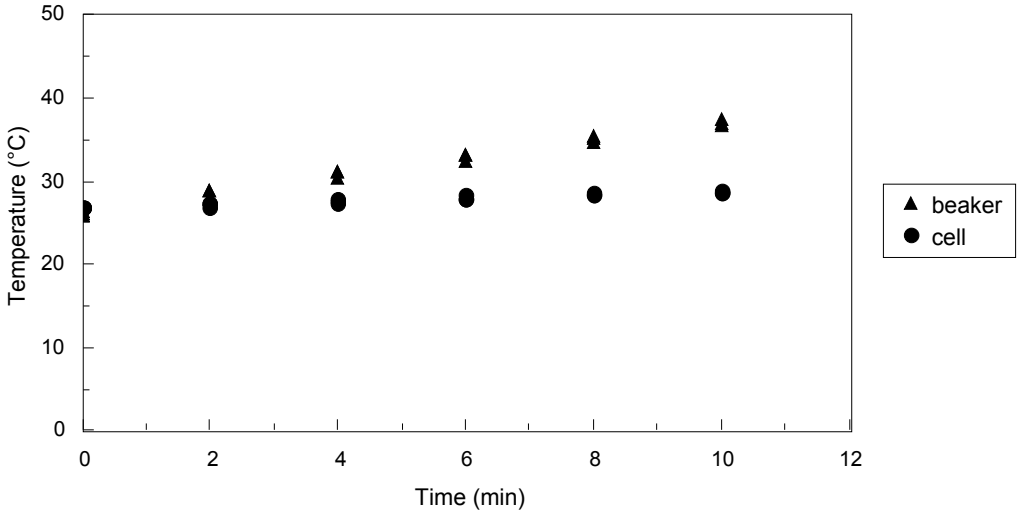

Figure A.7 : Comparison of temperature profiles measured during sonication with the low intensity horn in 500 mL of water in the ultrasonic cell and in a beaker (n = 3 per time period)

The lower temperature profile measured in the cell during sonication, shown in Figure A.7, indicates that less energy was transferred to the water in the cell than to the water in the beaker. The data presented in Figure A.7 is recorded in Table A.12.

Table A.12 : Temperatures measured during sonication with the low intensity horn in 500 mL of water in the ultrasonic cell and in a beaker

Time (min)	Temperature (°C)					
	ultrasonic cell			beaker		
0	26.8	27.0	27.0	25.9	26.2	26.5
2	27.0	27.3	27.3	28.0	29.0	29.0
4	27.5	27.9	27.7	30.5	31.2	31.2
6	28.0	28.3	28.0	32.5	33.2	33.1
8	28.4	28.6	28.3	34.8	35.4	35.3
10	28.7	28.8	28.7	36.8	37.1	37.5

Statistical analysis of the data presented in Figure A.7 is reported in Table F.6 in Appendix F. The maximum standard deviation in the temperatures measured in the ultrasonic cell and in a beaker are 0,20 and 0,58 °C, respectively.

Acoustic power transferred to both of the water samples was calculated using equation A.2. The rate of temperature increase $\left(\frac{dT}{dt}\right)$ was determined from regression over the 0 to 10 min data using the linear regression model

$$y = a + bx \qquad [A.7]$$

where coefficient *b*, the gradient of the regression line, represents the slope of the temperature profile. The calculated gradients of the temperature profiles during sonication in the ultrasonic cell and in a beaker (and the standard errors of the calculated values) are recorded in Table A.13.

Table A.13 : Comparison of the gradients of the temperature profiles measured in 500 mL of water during sonication with the low intensity horn in the ultrasonic cell and in a beaker

	Gradient of temperature profiles (°C min^{-1})	R^2
beaker	1,08 ± 0,03	0.991
ultrasonic cell	0,19 ± 0,01	0.957

Density (for mass calculation) and heat capacity were calculated at the average temperature of each of the temperature profiles. The acoustic power transferred during sonication with the low intensity horn to 500 mL of water in either the ultrasonic cell or a beaker is compared in Table A.14.

Table A.14 : Comparison of acoustic power transferred during sonication with the low intensity horn to 500 mL of water in the ultrasonic cell and in a beaker

	Water volume (mL)	Acoustic power (W)
beaker	500	37.7
ultrasonic cell	500	6.5

The acoustic power transferred to a water sample in the ultrasonic cell was approximately 17 % of that transferred to 500 mL of water in a beaker (Table A.14).

A.1.5 Mixing

The agitation induced in 500 mL of water by the ultrasonic horn was investigated using potassium permanganate crystals. The crystals were screened with a 600 μm sieve, three of the crystals that did not pass through the sieve were placed in 500 mL of water in a glass beaker. The water was sonicated with the horn at a transducer displacement of 11 μm. Pictures of the water after sonication for 2 and 5 s are presented in Figure A.8.

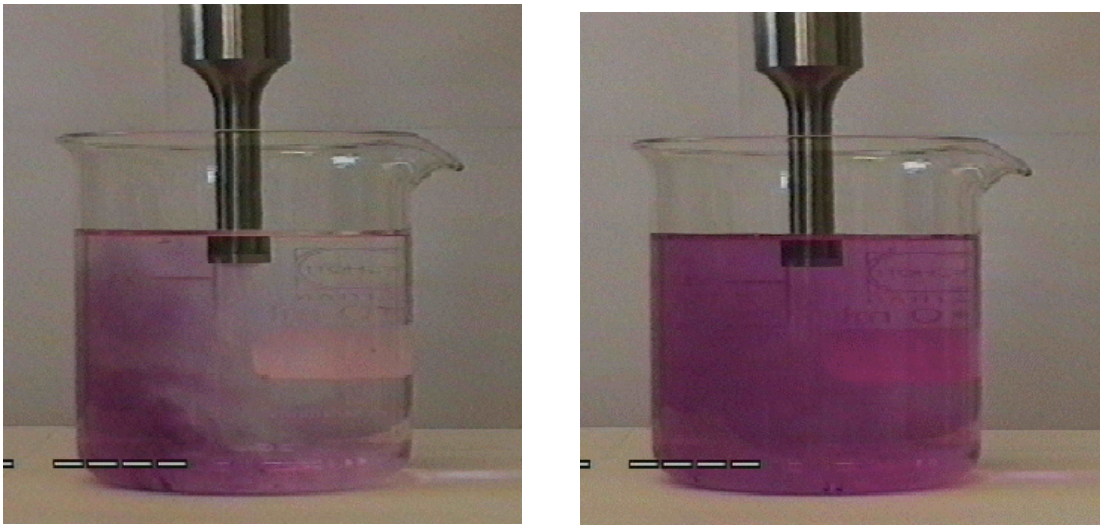

(a) (b)

Figure A.8 : Mixing of potassium permanganate crystals in 500 mL of water during sonication with the high intensity horn; (a) after 2 s and (b) after 5 s

A control was performed for comparison by adding potassium permanganate crystals to 500 mL of water in a beaker but without sonication. Pictures of the control after 10 and 60 min are presented in Figure A.9.

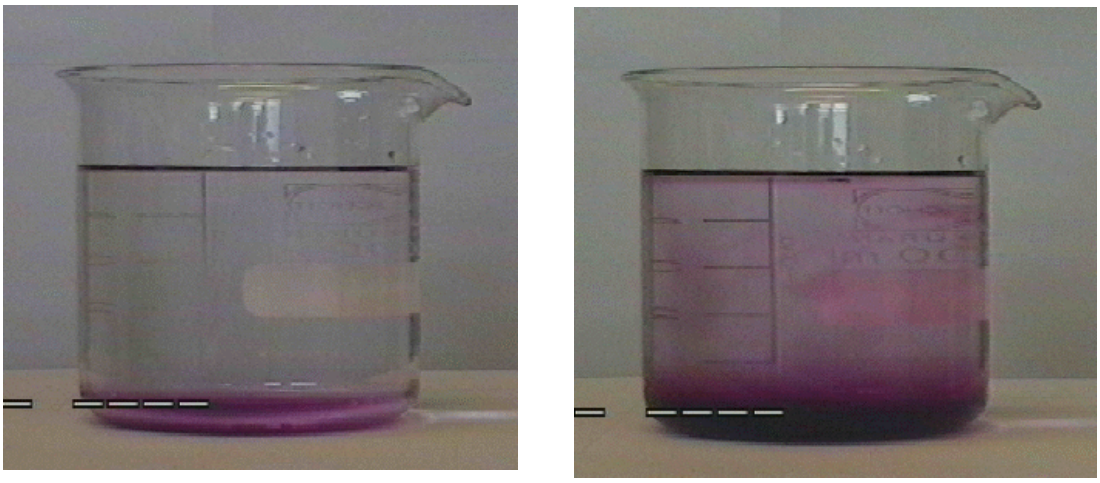

(a) (b)

Figure A.9 : Mixing of potassium permanganate crystals in 500 mL of water without sonication; (a) after 10 min and (b) after 60 min

A.1.6 Rotameter calibration

The flow rate of the gas bubbled through liquid samples in the ultrasonic cell was controlled by a rotameter. The rotameter was calibrated by measuring the flow rate of gas (in quadruple) with a bubble meter for each

rotameter setting from 1 to 10. The oxygen flow rate at each rotameter setting was measured at regulator pressures of 200 and 300 kPa. The oxygen flowrates are presented in Figure A.10.

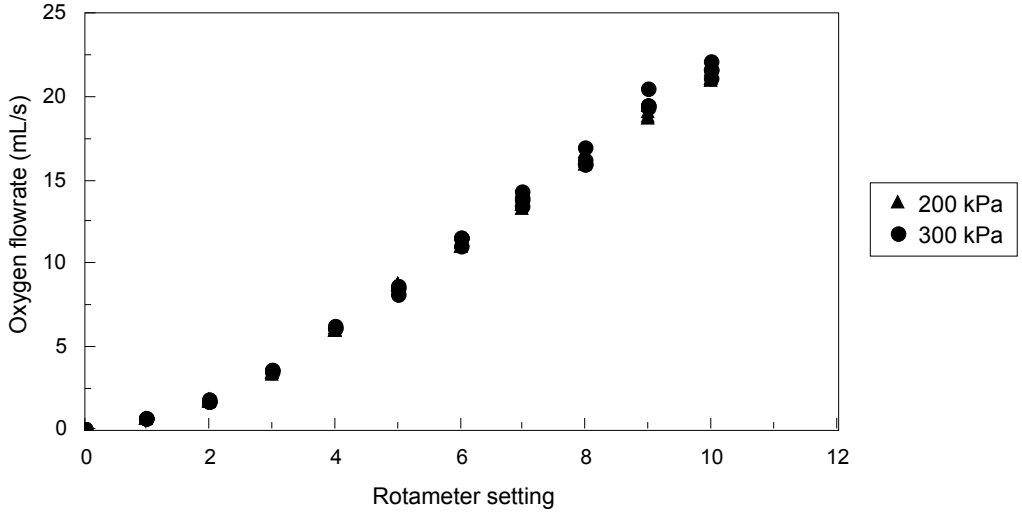

Figure A.10 : Rotameter calibration for oxygen at regulator pressures of 200 and 300 kPa (*n* = 4 per rotameter setting)

There is no significant difference at the lower rotameter settings, shown in Figure A.10, between the oxygen flowrates measured at regulator pressures of 200 or 300 kPa. The flow rate, 6,0 mL s^{-1}, used in gas experiments in the ultrasonic cell was obtained at the rotameter setting 4 with the regulator pressure set at 200 kPa. The flow rate at the rotameter setting 4 with the regulator pressure set at 100 kPa was also measured to be 6,0 mL s^{-1}. Minimal splashing occurred at this flow rate for a 500 mL volume of water. The data presented in Figure A.10 is recorded in Table A.15.

Table A.15 : Rotameter calibration for oxygen at regulator pressures of 200 and 300 kPa

Rotameter setting	Flow rate (mL s^{-1})							
	200 kPa				300 kPa			
1	0.7	0.7	0.8	0.7	0.7	0.7	0.7	0.7
2	1.7	1.7	1.8	1.8	1.7	1.7	1.7	1.8
3	3.5	3.5	3.4	3.4	3.6	3.5	3.6	3.6
4	6.1	6.0	6.0	6.0	6.2	6.1	6.2	
5	8.7	8.8	8.8	8.8	8.6	8.1	8.6	
6	11.1	11.1	11.3	11.0	11.6	11.6	11.1	11.5
7	13.8	13.3	13.6	13.6	14.3	13.8	14.0	13.4
8	16.7	16.3	16.3	16.0	17.0	16.0	16.2	16.0
9	19.5	18.7	18.9	19.1	20.5	19.5	19.4	19.5
10	21.0	21.2	21.2	21.7	22.1	21.6	21.7	21.2

Statistical analysis of the data presented in Figure A.10 is reported in Table F.7 in Appendix F. The maximum standard deviation in the flowrates of oxygen at regulator pressures of 200 and 300 kPa are 0,34 and 0,52 mL s^{-1}, respectively. The rotameter calibration was also performed for nitrogen at a regulator pressure of 200 kPa. A flow rate of 6,0 mL s^{-1}, as recorded in Table A.16, was obtained at a setting just below 4, approximately 3,7.

Table A.16 : Rotameter calibration for nitrogen at a regulator pressure of 200 kPa

Rotameter setting	Flow rate (mL s^{-1})					
2.0	2.0	1.9	2.0	2.0	2.0	
3.0	4.2	4.2	4.2	4.2	4.2	
3.5	5.2	5.1	5.1	5.1		
3.7	6.0	6.0	6.0	6.0	6.0	6.0
4.0	6.5	6.5	6.5	6.5	6.5	

Statistical analysis of the data recorded in Table A.16 is reported in Table F.8 in Appendix F. The maximum standard deviation in the flowrates of nitrogen is 0,05 mL s^{-1}.

A.2 OZONE EQUIPMENT

Ozone production by the Sorbios generator is determined by oxygen flow rate and power input. The flow rate for all experiments was maintained at 2,4 mL s^{-1} and ozone production was changed by varying the input of power. The Sorbios ozone generator was characterised by measuring the amount of ozone produced in 20 min at voltage settings of 100; 110; 130; 150; 170 and 200 V. A potassium iodide solution was used in the ultrasonic cell to react with all the ozone in the oxygen/ozone gas stream. Ozone concentration in solution was determined by titration with sodium thiosulphate as described in Section 5.3.2 of Chapter 5. Experiments were performed in triplicate. Statistical analysis of the dissolved ozone concentrations measured in solution during ozonation at voltages between 100 and 200 V is reported in Table F.9 in Appendix F. The maximum standard deviation in the measured ozone concentrations is 0,74 mg L^{-1}. The concentration of ozone in the incoming gas stream was calculated from the amount of ozone measured in solution over 20 min and the average flow rate of the oxygen/ozone gas stream. The concentration of ozone generated in an oxygen stream at voltages between 100 and 200 V is shown in Figure A.11.

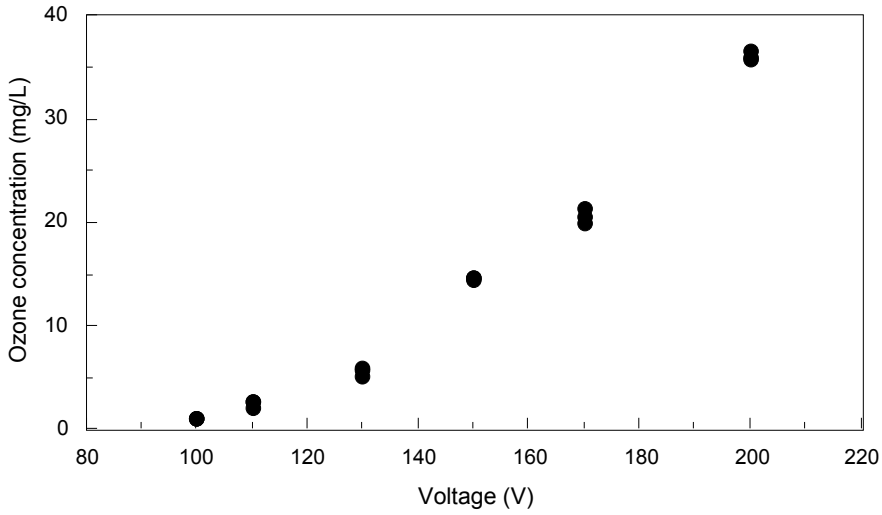

Figure A.11 : Ozone concentration in a 2,4 mL s^{-1} oxygen gas stream generated by a Sorbios ozone generator at voltage settings between 100 and 200 V (n = 3 per voltage)

Nebel reported that ozone generation, as shown in Figure A.11, varies exponentially with voltage applied to the high voltage electrode of ozone generators (Nebel, 1981). A voltage setting of 130 V was used as a standard voltage for ozone experiments. Ozone was also generated at voltage settings of 100, 150 and 170 V when the effect of ozone concentration on the degradation of atrazine was investigated. The data presented in Figure A.11 is recorded in Table A.17.

Table A.17 : Ozone concentration in a 2,4 mL s^{-1} oxygen gas stream generated by a Sorbios ozone generator at voltage settings between 100 and 200 V

Voltage (V)	Ozone concentration (mg L^{-1})		
100	1.2	1.2	1.1
110	2.0	2.8	2.7
130	5.2	5.8	6.1
150	14.6	14.6	14.7
170	20.6	21.5	20.1
200	36.7	35.9	36.1

The weight percentage of ozone generated in the oxygen/ozone gas stream is reported in Table A.18.

Table A.18 : Weight percentage of ozone in a 2,4 mL s^{-1} oxygen gas stream generated by a Sorbios ozone generator at voltage settings between 100 and 200 V

Voltage (V)	Weight percentage of ozone in gas (%)		
100	0.1	0.1	0.1
110	0.2	0.2	0.2
130	0.4	0.4	0.5
150	1.1	1.1	1.1
170	1.6	1.6	1.5
200	2.8	2.7	27.0

B

ANALYTICAL PROCEDURES

Analytical procedures used to determine concentrations of hydrogen peroxide, ozone, dissolved oxygen and atrazine are presented in this appendix. A copper-DMP (2,9-dimethyl-1,10-phenanthroline) method, described in Section B.1, was used to measure hydrogen peroxide concentration. Iodometric and indigo colorimetric methods, described in Section B.2, were used to determine ozone concentration. Dissolved oxygen concentration, described in Section B.3, was measured using an oxygen electrode. The high performance liquid chromatography technique used to determine atrazine concentration is presented in Section B.4.

B.1 HYDROGEN PEROXIDE MEASUREMENT

The hydrogen peroxide concentration of a solution could not be measured directly, a copper-DMP method was used to determine hydrogen peroxide concentration. A copper(I)-DMP complex is formed from the reaction between hydrogen peroxide and copper sulphate in the presence of an excess of DMP. The product is measured spectrophotometrically at a wavelength of 454 nm. A calibration curve was used to relate hydrogen peroxide concentration to absorbance at 454 nm. The calibration curve was constructed by plotting concentration of known hydrogen peroxide solutions versus the absorbance at 454 nm of the product formed by the reaction of the solutions with copper sulphate and DMP. A calibration curve was performed for each new batch of copper sulphate and DMP solutions. Three separate calibration curves were used throughout the investigation.

B.1.1 Calibration curve A

Three hydrogen peroxide stock solutions were prepared by pipetting 25 mL of a 30 % hydrogen peroxide solution (analytical reagent grade (AR); Saarchem) into a 250 mL volumetric flask. Total volume was made up with ultrapure water from a Millipore Milli Q System. The stock solutions were standardised by titration with a 3 840 mg L^{-1} potassium permanganate solution (AR; B. Owen Jones Chemicals) that had been standardised against a 6 801 mg L^{-1} sodium oxalate solution (AR; BDH Chemicals). Titrations were performed according to the standard methods reported in Vogel (Vogel, 1961). The concentrations of the three hydrogen peroxide stock solutions were 3 021, 3 045 and 3 031 mg L^{-1}, respectively. The stock solutions were diluted 500-fold to produce solutions of concentration 6,04; 6,09 and 6,06 mg L^{-1},

respectively, and 5 000-fold to produce solutions with concentrations of 0,604; 0,609 and 0,606 mg L^{-1}, respectively. A 3 078 mg L^{-1} copper sulphate stock solution (laboratory reagent grade (LAB); Saarchem) was prepared from the pentahydrate salt. The solution was standardised by titration, using the fast sulphon black indicator (Vogel 1961), against a 3 723 mg L^{-1} ethylenediaminetetraacetic acid (EDTA) solution (LAB; BDH Chemicals). A 10 001 mg L^{-1} DMP solution was prepared in ethanol (AR; Saarchem).

The calibration curve was produced by measuring the absorbance at a wavelength of 454 nm of a range of solutions of known hydrogen peroxide concentration. Absorbance was measured in a 10 mm glass cuvette with a Pharmacia Biotech Ultrospec 2000 spectrophotometer. The samples for absorbance measurement were prepared by mixing in a 10 mL volumetric flask 1 mL of the copper(II) sulphate solution, 1 mL of the ethanolic DMP solution and different volumes of the diluted hydrogen peroxide solutions. The volumes used of the 500-fold diluted hydrogen peroxide solutions were 1; 1,5; 2; 3 and 5 mL; volumes used of the 5 000-fold diluted hydrogen peroxide solutions were 1; 2; 4; 6 and 8 mL. Total volume was made-up with ultapure water. The procedure was repeated for the diluted solutions of each of the three hydrogen peroxide stock solutions. A control was performed by mixing 1 mL of the copper(II) sulphate solution, 1 mL of the ethanolic DMP solution and making up to total volume (10 mL) with ultrapure water. The calibration curve of absorbance (in absorbance units, AU) measured at 454 nm for different hydrogen peroxide concentrations (in mg L^{-1}) is shown in Figure B.1.

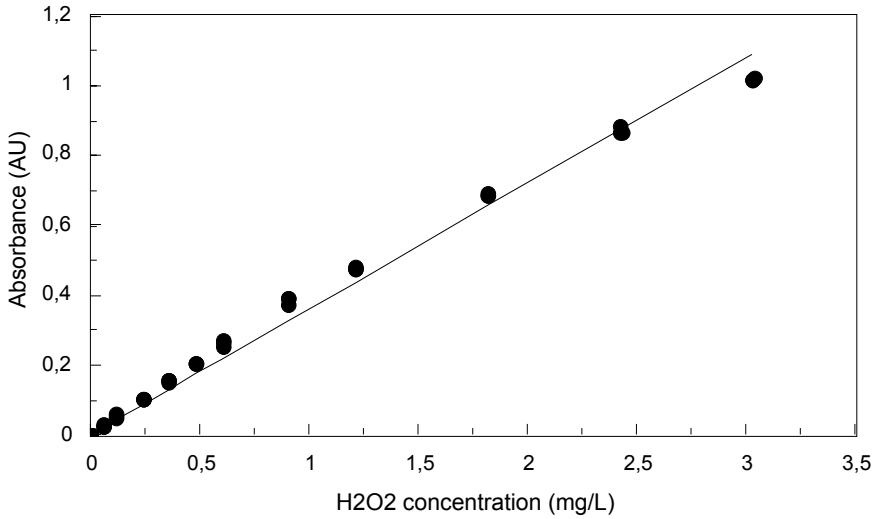

Figure B.1 : Hydrogen peroxide calibration curve A

The equation of the regression line of the data presented in Figure B.1 is

$$Absorbance = (0{,}3597 \pm 0{,}0047) \text{ x } [H_2O_2] \qquad [B.1]$$

The coefficient of determination (R^2) of the regression line is 0,987, thus, approximately 99 % of the variability in the data is accounted for with the regression equation B.1. The error (standard error of the *y* estimate divided by the mean of the sample data) in hydrogen peroxide concentrations calculated using equation B.1 from absorbance measured at 454 nm is 11 %. The data presented in Figure B.1 is recorded in Table B.1.

Table B.1 : Data for hydrogen peroxide calibration curve A

H_2O_2 stock solution A		H_2O_2 stock solution B		H_2O_2 stock solution C	
H_2O_2 concentration (mg L^{-1})	Absorbance (AU)	H_2O_2 concentration (mg L^{-1})	Absorbance (AU)	H_2O_2 concentration (mg L^{-1})	Absorbance (AU)
0.000	0.000	0.000	0.000	0.000	0.000
0.061	0.033	0.061	0.028	0.061	0.027
0.121	0.053	0.122	0.058	0.121	0.061
0.243	0.106	0.243	0.104	0.243	0.108
0.364	0.162	0.365	0.157	0.364	0.153
0.486	0.208	0.487	0.208	0.486	0.205
0.607	0.274	0.609	0.258	0.607	0.269
0.911	0.376	0.913	0.392	0.911	0.391
1.214	0.485	1.217	0.477	1.215	0.477
1.821	0.069	1.826	0.696	1.822	0.686
2.428	0.887	2.434	0.867	2.430	0.869
3.035	1.018	3.043	1.021	3.037	1.016

B.1.2 Calibration curve B

Hydrogen peroxide stock solutions were prepared for calibration curve B by pipetting 25 mL of a 30 % hydrogen peroxide solution (AR; Saarchem) into a 250 mL volumetric flask. Total volume was made up with ultrapure water. The stock solutions were standardised by titration with a 3 390 mg L^{-1} potassium permanganate solution (AR; B. Owen Jones Chemicals) that had been standardised against a 6 802 mg L^{-1} sodium oxalate solution (AR; BDH Chemicals). The concentrations of the three hydrogen peroxide stock solutions were 2 995, 3 017 and 3 008 mg L^{-1}, respectively. The stock solutions were diluted 500-fold to produce solutions of concentration 5,99; 6,03 and 6,02 mg L^{-1}, respectively, and 5 000-fold to produce solutions of concentration 0,599; 0,603 and 0,602 mg L^{-1}, respectively. A 3 075 mg L^{-1} copper sulphate stock solution (LAB; Saarchem) was prepared from the pentahydrate salt. The solution was standardised by

titration, using the fast sulphon black indicator, against a 3 724 mg L^{-1} ethylenediaminetetraacetic acid solution (LAB; BDH Chemicals). A 10 009 mg L^{-1} DMP solution was prepared in ethanol (AR; Saarchem).

The procedure to prepare a hydrogen peroxide calibration curve is detailed in Section B.1.1. The second calibration curve of absorbance (in absorbance units, AU) measured at 454 nm for different hydrogen peroxide concentrations (in mg L^{-1}) is shown in Figure B.2.

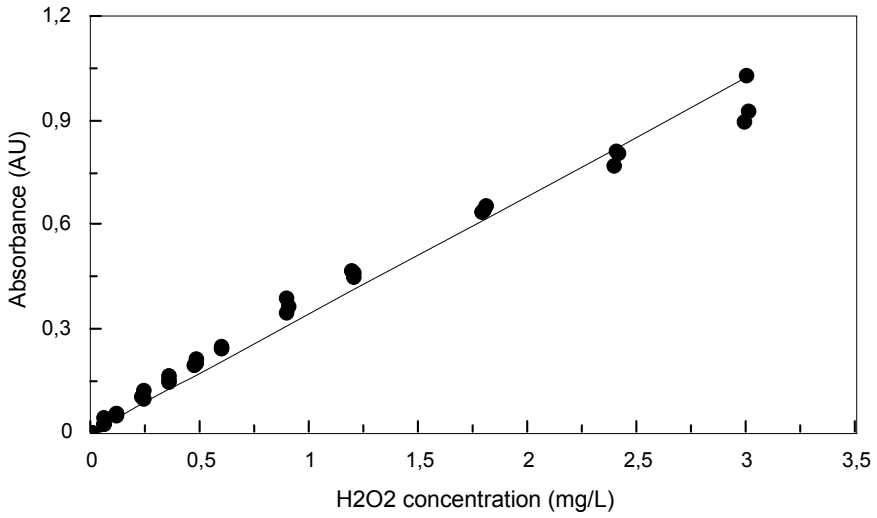

Figure B.2 : Hydrogen peroxide calibration curve B

The equation of the regression line of the data presented in Figure B.2 is

$$Absorbance = (0{,}3402 \pm 0{,}0056) \text{ x } [H_2O_2] \qquad [B.2]$$

The coefficient of determination (R^2) of the regression line is 0,979, thus, approximately 98 % of the variability in the data is accounted for with the regression equation B.2. The error in hydrogen peroxide concentrations calculated using equation B.2 from absorbance measured at 454 nm is 14 %. The data presented in Figure B.2 is recorded in Table B.2.

Table B.2 : Data for hydrogen peroxide calibration curve B

H_2O_2 stock solution A		H_2O_2 stock solution B		H_2O_2 stock solution C	
H_2O_2 concentration (mg L^{-1})	Absorbance (AU)	H_2O_2 concentration (mg L^{-1})	Absorbance (AU)	H_2O_2 concentration (mg L^{-1})	Absorbance (AU)
0.000	0.000	0.000	0.000	0.000	0.000
0.060	0.028	0.060	0.030	0.060	0.043
0.120	0.053	0.121	0.056	0.120	0.058
0.240	0.105	0.241	0.103	0.241	0.124
0.359	0.154	0.362	0.147	0.361	0.167
0.479	0.198	0.483	0.205	0.481	0.218
0.599	0.248	0.603	0.247	0.602	0.253
0.899	0.346	0.905	0.364	0.902	0.389
1.198	0.471	1.207	0.450	1.203	0.466
1.797	0.641	1.810	0.660	1.805	0.643
2.396	0.771	2.414	0.810	2.406	0.818
2.995	0.903	3.017	0.928	3.008	1.034

B.1.3 Calibration curve C

Hydrogen peroxide stock solutions were prepared for calibration curve B by pipetting 25 mL of a 30 % hydrogen peroxide solution (AR; Saarchem) into a 250 mL volumetric flask. Total volume was made up with ultrapure water. The stock solutions were standardised by titration with a 3 629 mg L^{-1} potassium permanganate solution (AR; B. Owen Jones Chemicals) that had been standardised against a 6 800 mg L^{-1} sodium oxalate solution (AR; BDH Chemicals). The concentrations of the three hydrogen peroxide stock solutions were 3 166, 3 065 and 3 047 mg L^{-1}, respectively. The stock solutions were diluted 500-fold to produce solutions of concentration 6,33; 6,13 and 6,09 mg L^{-1}, respectively, and 5 000-fold to produce solutions of concentration 0,633; 0,613 and 0,609 mg L^{-1}, respectively. A 3 090 mg L^{-1} copper sulphate stock solution (LAB; Saarchem) was prepared from the pentahydrate salt. The solution was standardised by titration, using the fast sulphon black indicator, against a 3 723 mg L^{-1} ethylenediaminetetraacetic acid solution (LAB; BDH Chemicals). A 10 006 mg L^{-1} DMP solution was prepared in ethanol (AR; Saarchem).

The procedure to prepare a hydrogen peroxide calibration curve is detailed in Section B.1.1. The second calibration curve of absorbance (in absorbance units, AU) measured at 454 nm for different hydrogen peroxide concentrations (in mg L^{-1}) is shown in Figure B.3.

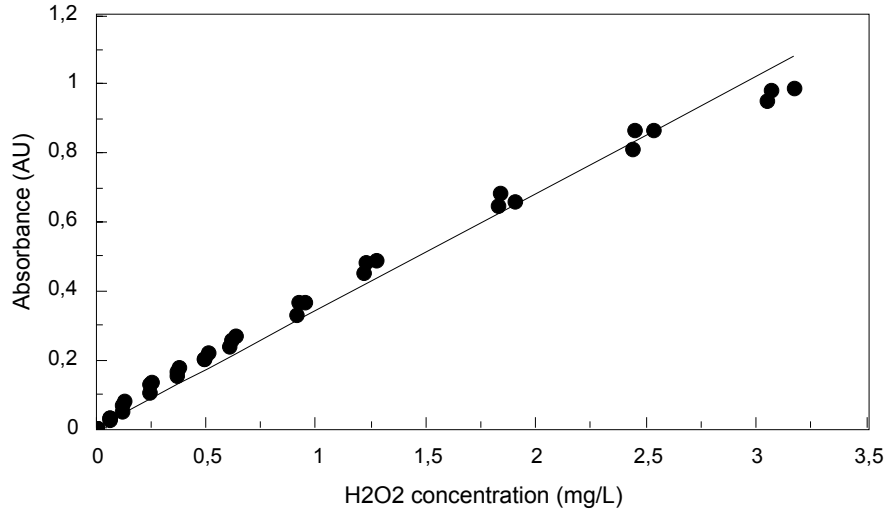

Figure B.3 : Hydrogen peroxide calibration curve C

The equation of the regression line through the data presented in Figure B.3 is

$$Absorbance = (0{,}3410 \pm 0{,}0053) \text{ x } [H_2O_2] \qquad [B.3]$$

The coefficient of determination (R^2) of the regression line is 0,981, thus, approximately 98 % of the variability in the data is accounted for with the regression equation B.3. The error in hydrogen peroxide concentrations calculated using equation B.3 from absorbance measured at 454 nm is 13 %. The data presented in Figure B.3 is recorded in Table B.3.

Table B.3 : Data for hydrogen peroxide calibration curve C

H_2O_2 stock solution A		H_2O_2 stock solution B		H_2O_2 stock solution C	
H_2O_2 concentration (mg L^{-1})	Absorbance (AU)	H_2O_2 concentration (mg L^{-1})	Absorbance (AU)	H_2O_2 concentration (mg L^{-1})	Absorbance (AU)
0.000	0.000	0.000	0.000	0.000	0.000
0.063	0.036	0.061	0.034	0.061	0.028
0.127	0.080	0.123	0.073	0.122	0.054
0.253	0.140	0.245	0.133	0.244	0.104
0.380	0.182	0.368	0.170	0.365	0.158
0.506	0.223	0.490	0.206	0.487	0.207
0.633	0.271	0.613	0.256	0.609	0.238
0.950	0.368	0.920	0.369	0.914	0.333
1.266	0.493	1.226	0.482	1.226	0.453
1.899	0.658	1.839	0.688	1.827	0.647
2.532	0.866	2.452	0.866	2.436	0.811
3.165	0.990	3.065	0.983	3.045	0.951

B.2 OZONE MEASUREMENT

Aqueous ozone concentration was determined using an iodometric (Eaton et al., 1995a) and indigo colorimetric method (Bader and Hoigné, 1981; Eaton et al., 1995b). The iodometric method is detailed in Section B.2.1 and the indigo colorimetric method in Section B.2.2.

B.2.1 Iodometric method

The iodometric method was used for daily characterisation to determine the rate of ozone generation. Experimental conditions were kept constant, however, the rate of ozone generation (at a voltage of 130 V) varied typically between 0,014 and 0,020 mg s^{-1} due to the daily fluctuation in oxygen flowrate between 2 and 3 mL s^{-1}. The % error in the daily rate of ozone generation during experimentation was calculated from the ozone mass balances reported in Section D.4 to be 7,5%. The rate of ozone generation was determined by bubbling ozone for 20 min through 500 mL of a 10 000 mg L^{-1} potassium iodide solution in the ultrasonic cell (AR; Merck). A 50 mL sample of the iodide solution post-ozonation was titrated against a 25 140 mg L^{-1} sodium thiosulphate solution (AR; PAL Chemicals) that had been standardised against a 4 904 mg L^{-1} potassium dichromate solution (GR; Merck). Titrations were performed according to Standard Methods (Eaton et al., 1995a). The iodometric method was also used in the series of ozone mass balances to determine the amount of ozone that passed through the ultrasonic cell and reacted with the 2 % potassium iodide solution in the gas washing bottles. The mass balances were performed over a 45 min period of ozonation. The total amount of ozone generated during a 45 min period was measured using a 16 000 mg L^{-1}

potassium iodide solution in the ultrasonic cell. The iodometric method can be used to determine ozone concentrations above 1 mg L^{-1} (Eaton et al., 1995a).

B.2.2 Indigo colorimetric method

Residual ozone in water or atrazine solutions in the ultrasonic cell was measured using the indigo colorimetric method. Indigo stock solution was prepared from potassium indigo trisulfonate (AR; Aldrich) and diluted 10-fold and 50-fold to prepare indigo reagents for the determination of different concentrations of ozone-containing solutions (Bader and Hoigné, 1981). The absorbance at a wavelength of 600 nm was measured of a solution prepared by mixing, in a 100 mL volumetric flask, 10 mL of the indigo reagent, a known volume of the ozone-containing solution so that the indigo solution was partially decolourised and distilled water to makeup total volume. Controls for the two reagents were performed by measuring absorbance at 600 nm of a solution prepared by mixing 10 mL of the indigo reagent and 90 mL of distilled water in a 100 mL volumetric flask. Ozone concentration was calculated from the difference in absorbance at 600 nm between that of the control and the sample, taking into account the volume of ozone-containing solution that used in the analysis (Eaton et al., 1995b) The indigo colorimetric method can be used to detect ozone concentrations down to 2 μg L^{-1} (Eaton et al., 1995b)

B.3 DISSOLVED OXYGEN MEASUREMENT

The oxygen electrode used to measure dissolved oxygen concentration was standardised daily for changes in atmospheric pressure and calibrated daily using oxygen-saturated water at 25 °C. The solubility concentration of oxygen in water at a pressure of 101,325 kPa and for temperatures between 0 and 40 °C is presented in Figure B.4 (International Critical Tables, 1928).

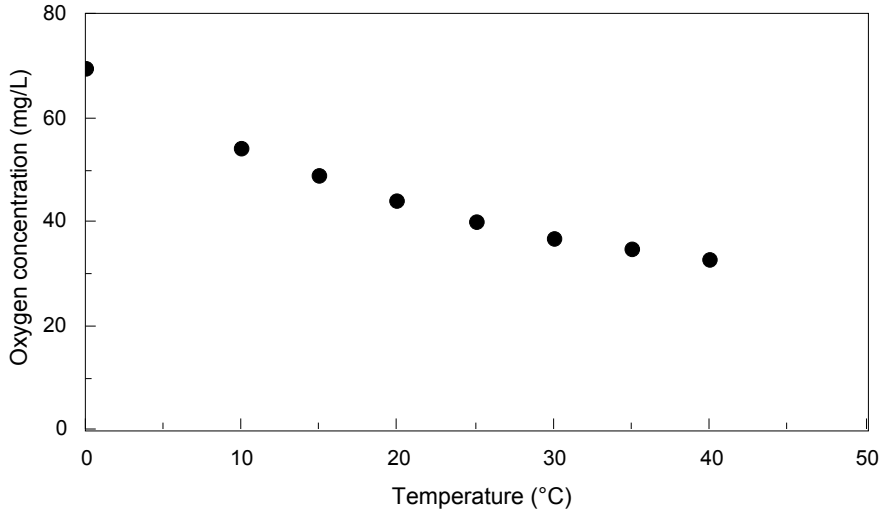

Figure B.4 : Solubility of oxygen in water at 101,325 kPa and temperatures between 0 and 40 °C (International Critical Tables, 1928)

The data presented in Figure B.4 is recorded in Table B.4.

Table B.4 : Solubility of oxygen in water at 101,325 kPa and temperatures between 0 and 40 °C (International Critical Tables, 1928)

Temperature (°C)	Oxygen concentration (mg L^{-1})
0	69.76
10	54.40
15	49.28
20	44.16
25	40.32
30	37.12
35	34.88
40	32.96

B.4 ATRAZINE MEASUREMENT

Atrazine concentration was measured using high performance liquid chromatography (HPLC). The HPLC system used a LiChrospher® RP-Select B (250 x 4 mm, 5 μm particles) column with a 70:30 (v/v) solvent mixture of methanol to water. The solvent was pumped at a flowrate of 0,6 mL min^{-1} through the column. The sample injection volume was 25 μL and absorbance was measured at a wavelength of 230 nm. The calibration curve was performed by injecting, in triplicate, atrazine (97 %; Sanachem) concentrations of 1; 2; 5; 10 and 20 mg L^{-1} through the HPLC system and recording the absorbance at 230 nm. The calibration curve is presented in Figure B.5.

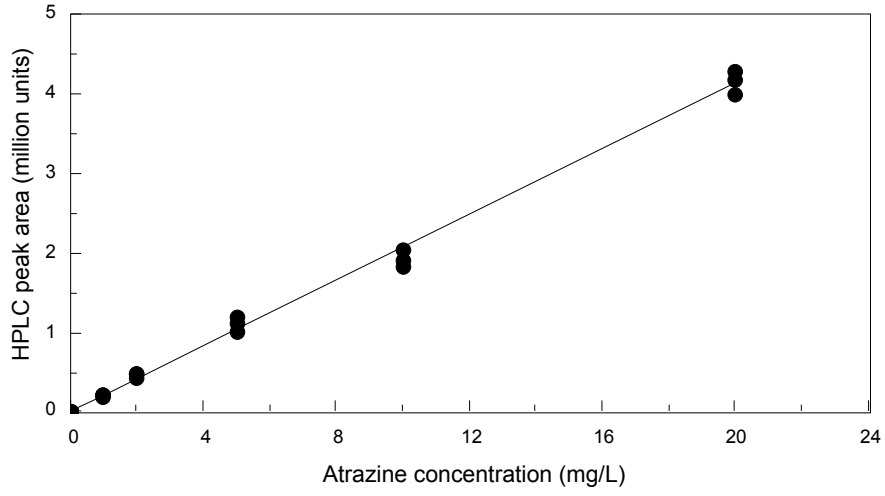

Figure B.5 : Atrazine calibration curve

The equation of the regression line through the data presented in Figure B.5 is

$$HPLC\ peak\ area = (206\ 479 \pm 2\ 443) \times [Atrazine] \quad [B.4]$$

The coefficient of determination (R^2) of the regression line is 0,996, thus, approximately 100 % of the variability in the data is accounted for with the regression equation B.5. The error in concentrations of atrazine calculated using equation B.5 of the calibration curve is 7 %. The data presented in Figure B.5 is recorded in Table B.5.

Table B.5 : Atrazine calibration curve data

H_2O_2 concentration ($mg\ L^{-1}$)	**HPLC peak area (units)**		
0	0	0	0
1	229,707	225,625	201,579
2	485,799	476,326	439,410
5	1,193,211	1,130,174	1,029,198
10	2,044,989	1,916,789	1,839,291
20	4,020,687	4,191,517	4,291,244

Statistical analysis of the data presented in Figure B.5 is reported in Table F.10 in Appendix F.

C

ULTRASOUND EXPERIMENTAL DATA

Data for the ultrasound process investigation discussed in Chapter 6 is recorded in this Appendix. Dissolved oxygen measurements are reported in Section C.1, hydrogen peroxide formation in Section C.2, hydrogen peroxide degradation in Section C.3, experiments using commercial hydrogen peroxide in Section C.4 and interval experiments in Section C.5.

C.1 DISSOLVED OXYGEN CONCENTRATION

The decrease in dissolved oxygen concentration in oxygen-saturated water was measured during sonication and when nitrogen was sparged through the water without sonication. The reduction in oxygen concentration (without sonication) was measured as a control. Oxygen-saturated water was prepared by sparging oxygen through the water at a flow rate of 6 mL s^{-1} for 10 min. Dissolved oxygen concentration was measured at time periods of 0; 5; 10; 20; 30; 45; 60; 90; 120; 150 and 180 min. Triplicate experiments were performed for each time period. The data recorded in Table C.1 is presented in Figure 6.1 in Chapter 6, statistical analysis of the data is reported in Table F.11 in Appendix F.

Table C.1 : Dissolved oxygen concentration in oxygen-saturated water during sonication, without sonication (control) and during nitrogen sparging without sonication

Time (min)	Oxygen concentration (mg L^{-1})								
	control			sonication			nitrogen		
0	37.2	40.1	40.0	40.3	37.7	36.7	40.3	39.9	36.4
5	35.3	37.7	35.3	30.3	29.2	28.1	2.8	3.0	3.1
15	32.6	33.2	32.4	23.6	22.7	24.3	1.9	1.6	1.8
30	29.7	-	29.9	20.8	20.7	21.2	1.8	1.5	1.4
45	-	28.8	29.0	-	18.0	19.7	-	-	-
60	27.6	27.7	28.0	17.2	17.2	17.7	-	1.7	1.5
90	26.1	25.7	25.5	14.4	14.2	14.3	-	-	-
120	25.1	-	25.3	13.4	12.8	13.3	-	2.0	1.8
150	24.4	24.5	24.9	12.0	-	12.2	-	-	-
180	-	24.2	23.8	11.2	-	-	-	1.5	1.4

The dissolved oxygen concentration of water saturated with air was measured for all solutions just before experimentation. Oxygen concentration varied between 8,3 and 12,3 mg L^{-1} (Table C.2) with an average of 10,0 mg L^{-1}. The standard deviation in the oxygen concentrations is 0,90 mg L^{-1}, statistical analysis of the data is reported in Table F.12 in Appendix F.

Table C.2 : Dissolved oxygen concentration in water saturated with air

Oxygen concentration (mg L^{-1})							
8.6	9.3	8.3	9.4	8.5	8.4	10.0	8.8
9.6	9.8	9.9	10.1	9.6	9.6	11.2	10.6
10.8	9.4	9.8	9.2	8.7	9.9	10.1	9.7
10.5	10.2	9.9	10.8	10.6	12.3	10.2	10.0
10.4	10.3	12.3	10.6	10.5	10.3	10.9	9.4

Dissolved oxygen concentration during sonication and saturation with oxygen, air and nitrogen was measured over a period of 40 min in the ultrasonic cell. The gases were sparged through 500 mL of water at a flow rate of 6 mL s^{-1} for 10 min prior to and during sonication. Oxygen concentration was measured at time periods of 0; 5; 10; 20 and 40 min; duplicate experiments were performed for each time period. A control was performed by measuring oxygen concentration during sonication of water with no gas sparging. The data recorded in Table C.3 is presented in Figure 6.2 in Chapter 6, statistical analysis of the data is reported in Table F.13 in Appendix F.

Table C.3 : Dissolved oxygen concentration in nitrogen-, air- and oxygen-saturated water during sonication in the ultrasonic cell at an acoustic power of 57 W

Time (min)	Oxygen concentration (mg L^{-1})							
	control		nitrogen		air		oxygen	
0	9.8	9.6	0.9	0.8	10.4	11.5	40.0	39.8
5	10.8	10.7	0.8	0.8	12.3	12.2	40.4	40.0
10	11.0	10.9	0.6	0.9	13.3	12.2	40.0	39.5
20	10.5	10.1	0.8	1.0	13.6	12.7	39.0	40.0
40	11.7	11.8	0.9	1.2	13.1	13.2	39.0	38.0

C.2 HYDROGEN PEROXIDE FORMATION

The formation of hydrogen peroxide during sonication in nitrogen-, air- and oxygen-saturated water was measured using the DMP method detailed in Section 5.3.1 of Chapter 5. The gases were sparged through the water at a flow rate of 6 mL s^{-1} for 10 min prior to and during sonication (at an acoustic power of 57 W) to

maintain a constant oxygen concentration in the water. Hydrogen peroxide concentration, reported in Table C.4, was measured at time periods of 0; 4; 8; 12; 16; 20; 30; 60; 120; 240; 480 and 960 min (16 h). Triplicate experiments were performed for each time period for each gas. A control was performed by measuring hydrogen peroxide concentration during the sonication of water with no gas sparging. The data recorded in Table C.4 is presented in Figure 6.3 in Chapter 6, statistical analysis of the data is reported in Table F.15 in Appendix F.

Table C.4 : Hydrogen peroxide formation in nitrogen-, air- and oxygen-saturated water during sonication in the ultrasonic cell for 16 h at an acoustic power of 57 W

Time (min)	H_2O_2 concentration (mg L^{-1})					
	control			nitrogen		
0	0.00	0.00	0.00	0.00	0.00	0.00
4	0.02	0.02	0.02	0.01	0.01	0.01
8	0.05	0.03	0.05	0.02	0.02	0.01
12	0.05	0.05	0.04	0.04	0.04	0.04
16	0.06	0.06	0.75	0.05	0.05	0.04
20	0.97	0.09	0.78	0.06	0.06	0.06
30	0.12	0.11	0.11	0.05	0.04	0.05
60	0.15	0.15	0.15	0.06	0.06	0.05
120	0.24	0.28	0.27	0.07	0.06	0.07
240	0.35	0.38	0.42	0.08	0.09	-
480	0.77	0.76	0.78	0.09	0.08	-
960	0.88	0.97	-	0.07	0.09	-
Time (min)	**H_2O_2 concentration (mg L^{-1})**					
	air			**oxygen**		
0	0.00	0.00	0.00	0.01	0.01	0.01
4	0.02	0.02	0.02	0.05	0.05	0.04
8	0.04	0.04	0.04	0.06	0.07	0.06
12	0.04	0.05	0.05	0.07	0.08	0.09
16	0.06	0.07	0.08	0.08	0.09	0.09
20	0.08	0.09	0.09	0.11	0.11	0.11
30	0.10	0.11	0.12	0.16	0.15	0.16
60	0.18	0.18	0.19	0.26	0.26	0.26
120	0.25	0.28	0.29	0.44	0.42	0.42
240	0.34	0.34	0.35	0.46	0.50	0.48
480	0.71	0.82	0.81	0.93	0.74	0.92
960	1.10	0.92	1.07	1.15	1.28	-

Hydrogen peroxide formation during sonication at an acoustic power of 24 W was measured in nitrogen-saturated water and a control. Water saturated with nitrogen was prepared by sparging nitrogen through the water for 10 min prior to and during sonication at a flow rate of 6 mL s^{-1}. A control was performed by measuring hydrogen peroxide concentration in water with no gas sparging. Hydrogen peroxide concentration was measured at time periods of 0; 4; 8; 12; 16; 20; 30; 60; 120; 240; 480 and 960 min. Triplicate experiments were performed for each time period. The data recorded in Table C.5 is presented in Figure 6.4 and Figure 6.5 in Chapter 6, statistical analysis of the data is reported in Table F.16 in Appendix F.

Table C.5 : Hydrogen peroxide formation in nitrogen-saturated water and the control during sonication in the ultrasonic cell at an acoustic power of 24 W

Time (min)	H_2O_2 concentration (mg L^{-1})					
	control			nitrogen		
0	0.00	0.00	0.00	0.00	0.00	0.00
4	0.02	0.01	0.10	0.01	0.01	0.01
8	0.02	0.02	0.02	0.02	0.03	0.02
12	0.02	0.03	0.03	0.03	0.04	0.03
16	0.04	0.04	0.04	0.05	0.05	0.05
20	0.05	0.05	0.06	0.05	0.05	0.06
30	0.07	0.07	0.07	0.06	0.06	0.05
60	0.14	0.13	0.14	0.05	0.06	0.05
120	0.24	0.24	0.25	0.06	0.06	0.07
240	0.44	0.43	0.42	0.07	0.07	0.08
480	0.77	0.72	0.73	-	-	-
960	0.98	-	-	-	-	-

C.3 HYDROGEN PEROXIDE DEGRADATION

Hydrogen peroxide is both formed and degraded by free radical reactions during sonication. The rate of hydrogen peroxide degradation was determined by sonicating water for 16 h at an acoustic power of 57 W to generate hydrogen peroxide. Hydrogen peroxide degradation after sonication was stopped was measured over 3 h. Hydrogen peroxide concentration was measured at time periods of 0; 5; 10; 20; 30; 60; 90; 120; 150 and 180 min. Nitrogen, air and oxygen were sparged through the water during the 3 h degradation period to investigate the effect of gas sparging upon the rate of hydrogen peroxide degradation. A control was performed by measuring hydrogen peroxide degradation in water with no gas sparging. Triplicate experiments were performed for the control and for each gas. Different hydrogen peroxide concentrations were produced during the 16 h period of sonication thus resulting in different initial concentrations for the

degradation experiments. The variation in initial concentration was removed, for comparison purposes, by normalising the data and dividing each concentration by the initial concentration for that particular experiment. The data recorded in Table C.6 is presented in Figure 6.7 in Chapter 6, statistical analysis of the data is reported in Table F.17 in Appendix F.

Table C.6 : Hydrogen peroxide degradation (normalised data) in nitrogen-, air- and oxygen-saturated water after sonication in the ultrasonic cell for 16 h at an acoustic power of 57 W

Time (min)	$[H_2O_2]$ / initial $[H_2O_2]$ ($mg\ L^{-1}/mg\ L^{-1}$)					
	control			nitrogen		
0	1.00	1.00	1.00	1.00	1.00	1.00
5	1.01	1.00	1.00	0.98	0.96	0.96
10	1.01	0.99	1.00	1.00	0.97	0.95
20	1.02	0.98	1.00	0.96	0.91	0.97
30	1.01	0.97	1.01	0.96	0.95	0.93
60	1.01	0.97	0.98	0.90	0.87	0.90
90	0.97	0.96	-	0.90	0.84	0.85
120	0.99	0.95	-	0.87	0.81	0.85
150	0.98	0.93	-	0.86	0.76	0.81
180	0.95	-	-	0.77	0.75	0.76
Time (min)	**$[H_2O_2]$ / initial $[H_2O_2]$ ($mg\ L^{-1}/mg\ L^{-1}$)**					
	air			**oxygen**		
0	1.00	1.00	1.00	1.00	1.00	1.00
5	0.96	0.94	1.02	0.95	1.01	0.95
10	0.96	0.94	0.98	0.97	1.02	0.95
20	0.95	0.93	0.98	0.95	0.98	0.95
30	0.96	0.93	0.94	0.95	0.99	0.95
60	0.89	0.87	0.91	0.91	0.93	0.91
90	0.87	0.86	-	0.87	0.90	0.88
120	0.82	0.80	0.84	0.84	0.88	0.83
150	0.79	0.78	0.79	0.83	0.83	0.80
180	0.75	0.74	0.78	0.79	0.79	0.78

The actual hydrogen peroxide concentrations are presented in Table C.7.

Table C.7 : Hydrogen peroxide degradation in nitrogen-, air- and oxygen-saturated water after

sonication in the ultrasonic cell for 16 h at an acoustic power of 57 W

Time (min)	$[H_2O_2]$ / initial $[H_2O_2]$ ($mg\ L^{-1}/mg\ L^{-1}$)					
	control			nitrogen		
0	0.38	0.44	0.47	0.71	1.02	1.25
5	0.38	0.44	0.47	0.69	0.98	1.20
10	0.38	0.44	0.47	0.71	0.99	1.18
20	0.38	0.43	0.47	0.68	0.93	1.21
30	0.38	0.43	0.48	0.68	0.97	1.16
60	0.38	0.42	0.46	0.64	0.89	1.12
90	0.37	0.42	0.45	0.64	0.86	1.07
120	0.38	0.42	0.41	0.62	0.83	1.06
150	0.37	0.41	0.41	0.61	0.78	1.01
180	0.36	0.39	0.41	0.55	0.77	0.95
Time (min)	**$[H_2O_2]$ / initial $[H_2O_2]$ ($mg\ L^{-1}/mg\ L^{-1}$)**					
	air			**oxygen**		
0	1.28	1.16	0.40	0.37	0.31	0.42
5	1.23	1.09	0.40	0.35	0.32	0.40
10	1.23	1.10	0.39	0.36	0.32	0.40
20	1.22	1.08	0.39	0.35	0.31	0.40
30	1.23	1.08	0.38	0.35	0.31	0.40
60	1.13	1.00	0.36	0.34	0.29	0.38
90	1.16	0.94	0.34	0.32	0.28	0.37
120	1.05	0.93	0.33	0.31	0.28	0.35
150	1.01	0.90	0.32	0.31	0.26	0.34
180	0.95	0.86	0.31	0.29	0.25	0.33

C.4 INTERVAL EXPERIMENTS

Ultrasonic reactors, such as the *Harwell* sonochemical reactor, are based on the concept of a flow loop system in which the reaction solution is circulated through a sonicated zone and a holding tank or reservoir. A flow loop system is advantageous if the limiting reagent of a reaction is retained in the sonicated zone or if the reagents exhibit a *memory* effect and remain activated after passing through the sonicated zone.

Interval experiments were performed to monitor hydrogen peroxide concentration when sonication was stopped for a certain time period and then restarted so as to simulate a flow loop system with the solution

moving in and out of a sonicated zone. Hydrogen peroxide concentration was measured in oxygen-saturated water at time periods of 0; 5; 10; 15; 20; 25; 30; 35; 40 and 45 min. Saturation was achieved by sparging oxygen through the water for 10 min prior to and during the 45 min experiment at a flow rate of 6 mL s^{-1}. The experiment was structured so that the water was sonicated for 15 min; sonication was stopped for the following 15 min and then restarted for a further 15 min. Sonication in the ultrasonic cell was performed at an acoustic power of 57 W. A control was performed in water with no gas sparging. All experiments were performed in triplicate. The data recorded in Table C.8 is presented in Figure 6.8 in Chapter 6, statistical analysis of the data is reported in Table F.18 in Appendix F.

Table C.8 : Hydrogen peroxide formation in oxygen-saturated water and a control in the ultrasonic cell during 15 min of sonication at an acoustic power of 57 W, 15 min without sonication and a further 15 min with sonication

Time (min)	Ultrasound	Hydrogen peroxide concentration (mg L^{-1})					
		control			oxygen		
0	on	0.00	0.00	0.00	0.00	0.01	0.00
5	on	0.04	0.04	0.03	0.05	0.06	0.05
10	on	0.06	0.06	0.06	0.08	0.09	0.09
15	on/off	0.08	0.08	0.08	0.11	0.11	0.11
20	off	0.08	0.07	0.07	0.11	0.11	0.10
25	off	0.80	0.07	0.08	0.11	0.12	0.11
30	off/on	0.08	0.07	0.08	0.11	0.10	0.11
35	on	0.11	0.10	0.11	0.14	0.13	0.13
40	on	0.12	0.12	0.13	0.16	0.16	0.17
45	on	0.14	0.15	0.14	0.19	0.19	0.19

Interval experiments were also performed to monitor the effect of a change in gas during sonication. An oxygen-saturated solution was prepared by sparging oxygen through the solution for 10 min prior to and during sonication at a flow rate of 6 mL s^{-1}. Sonication was performed with a 15 min period of oxygen saturation followed by a 15 min period with nitrogen saturation and a further 15 min period with oxygen saturation. Hydrogen peroxide concentration was measured at time periods of 0; 5; 10; 15; 20; 25; 30; 35; 40 and 45 min. Experiments for each time period were performed in triplicate. The data recorded in Table C.9 is presented in Figure 6.9 in Chapter 6, statistical analysis of the data is reported in Table F.19 in Appendix F.

Table C.9 : Hydrogen peroxide formation in water during sonication in the ultrasonic cell at an acoustic power of 57 W with 15 min of oxygen saturation, 15 min of nitrogen saturation and a further 15 min of oxygen saturation

Time (min)	Gas	Hydrogen peroxide concentration ($mg\ L^{-1}$)		
0	oxygen	0.00	0.01	0.01
5	oxygen	0.04	0.04	0.04
10	oxygen	0.09	0.08	0.08
15	oxygen/nitrogen	0.11	0.11	0.11
20	nitrogen	0.13	0.12	0.13
25	nitrogen	0.14	0.14	0.14
30	nitrogen/oxygen	0.15	0.15	0.14
35	oxygen	0.16	0.16	0.16
40	oxygen	0.19	0.18	0.18
45	oxygen	0.20	0.21	0.20

C.5 COMMERCIAL HYDROGEN PEROXIDE EXPERIMENTS

Hydrogen peroxide is used commercially for the oxidation of pollutants during water treatment. The use of ultrasound in combination with hydrogen peroxide facilitates the formation of hydroxyl radicals from hydrogen peroxide. Hydrogen peroxide concentration was measured during sonication for 1 h (at an acoustic power of 57 W) of approximate 0,25; 0,50 and 0,75 mg L^{-1} commercial hydrogen peroxide solutions (AR grade; Saarchem). The effect of gas on hydrogen peroxide concentration was investigated by sparging nitrogen, air and oxygen through the solutions for 10 min prior to and during sonication at a flow rate of 6 mL s^{-1}. A control was performed in water with no gas sparging. Hydrogen peroxide concentration was measured at time periods of 0; 5; 10; 20; 30 and 60 min. Experiments for each time period for each gas were performed in triplicate. The hydrogen peroxide concentrations measured during the sonication of a 0,28 mg L^{-1} hydrogen peroxide solution are recorded in Table C.10 and presented in Figure 6.10 in Chapter 6. Statistical analysis of the data is reported in Table F.20 in Appendix F.

Table C.10 : Hydrogen peroxide formation in nitrogen-, air- and oxygen-saturated 0,28 mg L^{-1} hydrogen peroxide solutions during sonication in the ultrasonic cell for 1 h

Time (min)	H_2O_2 concentration (mg L^{-1})					
	control			nitrogen		
0	0.28	0.27	0.28	0.28	0.27	0.28
5	0.28	0.29	0.28	0.25	0.26	0.26
10	0.30	0.30	0.29	0.25	0.26	0.25
20	0.33	0.32	0.33	0.25	0.24	0.24
30	0.34	0.35	0.35	0.26	0.26	0.27
60	0.40	0.40	0.41	0.25	0.26	0.26
Time (min)	**H_2O_2 concentration (mg L^{-1})**					
	air			**oxygen**		
0	0.28	0.27	0.27	0.29	0.29	0.29
5	0.29	0.28	0.27	0.30	0.30	0.29
10	0.29	0.30	0.29	0.33	0.33	0.31
20	0.33	0.34	0.32	0.37	0.36	0.37
30	0.35	0.35	0.34	0.42	0.41	0.40
60	0.41	0.42	0.42	0.56	0.57	0.55

The hydrogen peroxide concentrations measured during the sonication of a 0,43 mg L^{-1} hydrogen peroxide solution are recorded in Table C.11 and presented in Figure 6.11 in Chapter 6. Statistical analysis of the data is reported in Table F.21 in Appendix F.

Table C.11 : Hydrogen peroxide formation in nitrogen-, air- and oxygen-saturated 0,43 mg L^{-1} hydrogen peroxide solutions during sonication in the ultrasonic cell for 1 h

Time (min)	H_2O_2 concentration (mg L^{-1})					
	control			nitrogen		
0	0.42	0.42	0.45	0.42	0.44	0.43
5	0.46	0.45	0.45	0.44	0.44	0.44
10	0.46	0.45	0.45	0.43	0.44	0.42
20	0.48	0.48	0.48	0.43	0.42	0.42
30	0.50	0.50	0.51	0.41	0.42	0.42
60	0.58	0.58	0.59	0.40	0.40	0.39
Time (min)	**H_2O_2 concentration (mg L^{-1})**					
	air			**oxygen**		
0	0.42	0.42	0.42	0.45	0.43	0.44
5	0.45	0.45	0.45	0.47	0.46	0.47
10	0.46	0.45	0.44	0.47	0.48	0.47
20	0.48	0.47	0.47	0.51	0.50	0.50
30	0.51	0.50	0.49	0.52	0.52	0.53
60	0.57	0.57	0.59	0.61	0.62	0.63

The hydrogen peroxide concentrations measured during the sonication of a 0,72 mg L^{-1} hydrogen peroxide solution are recorded in Table C.12 and presented in Figure 6.12 in Chapter 6. Statistical analysis of the data is reported in Table F.22 in Appendix F.

Table C.12 : Hydrogen peroxide formation in nitrogen-, air- and oxygen-saturated 0,72 mg L^{-1} hydrogen peroxide solutions during sonication in the ultrasonic cell for 1 h

Time (min)	H_2O_2 concentration (mg L^{-1})					
	control			nitrogen		
0	0.73	0.73	0.72	0.73	0.73	0.73
5	0.71	0.73	0.71	0.71	0.71	0.70
10	0.74	0.73	0.73	0.69	0.69	0.69
20	0.75	0.74	0.78	0.68	0.68	0.67
30	0.80	0.79	0.78	0.69	0.68	0.68
60	0.82	0.81	0.82	0.64	0.63	0.63
Time (min)	**H_2O_2 concentration (mg L^{-1})**					
	air			**oxygen**		
0	0.71	0.71	0.72	0.71	0.72	0.73
5	0.72	0.73	0.74	0.77	0.76	0.76
10	0.74	0.75	0.75	0.77	0.78	0.77
20	0.77	0.76	0.76	0.76	0.75	0.77
30	0.78	0.78	0.78	0.78	0.78	0.79
60	0.80	0.81	0.81	0.83	0.86	0.85

D

OZONE EXPERIMENTAL DATA

Data for the ozone process investigation discussed in Chapter 7 is recorded in this Appendix. The dissolved ozone concentration in water is reported in Section D.1, ozone decomposition in Section D.2, the formation of hydrogen peroxide during ozonation in Section D.3 and ozone mass balances in Section D.4.

D.1 DISSOLVED OZONE CONCENTRATION

The dissolved ozone concentration in water was measured during ozonation, ozonation combined with sonication (at an acoustic power of 57 W), ozonation combined with hydrogen peroxide (40 mg L^{-1}) and ozonation combined with sonication and hydrogen peroxide. Water was saturated with ozone by sparging the ozone/oxygen gas stream through the diffuser of the ultrasonic cell. The ozone concentration in the 2,4 mL s^{-1} gas stream was 5,7 mg L^{-1} and the ozone production rate was 0,014 mg s^{-1} (Table 5.6 in Section 5.2). Dissolved ozone concentration in the solutions was measured at time periods of 0; 1; 2,5; 5; 10; 20; 40 and 60 min. Duplicate experiments were performed for each time period of the different experimental conditions. The dissolved ozone concentrations measured in water during ozonation, ozonation combined with sonication, ozonation combined with hydrogen peroxide and ozonation combined with sonication and hydrogen peroxide is recorded in Table D.1. The data recorded in Table D.1 is presented in Figure 7.1 in Chapter 7, statistical analysis of the data is reported in Table F.23 in Appendix F.

Table D.1 : Dissolved ozone concentration in water during ozonation (0,014 mg s^{-1}), ozonation combined with sonication (57 W), ozonation combined with hydrogen peroxide (40 mg L^{-1}) and ozonation combined with sonication and hydrogen peroxide

Time (min)	Ozone concentration (mg L^{-1})							
	ozone		ozone/uls		ozone/H_2O_2		ozone/uls/H_2O_2	
0	0.00	0.00	0.00	0.00	0.00	0.00	0.00	0.00
1	0.38	0.39	0.48	0.46	-	-	-	-
2.5	0.77	0.92	0.77	0.70	-	-	-	-
5	1.15	1.24	0.74	0.76	0.01	0.00	0.02	0.02
10	1.41	1.27	0.67	0.60	0.00	0.00	0.02	0.02
20	1.22	1.03	0.63	0.59	0.01	0.01	0.02	0.02
40	1.14	1.02	0.56	0.54	0.01	0.01	0.02	0.02
60	0.94	1.08	0.60	0.58	0.02	0.02	0.07	0.02

D.2 OZONE DECOMPOSITION

Ozone decomposition was measured in water saturated with ozone prepared by sparging the oxygen/gas gas through water in the ultrasonic cell for 20 min. The ozone concentration in the 2,4 mL s^{-1} gas stream was 5,7 mg L^{-1} and the ozone production rate was 0,014 mg s^{-1} (Table 5.6 in Section 5.2). Dissolved ozone concentration was measured over 40 min (after the 20 min saturation period) during ozonation, during sonication and when ozonation was combined with sonication. A control was performed by measuring dissolved ozone concentration after the 20 min saturation period without ozonation or sonication. Duplicate experiments were performed for each time period. The data recorded in Table D.2 is presented in Figure 7.3 in Chapter 7, statistical analysis of the data is reported in Table F.24 in Appendix F.

Table D.2 : Dissolved ozone concentration in water in the ultrasonic cell after a 20 min saturation period during ozonation (0,014 mg s^{-1}), sonication (57 W) and ozonation combined with sonication

Time (min)	Ozone concentration (mg L^{-1})							
	control		ozone		uls		ozone/uls	
0	1.44	1.57	1.22	1.03	0.97	0.92	1.57	1.44
2.5	-	-	-	-	0.44	0.46	-	-
5	1.40	-	-	-	0.28	0.27	1.40	-
10	1.37	1.40	-	-	0.13	0.13	1.37	1.40
20	1.22	1.27	1.14	1.02	0.07	0.04	1.22	1.27
40	1.40	1.29	0.94	1.08	-	-	1.40	1.29

D.3 HYDROGEN PEROXIDE FORMATION

Hydrogen peroxide formation in water was measured during ozonation, sonication and when ozonation was combined with sonication in the ultrasonic cell. Ozonation was performed at an ozone production rate of 0,014 mg s^{-1} and sonication at an acoustic power of 57 W. Hydrogen peroxide concentration was measured at time periods of 0; 5; 10; 20; 40 and 60 min. Duplicate experiments were performed for each time period. The data recorded in Table D.4 is presented in Figure 7.4 in Chapter 7, statistical analysis of the data is reported in Table F.25 in Appendix F.

Table D.3 : Hydrogen peroxide concentration in water in the ultrasonic cell during ozonation (0,014 mg s^{-1}), sonication (57 W) and ozonation combined with sonication

Time (min)	Hydrogen peroxide concentration (mg L^{-1})					
	ozone		uls		ozone/uls	
0	0.00	0.00	0.00	0.00	0.00	0.00
5	0.00	0.00	0.04	0.04	0.03	0.03
10	0.00	0.00	0.05	0.05	0.08	0.07
20	0.01	0.00	0.07	0.08	0.17	0.18
40	0.00	0.00	0.13	0.13	0.35	0.36
60	0.00	0.00	0.21	0.19	0.48	0.47

D.4 MASS BALANCES

Mass balances were performed to compare ozone decomposition over 45 min during ozonation, ozonation combined with sonication, ozonation combined with hydrogen peroxide and ozonation combined with sonication and hydrogen peroxide. Ozone decomposition was determined from the difference between the amount of ozone generated and the unreacted ozone in the system at the termination of the 45 min experiment. Ozonation was performed at an ozone production rate of 0,014 mg s^{-1}, sonication at an acoustic power of 57 W and hydrogen peroxide was added so as to prepare a 40 mg L^{-1} solution. Ozone and hydrogen peroxide concentrations were measured after the 45 min ozonation period except in solutions with added hydrogen peroxide (40 mg L^{-1}) where only ozone concentration was measured. The upper limit of the hydrogen peroxide concentrations that can be measured using the DMP method (described in Section 5.4.1) is 4,08 mg L^{-1}.

The amount of ozone generated in 45 min was determined from the reaction of ozone with a 16 000 mg L^{-1} potassium iodide solution in the ultrasonic cell and back titration with sodium thiosulphate as described in Section 5.4.2. The potassium iodide solution was sufficiently concentrated to ensure that all the ozone reacted and none passed through the ultrasonic cell. The amount of ozone generated in each mass balance (ozonation; ozonation combined with sonication; ozonation combined with hydrogen peroxide and ozonation combined with sonication and hydrogen peroxide) is recorded in Table D.4, statistical analysis of the data is reported in Table F.26 in Appendix F. The amount of ozone generated in 45 min was measured for each mass balance as fluctuations in daily conditions slightly altered the daily ozone production rate.

Table D.4 : Amount of ozone generated in 45 min in the ozonation, ozonation combined with sonication, ozonation combined with hydrogen peroxide and ozonation combined with sonication and hydrogen peroxide mass balance experiments

	Ozone mass (mg)			
	ozone	**ozone/uls**	**ozone/H_2O_2**	**ozone/uls/H_2O_2**
	55.8	55.1	53.5	54.2
	55.5	48.8	47.9	49.9
	52.5	47.9	45.7	48.3
	-	45.1	-	-
average	**54.6**	**49.2**	**49.0**	**50.8**

The amount of ozone generated in 45 min by the Sorbios ozone generator should have been the same for the same experimental conditions irrespective of when an experiment was performed. Fluctuations in daily conditions were, however, found to slightly alter the daily ozone production rate. The overall mean and standard deviation of the amount of ozone generated in 45 min as reported in Table D.4 was 50,8 and 3,82 mg L^{-1}, respectively (Table 5.26). Thus the % error in the daily amount of ozone generated in the Sorbios ozone generator is 7,5 %. The % error is calculated by dividing the standard deviation by the mean of the samples. The % error within the ozone generated in each mass balance is 3,3; 8,5; 8,3 and 6,1 %, respectively, for the ozonation, ozonation combined with sonication, ozonation combined with hydrogen peroxide and ozonation combined with sonication and hydrogen peroxide mass balances.

The total amount of unreacted ozone at the termination of an experiment was determined from the dissolved ozone in solution in the ultrasonic cell, the gas-phase ozone in the gas spaces in the system and the ozone that had passed through the system and reacted in the potassium iodide gas traps. The gas spaces in the system consists of the volume of the incoming gas line, the space above the liquid in the ultrasonic cell and the outgoing gas line to the potassium iodide traps. The volume of the gas spaces in the system is recorded in Table D.7.

Table D.5 : Volume of the gas spaces in the ultrasonic cell experimental setup

	Volume (mL)
incoming gas line	17
outgoing gas line	21
gas space in the ultrasonic cell	460
total volume	498

The residual ozone concentration in solution in the ultrasonic cell was measured according to the indigo calorimetric method described in Section 5.3.2. The ozone that passed through the ultrasonic cell and

reacted with the potassium iodide in the iodide traps, as shown in Figure 5.8 in Section 5.2, was measured according to the sodium thiosulphate method described in Section 5.3.2. The ozone concentration in the incoming gas line was determined separately from the concentration in the gas space in the ultrasonic cell and the outgoing gas line since ozone is transferred into solution where it can react or decompose. The ozone concentration in the incoming gas line is thus higher than the ozone concentration in the outgoing gas line since ozone is used up in solution. The ozone concentration in the incoming gas line was calculated from the amount of ozone generated over 45 min (recorded in Table D.4), the total volume of gas that passed through the system at a flow rate of 2,4 mL s^{-1} and the volume of the incoming gas line (17 mL). The ozone concentration in the gas space in the ultrasonic cell and the outgoing gas line was calculated from the amount of ozone reacted in the potassium iodide traps at the termination of the experiment (recorded in Table D.6), the total volume of gas that passed through the system at a flow rate of 2,4 mL s^{-1} and the volume of the space in the ultrasonic cell and the outgoing gas line (481 mL). Thus the total amount of ozone in the gas phase was calculated from the sum of the ozone in the incoming gas line and that in the gas space in the ultrasonic cell and the outgoing gas line.

The ozone and hydrogen peroxide measurements in water after ozonation, ozonation and sonication, ozonation and hydrogen peroxide and ozonation, sonication and hydrogen peroxide for 45 min are recorded in Table D.6. Experiments were performed in duplicate. Statistical analysis of the data recorded in Table D.6 is reported in Table F.27 in Appendix F.

Table D.6 : Ozone and hydrogen peroxide measurements in water after the 45 min ozonation, ozonation combined with sonication, ozonation combined with hydrogen peroxide, and ozonation combined with sonication and hydrogen peroxide mass balance experiments

	Ozone mass (mg)							
	ozone		**ozone/uls**		**ozone/H_2O_2**		**ozone/uls/H_2O_2**	
dissolved ozone in solution	0.64	0.60	0.21	0.23	0.00	0.08	0.04	0.05
gas-phase ozone	4.18	4.18	3.36	3.36	3.30	3.30	3.07	3.07
ozone in the KI traps	47.09	46.73	35.56	36.25	35.25	35.27	34.37	33.84
total	**51.91**	**51.51**	**39.13**	**39.84**	**38.55**	**38.65**	**37.48**	**36.96**
	Hydrogen peroxide concentration (mg L^{-1})							
	ozone		**ozone/uls**		**ozone/H_2O_2**		**ozone/uls/H_2O_2**	
H_2O_2 in solution	0.00	0.01	0.24	0.25	-	-	-	-

E

ATRAZINE EXPERIMENTAL DATA

Data for the atrazine experiments discussed in Chapter 8 is recorded in this Appendix. Atrazine chemistry during sonication, ozonation and in the presence of hydrogen peroxide is discussed in Section E.1. Mass balances are also reported in Section E.1. The investigation of atrazine degradation during sonication, ozonation and in the presence of hydrogen peroxide is reported in Section E.2. Identification of degradation products is detailed in Section E.4.

E.1 ATRAZINE CHEMISTRY

Atrazine concentration in a standing 5 mg L^{-1} solution was measured over 3 h as a degradation control at time periods of 0; 45; 90; 135 and 180 min. Atrazine concentration was also measured in a 5 mg L^{-1} atrazine solution when oxygen was sparged through the solution at a flow rate of 6 mL s^{-1}. Experiments were performed in triplicate. The data reported in Table E.1 is presented in Figure 8.1 in Chapter 8, statistical analysis of the data is reported in Table F.28 in Appendix F.

Table E.1 : Atrazine concentration in a 5 mg L^{-1} atrazine solution in the ultrasonic cell over 3 h in the absence of ultrasound without and with oxygen sparging

Time (min)	Atrazine concentration (mg L^{-1})					
	control			control with oxygen sparging		
0	5.4	5.1	5.9	4.8	4.9	4.9
45	5.3	4.9	5.6	5.0	4.7	4.9
90	5.0	5.1	5.5	4.9	4.5	5.1
135	5.2	5.0	4.9	4.9	5.2	5.2
180	5.4	5.5	5.2	4.8	4.9	4.7

Atrazine chemistry during ozonation is detailed in Section E.1.1 and with hydrogen peroxide addition in Section E.1.2. Mass balances are reported in Section E.1.3.

E.1.1 Ozone

The dissolved ozone concentration in a 5 mg L^{-1} atrazine solution was measured during ozonation, ozonation combined with sonication (at an acoustic power of 57 W), ozonation combined with hydrogen peroxide

(40 mg L^{-1}) and ozonation combined with sonication and hydrogen peroxide. The atrazine solution was saturated with ozone by sparging the ozone/oxygen gas stream through the diffuser of the ultrasonic cell. The ozone concentration in the 2,4 mL s^{-1} gas stream was 5,7 mg L^{-1} and the ozone production rate was 0,014 mg s^{-1} (Table 5.6 in Section 5.2). Dissolved ozone concentration in the solutions was measured at time periods of 0; 1; 2,5; 5; 10; 20; 40 and 60 min. Duplicate experiments were performed for each time period of the different experimental conditions. The dissolved ozone concentrations measured in a 5 mg L^{-1} atrazine solution during ozonation, ozonation combined with sonication, ozonation combined with hydrogen peroxide and ozonation combined with sonication and hydrogen peroxide is recorded in Table E.2. The data recorded in Table E.2 is presented in Figure 8.4 in Chapter 8, statistical analysis of the data is reported in Table F.29 in Appendix F.

Table E.2 : Dissolved ozone concentration in a 5 mg L^{-1} atrazine solution during ozonation (0,014 mg s^{-1}), ozonation combined with sonication (57 W), ozonation combined with hydrogen peroxide (40 mg L^{-1}) and ozonation combined with sonication and hydrogen peroxide

Time (min)	Ozone concentration (mg L^{-1})							
	ozone		ozone/uls		ozone/H_2O_2		ozone/uls/H_2O_2	
0	0.00	0.00	0.00	0.00	0.00	0.00	0.00	0.00
1	0.31	0.27	0.37	0.34	-	-	-	-
2.5	0.56	0.58	0.41	0.38	0.23	0.24	0.14	0.12
5	0.71	0.67	0.35	0.40	0.40	0.36	0.23	0.20
10	0.58	0.58	0.37	0.35	0.39	0.32	0.16	0.18
20	0.58	0.56	0.36	0.33	0.48	0.36	0.17	0.12
40	0.57	0.59	0.40	0.36	0.31	0.35	0.10	0.08
60	0.43	0.50	0.35	0.31	0.43	0.35	0.05	0.04

E.1.2 Hydrogen peroxide

Hydrogen peroxide formation in a 5 mg L^{-1} atrazine solution was investigated during ozonation, sonication and when ozonation was combined with sonication. Ozonation was performed at an ozone production rate of 0,014 mg s^{-1} and sonication at an acoustic power of 57 W. Hydrogen peroxide concentration was measured at time periods of 0; 5; 10; 20; 40 and 60 min. Duplicate experiments were performed for each time period. The data recorded in Table E.3 is presented in Figure 8.6 in Chapter 8, statistical analysis of the data is reported in Table F.30 in Appendix F.

Table E.3 : Hydrogen peroxide concentration in a 5 mg L^{-1} atrazine solution in the ultrasonic cell

during ozonation (0,014 mg s^{-1}), sonication (57 W) and ozonation combined with sonication

Time (min)	Hydrogen peroxide concentration (mg L^{-1})					
	ozone		uls		ozone/uls	
0	0.00	0.00	0.00	0.00	0.00	0.00
5	0.18	0.18	0.03	0.03	0.23	0.20
10	0.34	0.34	0.04	0.05	0.40	0.41
20	0.67	0.67	0.09	0.09	0.73	0.69
40	1.17	1.18	0.19	0.16	1.21	1.22
60	1.62	1.66	0.20	0.19	1.53	1.61

E.1.3 Mass balances

Mass balances in a 5 mg L^{-1} atrazine solution were performed over a 45 min period of ozonation, ozonation combined with sonication, ozonation combined with hydrogen peroxide and ozonation combined with sonication and hydrogen peroxide to relate atrazine degradation to ozone decomposition. The amount of ozone decomposed or consumed in the oxidation of atrazine is calculated from the difference between the amount of ozone generated in 45 min and the unreacted ozone in the system at the termination of the experiment. The total amount of unreacted ozone consists of the dissolved ozone in solution in the ultrasonic cell, the ozone in the gas spaces of the system and the ozone that passed through the system and reacted with the potassium iodide in the gas traps. Ozonation was performed at an ozone production rate of 0,014 mg s^{-1}, sonication at an acoustic power of 57 W and hydrogen peroxide was added so as to prepare a 40 mg L^{-1} solution. Ozone and hydrogen peroxide concentrations were measured after the 45 min period except in solutions with added hydrogen peroxide where only ozone concentration was measured. The upper limit of the hydrogen peroxide concentrations that can be measured using the DMP method (described in Section 5.4.1) is 4,08 mg L^{-1}.

The measurement of the amount of ozone generated in 45 min for the different mass balances is detailed in Section D.4 and summarised in Table D.4. The measurement of unreacted ozone in the system at the termination of the experiments is also detailed in Section D.4. The ozone, hydrogen peroxide and atrazine measurements in a 5 mg L^{-1} atrazine solution after 45 min of ozonation, ozonation combined with sonication, ozonation combined with hydrogen peroxide and ozonation combined with sonication and hydrogen peroxide are recorded in Table E.4. Statistical analysis of the data recorded in Table D.4 is reported in Table F.31 in Appendix F. The mass balance measurements in water are recorded in Table D.6 in Section D.4.

Table E.4 : Ozone, hydrogen peroxide and atrazine measurements in a 5 mg L^{-1} atrazine solution

after the 45 min ozonation, ozonation combined with sonication, ozonation combined with hydrogen peroxide and ozonation combined with sonication and hydrogen peroxide mass balance experiments

	Ozone mass (mg)								
	ozone		**ozone/uls**		**ozone/H_2O_2**			**ozone/uls/H_2O_2**	
dissolved ozone in solution	0.16	0.23	0.12	0.11	0.14	0.22	0.20	0.02	0.01
gas-phase ozone	3.82	3.82	2.89	2.89	3.18	3.18	3.18	2.67	2.67
ozone in the KI traps	43.42	45.56	30.65	30.34	33.61	34.39	33.68	29.42	29.64
total	**47.40**	**49.61**	**33.66**	**33.34**	**36.93**	**37.79**	**37.06**	**32.11**	**32.32**
	Hydrogen peroxide concentration (mg L^{-1})								
	ozone		**ozone/uls**		**ozone/H_2O_2**			**ozone/uls/H_2O_2**	
H_2O_2 in solution	1.14	1.25	1.41	1.36	-	-	-	-	-
	Atrazine concentration (mg L^{-1})								
	ozone		**ozone/uls**		**ozone/H_2O_2**			**ozone/uls/H_2O_2**	
initial concentration	5.2	5.1	5.3	5.0	6.4	6.5	6.0	6.1	6.1
final concentration	3.8	3.8	3.4	3.5	3.7	3.5	3.8	4.0	3.9

E.2 ATRAZINE DEGRADATION

Atrazine degradation was investigated during sonication, ozonation and with hydrogen peroxide. Degradation during sonication is reported in Section E.2.1, during ozonation in Section E.2.2 and with hydrogen peroxide in Section E.2.3.

E.2.1 Ultrasound

The ultrasonic degradation of atrazine was investigated by sonicating solutions of initial concentration 5, 10 and 20 mg L^{-1} in the ultrasonic cell for 3 h at an acoustic power of 57 W. Atrazine concentration was measured using the HPLC method described in Section 5.4.4. The data reported in Table E.5 is presented in Figure 8.7 in Chapter 8, statistical analysis of the data is reported in Table F.32 in Appendix F.

Table E.5 : Atrazine concentration in a 5, 10 and 20 mg L^{-1} atrazine solution during sonication in the ultrasonic cell at an acoustic power of 57 W over 3 h

Time (min)	Atrazine concentration (mg L^{-1})								
	5 mg L^{-1} solution			10 mg L^{-1} solution			20 mg L^{-1} solution		
0	5.4	5.9	6.1	10.9	11.9	11.5	20.9	20.4	20.6
45	5.6	5.0	4.8	10.7	11.0	10.9	21.8	20.3	21.5
90	5.1	4.7	4.9	10.6	10.7	11.2	20.6	20.1	20.0
135	4.9	4.7	4.2	10.6	9.8	10.5	21.6	20.5	21.1
180	4.2	4.4	4.2	10.1	9.6	9.6	20.8	18.8	18.4

A concentration of 5 mg L^{-1} was used as the initial concentration for all further atrazine experiments. Atrazine degradation is through a radical reaction process. The degradation of atrazine in the presence and absence of oxygen was investigated by sparging oxygen and nitrogen at a flow rate of 6 mL s^{-1} through the atrazine solution during sonication. The data reported in Table E.6 is presented in Figure 8.8 in Chapter 8, statistical analysis of the data is reported in Table F.34 in Appendix F.

Table E.6 : Effect of oxygen and nitrogen sparging on the degradation of atrazine in a 5 mg L^{-1} atrazine solution during sonication in the ultrasonic cell at an acoustic power of 57 W over 3 h

Time (min)	Atrazine concentration (mg L^{-1})					
	nitrogen			oxygen		
0	5.1	5.1	5.6	5.3	5.3	5.2
45	5.4	5.1	4.9	4.8	4.9	5.0
90	4.6	4.9	5.6	4.7	4.7	4.8
135	5.4	5.4	4.9	4.5	4.5	4.6
180	4.7	4.8	5.3	4.1	3.8	4.2

E.2.2 Ozone

The atrazine degradation during ozonation in the ultrasonic cell was investigated by measuring atrazine concentration over 3 h at ozone production rates of 0,003; 0,014; 0,030 and 0,047 mg s^{-1} (Table 5.6 in Chapter 5). Atrazine concentration was measured at time periods of 0; 15; 30; 45; 90; 135 and 180 min. Experiments were performed in duplicate. The data for the degradation of atrazine during ozonation is recorded in Table E.7. The data recorded in Table E.7 is presented in Figure 8.9 in Chapter 8, statistical analysis of the data is reported in Table F.35 in Appendix F.

Table E.7 : Atrazine concentration in a 5 mg L^{-1} atrazine solution during ozonation over 3 h at

ozone production rates of 0,003; 0,014; 0,030 and 0,047 mg s^{-1}

Time (min)	Atrazine concentration (mg L^{-1})							
	100 V		130 V		150 V		170 V	
0	5.0	4.9	5.2	5.1	5.0	5.2	5.3	4.9
15	4.7	4.7	4.7	4.7	4.1	4.1	3.8	3.5
30	4.4	4.4	4.5	4.5	3.6	3.9	2.3	2.3
45	4.2	4.0	4.2	4.4	2.5	2.8	1.8	1.8
90	3.5	3.5	3.8	3.4	2.3	2.1	1.0	0.9
135	3.1	3.2	3.0	3.0	1.3	1.4	0.5	0.7
180	2.8	2.7	2.4	2.5	0.9	1.0	0.1	0.2

Atrazine degradation was also investigated when ozonation of a 5 mg L^{-1} atrazine solution was combined with sonication at an acoustic power of 57 W. Atrazine concentration was measured at time periods of 0; 15; 30; 45; 90; 135 and 180 min. Experiments were performed in triplicate. The data for the degradation of atrazine during ozonation combined with sonication in Table E.8. The data recorded in Table E.8 is presented in Figure 8.11, statistical analysis is reported in Table F.36 in Appendix F.

Table E.8 : Atrazine concentration in a 5 mg L^{-1} atrazine solution during ozonation over 3 h at ozone production rates of 0,003; 0,014; 0,030 and 0,047 mg s^{-1} combined with sonication at an acoustic power of 57 W

Time (min)	Atrazine concentration (mg L^{-1})					
	100 V			130 V		
0	4.8	4.8	-	5.3	5.0	4.9
15	3.9	3.8	-	4.2	4.4	4.5
30	3.7	3.7	-	3.9	4.1	4.0
45	3.5	3.4	-	3.3	3.4	3.5
90	3.2	3.2	-	2.1	2.3	2.3
135	2.9	3.0	-	1.7	2.0	1.9
180	2.8	2.5	-	1.3	1.6	1.7
Time (min)	**Atrazine concentration (mg L^{-1})**					
	150 V			**170 V**		
0	5.3	5.2	5.1	4.9	4.9	4.9
15	3.7	3.7	3.7	2.9	3.2	3.0
30	2.8	2.9	2.7	2.0	2.2	2.2
45	2.3	2.2	2.2	1.4	1.5	1.5
90	1.6	1.6	1.8	0.5	0.5	0.5
135	1.0	1.1	1.1	0.1	0.1	0.2
180	0.6	0.6	0.6	0.0	0.0	0.0

Comparisons of atrazine degradation in a 5 mg L^{-1} atrazine solution during ozonation at ozone production rates of 0,003; 0,014; 0,030 and 0,047 mg s^{-1}, sonication at an acoustic power of 57 W and ozonation combined with sonication are shown in Figure E.1 to Figure E.4.

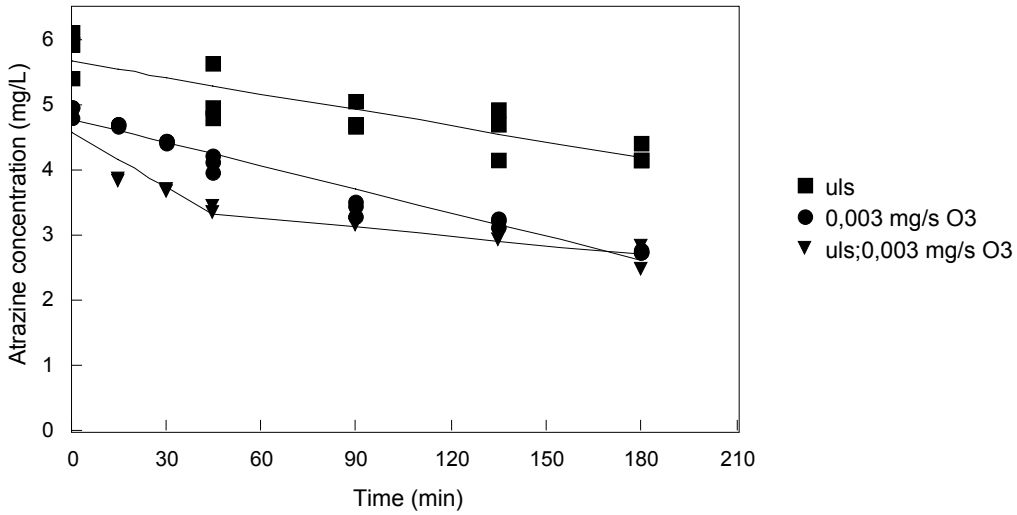

Figure E.1 : Atrazine degradation in a 5 mg L^{-1} atrazine solution over 3 h during ozonation (0,003 mg s^{-1}), sonication (57 W) and ozonation combined with sonication

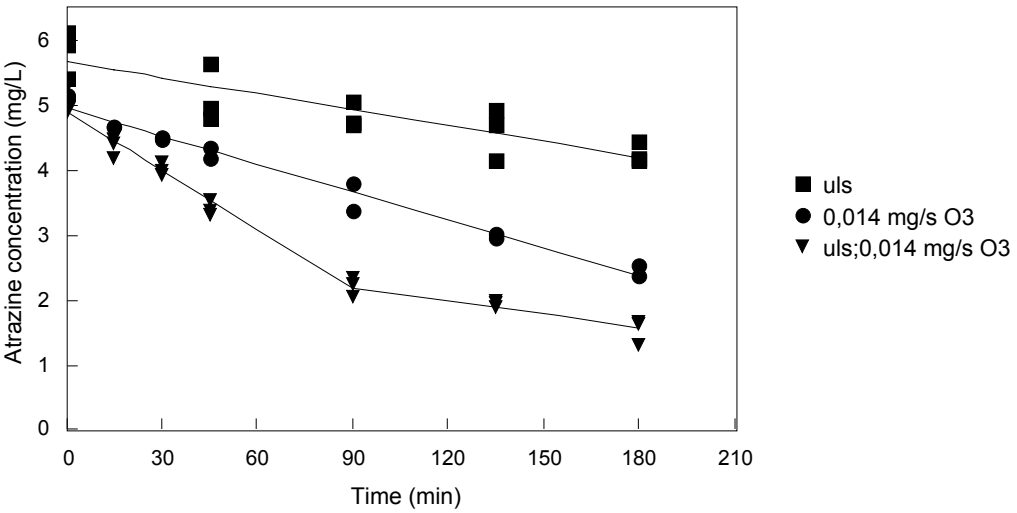

Figure E.2 : Atrazine degradation in a 5 mg L^{-1} atrazine solution over 3 h during ozonation (0,014 mg s^{-1}), sonication (57 W) and ozonation combined with sonication

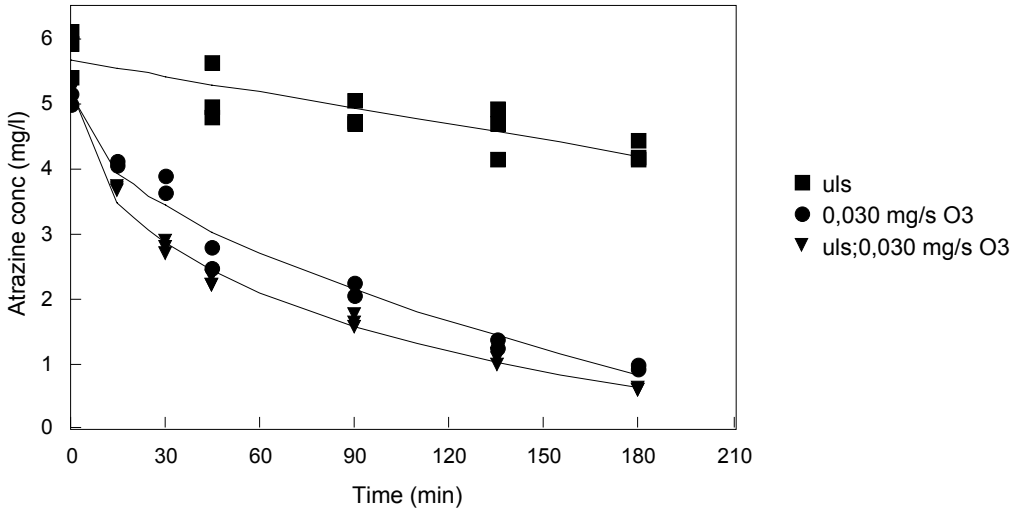

Figure E.3 : Atrazine degradation in a 5 mg L^{-1} atrazine solution over 3 h during ozonation (0,030 mg s^{-1}), sonication (57 W) and ozonation combined with sonication

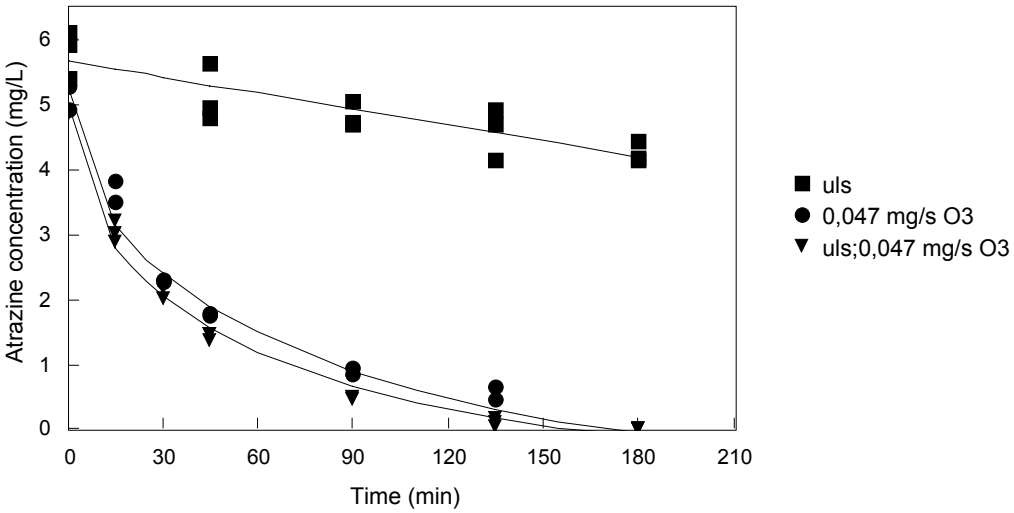

Figure E.4 : Atrazine degradation in a 5 mg L^{-1} atrazine solution over 3 h during ozonation (0,047 mg s^{-1}), sonication (57 W) and ozonation combined with sonication

E.2.3 Hydrogen peroxide

The oxidation of organic pollutants during water treatment with advanced oxidation processes such as ultrasound or ozone is enhanced with the addition of hydrogen peroxide due to the generation of additional free radicals. The molar ratio of ozone to hydrogen peroxide for optimal atrazine oxidation is reported in literature to vary between 1,5 and 3 (Beltrán et al., 1998; Meijers et al., 1993; Paillard et al., 1991). The hydrogen peroxide concentration used in the atrazine investigation was selected based on the atrazine degradation obtained over 45 min in solutions during ozonation with different hydrogen peroxide

concentrations. A hydrogen peroxide concentration of 27 mg L^{-1} is equivalent to a 2:1 molar ratio of ozone to hydrogen peroxide at an ozone production rate of 0,014 mg s^{-1}. A 5 mg L^{-1} atrazine solution was ozonation in the ultrasonic cell at an ozone production rate of 0,014 mg s^{-1} with hydrogen peroxide concentrations of 0, 1, 5, 10, 25 and 50 mg L^{-1}. The different hydrogen peroxide concentrations were prepared by dilution from a 3 072 mg L^{-1} peroxide stock solution that had been titrated against potassium permanganate. The experiments were performed in duplicate. The fraction of undegraded atrazine after ozonation for 45 min with the different hydrogen peroxide concentrations is presented in Figure E.5. The data presented in Figure E.5 is recorded in Table E.9, statistical analysis of the data is reported in Table F.37 in Appendix F.

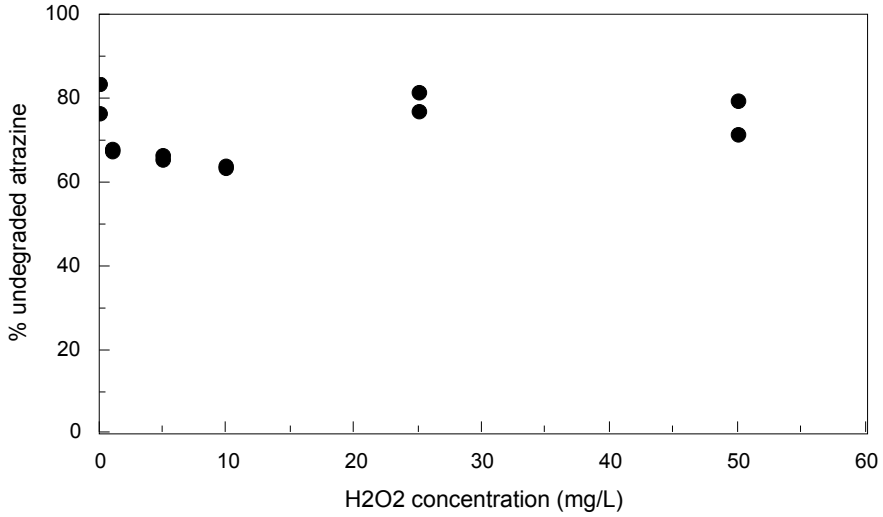

Figure E.5 : Fraction of undegraded atrazine in a 5 mg L^{-1} atrazine solution after ozonation (0,014 mg s^{-1}) for 45 min with hydrogen peroxide concentrations of 1, 5, 10, 25 and 50 mg L^{-1}

Table E.9 : Fraction of undegraded atrazine in a 5 mg L^{-1} atrazine solution after ozonation (0,014 mg s^{-1}) for 45 min with hydrogen peroxide concentrations of 1, 5, 10, 25 and 50 mg L^{-1}

H_2O_2 concentration (mg L^{-1})	Atrazine concentration (mg L^{-1})					
	Initial conc	Final conc	% undegraded	Initial conc	Final conc	% undegraded
0	5.0	3.9	78	4.4	3.7	84
1	4.9	3.3	67	4.7	3.2	68
5	4.5	3.0	66	4.9	3.2	65
10	4.8	3.1	64	5.0	3.2	64
25	4.5	3.7	82	4.7	3.6	77
50	4.9	3.9	80	5.6	4.0	71

Atrazine degradation over a period of 45 min was greatest, shown in Figure E.5, when ozonation was performed with a hydrogen peroxide concentration of 10 mg L^{-1}. A hydrogen peroxide concentration of 40 mg L^{-1} was thus used for ozonation and sonication experiments over a period of 3 h. Ozonation was performed at an ozone production rate of 0,014 mg s-1 and sonication at an acoustic power of 57 W. Atrazine concentration was measured at time periods of 0; 15; 30; 45; 90; 135 and 180 min with hydrogen peroxide addition, hydrogen peroxide combined with sonication, hydrogen peroxide combined with ozonation and hydrogen peroxide combined with both sonication and ozonation. The experiments were performed in triplicate. The data recorded in Table E.10 is presented in Figure 8.14 in Chapter 8, statistical analysis of the data is reported in Table F.38 in Appendix F.

Table E.10 : Atrazine concentration in a 5 mg L^{-1} atrazine solution with 40 mg L^{-1} hydrogen peroxide, hydrogen peroxide combined with sonication (57 W), hydrogen peroxide combined with ozonation (0,014 mg s^{-1}) and hydrogen peroxide combined with sonication and ozonation

Time (min)	Atrazine concentration (mg L^{-1})					
	H_2O_2			uls/H_2O_2		
0	4.9	5.2	5.0	5.0	5.0	-
45	4.8	5.1	5.0	4.4	4.4	-
90	4.8	4.5	4.7	4.1	4.0	-
135	4.5	4.9	4.9	3.3	3.3	-
180	4.6	4.8	4.5	3.0	2.8	-
Time (min)	**Atrazine concentration (mg L^{-1})**					
	O_3/H_2O_2			uls/O_3/H_2O_2		
0	5.5	5.4	5.7	5.2	5.1	5.1
15	4.4	4.5	4.1	4.4	4.2	4.1
30	3.9	3.8	3.8	4.1	4.0	4.0
45	3.7	3.3	3.4	3.9	3.7	3.5
90	2.5	2.7	2.7	3.0	2.8	2.7
135	2.1	2.1	2.2	2.8	2.5	3.0
180	1.4	1.7	1.7	2.7	2.6	2.7

Comparisons of atrazine degradation in a 5 mg L^{-1} atrazine solution during sonication with and without hydrogen peroxide, ozonation with and without hydrogen peroxide and sonication combined with ozonation with and without hydrogen peroxide are shown in Figure E.6 to Figure E.8.

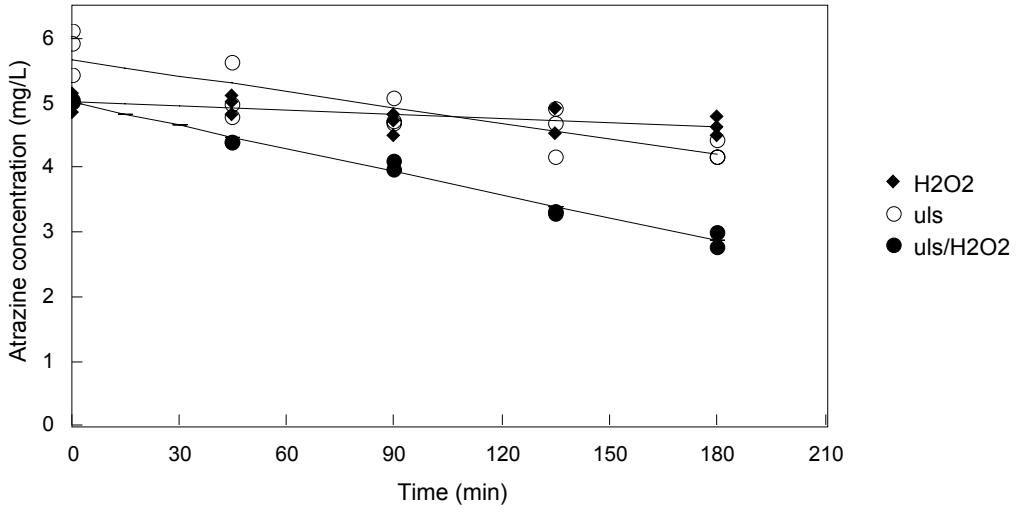

Figure E.6 : Atrazine degradation in a 5 mg L^{-1} atrazine solution with 40 mg L^{-1} hydrogen peroxide, sonication (57 W) and sonication combined with hydrogen peroxide

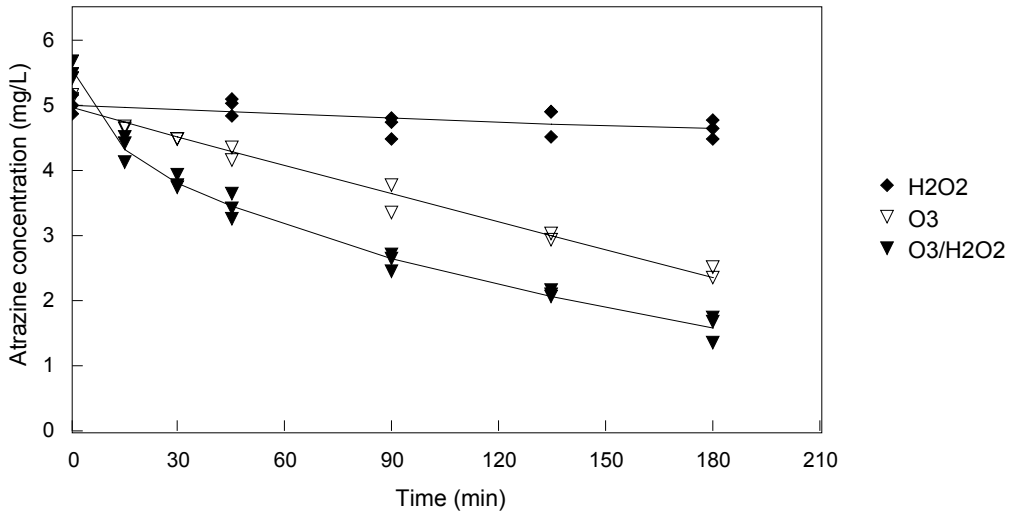

Figure E.7 : Atrazine degradation in a 5 mg L^{-1} atrazine solution with 40 mg L^{-1} hydrogen peroxide, ozonation (0,014 mg s^{-1}) and ozonation combined with hydrogen peroxide

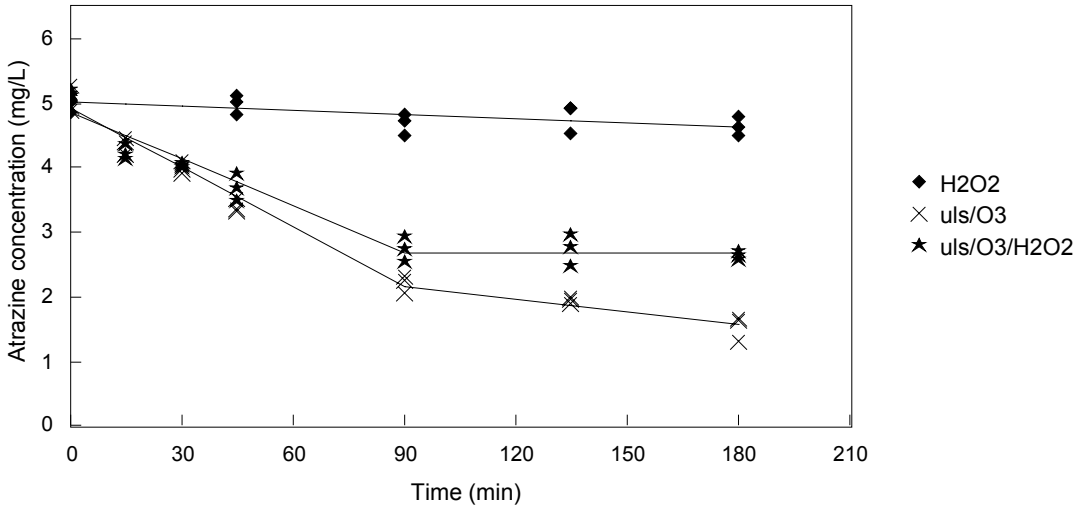

Figure E.8 : Atrazine degradation in a 5 mg L^{-1} solution with 40 mg L^{-1} hydrogen peroxide, sonication (57 W) combined with ozonation (0,014 mg s^{-1}) and sonication combined with ozonation and hydrogen peroxide

E.3 PRODUCT IDENTIFICATION

The HPLC method described in Section 5.4.4 was used to measure atrazine concentration during the degradation experiments discussed in Section 8.2. Product peaks appeared on the HPLC chromatograms as the concentration of atrazine decreased. The chromatogram of an unreacted 5 mg L^{-1} atrazine solution is presented in Figure E.9.

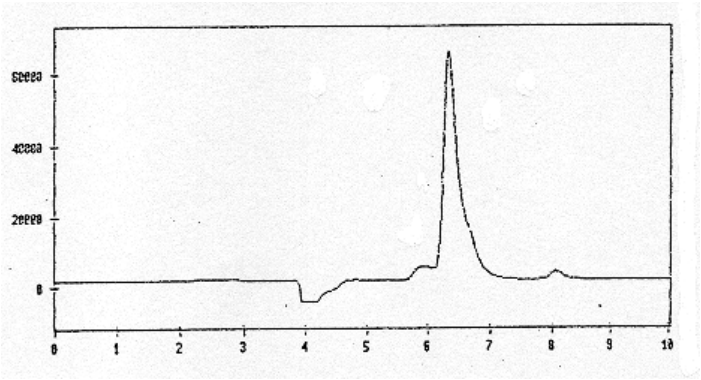

Figure E.9 : HPLC chromatogram of a 5 mg L^{-1} atrazine solution

The retention time of atrazine on the chromatograms for the HPLC analysis system, as shown in Figure E.9, is approximately 6,5 min, although some variation occurred on a daily basis. The blimp at a retention time of 8 min was an impurity in the atrazine feedstock (97 %) since it was evident on all chromatograms, even for a new atrazine feedstock obtained from Sanachem.

Gas chromatography-mass spectrometry (GC-MS) was used for the identification of degradation products. Analysis of atrazine samples after 3 h of sonication, ozonation and sonication combined with ozonation was performed at the CSIR and the Rand Afrikaans University (RAU). GC-MS analysis at the CSIR was performed on a Varian 2000 instrument with Saturn software. GC-MS analysis at RAU was performed on a Saturn 3 ion trap instrument with a J&W DB 1 column. The flow rate of ultrapure helium, the carrier gas, was 0,94 mL min^{-1}, a split ratio of 13:1 helium to sample was used. The injection sample volume was 3 μL and the temperature was ramped from 40 °C to 270 °C at a rate of 10 °C min^{-1} (Vorster, 2000). The GC-MS chromatograms (analysis performed at RAU) of the sonication, ozonation and sonication combined with ozonation samples are presented in Figure E.10.

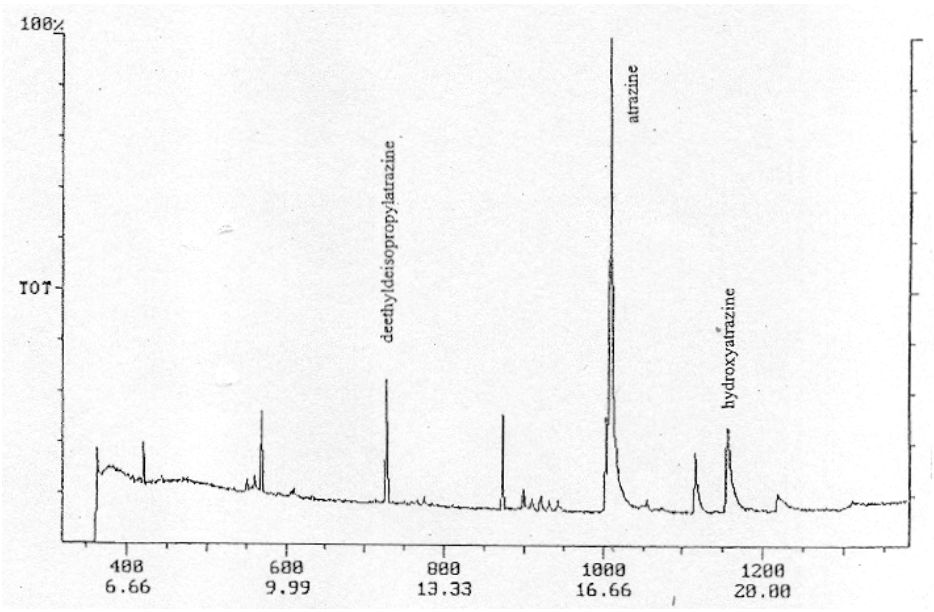

(a) ultrasound

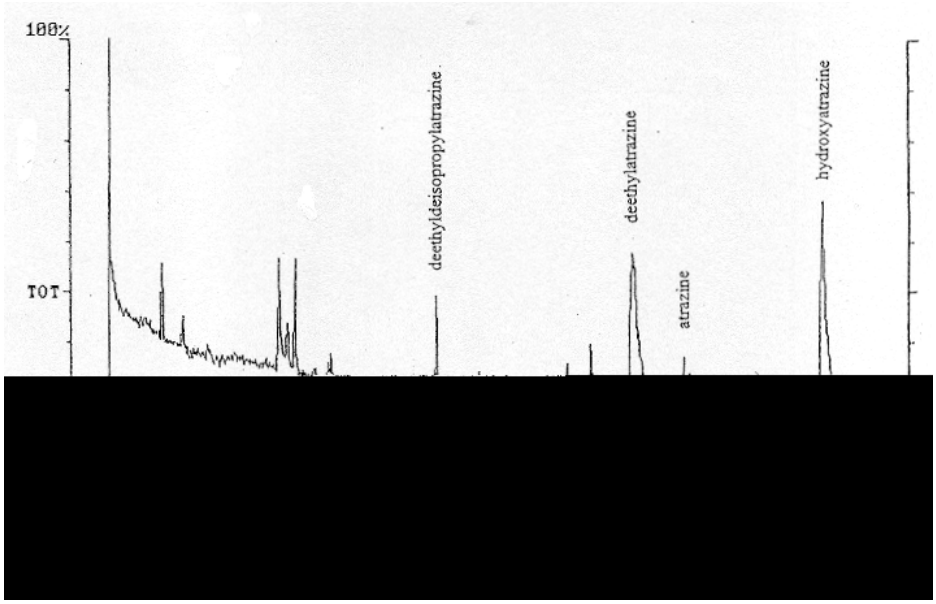

(b) ozone

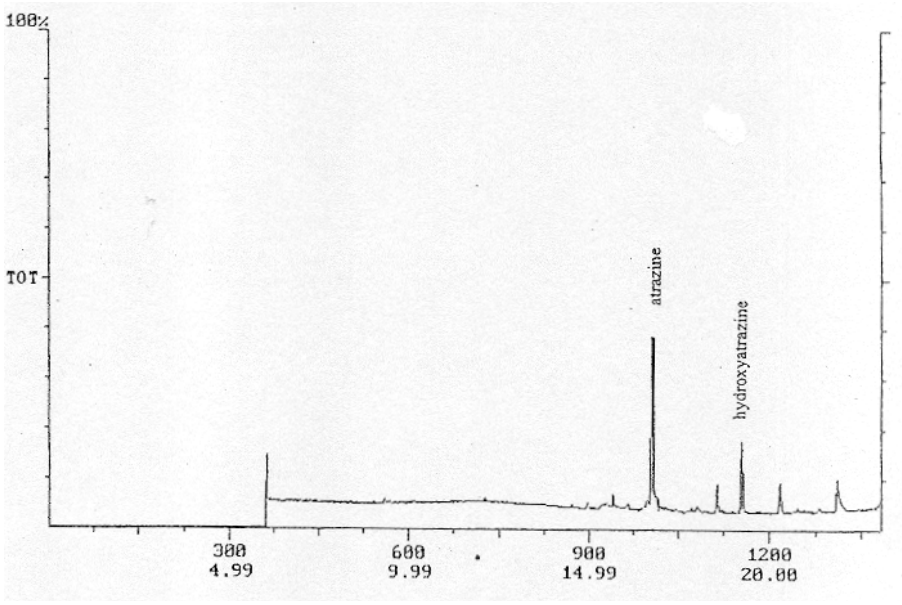

(c) ultrasound/ozone

Figure E.10 : GC-MS chromatograms of a 5 mg L^{-1} atrazine solution after sonication (57 W), ozonation (0,047 mg s^{-1}) and sonication combined with ozonation for 3 h

F

STATISTICAL ANALYSIS

Statistics is a valuable tool for engineers and scientists to use in the development of new products or the investigation of operation variables to optimise product and process quality (Kyle, 1995). Good engineering practise combines statistical thinking and tools with sound engineering theory. Statistical tools include experimental design to identify a data collection strategy, descriptive statistics such as sample mean and standard deviation, regression models to indicate correlation between variables and tests indicating variability and uncertainty (Vining, 1998).

Important statistics of a test sample are the sample mean $\bar{x}$ and the sample standard deviation, s. The sample mean is a measure of the central tendency of the data, the average value, and the standard deviation a measure of the spread or variation in the sample data, it reflects the average distance between a particular point and the sample mean (Kyle, 1995). The sample mean and standard deviation are defined as

$$\bar{x} = \frac{1}{n} \sum_{i=1}^{n} x_i \qquad [F.1]$$

$$s = \sqrt{\frac{\Sigma(x_i - \bar{x})^2}{n-1}} \qquad [F.2]$$

where n is the sample size and x_i a sample point (Vining, 1998).

The confidence interval of a calculated statistic is the range around the calculated value, at a particular confidence level (typically 95 or 99 %), that contains the true value. A confidence level of 95 % indicates that the range will contain the true value 95 % of the time. The width of the confidence interval is determined by the level of confidence (the higher the required confidence the wider the interval) and the variability of the data (the higher the data variability the wider the interval). The confidence interval

$$\bar{x} \pm t_{df,\,\alpha/2} \frac{s}{\sqrt{n}} \qquad [F.3]$$

is defined as the interval with 100 x (1 - α) % confidence (α is 0,05 for a 95 % confidence) of a population mean where $\bar{x}$ is the sample mean, s the sample standard deviation, n the sample size and $t_{df,\,\alpha/2}$ the value

from a *t*-table that corresponds to the right-hand tail of $\alpha/2$ for a *t*-distribution with *df* degrees of freedom (Vining, 1998). The term $\frac{s}{\sqrt{n}}$ is defined as the standard error of the estimate of the population mean.

The adequacy of a regression model of a set of experimental data is determined by the coefficient of determination, R^2 (Vining, 1998). The coefficient of determination is the proportion of total variability explained by the regression model and has a value $0 \leq R^2 \leq 1$. R^2 is close to 1 for models that fit experimental data well and close to 0 for models that fit experimental data poorly.

$$R^2 = \frac{SS_{reg}}{SS_{total}} = \frac{SS_{total} - SS_{res}}{SS_{total}} = 1 - \frac{SS_{res}}{SS_{total}} \quad [F.4]$$

where SS_{total} is the overall variability in data, SS_{reg} the variability explained by the regression model and SS_{res} the variability left unexplained and usually attributed to error (Vining, 1998). The values of SS_{total} and SS_{res} are calculated from the measured dependent variable y, the variable mean $\bar{y}$ and the prediction of the variable using the regression model $\hat{y}$ (Vining, 1998).

$$SS_{res} = \sum_{i=1}^{n} (y_i - \hat{y}_i)^2 \quad [F.5]$$

$$SS_{total} = \sum_{i=1}^{n} (y_i - \bar{y})^2 \quad [F.6]$$

Statistical analysis performed in the investigation includes the calculation of means and standard deviations, regression models to determine relationships between variables and experimental designs to determine the interaction between independent variables on the response of the dependent variable. Tables of calculated sample means, 95% confidence limits of the means and standard deviations are recorded in this appendix. Regression models and experimental designs are discussed in the appropriate chapters.

Statistical analysis of experiments performed for equipment characterisation is presented in Section F.1 and for the analytical procedures in Section F.2. Statistical analysis of the ultrasound experiments is presented in Section F.3, ozone experiments in Section F.4 and atrazine experiments in Section F.5.

F.1 EQUIPMENT CHARACTERISATION

Statistical analysis of the experimental data for the characterisation of equipment (recorded in Appendix A) is presented in this section.

F.1.1 Evaluation of machining the surface of a horn tip

Table F.1 : Statistical analysis of the formation of hydrogen peroxide during sonication with a new and a machined horn tip (Table A.1; Figure A.1)

Transducer vibration (μm)	New horn tip				
	valid N	mean (mg L^{-1})	-95 % confidence limit (mg L^{-1})	+95 % confidence limit (mg L^{-1})	std deviation (mg L^{-1})
0	3	0.00	-	-	0.000
2	3	0.02	0.01	0.03	0.003
4	3	0.04	0.02	0.06	0.009
6	3	0.06	0.04	0.08	0.009
8	3	0.08	0.07	0.09	0.005
10	3	0.10	0.09	0.10	0.003
11	3	0.10	0.09	0.11	0.004
12	3	0.11	0.10	0.12	0.003
	Machined horn tip				
0	3	0.00	-	-	0.000
2	3	0.02	0.00	0.03	0.006
4	3	0.05	0.03	0.06	0.004
6	3	0.07	0.05	0.08	0.005
8	3	0.08	0.07	0.09	0.003
10	3	0.10	0.09	0.10	0.002
11	3	0.11	0.10	0.12	0.004
12	3	0.11	0.10	0.10	0.004

F.1.2 Acoustic power measurement

Table F.2 : Statistical analysis of the measured acoustic power of the sonication experiments (Table A.3)

	5 μm				
Time (min)	valid N	mean (W)	-95 % confidence limit (W)	+95 % confidence limit (W)	std deviation (W)
0	3	24.6	23.7	25.5	0.36
1	3	24.4	24.0	24.8	0.17
2	3	24.4	24.0	24.8	0.17
3	3	24.3	23.6	24.9	0.25
4	3	24.3	23.6	24.9	0.25
5	3	24.3	23.6	24.9	0.25
6	3	24.2	23.8	24.5	0.15
7	3	24.2	23.8	24.5	0.15
8	3	24.1	23.8	24.4	0.12
9	3	24.0	23.6	24.3	0.15
10	3	23.9	23.3	24.4	0.23

Table F.2 cont.

Time (min)	valid N	mean (W)	-95 % confidence limit (W)	+95 % confidence limit (W)	std deviation (W)
			8 μm		
0	3	39.8	39.1	40.6	0.29
1	3	39.4	39.0	39.8	0.17
2	3	39.3	38.6	40.1	0.29
3	3	39.3	38.6	39.9	0.25
4	3	39.2	38.6	39.9	0.25
5	3	39.2	38.6	39.9	0.25
6	3	39.2	38.4	39.9	0.29
7	3	39.2	38.4	39.8	0.29
8	3	39.1	38.7	39.5	0.17
9	3	39.2	38.4	39.9	0.29
10	3	39.0	38.4	39.7	0.25
			11 μm		
0	3	57.7	53.7	61.7	1.61
1	3	57.6	53.9	61.3	1.49
2	3	57.4	54.0	60.9	1.40
3	3	57.3	53.5	61.1	1.53
4	3	57.1	53.4	60.8	1.49
5	3	56.8	53.0	60.6	1.52
6	3	56.5	52.4	60.6	1.67
7	3	56.2	51.6	60.9	1.86
8	3	56.2	51.8	60.5	1.76
9	3	55.6	50.7	60.5	1.97
10	3	55.5	51.0	60.0	1.80

Table F.3 : Statistical analysis of the measured temperatures in 500 mL water in an insulated vessel during sonication at transducer displacement amplitudes of 5, 8 and 11 μm (Table A.5; Figure A.3)

Time (min)	valid N	mean (°C)	-95 % confidence limit (°C)	+95 % confidence limit (°C)	std deviation (°C)
			5 μm		
0	3	23.7	23.6	23.9	0.06
1	3	24.2	23.8	24.5	0.15
2	3	24.8	24.6	25.0	0.10
3	3	25.4	25.1	25.7	0.12
4	3	26.0	25.8	26.1	0.06
5	3	26.6	-	-	0.00
6	3	27.1	27.0	27.3	0.06
7	3	27.8	27.6	27.9	0.06
8	3	28.3	28.1	28.5	0.10
9	3	28.9	28.8	29.1	0.06
10	3	29.4	29.1	29.8	0.15
12	3	30.3	29.7	31.0	0.25
14	3	31.3	30.5	32.0	0.31
16	3	32.1	31.3	32.8	0.31

Table F.3 cont.

Time (min)	valid N	mean (°C)	-95 % confidence limit (°C)	+95 % confidence limit (°C)	std deviation (°C)
			5 μm		
18	3	32.8	32.1	33.5	0.26
20	3	33.5	32.7	34.2	0.29
25	3	35.5	34.3	36.8	0.49
30	3	37.5	36.1	38.8	0.55
35	3	39.3	38.0	40.6	0.53
40	3	41.0	39.6	42.4	0.57
			8 μm		
0	3	23.9	23.6	24.2	0.11
1	3	24.6	23.9	25.3	0.31
2	3	25.6	24.7	26.5	0.36
3	3	26.6	25.7	27.5	0.36
4	3	27.6	26.5	28.6	0.41
5	3	28.5	27.6	29.4	0.36
6	3	29.4	28.4	30.4	0.40
7	3	30.4	29.4	31.4	0.40
8	3	31.3	30.5	32.2	0.35
9	3	32.3	31.6	33.0	0.30
10	3	33.2	32.3	34.0	0.35
12	3	35.1	34.2	36.0	0.36
14	3	36.9	36.0	37.8	0.36
16	3	38.7	37.8	39.7	0.38
18	3	40.6	39.7	41.5	0.36
20	3	42.4	41.5	43.3	0.36
25	3	46.6	45.7	47.5	0.35
30	3	50.1	49.9	51.5	0.32
35	3	54.5	53.6	55.5	0.38
40	3	58.3	58.1	58.4	0.06
			11 μm		
0	3	23.5	22.2	24.7	0.50
1	3	24.7	23.6	25.9	0.45
2	3	26.1	24.7	27.5	0.56
3	3	27.5	26.2	28.7	0.50
4	3	28.9	27.5	30.3	0.56
5	3	30.3	29.2	31.5	0.45
6	3	31.7	30.7	32.7	0.40
7	3	33.1	32.1	34.1	0.40
8	3	34.4	33.6	35.3	0.35
9	3	35.8	35.0	36.7	0.35
10	3	37.2	36.2	38.2	0.40
12	3	39.9	39.3	40.6	0.25
14	3	42.6	41.8	43.3	0.31
16	3	45.1	44.5	45.6	0.25
18	3	47.6	47.1	48.2	0.21
20	3	50.1	49.9	50.3	0.10
25	3	55.9	55.6	56.2	0.11
30	3	61.4	61.1	61.7	0.12
35	3	66.4	66.1	66.7	0.12
40	3	70.8			0.00

F.1.3 Volume experiments with the low intensity ultrasonic horn

Table F.4 : Statistical analysis of the formation of hydrogen peroxide in water volumes of 100 to 1 000 mL during sonication with the low intensity ultrasonic horn (Table A.7; Figure A.4)

Time (min)	valid N	mean ($mg\ L^{-1}$)	-95 % confidence limit ($mg\ L^{-1}$)	+95 % confidence limit ($mg\ L^{-1}$)	std deviation ($mg\ L^{-1}$)
100 mL					
0	2	0.00	-	-	0.000
2	2	0.11	0.06	0.16	0.006
4	2	0.19	0.17	0.21	0.002
6	2	0.27	0.10	0.44	0.019
8	2	0.32	0.21	0.45	0.013
10	2	0.37	-	-	0.000
15	2	0.46	0.34	0.58	0.013
20	2	0.55	0.47	0.64	0.009
200 mL					
0	2	0.00	-	-	0.000
2	2	0.07	0.00	0.16	0.011
4	2	0.11	0.05	0.18	0.007
6	2	0.15	0.13	0.17	0.002
8	2	0.19	0.16	0.22	0.004
10	2	0.23	0.20	0.26	0.004
15	2	0.27	0.16	0.39	0.013
20	2	0.33	0.21	0.45	0.013
300 mL					
0	2	0.00	-	-	0.000
2	2	0.04	0.01	0.08	0.004
4	2	0.08	0.05	0.11	0.004
6	2	0.10	0.00	0.20	0.011
8	2	0.13	0.12	0.15	0.002
10	2	0.15	0.10	0.20	0.006
15	2	0.20	0.05	0.35	0.017
20	2	0.23	-	-	0.000
400 mL					
0	2	0.00	-	-	0.000
2	2	0.05	0.03	0.07	0.002
4	2	0.07	-	-	0.000
6	2	0.10	0.03	0.16	0.007
8	2	0.11	0.09	0.13	0.002
10	2	0.13	-	-	0.000
15	2	0.17	0.14	0.21	0.004
20	2	0.20	0.15	0.25	0.006
500 mL					
0	2	0.00	-	-	0.000
2	2	0.03	-	-	0.000
4	2	0.04	0.00	0.07	0.004
6	2	0.07	0.00	0.13	0.007
8	2	0.08	0.06	0.09	0.002
10	2	0.10	-	-	0.000
15	2	0.14	0.07	0.21	0.007
20	2	0.17	0.14	0.20	0.004

Table F.4 cont.

Time (min)	valid N	mean (mg L^{-1})	-95 % confidence limit (mg L^{-1})	+95 % confidence limit (mg L^{-1})	std deviation (mg L^{-1})
600 mL					
0	2	0.00	-	-	0.000
2	2	0.03	0.00	0.06	0.004
4	2	0.04	-	-	0.000
6	2	0.05	0.03	0.07	0.002
8	2	0.07	-	-	0.000
10	2	0.09	0.02	0.17	0.009
15	2	0.11	0.08	0.15	0.004
20	2	0.15	0.06	0.23	0.009
700 mL					
0	2	0.00	-	-	0.000
2	2	0.02	0.00	0.09	0.007
4	2	0.04	0.02	0.06	0.002
6	2	0.05	0.02	0.08	0.004
8	2	0.06	0.02	0.09	0.004
10	2	0.08	0.04	0.11	0.004
15	2	0.10	0.08	0.12	0.002
20	2	0.12	0.04	0.20	0.009
800 mL					
0	2	0.00	-	-	0.000
2	2	0.02	0.00	0.05	0.004
4	2	0.03	0.00	0.06	0.004
6	2	0.04	0.00	0.09	0.006
8	2	0.06	0.00	0.14	0.009
10	2	0.07	0.00	0.14	0.007
15	2	0.10	-	-	0.000
20	2	0.13	0.08	0.18	0.006
900 mL					
0	2	0.00	-	-	0.000
2	2	0.03	0.00	0.06	0.004
4	2	0.03	0.00	0.07	0.004
6	2	0.05	0.02	0.08	0.004
8	2	0.05	0.00	0.10	0.006
10	2	0.07	0.03	0.10	0.004
15	2	0.10	-	-	0.000
20	2	0.11	0.07	0.14	0.004
1 000 mL					
0	2	0.00	-	-	0.000
2	2	0.01	0.00	0.03	0.002
4	2	0.03	-	-	0.000
6	2	0.04	0.00	0.07	0.004
8	2	0.04	0.00	0.09	0.006
10	2	0.06	0.00	0.14	0.009
15	2	0.08	0.00	0.21	0.014
20	2	0.10	-	-	0.000

Table F.5 : Statistical analysis of the temperature measurements in water volumes of 100 to

1 000 mL during sonication with the low intensity ultrasonic horn (Table A.10)

Time (min)	valid N	mean (°C)	-95 % confidence limit (°C)	+95 % confidence limit (°C)	std deviation (°C)
			100 mL		
0	3	24.8	23.8	25.9	0.42
2	3	36.6	35.4	37.7	0.47
4	3	45.0	44.1	45.9	0.35
6	3	52.1	49.9	54.2	0.86
8	3	57.9	55.1	60.8	1.14
10	3	64.2	60.4	67.9	1.51
			200 mL		
0	3	24.2	23.1	25.3	0.44
2	3	30.5	28.5	32.5	0.81
4	3	35.3	32.9	37.7	0.95
6	3	39.8	37.8	41.8	0.79
8	3	44.5	42.8	46.2	0.69
10	3	48.6	46.7	50.5	0.78
			300 mL		
0	3	24.0	23.4	24.7	0.25
2	3	28.0	26.9	29.1	0.46
4	3	31.4	29.7	33.2	0.70
6	3	34.7	33.0	36.4	0.70
8	3	38.1	36.6	39.6	0.60
10	3	41.0	38.6	43.4	0.95
			400 mL		
0	3	25.6	24.6	26.6	0.40
2	3	28.4	27.3	29.5	0.46
4	3	31.1	30.3	31.9	0.32
6	3	33.7	33.0	34.4	0.26
8	3	36.0	35.3	36.7	0.26
10	3	38.2	37.3	39.1	0.35
			500 mL		
0	3	26.2	25.5	26.9	0.30
2	3	28.7	27.2	30.1	0.58
4	3	31.0	30.0	32.0	0.40
6	3	32.9	32.0	33.9	0.38
8	3	35.2	34.4	36.0	0.32
10	3	37.1	36.3	38.0	0.35
			600 mL		
0	3	26.3	25.3	27.4	0.42
2	3	28.5	27.4	29.7	0.46
4	3	30.3	29.6	31.1	0.29
6	3	32.2	31.3	33.2	0.38
8	3	33.8	32.5	35.0	0.49
10	3	35.7	34.4	37.0	0.52

Table F.5 cont.

700 mL					
Time (min)	valid N	mean (°C)	-95 % confidence limit (°C)	+95 % confidence limit (°C)	std deviation (°C)
0	3	26.5	26.0	27.0	0.20
2	3	28.2	27.7	28.8	0.21
4	3	29.5	28.4	30.6	0.44
6	3	31.1	30.8	31.5	0.15
8	3	32.7	32.1	33.2	0.23
10	3	34.1	33.9	34.2	0.06
800 mL					
0	3	24.5	23.8	25.2	0.30
2	3	25.7	25.4	26.0	0.12
4	3	27.3	26.7	27.8	0.21
6	3	28.7	28.4	29.0	0.12
8	3	29.9	29.6	30.2	0.12
10	3	31.1	30.8	31.5	0.15
900 mL					
0	3	24.4	23.5	25.2	0.35
2	3	25.7	24.9	26.5	0.32
4	3	26.5	25.4	27.6	0.46
6	3	28.2	27.3	29.0	0.35
8	3	29.4	28.1	30.7	0.53
10	3	30.5	29.4	31.6	0.44
1 000 mL					
0	3	25.9	25.7	26.1	0.10
2	3	27.0	26.8	27.2	0.10
4	3	28.2	27.6	28.7	0.21
6	3	29.2	28.6	29.9	0.25
8	3	30.3	29.5	31.0	0.31
10	3	31.3	30.5	32.0	0.31

F.1.4 Acoustic power reduction due to the ultrasonic cell lid design

Table F.6 : Statistical analysis of the comparison of measured temperatures during sonication with the low intensity horn in 500 mL of water in the ultrasonic cell and in a beaker (Table A.12; Figure A.7)

Ultrasonic cell					
Time (min)	valid N	mean (°C)	-95 % confidence limit (°C)	+95 % confidence limit (°C)	std deviation (°C)
0	3	26.9	26.6	27.2	0.12
2	3	27.2	26.8	27.6	0.17
4	3	27.7	27.2	28.2	0.20
6	3	28.1	27.7	28.5	0.17
8	3	28.4	28.1	28.8	0.15
10	3	28.7	28.6	28.9	0.06

Table F.6 cont.

Beaker					
Time (min)	valid N	mean (°C)	-95 % confidence limit (°C)	+95 % confidence limit (°C)	std deviation (°C)
0	3	26.2	25.5	26.9	0.30
2	3	28.7	27.3	30.1	0.58
4	3	31.0	30.0	32.0	0.40
6	3	32.9	32.0	33.9	0.38
8	3	35.2	34.4	36.0	0.32
10	3	37.1	36.3	38.0	0.35

F.1.5 Rotameter calibration

Table F.7 : Statistical analysis of the rotameter calibration for oxygen at regulator pressures of 200 and 300 kPa (Table A.15; Figure A.10)

200 kPa					
Rotameter setting	valid N	mean (mL s^{-1})	-95 % confidence limit (mL s^{-1})	+95 % confidence limit (mL s^{-1})	std deviation (mL s^{-1})
0	1	0.0	-	-	-
1	4	0.7	0.7	0.8	0.01
2	4	1.7	1.7	1.8	0.03
3	4	3.4	3.4	3.5	0.05
4	4	6.0	6.0	6.1	0.05
5	4	8.8	8.7	8.8	0.04
6	4	11.1	10.9	11.3	0.13
7	4	13.6	13.2	13.9	0.21
8	4	16.3	15.9	16.8	0.29
9	4	19.1	18.5	19.6	0.34
10	4	21.3	20.8	21.8	0.30
300 kPa					
0	1	0.0	-	-	-
1	4	0.7	0.7	0.7	0.01
2	4	1.7	1.7	1.8	0.03
3	4	3.6	3.5	3.7	0.06
4	4	6.2	6.1	6.2	0.03
5	4	8.4	7.8	9.1	0.25
6	4	11.5	11.1	11.8	0.24
7	4	13.9	13.3	14.5	0.38
8	4	16.3	15.5	17.1	0.48
9	4	19.7	18.9	20.6	0.52
10	4	21.7	21.1	22.2	0.37

Table F.8 : Statistical analysis of the rotameter calibration for nitrogen at a regulator pressure of 200 kPa (Table A.16)

Rotameter setting	Flow rate				
	valid N	mean (mL s^{-1})	-95 % confidence limit (mL s^{-1})	+95 % confidence limit (mL s^{-1})	std deviation (mL s^{-1})
2.0	5	2.0	1.9	2.1	0.05
3.0	5	4.2	4.2	4.2	0.04
3.5	4	5.1	5.1	5.2	0.03
3.7	6	6.0	6.0	6.0	0.03
4.0	5	6.5	6.5	6.5	0.01

F.1.6 Ozone generator calibration

Table F.9 : Statistical analysis of the dissolved ozone concentration in solution during ozonation with ozone generated by a Sorbios ozone generator in a 2,4 mL s^{-1} oxygen gas stream at voltage settings between 100 and 200 V (Table A.17; Figure A.11)

Voltage (V)	Ozone concentration				
	valid N	mean (mg L^{-1})	-95 % confidence limit (mg L^{-1})	+95 % confidence limit (mg L^{-1})	std deviation (mg L^{-1})
100	3	7.7	7.2	8.3	0.23
110	3	14.7	14.0	15.3	0.27
130	3	34.5	32.6	36.3	0.74
150	3	73.2	72.6	73.7	0.23
170	3	111.9	110.3	113.6	0.68
200	3	178.4	172.5	184.3	2.39

F.2 ANALYTICAL PROCEDURES

Statistical analysis of information recorded in Appendix B is presented in this section. Means and standard deviations were not calculated for the hydrogen peroxide calibration curves since three stock solutions with slightly different concentrations were used to prepare each calibration curve. The calibration curves were not prepared from triplicate injections of the same solution.

Table F.10 : Statistical analysis of the atrazine calibration curve (Table B.5; Figure B.5)

Atrazine concentration (mg L^{-1})	Peak area				
	valid N	mean (units)	-95 % confidence limit (units)	+95 % confidence limit (units)	std deviation (units)
0	3	0	-	-	0
1	3	218,170	181,214	256,727	15,199
2	3	467,178	406,292	528,065	24,510
5	3	1,117,528	912,004	1,323,052	82,734
10	3	1,933,690	1,675,624	2,191,755	103,885
20	3	4,167,816	3,827,919	4,507,713	136,827

F.3 ULTRASOUND EXPERIMENTS

Statistical analysis of the ultrasound experimental data recorded in Appendix C is presented in this section.

F.3.1 Dissolved oxygen concentration

Table F.11 : Statistical analysis of the dissolved oxygen concentration in oxygen-saturated water during sonication, without sonication (control) and during nitrogen sparging without sonication (Table C.1; Figure 6.1)

Time (min)	valid N	mean (mg L^{-1})	-95 % confidence limit (mg L^{-1})	+95 % confidence limit (mg L^{-1})	std deviation (mg L^{-1})
Control					
0	3	39.1	35.0	43.2	1.65
5	3	36.1	32.7	39.5	1.39
15	3	32.7	32.0	33.8	0.42
30	2	29.8	28.5	31.1	0.14
45	2	28.9	27.6	30.2	0.14
60	3	27.8	27.2	28.3	0.21
90	3	25.8	25.0	26.5	0.31
120	2	25.2	23.9	26.5	0.14
150	3	24.6	23.9	25.3	0.26
180	2	24.0	21.5	26.5	0.28
Sonication					
0	3	38.2	33.6	42.8	1.85
5	3	29.2	26.5	31.9	1.10
15	3	23.5	21.5	25.5	0.80
30	3	20.9	20.2	21.6	0.26
45	2	18.9	8.0	29.7	1.20
60	3	17.4	16.6	18.1	0.29
90	3	14.3	14.1	14.5	0.10
120	3	13.2	12.4	14.0	0.32
150	2	12.1	10.8	13.4	0.14
180	1	11.2	-	-	-
Nitrogen					
0	3	38.9	33.5	44.2	2.15
5	3	3.0	2.6	3.3	0.15
15	3	1.8	1.4	2.1	0.15
30	3	1.6	1.0	2.1	0.21
45	0	-	-	-	-
60	2	1.6	0.3	2.9	0.14
90	0	-	-	-	-
120	2	1.9	0.6	3.2	0.14
150	0	-	-	-	-
180	2	1.5	0.8	2.1	0.07

Table F.12 : Statistical analysis of the dissolved oxygen concentration in water saturated with air (Table C.2)

valid N	mean ($mg\ L^{-1}$)	-95 % confidence limit ($mg\ L^{-1}$)	+95 % confidence limit ($mg\ L^{-1}$)	std deviation ($mg\ L^{-1}$)
40	10.0	9.7	10.3	0.90

Table F.13 : Statistical analysis of the dissolved oxygen concentration in nitrogen-, air- and oxygen-saturated water during sonication in the ultrasonic cell at an acoustic power of 57 W (Table C.3; Figure 6.2)

Time (min)	valid N	mean ($mg\ L^{-1}$)	-95 % confidence limit ($mg\ L^{-1}$)	+95 % confidence limit ($mg\ L^{-1}$)	std deviation ($mg\ L^{-1}$)
Control					
0	2	9.7	8.4	11.0	0.14
5	2	10.8	10.1	11.4	0.07
10	2	11.0	10.3	11.6	0.07
20	2	10.3	7.8	12.8	0.28
40	2	11.8	11.1	12.4	0.07
Nitrogen					
0	2	0.9	0.2	1.5	0.07
5	2	0.8	-	-	0.00
10	2	0.8	0.0	2.7	0.21
20	2	0.9	0.0	2.2	0.14
40	2	1.1	0.0	3.0	0.21
Air					
0	2	11.0	4.0	17.9	0.78
5	2	12.3	11.6	12.9	0.07
10	2	12.8	5.8	19.7	0.78
20	2	13.2	7.4	18.9	0.64
40	2	13.2	12.5	13.8	0.07
Oxygen					
0	2	39.9	38.6	41.1	0.14
5	2	40.2	37.7	42.7	0.28
10	2	39.8	36.6	42.9	0.35
20	2	39.5	33.1	45.9	0.71
40	2	38.5	32.1	44.9	0.71

Table F.14 : Overall statistical analysis of the dissolved oxygen concentration in nitrogen-, air- and oxygen-saturated water during sonication in the ultrasonic cell (Table C.3; Figure 6.2)

Gases	valid N	mean ($mg\ L^{-1}$)	-95 % confidence limit ($mg\ L^{-1}$)	+95 % confidence limit ($mg\ L^{-1}$)	std deviation ($mg\ L^{-1}$)
control	10	10.7	10.2	11.2	0.73
nitrogen	10	0.9	0.8	1.0	0.16
air	10	12.5	11.8	13.1	0.96
oxygen	10	39.6	39.1	40.1	0.71

F.3.2 Hydrogen peroxide formation

Table F.15 : Statistical analysis of the formation of hydrogen peroxide in nitrogen-, air- and oxygen-saturated water during sonication in the ultrasonic cell for 16 h at an acoustic power of 57 W (Table C.4; Figure 6.3)

Time (min)	valid N	mean (mg L^{-1})	-95 % confidence limit (mg L^{-1})	+95 % confidence limit (mg L^{-1})	std deviation (mg L^{-1})
Control					
0	3	0.00	-	-	0.000
4	3	0.02	-	-	0.000
8	3	0.04	0.02	0.06	0.008
12	3	0.05	0.04	0.06	0.003
16	3	0.07	0.05	0.08	0.006
20	3	0.09	0.06	0.11	0.010
30	3	0.11	0.10	0.13	0.007
60	3	0.15	0.15	0.15	0.001
120	3	0.26	0.21	0.32	0.023
240	3	0.38	0.29	0.47	0.035
480	3	0.77	0.75	0.79	0.008
960	2	0.92	0.39	1.46	0.060
Nitrogen					
0	3	0.00	0.00	0.01	0.002
4	3	0.01	0.00	0.10	0.001
8	3	0.02	0.01	0.03	0.004
12	3	0.04	0.03	0.05	0.004
16	3	0.04	0.04	0.05	0.002
20	3	0.06	0.05	0.07	0.004
30	3	0.05	0.04	0.06	0.005
60	3	0.06	0.04	0.07	0.006
120	3	0.06	0.06	0.07	0.002
240	2	0.09	0.02	0.15	0.007
480	2	0.09	0.04	0.14	0.005
960	2	0.08	0.00	0.19	0.012
Air					
0	3	0.00	0.00	0.01	0.002
4	3	0.02	0.01	0.02	0.001
8	3	0.04	0.04	0.05	0.001
12	3	0.05	0.04	0.05	0.003
16	3	0.07	0.06	0.09	0.006
20	3	0.09	0.08	0.09	0.002
30	3	0.11	0.08	0.13	0.010
60	3	0.18	0.17	0.20	0.006
120	3	0.28	0.23	0.32	0.020
240	3	0.34	0.33	0.36	0.006
480	3	0.78	0.63	0.93	0.061
960	3	1.03	0.79	1.27	0.097

Table F.15 cont.

Oxygen					
Time (min)	valid N	mean (mg L^{-1})	-95 % confidence limit (mg L^{-1})	+95 % confidence limit (mg L^{-1})	std deviation (mg L^{-1})
0	3	0.01	0.01	0.02	0.002
4	3	0.04	0.03	0.06	0.006
8	3	0.06	0.05	0.08	0.007
12	3	0.08	0.06	0.10	0.008
16	3	0.09	0.08	0.10	0.005
20	3	0.11	0.10	0.11	0.001
30	3	0.16	0.14	0.17	0.006
60	3	0.26	0.25	0.26	0.003
120	3	0.43	0.41	0.45	0.009
240	3	0.48	0.44	0.52	0.016
480	3	0.86	0.59	1.13	0.108
960	2	1.21	0.38	2.05	0.093

Table F.16 : Statistical analysis of the formation of hydrogen peroxide in nitrogen-saturated water and the control during sonication in the ultrasonic cell at an acoustic power of 24 W (Table C.5; Figure 6.4; Figure 6.5)

Control					
Time (min)	valid N	mean (mg L^{-1})	-95 % confidence limit (mg L^{-1})	+95 % confidence limit (mg L^{-1})	std deviation (mg L^{-1})
0	3	0.00	-	-	0.000
4	3	0.01	0.00	0.02	0.004
8	3	0.02	-	-	0.000
12	3	0.03	0.02	0.04	0.004
16	3	0.04	0.03	0.05	0.003
20	3	0.05	0.04	0.07	0.006
30	3	0.07	0.06	0.08	0.003
60	3	0.14	0.13	0.14	0.003
120	3	0.24	0.23	0.26	0.006
240	3	0.42	0.40	0.45	0.009
480	3	0.74	0.67	0.80	0.026
960	1	0.98	-	-	-
Nitrogen					
0	3	0.00	-	-	0.000
4	3	0.01	-	-	0.000
8	3	0.02	0.02	0.03	0.002
12	3	0.03	0.03	0.04	0.003
16	3	0.05	0.04	0.05	0.002
20	3	0.05	0.04	0.06	0.004
30	3	0.06	0.05	0.07	0.004
60	3	0.05	0.05	0.06	0.003
120	3	0.06	0.05	0.07	0.003
240	3	0.07	0.06	0.09	0.004

F.3.3 Hydrogen peroxide degradation

Table F.17 : Statistical analysis of the degradation of hydrogen peroxide (normalised data) in nitrogen-, air- and oxygen-saturated water after sonication in the ultrasonic cell for 16 h at an acoustic power of 57 W (Table C.6; Figure 6.7)

Time (min)	valid N	mean	-95 % confidence limit	+95 % confidence limit	std deviation
Control					
0	3	1.00	-	-	0.000
5	3	1.00	0.99	1.01	0.004
10	3	1.00	0.99	1.02	0.006
20	3	1.00	0.96	1.05	0.018
30	3	1.00	0.94	1.05	0.021
60	3	0.98	0.93	1.04	0.021
90	2	0.97	0.81	1.14	0.019
120	2	0.97	0.69	1.25	0.031
150	2	0.95	0.61	1.29	0.038
180	1	0.95	-	-	-
Nitrogen					
0	3	1.00	-	-	0.000
5	3	0.97	0.94	1.00	0.012
10	3	0.97	0.91	1.03	0.025
20	3	0.95	0.87	1.02	0.030
30	3	0.95	0.91	0.98	0.015
60	3	0.89	0.86	0.92	0.014
90	3	0.86	0.79	0.94	0.030
120	3	0.84	0.76	0.92	0.032
150	3	0.81	0.70	0.92	0.046
180	3	0.76	0.73	0.79	0.012
Air					
0	3	0.00	-	-	0.000
5	3	0.97	0.87	1.07	0.040
10	3	0.96	0.92	1.01	0.018
20	3	0.95	0.89	1.01	0.025
30	3	0.94	0.90	0.99	0.018
60	3	0.89	0.83	0.95	0.024
90	2	0.87	0.80	0.94	0.008
120	3	0.82	0.77	0.86	0.018
150	3	0.79	0.77	0.81	0.009
180	3	0.76	0.70	0.81	0.023
Oxygen					
0	3	1.00	-	-	0.000
5	3	0.97	0.89	1.05	0.032
10	3	0.98	0.89	1.06	0.036
20	3	0.96	0.92	1.00	0.016
30	3	0.96	0.90	1.02	0.025
60	3	0.92	0.89	0.94	0.012
90	3	0.88	0.83	0.93	0.020
120	3	0.85	0.79	0.92	0.026
150	3	0.82	0.77	0.86	0.018
180	3	0.78	0.78	0.79	0.003

F.3.4 Interval experiments

Table F.18 : Statistical analysis of the formation of hydrogen peroxide in oxygen-saturated water and a control in the ultrasonic cell during 15 min of sonication, 15 min without sonication and a further 15 min with sonication (Table C.8; Figure 6.8)

Time (min)	valid N	mean (mg L^{-1})	-95 % confidence limit (mg L^{-1})	+95 % confidence limit (mg L^{-1})	std deviation (mg L^{-1})
Control					
0	3	0.00	-	-	0.000
5	3	0.04	0.03	0.04	0.003
10	3	0.06	0.05	0.07	0.003
15	3	0.08	0.07	0.08	0.002
20	3	0.08	0.07	0.08	0.003
25	3	0.08	0.07	0.09	0.004
30	3	0.08	0.07	0.08	0.003
35	3	0.10	0.10	0.11	0.002
40	3	0.12	0.11	0.14	0.006
45	3	0.14	0.14	0.15	0.003
Oxygen					
0	3	0.01	0.00	0.03	0.008
5	3	0.05	0.05	0.06	0.003
10	3	0.09	0.08	0.10	0.004
15	3	0.11	0.10	0.12	0.003
20	3	0.11	0.10	0.12	0.004
25	3	0.11	0.10	0.13	0.006
30	3	0.11	0.09	0.12	0.006
35	3	0.13	0.12	0.14	0.003
40	3	0.16	0.15	0.18	0.006
45	3	0.19	0.18	0.20	0.004

Table F.19 : Statistical analysis of the formation of hydrogen peroxide in water during sonication in the ultrasonic cell with 15 min of oxygen saturation, 15 min of nitrogen saturation and a further 15 min of oxygen saturation (Table C.9; Figure 6.9)

Time (min)	Gas	valid N	mean (mg L^{-1})	-95 % confidence limit (mg L^{-1})	+95 % confidence limit (mg L^{-1})	std deviation (mg L^{-1})
0	O_2	3	0.01	0.00	0.01	0.003
5	O_2	3	0.04	0.03	0.05	0.003
10	O_2	3	0.08	0.07	0.09	0.003
15	O_2/N_2	3	0.11	0.10	0.12	0.004
20	N_2	3	0.13	0.12	0.14	0.004
25	N_2	3	0.14	0.13	0.15	0.003
30	N_2/O_2	3	0.15	0.14	0.16	0.004
35	O_2	3	0.16	0.15	0.17	0.004
40	O_2	3	0.18	0.17	0.19	0.004
45	O_2	3	0.20	0.19	0.21	0.004

F.3.5 Commercial hydrogen peroxide experiments

Table F.20 : Statistical analysis of the formation of hydrogen peroxide in nitrogen-, air- and oxygen-saturated 0,28 mg L^{-1} hydrogen peroxide solutions during sonication in the ultrasonic cell for 1 h at an acoustic power of 57 W (Table C.10; Figure 6.10)

Time (min)	valid N	mean (mg L^{-1})	-95 % confidence limit (mg L^{-1})	+95 % confidence limit (mg L^{-1})	std deviation (mg L^{-1})
Control					
0	3	0.28	0.27	0.29	0.003
5	3	0.28	0.26	0.30	0.008
10	3	0.30	0.29	0.30	0.003
20	3	0.33	0.31	0.34	0.004
30	3	0.25	0.32	0.37	0.009
60	3	0.40	0.40	0.41	0.003
Nitrogen					
0	3	0.28	0.26	0.29	0.006
5	3	0.25	0.25	0.26	0.002
10	3	0.25	0.24	0.27	0.006
20	3	0.25	0.23	0.26	0.006
30	3	0.26	0.24	0.28	0.008
60	3	0.25	0.24	0.27	0.004
Air					
0	3	0.27	0.27	0.28	0.003
5	3	0.28	0.26	0.29	0.006
10	3	0.29	0.28	0.31	0.007
20	3	0.33	0.31	0.35	0.009
30	3	0.34	0.33	0.36	0.006
60	3	0.41	0.40	0.43	0.007
Oxygen					
0	3	0.29	0.28	0.30	0.003
5	3	0.29	0.29	0.30	0.003
10	3	0.32	0.30	0.35	0.009
20	3	0.37	0.36	0.37	0.003
30	3	0.41	0.40	0.43	0.006
60	3	0.56	0.54	0.58	0.009

Table F.21 : Statistical analysis of the formation of hydrogen peroxide in nitrogen-, air- and oxygen-saturated 0,43 mg L^{-1} hydrogen peroxide solutions during sonication in the ultrasonic cell for 1 h at an acoustic power of 57 W (Table C.11; Figure 6.11)

Time (min)	valid N	mean (mg L^{-1})	-95 % confidence limit (mg L^{-1})	+95 % confidence limit (mg L^{-1})	std deviation (mg L^{-1})
Control					
0	3	0.43	0.39	0.47	0.017
5	3	0.45	0.43	0.47	0.008
10	3	0.45	0.44	0.46	0.004
20	3	0.48	0.47	0.48	0.001
30	3	0.50	0.49	0.52	0.007
60	3	0.58	0.57	0.60	0.005

Table F.21 cont.

Time (min)	valid N	mean (mg L^{-1})	-95 % confidence limit (mg L^{-1})	+95 % confidence limit (mg L^{-1})	std deviation (mg L^{-1})
Nitrogen					
0	3	0.43	0.42	0.45	0.006
5	3	0.44	0.43	0.45	0.002
10	3	0.43	0.41	0.46	0.010
20	3	0.42	0.40	0.45	0.009
30	3	0.42	0.40	0.43	0.008
60	3	0.40	0.39	0.41	0.004
Air					
0	3	0.42	0.42	0.43	0.001
5	3	0.45	0.44	0.46	0.003
10	3	0.45	0.43	0.47	0.007
20	3	0.48	0.46	0.49	0.005
30	3	0.50	0.49	0.52	0.007
60	3	0.58	0.54	0.61	0.014
Oxygen					
0	3	0.44	0.42	0.46	0.007
5	3	0.47	0.46	0.48	0.004
10	3	0.47	0.46	0.49	0.005
20	3	0.50	0.48	0.52	0.008
30	3	0.52	0.52	0.53	0.004
60	3	0.62	0.60	0.65	0.010

Table F.22 : Statistical analysis of the formation of hydrogen peroxide in nitrogen-, air- and oxygen-saturated 0,72 mg L^{-1} hydrogen peroxide solutions during sonication in the ultrasonic cell for 1 h at an acoustic power of 57 W (Table C.12; Figure 6.12)

Time (min)	valid N	mean (mg L^{-1})	-95 % confidence limit (mg L^{-1})	+95 % confidence limit (mg L^{-1})	std deviation (mg L^{-1})
Control					
0	3	0.73	0.71	0.75	0.008
5	3	0.72	0.69	0.75	0.011
10	3	0.73	0.73	0.74	0.003
20	3	0.75	0.71	0.80	0.020
30	3	0.79	0.76	0.82	0.011
60	3	0.82	0.81	0.82	0.003
Nitrogen					
0	3	0.73	0.72	0.74	0.004
5	3	0.71	0.68	0.73	0.009
10	3	0.69	0.68	0.70	0.003
20	3	0.68	0.66	0.69	0.005
30	3	0.68	0.66	0.70	0.007
60	3	0.63	0.62	0.65	0.004

Table F.22 cont.

Time (min)	valid N	mean (mg L^{-1})	-95 % confidence limit (mg L^{-1})	+95 % confidence limit (mg L^{-1})	std deviation (mg L^{-1})
Air					
0	3	0.71	0.70	0.72	0.004
5	3	0.73	0.71	0.75	0.009
10	3	0.75	0.74	0.75	0.002
20	3	0.76	0.75	0.78	0.005
30	3	0.78	0.77	0.79	0.003
60	3	0.81	0.78	0.83	0.009
Oxygen					
0	3	0.72	0.70	0.74	0.008
5	3	0.76	0.75	0.78	0.006
10	3	0.78	0.77	0.78	0.003
20	3	0.76	0.74	0.78	0.007
30	3	0.78	0.77	0.79	0.004
60	3	0.85	0.81	0.88	0.015

F.4 OZONE EXPERIMENTS

Statistical analysis of the ozone experimental data recorded in Appendix D is presented in this section.

F.4.1 Dissolved ozone concentration

Table F.23 : Statistical analysis of the measured dissolved ozone concentration in water during ozonation (0,014 mg s^{-1}), ozonation combined with sonication (57 W), ozonation combined with hydrogen peroxide (40 mg L^{-1}) and ozonation combined with sonication and hydrogen peroxide (Table D.1; Figure 7.1)

Time (min)	valid N	mean (mg L^{-1})	-95 % confidence limit (mg L^{-1})	+95 % confidence limit (mg L^{-1})	std deviation (mg L^{-1})
Ozone					
0	2	0.00	-	-	0.000
1	2	0.39	0.33	0.44	0.006
2.5	2	0.85	0.00	1.82	0.108
5	2	1.20	0.62	1.77	0.063
10	2	1.34	0.45	2.23	0.099
20	2	1.13	0.00	2.33	0.134
40	2	1.08	0.32	1.84	0.084
60	2	1.01	0.10	1.92	0.101
Ozone/ultrasound					
0	0	0.00	-	-	0.000
1	2	0.47	0.35	0.59	0.013
2.5	2	0.73	0.25	1.22	0.054
5	2	0.75	0.63	0.87	0.013
10	2	0.63	0.21	1.06	0.047
20	2	0.61	0.36	0.86	0.028
40	2	0.55	0.43	0.67	0.013
60	2	0.59	0.47	0.71	0.013

Table F.23 cont.

Ozone/hydrogen peroxide					
Time (min)	valid N	mean (mg L^{-1})	-95 % confidence limit (mg L^{-1})	+95 % confidence limit (mg L^{-1})	std deviation (mg L^{-1})
0	2	0.00	-	-	0.000
5	2	0.00	0.00	0.02	0.001
10	2	0.00	0.00	0.02	0.002
20	2	0.01	-	-	0.000
40	2	0.01	-	-	0.000
60	2	0.02	0.01	0.03	0.001
Ozone/ultrasound/hydrogen peroxide					
0	2	0.00	-	-	0.000
5	2	0.02	0.01	0.03	0.001
10	2	0.02	0.01	0.03	0.001
20	2	0.02	-	-	0.000
40	2	0.02	-	-	0.000
60	2	0.05	0.00	0.31	0.030

F.4.2 Ozone decomposition

Table F.24 : Statistical analysis of the dissolved ozone concentration in water in the ultrasonic cell after a 20 min saturation period during ozonation (0,014 mg s^{-1}), sonication (57 W) and ozonation combined with sonication (Table D.2; Figure 7.3)

Control					
Time (min)	valid N	mean (mg L^{-1})	-95 % confidence limit (mg L^{-1})	+95 % confidence limit (mg L^{-1})	std deviation (mg L^{-1})
0	2	1.51	0.70	2.31	0.090
5	1	1.40	-	-	-
10	2	1.38	1.18	1.58	0.023
20	2	1.25	0.94	1.55	0.034
40	2	1.34	0.64	2.05	0.078
Ozone					
0	2	1.13	0.00	2.33	0.134
20	2	1.08	0.32	1.84	0.085
40	2	1.01	0.10	1.92	0.101
Ultrasound					
0	0	0.94	0.65	1.24	0.033
2.5	2	0.45	0.33	0.57	0.013
5	2	0.28	0.21	0.34	0.007
10	2	0.13	0.12	0.14	0.001
20	2	0.06	0.00	0.25	0.022
Ozone/ultrasound					
0	2	0.00	0.54	1.75	0.067
2.5	2	0.53	0.00	1.07	0.060
5	2	0.52	0.00	1.55	0.115
10	2	0.46	0.34	0.58	0.013
20	2	0.46	0.43	0.49	0.004
40	2	0.40	0.22	0.59	0.021

F.4.3 Hydrogen peroxide formation

Table F.25 : Statistical analysis of the formation of hydrogen peroxide in water in the ultrasonic cell during ozonation (0,014 mg s^{-1}), sonication (57 W) and ozonation combined with sonication (Table D.4; Figure 7.4)

Time (min)	valid N	mean (mg L^{-1})	-95 % confidence limit (mg L^{-1})	+95 % confidence limit (mg L^{-1})	std deviation (mg L^{-1})
Ozone					
0	2	0.00	-	-	0.000
5	2	0.00	-	-	0.000
10	2	0.00	0.00	0.02	0.002
20	2	0.00	0.00	0.02	0.002
40	2	0.00	-	-	0.000
60	2	0.00	-	-	0.000
Ultrasound					
0	2	0.00	-	-	0.000
5	2	0.04	0.02	0.06	0.002
10	2	0.05	0.03	0.07	0.002
20	2	0.07	0.04	0.11	0.004
40	2	0.13	0.09	0.17	0.004
60	2	0.20	0.07	0.33	0.015
Ozone/ultrasound					
0	2	0.00	-	-	0.000
5	2	0.03	0.00	0.07	0.004
10	2	0.08	0.04	0.11	0.004
20	2	0.18	0.08	0.27	0.010
40	2	0.35	0.26	0.45	0.010
60	2	0.48	0.44	0.51	0.004

F.4.4 Mass balances

Table F.26 : Statistical analysis of the measured ozone input in the 45 min ozonation, ozonation combined with sonication, ozonation combined with hydrogen peroxide and ozonation combined with sonication and hydrogen peroxide mass balance experiments (Table D.4)

Mass balance experiment	Ozone input				
	valid N	mean (mg)	-95 % confidence limit (mg)	+95 % confidence limit (mg)	std deviation (mg)
ozone	3	54.6	50.1	59.1	1.82
ozone/uls	4	49.2	42.5	55.9	4.21
ozone/H_2O_2	3	49.0	38.9	59.1	4.07
ozone/uls/H_2O_2	3	50.8	43.2	58.5	3.08
total	**13**	**50.8**	**48.5**	**53.1**	**3.82**

Table F.27 : Statistical analysis of the ozone and hydrogen peroxide measurements in water after the 45 min ozonation, ozonation combined with sonication, ozonation combined with hydrogen peroxide, and ozonation combined with sonication and hydrogen peroxide mass balance experiments (Table D.6)

	valid N	mean ($mg\ L^{-1}$)	-95 % confidence limit ($mg\ L^{-1}$)	+95 % confidence limit ($mg\ L^{-1}$)	std deviation ($mg\ L^{-1}$)
Ozone					
dissolved ozone (mg)	2	0.62	0.42	0.81	0.021
gas-phase ozone (mg)	2	4.84	-	-	0.000
ozone in KI traps (mg)	2	46.92	44.56	49.27	0.262
H_2O_2 in solution ($mg\ L^{-1}$)	2	0.01	0.00	0.07	0.007
Ozone/ultrasound					
dissolved ozone (mg)	2	0.22	0.07	0.37	0.017
gas-phase ozone (mg)	2	4.55	-	-	0.000
ozone in KI traps (mg)	2	35.91	31.56	40.26	0.484
H_2O_2 in solution ($mg\ L^{-1}$)	2	0.23	0.00	0.49	0.029
Ozone/H_2O_2					
dissolved ozone (mg)	2	0.04	0.00	0.53	0.054
gas-phase ozone (mg)	2	4.53	-	-	0.000
ozone in KI traps (mg)	2	35.26	35.13	35.39	0.014
Ozone/ultrasound/H_2O_2					
dissolved ozone (mg)	2	0.04	0.00	0.09	0.006
gas-phase ozone (mg)	2	4.50	-	-	0.000
ozone in KI traps (mg)	2	34.10	30.77	37.44	0.371

F.5 ATRAZINE EXPERIMENTS

Statistical analysis of the atrazine experimental data recorded in Appendix E is presented in this section.

F.5.1 Atrazine chemistry

Table F.28 : Statistical analysis of the atrazine concentration in a 5 $mg\ L^{-1}$ atrazine solution in the ultrasonic cell over 3 h in the absence of ultrasound without and with oxygen sparging (Table E.1; Figure 8.1)

Time (min)	valid N	mean ($mg\ L^{-1}$)	-95 % confidence limit ($mg\ L^{-1}$)	+95 % confidence limit ($mg\ L^{-1}$)	std deviation ($mg\ L^{-1}$)
Control					
0	3	5.5	4.4	6.5	0.42
45	3	5.3	4.5	6.1	0.31
90	3	5.2	4.5	5.9	0.27
135	3	5.0	4.7	5.4	0.15
180	3	5.4	5.0	5.7	0.14

Table F.28 cont.

Oxygen					
Time (min)	valid N	mean (mg L^{-1})	-95 % confidence limit (mg L^{-1})	+95 % confidence limit (mg L^{-1})	std deviation (mg L^{-1})
0	3	4.9	4.7	5.1	0.08
45	3	4.9	4.6	5.2	0.12
90	3	4.8	4.0	5.7	0.34
135	3	5.1	4.6	5.6	0.21
180	3	4.8	4.5	5.0	0.10

F.5.1.1 Ozone

Table F.29 : Statistical analysis of the measured dissolved ozone concentration in a 5 mg L^{-1} atrazine solution during ozonation (0,014 mg s^{-1}), ozonation combined with sonication (57 W), ozonation combined with hydrogen peroxide (40 mg L^{-1}) and ozonation combined with sonication and hydrogen peroxide (Table E.2; Figure 8.4)

Ozone					
Time (min)	valid N	mean (mg L^{-1})	-95 % confidence limit (mg L^{-1})	+95 % confidence limit (mg L^{-1})	std deviation (mg L^{-1})
0	2	0.00	-	-	0.000
1	2	0.29	0.00	0.59	0.033
2.5	2	0.57	0.45	0.69	0.013
5	2	0.69	0.44	0.93	0.027
10	2	0.58	-	-	0.000
20	2	0.57	0.45	0.69	0.013
40	2	0.58	0.46	0.70	0.013
60	2	0.46	0.04	0.88	0.047
Ozone/ultrasound					
0	0	0.00	-	-	0.000
1	2	0.35	0.12	0.59	0.026
2.5	2	0.39	0.19	0.60	0.023
5	2	0.38	0.04	0.71	0.037
10	2	0.36	0.26	0.46	0.011
20	2	0.34	0.12	0.56	0.025
40	2	0.38	0.15	0.62	0.026
60	2	0.33	0.06	0.60	0.030
Ozone/hydrogen peroxide					
0	2	0.00	-	-	0.000
2.5	2	0.24	0.17	0.31	0.008
5	2	0.38	0.15	0.62	0.026
10	2	0.36	0.00	0.81	0.051
20	2	0.42	0.00	1.17	0.084
40	2	0.33	0.11	0.55	0.025
60	2	0.39	0.00	0.92	0.059
Ozone/ultrasound/hydrogen peroxide					
0	2	0.00	-	-	0.000
2.5	2	0.13	0.01	0.25	0.013
5	2	0.21	0.00	0.43	0.024
10	2	0.17	0.09	0.25	0.009
20	2	0.15	0.00	0.42	0.030
40	2	0.09	0.00	0.21	0.013
60	2	0.04	0.02	0.06	0.002

F.5.1.2 Hydrogen peroxide

Table F.30 : Statistical analysis of the formation of hydrogen peroxide in a 5 mg L^{-1} atrazine solution in the ultrasonic cell during ozonation (0,014 mg s^{-1}), sonication (57 W) and ozonation combined with sonication (Table E.3; Figure 8.6)

Time (min)	valid N	mean (mg L^{-1})	-95 % confidence limit (mg L^{-1})	+95 % confidence limit (mg L^{-1})	std deviation (mg L^{-1})
Ozone					
0	2	0.00	-	-	0.000
5	2	0.18	0.14	0.22	0.004
10	2	0.34	0.32	0.36	0.002
20	2	0.67	0.63	0.71	0.004
40	2	1.18	1.14	1.21	0.004
60	2	1.64	1.38	1.90	0.029
Ultrasound					
0	0	0.00	-	-	0.000
5	2	0.03	0.01	0.05	0.002
10	2	0.04	0.01	0.08	0.004
20	2	0.09	-	-	0.000
40	2	0.17	0.00	0.38	0.023
60	2	0.19	0.14	0.25	0.006
Ozone/ultrasound					
0	2	0.00	-	-	0.000
5	2	0.22	0.05	0.38	0.019
10	2	0.40	0.33	0.48	0.008
20	2	0.71	0.45	0.97	0.030
40	2	1.22	1.18	1.25	0.004
60	2	1.57	1.09	2.06	0.054

F.5.1.3 Mass balances

Table F.31 : Statistical analysis of the ozone, hydrogen peroxide and atrazine measurements in a 5 mg L^{-1} atrazine solution after the 45 min ozonation, ozonation combined with sonication, ozonation combined with hydrogen peroxide and ozonation combined with sonication and hydrogen peroxide mass balance experiments (Table E.4)

	valid N	mean (mg L^{-1})	-95 % confidence limit (mg L^{-1})	+95 % confidence limit (mg L^{-1})	std deviation (mg L^{-1})
Ozone					
dissolved ozone (mg)	2	0.20	0.00	0.64	0.049
gas-phase ozone (mg)	2	4.84	-	-	0.000
ozone in KI traps (mg)	2	44.49	30.95	58.02	1.506
H_2O_2 in solution (mg L^{-1})	2	1.20	0.50	1.89	0.078
initial atrazine (mg L^{-1})	2	5.16	4.91	5.41	0.028
final atrazine (mg L^{-1})	2	3.83	-	-	0.000

Table F.31 cont.

	valid N	mean (mg L^{-1})	-95 % confidence limit (mg L^{-1})	+95 % confidence limit (mg L^{-1})	std deviation (mg L^{-1})
Ozone/ultrasound					
dissolved ozone (mg)	2	0.00	0.00	0.20	0.045
gas-phase ozone (mg)	2	4.55	-	-	0.000
ozone in KI traps (mg)	2	30.61	29.96	31.26	0.262
H_2O_2 in solution (mg L^{-1})	2	1.41	1.29	1.52	0.045
initial atrazine (mg L^{-1})	2	5.12	4.80	5.43	0.127
final atrazine (mg L^{-1})	2	3.38	3.10	3.66	0.114
Ozone/H_2O_2					
dissolved ozone (mg)	2	0.18	0.08	0.29	0.041
gas-phase ozone (mg)	2	4.53	-	-	0.000
ozone in KI traps (mg)	2	33.89	32.81	34.97	0.434
initial atrazine (mg L^{-1})	2	6.33	5.67	7.00	0.270
final atrazine (mg L^{-1})	2	3.66	3.27	4.05	0.158
Ozone/ultrasound/H_2O_2					
dissolved ozone (mg)	2	0.02	0.00	0.05	0.004
gas-phase ozone (mg)	2	4.50	-	-	0.000
ozone in KI traps (mg)	2	29.53	28.16	30.89	0.152
initial atrazine (mg L^{-1})	2	6.08	5.87	6.28	0.023
final atrazine (mg L^{-1})	2	3.96	3.79	4.12	0.019

F.5.2 Atrazine degradation

F.5.2.1 Ultrasound

Table F.32 : Statistical analysis of the atrazine concentration measured in a 5, 10 and 20 mg L^{-1} atrazine solution during sonication in the ultrasonic cell at an acoustic power of 57 W over 3 h (Table E.5; Figure 8.7)

Time (min)	valid N	mean (mg L^{-1})	-95 % confidence limit (mg L^{-1})	+95 % confidence limit (mg L^{-1})	std deviation (mg L^{-1})
5 mg L^{-1}					
0	3	5.8	4.9	6.7	0.36
45	3	5.1	4.0	6.2	0.44
90	3	4.8	4.3	5.4	0.21
135	3	4.6	3.6	5.6	0.39
180	3	4.3	3.9	4.6	0.15
10 mg L^{-1}					
0	3	11.4	10.2	12.6	0.48
45	3	10.8	10.5	11.2	0.16
90	3	10.8	10.1	11.5	0.30
135	3	10.3	9.3	11.4	0.42
180	3	9.8	9.0	10.6	0.32

Table F.32 cont.

20 mg L^{-1}					
Time (min)	valid N	mean (mg L^{-1})	-95 % confidence limit (mg L^{-1})	+95 % confidence limit (mg L^{-1})	std deviation (mg L^{-1})
0	3	20.6	20.0	21.2	0.24
45	3	21.2	19.2	23.2	0.80
90	3	20.2	16.5	21.0	0.32
135	3	21.1	19.6	22.5	0.57
180	3	19.3	16.2	22.5	1.27

Table F.33 : Statistical analysis of the initial concentration of the 5 mg L^{-1} atrazine solutions used in the atrazine investigation

valid N	mean (mg L^{-1})	-95 % confidence limit (mg L^{-1})	+95 % confidence limit (mg L^{-1})	std deviation (mg L^{-1})
66	5.2	5.1	5.3	0.43

Table F.34 : Statistical analysis of the effect of oxygen and nitrogen sparging on the degradation of atrazine in a 5 mg L^{-1} atrazine solution during sonication in the ultrasonic cell at an acoustic power of 57 W over 3 h (Table E.6; Figure 8.8)

Nitrogen					
Time (min)	valid N	mean (mg L^{-1})	-95 % confidence limit (mg L^{-1})	+95 % confidence limit (mg L^{-1})	std deviation (mg L^{-1})
0	3	5.3	4.5	6.0	0.30
45	3	5.1	4.6	5.7	0.21
90	3	5.0	3.8	6.3	0.51
135	3	5.2	4.5	5.9	0.28
180	3	4.9	4.2	5.6	0.29
Oxygen					
0	0	5.3	5.0	5.5	0.08
45	3	4.9	4.6	5.2	0.12
90	3	4.8	4.6	4.9	0.05
135	3	4.5	4.4	4.7	0.06
180	3	4.0	3.5	4.5	0.20

F.5.2.2 Ozone

Table F.35 : Statistical analysis of the atrazine concentration in a 5 mg L^{-1} atrazine solution during ozonation at ozone production rates of 0,003; 0,014; 0,030 and 0,047 mg s^{-1} (Table E.7; Figure 8.9)

0,003 mg s^{-1}					
Time (min)	valid N	mean (mg L^{-1})	-95 % confidence limit (mg L^{-1})	+95 % confidence limit (mg L^{-1})	std deviation (mg L^{-1})
0	2	5.0	4.9	5.1	0.01
45	2	4.1	2.5	5.7	0.18
90	2	3.5	3.0	4.0	0.06
135	2	3.2	2.5	3.9	0.08
180	2	2.7	2.6	2.8	0.01

Table F.35 cont.

Time (min)	valid N	mean (mg L^{-1})	-95 % confidence limit (mg L^{-1})	+95 % confidence limit (mg L^{-1})	std deviation (mg L^{-1})
0,014 mg s^{-1}					
0	2	5.1	4.7	5.6	0.05
45	2	4.3	3.1	5.4	0.13
90	2	3.6	0.9	6.3	0.30
135	2	3.0	2.5	3.5	0.05
180	2	2.5	1.4	3.5	0.11
0,030 mg s^{-1}					
0	2	5.1	4.0	6.2	0.12
45	2	2.6	0.6	4.6	0.22
90	2	2.2	0.9	3.4	0.14
135	2	1.3	0.6	2.0	0.08
180	2	0.9	0.5	1.4	0.05
0,047 mg s^{-1}					
0	2	5.1	2.9	7.3	0.25
45	2	1.8	1.6	2.0	0.02
90	2	0.9	0.2	1.6	0.07
135	2	0.6	0.0	1.9	0.15
180	2	0.2	0.0	0.3	0.02

Table F.36 : Statistical analysis of the atrazine concentration in a 5 mg L^{-1} atrazine solution during ozonation over 3 h at ozone production rates of 0,003; 0,014; 0,030 and 0,047 mg s^{-1} and sonication at an acoustic power of 57 W (Table E.8; Figure 8.11)

Time (min)	valid N	mean (mg L^{-1})	-95 % confidence limit (mg L^{-1})	+95 % confidence limit (mg L^{-1})	std deviation (mg L^{-1})
Ultrasound/0,003 mg s^{-1} ozone					
0	2	4.8	4.7	4.8	0.01
45	2	3.4	2.9	3.9	0.06
90	2	3.2	3.1	3.3	0.01
135	2	3.0	2.5	3.4	0.05
180	2	2.7	0.5	4.9	0.25
Ultrasound/0,014 mg s^{-1} ozone					
0	3	5.1	4.5	5.6	0.21
45	3	3.4	3.1	3.7	0.11
90	3	2.2	1.9	2.6	0.14
135	3	2.0	1.8	2.1	0.05
180	3	1.5	1.1	2.0	0.19
Ultrasound/0,030 mg s^{-1} ozone					
0	3	0.0	5.0	5.4	0.09
45	3	2.3	2.1	2.4	0.07
90	3	1.7	1.4	1.9	0.11
135	3	1.1	0.9	1.3	0.08
180	3	0.6	0.6	0.6	0.01

Table F.36 cont.

Ultrasound/0,047 mg s^{-1} ozone					
Time (min)	valid N	mean (mg L^{-1})	-95 % confidence limit (mg L^{-1})	+95 % confidence limit (mg L^{-1})	std deviation (mg L^{-1})
0	3	0.0	4.9	4.9	0.02
45	3	1.4	1.3	1.6	0.06
90	3	0.5	0.4	0.5	0.02
135	3	0.1	0.0	0.2	0.05
180	3	0.0	-	-	0.00

F.5.2.3 Hydrogen peroxide

Table F.37 : Statistical analysis of the fraction of undegraded atrazine in a 5 mg L^{-1} atrazine solution after ozonation (0,0014 mg s^{-1}) for 45 min with hydrogen peroxide concentrations of 1, 5, 10, 25 and 50 mg L^{-1} (Table E.9; Figure E.5)

H_2O_2 (mg L^{-1})	valid N	mean (%)	-95 % confidence limit (%)	+95 % confidence limit (%)	std deviation (%)
0	2	81	42	120	4.3
1	2	68	63	72	0.5
5	2	66	57	75	1.0
10	2	64	61	68	0.4
25	3	79	44	115	4.0
50	3	76	24	127	5.8

Table F.38 : Statistical analysis of the atrazine concentration in a 5 mg L^{-1} atrazine solution with 40 mg L^{-1} hydrogen peroxide, hydrogen peroxide combined with sonication (57 W), hydrogen peroxide combined with ozonation (0,014 mg s^{-1}) and hydrogen peroxide combined with sonication and ozonation (Table E.10; Figure 8.14)

H_2O_2					
Time (min)	valid N	mean (mg L^{-1})	-95 % confidence limit (mg L^{-1})	+95 % confidence limit (mg L^{-1})	std deviation (mg L^{-1})
0	3	5.0	4.7	5.4	0.14
45	3	5.0	4.6	5.3	0.14
90	3	4.7	4.3	5.1	0.17
135	3	4.8	4.2	5.4	0.23
180	3	4.6	4.3	5.0	0.14
Ultrasound/H_2O_2					
0	0	0.0	4.9	5.2	0.02
45	2	4.4	4.3	4.5	0.01
90	2	4.1	3.2	4.9	0.09
135	2	3.3	3.1	3.5	0.02
180	2	2.9	1.4	4.4	0.17

Table F.38 cont.

Time (min)	valid N	mean (mg L^{-1})	-95 % confidence limit (mg L^{-1})	+95 % confidence limit (mg L^{-1})	std deviation (mg L^{-1})
Ozone/H_2O_2					
0	3	0.0	5.2	5.8	0.12
15	3	4.4	3.9	4.8	0.19
30	3	3.8	3.6	4.1	0.09
45	3	3.4	3.0	3.9	0.20
90	3	2.6	2.3	2.9	0.13
135	3	2.1	2.0	2.2	0.04
180	3	1.6	1.1	2.1	0.21
Ultrasound/ozone/H_2O_2					
0	0	5.2	5.0	5.3	0.05
15	3	4.2	3.9	4.5	0.12
30	3	4.0	4.0	4.1	0.03
45	3	3.7	3.1	4.3	0.22
90	3	2.8	2.3	3.2	0.19
135	3	2.7	2.1	3.4	0.24
180	3	2.6	2.5	2.8	0.07

G

FREE RADICAL REACTIONS

Free radicals contain an unpaired electron, they are thus extremely reactive and in general exist only for a short time period. Free radical chemistry is described in Section G.1 and the free radical reactions that occur during photolysis and radiolysis and may also occur during sonication are listed in Section G.2.

G.1 FREE RADICAL CHEMISTRY

Free radical reactions can be broadly classified as radical combination processes, where two radicals react to produce non-radical products in which all electrons are paired, and radical transfer processes which generate a new radical that reacts further with molecules around it, often propagating a chain of radical reactions (Huang et al., 1974).

Combination or coupling:

The combination of two radicals, shown in Scheme G.1, leads to bond formation. The process is extremely fast and requires little or no activation energy. Radical concentrations in solution are extremely low and combination reactions are thus, in general, not as important as transfer reactions with the solvent. Reaction conditions, however, are favourable when free radicals are formed in pairs in close proximity to each other within the solvent cage (Huang et al., 1974).

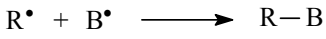

Scheme G.1

Disproportionation:

The transfer of a β-hydrogen atom from one radical to another generating non-radical products is known as disproportionation. The process is energetically favourable since two bonds are formed for one that is broken (Huang et al., 1974).

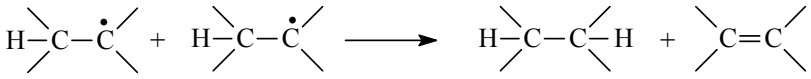

Scheme G.2

Redox reactions:

Radicals are both formed and destroyed in one-electron transfer redox reactions. Anions are produced during the reduction of radicals by transition metal ions while cations, shown in Scheme G.3, are produced during oxidation (Huang et al., 1974).

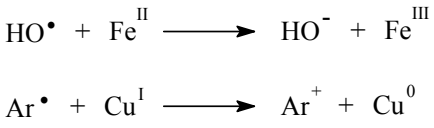

Scheme G.3

Displacement:

Displacement similar to ionic displacement (S_N reactions) rarely occurs in radical chemistry except for the abstraction of hydrogen and halogen atoms (Huang et al., 1974).

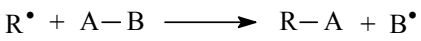

Scheme G.4

Addition:

A more stable radical is formed from the addition of a radical to an unsaturated compound, as shown in Scheme G.5. Radical polymerisation is initiated when the generated radical reacts with another molecule of the unsaturated substrate (Huang et al., 1974).

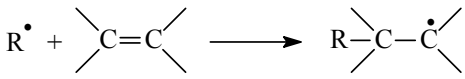

Scheme G.5

Fragmentation:

A smaller radical and an unsaturated molecule are formed when a radical breaks down by the scission of a bond β to the radical centre (Huang et al., 1974).

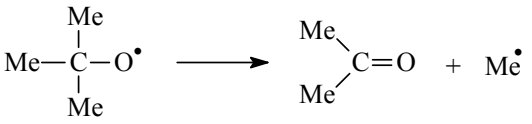

Scheme G.6

Insertion:

The insertion reaction is peculiar to carbenes and nitrenes. The insertion of methylene (H_2C:) into the C-H bonds of pentane, as shown in Scheme G.7, produces isomeric hexanes (Huang et al., 1974).

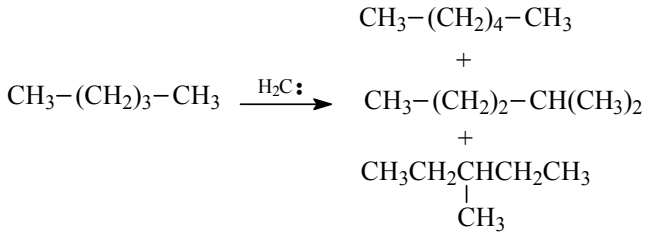

Scheme G.7

G.2 RADICAL REACTIONS

The conditions in the cavitation bubbles during sonication are similar to that initiated during radiolysis and photolysis. Radical reactions occurring during radiolysis and photolysis can thus occur during sonication. The reactions proposed by Spinks and Woods that occur during the radiolysis of water include the reactions listed in Scheme G.8 (Spinks and Woods, 1976).

$$H_2O + h\nu \rightarrow H^{\bullet} + HO^{\bullet} \quad [a]$$

$$H_2O + h\nu \rightarrow H_2 + O \quad [b]$$

$$H^{\bullet} + HO^{\bullet} \rightarrow H_2O \quad [c]$$

$$H^{\bullet} + H^{\bullet} \rightarrow H_2 \quad [d]$$

$$HO^{\bullet} + HO^{\bullet} \rightarrow H_2O_2 \quad [e]$$

$$H^{\bullet} + HO^{\bullet} \rightarrow H_2 + O \quad [f]$$

$$HO^{\bullet} + HO^{\bullet} + M \rightarrow H_2O + O \quad [g]$$

$$O + HO^{\bullet} \rightarrow H^{\bullet} + O_2 \quad [h]$$

$$HO^{\bullet} + H_2 \rightarrow H_2O + H^{\bullet} \quad [i]$$

$$O + H_2O \rightarrow H_2O_2 \quad [j]$$

$$O + H_2O \rightarrow 2HO^{\bullet} \quad [k]$$

$$H^{\bullet} + H_2O_2 \rightarrow H_2O + HO^{\bullet} \quad [m]$$

$$HO^{\bullet} + H_2O_2 \rightarrow H_2O + HO_2^{\bullet} \quad [n]$$

$$HO_2^{\bullet} \rightleftharpoons O_2^{\bullet -} + H^+ \quad [o]$$

$$HO^{\bullet} \rightleftharpoons O^{\bullet -} + H^+ \quad [p]$$

$$H_2O_2 \rightleftharpoons HO_2^- + H^+ \quad [q]$$

$$H^- + H_2O \rightarrow HO^- + H_2 \quad [r]$$

$$HO^+ + H_2O \rightarrow H_3O^+ + O \quad [s]$$

$$H^{\bullet} + O_2 \rightarrow HO_2^{\bullet} \quad [t]$$

$$2O_2^- + 2H^+ \rightarrow H_2O_2 + O_2 \quad [u]$$

$$H^{\bullet} + H^{\bullet} \rightarrow H_2 \quad [v]$$

$$HO^{\bullet} + HO^{-} \rightarrow H_2O + O^{-} \quad [w]$$

Scheme G.8

The radical reactions proposed by Lii and co-workers that occur in a pulse irradiated Ar-H_2O-O_2 system during radiation with a high-pressure xenon lamp are listed in Scheme G.9 (Lii et al., 1980).

$$HO^{\bullet} + HO_2^{\bullet} \rightarrow O_2 + H_2O \quad [a]$$

$$HO^{\bullet} + HO^{\bullet} \rightarrow O + H_2O \quad [b]$$

$$HO^{\bullet} + HO^{\bullet} \rightarrow H_2O_2 \quad [c]$$

$$O_2 + O \rightarrow O_3 \quad [d]$$

$$H^{\bullet} + O_2 \rightarrow HO_2^{\bullet} \quad [e]$$

$$HO_2^{\bullet} + HO_2^{\bullet} \rightarrow O_2 + H_2O_2 \quad [f]$$

$$HO^{\bullet} + H_2O_2 \rightarrow HO_2^{\bullet} + H_2O \quad [g]$$

$$O_3 + HO^{\bullet} \rightarrow O_2 + HO_2^{\bullet} \quad [h]$$

$$O + HO_2^{\bullet} \rightarrow O_2 + HO^{\bullet} \quad [i]$$

$$H^{\bullet} + HO_2^{\bullet} \rightarrow O_2 + H_2 \quad [j]$$

$$H^{\bullet} + HO_2^{\bullet} \rightarrow HO^{\bullet} + HO^{\bullet} \quad [k]$$

$$H^{\bullet} + HO_2^{\bullet} \rightarrow O + H_2O \quad [l]$$

$$H^{\bullet} + HO^{\bullet} \rightarrow H_2O \quad [m]$$

$$O + HO^{\bullet} \rightarrow H^{\bullet} + O_2 \quad [n]$$

Scheme G.9

The radical reactions proposed by Gonzalez and Mártire that occur during the UV photolysis of alkaline solutions of hydrogen peroxide are listed in Scheme G.10 (Gonzalez and Mártire, 1997).

$$O^{\bullet -} + O_2 \rightarrow O_3^{\bullet -} \quad [a]$$

$$HO^{\bullet} \rightleftharpoons O^{\bullet -} + H^{+} \quad [b]$$

$$O_3^{\bullet -} \rightarrow O^{\bullet -} + O_2 \quad [c]$$

$$O^{\bullet -} + O_3^{\bullet -} \rightarrow O_2^{\bullet -} + O_2^{\bullet -} \quad [d]$$

$$H_2O_2 \rightleftharpoons HO_2^{-} + H^{+} \quad [e]$$

$$HO^{\bullet} + HO_2^{-} \rightarrow O_2^{\bullet -} + H_2O \quad [f]$$

$$O^{\bullet -} + HO_2^{-} \rightarrow O_2^{\bullet -} + HO^{-} \quad [g]$$

$$HO^{\bullet} + HO^{\bullet} \rightarrow HO_2^{-} + H^{+} \quad [h]$$

$$O^{\bullet -} + HO^{\bullet} \rightarrow HO_2^{-} \quad [i]$$

$$O^{\bullet -} + O^{\bullet -} + H_2O \rightarrow HO_2^{-} + HO^{-} \quad [j]$$

$$HO^{\bullet} + O_2^{\bullet -} \rightarrow O_2 + HO^{-} \quad [k]$$

$$HO^{\bullet} + O_3^{\bullet -} \rightarrow H^+ + 2O_2^{\bullet -} \quad [m]$$

$$HO^{\bullet} + O_3^{\bullet -} \rightarrow HO^- + O_3 \quad [n]$$

$$O^{\bullet -} + O_2^{\bullet -} + H_2O \rightarrow O_2 + 2HO^- \quad [o]$$

$$O_2^{\bullet -} + O_2^{\bullet -} + H_2O \rightarrow O_2 + HO^- + HO_2^- \quad [p]$$

$$O_2^{\bullet -} + H_2O_2 \rightarrow HO^- + HO^{\bullet} + O_2 \quad [q]$$

$$O_2^{\bullet -} + HO_2^- \rightarrow O^{\bullet -} + HO^- + O_2 \quad [r]$$

$$O_3^{\bullet -} + O_2^{\bullet -} + H_2O \rightarrow 2HO^- + 2O_2 \quad [s]$$

$$O_3 + HO^- \rightarrow O_2 + HO_2^- \quad [t]$$

$$O_3 + O^{\bullet -} \rightarrow O_2 + O_2^{\bullet -} \quad [u]$$

$$O_3 + O_2^{\bullet -} \rightarrow O_2 + O_3^{\bullet -} \quad [v]$$

Scheme G.10

The radical reactions proposed by Podolske and Johnston that occur during the photolysis of ozone are listed in Scheme G.11 (Podolske and Johnston, 1983).

$$O + O_3 \rightarrow O_2 + O_2 \quad [a]$$

$$O + O_2 + H_2O \rightarrow O_3 + H_2O \quad [b]$$

$$O + O_2 + He \rightarrow O_3 + He \quad [c]$$

$$O + O_2 + O_2 \rightarrow O_3 + O_2 \quad [d]$$

$$O + O_2 + O_3 \rightarrow O_3 + O_3 \quad [e]$$

$$O + HO^{\bullet} \rightarrow H^{\bullet} + O_2 \quad [f]$$

$$O + HO_2^{\bullet} \rightarrow HO^{\bullet} + O_2 \quad [g]$$

$$O + H_2O_2 \rightarrow HO^{\bullet} + HO_2^{\bullet} \quad [h]$$

$$HO^{\bullet} + O_3 \rightarrow HO_2^{\bullet} + O_2 \quad [i]$$

$$HO^{\bullet} + HO^{\bullet} \rightarrow H_2O + O \quad [j]$$

$$HO^{\bullet} + HO^{\bullet} \rightarrow H_2O_2 \quad [k]$$

$$HO^{\bullet} + H_2O_2 \rightarrow HO_2^{\bullet} + H_2O \quad [l]$$

$$HO_2^{\bullet} + O_3 \rightarrow HO^{\bullet} + O_2 + O_2 \quad [m]$$

$$HO_2^{\bullet} + HO_2^{\bullet} \rightarrow O_2 + H_2O_2 \quad [n]$$

$$H^{\bullet} + O_3 \rightarrow HO^{\bullet} + O_2 \quad [o]$$

$$H^{\bullet} + O_2 + He \rightarrow HO_2^{\bullet} + He \quad [p]$$

$$H^{\bullet} + O_2 + H_2O \rightarrow HO_2^{\bullet} + H_2O \quad [q]$$

$$H^{\bullet} + O_2 + O_2 \rightarrow HO_2^{\bullet} + O_2 \quad [r]$$

$$HO^{\bullet} + HO_2^{\bullet} \rightarrow O_2 + H_2O \quad [s]$$

Scheme G.11

H

SUMMARY OF RADICAL REACTIONS

Free radical reactions are repeated from the literature chapters to facilitate the discussion and comparison of the reactions occurring sonication, ozonation and with the addition of hydrogen peroxide.

H.1 RADICAL REACTIONS: ULTRASOUND

$$H_2O \rightarrow HO^{\bullet} + H^{\bullet}$$

Scheme 2.1

$$H^{\bullet} + HO^{\bullet} \rightarrow H_2O \quad [a]$$
$$HO^{\bullet} + HO^{\bullet} \rightarrow H_2O_2 \quad [b]$$
$$H^{\bullet} + H^{\bullet} \rightarrow H_2 \quad [c]$$

Scheme 2.2

$$H^{\bullet} + O_2 \rightarrow HO_2^{\bullet} \quad [a]$$
$$HO_2^{\bullet} + H^{\bullet} \rightarrow H_2O_2 \quad [b]$$
$$HO_2^{\bullet} + HO_2^{\bullet} \rightarrow H_2O_2 + O_2 \quad [c]$$

Scheme 2.3

$$HO^{\bullet} + HO_2^{\bullet} \rightarrow H_2O + O_2 \quad [a]$$
$$HO^{\bullet} + HO^{\bullet} \rightarrow H_2O + O^{\bullet} \quad [b]$$
$$O^{\bullet} + H_2O \rightarrow H_2O_2 \quad [c]$$
$$HO^{\bullet} + HO^{\bullet} \rightarrow H_2 + O_2 \quad [d]$$

Scheme 2.4

H.2 RADICAL REACTIONS: OZONE

Initiation step

$O_3 + HO^- \xrightarrow{k_i} O_2^{\bullet -} + HO_2^{\bullet}$	$k_i = 70\ M^{-1}\ s^{-1}$	[a]

Propagation steps

$HO_2^{\bullet} \rightleftharpoons O_2^{\bullet -} + H^+$	$pK_a = 4,8$	[b]
$O_3 + O_2^{\bullet -} \xrightarrow{k_1} O_3^{\bullet -} + O_2$	$k_1 = 1,6 \times 10^9\ M^{-1}\ s^{-1}$	[c]
$O_3^{\bullet -} + H^+ \overset{k_2}{\rightleftharpoons} HO_3^{\bullet}$	$k_2 = 5,2 \times 10^{10}\ M^{-1}\ s^{-1}$	[d]
$HO_3^{\bullet} \xrightarrow{k_3} HO^{\bullet} + O_2$	$k_3 = 1,1 \times 10^5\ M^{-1}\ s^{-1}$	[e]
$O_3 + HO^{\bullet} \xrightarrow{k_4} HO_4^{\bullet}$	$k_4 = 2 \times 10^9\ M^{-1}\ s^{-1}$	[f]
$HO_4^{\bullet} \xrightarrow{k_5} HO_2^{\bullet} + O_2$	$k_5 = 2,8 \times 10^4\ M^{-1}\ s^{-1}$	[g]

Termination steps

$HO_4^{\bullet} + HO_4^{\bullet} \rightarrow H_2O_2 + 2O_3$		[h]
$HO_4^{\bullet} + HO_3^{\bullet} \rightarrow H_2O_2 + O_3 + O_2$		[i]

Scheme 3.3

H.3 RADICAL REACTIONS: OZONE/HYDROGEN PEROXIDE

Initiation steps

$O_3 + HO^- \xrightarrow{k_i} O_2^{\bullet -} + HO_2^{\bullet}$	$k_i = 70\ M^{-1}\ s^{-1}$	[a]
$HO_2^{\bullet} \rightleftharpoons O_2^{\bullet -} + H^+$	$pK_a = 4,8$	[b]
$H_2O_2 \rightleftharpoons HO_2^- + H^+$	$pK = 11,8$	[c]
$O_3 + HO_2^- \xrightarrow{k'_i} O_3^{\bullet -} + HO_2^{\bullet}$	$k'_i = 2,8 \times 10^6\ M^{-1}\ s^{-1}$	[d]

Propagation steps

$O_3 + O_2^{\bullet -} \xrightarrow{k_1} O_3^{\bullet -} + O_2$	$k_1 = 1,6 \times 10^9\ M^{-1}\ s^{-1}$	[e]
$O_3^{\bullet -} + H^+ \overset{k_2}{\rightleftharpoons} HO_3^{\bullet}$	$k_2 = 5,2 \times 10^{10}\ M^{-1}\ s^{-1}$	[f]
$HO_3^{\bullet} \xrightarrow{k_3} HO^{\bullet} + O_2$	$k_3 = 1,1 \times 10^5\ M^{-1}\ s^{-1}$	[g]
$O_3 + HO^{\bullet} \xrightarrow{k_4} O_2 + HO_2^{\bullet}$	$k_4 = 2,0 \times 10^9\ M^{-1}\ s^{-1}$	[h]
$HO^{\bullet} + H_2O_2 \xrightarrow{k_5} O_2^{\bullet -} + H_2O + H^+$	$k_5 = 2,7 \times 10^7\ M^{-1}\ s^{-1}$	[i]
$HO^{\bullet} + HO_2^- \xrightarrow{k_6} O_2^{\bullet -} + H_2O$	$k_6 = 7,5 \times 10^9\ M^{-1}\ s^{-1}$	[j]

Termination steps

$HO^{\bullet} + B \xrightarrow{k_{HO,B}} B'_{oxid}$		[k]
$O_3 + B \xrightarrow{k_d} B_{oxid}$		[l]

Scheme 3.6